

LAWRENCE TECHNOLOGICAL UNIVERSITY



INSPECTION AND DETERIORATION OF BRIDGE DECKS CONSTRUCTED USING STAY-IN-PLACE METAL FORMS AND EPOXY-COATED REINFORCEMENT

by

**Dr. Nabil Grace, Principal Investigator
and Dr. Jim Hanson, Co-Principal Investigator**

Submitted to

Roger D. Till, Engineer of Structural Research

Testing and Research Section
Construction and Technology Division
Contract # 2002-0134

Department of Civil Engineering
Lawrence Technological University
Southfield, MI 48075-1058, USA

October, 2004

1. Report No. Research Report R	2. Government Accession No.	3. MDOT Project Manager Roger Till	
4. Title and Subtitle Inspection and Deterioration of Bridge Decks Constructed Using Stay-in-Place Metal Forms and Epoxy-Coated Reinforcement		5. Report Date October 2004	
7. Author(s) Dr. Nabil Grace, Dr. Jim Hanson, and Hany AbdelMessih		6. Performing Organization Code	
9. Performing Organization Name and Address Lawrence Technological University 21000 West Ten Mile Rd. Southfield. MI 48075		8. Performing Org Report No.	
12. Sponsoring Agency Name and Address Michigan Department of Transportation Construction and Technology Division P.O. Box 30049 Lansing, MI 48909		10. Work Unit No. (TRAIS)	
		11. Contract Number: 2002-0134	
		11(a). Authorization Number:	
15. Supplementary Notes		13. Type of Report & Period Covered Research Report 2002 - 2004	
		14. Sponsoring Agency Code	
16. Abstract <p>A comprehensive research investigation was conducted to evaluate the use of Stay-in-Place Metal Forms (SIPMFs) in construction of concrete bridge decks. The objectives of this research project were to establish the state-of-the-practice for use and performance of SIPMFs for bridge decks, to evaluate the field performance of bridge decks with and without SIPMFs, and to investigate the behavior of environmentally conditioned large-scale laboratory bridge deck specimens with and without SIPMFs.</p> <p>A survey was developed and administered to all DOTs to examine the state-of-the-practice of using SIPMFs for concrete bridge deck construction. Additionally, a field investigation was conducted to evaluate the performance of existing concrete bridge decks constructed with and without SIPMFs. This field investigation included visual inspection of 10 bridge decks and laboratory investigation of full-depth cores obtained from the inspected bridge decks. The cores were investigated using visual inspection, compressive strength tests, and ultrasonic tests.</p> <p>A laboratory durability investigation was conducted on 24 large-scale bridge deck slab specimens with and without SIPMF. Four specimens were used as control specimens, and the remaining 20 specimens were subjected to either freeze/thaw exposure and repeated load cycles or salt-water exposure and repeated load cycles. All specimens were constructed using epoxy-coated steel reinforcing. At various stages before, during, and after the environmental exposures, ultrasonic pulse-echo testing was used to determine the quality of contact between the SIPMFs and concrete for specimens with SIPMFs. Furthermore, after the completion of the environmental exposure, ultrasonic through-transmission testing was used to assess the condition of the concrete for all specimens.</p> <p>Overall, a statistical bias was present in the results of the survey as a function of climate region. Apparent equivalency of deck performance was observed using field inspection as well as visual inspection, compressive strength, and pulse-velocity profiles of the cores. Small changes in the performance of bridge deck specimens with and without SIPMF were measured during the structural and ultrasonic laboratory test programs.</p>			
17. Key Words		18. Distribution Statement No restrictions. This document is available to the public through the Michigan Department of Transportation.	
19. Security Classification (report) Unclassified	20. Security Classification (Page) Unclassified	21. No of Pages 359	22. Price

Michigan Department of Transportation

Roger D. Till, *Project Coordinator*
Materials and Technology Laboratories

Eric Burns
Materials and Technology Laboratories

Dave Juntunen
Construction

Chuck Occhinto
Design

John Staton
Materials

Lawrence Technological University

Nabil Grace, *Project Advisor*

Jim Hanson, *Project Advisor*

Hany I. AbdelMessih, *Graduate Research Assistant*

MDOT Contract Number: 2002 – 0134

Principal Investigator:	Nabil Grace, LTU
Co-Principal Investigator:	Jim Hanson, LTU
Project Coordinator:	Roger D. Till, MDOT

October, 2004

Key words:

- bridge deck
- crack
- deck slab
- deterioration
- durability
- epoxy
- formwork
- freeze/thaw
- metal form
- pulse-echo
- stay-in-place metal form (SIPMF)
- salt solution
- through-transmission
- ultrasonic
- ultrasonic velocity

Department of Civil Engineering
Lawrence Technological University
21000 West Ten Mile Rd.
Southfield, MI 48075
Tel: 1-248-204-2545
Fax: 1-248-204-2568

The publication of this report does not necessarily indicate approval or endorsement of the findings, opinions, conclusions, or recommendations either inferred or specifically expressed herein, by the Regents of the Lawrence Technological University or the Michigan Department of Transportation.

ACKNOWLEDGEMENT

The research described in this report was supported by a grant from the Michigan Department of Transportation. Matching funds for student tuition and for equipment were provided by Lawrence Technological University.

The support provided by Roger Till, project coordinator of the Michigan Department of Transportation, is greatly appreciated.

The laboratory assistance provided by Mike Bellini, Charles Elder, Walid Farahat, Azmi Guirguis, Steve Mckinnon, Sreejith Puravankara, Saju Sachidanandan, Drew Weller, is greatly appreciated.

The opinions expressed in this report are those of the authors and do not necessarily reflect the views of the sponsors.

TABLE OF CONTENTS

EXECUTIVE SUMMARY	viii
CHAPTER 1: INTRODUCTION	1
CHAPTER 2: LITERATURE REVIEW	3
2.1 BRIDGE DECK CONSTRUCTION	3
2.2 CONCRETE BRIDGE DECK DESIGN	4
2.3 DETERIORATION OF CONCRETE BRIDGE DECKS	6
2.4 DETERIORATION OF CONCRETE	8
2.5 STEEL CORROSION	9
2.6 FREEZE/THAW DETERIORATION	13
2.7 ASSESSMENT OF CONCRETE	15
2.8 NONDESTRUCTIVE TESTING METHODS	17
2.9 ULTRASONIC TEST METHODS	17
CHAPTER 3: INSPECTION AND CORING OF BRIDGE DECK SLABS	27
3.1 INTRODUCTION	27
3.2 FIELD INSPECTION AND CORING	27
3.2.1 Selection of Bridge decks	27
3.2.2 Coring Procedures	29
3.2.3 Field Inspection Procedures	31
3.2.4 Procedures for Inspection of Cores	31
3.3 INSPECTION RESULTS	35
3.3.1 Bridge Deck Number 1: Structure No. R01-13012 (No SIPMF)	35
3.3.2 Bridge Deck Number 2: Structure No. S03-81041 (No SIPMF)	43
3.3.3 Bridge Deck Number 3: Structure No. B01-82194 (No SIPMF)	53
3.3.4 Bridge Deck Number 4: Structure No. S11-82022 (No SIPMF)	62
3.3.5 Bridge Deck Number 5: Structure No. S09-82022 (No SIPMF)	68
3.3.6 Bridge Deck Number 6: Structure No. R01-13012 (SIPMF)	74
3.3.7 Bridge Deck Number 7: Structure No. S03-81041 (SIPMF)	83
3.3.8 Bridge Deck Number 8: Structure No. B01-82194 (SIPMF)	91
3.3.9 Bridge Deck Number 9: Structure No. S10-82022 (SIPMF)	99
3.3.10 Bridge Deck Number 10: Structure No. R03-25132 (SIPMF)	106
3.4 SUMMARY OF BRIDGE DECK INSPECTION AND CORING	116
3.4.1 Field Inspection	116
3.4.2 Inspection of Cores	121
3.5 SUMMARY OF INSPECTION AND CORING	137
CHAPTER 4: TEST PROGRAM	139
4.1 INTRODUCTION	139
4.2 OVERVIEW OF TEST PROGRAM	139
4.3 TEST SPECIMENS	144
4.3.1 Materials	144
4.3.2 Specimens Geometry and Fabrication	145

4.4 ENVIRONMENTAL CONDITIONING	152
4.4.1 Service Load Exposure	152
4.4.2 Freeze/Thaw Cycles	159
4.4.3 Salt-Water Exposure	164
4.4.4 Repeated Load Cycles	168
4.5 ULTRASONIC TESTS	172
4.5.1 Pulse-Echo	172
4.5.2 Through-Transmission	181
4.6 ULTIMATE LOAD TESTS	188
CHAPTER 5: RESULTS AND DISCUSSION	191
5.1 INTRODUCTION	191
5.2 COMPRESSIVE STRENGTH OF CONCRETE	191
5.3 SPECIMENS WITH SIPMF	193
5.3.1 Service Load Test Results	193
5.3.2 Ultrasonic Pulse-Echo Test Results	196
5.3.3 Ultrasonic Through-Transmission Results	227
5.3.4 Ultimate Load Test Results	238
5.4 SPECIMENS WITHOUT SIPMF	245
5.4.1 Service Load Test Results	245
5.4.2 Ultrasonic Through-Transmission Results	247
5.4.3 Ultimate Load Test Results	258
5.5 COMPARISON BETWEEN SPECIMENS WITH AND WITHOUT SIPMF	265
5.5.1 Ultrasonic Through-Transmission Results Comparison	265
5.5.2 Ultimate Load Test Results Comparison	273
5.5.3 Correlation between Ultrasonic and Structural Test Results	276
CHAPTER 6: FIELD IMPLEMENTATION	277
6.1 INTRODUCTION	277
6.2 THROUGH-TRANSMISSION TECHNIQUE	277
6.3 PULSE-ECHO TECHNIQUE	277
6.4 SUITABILITY OF FIELD IMPLEMENTATION	286
CHAPTER 7: SUMMARY AND CONCLUSIONS	287
REFERENCES	293
APPENDIX A: SURVEY REPORT	299
APPENDIX B: PROGRAM FOR ARRIVAL TIME CALCULATION	343
APPENDIX C: SALT SOLUTION COMPOSITION	349

EXECUTIVE SUMMARY

A comprehensive research investigation was conducted to evaluate the use of Stay-in-Place Metal Forms (SIPMFs) in construction of concrete bridge decks. This type of formwork is left in place subsequent to construction of a bridge deck and becomes part of the permanent bridge deck structure. The presence of the formwork may affect the quality and performance of the concrete during service. Benefits of SIPMFs include reduced labor costs and construction time as well as increased construction safety. Disadvantages of using SIPMFs have been identified as: difficulty in inspecting the underside of concrete decks after construction for maintenance purposes, corrosion of the forms, and presence of excess moisture content in the concrete. The objectives of this research project were to establish the state-of-the-practice for use and performance of SIPMFs for bridge decks, to evaluate the field performance of bridge decks with and without SIPMFs, and to investigate the behavior of environmentally conditioned, large-scale laboratory bridge deck specimens with and without SIPMFs.

A survey was developed and administered to all DOTs to examine the state of the practice of using SIPMFs for concrete bridge deck construction. Additionally, a field investigation was conducted to evaluate the performance of existing concrete bridge decks constructed with and without SIPMFs. This field investigation included visual inspection of 10 bridge decks and laboratory investigation of full-depth cores obtained from the inspected bridge decks. The cores were investigated using visual inspection, compressive strength tests, and ultrasonic tests. The compressive strength tests provided overall strength for the concrete used in the inspected bridges. The ultrasonic tests provided means for evaluating the quality of concrete through the depth of bridge deck. A laboratory durability investigation was conducted on 24 large-scale bridge deck slab specimens with and without SIPMFs. Four specimens were used as control specimens, and the remaining 20 specimens were subjected to either freeze/thaw exposure and repeated load cycles or salt-water exposure and repeated load cycles. At various stages before, during, and after the environmental exposure, ultrasonic pulse-echo testing was used to determine the quality of contact between the SIPMFs and concrete for specimens with SIPMFs. Furthermore, after the completion of the environmental exposure, ultrasonic through-transmission testing was used to assess the condition of the concrete for all specimens. These tests were followed by the ultimate load tests.

Overall, a statistical bias was present in the results of the national survey as a function of climate region. Virtual equivalency of deck performance was observed using field inspection, visual inspection of cores, compressive strength of cores, and pulse-velocity profile of the cores. Small changes in the performance of bridge deck specimens with and without SIPMFs were measured during the structural and ultrasonic laboratory test programs.

CHAPTER 1 : INTRODUCTION

Various types of formwork are used for construction of concrete bridge decks. Stay-in-place metal forms (SIPMFs) are one of the commonly used types of formwork. This type of formwork is left in place subsequent to construction of a bridge deck and becomes part of the permanent bridge deck structure. The presence of the formwork may affect the quality and performance of the concrete during service. Several research investigations related to SIPMFs were conducted in the early and mid-1970s. Some design modifications have occurred since this earlier research was conducted.

Benefits of SIPMFs include reduced labor costs and construction time, as well as increased construction safety. Construction can be accelerated using SIPMFs since the formwork is lightweight, generally prefabricated, simple to construct, and does not require removal subsequent to the placement of concrete. In addition, safety hazards can be reduced by using SIPMFs. This is particularly applicable to bridge decks constructed over features such as electrified rail lines, heavy highway traffic, deep ravines, or other hazardous locations. Disadvantages of using SIPMFs have been identified as: difficulty in inspecting the underside of concrete decks after construction for maintenance purposes, corrosion of the forms, and presence of excess moisture content in the concrete. Nevertheless, the advantages of SIPMFs are significant, which has led to increased use in recent decades.

The need to understand and to determine the durability for bridge decks that have SIPMFs and epoxy-coated reinforcement and their mode of deterioration is of great importance since at least 75 percent of decks in Michigan are cast using SIPMFs. Furthermore, due to the fact that the SIPMFs hide the bottom of the deck slab, practical and feasible inspection approaches need to be available for routine bridge inspection.

Deterioration of concrete due to salt-water exposure, freeze/thaw cycles, and repeated loads is generally well documented. The effects of these exposure conditions on the durability of concrete have been investigated. However, the influence of SIPMFs on durability of concrete bridge deck systems incorporating epoxy-coated steel reinforcement has not been commonly reported.

The objectives of this research project were to establish the state-of-the-practice for use and performance of SIPMFs for bridge decks, to evaluate the field performance of bridge decks with and without SIPMFs, and to investigate the behavior of environmentally conditioned large-scale laboratory bridge deck specimens with and without SIPMFs. To establish the state-of-the-practice of this construction method, a comprehensive survey was developed and administered to all United States DOTs. Field performance was investigated using visual inspection of selected Michigan bridge decks with and without SIPMFs and using laboratory investigation of full-depth cores from these bridge decks (including visual inspection, ultrasonic tests, and mechanical tests). Large-scale laboratory bridge deck specimens were constructed for evaluating the durability of bridge decks with and without SIPMFs when exposed to combined environmental exposures of a) salt-water and repeated load and b) freeze/thaw cycles and repeated load. These specimens were subjected to varying degrees of environmental exposure and tested using through-transmission ultrasonic tests (to determine condition of concrete), pulse-echo ultrasonic tests (to determine the quality of contact between concrete and SIPMF), and 4-point flexural tests (to determine ultimate load).

This report provides details related to this investigation. A literature review is presented in Chapter 2. The field inspection and coring test program is presented in Chapter 3. An overview of the laboratory experimental test program is presented in Chapter 4. Results from the laboratory experimental test program are presented in Chapter 5. Materials related to field implementation of laboratory methods are presented in Chapter 6. Conclusions from the entire research project are outlined in Chapter 7. The appendices to this report include the survey report and other supporting documents.

CHAPTER 2 : LITERATURE REVIEW

2.1 BRIDGE DECK CONSTRUCTION

Specifications for permanent steel bridge deck forms for concrete deck slabs were outlined by the United States Federal Highway Administration (FHWA 1972). Use of permanent forms are promoted for bridge decks over features such as electrified rail lines, heavy highway traffic, deep ravines, or other hazardous locations to increase the safety level associated with construction activity. The FHWA Instructional Memorandum 40-3-72 (FHWA 1972) provides design criteria for loading, material specifications, allowable deflections, and construction and inspection details. This instructional memorandum was deleted in 1984 because states had developed their own design/construction requirements for permanent steel forms. Although developed by each state, the design and construction requirements have generally remained consistent with the original FHWA specifications. A few design features (as specified by one or more of the following states: New York, Pennsylvania, or Indiana) are outlined in Table 2.1.

Table 2.1. Design Features for Permanent Steel Forms

Design Feature	Specification
Material Type	Conform to ASTM A446, Grades A through E
Material Coating	Conform to ASTM A525, Coating Class G165
Allowable Deflection	L/180 or 1/2 in. whichever is less (for 10 ft or shorter spans) L/240 or 3/4 in. whichever is less (for spans greater than 10 ft)
Dead Load	Additional 15 psf to account for weight of form and concrete in valley of form
Live Load for construction activity	50 psf
Reinforcement cover	Minimum 1 in. cover required between form and reinforcing steel
Inspection Requirement	Hammer sounding after initial set of concrete

Cady and Renton (1975) reported that although the use of SIPMF decks was common in roughly 12 states in 1975, the widespread use throughout the United States was limited due to three primary reasons: 1) Increased probability of freeze/thaw damage due to increased moisture

retention, 2) Potential danger and unsightliness due to possible corrosion of the forms with time, and 3) Difficulty in inspecting the concrete on the underside of the deck. When compared to precast stay-in-place forms, Taly (1998) reports that another drawback of the SIPMF is that their use does not replace or reduce the transverse slab reinforcing steel because no composite action is developed using these forms.

2.2 CONCRETE BRIDGE DECK DESIGN

Bridges represent a critical component of the infrastructure and extensive deterioration is a cause of great concern for the United States in terms of both public safety and economic burden. The efficient design of bridges is critical for the ongoing rehabilitation of the United States infrastructure. The timing for rehabilitation is acute as the projected, normalized mean service life of bridges on Interstate and U.S. routes (that were built between 1968 and 1972) is 34 years (Kirkpatrick et al. 2001).

Formwork for concrete construction is necessary to provide control of shape, position and alignment of the concrete structure. The formwork must support its own weight, the weight of freshly placed concrete, and live loads associated with construction activity and equipment. Design of formwork must provide quality, safety, and economy. Three common types of formwork for concrete bridge construction include 1) constructing forms in place using plywood and lumber, to be removed after the concrete has gained adequate strength, 2) using precast, prestressed panel subdecks that become an integral part of the completed deck thickness, and 3) using permanent galvanized steel forms (Hilton 1975). Much of the development of formwork in the United States and Canada has been driven by the high costs of labor in these countries (Hurd 1995). Therefore, the development of formwork in the United States is not entirely consistent with formwork development in other countries. Formwork typically constitutes 35 to 60% of the total cost of the concrete structure (Hurd 1995). Therefore, economical developments have been adopted by the construction industry including increasing prefabrication, assembly in large units, and reusing the forms. Permanent or stay-in-place forms present strong economical benefits by reducing labor costs and construction time.

Metal deck, precast concrete, wood, plastics, fiberboard, and reinforced water-repellent paper have all been used as materials for stay-in-place forms. Construction techniques using Stay-in-Place-Metal-Forms (SIPMFs) have been developed and widely used in bridge construction (Hilton 1975, Cady and Renton 1975, Taly 1998). In a survey of 38 states conducted by Hilton (1975), 35 states responded, 8 states permitted the use of SIPMF, 13 states permitted the use of SIPMF on some contracts, 6 states permitted only in special situations, and 8 states had not permitted their use. This data represents bridge construction status as of 1974.

Use of SIPMF provides accelerated construction due to the reduction in labor associated with formwork. Another benefit of SIPMF is the reduced safety hazard experienced using these forms for construction (Taly 1998, Hilton 1975). Although corrugated metal deck forms cannot take the place of negative reinforcing (top steel), special geometries of metal deck forms can be designed to combine form and positive reinforcing in one piece. This is accomplished by increasing the depth of the corrugations and providing raised lugs on the corrugations (Hurd 1995).

Notable drawbacks of using SIPMF cited in the 1974 survey (Hilton 1975) include: 1) the increased cost of future bridge widening or reconstruction work due to the removal of the SIPMF, 2) some difficulty with flexibility of placement of the steel forms, 3) increased difficulty in numerous construction activities as compared to using wooden forms (such as adhering insulation for cold-weather concreting or use of reinforcing steel tie-downs), 4) rusting of the forms (both before construction and after a few years' service), 5) increased corrosion of top flange due to drainage configuration driven by SIPMF, 6) presence of excess moisture content in the concrete, 7) bridge design needs to be modified to accommodate loads associated with forms and concrete in the valleys of the forms, 8) excessive deflections due to thin forms being used, 9) forms do not bond to concrete, and 10) underside of concrete decks cannot be visually inspected after construction or for maintenance purposes. Although these drawbacks are of varying critical degree, the number of survey responses that demonstrated concern appears to be significant.

Various investigations related to SIPMF have addressed some of these drawbacks with field observations or experimental test programs. Scaling and spalling have been reported to be roughly equivalent between bridges using SIPMF or conventional formwork (Hilton 1975).

2.3 DETERIORATION OF CONCRETE BRIDGE DECKS

Bridge deck deterioration is the most frequent reason for categorizing a bridge as structurally deficient (Tsiatas and Robinson, 2002). Primary defects of bridge decks include surface spalling, scaling, and transverse cracking. Other, generally less critical defects include joint spalls, pop-outs, other types of cracking, and wear.

Cracks provide an indicator for deterioration of bridge decks. Tsiatas and Robinson (2002) present three categories of cracks in bridge components: inadequate structural performance cracks, inadequate material performance cracks and acceptable cracks. Details related to the formation of these cracks are depicted in Table 2.2. Cracking of structural concrete presents multiple problems. The first is the decrease in structural integrity of the bridge component. Secondly, the cracking creates a flow path for infiltration of chlorides. Tsiatas and Robinson (2002) indicated that cracks having widths as small as 0.1 to 0.2 mm allow penetration of water and chloride solutions.

The predominant form of bridge deck cracking is transverse cracking (Ramey and Wright 1997), which generally occurs over transverse reinforcing bars in regions of negative moment in continuous spans (in the top region of the deck). Overall, cracking is greater in continuous spans (than simple spans), greater in longer spans (than shorter spans), and greater in older decks (than newer decks). Alampalli et al. (2002) reported a direct correlation between severity of cracking and severity of vibrations. Strategies for reducing the amount of cracking include: using smaller than number 5 reinforcing bars, experimenting with reinforcing bar arrangements, avoiding splicing transverse steel when possible, increasing deck thickness, standardizing deck thickness, increasing concrete cover to at least 2.5 in. when deicing salts are used, limiting w/c ratio to 0.4 to 0.45, and maintaining control on materials (Ramey et al. 1997).

Table 2.2. Categories of Cracks and Corresponding Mechanisms of Formation (Tsiatas and Robinson 2002)

Category of Crack	Inducing Mechanism
Inadequate structural performance	excessive foundation settlement, excessive loading or construction overloads, excessive stresses due to thermal gradients, inadequate design or detailing, poor construction practices.
Inadequate material performance	plastic shrinkage, drying shrinkage, reinforcement corrosion, freeze/thaw cycles, wet/dry cycles, chemical reaction
Acceptable	cracks that must develop to properly distribute tensile stresses according to current design criteria.

Cady and Renton (1975) performed an extensive investigation related to the durability of steel formed, sealed bridge decks. Twelve simulated bridge deck slabs were constructed and subjected to freeze/thaw tests and outdoor exposure tests. Cady and Renton (1975) used visual inspection and pulse velocity techniques for assessing degradation in the deck slabs over the exposure period. In this investigation, steel formed deck slabs behaved no differently in freeze/thaw testing than wood formed decks. The separation between metal form and concrete was documented for some of the test specimens of the investigation (Cady and Renton 1975) and it was determined that this separation had no apparent effect on the durability of either the deck or the form. The condition of concrete after removal of the metal forms was generally observed as excellent in this test program (Cady and Renton 1975).

It was observed in New York that surface spalling was the most serious defect encountered due to the frequency of occurrence (Chamberlin et al. 1972). A hypothesis that transverse cracking allows the infiltration of chlorides, which produces further problems associated with corrosion and spalling, was not supported by the observation data (a strong correlation between both transverse cracking and spalling at the same bridge was not present).

Of the different types of deterioration, transverse cracking was found to be highly dependent on the age of the bridge, whereas spalling was moderately dependent, and scaling was slightly dependent on age of bridge. In the New York study, 33% of conventional bridge decks exhibited transverse cracking whereas only 22% of bridge decks constructed with SIPMF exhibited transverse cracking. In addition, the SIPMF bridge decks exhibited approximately

33% less cracking than bridges that were constructed using conventional techniques (Chamberlin et al. 1972).

2.4 DETERIORATION OF CONCRETE

Deterioration of concrete occurs due to chemical attack and by exposure to physical attack such as freeze-thaw cycles. The implications of concrete bridge deck deterioration are the need for repair and ultimately replacement. The success of bridge decks can be measured by the years of maintenance-free service that is provided (Young et al. 1998). Kirkpatrick et al. (2001) cite that the time to the first repair of a bridge deck commonly occurs when 2.5% of the surface area of the worst-condition span lane has deteriorated.

Preliminary stages of concrete deterioration can occur without visible evidence. The initial deterioration can compromise the structure of the concrete and make the structure vulnerable to further attack (Young et al. 1998).

Four common types of chemical attack of concrete are acid attack, carbonation, alkali-aggregate reaction, and sulfate attack. Acid attack is a mode of chemical attack that is generally present only due to external sources such as in waste containment applications. Carbonation is caused by atmospheric carbon dioxide dissolving in concrete pore water and creating an acidic solution (Mays 1992). Although the shrinkage associated with carbonation can actually increase the chemical stability and strength of concrete (Kosmatka and Panarese 1988), the lower pH present after this reaction can allow corrosion of the reinforcing steel (corrosion can begin when the pH reaches values less than approximately 11.5) [Mays 1992]. Alkali-aggregate reaction is a result of the high pH in concrete paste (pH of approximately 13) or external alkaline source reacting with certain rocks (Young et al. 1998). The reaction causes loss of integrity of the affected aggregates and ultimately swelling, pressure build-up, and subsequent cracking. A strategy for controlling alkali-aggregate reaction is to spread the reactive silica throughout the concrete avoiding localized concentrations. Sulfate attack is another type of chemical attack in concrete that occurs in two stages. First, sulfate ions penetrate into the concrete and react to form gypsum. Second, the gypsum further reacts to form ettringite, which causes volume expansion and subsequent cracking. Control of sulfate attack is possible by lowering the

permeability of the concrete (to control stage 1) and lowering the C_3A content (to control stage 2). These effects can be accomplished by using a lower water/cement ratio, applying proper moist curing conditions, using mineral admixtures (all affecting permeability), and using low C_3A content cement (Type V or Type II).

The deterioration of concrete is strongly influenced by the microstructure of the concrete and void space distribution within the structure. Porosity is commonly related to the permeability of porous media. Although the porosity of concrete is generally greater than that of natural rock, the permeability of concrete can generally be lower due to the pore space distribution (Young et al. 1998). Concrete contains discontinuous pore space forcing water to flow by the mechanism of diffusion rather than by advection. Also, aggressive agents such as chloride ions can penetrate the concrete surface by the mechanism of diffusion. In general, surface attack of concrete is generally slow.

The two modes of attack to be described herein include 1) steel corrosion induced primarily by salt-water exposure and 2) freeze-thaw cycles, both predominant mechanisms in northern climates where de-icing salts are used on roadways. ASTM C666, Test for Resistance of Concrete to Freezing and Thawing (Procedures A and B), is used to assess the durability of concrete to freeze/thaw cycles. Results from the freeze/thaw exposures are typically evaluated by evaluating one or more of the following measures: 1) reduction in dynamic modulus of elasticity, 2) loss in compressive or flexural strength, 3) loss in weight, 4) change in visual appearance, and 5) expansion of the specimen (Waddell and Dobrowolski 1993).

2.5 STEEL CORROSION

Corrosion is defined as the destructive and unintentional attack of a metal. It is electrochemical and ordinarily begins at the surface (Callister 1997). Corrosion is the most frequent and serious form of degradation of reinforced concrete (Taly 1998). The corrosion of steel causes deterioration of concrete. The product of steel corrosion, rust, has a volume several times greater than the metallic iron from which it was formed, which causes pressure build-up and cracking in the concrete (Mays 1992). Young et al. (1998) reported that 0.1 to 0.5 mm of

corrosion is sufficient to cause concrete cracking. The resulting cracks appear in an orientation parallel to the reinforcing steel.

Four main causes for corrosion include carbonation or sulphation, chloride attack, inadequate cover, and presence of cracks. The effects of corrosion include cracking or spalling, rust staining, corrosion of reinforcing steel, excessive deflection, and ultimately, failure of structural members. Prevention of corrosion must address two factors of environmental factors: those affecting the concrete structure and those affecting the reinforcing steel.

When reinforcing bars are placed in fresh concrete, a protective, thin coating of ferrous hydroxide is formed. The high pH of the concrete leads to the spontaneous formation of a “passivation film” (Young et al. 1998). Chlorides are the most common ion to break down this passive protective layer (Taly 1998). Carbonation (a process causing reduction of pH to below 11) is another means of depassivation, although it is rare in the United States (Young et al. 1998).

The singlemost destructive factor promoting corrosion of reinforcement is deicing salts (Cady and Renton 1975). The deicing agents cause detrimental effects on the concrete structures leading to scaling. The use of air-entrained concrete can resist satisfactorily the scaling associated with deicing deterioration of concrete. Some deicing agents containing primarily ammonium nitrate and ammonium sulfate are particularly problematic for concrete deterioration (Waddell and Dobrowolski 1993). Chloride distribution in bridge decks has been measured with depth in various investigations. Cady and Renton (1975) report that the chloride ion concentration was found to be negligible beyond 1.5 in. depth when measured on three bridges after seven years of service.

This deterioration is caused from inadequate concrete, inadequate cover to the reinforcement, or presence of impurities. In general, well-placed good quality concrete (characterized by low w/c ratio) will be sufficient to prevent corrosion (Taly 1998). A low w/c ratio produces concrete having lower permeability, limiting the infiltration of impurities. With superplasticizers, it is now possible to have w/c ratios as low as 0.37 – 0.38. The presence of water has a dramatic influence on the rates and extent of deterioration in concrete. When

exposed to both water and oxygen, unprotected steel will corrode. AASHTO 8.22 requires 2.5 in. of cover on top and 1.0 in. of cover on the bottom of deck slabs that have no positive corrosion protection and are frequently exposed to deicing salts (Taly 1998).

The diffusion coefficient for chloride ions plays a critical role in affecting service life of bridge decks. Surface chloride concentration (acid soluble concentration of chlorides) was measured by Kirkpatrick et al. (2001) to occur to a depth of 12.7 mm below the deck surface. The depth of chloride ion penetration in intact concrete is dependent on the diffusion coefficient. Lowering the diffusion coefficient in concrete (which can be achieved in part by using supplemental cementitious materials such as fly ash or slag) can be highly effective at prolonging the service life of bridge decks. Evidence for this effect is predicted using statistical diffusion cracking model produced by Kirkpatrick et al. (2001). The model developed predicts that the time for diffusion to occur and the time for corrosion-induced cracking to occur. A model simulation of bridges built between 1981 and 1994 predicts 47 to 65 years before rehabilitation is required, depending on method of mathematical analysis conducted. This prediction demonstrates a substantial improvement over bridges constructed approximately 20 years earlier. Other stochastic models have been developed to assess the durability and service life of concrete structures (Sarja and Vesikari 1996).

The geometry and type of reinforcing bars can also influence the onset and propagation of corrosion. Mohammed reported that deformed reinforcing bars are more prone to corrosion than plain bars. Kirkpatrick et al. (2001) indicated that typical time of corrosion is approximately 4-6 years for bare reinforcement whereas an additional 1-7 years is estimated for use of epoxy coated reinforcement. The use of various sealers and coatings has also been investigated for preventing deterioration of concrete structures (Ibrahim et al. 1999).

In order for corrosion to occur in the lower reinforcing or the SIPMF, the chloride ions would have to migrate a distance equal to the depth of the slab if introduction of the chlorides was occurring on the top surface of the deck slab. Macrofeatures (such as fractures, cracks, and defects) have a significant impact on the hydraulic conductivity of porous media (Benson et al. 1997). Similar behavior is expected for flow characteristics in concrete. Therefore, if cracking is present in the concrete structure, the introduction of chloride ions from the top surface of the

deck can be greatly accelerated. Alternatively, chloride ions can be introduced to the lower region of the bridge deck through expansion joints or by splashing upward from the roadway beneath the bridge.

Experimental and modeling work has been conducted to assess and predict the formation of cracks in concrete due to corrosion. Mohammed et al. (2000) conducted experiments to assess the influence of crack width on the rate of corrosion. Mohammed et al. (2000) reported that the simple presence of cracks is more critical than the width of cracks. Francois and Arligui (1998) conducted 12-year salt fog exposure tests on 3-m long beams to establish a relationship between cracking in loaded beams and the corrosion of reinforcing steel. Beams were removed from the exposure conditions at various intervals to assess chloride penetration profiles, steel corrosion maps, flexural strength, concrete microstructure, and steel/concrete interfaces. Francois and Arligui (1998) made a distinction between cracks caused by service loads (“primary cracks”) and cracks caused by rust formation and associated volume changes (“secondary cracks”). Similar to Mohammed et al. (2000), Francois and Arligui (1998) found that corrosion is not influenced by crack width (within the range of cracks produced by service loads, <0.5 mm crack width). In addition, both w/c ratio of the concrete and load level applied to the structure play more significant roles in defining corrosion onset and propagation than width of cracks (Mohammed et al. 2000, Francois and Arligui 1998). Increased loads produce damage to both the paste/aggregate interface and the steel/concrete interface. After initiation of corrosion, the surrounding conditions (mostly related to physical and chemical condition of concrete) predominate over the presence of cracks (Mohammed et al. 2000)

Leung (2001) developed a fracture-mechanics based physical model to predict the size of cracks formed due to expansion of steel associated with corrosion. Stewart and Rosowski (1998) developed a structural reliability model including interaction between transverse cracking, diffusion of chlorides, corrosion initiation, corrosion propagation, and serviceability limits (such as spalling).

A relationship between extent of corrosion and load carrying capacity of decks has not been well established (Almusallam et al. 1996). Loss of strength due to corrosion is due to a loss in cross section and a degradation of the bond with the concrete. Almusallam et al. (1996)

prepared test slabs and induced artificially accelerated corrosion. The slabs were loaded in flexure after varying degrees of corrosion. An initial increase in ultimate strength was observed and attributed to increased frictional bond between the steel and the concrete due to growth of film rust. The results of these tests are shown in Figure 2.1. Almusallam et al. (1996) observed similar modes of failure for low corrosion specimens to control specimens (no corrosion present). Higher degrees of corrosion led to a progressive loss of ductility. At 60% corrosion, the slabs demonstrated equivalent strength to unreinforced slabs (Almusallam et al. 1996). In another study related to mode of failure of corroded sections, Enright and Frangopol (2000) observed that bridges subjected to corrosion may be more vulnerable to shear failure than to flexural failure due to a variety of controlling factors including steel placement, influence of corrosion, and interaction with concrete.

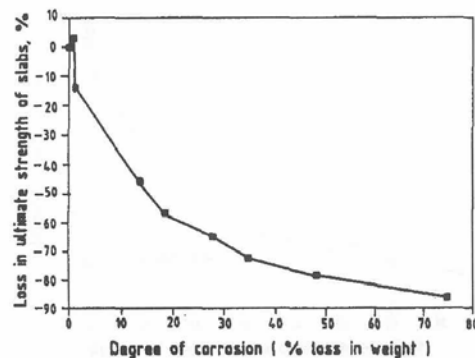


Figure 2.1. Loss in ultimate strength of slabs with varying degrees of corrosion (Almusallam et al. 1996)

2.6 FREEZE/THAW DETERIORATION

The presence of water is required for the action of freeze/thaw cycles to be detrimental to concrete structures. Freezing causes a 9% expansion in volume of water. This freezing action is most detrimental when the pores within the concrete structure are fully or nearly saturated. In this case, pressure builds up against the solid component causing localized fractures. If water can move as little as 0.2 mm, stresses are reduced preventing this fracturing (Young et al. 1998). The accepted solution to this problem is the use of air entraining agents, which produce bubbles spaced at less than 0.2 mm. Four types of voids have been identified by Cordon (1979): gel pores, capillary cavities, entrained air, and entrapped air. Gel pores are interstitial cavities among hydration products and are approximately 1.5 – 2.0 mm diameter. Capillary cavities are

formed by excess water not used by hydration and are approximately 500 mm diameter. Entrained air voids are tiny spherical bubbles (0.001 – 1.0 mm diameter). Entrapped air voids are generally larger and form if the concrete is not completely compacted. The voids need to be full of water for freeze/thaw cycles to be detrimental (Cordon 1979).

Other aspects of aggregates affect the freeze/thaw resistance of concrete including pore size distribution and presence of impurities. Some aggregates have pore structures that are susceptible to freeze/thaw deterioration if frozen when wet. This type of aggregate is widespread in midwestern states (Young et al. 1998). Koubaa and Snyder (2001) reported that grain size of aggregates alone is not sufficient as an indicator of freeze/thaw resistance. Fine pores are more prone to causing freeze/thaw deterioration than larger pores. In general, fine grained materials contain finer pore structures. D-cracking, a common freeze/thaw deterioration symptom caused by aggregate deterioration, is critical in some states (Koubaa and Snyder 2001). Young et al. (1998) reported that D-cracking causes considerable damage underneath bridge decks that is present 8-12 years after placement.

Mohammed et al. (2000) reported results from a 55-year freeze/thaw investigation. It was observed that although air entrainment improves freeze/thaw resistance, it does not entirely prevent freeze/thaw damage. It was shown that air entrainment admixture effectively delays the onset of freeze/thaw deterioration. In addition, Mohammed et al. (2000) reported that the type of Portland cement affects freeze/thaw resistance (Type III demonstrated the worst resistance) and that integrating air entrainment with the cement was more effective than adding it in solution. Rangaraju (2002) reported excessive premature freeze/thaw damage on a section of pavement that was attributed to a poor air void system. The main reasons for the poor air void structure were non-uniform vibration of the concrete and an in-filling of air voids upon repeated freeze/thaw cycles.

Presence of salt in aggregates can affect the adsorption potential, increasing adsorbed water potential up to 10% greater than similar aggregates without salt (Ahmed and Ahmed 1996). Cady and Carrier (1971) measured higher moisture contents in a sealed, steel-formed deck than a similar wood-formed deck. The steel-formed deck had higher moisture content at the center and bottom of the deck than at the top. Both decks exhibited lower moisture contents

than pavement slabs on well-draining granular base material (Cady and Carrier 1971). The trend of moisture content through depth of the various slabs is presented in Figure 2.2. Although at higher moisture contents, pavement slabs generally exhibit less deterioration than bridge decks. The heat capacity of the surrounding soil prevents excessive freeze/thaw cycling that can occur in bridge decks.

2.7 ASSESSMENT OF CONCRETE

Assessment of the mechanical properties of concrete can be accomplished by conducting destructive testing or by using non-destructive methods. Destructive testing provides a direct measurement of mechanical properties but is generally not practical for testing existing components of the infrastructure. Destructive tests can be conducted on molded cylinders, sampled cores, or molded beams of concrete. Numerous standardized test methods are available for testing concrete strength, durability, permeability, and physical composition (Kosmatka and Panarese 1988).

Permeability represents an index property for concrete durability. A higher coefficient of permeability in the concrete will provide a condition for increased infiltration of reagents to the concrete structure. Permeability is a function of the pore structure of the concrete. Methods for assessing permeability include hydraulic permeability, air/gas permeability, capillary suction, chloride ion penetration, rapid test for permeability to chloride, initial surface absorption, and the Figg test (Yaman et al. 2001). Permeability is related to the interconnected void structure. Of the void types identified by Cordon (1979), capillary voids are the most problematic for allowing flow of water because gel pores are too small and entrained air voids are discontinuous.

Another index parameter representing the void structure or soundness of concrete is the ultrasonic pulse velocity. ASTM Test Method for Pulse Velocity through Concrete is used to measure the velocity of a compression wave through concrete. When analyzed using the theory of wave transmission, compared to similar tests conducted on a variety of materials, and compared to conventional destructive strength tests, the velocity measurement can provide information related to the physical properties (elastic parameters) and condition of the concrete specimen (uniformity and degree of cracking).

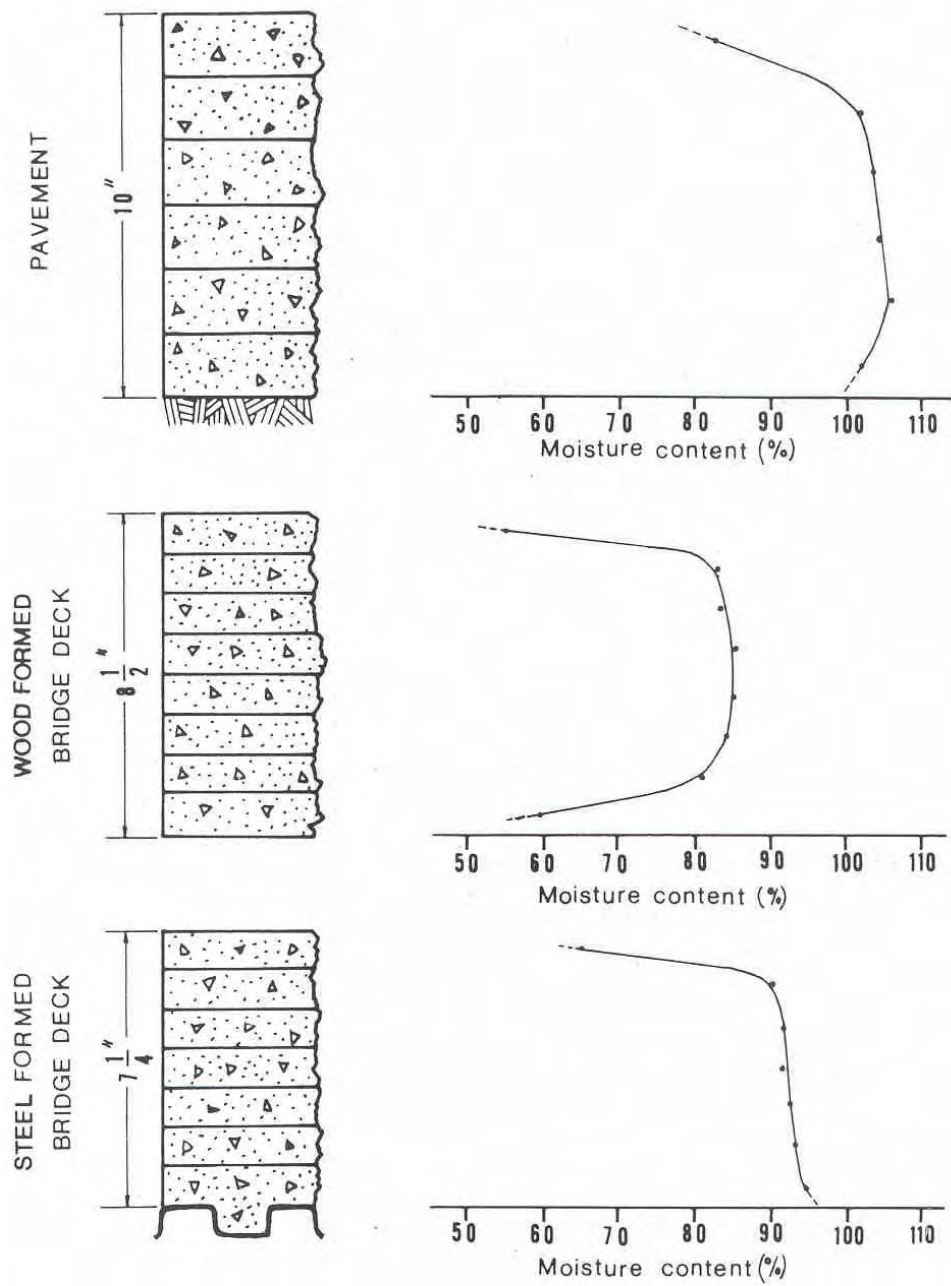


Figure 2.2. Moisture Distribution in a Pavement and Bridge Decks (Cady and Renton 1975)

2.8 NONDESTRUCTIVE TESTING METHODS

Nondestructive test methods can be used to evaluate a material or structure without significantly damaging it. Benefits of nondestructive test methods include allowing for repeated testing of the same sample over time as well as allowing for testing existing components of infrastructure. Nondestructive methods have been extensively used to evaluate civil engineering materials. There are many types of nondestructive methods including: acoustic emission, computer tomography, infrared emissions, multiple chain drag, embedded optical fibers, nuclear radiation techniques, radar, magnetic methods, impact echo, impulse-response, cross-hole sonic logging, impulse radar, half cell potential, linear polarization, and ultrasound (Rens and Greiman 1997 and Davis 1999). Various nondestructive methods have been applied to evaluating the relative strength of hardened concrete. Common methods include rebound, penetration, pullout, dynamic or vibration, X-rays, gamma radiography, neutron moisture gages, magnetic cover meters, electricity, microwave absorption, and acoustic emissions (Kosmatka and Panarese 1988). It is important to recognize that many of these methods do not provide any direct measurement of engineering properties, thus the development of accurate empirical relationships may limit their application. Many tests of concrete provide an index property, from which other properties can be inferred.

The following discussion will emphasize ultrasound because this is the method that has been selected for the current research program. Advantages of ultrasonic testing techniques include: the method is nondestructive, the method is easily and rapidly performed, and important engineering properties of materials can be evaluated using ultrasonic methods.

2.9 ULTRASONIC TEST METHODS

Ultrasound is the term given to sound waves that have frequencies greater than the audible range for humans. The audible range is characterized by frequencies that fall between the range of approximately 20 Hz and 20,000 Hz (Bray and McBride 1992). Ultrasonics can be used for a variety of engineering applications. Ensminger (1988) distinguishes between low-intensity ultrasonic applications (generally used for assessing material properties) and high-intensity ultrasonic applications (for producing an effect on a medium such as cleaning or mixing). Most

practical use of ultrasonic frequencies for material assessment and flaw detection in material is accomplished with frequencies between 50 kHz and 20 MHz.

Ultrasonic testing involves sending a wave from an external surface into a material and then analyzing the resulting wave. The speed of wave propagation is related to both the wave properties and the elastic parameters of the material. In terms of wave properties, the velocity of wave propagation (C) is expressed in m/s and is related to frequency (f) and wavelength (λ) by the relationship presented in Equation 1.

$$\lambda = \frac{C}{f} \quad (1)$$

In terms of elastic properties, the wave velocity is described by Equation 2.

$$C = \sqrt{\frac{E(1-\sigma)}{\rho(1+\sigma)(1-2\sigma)}} \quad (2)$$

where:

C = wave velocity
 E = Modulus of Elasticity
 σ = Poisson's Ratio
 ρ = density

An important parameter affecting the transmission and reflection of ultrasonic energy at boundaries is the characteristic acoustic impedance (Z), defined as the product of density (ρ) and velocity (C) [Equation 3].

$$Z = \rho C \quad (3)$$

Piezoelectric transducers are the most common method of achieving ultrasonic signals for material testing (Bray and McBride 1992). A piezoelectric transducer will develop an electric signal or voltage when deformed and conversely, will deform when subjected to an electric signal or voltage. Transducers can be designed and specified to handle a wide variety of material testing applications. As the ultrasonic beam propagates through the material, the initial

interference of individual waves from the transducer face produces a near-field effect. It is best to conduct tests analyzing regions beyond the near-field. A wave front of nearly uniform intensity is formed in the far-field. The extent of the near field is a function of both transducer geometry and wavelength (Bray and McBride 1992). A coupling agent is required between the ultrasonic transducer and the testing medium. Presence of the coupling agent allows for transmission of the wave into the test medium (rather than being reflected off the surface).

The behavior of ultrasonic energy is similar in many ways to that of light (and other electromagnetic energy) [Ensminger 1998]. Concepts of refraction, reflection, scattering, and diffraction are common to these forms of energy. The general wave equation describes the propagation of a sinusoidal wave through an elastic medium. The resulting oscillation of the system can be described by Equation 4:

$$P = \left(\frac{F^2}{Z_m} \right) \cos(\omega t) \cos(\omega t - \phi) \quad (4)$$

where:

- P = instantaneous power
- F = driving force
- Z_m = complex mechanical impedance of system
- $\omega = 2\pi f$
- f = frequency of oscillations
- ϕ = phase angle between the driving force and velocity
- t = time

Ultrasonic testing involves the transfer of mechanical disturbance through a medium. Measurements are conducted to evaluate the velocity of ultrasonic waves passing through a material, the amount of wave attenuation, and the frequency response of a transmitted wave. Sound waves result from a disturbance or vibration in a medium. Rigidity of the transmitting medium affects the speed of the wave propagation. The system required for conducting ultrasonic tests includes a pulse generator, transmitting transducer, receiving transducer, and a data acquisition system that contains various electronic components to amplify, filter, process, and record the signals.

There are inherent shortcomings with regard to using ultrasonic tests with concrete. Specifically, only a range of potential strengths can be approximated for a range of velocities. Additionally, there are small micro-defects that can exist and go undetected by this testing method because waveforms can be larger than these defects. In that case, waves may propagate through the defect and show no reflection or loss of velocity (Popovics and Popovics 1992). Additional disadvantages of ultrasonic testing include: difficulty in transference of energy on rough surfaces, impracticality of inspecting complex shapes, and difficulty in detecting small or tight flaws such as cracks (Bray and McBride 1992).

Ultrasonic testing produces different types of waves after a pulse is introduced into a medium. These waves are categorized by their direction and type of propagation. Primary waves (P-waves), also known as compression waves or longitudinal waves, travel in the direction of propagation. Secondary waves (S-waves), also known as shear waves, travel normal to the direction of propagation. Rayleigh waves are a third wave type and travel along surface waves. Figure 3 shows typical deformation caused by the propagation of the three wave types. The arbitrary wavelength in the figure is denoted by the variable λ .

Pulse-echo and through-transmission techniques are two common types of testing setups that are used for ultrasonics. The through-transmission technique utilizes two transducers, one that acts as a transmitter and the other as a receiver. Materials with high attenuation generally are tested with this method. In the event that two opposing surfaces of a material or medium are unavailable, a surface-transmission or pulse-echo arrangement is used (Inci 2001). Figure 2.4 shows common testing set-ups for the through-transmission and surface-transmission techniques. Pulse-echo uses one transducer that acts as both the emitter and receiver. With this method, the incident wave reflects and refracts when it hits a boundary or a discontinuity or defect, and is received back at the single transducer. This technique is often used in the determination of metal thickness and defect detection.

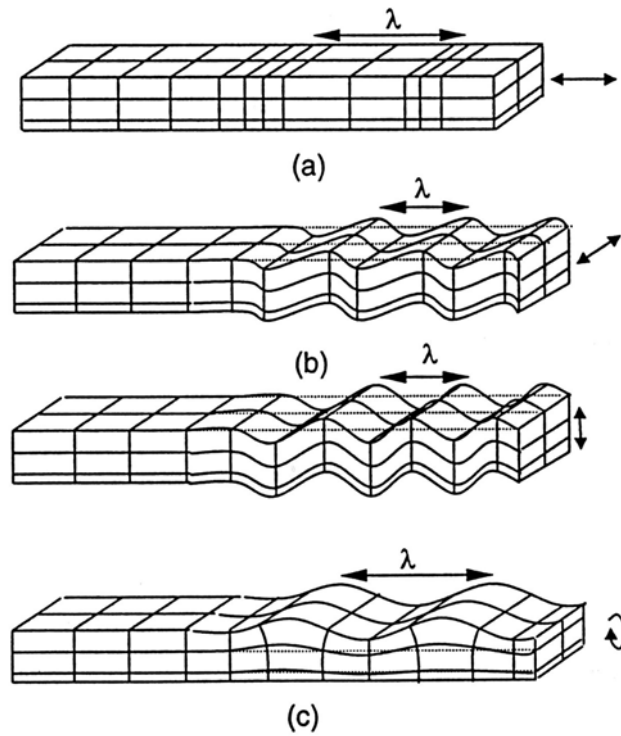


Figure 2.3. Ultrasonic Waveforms (a) Primary Waves, (b) Shear Waves (two polarizations), (c) Rayleigh Waves (Inci 2001)

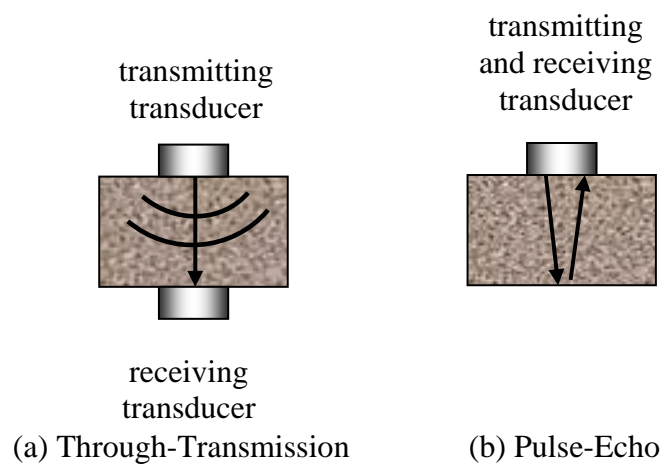


Figure 2.4. Ultrasonic Wave Propagation for (a) Through-Transmission and (b) Pulse-Echo Arrangement

Ultrasonics have been utilized to evaluate mechanical properties of civil engineering materials including wood, steel, plastics, soils, and concrete. Ultrasonic investigations of metals have been documented extensively for a wide variety of applications including defect detection, weld quality inspection, and thickness measurements (Ensminger 1988, Krautkramer and Krautkramer 1990). Ultrasonics have been used to analyze plastic products such as geosynthetics for density, thickness, and presence of defects and aging effects (Yesiller and Sungur 2001, Yesiller and Cekic 2001). Evaluation of soils and earthen materials has been limited, although direct correlations between modulus of elasticity and pulse velocity have been demonstrated for stabilized soil mixtures (Yesiller et al. 2001). Ultrasonic tests on concrete have been performed to assess the quality of concrete and presence of large voids (Kamada et al. 1997, Rens et al. 1997, Krautkramer and Krautkramer 1990). Table 2.3 shows typical densities and velocities of common civil engineering materials. General trends can be observed that with higher densities, higher velocities are typical (although there are exceptions).

Table 2.3. Acoustic Velocity in Civil Engineering Materials (Bray and McBride, 1992)

Material	Density (g/cm³)	P-Wave Velocity (m/s)
Aluminum	2.7	6,300
Steel	7.7	5,900
Concrete (at 28 days)	2.4	4,500
Polyethylene	0.90	1,950

Because concrete causes relatively high levels of attenuation of ultrasonic energy, the dimensions of samples to be monitored are somewhat limited (Krautkramer and Krautkramer 1990). Pulse velocity is a common test conducted for concrete (Kamada et al. 1997, Rens et al. 1997, Hearn and Shim 1998) and fairly refined qualitative correlations exist between pulse velocity and quality of concrete (Table 2.4). Inherent problems with interpretation of pulse velocity results for concrete include inhomogeneity in material composition, changing structure with time due to the hydration process, and presence of reinforcing steel.

Table 2.4. Correlation between Ultrasonic Pulse Velocity and Quality of Concrete (Krautkramer and Krautkramer 1990)

Pulse Velocity (m/s)	Quality of Concrete
Above 4,600	Very Good
3,600 – 4,600	Good
3,000 – 3,600	Moderate to Questionable
2,100 – 3,000	Poor
Below 2,100	Very Poor

Internal voids, cracks, and discontinuities can reduce the pulse velocity within a material due to diffraction around the crack causing delay of travel of the pulse (Krautkramer and Krautkramer 1990).

Using ultrasound, it is possible to obtain quantitative information in regards to the status of concrete by effective analysis of the frequency spectrum. The main parameters directly affecting the results include: testing frequency, sampling length and interval and scanning baseline (Wei-Du 1992). Pulse velocities of the concrete samples were shown to increase with respect to time for many high strength concrete samples. An exponential relationship between the ultrasonic velocity and compressive strength of the concrete tested is demonstrated (Ravindrarajah 1992).

Through-transmission techniques have been used in evaluation of precast bridge sections. These tests were conducted to investigate and determine engineering properties such as estimated concrete strength, and detection of imperfections in the concrete. Field application requires that a predetermined grid be tested to insure proper sampling of the concrete for determination of the properties. This method has been shown to be both economical and rapid for field evaluation of these sections (Olson 1992 and Millstein and Sabnis 1983).

Yaman et al. (2001) developed a theoretical relationship between ultrasonic pulse velocity and rapid test for permeability to chloride (RCPT). Bridge deck test specimens were prepared in the laboratory at various water/cement ratios to assess a variety of concrete pore structures. These samples were monitored for ultrasonic pulse velocity over the duration of

curing. These samples were considered control specimens and compared to similar measurements conducted in the field. The reduction in pulse velocity measured in the field was a function of deterioration of the bridge decks. Permeability tests were also conducted in the field to confirm the loss of soundness of the concrete (Yaman et al. 2001). Yaman et al. (2001) conducted ultrasonic measurements in the laboratory and the field using ASTM C597. For field measurements, a template was used for repeatable placement of the pulsing and receiving transducers.

Use of ultrasonics has been reported for assessing concrete condition (Mamlouk and Zaniewski 1999), membrane condition (Hearn and Shim 1998), and bridge substructure condition (Rens and Transdue 1998). Recent developments in ultrasonic technology include equipment advances and analysis techniques for continued development of ultrasonic techniques for assessing material conditions. Pla-Rucki and Eberhard (1995) reported the development of a rolling ultrasonic pulse velocity scanner that provides an opportunity for greatly accelerating measurements of entire structures. A similar system has been developed in France for ultrasonic assessment of prefabricated bituminous geomembranes (Chaignon 2002). Ultrasonic techniques using spread spectrum techniques show promise for improving sensitivity of pulse-echo methods. The direct sequence spread spectrum ultrasonic evaluation involves applying an intentionally arbitrary (random) signal to establish an overall “fingerprint” of the entire structure. By monitoring with time, changes (e.g., deterioration) can be tracked (Rens et al. 1997). Kamada et al. (1997) have reported using Acoustic Emission (AE) receiving sensors to improve resolution of ultrasonic investigations. In addition, Kamada et al. (1997) has reported work related to analyzing the amplitude of the received ultrasonic signal for analysis. Although achieving an accurate measurement of amplitude is difficult (Kamada et al. 1997), a normalized analysis method allows comparison to nondeteriorated samples.

Measuring attenuation of ultrasonic signals can be used for assessing various material properties (Krautkramer and Krautkramer 1990). In general, attenuation occurs due to diffraction at discontinuities. A range of ultrasonic response for a variety of materials is presented in Figure 2.5. Measuring attenuation can be effective for measuring contact or bond interface between layered systems (Figure 2.6).

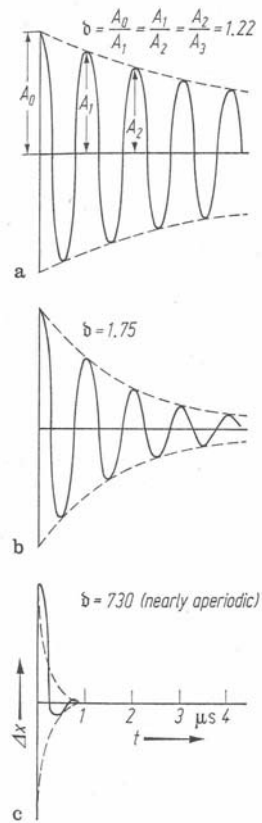


Figure 2.5. Attenuation of ultrasonic wave in various materials (Krautkramer and Krautkramer 1990)

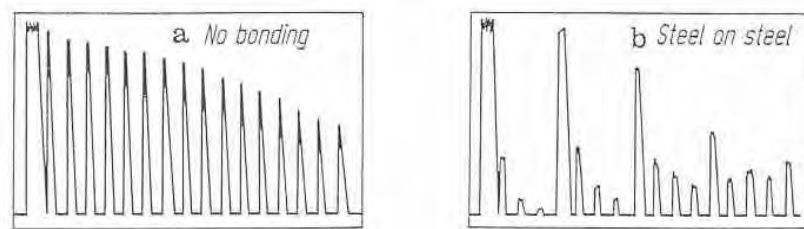


Figure 2.6. Ultrasonic response for various degrees of bonding (Krautkramer and Krautkramer 1990)

CHAPTER 3 : INSPECTION AND CORING OF BRIDGE DECK SLABS

3.1 INTRODUCTION

Coring and inspection were conducted on ten bridge decks, five with stay-in-place metal forms (SIPMF) and five without SIPMF. Five full-depth cores were taken from each bridge deck. A total of 50 cores were obtained for the investigation. The bridges were selected by the research team and approved by MDOT engineers. Since three of the selected bridges had regions both with and without SIPMF, only seven individual bridge structures were required to obtain the appropriate cores. McDowell and Associates, in collaboration with FMG Concrete Sawing, were retained as subcontractors to LTU for this phase of study. McDowell and Associates obtained permits from appropriate agencies prior to coring. The traffic control was conducted in accordance with MDOT guidelines. Inspection and coring were generally performed during weekends to avoid heavy traffic periods. A majority of the field work was completed in May and June 2002.

The concrete cores were transported to the laboratory for evaluation of structural condition and assessment of condition of concrete. The cores were assessed visually, nondestructively, and destructively. Inspection indices were developed for quantitative comparison of field inspection, visual inspection, and nondestructive evaluation. The procedures for coring, field inspection, and laboratory investigation are first presented. Then, data are presented for all inspection procedures on a bridge-by-bridge basis. Finally, a summary of the comparison between the deck slabs with and without SIPMF is presented based on the inspection and investigation of the cores.

3.2 FIELD INSPECTION AND CORING

3.2.1 Selection of Bridge Decks

The details of the bridges selected for coring and inspection are presented in Table 3.1 MDOT structure number, the year of construction, the facility carried, the type of the deck slab (with or without SIPMF), the lane description, and the date of visit are provided.

Table 3.1. Selected bridges for inspection and coring

Bridge Deck Number	MDOT Structure (Year of Construction)	Facility Carried	Age at Inspection (years)	Structural and Steel Reinforcement Bars Details	ADT	CADT**	Date of Coring
1	R01-13012 (1981)	NB S. Washington Ave.	21	- No SIPMF, 4-lane (2-way traffic), 8-span, 713 ft total length, steel girders - Epoxy-coated steel (brown)	16,000	310	June 8, 2002
2	S03-81041 (1975)	NB Rawsonville Rd.	27	- No SIPMF, 4-lane (2-way traffic), 4-span, 303 ft total length, steel girders - Not epoxy-coated steel	24,000*	(--)	May 11, 2002
3	B01-82194 (1966)	SB I-75	36	- No SIPMF, 4-lane, 106-span, 9,246 ft total length, concrete girders - Not epoxy-coated steel	85,100	12,000	May 18, 2002
4	S11-82022 (1962)	WB I-94	40	- No SIPMF, 3-lane, 3-span, 137 ft total length, concrete girders - Epoxy-coated steel (green)	132,000	16,600	May 4, 2002
5	S09-82022 (1962)	EB I-94	40	- No SIPMF, 4-lane, 4-span, 237 ft total length, steel girders - Epoxy-coated steel (green)	130,000	16,600	May 4, 2002
6	R01-13012 (1981)	NB S. Washington Ave.	21	- SIPMF, 4-lane (2-way traffic), 8-span, 713 ft total length, steel girders - Epoxy-coated steel (brown)	16,000	310	June 8, 2002
7	S03-81041 (1975)	NB Rawsonville Rd.	27	- SIPMF, 4-lane (2-way traffic), 4-span, 303 ft total length, steel girders - Not epoxy-coated steel	24,000*	(--)	May 11, 2002
8	B01-82194 (1966)	SB I-75	36	- SIPMF, 4-lane, 106-span, 9,246 ft total length, concrete girders - Not epoxy-coated steel	85,100	12,000	May 18, 2002
9	S10-82022 (1962)	WB I-94	40	- SIPMF, 3-lane, 4-span, 237 ft total length, steel girders - Not epoxy-coated steel	132,000	16,600	May 4, 2002
10	R03-25132 (1976)	NB I-475	26	- SIPMF, 3-lane, 4-span, 382 ft (116.5 m) total length, steel girders - Epoxy-coated steel (green)	40,800	2,000	June 6, 2002

** Commercial ADT

* approximation based on nearby location

(--) data not available

Bridge decks are labeled with numbers for reference discussion through the report. Bridge Numbers 1 through 5 represent bridge decks without SIPMF, whereas Bridge Numbers 6 through 10 represent bridge decks with SIPMF.

The three bridges that were constructed using a combination of formwork systems (Bridge Deck Numbers 1 and 6; 2 and 7; and 3 and 8) allowed for direct comparison of measured parameters eliminating the effects of bridge age, traffic loading, and environmental conditions. These three sets of bridge decks are referred to as direct comparison decks throughout this report.

3.2.2 Coring Procedures

The steps involved in coring each bridge were: identification of coring locations, coring the full depth of bridge deck, and plugging the holes.

Identification of Coring Locations

In most cases cores were taken from near the end spans of each bridge to facilitate handling of the cores. In particular, coring in the first span of the bridge allows for access from beneath the bridge deck to capture the core after drilling and prevents the full depth cores from dropping on the roadway below the bridge. The coring locations were selected randomly in regions of the bridge decks containing cracks.

Coring the Full Depth of Bridge Deck

The coring apparatus consisted of a core drill with diamond-impregnated bits attached to a core barrel for obtaining cylindrical core specimens. The full depth cores were 3.75 in. diameter. The coring procedure is shown in Figure 3.1. The drilled cores were either collected from the top or from the bottom of the bridge deck depending on accessibility. Collection of cores is shown in Figure 3.1.

Plugging the Holes

Procedures were established for preparing the holes for plugging and subsequently filling the holes with concrete mixture. Prior to drilling the full depth core, a circular ring was formed by coring to a depth of 2 in. using a 6 in. diameter core barrel. Subsequent to full-depth coring, a circular ring was removed to provide a shelf for support of the reinforcement (Figure 3.2).

To fill the hole left after the extraction of the core, the hole had to be filled with concrete using a simple reinforcement arrangement to ensure that the plug will not crack or separate from the deck. Reinforcement details are shown in Figure 3.2. Before casting, the opening had to be blocked from underneath using a plug. Circular plastic covers, conical wooden blocks, and plastic-rubber blocks were used for this test program.

The reinforced hole was then plugged using ready-mix concrete “DURAPATCH HIWAY” (which sets in 10 minutes). The concrete for the plug was rodded after placement.



a. Coring



b. Collecting the core from the top



c. Collecting the core from the bottom

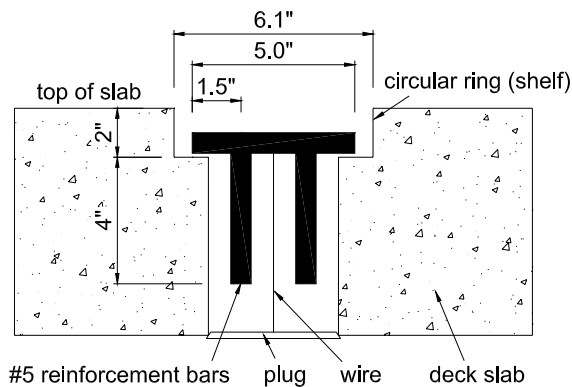


d. Resulting hole in a concrete deck slab without SIPMF, view from below



e. Resulting hole in a concrete deck slab with SIPMF, view from below

Figure 3.1. Coring procedures



a. Schematic diagram of reinforcement for plug



b. Reinforcement unit

Figure 3.2. Reinforcement details.

3.2.3 Field Inspection Procedures

The condition of the concrete decks of all of the bridges investigated in this study was evaluated using visual inspection. This inspection consisted of evaluating the deterioration on the wearing and the bottom surfaces. The types of deterioration assessed for visual inspection are cracking on the top and bottom surfaces of the bridge decks, presence of traces of rust, salt or other deicing agent on the bridge deck, and deterioration of bridge deck supports. For the bridges with SIPMF, rust of the metal forms was analyzed. Cracks on the top surface for each bridge deck were mapped in the rectangular region of coring for an area extending approximately 2 ft beyond coring locations in each direction.

3.2.4 Procedures for Inspection of Cores

Visual Inspection

Visual inspection of the cores was used to determine general physical characteristics and overall condition of the cores that were obtained for the test program. All cores were inspected visually. The reinforcing steel was assessed for presence and condition of epoxy coating and extent of rust. The concrete was assessed for quantity, size, and alignment of cracking; quantity and size of voids; quantity and size of honeycombing; and porosity of aggregate and cement paste. Slag was used as aggregate on a number of bridge decks and higher porosities were expected for these conditions. SIPMFs were assessed for extent of rust. One of the cores for each

location was sliced vertically, and it was subjected to visual inspection to assess the consistency of the concrete condition on the outer and inner faces.

Compressive Strength Testing

Compressive strength is a common parameter used for quality control and quality assessment of concrete. Compressive strength tests were conducted on specimens obtained from the cores. Two of the cores from each bridge deck were selected for compressive strength testing. Cores were prepared for compressive strength testing by removing top and bottom portions of core (by sawcutting) to provide a 2:1 length:diameter ratio. The specimens had a length of 7.5 in. Sulfur caps were used for the compressive strength testing (ASTM C617-98). A vertical strain gauge was installed on the side of the core to measure the initial modulus of elasticity of the concrete. Finally compressive strength tests were conducted in accordance with ASTM C39/ C39M-99.

Ultrasonic Testing

Ultrasonic testing was used in the test program to further assess the quality and condition of concrete. In particular, variation of concrete condition with depth was determined since this was not possible using compressive strength tests. Tests were conducted using commercially available hardware (Figure 3.3). The measurement system consisted of two P-wave transducers, a pulser-receiver, and a data acquisition system. The narrowband transducers operated at 100-kHz-center frequency. The 10-MHz-bandwidth pulser-receiver contained a high-voltage pulser and a high-gain receiver. The low-frequency transducers and high-voltage, high-gain pulser-receiver were particularly selected for testing concrete, which is a highly attenuating material. The data acquisition system consisted of a computer equipped with an analog-to-digital converter board with 50 MHz sampling rate and a digital oscilloscope software that was used for viewing waveforms and adjusting data acquisition parameters.

The cores were cut into disks with thicknesses ranging from approximately 1 to 3 in. using a concrete saw for ultrasonic testing. Generally, six to eight pulse velocity test specimens were obtained from each core designated for ultrasonic testing. Ultrasonic pulse velocity was determined on specimens obtained from the cores using the through transmission test method in

accordance with ASTM C597-97 (Figure 3.3). Three repeated ultrasonic measurements were made on each specimen by placing one transducer at the center of the top surface and one transducer at the center of the bottom surface of the specimen. Transit time for wave propagation was identified as the first major deviation in the amplitude of a waveform (on an amplitude vs. time record) using statistical analysis. A waveform obtained in air was subtracted from the waveforms obtained on test specimens to provide a baseline for deviation in amplitude. Then, the initial portion of the modified waveform was analyzed to determine the level of noise in the signal prior to arrival of the waveform from the test specimen. First arrival was identified as the first occurrence of deviation of amplitude by more than 3 standard deviations from the mean amplitude of the initial portion of the waveform. The resolution for transit time measurements was $0.04\ \mu\text{s}$. The wave travel path was measured as the thickness of the slice using a custom-made micrometer with a resolution of 0.001 in. Therefore, based on an adaptation of Taylor's Theorem to the propagation of uncertainty, the maximum error in pulse velocity calculations was 1.2%.

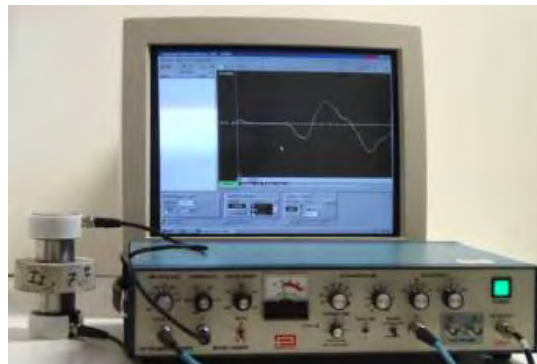


Figure 3.3. Test setup for through-transmission ultrasonic measurements of slices of cores

Two cores from each bridge deck were selected for nondestructive testing. The cores were sliced horizontally, and ultrasonic velocity was measured on individual slices of each core to obtain a profile of the pulse velocity through its depth. A summary of the laboratory test program for the cores is presented in Table 3.2.

Table 3.2. Summary of laboratory test program for cores

Formwork	Bridge Deck Number	MDOT Structure	Core	Type of Test
No SIPMF	1	R01-13012	1a 1b 1c 1d 1e	Compressive Strength Vertically Sliced for Visual Inspection Through Transmission Compressive Strength Through Transmission
	2	S03-81041	2a 2b 2c 2d 2e	Through Transmission Compressive Strength Vertically Sliced for Visual Inspection Through Transmission Compressive Strength
	3	B01-82194	3a 3b 3c 3d 3e	Through Transmission Compressive Strength Compressive Strength Through Transmission Vertically Sliced for Visual Inspection
	4	S11-82022	4a 4b 4c 4d 4e	Vertically Sliced for Visual Inspection Compressive Strength Through Transmission Compressive Strength Through Transmission
	5	S09-82022	5a 5b 5c 5d 5e	Compressive Strength Vertically Sliced for Visual Inspection Through Transmission Compressive Strength Through Transmission
SIPMF	6	R01-13012	6a 6b 6c 6d 6e	Vertically Sliced for Visual Inspection Through Transmission Compressive Strength Through Transmission Compressive Strength
	7	S03-81041	7a 7b 7c 7d 7e	Through Transmission Compressive Strength Through Transmission Compressive Strength Vertically Sliced for Visual Inspection
	8	B01-82194	8a 8b 8c 8d 8e	Through Transmission Vertically Sliced for Visual Inspection Through Transmission Compressive Strength Compressive Strength
	9	S10-82022	9a 9b 9c 9d 9e	Through Transmission Through Transmission Vertically Sliced for Visual Inspection Compressive Strength Compressive Strength
	10	R03-25132	10a 10b 10c 10d 10e	Through Transmission Vertically Sliced for Visual Inspection Compressive Strength Through Transmission Compressive Strength

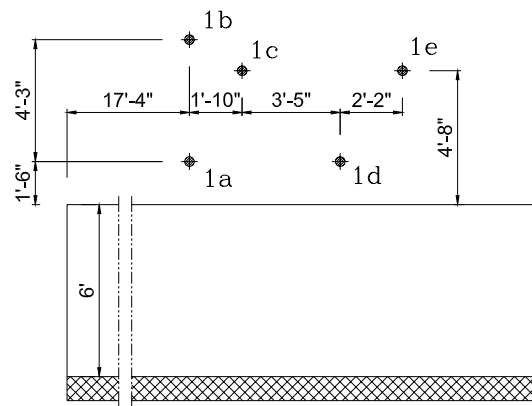
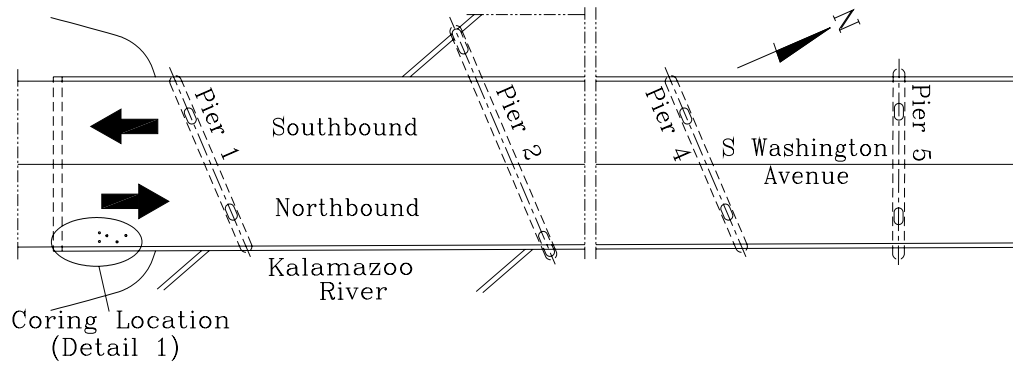
3.3 INSPECTION RESULTS

Results from the bridge inspection and laboratory investigation of the cores are presented in the following section on a bridge-by-bridge basis. This section of the report describes in detail the bridges that were selected and examined (Table 3.1). For each bridge, two sections are presented: a *Field Inspection* section and an *Inspection of Cores* section. The *Field Inspection* section includes the inspection date, bridge location, traffic details, structural description of the bridge deck, coring locations, map of cracks, and assessments of bridge deck condition. The *Inspection of Cores* section includes three parts: visual inspection, compressive strength test results, and ultrasonic test results.

3.3.1 Bridge Deck Number 1: Structure No. R01-13012 (No SIPMF)

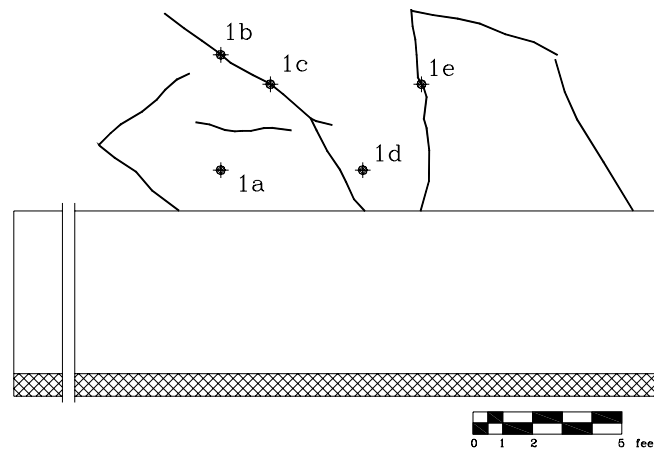
Field Inspection

The location of the 2-way 2-lane bridge was at the northbound lane of S. Washington Avenue over Kalamazoo River and train tracks in Battle Creek. The bridge has 8 spans. Beginning from the abutment at the north of the bridge, the first, second, third, fourth, and eighth spans of the deck slab are composed of concrete slabs without SIPMF. Nine steel beams support the deck slabs of the northbound and southbound lanes. Steel beams are supported on two abutments and seven piers. The structural system of the piers is composed of a concrete girder and 2 columns. Six of the concrete girders have one span and double cantilever. The seventh girder has one span without cantilever. The top and bottom steel reinforcement bars used in the deck slab were coated with brown epoxy. Five cores were taken from the first span (southwestern part of the bridge) in the concrete deck slab without SIPMF. Coring locations for Bridge Deck Number 1 are presented in Figure 3.4. A map of cracks in the region of coring for Bridge Deck Number 1 is presented in Figure 3.5. Detailed photographs of bridge deck inspection are presented in Figures 3.6 through 3.9.



Detail 1

Figure 3.4. Coring locations for Bridge Deck Number 1 (Structure No. R01-13012)

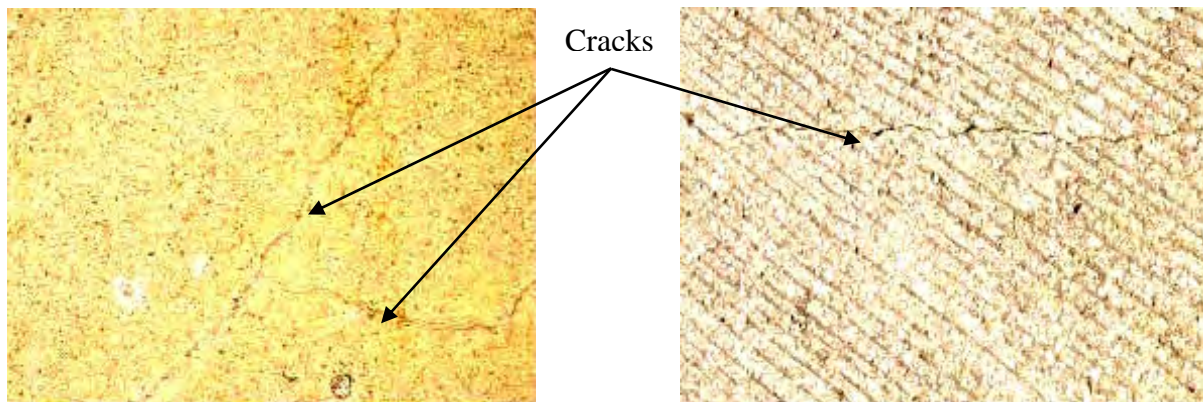


Detail 1

Figure 3.5. Map of cracks at coring locations for Bridge Deck Number 1 (Structure No. R01-13012)

Cracks were found at the top surface of the road and the curbs as shown in Figure 3.6. The cracks propagated longitudinally, transversely, and diagonally along the entire length of the bridge. The cracks were found at the sides of the deck slabs as shown in Figure 3.7. A different type of concrete (as indicated by the difference in color) was encountered at the sides of the joints in the top surface (Figure 3.8).

The bottom surface of the deck slab had cracks propagated transversely, longitudinally and diagonally (Figures 3.9 a, b and c). A thick layer of light colored material filled the cracks and spread in the direction of the bridge slope (Figure 3.9d). Some of the cracks also had corrosion traces. The drainage holes had corrossions in the deck without SIPMF (Figure 3.9e).



a. Longitudinal and transverse cracks

b. Diagonal cracks

Figure 3.6. Cracks propagated on the top surface



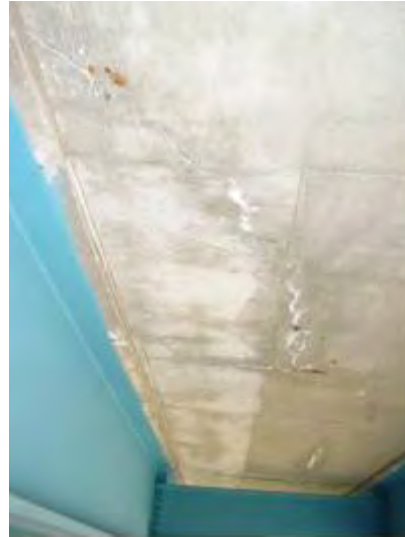
Figure 3.7. Cracks propagated through the sides



Figure 3.8. Different types of concrete around the joints



a. Diagonal cracks with white traces



b. Longitudinal cracks with white traces



c. Transverse cracks with white traces



d. Cracks with corrosion and white traces in the direction of slope



e. Rust traces from reinforcement around the drainage holes

Figure 3.9. Cracks, rust, and white traces propagated on the bottom surface

Inspection of Cores

The visual inspection of cores indicated that all of the cores had no wearing surface at the top surface. The steel reinforcement was coated with brown epoxy and generally showed severe signs of rust. Several voids were encountered. The coarse aggregate was well bonded to the concrete. The heights of the cores were not significantly different thus indicating uniformity of the bridge deck. The five cores removed from Bridge Deck Number 1 are presented in Figure 3.10. Each Core was carefully inspected and illustrated as follows:



Figure 3.10. The 5 cores taken from Bridge Deck Number 1 (Structure No. R01-13012)

Details of the visual inspection of the cores follow:

Core 1a (Figure 3.11)

- 10.0 in. height.
- Part of the edge of the core at the bottom was fractured during the coring.
- Two locations of honeycombing of approximate length of 0.3 in. were encountered at 2.5 in. and 3.0 in. from the bottom.
- Large voids of average diameter of 0.2 in. were located 3.0, 4.5, 5.0, and 6.2 in. from the bottom.



Figure 3.11. Core 1a shows large region of honeycombing

Core 1b (Figures 3.12-3.13)

- 10.0 in. height.
- A crack of average width of 0.05 in. extends the entire length of the core.
- Four axial cuts in the reinforcement were present at 4.5 and 7.5 in. from the top.
- The exposed reinforcement showed severe signs of rust.
- A large region containing honeycombing of approximate width 0.4 in. was located 5.2 in. from the top.



Figure 3.12. Core 1b shows rust in reinforcement



Figure 3.13. Core 1b longitudinal crack

Core 1c (Figures 3.14-3.15)

- 10.0 in. height.
- The core was cracked and split by a lateral crack at the location of the reinforcement at 4.0 in. from top.
- A crack of average width of 0.05 in. extends the entire length of the core.
- Four axial cuts in the reinforcement showed severe signs of rust.
- Part of the edge of the bottom of the core was fractured during coring.
- Two locations of honeycombing of average width of 0.3 in. located 2.5 in. and 5.0 in. from top.
- Two large voids of average diameter of 0.3 in. were located 7.0 in. and 8.0 in. from top.



Figure 3.14. Core 1c transverse and longitudinal cracks



Figure 3.15. Core 1c rust in steel

Core 1d (Figure 3.16)

- 10.1 in. height.
- Two axial cuts in the reinforcement located 8.8 in. from the top.
- One longitudinal cut in the reinforcement located 4.8 in. from the top.
- Two large voids of average diameter of 0.3 in. located 5.3 in. from the top.
- Exposed steel reinforcement showed slight signs of rust.



Figure 3.16. Core 1d

Core 1e (Figures 3.17-3.18)

- 10.2 in. height.
- The core was cracked and split into three segments by two lateral cracks; both at the locations of the reinforcement. The cracks are located 4.5 in. and 8.3 in. from the top.
- Two longitudinal cuts in the reinforcement located 4.5 in. and 8.3 in. from the top.
- The exposed reinforcement showed severe signs of rust.
- Part of the concrete was fractured at the crack located 8.3 in. from the top.
- A crack of average width of 0.03 in. width propagated along the entire depth of the core.
- Two large voids of average diameter of 0.3 in. located 5.8 in. and 7.8 in. from the top.



Figure 3.17. Core 1e cracks at the reinforcement bars



Figure 3.18. Core 1e rust in the reinforcement bar

The stress-strain curves for Cores 1a and 1d are presented in Figure 3.19, and the curves for pulse velocity through the depth for Cores 1c and 1e are presented in Figure 3.20. Due to fractures in the specimen, the velocity measurements were not obtained for all slices of Cores 1c and 1e.

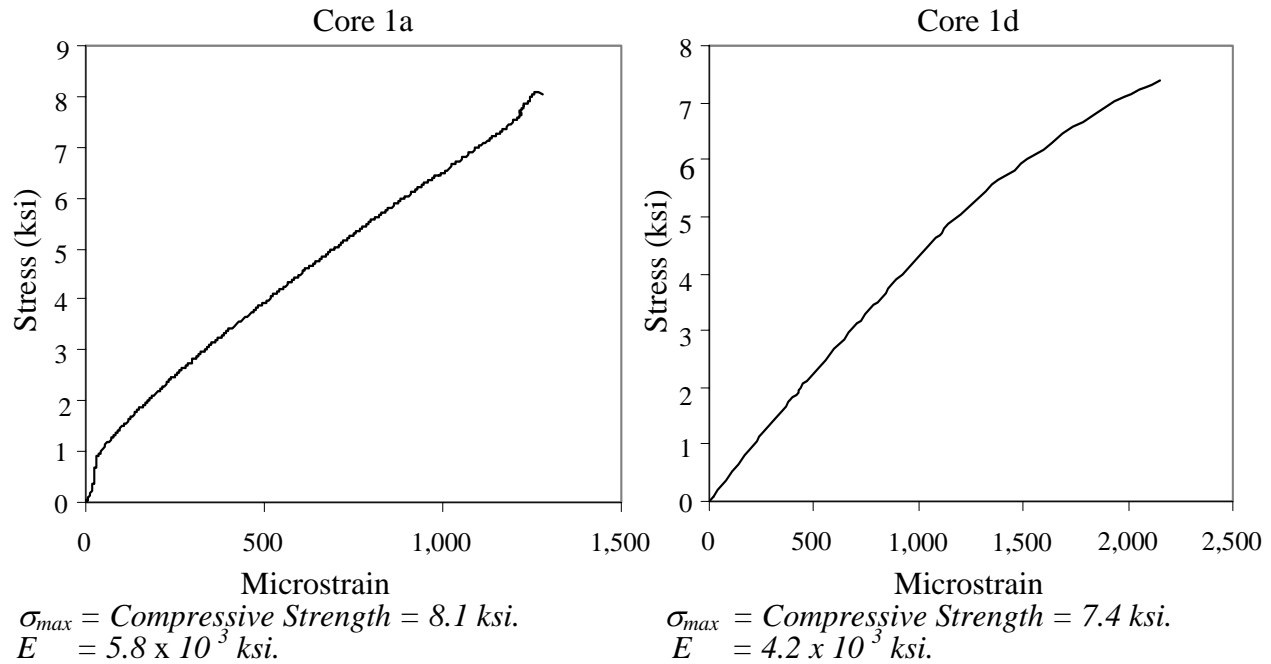


Figure 3.19. Compressive strength test results for Cores 1a and 1d
(S. Washington Ave., Bridge Deck Number 1, Structure No. R01-13012, No SIPMF)

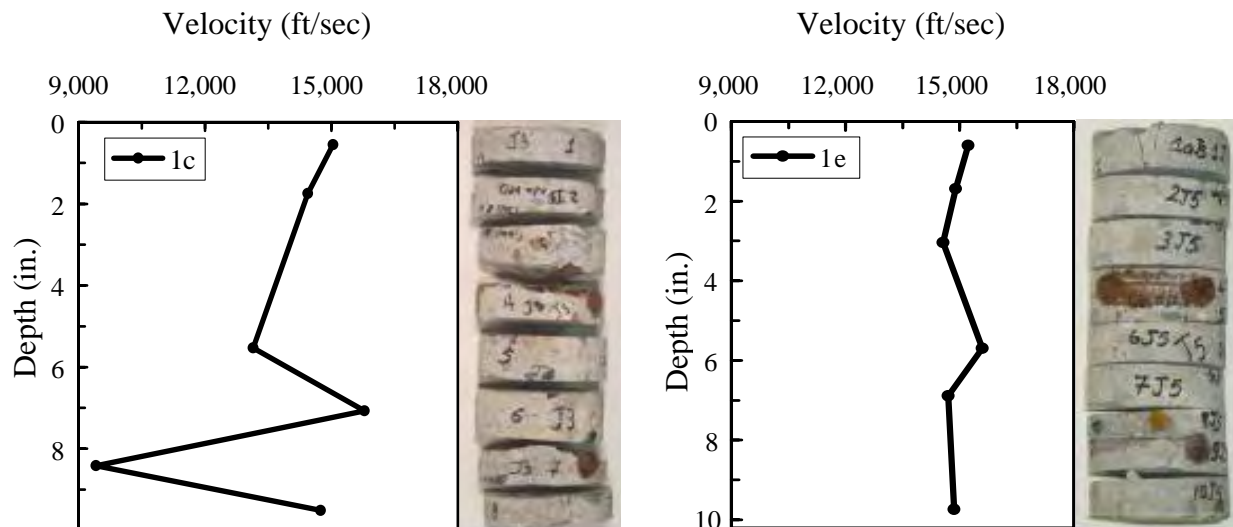


Figure 3.20. Ultrasonic velocity with core depth for Cores 1c and 1e
(S. Washington Ave., Bridge Deck Number 1, Structure No. R01-13012, No SIPMF)

3.3.2 Bridge Deck Number 2: Structure No. S03-81041 (No SIPMF)

Field Inspection

The location of the 2-way 4-lane bridge was at the northbound lane of Rawsonville Road over I-94 Freeway in Belleville. The bridge has 4 spans of 44'-11", 106'-7", 115'-0" and 36'-6" lengths. The deck slabs are made of concrete slabs without SIPMF for the first and fourth spans. Deck slabs are supported by eight steel beams, which are supported on two abutments and three piers. The structural system of the piers is composed of a concrete girder supported by eight columns. The top and bottom steel reinforcement bars used in the deck slab were not epoxy-coated steel. Five cores were taken at the eastern shoulder of the northbound lane of Rawsonville over I-94 near the parapet of the bridge. The cores were from the portion of concrete deck slab without SIPMF. Coring locations for Bridge Deck Number 2 are presented in Figure 3.21. A map of cracks in the region of coring for Bridge Deck Number 2 is presented in Figure 3.22. Detailed photographs of bridge deck inspection are presented in Figures 3.23 through 3.31.

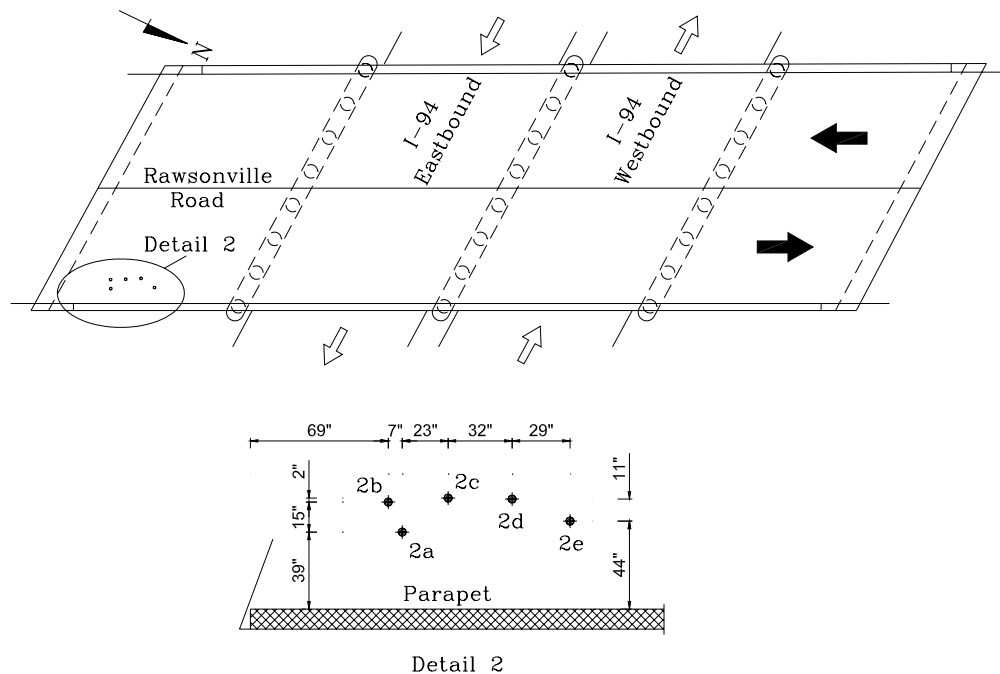


Figure 3.21. Coring locations for Bridge Deck Number 2
(Structure No. S03-81041)

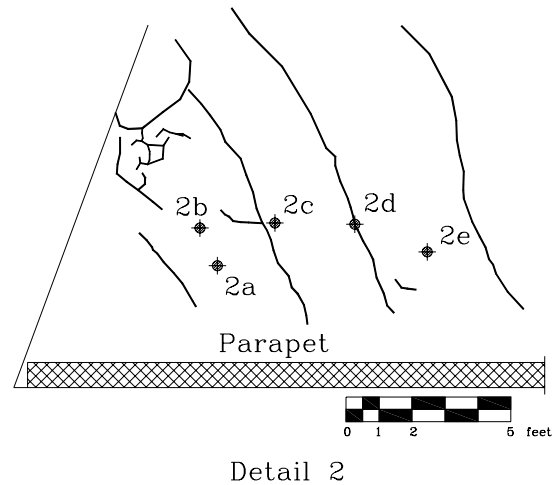


Figure 3.22. Map of cracks at coring locations for Bridge Deck Number 2
(Structure No. S03-81041)

Major cracks were found at the top surface of the concrete slabs at the first and fourth spans (Figure 3.23). These cracks penetrated the entire slab thickness (Figure 3.24). In many locations along the bridge, the concrete curbs were deteriorated and the steel reinforcement bars were uncovered (Figure 3.25). White and rust traces were observed underneath the concrete slab, along the side of the bridge, and at the location of the steel hanger rods supporting PVC conduit for telephone wires (Figures 3.26 to 3.29). Traces of corrosion existed at the location of the first and second joints (Figure 3.30). For the abutment located at the north of the bridge, cracks, white traces and traces of corrosion in steel reinforcements existed at the middle and extreme bays (Figure 3.31).



a. Diagonal cracks



b. Transverse cracks with rust traces

Figure 3.23. Cracks on the top surface



Figure 3.24. Cracks through the slab thickness



Figure 3.25. Severe deterioration of the curb



a. Longitudinal crack



b. Diagonal and Transverse cracks

Figure 3.26. Cracks at the bottom surface of the slab



Figure 3.27. White traces on the bottom surface



Figure 3.28. Rust traces on the bottom surface



Figure 3.29. Honeycombing at the bottom surface of the slab



Figure 3.30. Deterioration of the concrete cover and rust traces at the joint



a. Water leakage



b. Cracks and rust traces

Figure 3.31. Deterioration of the deck slab at the north abutment

Inspection of Cores

The visual inspection of cores from Bridge Deck Number 2 indicated that the bridge had no separate wearing surface at the top surface and the top surface of all cores had a grooved texture. The steel reinforcement was not coated and had traces of rust. Many voids were encountered with an average diameter of 0.3 in. The coarse aggregate was well bonded to the concrete. The cement paste had high porosity. Slag as well as conventional aggregates were used in the deck slab. All of the cores had approximately the same height of average 9.8 ± 0.3 in. The five cores that were taken are shown in Figure 3.32.



Figure 3.32. The 5 cores taken from Bridge Deck Number 2 (Structure No. S03-81041)

Core 2a (Figures 3.33-3.34)

- 9.8 in. height.
- Many voids of average diameter of 0.3 in. were encountered.
- Two axial cuts in the reinforcement bars located 4.5 in. from the top surface.
- Three longitudinal cuts in the reinforcement located 3.8, 7.0 and 8.3 in. from the top.
- Two full depth cracks.
- Slag as well as conventional aggregates were used; and cement paste had high porosity.
- One longitudinally cut in the steel reinforcement bar located 3.5 in. from the top.
- All exposed steel reinforcement bars showed signs of rust.



Figure 3.33. Core 2a reinforcement bars are rusted



Figure 3.34. Core 2a crack propagated through the depth of the core

Core 2b (Figures 3.35-3.36)

- 10.0 in. height.
- Slag as well as conventional aggregates were used; and cement paste had high porosity.
- Four locations of honeycombing present with average width of 0.5 in. and located approximately 3.5 in. from the top.
- Two axial cuts in the reinforcement bars located 4.5 in. from the top.

- One longitudinal cut in the reinforcement bars located 8.5 in. from the top.
- The exposed reinforcement bars showed traces of rust.



Figure 3.35. Core 2b



Figure 3.36. Core 2b rust in the reinforcement bars

Core 2c (Figures 3.37-3.41)

- 9.8 in. height.
- Slag as well as conventional aggregates was used; and cement paste had high porosity.
- Core was broken at 8.0 in. from the top surface due to crack existing horizontally in the slab thickness. The existing crack is shown in Figure 3.40.
- Two locations of honeycombing with average width of 0.4 in. were located approximately 1 in. and 6.8 in. from the top.



Figure 3.37. Crack in the thickness of the slab (Core 2c location)



Figure 3.38. Presence of horizontal crack in Core 2c



Figure 3.39. Core 2c



Figure 3.40. Core 2c rust traces



Figure 3.41. Core 2c honeycombing in the concrete

Core 2d (Figures 3.42 to 3.44)

- 9.8 in. height.
- Slag as well as conventional aggregates were used; and cement paste had high porosity.
- Core was broken at 8.0 in. from the top surface at the location of the steel reinforcement bar.
- The exposed steel bar at the fracture location showed severe signs of rust and concrete deterioration.
- Four axial cuts in the reinforcement bars located 3.8 in. and 8.0 in. from the top.
- Horizontal fracture plane in the core located 4.5 in. from the top. The crack width is approximately 0.08 in.
- One hairline crack propagated along the entire length of the core and through the surface.



Figure 3.42. Core 2d after collecting it



a. Core was broken at the bottom



b. Reinforcement bars are rusted

Figure 3.43. Deterioration of Core 2d



a. Rust traces



b. White traces on the bottom surface

Figure 3.44. Deterioration of Core 2d

Core 2e (Figure 3.45)

- 9.5 in. height.
- Slag as well as conventional aggregates were used; and cement paste had high porosity.
- Many large voids of 0.4 in. average diameter located 3.8 in., 5.0 in. and 6.8 in. from the top.



a. High porosity



b. Large voids

Figure 3.45. Core 2e

The stress-strain curves for Cores 2b and 2e are presented in Figure 3.46, and the curves for pulse velocity through the depth for Cores 2a and 2d are presented in Figure 3.47. Due to fractures in the specimen, the velocity measurements were not obtained for all slices of Core 2d.

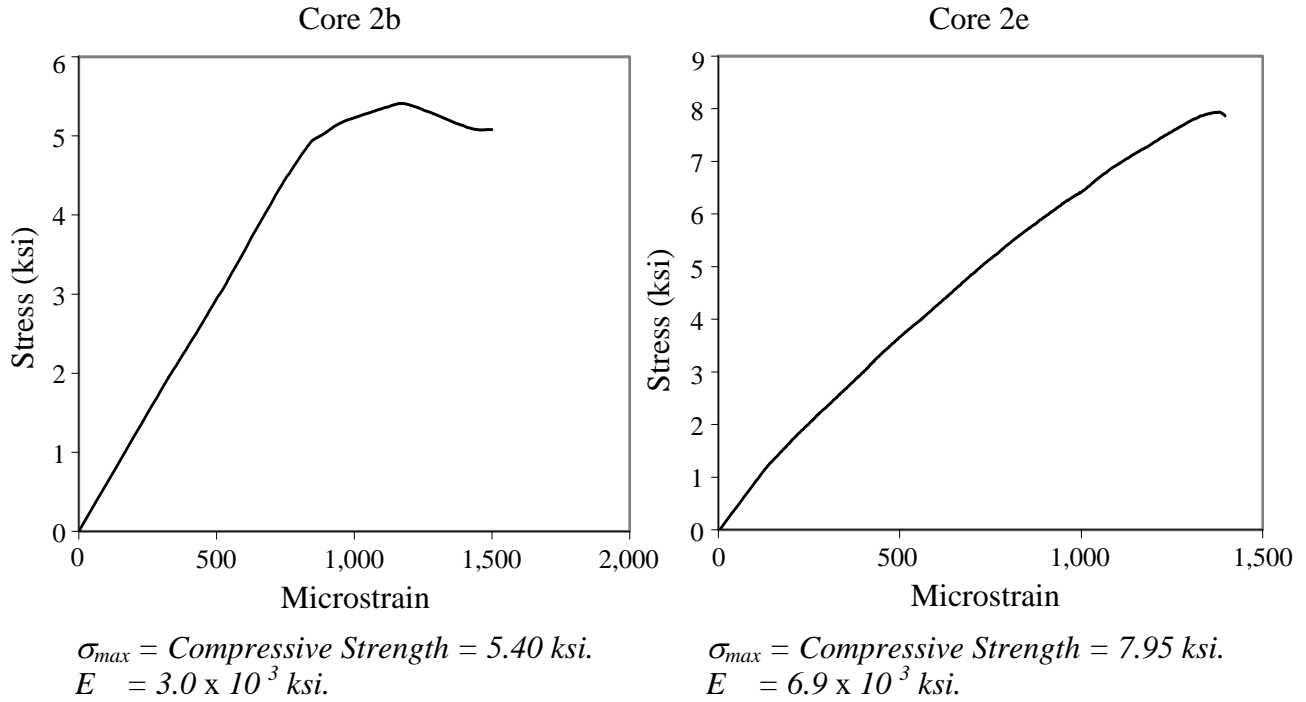


Figure 3.46. Compressive strength test results for Cores 2b and 2e (Rawsonville Rd., Bridge Deck Number 2, Structure No. S03-81041, No SIPMF)

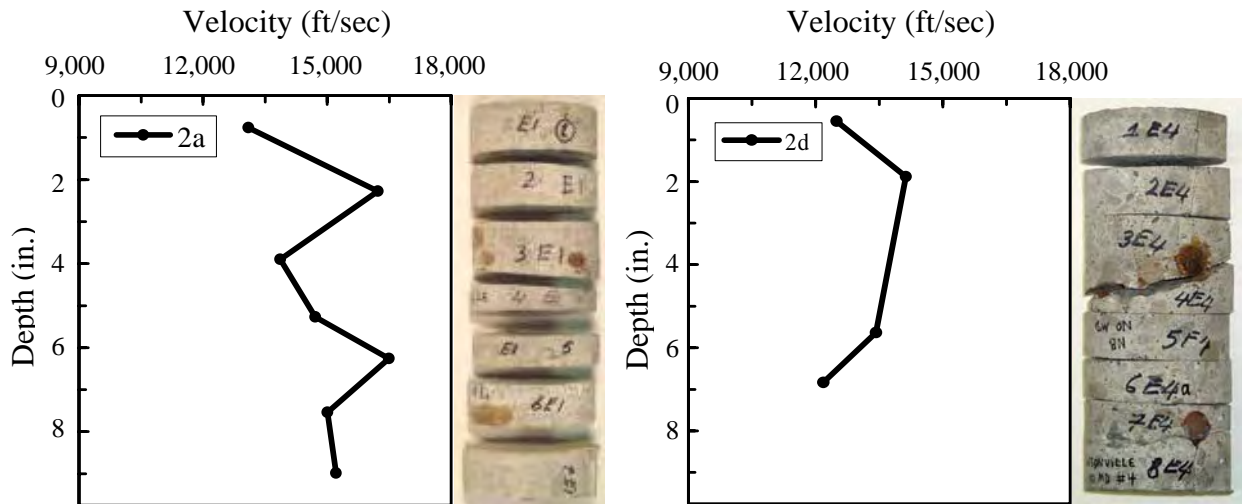


Figure 3.47. Ultrasonic velocity with core depth for Cores 2a and 2d (Rawsonville Rd., Bridge Deck Number 2, Structure No. S03-81041, No SIPMF)

3.3.3 Bridge Deck Number 3: Structure No. B01-82194 (No SIPMF)

Field Inspection

The location of the 4-lane bridge is at the southbound lane of I-75 over Dearborn Street in Detroit. The bridge has 106 spans. Some spans of the deck slabs were composed of concrete slabs without SIPMF and the other slabs were constructed with SIPMF. Deck slabs are supported by seven steel beams, which are laying on two abutments and 105 piers. The structural system of the piers was composed of a concrete girder and four columns. The top and bottom steel reinforcement bars used in the deck slab were not epoxy-coated steel. Five cores were taken at the northwestern shoulder of the southbound of I-75 over Dearborn. The cores were from the concrete deck slab without SIPMF. Coring locations for Bridge Deck Number 3 are presented in Figure 3.48. A map of cracks in the region of coring for Bridge Deck Number 3 is presented in Figure 3.49. Detailed photographs of bridge deck inspection are presented in Figures 3.50 through 3.54.

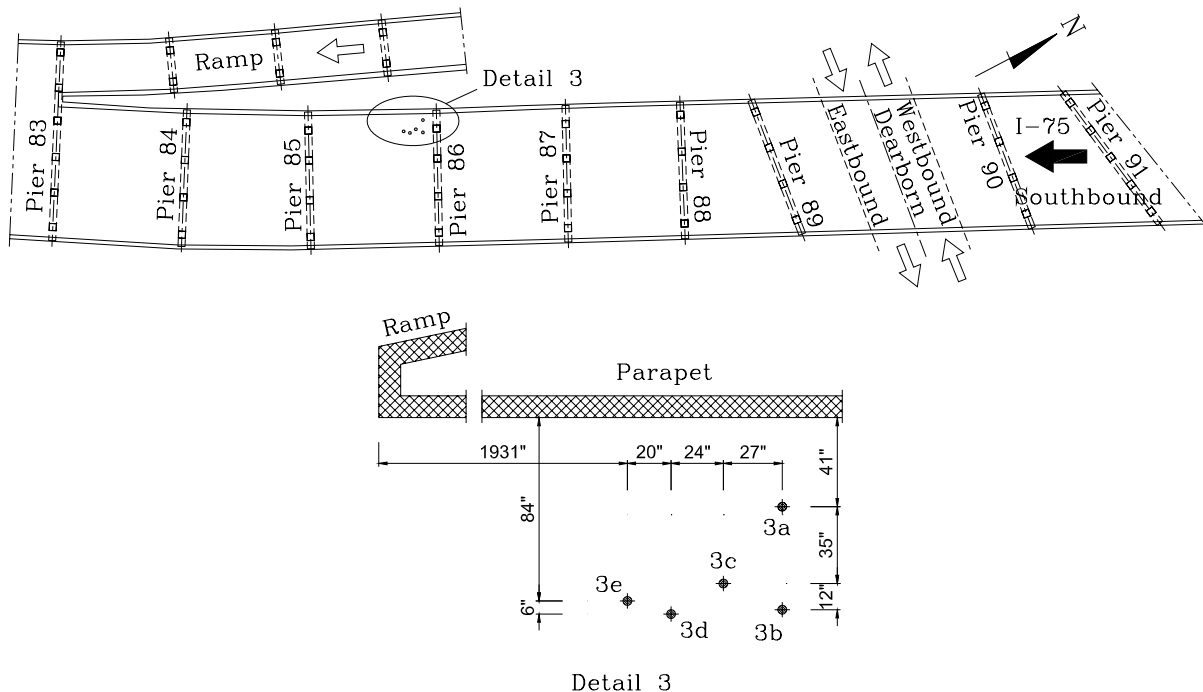
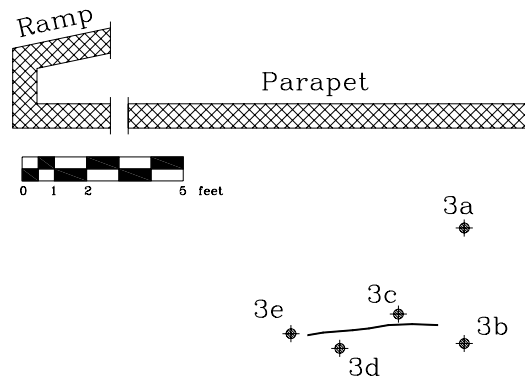


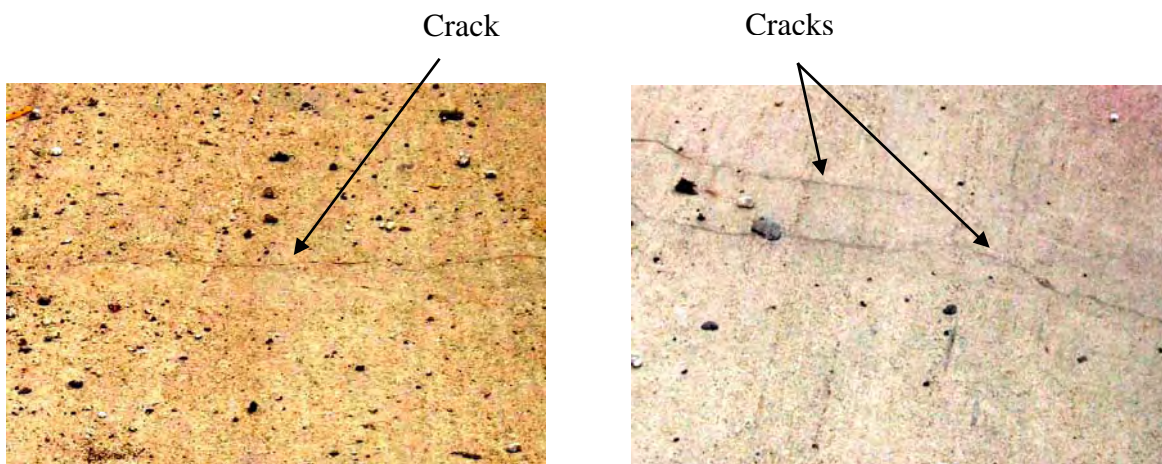
Figure 3.48. Coring locations for Bridge Deck Number 3 (Structure No. B01-82194)



Detail 3

Figure 3.49. Map of cracks at coring locations for Bridge Deck Number 3
(Structure No. B01-82194)

An inspection of the bridge was conducted for the top and bottom surfaces of the deck slab, steel beams and piers. Cracks were observed at the top surface of the concrete slabs (Figure 3.50). Cracks propagated transversely and longitudinally dividing the surface into small rectangles (approximately one square foot each) as shown in Figure 3.51. White and rust traces were encountered underneath the concrete slab (Figure 3.51). White traces were also encountered around the drainage pipe at the bottom surface (Figure 3.51). In some locations, the concrete cover was deteriorated and the steel reinforcement bars were exposed and rusted (Figure 3.52). The bottom surface of the cantilever deck slabs had white traces and the reinforcement bars had corrosion traces (Figure 3.53).



a. Transverse crack

b. Transverse and longitudinal cracks

Figure 3.50. Cracks propagated on the top surface



a. Transverse cracks and white traces



b. Transverse and longitudinal cracks



c. Cracks and white traces (small rectangles)



d. White traces around drainage opening

Figure 3.51. Cracks and white traces propagated on the bottom surface of the slab



a. Deteriorated concrete cover and rust traces



b. Reinforcement bars rusted

Figure 3.52. Corrosion in the reinforcement bars at the bottom surface of the slab



a. White traces



b. Rust and white traces



c. Rust and white traces

Figure 3.53. White and rust traces at the bottom surface of the cantilever slabs



a. Deteriorated concrete cover



b. Rust traces

Figure 3.54. Deterioration at the bottom surface of deck slabs

Inspection of Cores

The visual inspection of cores from Bridge Deck Number 3 indicated that all of the cores except for two cores had no separate wearing surface at the top surface. The top surface was grooved for all of the cores. The steel reinforcement was not epoxy-coated and some of the reinforcement had traces of rust. No regions containing high porosity were observed. Slag as well as conventional aggregates were used. The coarse aggregate was well bonded to the concrete. The heights of the cores varied from 9.3 to 12.3 in. indicating non-uniformity of the bridge deck thickness. Five cores were taken from the concrete deck slab without SIPMF. The cores are shown in Figure 3.55.



Figure 3.55. The 5 cores that were taken from Bridge Deck Number 3
(Structure No. B01-82194)

Core 3a (Figure 3.56)

- 12.3 in. height.
- Part of the connection between the steel beam and the slab was cut and there were traces of corrosion on it.
- Six axial cuts located 4.8, 8.0 and 9.0 in. from top.
- One longitudinal cut located 3.8 in. from top.
- Five locations of honeycombing of average diameter of 0.2 in. located 5.0, 5.5, 6.0 and 8.0 in. from top.
- There was a large void of diameter 0.4 in. and depth of 3.5 in. located the bottom of the core at the location of the connection with the steel beam.
- Slag as well as conventional aggregates were used.



a. Broken bottom



b. Large void and rust at the bottom



c. Rusted reinforcement bars

Figure 3.56. Core 3a

Core 3b (Figures 3.57-3.58)

- 10.5 in. height.
- Two longitudinal cuts in the reinforcement bars located 2.0 in. from top.
- Many entrapped air voids of average diameter 0.3 in. were observed along the length of the core.
- Slag as well as conventional aggregates were used.
- Traces of rust were observed on the exposed steel reinforcement.

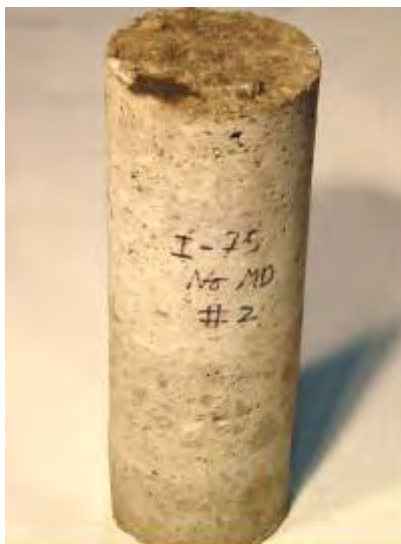


Figure 3.57. Core 3b



Figure 3.58. Core 3b voids and rust in the reinforcement

Core 3c (Figures 3.59-3.60)

- 9.3 in. height.
- Slag as well as conventional aggregates were used; and cement paste had high porosity.
- Four axial cut in the reinforcement located 7.0 and 7.8 in. from the top.
- Three large voids of average diameter 0.4 in. located 2.8 and 6.0 in. from top.
- Steel reinforcement had rust traces.

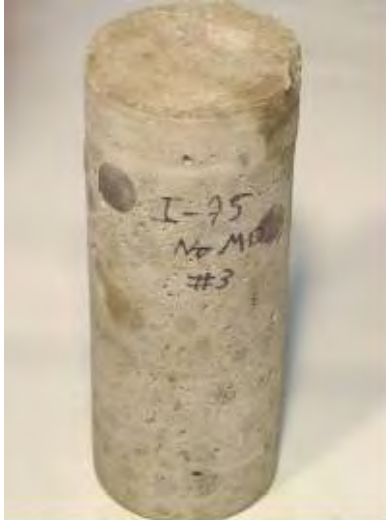


Figure 3.59. Core 3c



Figure 3.60. Core 3c high porosity

Core 3d (Figures 3.61 to 3.63)

- 10.0 in. height.
- The core showed that it was cast in two different layers of concrete: an interface existed 4.0 in. from top.
- Slag as well as conventional aggregates were used.
- Two longitudinal cuts in the reinforcement were observed at 7.3 and 8.0 in. from the top.
- Many voids of average diameter 0.2 in. were distributed along the length of the core.
- Three regions containing honeycombing existed at 1.5, 5.8 and 6.0 in. from top.
- Steel reinforcement bars had traces of rust.
- One large void (0.3 in. diameter) was present 1.3 in. from top.

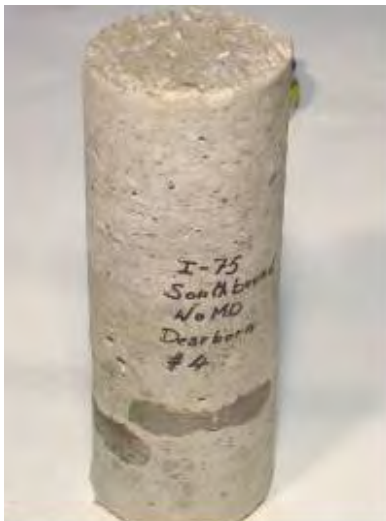


Figure 3.61. Core 3d



Figure 3.62. Core 3d wearing surface

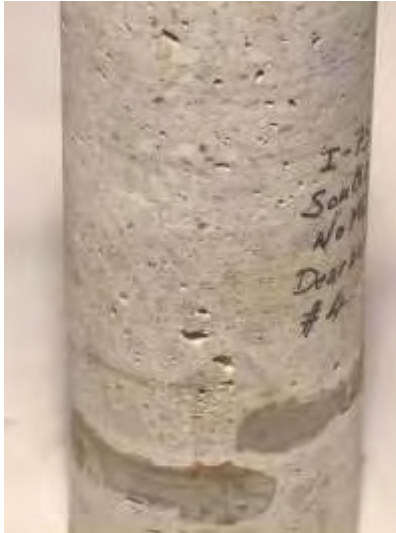


Figure 3.63. Voids in Core 3d

Core 3e (Figures 3.64 to 3.66)

- 9.3 in. height.
- One longitudinal cut in the reinforcement located 7.3 in. from top.
- Two axial cuts in the reinforcement located 3.0 in. from the top.
- Traces of rust were observed in the exposed steel reinforcement.
- Slag as well as conventional aggregates were used.
- The bottom surface of the core had a pop-out of diameter 0.1 in. and 0.2 in. depth and had rust traces in it.
- Four regions of honeycombing existed at 1.0, 2.5, 2.8 and 8.0 in. from top. These regions were of average diameter of 0.2 in.
- One location of honeycombing was near the reinforcement bar and had traces of rust in it.
- The bottom surface was partially damaged.

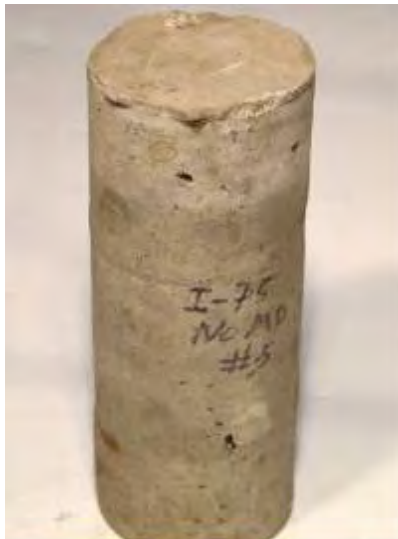


Figure 3.64. Wearing surface
Core 3e



Figure 3.65. Rust in steel bars
Core 3e



Figure 3.66. Pop-out in concrete
Core 3e

The stress-strain curves for Cores 3b and 3c are presented in Figure 3.67. The curves for pulse velocity through the depth for Cores 3a and 3d are presented in Figure 3.68.

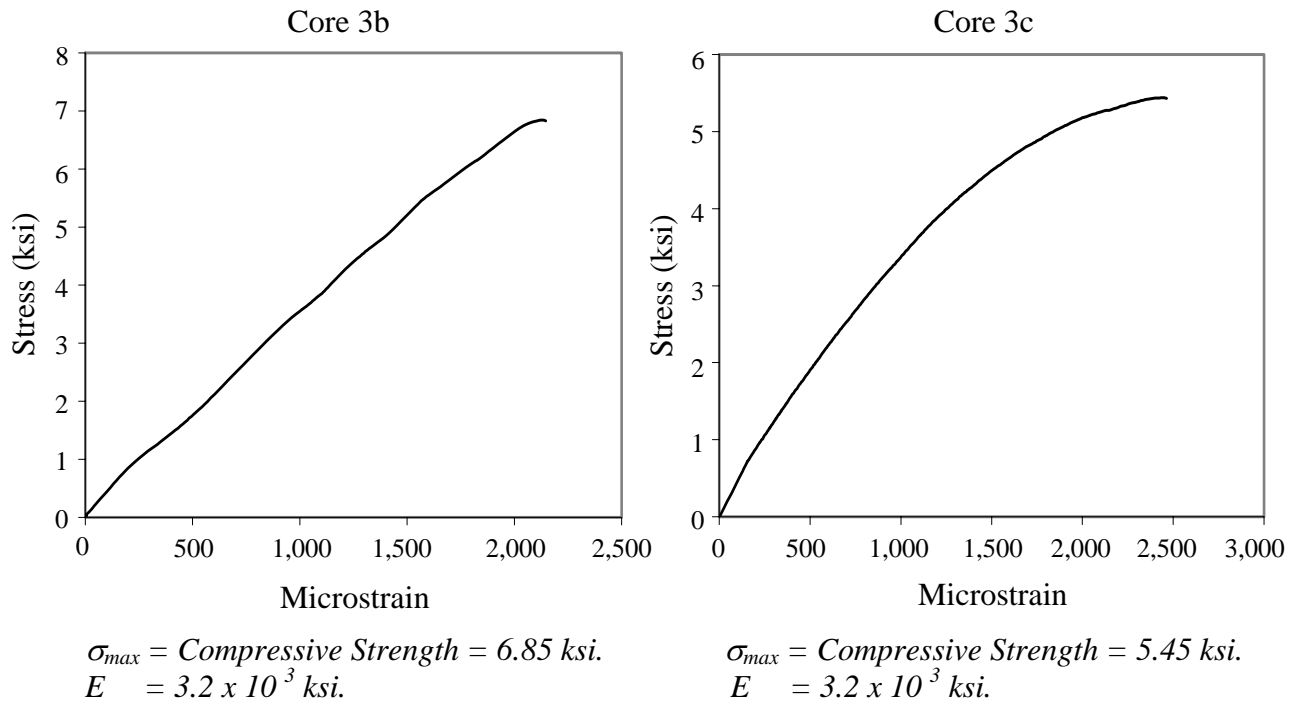


Figure 3.67. Compressive strength test results for Cores 3b and 3c (I-75, Bridge Deck Number 3, Structure No. B01-82194, No SIPMF)

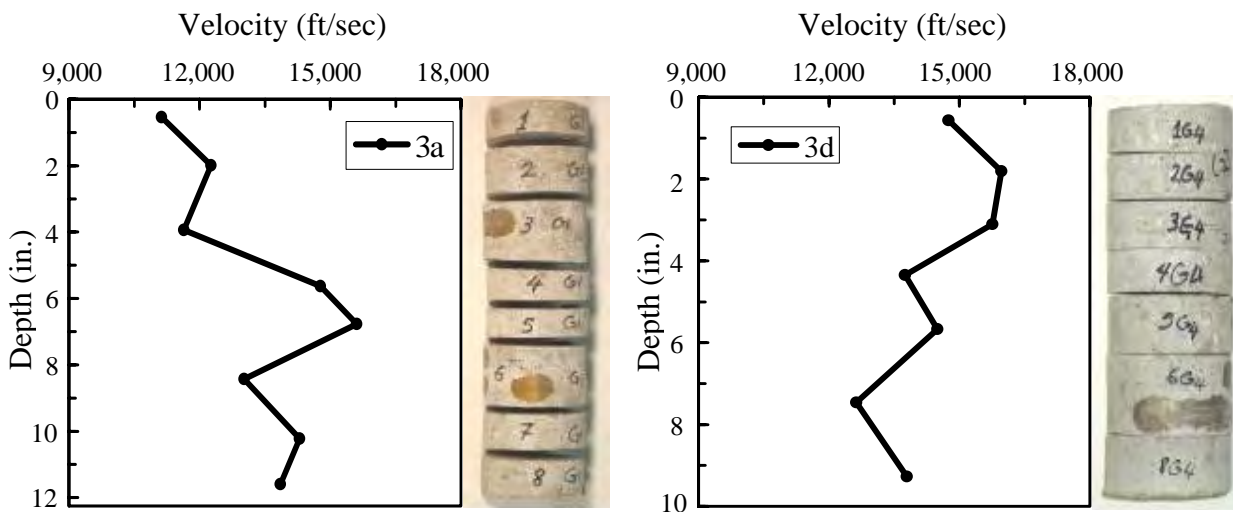


Figure 3.68. Ultrasonic velocity with core depth for Cores 3a and 3d (I-75, Deck Slab Number 3, Structure No. B01-82194, No SIPMF)

3.3.4 Bridge Deck Number 4: Structure No. S11-82022 (No SIPMF)

Field Inspection

The location of the 3-lane bridge is at the intersection of the westbound lane of I-94 over Beech Daly Road in Taylor. The bridge has 3 spans of 47'-3", 43'-2" and 46'-5" lengths. The structural system of the bridge consists of a concrete deck slab and concrete girders supported by two abutments and two piers. The top and bottom steel reinforcement bars used in the deck slab were coated with green epoxy. Five cores were taken from the northern shoulder of westbound I-94 over Beech Daly Road near the parapet of the bridge. Coring locations for Bridge Deck Number 4 are presented in Figure 3.69. A map of cracks in the region of coring for Bridge Deck Number 4 is presented in Figure 3.70. Detailed photograph of bridge deck inspection is presented in Figure 3.71.

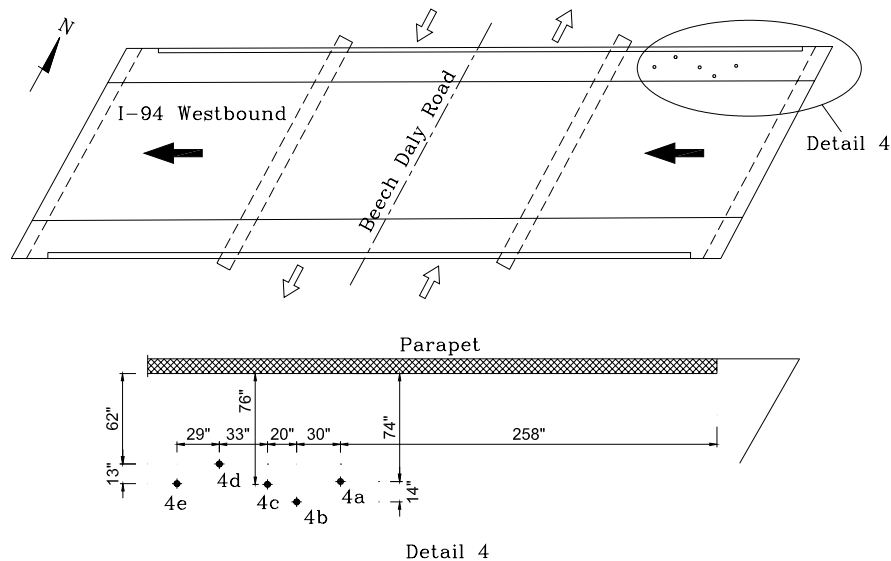


Figure 3.69. Coring locations for Bridge Deck Number 4 (Structure No. S11-82022)

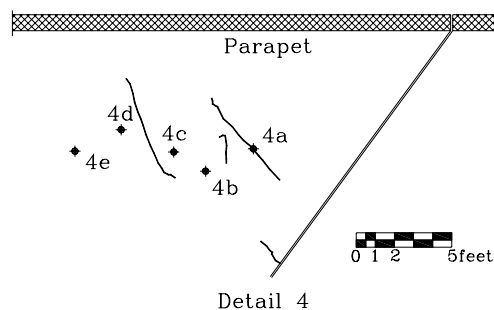


Figure 3.70. Map of cracks at coring location for Bridge Deck Number 4 (Structure No. S11-82022)

The top and bottom surfaces of the deck and beams were visually inspected. Cracks were observed at the top and bottom surfaces of the concrete slab and white traces were observed at the side of beams of the bridge. The cracks and white traces were minor and randomly propagated. The concrete condition generally appeared good.



Figure 3.71. Good concrete condition

Inspection of Cores

The visual inspection of cores from Bridge Deck Number 4 indicated that the concrete was placed at once, as there were no signs of a separate wearing surface. The steel appeared in excellent condition and was coated with green epoxy that was also in excellent condition. However, two cores were cracked at the reinforcement location and the steel had no traces of concrete adhering to it. The coarse aggregate was well bonded to the concrete and no regions of high porosity were observed; however, numerous entrapped air voids were observed. All of the cores had approximately the same height of average 9.8 ± 0.2 in. which indicates bridge uniformity. The five cores are shown in Figure 3.72.



Figure 3.72. The 5 cores that were taken from Bridge Deck Number 4 (Structure No. S11-82022)

Core 4a (Figure 3.73)

- 9.8 in. height.
- A full depth crack propagated all through the height and cross section of the core.
- Steel bars were observed at 4 in. and 8 in. from the top.



a. Reinforcement bars



b. Crack propagated through the height

Figure 3.73. Two sides of Core 4a showing a crack all along the depth of the core

Core 4b (Figure 3.74)

- 9.8 in. height.
- A groove existed on the surface.
- Numerous voids of approximately 0.3 in. diameter.
- A #4 steel bar was observed located 3.5 in. from the top.



Figure 3.74. A few large voids near the mid-height and reinforcing steel were observed in Core 4b

Core 4c (Figure 3.75)

- 9.8 in. height.
- Core fractured at the reinforcement located 3.8 in. from the top.
- Numerous voids of approximately 0.1 in. diameter.



Figure 3.75. Core 4c fractured at the reinforcement location

Core 4d (Figure 3.76)

- 9.9 in. height.
- Overall, good concrete quality.



Figure 3.76. Core 4d

Core 4e (Figures 3.77-3.78)

- 9.6 in. height.
- Core fractured at the reinforcement located 4 in. from the top.
- Core appeared more porous than the other cores from this bridge deck.
- Numerous entrapped air voids with an average diameter of 0.15 in. were observed.



Figure 3.77. Exposed reinforcement where core fractured in Core 4e



Figure 3.78. Voids observed in Core 4e

The stress-strain curves for Cores 4b and 4d are presented in Figure 3.79, and the curves for pulse velocity through the depth for Cores 4c and 4e are presented in Figure 3.80. Due to fractures in the specimen, the velocity measurements were not obtained for all slices of Cores 4c and 4e.

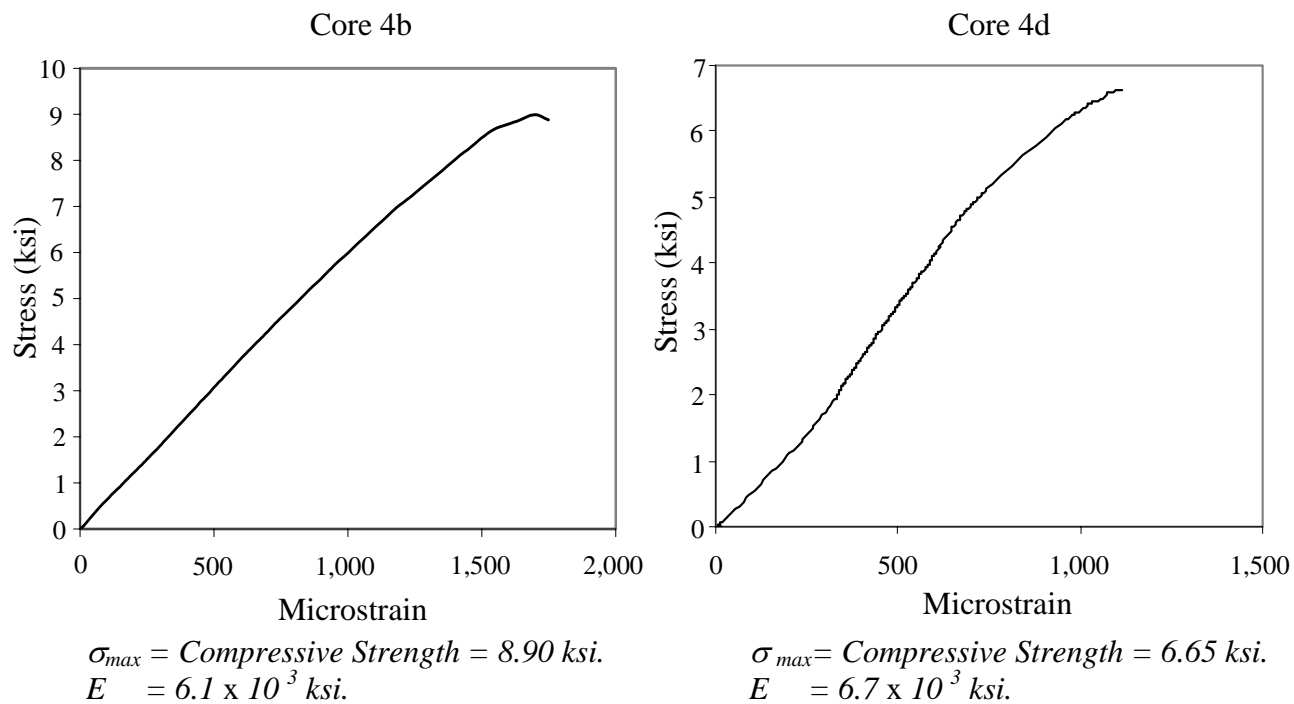


Figure 3.79. Compressive strength test results for Cores 4b and 4d (I-94, Bridge Deck Number 4, Structure No. S11-82022, No SIPMF)

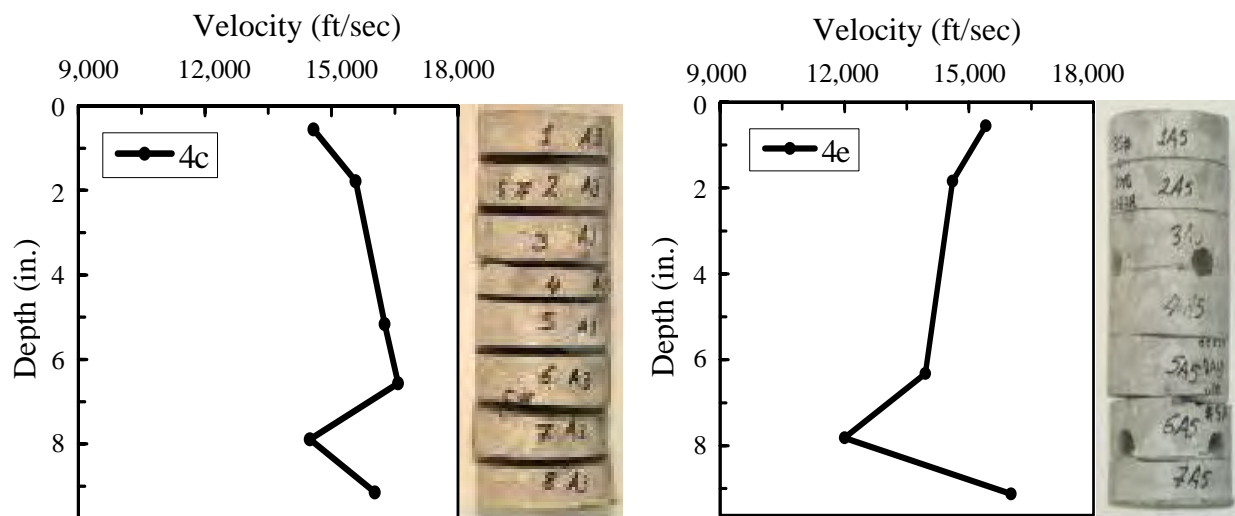


Figure 3.80. Ultrasonic velocity with core depth for Cores 4c and 4e (I-94, Bridge Deck Number 4, Structure No. S11-82022, No SIPMF)

3.3.5 Bridge Deck Number 5: Structure No. S09-82022 (No SIPMF)

Field Inspection

The location of the 4-lane bridge is at the intersection of the eastbound lane of I-94 over Ecorse Road in Taylor. The bridge has 4 spans of 53'-6", 65'-0", 65'-0" and 53'-6" lengths. The bridge is composed of a concrete slab deck and steel girders supported by two abutments and three piers. The top and bottom steel reinforcement bars used in the deck slab were coated with green epoxy. Five cores were taken from the southern shoulder of eastbound I-94 over Ecorse Road near the parapet of the bridge. The cores were from deck slab without SIPMF. Coring locations for Bridge Deck Number 5 are presented in Figure 3.81. A map of cracks in the region of coring for Bridge Deck Number 5 is presented in Figure 3.82. Detailed photographs of bridge deck inspection are presented in Figures 3.83 and 3.84.

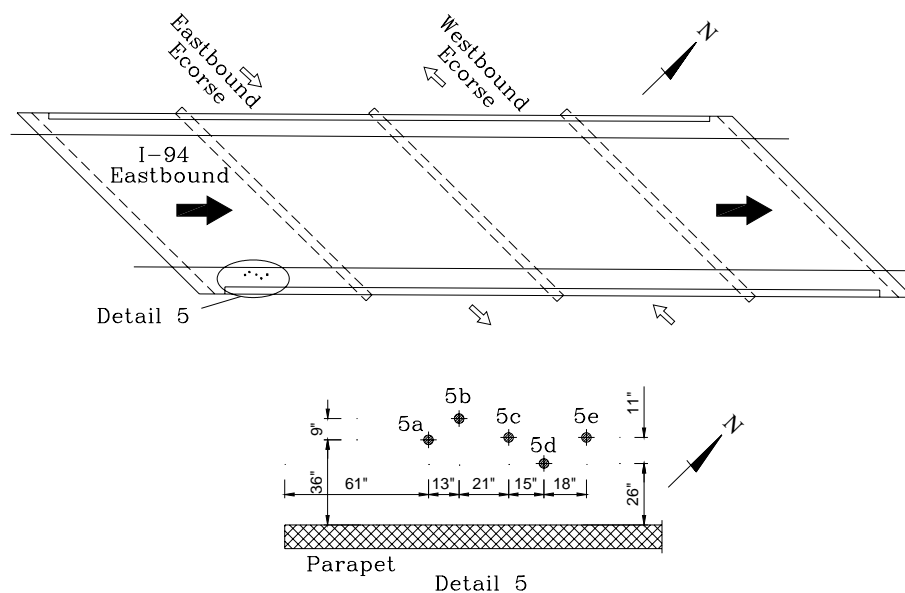


Figure 3.81. Coring locations for Bridge Deck Number 5
(Structure No. S09-82022)

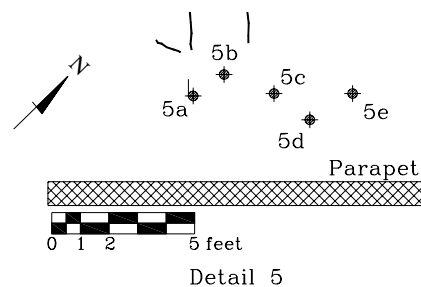
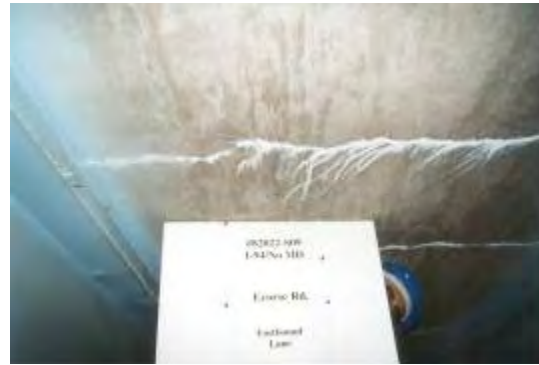


Figure 3.82. Map of cracks at coring locations for Bridge Deck Number 5
(Structure No. S09-82022)

Cracks were observed at the top surface of the concrete slab. White traces were observed underneath the concrete slab at approximately 4 ft. intervals as shown in Figures 3.83 and 3.84.



a. White traces at approximately 4 ft



b. White traces with transverse crack

Figure 3.83. White traces at the bottom surface of the deck



Figure 3.84. White traces near coring location

Inspection of Cores

The visual inspection of cores from Bridge Number 5 indicated that the bridge had no separate wearing surface at the top surface. The top surface of all of the cores had a grooved texture. The steel reinforcement bars were coated with green epoxy and had slight traces of rust. The coarse aggregate was well bonded to the concrete, which had no porosity however few voids were encountered. All of the cores had approximately the same height of average 9.4 ± 0.2 in. which indicates bridge uniformity. The five cores that were taken are shown in Figure 3.85.



Figure 3.85. The 5 cores that were taken from Bridge Deck Number 5 (Structure No. S09-82022)

Core 5a (Figure 3.86)

- 9.5 in. height.
- One large void of 0.6 in. located 2.0 in. from the top.
- Axial section of a steel reinforcement #4 appeared at 3.3 in. from the top.
- Exposed steel showed traces of rust.



Figure 3.86. Core 5a with a large void

Core 5b (Figure 3.87)

- 9.5 in. height.
- Two axial sections of a steel reinforcement #4 observed at 3.3 in. from the top.
- One axial section of a steel reinforcement #5 observed at 4.0 in. from the top.
- Traces of rust were observed in exposed steel reinforcement.
- One large void of 0.5 in. diameter located 5.5 in. from the top.

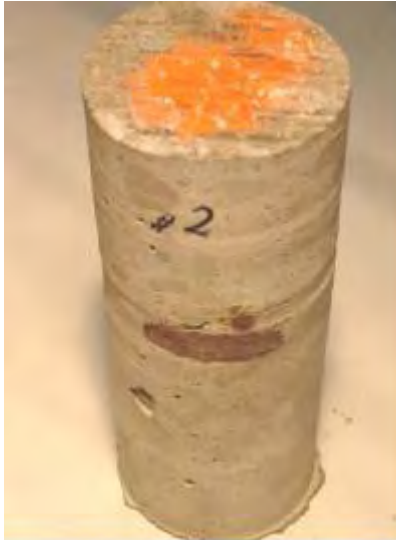


Figure 3.87. Core 5b with a large void and rust in the reinforcement

Core 5c (Figures 3.88-3.89)

- 9.5 in. height.
- Two axial sections of steel reinforcement located 7.8 in. from the top.
- Two longitudinal sections of steel reinforcement located 3.8 and 6.8 in. from the top.
- Exposed reinforcement bars had traces of rust.
- Honeycombing in regions of average width 0.5 in.
- Many entrapped air voids of average dimension 0.2 in.
- Two longitudinal hair cracks observed along the entire length of the core.



Figure 3.88. Presence of honeycombing in Core 5c



Figure 3.89. Hairline crack along surface of core in Core 5c

Core 5d (Figure 3.90)

- 9.2 in. height.
- Some reinforcement bars had rust traces while others did not.
- Many voids of average diameter 0.2 in.
- Five axial sections of reinforcement bars located 3.8, 4.0, 7.0, 7.8 and 8.0 in. from the top.
- The core was partially damaged in the coring from the bottom surface.



Figure 3.90. Damage of bottom region of Core 5d

Core 5e (Figure 3.91)

- 9.3 in. height.
- Many voids of average diameter 0.2 in.
- Two large voids located 2.0 and 4.5 in. from the top surface.
- Two axial sections of reinforcement bars located 3.8 in. from the top.
- Three longitudinal sections of reinforcement bars located 3.3, 6.8 and 7.5 in. from the top surface.
- Rust traces were observed in reinforcement bars.

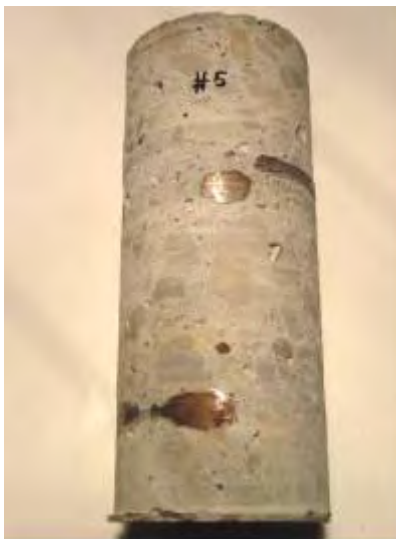
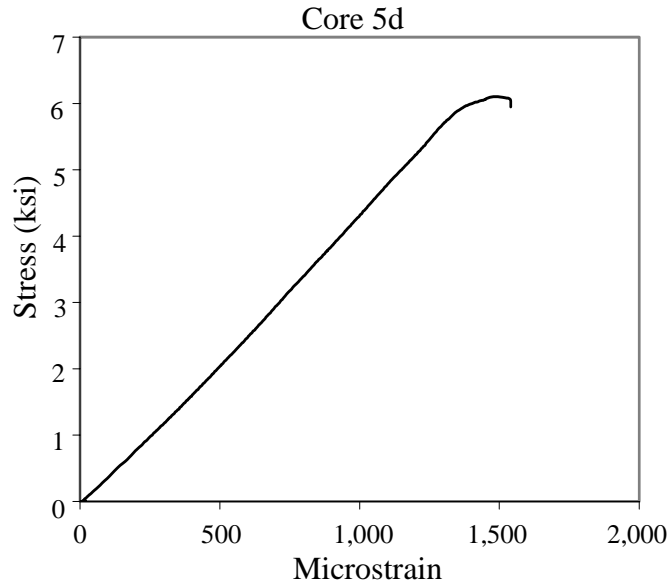


Figure 3.91. Core 5e with rust traces in reinforcement bars

The stress-strain curve for Core 5d is presented in Figure 3.92. The compression strength test for Core 5a resulted in a rapid failure and extremely low compression strength. A plot is not shown for this test. The curves for pulse velocity through the depth for Cores 5c and 5e are presented in Figure 3.93.



$$\sigma_{max} = \text{Compressive Strength} = 6.10 \text{ ksi.}$$

$$E = 4.2 \times 10^3 \text{ ksi.}$$

Figure 3.92. Compressive strength test results for Core 5d
(I-94, Bridge Deck Number 5, Structure No. S09-82022, No SIPMF)

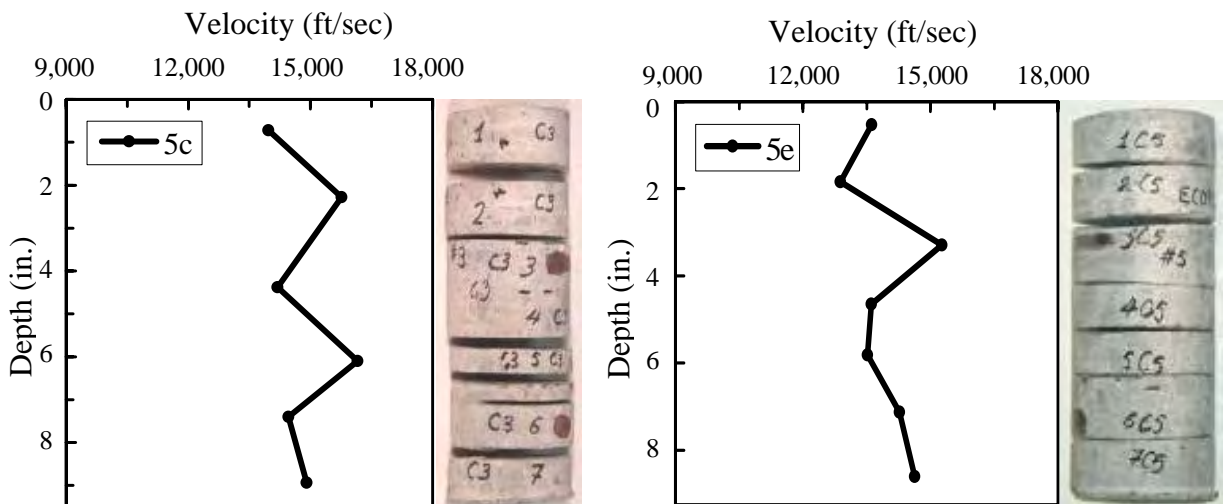


Figure 3.93. Ultrasonic velocity with core depth for Cores 5c and 5e
(I-94, Deck Slab Number 5, Structure No. S09-82022, No SIPMF)

3.3.6 Bridge Deck Number 6: Structure No. R01-13012 (SIPMF)

Field Inspection

The location of the 2-way 2-lane bridge deck is at the northbound lane of S. Washington Avenue over Kalamazoo River and train tracks in Battle Creek. The bridge has 8 spans. Beginning from the abutment at the north of the bridge, the fifth, sixth and seventh spans are composed of concrete slabs with SIPMF. Nine steel beams support the deck slabs of the northbound and southbound lanes. Steel beams are supported on two abutments and seven piers. The structural system of the piers is composed of a concrete girder and 2 columns. Six of the concrete girders have one span and double cantilever. The seventh girder has one span without cantilever. The top and bottom steel reinforcement bars used in the deck slab were coated with brown epoxy. Five cores were taken from the fifth span (northeastern part of the bridge) in the concrete deck slab with SIPMF. Coring locations for Bridge Deck Number 6 are presented in Figure 3.94. A map of cracks in the region of coring for Bridge Deck Number 6 is presented in Figure 3.95. Detailed photographs of bridge deck inspection are presented in Figures 3.96 through 101.

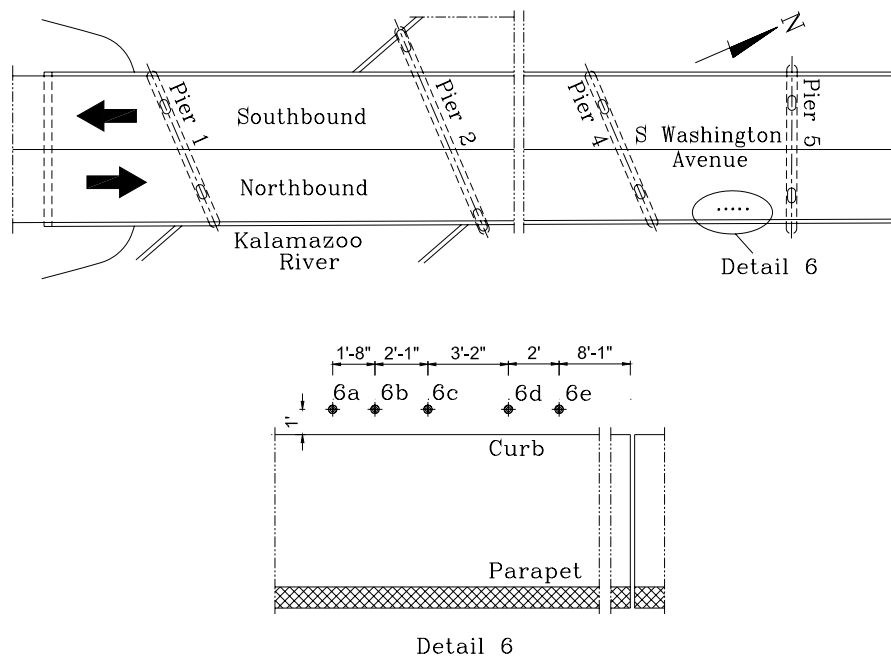
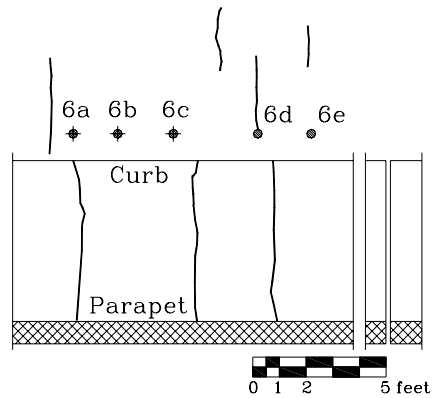


Figure 3.94. Coring locations for Bridge Deck Number 6
(Structure No. R01-13012)



Detail 6

Figure 3.95. Map of cracks at coring locations for Bridge Deck Number 6 (Structure No. R01-13012)

An inspection of the bridge was conducted for the top and bottom surfaces of the deck slab, steel beams, piers and abutments. The cracks propagated longitudinally, transversely or diagonally through the bridge. Some of the top surface cracks were accompanied by corrosion of the SIPMF indicating that these cracks were full depth cracks as shown in Figures 3.96 and 3.97. A different type of concrete (as indicated by a difference in color) was encountered at the sides of the joints in the top surface (Figure 3.98). The SIPMF at bottom surface of the deck slab was corroded diagonally and transversely at the same location of the top cracks (Figure 3.99). The connections between the SIPMF and the steel beams showed rust accompanied with white traces as shown in Figure 3.100. The drainage holes had corrosions in the deck with SIPMF (Figure 3.101)

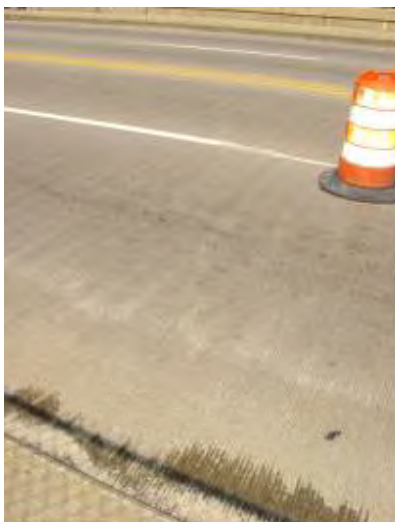


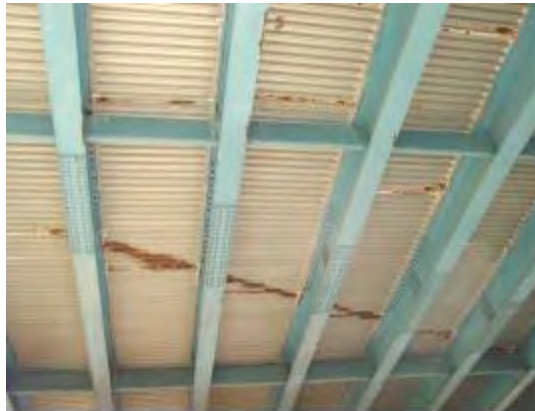
Figure 3.96. Cracks propagated on the top surface of the deck slab



Figure 3.97. Corrosion at the SIPMF



Figure 3.98. Different types of concrete around the joints



a. Corrosion in the SIPMF oriented diagonally



b. Corrosion in the SIPMF oriented transversely

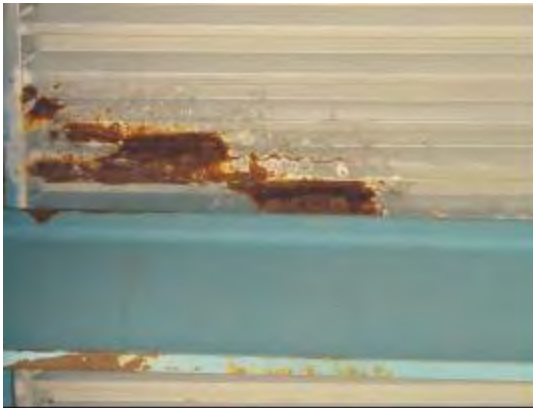


c. Corrosion and white traces in the SIPMF

Figure 3.99. Corrosion in the SIPMF is oriented diagonally and transversely



a. Corrosion and white traces near the connection



b. Corrosion in SIPMF near connection
between main and bracing beams



c. Corrosion in SIPMF and steel beam
at the connection

Figure 3.100. Corrosion and white traces at the connection between SIPMF and steel beams



Figure 3.101. Corrosion around the hole in the deck with SIPMF

Inspection of Cores

The visual inspection of the cores from Bridge Number 6 indicated that all of the cores had a wearing surface of 2.3 in. at the top as indicated by the change in concrete color and the aggregate size. This wearing surface had a higher porosity than the rest of the core. The top surface was grooved for all of the cores. The steel reinforcement was coated with brown epoxy and some of the exposed reinforcement bars had rust traces. The coarse aggregate was well bonded to the concrete. Regions of high porosity and large voids were observed. The SIPMFs for all of the cores are separated from the concrete without leaving concrete traces adhering to its inner face. The height of the cores did not vary thus indicating uniformity of the bridge. The five cores that were taken are shown in Figure 3.102.



Figure 3.102. The 5 cores that were taken from Bridge Deck Number 6 (Structure No. R01-13012)

Core 6a (Figure 3.103)

- 10.0 in. height.
- Two axial cuts in the reinforcement located 4.3 in. from the top.
- One longitudinal cut in the reinforcement located 8.3 in. from the top.
- Reinforcement bars had signs of rust.
- The SIPMF was separated from the core.
- Part of the concrete in the region of the valley of the SIPMF was broken at 10.8 in. from the top during coring.
- Two regions of honeycombing of average width of 0.3 in. were located 5.8 in. and 9.3 in. from the top.



Figure 3.103. Core 6a broken concrete in the region of the valley of the SIPMF and separated SIPMF

Core 6b (Figure 3.104)

- 10.0 in. height.
- SIPMF was separated from the core.
- One longitudinal cut in the reinforcement located 5.0 in. from the top.
- High porosity.
- Many large voids of average diameter of 0.2 in.
- Three regions of honeycombing of average width of 0.3 in. were located 3.8, 5.0 and 5.8 in. from the top.



Figure 3.104. Core 6b many honeycombing and rust in the reinforcement bars

Core 6c (Figure 3.105)

- 10.0 in. height.
- The concrete in the region of the valley of the SIPMF was partially broken during the coring.
- SIPMF separated from the core.
- The concrete had high porosity.

- Many large entrapped air voids of average diameter of 0.2 in. were observed.
- Seven locations of honeycombing of average width of 0.3 in. were located 3.0, 3.5, 5.5, 6.5, 6.8, and 8.0 inches from the top.
- Reinforcement bars had rust traces.



Figure 3.105. Core 6c crack
at the reinforcement

Core 6d (Figures 3.106-3.107)

- 10.0 in. height.
- Lateral crack caused splitting at 4.5 in. from the top at the location of the reinforcement, which showed traces of corrosion.
- Four axial sections of reinforcement bars located 4.5 and 8.5 in. from the top.
- SIPMF separated from the core.
- The SIPMF left signs of rust on the surface of contact with the concrete.
- Reinforcement bars had rust traces.
- Four locations of honeycombing of average width of 0.3 in. were located 6.0, 7.5, 8.5 and 9.3 in. from the top.



Figure 3.106. Core 6d rust at the reinforcement bar



Figure 3.107. Core 6d rust on the SIPMF

Core 6e (Figure 3.108)

- 10.0 in. height.
- High porosity.
- Many large voids of average diameter 0.2 in.
- SIPMF was separated during the coring.
- Two locations of honeycombing of average width of 0.3 in. were located 5.5 and 8.3 in. from the top.



Figure 3.108. Core 6e many locations of entrapped air

The stress-strain curve for Cores 6c and 6e are presented in Figure 3.109, and the curves for pulse velocity through the depth for Cores 6b and 6d are presented in Figure 3.110. Due to fractures in the specimen, the velocity measurements were not obtained for all slices of Core 6d.

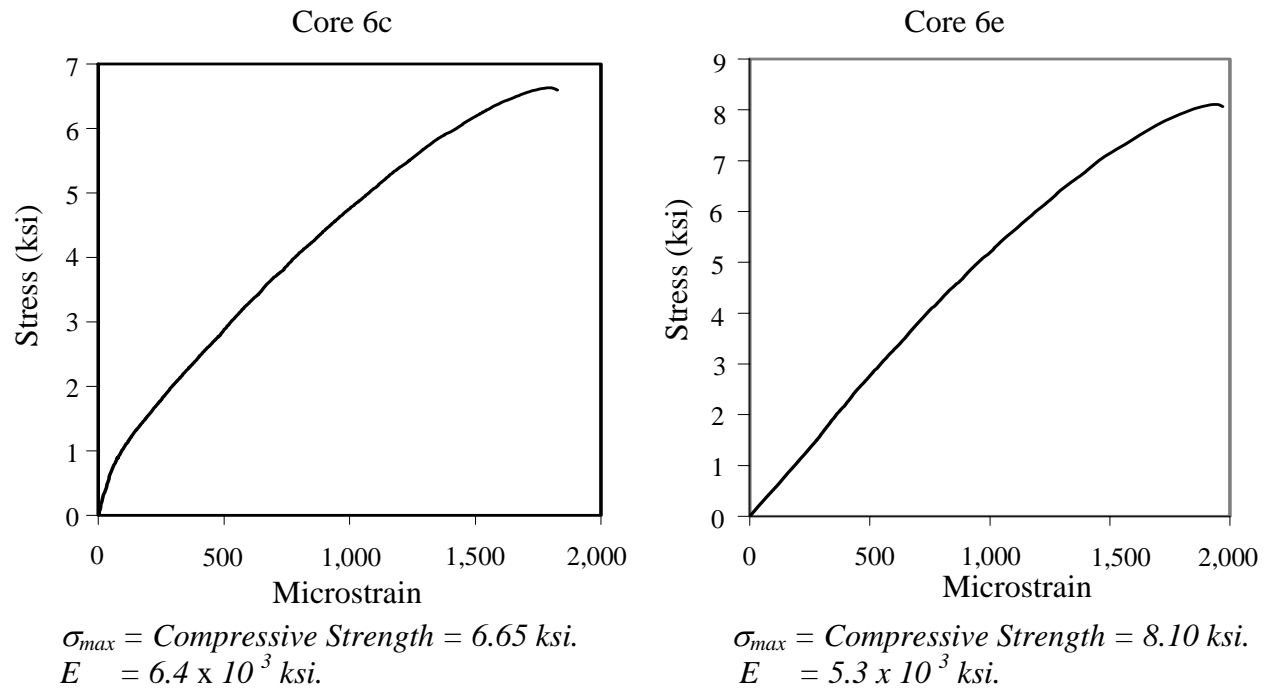


Figure 3.109. Compressive strength test results for Cores 6c and 6e
(S. Washington Ave., Bridge Deck Number 6, Structure No. R01-13012, SIPMF)

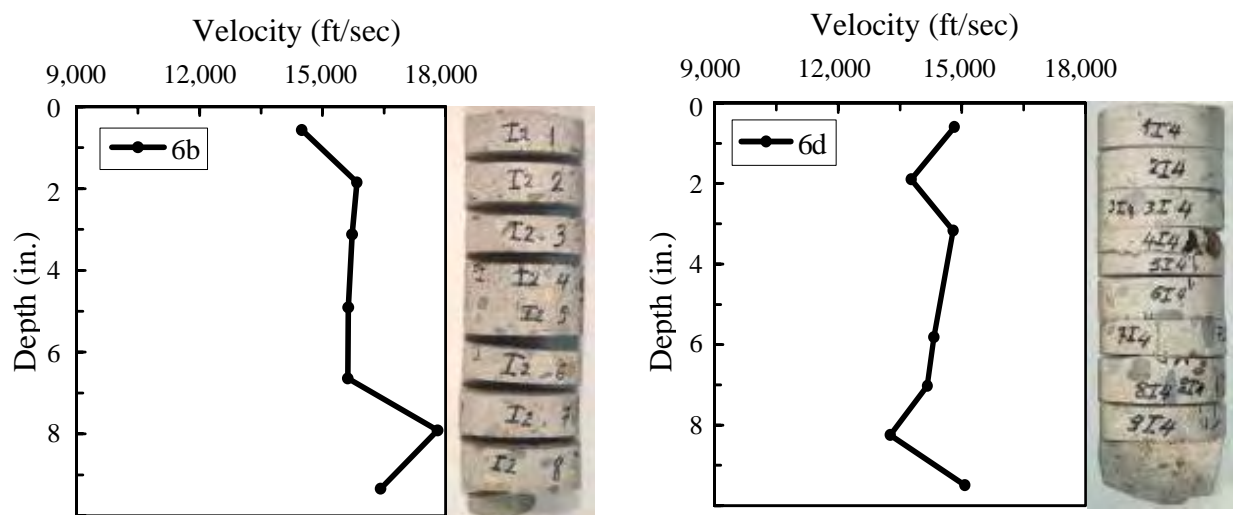


Figure 3.110. Ultrasonic velocity with core depth for Cores 6b and 6d
(S. Washington Ave., Bridge Deck Number 6, Structure No. R01-13012, SIPMF)

3.3.7 Bridge Deck Number 7: Structure No. S03-81041 (SIPMF)

Field Inspection

The location of the 2-way, 4-lane bridge is at the northbound lane of Rawsonville Road over I-94 Freeway in Belleville. The bridge has 4 spans of 44'-11", 106'-7", 115'-0" and 36'-6" lengths. The deck slabs are made of concrete slabs with SIPMF for the second and third slabs. Deck slabs are supported by eight steel beams, which are supported on two abutments and three piers. The structural system of the piers is composed of a concrete girder supported by eight columns. The top and bottom steel reinforcement bars used in the deck slab were not epoxy-coated steel. Five cores were taken at the eastern shoulder of the northbound lane of Rawsonville over I-94 near the parapet of the bridge. The cores were from the concrete deck slab with SIPMF. Coring locations for Bridge Deck Number 7 are presented in Figure 3.111. A map of cracks in the region of coring for Bridge Deck Number 7 is presented in Figure 3.112. Detailed photographs of bridge deck inspection are presented in Figures 3.113 through 3.115.

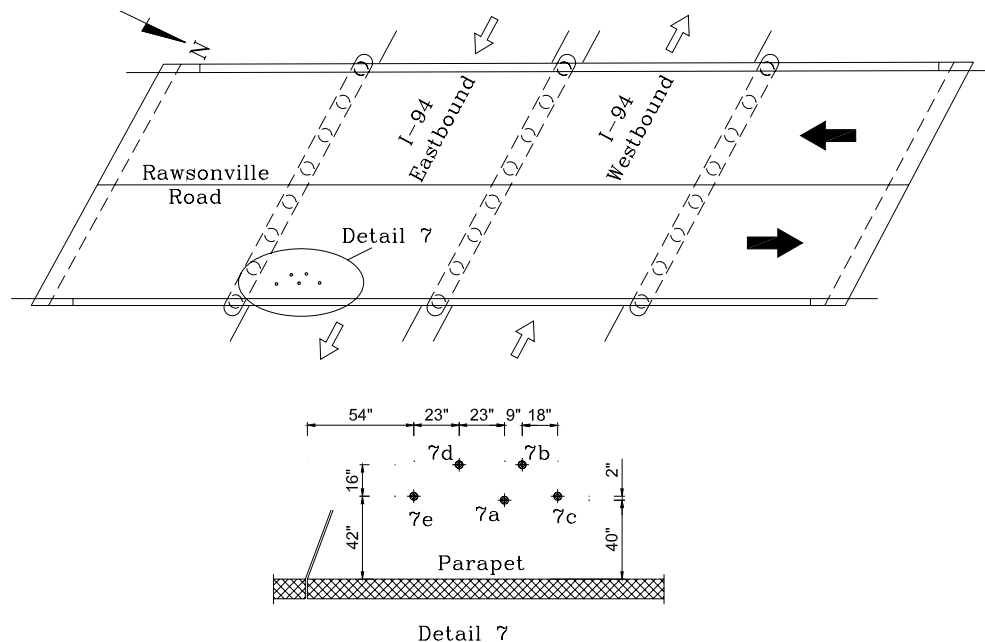


Figure 3.111. Coring locations for Bridge Deck Number 7
(Structure No. S03-81041)

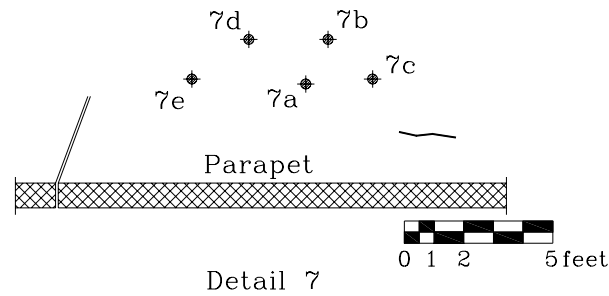


Figure 3.112. Map of cracks at coring locations for Bridge Deck Number 7 (Structure No. S03-81041)

A deteriorated section of approximately 2 in. depth and 2 feet in diameter existed in the top surface of the bridge (Figure 3.113). In many locations along the bridge, the concrete curbs were deteriorated and the steel reinforcement bars were uncovered (Figure 3.114). The SIPMF was in good condition (Figure 3.115).



a. Large depression in bridge deck



b. Depth of large depression

Figure 3.113. Deteriorated section in the deck slab



a. Severe deterioration along the curb



b. Deteriorated section and white traces

Figure 3.114. Severe deterioration on the curbs



Figure 3.115. Good condition of SIPMF

Inspection of Cores

The visual inspection of cores from Bridge Number 7 indicated that the bridge had no separate wearing surface at the top surface. The steel reinforcement was not epoxy-coated and had traces of rust. The coarse aggregate was well bonded to the concrete. The cement paste had high porosity. Slag was used as aggregates in the deck slab. The SIPMFs for all of the cores were separated from the concrete (without leaving big traces adhering to its inner face). All of the cores had approximately the same height of average 9.3 ± 0.2 in. (not including concrete placed in the valley of the corrugation of the SIPMF) which indicates bridge uniformity. The five cores are shown in Figure 3.116.



Figure 3.116. The 5 cores that were taken from Bridge Deck Number 7 (Structure No. S03-81041)

Core 7a (Figures 3.117-3.118)

- 9.3 in. height.
- The concrete in the region of the valley of the SIPMF was broken during coring.
- Slag was used as aggregates in the deck slab; and cement paste had high porosity.
- One longitudinal cut in the steel reinforcement bar located 3.5 in. from top.
- Reinforcement bar had signs of rust.
- SIPMF was separated from the concrete and had 2 overlapping sections.



Figure 3.117. Core 7a is broken and reinforcement bar is rusted

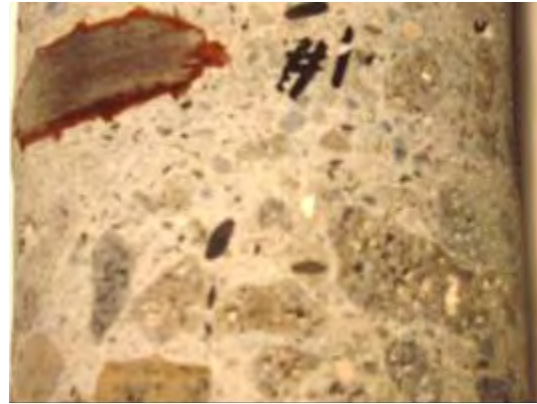


Figure 3.118. Core 7a reinforcement is rusted and concrete is porous

Core 7b (Figure 3.119)

- 9.3 in. height (11.5 in. with the concrete in the region of the valley of the SIPMF).
- Large entrapped air voids of approximately 0.3 in. diameter occurred at the concrete in the region of the valley of the SIPMF at 0.8 and 1.5 in. from bottom.
- Four axial cuts in the steel reinforcement bars located 3.5, 3.8, 7.8, and 8.0 in. from top.
- SIPMF was separated with 2 overlapping sections.
- Slag was used as aggregates in the deck slab.



Figure 3.119. Core 7b shows large entrapped air voids and overlap of SIPMF sections

Core 7c (Figure 3.120)

- 9.0 in. height (11.8 in. with the concrete in the region of the valley of the SIPMF).
- Slag was used as aggregates in the deck slab; and cement paste had high porosity.
- Many large voids of 0.3 in. average diameter.
- Two axial cuts in the steel reinforcement bars located 3.8 in. from top.
- One longitudinal reinforcement bar located 7.8 in. from top.
- Reinforcement bars had signs of rust.
- SIPMF separated from the core.
- Concrete in the region of the valley of the SIPMF was damaged during the coring.



Figure 3.120. Core 7c shows the broken concrete in the region of the valley of the SIPMF and the rust in the reinforcement bars

Core 7d (Figure 3.121)

- 9.5 in. height (12.0 in. with the concrete in the region of the valley of the SIPMF).
- Concrete in the region of the valley of the SIPMF was broken during the coring.
- Slag was used as aggregates in the deck slab; and cement paste had high porosity.
- Large voids of average diameter 0.4 in. occurred 4.3, 6.0, and 8.0 in. from top.
- Two axial sections of reinforcement bars located 8.0 in. from top.
- Two longitudinal sections of reinforcement located 3.8 in. from top.
- Reinforcement bars had signs of rust.
- SIPMF separated from the core.
- Region of honeycombing observed 2.8 in. from top.



a. Broken concrete in the region of the valley of the SIPMF



b. Rust in the reinforcement bar

Figure 3.121. Core 7d

Core 7e (Figure 3.122)

- 9.5 in. height (11.0 in. with the concrete in the region of the valley of the SIPMF).
- The concrete in the region of the valley of the SIPMF was broken during the coring.
- Slag was used as aggregates in the deck slab; and cement paste had high porosity.
- Large entrapped air voids of average diameter 0.2 in. occurred 3.0 in. from top.
- Two longitudinal sections of reinforcement occurred at 4.0 in. and 8.0 in. from top.
- Reinforcement bars have signs of rust.
- SIPMF was separated during the coring.



Figure 3.122. Broken concrete in the region of the valley of the SIPMF and the rust in the reinforcement bars in Core 7e

The stress-strain curves for Cores 7b and 7d are presented in Figure 3.123, and the curves for pulse velocity through the depth for Cores 7a and 7c are presented in Figure 3.124.

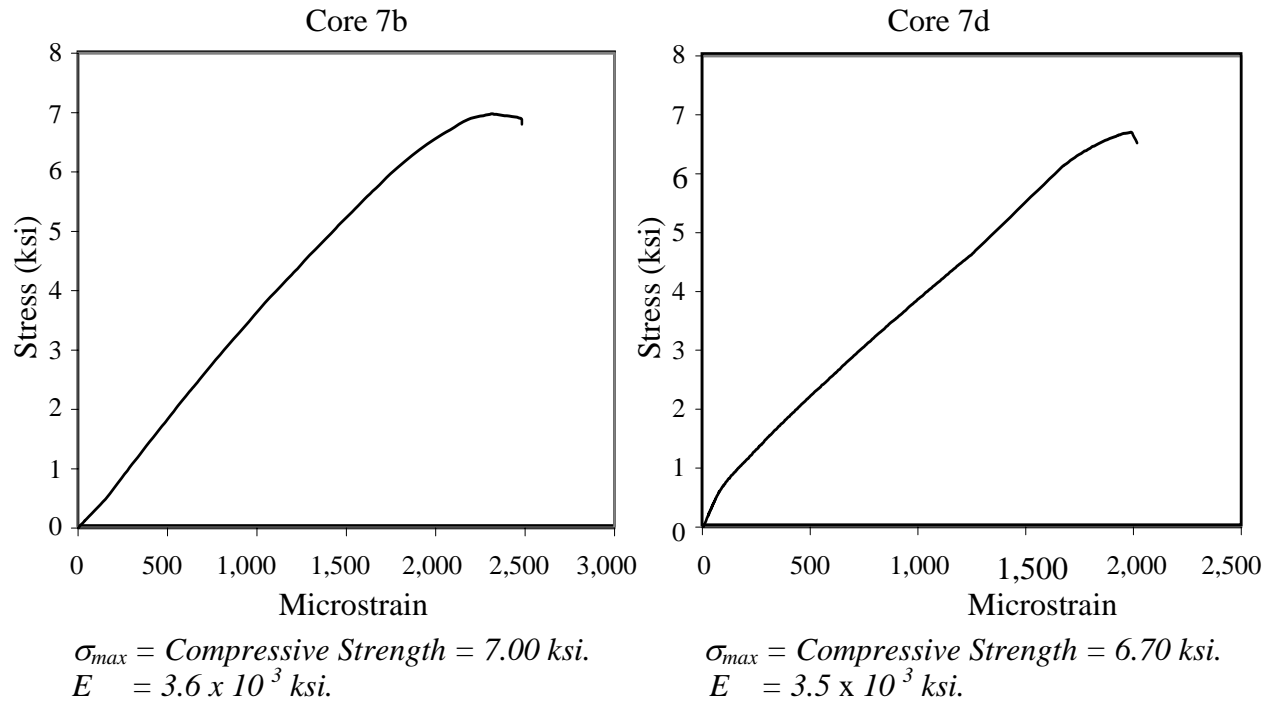


Figure 3.123. Compressive strength test results for Cores 7b and 7d
(Rawsonville Rd., Bridge Deck Number 7, Structure No. S03-81041, SIPMF)

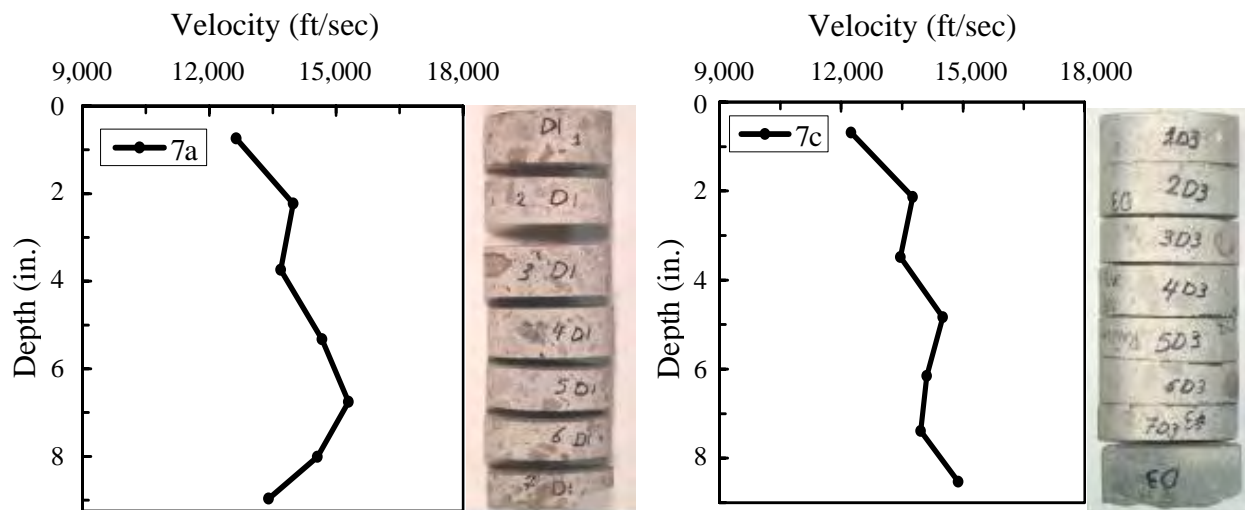


Figure 3.124. Ultrasonic velocity with core depth for Cores 7a and 7c
(Rawsonville Rd., Bridge Deck Number 7, Structure No. S03-81041, SIPMF)

3.3.8 Bridge Deck Number 8: Structure No. B01-82194 (SIPMF)

Field Inspection

The location of the 4-lane bridge is at the southbound lane of I-75 over Dearborn Street in Detroit. The bridge had 106 spans. Some spans of the deck slabs were constructed with SIPMF. Deck slabs are supported by seven steel beams, which are laying on two abutments and 105 piers. The structure system of the piers was composed of a concrete girder and four columns. The top and bottom steel reinforcement bars used in the deck slab were not epoxy-coated steel. Five cores were taken at the northwestern shoulder of the southbound of I-75 over Dearborn. The cores were from the concrete deck slab with SIPMF. Coring locations for Bridge Deck Number 8 are presented in Figure 3.125. A map of cracks in the region of coring for Bridge Deck Number 8 is presented in Figure 3.126. Detailed photographs of bridge deck inspection are presented in Figures 3.127 through 3.130.

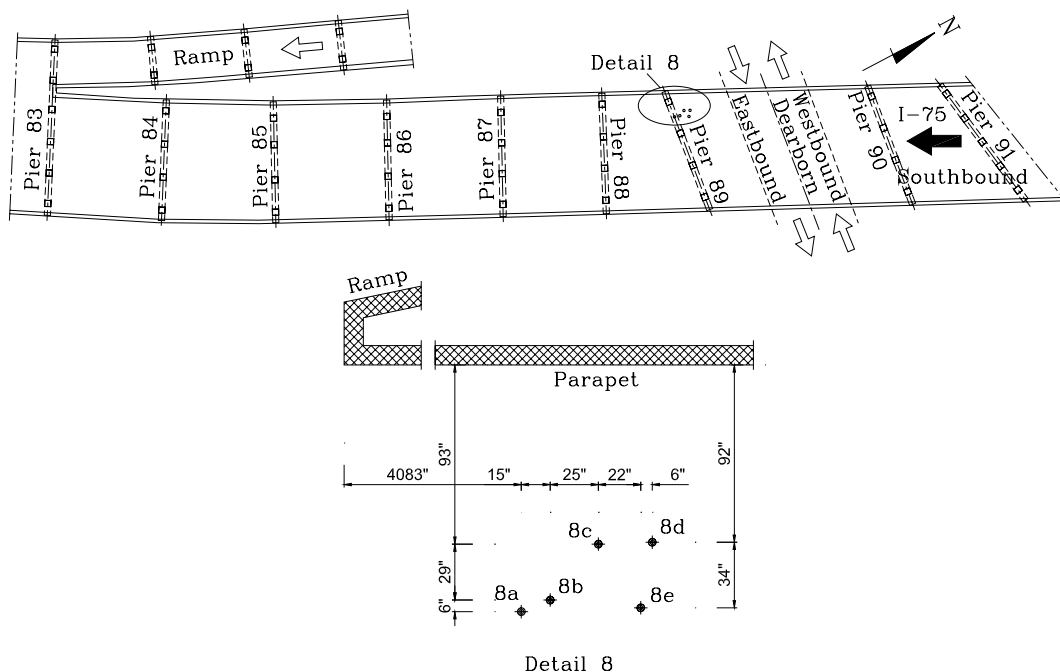


Figure 3.125. Coring locations for Bridge Deck Number 8
(Structure No. B01-82194)

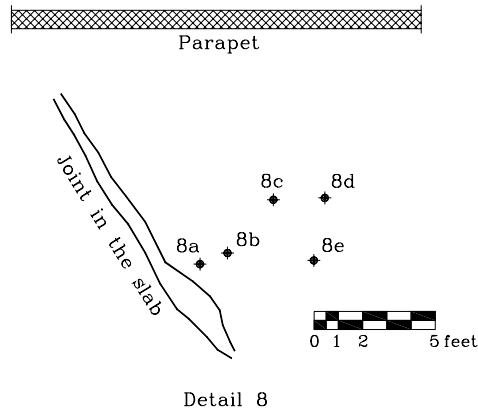


Figure 3.126. Map of cracks at coring locations for Bridge Deck Number 8 (Structure No. B01-82194)

Cracks were found at the top surface of the concrete slabs. Cracks were propagated transversely and longitudinally (Figure 3.127). Deterioration was encountered in the joints between deck slabs (Figure 3.128). Wide regions of corrosion were found at the bottom surface of the SIPMF concrete placed in the valley of the corrugation of the SIPMFs (Figure 3.129). Traces of steel rust existed in the connections between the SIPMF and the steel girders (Figure 3.130).



a. Longitudinal Crack



b. Diagonal and transverse cracks

Figure 3.127. Top cracks propagated on the top surface of the slab



Figure 3.128. Deterioration in the joint



a. Rust traces in SIPMF



b. General view of the rusted SIPMFs

Figure 3.129. Corrosion in the SIPMF



Figure 3.130. Rust in the connection between steel girders and SIPMFs

Inspection of Cores

The visual inspection of the cores from Bridge Number 8 indicated that the bridge had a wearing surface of average 1.5 in. thickness at the top surface as shown by the different size of aggregates used. This wearing surface had a higher porosity than the rest of the core, and conventional aggregates were used for the wearing surface. Slag was used as aggregates in the remaining part of the core. The coarse aggregate was well bonded to the concrete. No regions of high porosity were observed. Many entrapped air voids were encountered and had an average diameter of 0.2 in. Many regions of honeycombing existed in all of the cores. The top surface was grooved for all of the cores. The steel reinforcement was not coated with epoxy. Some of the exposed reinforcement bars had rust traces while others were in good condition. The SIPMFs for all of the cores were separated from the concrete without leaving concrete traces adhering to its inner face. The height of the cores varied indicating non-uniformity of the bridge deck thickness. The five cores that were taken are shown in Figure 3.131.



Figure 3.131. The 5 cores that were taken from Bridge Deck Number 8
(Structure No. S03-81041)

Core 8a (Figures 3.132-3.133)

- 12.5 in. height.
- The concrete in the region of the valley of the SIPMF was broken during coring.
- Three longitudinal cuts through steel reinforcement bar located 5.5 and 6.5 in. from the top were observed.
- Two regions of honeycombing of average diameter 0.6 in. were observed at 3.5 and 9.5 in. from the top surface.
- One bar had minor rust traces while the others did not.
- The reinforcement bars were epoxy coated.
- SIPMF was separated from the concrete.
- The connection between the concrete and the bracing angle had traces of rust.



Figure 3.132. Core 8a



Figure 3.133. Core 8a honeycombing and large single void in the concrete

Core 8b (Figure 3.134)

- 9.5 in. height (11.6 in. with the concrete in the region of the valley of the SIPMF).
- The concrete in the region of the valley of the SIPMF was broken during coring.
- Two longitudinal cuts in the reinforcement located 5.0 in. and 8.5 in. from top.
- One region of honeycombing of approximate width of 0.4 in. located 5.5 in. from top.
- Two large voids of average diameter 0.5 in. located 5.0 in. and 7.5 in. from top.
- The wearing surface had very high porosity and many voids of average diameter 0.3 in.
- SIPMF was separated.
- Steel reinforcement bars were in good condition.



a. Rust traces



b. Large region of voids

Figure 3.134. Core 8b with large region of voids and rust in the reinforcement bars

Core 8c (Figure 3.135)

- 9.0 in. height (10.5 in. with the concrete in the region of the valley of the SIPMF).
- The concrete in the region of the valley of the SIPMF was partially broken during the coring.
- Three longitudinal cuts in the reinforcement located 4.5, 6.5, and 8.3 in. from top.
- Large entrapped air voids of average diameter 0.3 in. located 5.0, 5.5, 5.8, and 6.0 in. from top were observed.
- SIPMF separated from the core.
- Slag was used as aggregates; and cement paste had high porosity.
- The wearing surface had higher porosity and more voids.
- Steel reinforcement bars were in good condition.



Figure 3.135. Core 8c

Core 8d (Figure 3.136)

- 9.0 in. height (11.0 in. with the concrete in the region of the valley of the SIPMF).
- One longitudinal cut of reinforcement bar located 3.5 in. from the top.
- Five axial sections of reinforcement bars located 4.0, 4.5, 6.5, 6.8 and 7.5 in. from top.
- SIPMF separated from the core and cut to two parts.
- Slag was used as aggregates; and cement paste had high porosity.
- Wearing surface had entrapped air voids of average diameter 0.5 in. located 2.3 and 5.8 from top.
- Steel reinforcement bars were in good condition.



a. High porosity



b. Entrapped air voids in the wearing surface

Figure 3.136. Core 8d with the high porosity of the concrete

Core 8e (Figure 3.137)

- 9.1 in. height (11.0 in. with the concrete in the region of the valley of the SIPMF).
- Concrete in the region of the valley of the SIPMF was partially broken during the coring.
- Slag was used as aggregates; and cement paste had high porosity.
- The wearing surface has higher porosity than remainder of the core.
- Three Large voids of average diameter 0.2 in. observed 5.0 and 7.0 in. from top.
- Six axial cuts in the steel reinforcement bars 4.5, 5, 8, and 8.5 in. from top.
- One of the axial cuts in the reinforcement bars had slight traces of rust while the others were in good condition.
- SIPMF was separated during the coring.



Figure 3.137. Core 8e with the broken concrete in the region of the valley of the SIPMF

The stress-strain curves for Cores 8d and 8e are presented in Figure 3.138. The curves for pulse velocity through the depth for Cores 8a and 8c are presented in Figure 3.139.

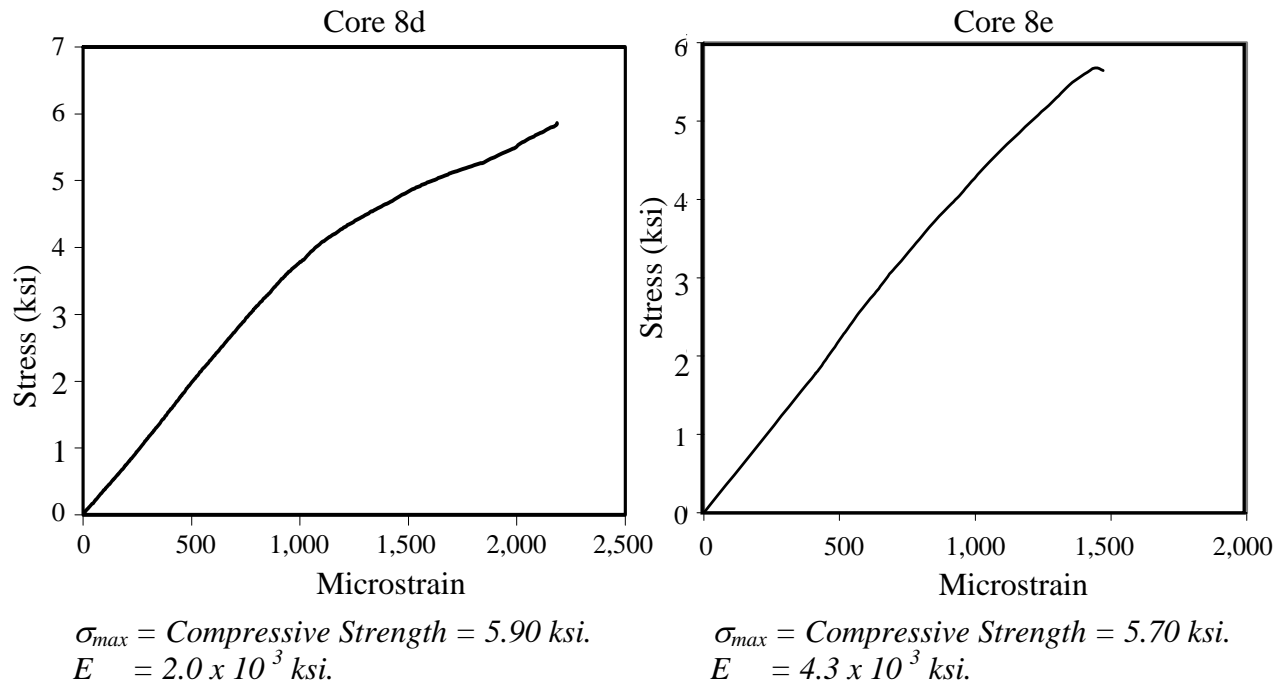


Figure 3.138. Compressive strength test results for Cores 8d and 8e (I-75, Bridge Deck Number 8, Structure No. B01-82194, SIPMF)

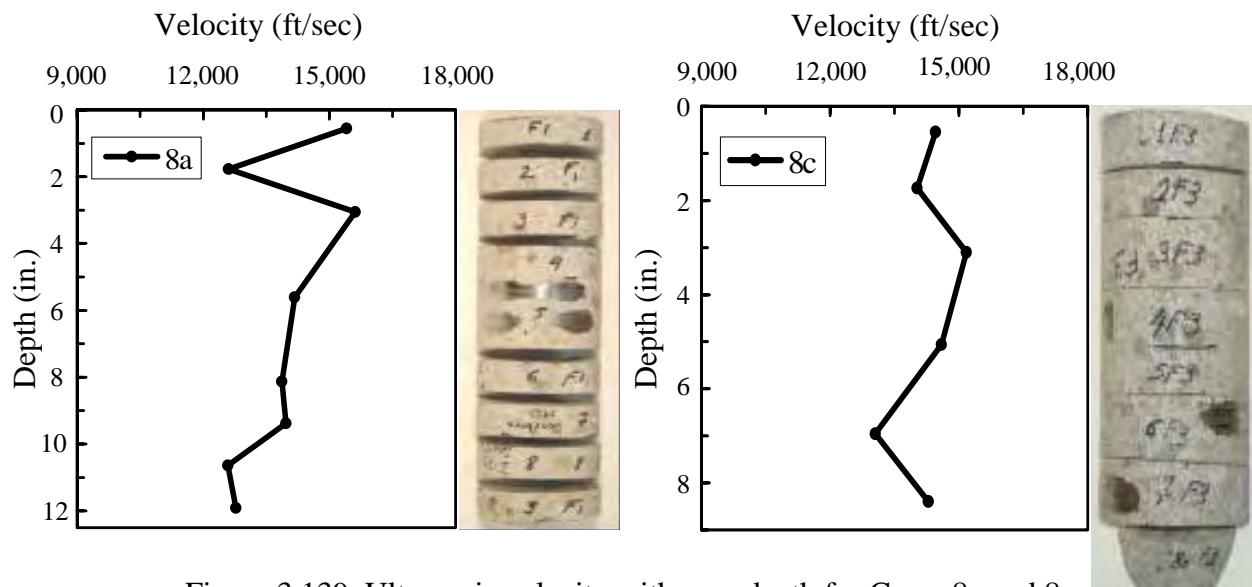


Figure 3.139. Ultrasonic velocity with core depth for Cores 8a and 8c (I-75, Bridge Deck Number 8, Structure No. B01-82194, SIPMF)

3.3.9 Bridge Deck Number 9: Structure No. S10-82022 (SIPMF)

Field Inspection

The location of the 3-lane bridge is at the intersection of the westbound lane of I-94 over Ecorse Road in Taylor. The bridge has 4 spans of 53'-6", 65'-0", 65'-0" and 53'-6" lengths. The structural system of the bridge consists of a concrete slab on metal deck and steel girders supported by three abutments and two piers. The top and bottom steel reinforcement bars used in the deck slab were not epoxy-coated steel. Five cores were taken from the northern shoulder of westbound lane I-94 over Ecorse Road near the parapet of the bridge. The detail of the coring locations on the bridge is shown in the schematic diagram of Figure 3.140. Coring locations for Bridge Deck Number 9 are presented in Figure 3.140. A map of cracks in the region of coring for Bridge Deck Number 9 is presented in Figure 3.141. Detailed photographs of bridge deck inspection are presented in Figures 3.142 through 3.145.

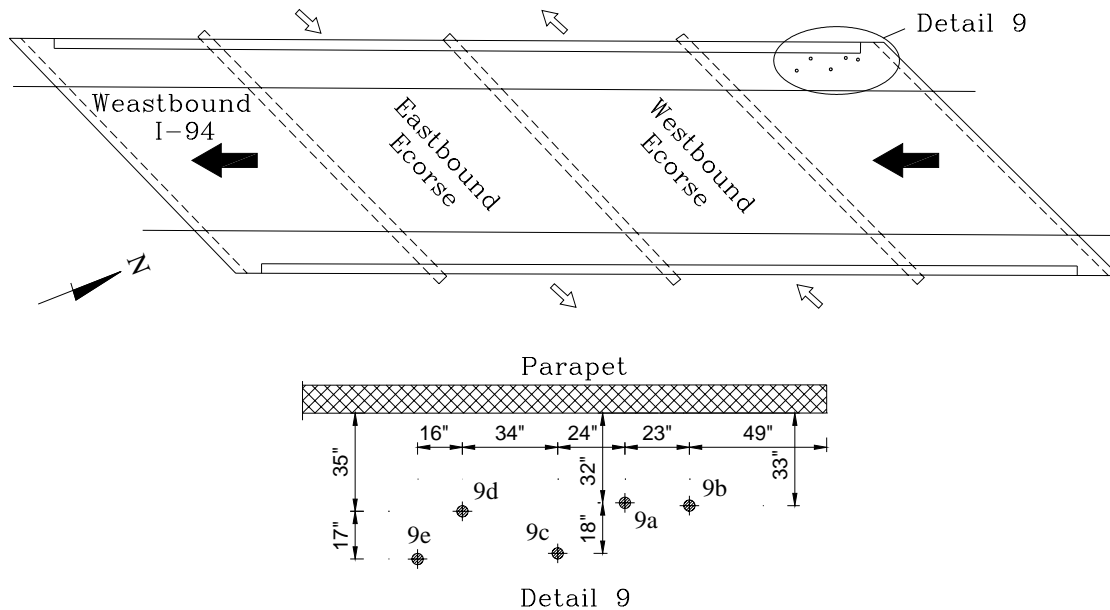


Figure 3.140. Coring locations for Bridge Deck Number 9
(Structure No. S10-82022)

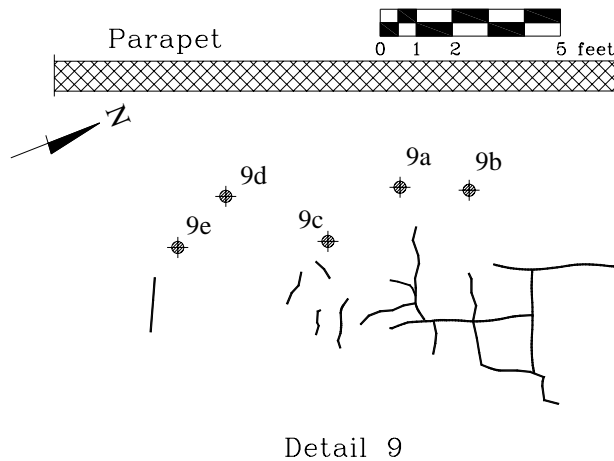


Figure 3.141. Map of cracks at coring locations for Bridge Deck Number 9
(Structure No. S10-82022)

The top and bottom surfaces of the deck slab were visually inspected. Propagated cracks were observed at the top surface of the concrete slab as shown in Figure 3.142. Corrosion in the steel forms was observed near the northeast abutment, at the connection between steel beams and the form and around the concrete in the region of the valley of the SIPMFs (Figure 3.143). In some specific regions corrosion was so excessive that the steel forms were completely damaged and the concrete was exposed as shown in Figure 3.144. White traces and rust traces were seen on the side of the edge beam as shown in Figure 3.145.



Figure 3.142. Cracks at the top surface



Figure 3.143. Traces of corrosion in SIPMF



Figure 3.144. Excessive corrosion in SIPMF



Figure 3.145. White traces and rust traces at Cracks

Inspection of Cores

The visual inspection of cores from Bridge Number 9 indicated that the bridge had a 2.0 in. thick wearing surface. The top surface of all of the cores taken had a grooved texture. The steel reinforcement was not coated with epoxy and had traces of rust at the interface between steel and concrete. The coarse aggregate was well bonded to the concrete. The wearing surface had higher porosity and there were many voids. All of the cores had approximately the same height of average 9.4 ± 0.2 in. which indicates bridge uniformity. The five cores that were taken are shown in Figure 3.146.



Figure 3.146. The 5 cores taken from Bridge Deck Number 9 (Structure No. S10-82022)

Core 9a (Figures 3.147-3.148)

- 9.7 in. height (11.3 in. with the concrete in the region of the valley of the SIPMF)
- Core fractured at the bottom steel reinforcement located approximately 7.5 in. from top.
- Axial section of a steel bar located 3.8 in. from top showed traces of rust.
- The SIPMF separated from the concrete.



Figure 3.147. Core 9a fractured at reinforcement location



Figure 3.148. Core 9a rust in the reinforcement bar

Core 9b (Figure 3.149)

- 9.3 in. height (11.3 in. with the concrete in the region of the valley of the SIPMF).
- Core broke at the bottom steel reinforcement located approximately 7.5 in. from top.
- Axial section of a steel bar located 3.8 in. from top showed traces of rust.
- The SIPMF separated from the concrete and consisted of two overlapping parts.
- The reinforcing steel had rust traces on its boundary.



a. Broken at reinforcement location



b. Rust in the reinforcing steel

Figure 3.149. Core 9b

Core 9c (Figures 3.150-3.151)

- 9.4 in. height
- Axial section of a steel bar located 3.8 in. from top showed traces of rust.

- The SIPMF separated from the concrete and was damaged during the coring.
- The reinforcing steel had rust traces on its boundary.
- Part of the concrete in the region of the valley of the SIPMF was damaged during the coring.
- Large entrapped air voids of average width 0.3 in. were observed on the surface of the core.



Figure 3.150. Core 9c



Figure 3.151. Core 9c Large voids and rust in the reinforcing steel

Core 9d (Figures 3.152-3.153)

- 9.4 in. height.
- The SIPMF separated from the concrete.
- SIPMF had rust traces on the surface that was in contact with the concrete.
- Part of the concrete in the region of the valley of the SIPMF was broken during the coring.
- Large voids of average diameter 0.3 in. were observed.



Figure 3.152. Core 9d



Figure 3.153. Core 9d rust traces on SIPMF and concrete

Core 9e (Figures 3.154 to 3.156)

- 9.5 in. height.
- The SIPMF separated from the concrete.
- SIPMF had rust traces on the surface that is in contact with the concrete specifically at the location of the voids on the concrete surface.
- Part of the concrete in the region of the valley of the SIPMF was broken during the coring.
- Hairline cracks were observed on the top (surface layer) of the core.



Figure 3.154. Core 9e



Figure 3.155. Core 9e rust traces on the SIPMF at the entrapped air voids



Figure 3.156. Core 9e hairline cracks at the top surface layer of the deck

The stress-strain curves for Cores 9d and 9e are presented in Figure 3.157, and the curves for pulse velocity through the depth for Cores 9a and 9b are presented in Figure 3.158. Due to fractures in the specimen, the velocity measurements were not obtained for all slices of cores No. 9a and 9b.

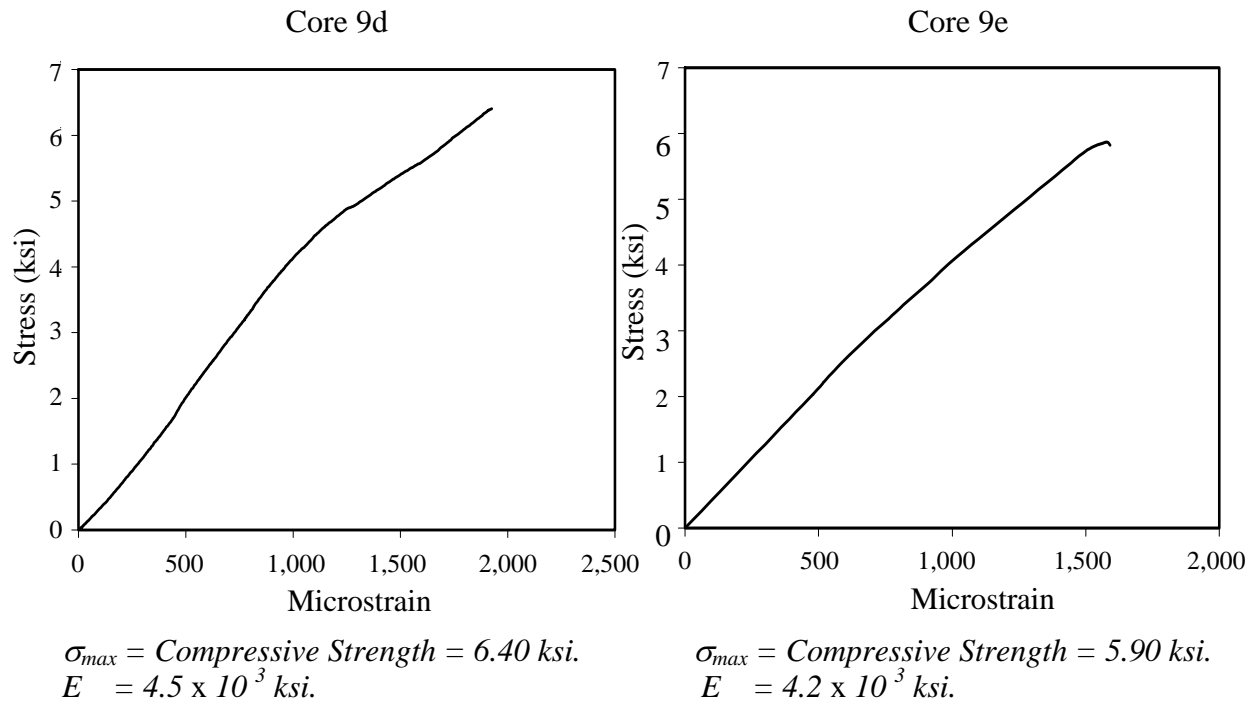


Figure 3.157. Compressive strength test results for Cores 9d and 9e
(I-94, Bridge Deck Number 9, Structure No. S10-82022, SIPMF)

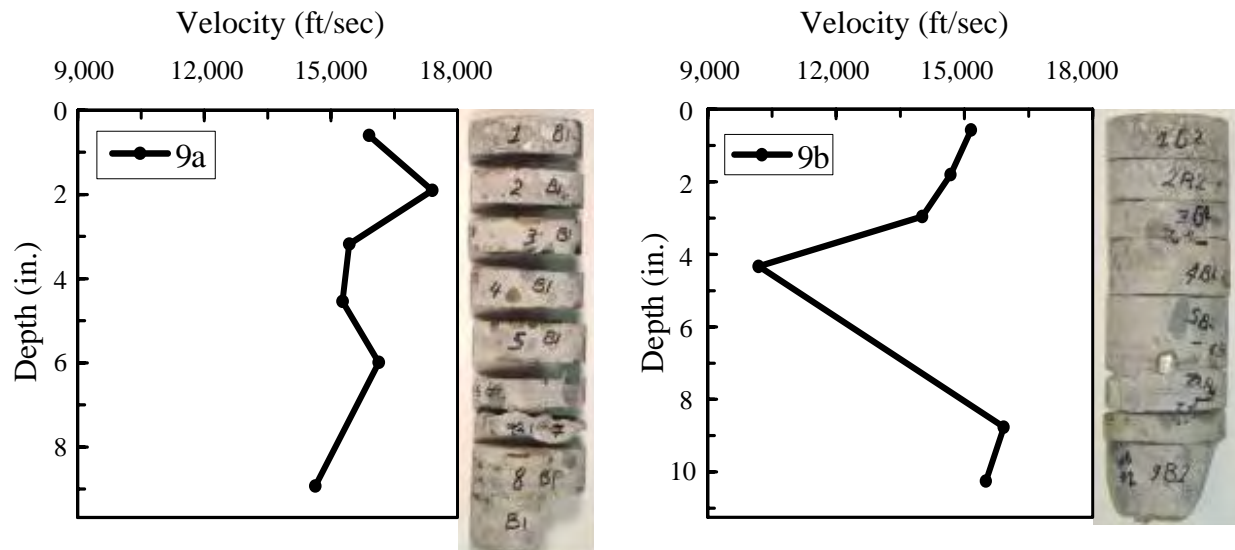


Figure 3.158. Ultrasonic velocity with core depth for Cores 9a and 9b
(I-94, Bridge Deck Number 9, Structure No. 82022-S10, SIPMF)

3.3.10 Bridge Deck Number 10: Structure No. R03-25132 (SIPMF)

Field Inspection

The location of the 3-lane bridge was at the northbound lane of 475 over Pierson Road and train tracks in Flint. The bridge had 4 spans at the northbound lane and 3 spans at the southbound lane. Spans of the deck slabs were composed of concrete slabs with SIPMF. Eight steel beams supported deck slabs of the northbound lanes and nine steel beams supported deck slabs of the southbound lanes. Steel beams were supported on two abutments, three piers for the northbound lanes and two piers for the southbound lanes. The structural system of the piers was composed of a concrete girder and columns. The top and bottom steel reinforcement bars used in the deck slab were coated with green epoxy. Five cores were taken at the northeastern shoulder of the northbound lanes of 475 over Pierson Road and train tracks. Coring locations for Bridge Deck Number 10 are presented in Figure 3.159. A map of cracks in the region of coring for Bridge Deck Number 10 is presented in Figure 3.160. Detailed photographs of bridge deck inspection are presented in Figures 3.161 through 3.170.

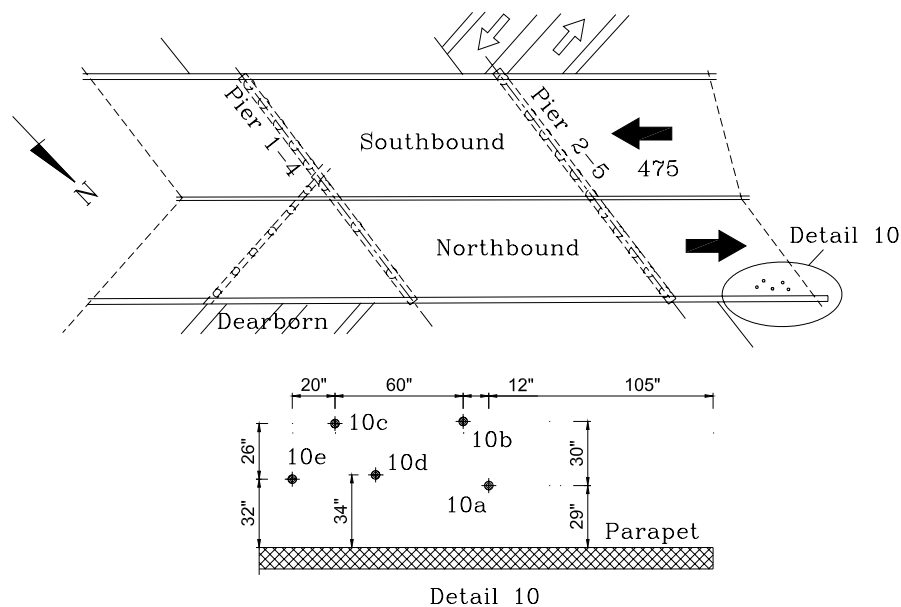


Figure 3.159. Coring locations for Bridge Deck Number 10
(Structure No. R03-25132)

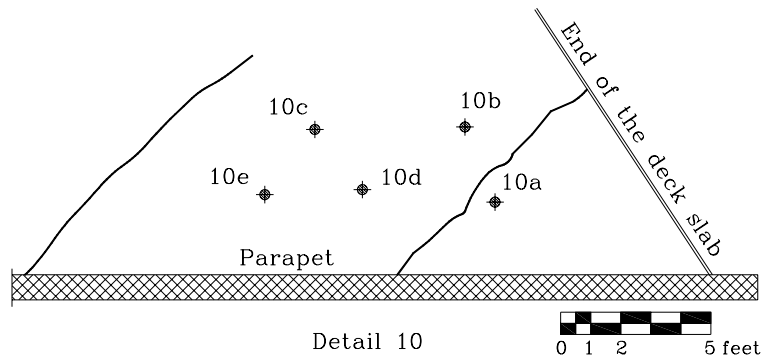


Figure 3.160. Map of cracks at coring locations for Bridge Deck Number 10 (Structure No. R03-25132)

Cracks were observed at the top surface of the concrete slabs. The propagation of cracks was transversely and diagonally across the entire bridge deck as shown in Figures 3.161 and 3.162. Some of the major cracks were found around the joints (Figure 3.163). In some locations the cracks in the parapet were at the same place as in the slab continuing through the entire depth of the deck slab (Figure 3.164). A different type of concrete was encountered at the sides of the joints in the parapet and the top surface as shown in Figure 3.165.

White and rust traces were encountered underneath the deck slab in the SIPMF. Major traces were observed at the overlap between SIPMFs and at the connection between the deck slab and the abutment. The holes where screws were fixing the SIPMF had some of white and rust traces. In some locations, the connection between the steel beams and the SIPMF had white traces (Figure 3.166). The bottom surface of the cantilever parts of the deck slabs had white and rust traces as shown in Figure 3.167.

Vertical traces of corrosion were observed on the webs of the steel beams (Figure 3.168). Corrosion and white traces were found at the connection between steel beams and the SIPMF (Figure 3.169). In some locations, major traces of corrosion were found at the connection between the SIPMF and the abutment walls, as shown in Figure 3.170.



Figure 3.161. Top cracks propagated transversely in the slab

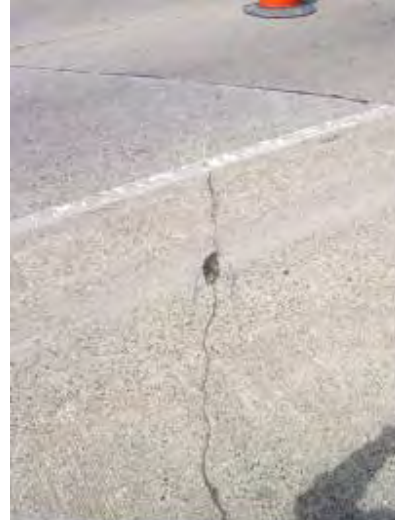


Figure 3.162. Top cracks propagated diagonally in the slab



Figure 3.163. Top cracks propagated around the joint



Figure 3.164. Cracks with white traces propagated in the parapet and the whole depth of the slab



Figure 3.165. Different types of concrete around the joints



a. White traces



b. White and rust traces

Figure 3.166. Corrosion and white traces in the SIPMF



Figure 3.167. Corrosion and white traces on the bottom face of the cantilever slabs



Figure 3.168. Corrosion traces underneath the steel beams



Figure 3.169. White and corrosion traces at the connection between steel beams and the SIPMF



Figure 3.170. White and corrosion traces at the connection between SIPMF and the abutment

Inspection of Cores

The visual inspection of the cores indicated that the bridge had a wearing surface of average 1.5 in. thickness at the top surface as shown by the different size of aggregates used. This wearing surface had a higher porosity than the rest of the core. The top surface was grooved for all of the cores. The steel reinforcement was coated with green epoxy. Some of the exposed reinforcement bars had rust traces while others were in good condition. The coarse aggregate was well bonded to the concrete. No regions of high porosity were observed. Many entrapped air voids were encountered that had an average diameter of 0.2 in. Many regions of honeycombing existed in all of the cores. The SIPMFs for all of the cores are separated from the concrete without leaving concrete traces adhering to its inner face. Cores had approximately the same height of average 9.5 ± 0.2 in. which indicates bridge deck thickness uniformity. The five cores that were taken are shown in Figure 3.171.



Figure 3.171. The 5 cores that were taken from Bridge Deck Number 10 (Structure No. R03-25132)

Core 10a (Figures 3.172-3.175)

- 9.7 in. height (12.0 with the concrete in the region of the valley of the SIPMF).
- The concrete in the region of the valley of the SIPMF was partially broken during coring.
- Six axial sections in the steel reinforcement bar located 4.0, 7.3, and 8.0 in. from top.
- One region of honeycombing of 0.4 in. diameter located 8.3 in. from the top surface.
- Many small voids of average diameter of 0.2 in. were observed.
- One reinforcement bar had minor rust traces while the other did not.
- SIPMF was separated from the core.
- Large horizontal crack was observed at 8.0 in. from top.



Figure 3.172. Core 10a



Figure 3.173. Core 10a concrete placed in the valley of the corrugation of the SIPMF partially broken



Figure 3.174. Core 10a horizontal crack.



Figure 3.175. Core 10a small voids in the concrete

Core 10b (Figure 3.176)

- 9.5 in. height (12.0 in. with the concrete in the region of the valley of the SIPMF).
- The core was broken during coring at reinforcement location (4.0 in. from top).
- One longitudinal cut in the reinforcement located 7.3 in. from top.
- Four axial sections in the reinforcement located 4.0 and 8.0 in. from top.
- SIPMF was separated from the core.
- Steel reinforcement bars had traces of corrosion.
- The concrete in the region of the valley of the SIPMF was partially broken.
- Small voids of 0.1 in. were observed throughout the entire core.



a. Broken Core



b. The concrete in the region of the valley of the SIPMF was partially broken

Figure 3.176. Core 10b with the concrete in the region of the valley of the SIPMF partially broken

Core 10c (Figure 3.177)

- 9.5 in. height (11.0 in. with the concrete in the region of the valley of the SIPMF).
- Many small voids existed of average dimensions 0.2 in.
- SIPMF separated from the core.
- No steel reinforcement bars existed.



Figure 3.177. Core 10c

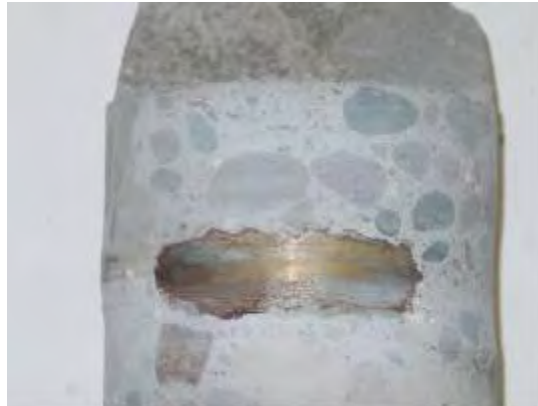
Core 10d (Figure 3.178)

- 9.5 in. height (12.0 in. with the concrete in the region of the valley of the SIPMF).

- Two longitudinal cuts of reinforcement bars: one was located 4.3 in. from the top and separated from the core and the other one was located 7.8 in. from top.
- Two axial sections of reinforcement bars located 4.8 in. from top.
- SIPMF separated from the core.
- Many small voids of average diameter of 0.1 in. were propagated at the entire surface.
- Steel reinforcement bars had traces of corrosion.
- Core was broken at 4.5 in. from top at the reinforcement location.
- One large region of honeycombing of 0.5 in. diameter located 3.5 in. from top.
- The concrete in the region of the valley of the SIPMF was broken during coring.



a. Core was broken



b. Reinforcement bar had traces of corrosion

Figure 3.178. Core 10d with corrosion in the reinforcement

Core 10e (Figure 3.179)

- 9.3 in. height (11.5 in. with the concrete in the region of the valley of the SIPMF).
- High porosity in the aggregate and cement paste.
- Many voids of 0.2 in. were observed.
- One region of honeycombing of 0.3 in. diameter was observed 8.6 in. from top.
- SIPMF was separated during the coring.
- One longitudinal cut of reinforcement bar located 4.5 in. from top.
- Traces of corrosion on the exposed reinforcing steel.



a. High porosity



b. Region of honeycombing

Figure 3.179. Core 10e with honeycombing

The stress-strain curves for Cores 10c and 10e are presented in Figure 3.180, and the curves for pulse velocity through the depth for Cores 10a and 10d are presented in Figure 3.181. Due to fractures in the specimen, the velocity measurements were not obtained for all slices of Cores 10a and 10d.

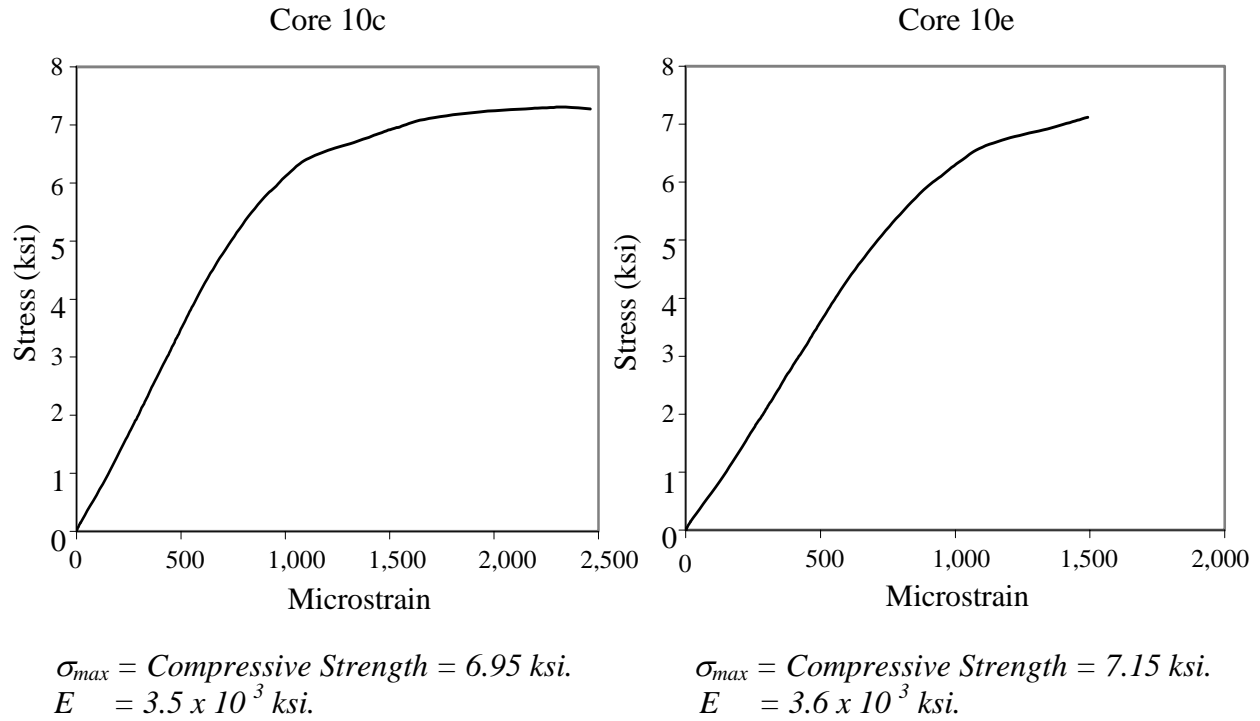


Figure 3.180. Compressive strength test results for Cores 10c and 10e
(I-475, Bridge Deck Number 10, Structure No. R03-25132, SIPMF)

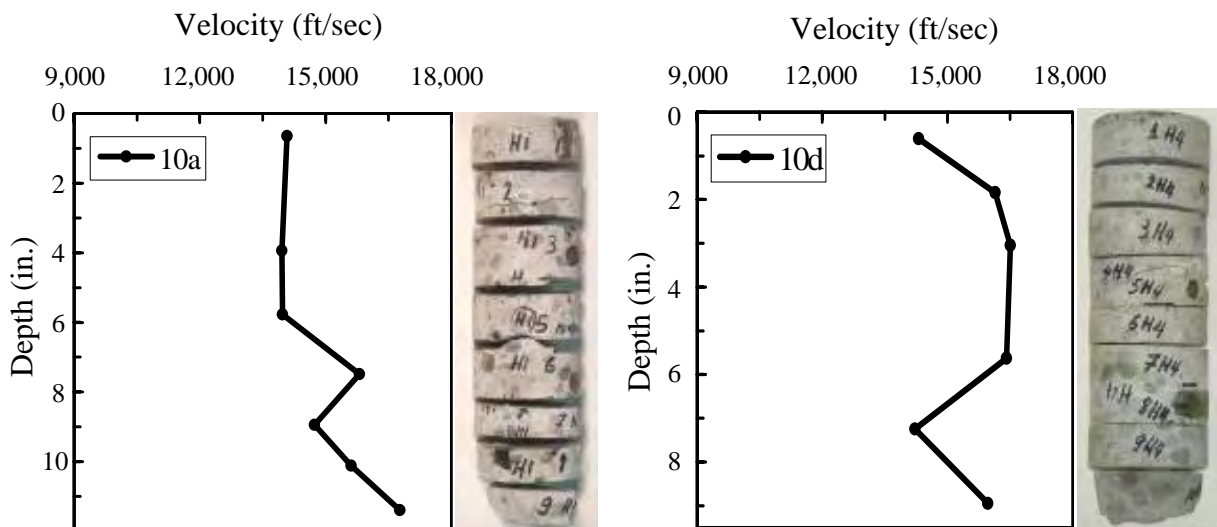


Figure 3.181. Ultrasonic velocity with core depth for Cores 10a and 10d
(I-475, Structure No. R03-25132, SIPMF)

3.4 SUMMARY OF BRIDGE DECK INSPECTION AND CORING

The test program included investigation of seven concrete bridges located in Michigan. Two of the bridges were constructed without using SIPMF and two of the bridges were constructed using entirely SIPMFs. The remaining three bridges had sections constructed without SIPMFs and sections constructed with SIPMFs. The test program was designed such that of a total of ten concrete bridge decks, five decks constructed without SIPMFs (Bridge Deck Number 1 through 5) and five decks constructed with SIPMFs (Bridge Deck Number 6 through 10), were analyzed and compared. Structural configuration and traffic loading information for the inspected bridges are presented in Table 3.1.

Comparisons were made using visual inspection, compressive strength tests, and ultrasonic pulse velocity tests. Inspection indices were developed to quantify visual inspection test results (both for bridge decks and cores). Statistical analysis was used to compare all of the test results obtained for decks constructed without SIPMF and with SIPMF.

3.4.1 Field Inspection

Varying degrees of deterioration were observed in the bridge decks. Overall, the wearing surfaces of the decks were generally in acceptable to good condition. Deterioration was observed in the form of cracking on the wearing surface, cracking on the bottom surface of the bridge decks, staining from apparent migration of salt or other deicing agents, and rusting of bridge deck supports. For the bridges with SIPMF, some deterioration of the SIPMFs was observed, usually in the form of rusting. Rusting was most commonly observed in areas surrounding the drainage structures of the bridge decks. In some cases, a direct correlation between the geometry of the top surface cracks on the bridge decks and bottom surface corrosion patterns in the SIPMFs directly beneath the concrete cracks was observed.

Cracks on the wearing surface for each bridge deck were mapped in the region of coring. Crack density was calculated as length of cracks (in.) per unit area of deck (square feet). Crack densities were computed for transverse cracks and total cracks as shown in Table 3.3.

Table 3.3. Summary of crack density for bridge decks

Formwork	Bridge Deck Number	MDOT Structure (Year of construction)	Area (ft ²)	Transverse Cracks (in.)	Transverse Crack Density (in. / ft ²)	Total Cracks (in.)	Total Crack Density (in. / ft ²)
No SIPMF	1	R01-13012 (1981)	147.1	312.8	2.1	513.9	3.5
	2	S03-81041 (1975)	185.4	536.0	2.9	605.8	3.3
	3	B01-82194 (1966)	137.3	0.0	0.0	53.5	0.4
	4	S11-82022 (1962)	208.7	180.1	0.9	180.1	0.9
	5	S09-82022 (1962)	67.1	40.0	0.6	40.0	0.6
SIPMF	6	R01-13012 (1981)	148.0	342.0	2.3	342.0	2.3
	7	S03-81041 (1975)	103.2	0.0	0.0	22.9	0.2
	8	B01-82194 (1966)	251.7	344.6	1.4	344.6	1.4
	9	S10-82022 (1962)	167.0	198.1	1.2	324.3	1.9
	10	R03-25132 (1976)	152.1	235.4	1.6	235.4	1.6

The transverse crack density observed ranged from 0 to 2.9 in./ft². The average transverse crack density observed for both with SIPMF and without SIPMF decks was 1.3 in./ft². The total crack density observed ranged from 0.2 to 3.5 in./ft². The average total crack density observed for decks without SIPMF was 1.7 in./ft² and for decks with SIPMF was 1.5 in./ft². Even though the observed transverse crack densities were essentially identical for the two bridge deck systems, approximately 16% more total cracks were observed in decks without SIPMF than decks with SIPMF. A summary of crack densities is presented in Table 3.4.

Table 3.4. Crack density comparison between No SIPMF and SIPMF deck slabs

Formwork	Bridge Deck Number	Transverse Crack Density (in. / ft ²)	Total Crack Density (in. / ft ²)
No SIPMF	1	2.13	3.49
	2	2.89	3.27
	3	0.00	0.39
	4	0.86	0.86
	5	0.60	0.60
	Average =	1.30	1.72
SIPMF	6	2.31	2.31
	7	0.00	0.22
	8	1.37	1.37
	9	1.19	1.94
	10	1.55	1.55
	Average =	1.28	1.48

A field inspection index (*FII*) was developed that was used to rate the condition of the bridge decks based on visual inspection. The parameter was determined using visual inspection and rating of various characteristics of the bridge decks including crack density (transverse, longitudinal, and total cracks), SIPMF condition, presence of full-depth cracks, spalling, salt traces, rust traces, condition of joints, condition of drainage openings, condition of girders, and condition of curbs. A numerical value is specified to indicate the condition of the various bridge characteristics. The value of *FII* is calculated by dividing the summation of the numerical values for all of the characteristics by the summation of the maximum potential numerical values, and converting to a percentage (by multiplying by 100). This parameter has a potential range of 0 to 100 (poor to excellent) that represents the overall quality of a bridge deck. *FII* ranged from 39 to 90 for bridge decks without SIPMF (Table 3.5). The average *FII* for decks without SIPMF was 60. *FII* ranged from 46 to 66 for bridge decks with SIPMF (Table 3.6). The average for bridge decks with SIPMF was 59.

Overall, deterioration was observed in both types of bridge decks (with and without SIPMF) and conclusive correlations between bridge deck type and level and mechanism of deterioration were not evident. The condition of the bridge decks constructed with and without SIPMFs was essentially similar based on visual inspection using crack densities and *FII*.

Table 3.5. Field Inspection Index (*FII*) for No SIPMF deck slabs

No SIPMF																			
Bridge Deck Number	MDOT Structure	Year of Construction	Facility Carried	Cracks							Spalling of concrete	Salt Traces	Rust Traces for reinforcement	Joint Deterioration	Drainage Openings	Girder Condition	Curb Condition	Σ	FII FII = (Σ / 210) * 100
				Top Cracks			Bottom Cracks			Full Depth Crack									
				Transverse	Longitudinal	Diagonal	Transverse	Longitudinal	Diagonal										
				10	10	10	10	10	10										
1	R01-13012	1981	NB S.Washington Ave	3	3	3	3	3	3	3	20	3	15	10	10	17	5	101	48
2	S03-81041	1975	NB Rawsonville Rd.	3	9	3	3	9	3	3	10	5	5	10	20	13	3	99	47
3	B01-82194	1966	SB I-75	3	5	4	3	5	4	3	15	5	5	5	5	10	10	82	39
4	S11-82022	1962	WB I-94	7	9	7	7	9	7	17	20	17	20	18	20	20	10	188	90
5	S09-82022	1962	EB I-94	3	9	9	3	9	9	5	20	5	15	20	20	20	10	157	75
Average				3.8	7.0	5.2	3.8	7.0	5.2	6.2	17.0	7.0	12.0	12.6	15.0	16.0	7.6	125.4	60

Table 3.6. Field Inspection Index (*FII*) for SIPMF deck slabs

SIPMF																	
Bridge Deck Number	MDOT Structure No.	Year of Construction	Facility Carried	Top Cracks			SIPMF Status	Full Depth Crack	Spalling of concrete	Salt Traces	Rust Traces for reinforcement	Joint Deterioration	Drainage Openings	Girder Condition	Curb Condition	Σ	<i>FII</i> $FII = (\Sigma / 210) * 100$
				Transverse	Longitudinal	Diagonal											
				10	10	10											
6	R01-13012	1981	NB S.Washington Ave.	3	3	3	7	3	20	5	20	10	3	15	5	97	46
7	S03-81041	1975	NB Rawsonville Rd.	5	8	6	20	10	7	10	17	10	20	18	3	134	64
8	B01-82194	1966	SB I-75	3	5	4	10	5	15	5	20	0	20	15	10	112	53
9	S10-82022	1962	WB I-94	4	4	3	10	10	10	10	20	17	20	17	10	135	64
10	R03-25132	1976	NB I-475	5	7	5	20	15	15	10	17	10	20	10	5	139	66
Average				4.0	5.4	4.2	13.4	8.6	13.4	8.0	18.8	9.4	16.6	15.0	6.6	123.4	59

3.4.2 Inspection of Cores

Visual Inspection

Visual inspection of the cores was used to determine general physical characteristics and overall condition of the cores that were obtained for the test program. A visual inspection index (*VII*) was developed to quantify the condition of cores based on visual inspection. The parameter was determined using visual inspection and rating of various characteristics of the reinforcing steel (when present in a core), concrete, and SIPMF. The characteristics analyzed for reinforcing steel were presence and condition of epoxy coating, and extent of rust. The characteristics analyzed for concrete were quantity, size, and alignment of cracking; quantity and size of voids; quantity and size of honeycombing; and porosity of aggregate and cement paste. The characteristics analyzed for SIPMF were the extent of rust. A numerical value is specified to indicate the condition of the various characteristics. The value of *VII* is calculated by dividing the summation of the numerical values for all of the characteristics by the summation of the maximum potential numerical values, and converting to a percentage (by multiplying by 100). This parameter has a potential range of 0 to 100 (poor to excellent) that represents the overall quality of a core. *VII* ranged from 52 to 88 for bridge decks without SIPMF. The average *VII* for decks without SIPMF was 68. *VII* ranged from 64 to 78 for bridge decks with SIPMF. The average *VII* for bridge decks with SIPMF was 69.

The observations from the visual inspection of the sliced core with depth for each bridge deck were similar to the visual inspection observations of the five intact cores for that particular deck. Overall, based on visual inspection of the cores, a correlation between bridge deck type and condition of the cores was not evident. The condition of the bridge decks constructed with and without SIPMFs was essentially similar based on visual inspection using *VII*.

Table 3.7. Visual Inspection Index (VII) for cores from No SIPMF deck slabs

No SIPMF																
Bridge Deck Number	MDOT Structure	Year of Construction	Facility Carried	Core	Steel	Concrete								Σ	VII VII = (Σ / 27) * 100	Average VII
					Condition of Rust	Porosity		Honeycombing		Cracks		Voids				
						Concrete	Aggregate	Quantity	Size	Quantity	Size	Quantity	Size			
					3	3	3	3	3	3	3	3	3	27		
1	R01-13012	1981	NB S.Washington Ave.	1a	2	2	2	2	1.5	3	3	1	2	18.5	69	52
				1b	0	2	2	2	2	2	0	1	1.5	12.5	46	
				1c	0	2	2	1	1	0	0	1	1	8.0	30	
				1d	2	2	2	2	2	3	3	1.5	2	19.5	72	
				1e	0	2	2	2	2	0	0	2	2	12.0	42	
2	S03-81041	1975	NB Rawsonville Rd.	2a	1	1	1	3	3	3	3	1	2	18.0	67	54
				2b	1	1	1	1	1	1	1.5	3	3	13.5	50	
				2c	1	1	1	1.5	1.5	2	0	3	3	14.0	52	
				2d	0	0	0	3	3	0	0	2	2	10.0	37	
				2e	1	1	1	3	3	3	3	1	1	17.0	63	
3	B01-82194	1966	SB I-75	3a	1.5	2	2	1	1.5	3	3	2	1	17.0	63	70
				3b	1.5	2	2	3	3	3	3	1	2	20.5	76	
				3c	2	2	2	2	1.5	3	3	1.5	1.5	18.5	69	
				3d	2	2	2	1	1.5	3	3	1	1.5	17.0	63	
				3e	2	2	2	1.5	2	3	3	3	3	21.5	80	
4	S11-82022	1962	WB I-94	4a	3	3	3	3	3	2	1	3	3	24.0	89	88
				4b	3	3	3	3	3	3	3	2	2	25.0	93	
				4c	3	3	3	3	3	2	1	2	2	22.0	81	
				4d	3	3	3	3	3	3	3	3	3	27.0	100	
				4e	3	1.5	2.5	3	3	2	1.5	2	2.5	21.0	78	
5	S09-82022	1962	EB I-94	5a	2.5	2.5	2.5	3	3	3	3	2	1	22.5	83	74
				5b	2	2.5	2.5	3	3	3	3	2	1	22.0	81	
				5c	2	2	2	2	2	1	1.5	1	1.5	15.0	56	
				5d	2	2	2	3	3	3	3	1.5	2	21.5	80	
				5e	2	1	2	3	3	3	3	1	1.5	19.5	72	

Table 3.8. Visual Inspection Index (VII) for cores from SIPMF deck slabs

SIPMF																	
Bridge Deck Number	MDOT Structure	Year of Construction	Facility Carried	Core	Steel	Concrete								SIPMF	Σ	VII VII = (Σ / 30) * 100	Average VII
					Condition of Rust	Porosity		Honeycombing		Cracks		Voids					
						Concrete	Aggregate	Quantity	Size	Quantity	Size	Quantity	Size	Condition of Rust			
						3	3	3	3	3	3	3	3				
6	R01-13012	1981	NB S.Washington Ave.	6a	2.5	1.5	1.5	1.5	2	2	1	3	3	3	21.0	70	65
				6b	2.5	1.5	1.5	1.5	1.5	3	3	1.5	2	3	21.0	70	
				6c	2.5	1.5	1.5	1.5	1.5	2	2	2	2	3	19.5	65	
				6d	1.5	1.5	1.5	1.5	1.5	1	1	3	3	1	16.5	55	
				6e	1.5	2	2	2	2	2	2	2	2	2.5	20.0	67	
7	S03-81041	1975	NB Rawsonville Rd.	7a	1	1	1	3	3	3	3	3	3	3	24.0	80	67
				7b	1	1	1	3	3	3	3	1	1	3	20.0	67	
				7c	1	1	1	3	3	3	3	0	1	3	19.0	63	
				7d	1	1	1	2	1	3	3	1	0	3	16.0	53	
				7e	1	1	1	3	3	3	3	2	1	3	21.0	70	
8	B01-82194	1966	SB I-75	8a	2.5	2	2	2	1	2	2	2	2	3	20.5	68	64
				8b	2	2	2	2	1	2	2	1	1	3	18.0	60	
				8c	3	1	1	3	3	2	2	0	1	3	19.0	63	
				8d	3	1	1	3	3	3	3	1	0	3	21.0	70	
				8e	2	1	1	1	2	2	2	1	2	3	17.0	57	
9	S10-82022	1962	WB I-94	9a	2	2	3	3	3	2	1	3	3	3	25.0	83	78
				9b	2	2	3	3	3	1	1	3	3	3	24.0	80	
				9c	2	2	3	3	3	3	3	0	0	3	22.0	73	
				9d	2	2	3	3	3	3	3	2	0	2	23.0	77	
				9e	2	2	3	3	3	0	2	3	3	2	23.0	77	
10	R03-25132	1976	NB I-475	10a	2.5	2.5	2.5	2	2	1.5	1.5	1	2	3	20.5	68	72
				10b	2.5	2.5	2.5	3	3	1	1	1	1	3	20.5	57	
				10c	3	2.5	2.5	3	3	3	3	1	2	3	26.0	87	
				10d	2.5	2.5	2.5	2	1.5	2	1	1	2	3	20.0	67	
				10e	2.5	1.5	1.5	2	1.5	3	3	1	2	3	21.0	70	

Compressive Strength Testing

Compression strength tests were conducted on two cores from each bridge deck. The summary of compressive strength test results is presented in Table 3.9. Compressive strength of the concrete cores ranged from 5.40 to 8.90 ksi for bridge decks without SIPMF. The average compressive strength of concrete from decks without SIPMF was 6.98 ksi. Compressive strength of concrete cores ranged from 5.70 to 8.10 ksi for bridge decks with SIPMF. The average compressive strength of concrete cores from bridge decks with SIPMF was 6.65 ksi. The compressive strengths for the bridge decks were compared statistically to determine equivalency between the bridge deck systems. A student's t-test was conducted to compare the compressive strengths for decks constructed with and without SIPMFs based on the values provided in Table 3.9. The data were compared using a two-tailed analysis with a 95% confidence interval. The t_{critical} value for this dataset was equal to 2.16 and the t-statistic was calculated to be 0.72. The compressive strengths of the two types of bridge decks were deemed statistically similar, as the t-statistic was less than t_{critical} . Further analysis was conducted using direct comparison decks. The variation in compressive strength between the paired direct comparison data sets (Bridge Deck Number 1 and 6; 2 and 7; and 3 and 8) was calculated by dividing the difference between the average compressive strength of the decks with SIPMF and decks without SIPMF with the compressive strength of the decks without SIPMF. The variation was determined to be in the range of -6% to +3%. The low variation in compressive strength between the paired deck systems also indicates the similarity of the two bridge deck systems.

The modulus of elasticity (Young's modulus) of the concrete cores ranged from 30,000 to 69,000 ksi for bridge decks without SIPMF. The average modulus of elasticity of concrete for bridge decks without SIPMF was 48,000 ksi. The modulus of elasticity of the concrete cores ranged from 20,000 to 64,000 ksi for bridge decks with SIPMF. The average modulus of elasticity of concrete for bridge decks with SIPMF was 40,900 ksi. The average modulus of elasticity of the concrete cores from bridge decks without SIPMF was higher than from bridge decks with SIPMF by 17.6 %.

Table 3.9. Summary of compressive strength test results

Formwork	Bridge Deck Number	MDOT Structure (Year of Construction)	Facility Carried	Core	Compressive Strength (ksi)	Average Compressive Strength (ksi)	Young's Modulus (ksi)	Average Young's Modulus (ksi)
No SIPMF	1	R01-13012 (1981)	NB S.Washington Ave.	1a	8.10	7.75	5,800	5,000
				1d	7.40		4,200	
	2	S03-81041 (1975)	NB Rawsonville Rd.	2b	5.40	6.70	3,000	4,950
				2e	7.95		6,900	
	3	B01-82194 (1966)	SB I-75	3b	6.85	6.15	3,200	3,200
				3c	5.45		3,200	
	4	S11-82022 (1962)	WB I-94	4b	8.90	7.80	6,100	6,400
				4d	6.65		6,700	
	5	S09-82022 (1962)	EB I-94	5a	--	6.10	--	4,200
				5d	6.10		4,200	
SIPMF	6	R01-13012 (1981)	NB S.Washington Ave.	6c	6.65	7.40	6,400	5,850
				6e	8.10		5,300	
	7	S03-81041 (1975)	NB Rawsonville Rd	7b	7.00	6.85	3,600	3,550
				7d	6.70		3,500	
	8	B01-82194 (1966)	SB I-75	8d	5.90	5.80	2,000	3,150
				8e	5.70		4,300	
	9	S10-82022 (1962)	WB I-94	9d	6.40	6.15	4,500	4,350
				9e	5.90		4,200	
	10	R03-25132 (1976)	NB I-475	10c	6.95	7.05	3,500	3,550
				10e	7.15		3,600	

(--) indicates no data available

Ultrasonic Testing

Ultrasonic velocity was measured on individual slices of each core. The ultrasonic measurements for each core are presented at the end of each coring location section. All of the ultrasonic data (velocity vs. depth) obtained in the test program is presented in Figures 3.182 through 3.184. Numbers are used to indicate bridge deck number and letters are used to indicate core number for a given bridge in the legends of Figures 3.182 through 3.184. Average linear trends are shown on Figure 3.184. Average velocities for cores were calculated as weighted averages obtained by taking into consideration the thickness and corresponding pulse velocity of each slice from a core. This approach was used as the thicknesses of specimens obtained for a core were variable.

To better quantify the results of this analysis, a parameter termed Quality Index (*QI*) was introduced. The profile of wave velocity with depth can be quantified by taking the product of incremental wave velocity (for a given slice) and length of that particular slice. This is effectively represented as area contained by the velocity vs. length (along a core) plot. This area, considered alone, would bias results of longer cores. Therefore, a normalization of the quantity was achieved by dividing this summed area by total length of the core. The normalized value, *QI*, had units consistent with velocity (ft/s) and represented a weighted average of the wave velocity with depth over the entire profile (Figure 3.185). This parameter provided an effective means for comparison of the integrity of concrete between different cores. The results of this analysis are presented in Tables 3.10-3.14. The *QI* representing all bridge deck cores with SIPMF (calculated for the total length of all analyzed cores from bridge decks with SIPMF) was 14,563 ft/s (Table 3.17). The *QI* representing all bridge deck cores without SIPMF (calculated for the total length of all analyzed cores from bridge decks without SIPMF) was 14,290 ft/s (Table 3.15). Even though the *QI* for bridge decks with SIPMF was greater than *QI* for bridge decks without SIPMF, the difference in *QI* between the two bridge deck systems was considered negligible (1.91%). Results from the through-transmission ultrasonic measurements demonstrated the similarity of the integrity of the concrete in the two bridge deck systems.

The average *QI* for all of the cores tested in the study was 14,440 ft/s. The average *QI* for cores obtained from bridge decks without SIPMF was 14,315 ft/s and the average *QI* for

cores obtained from bridge decks with SIPMF was 14,565 ft/s. The average QI for the bridge decks were compared statistically to determine equivalency between the decks. A student's t-test was conducted to compare the average QI for decks constructed with and without SIPMFs based on the values provided in Tables 3.15 and 3.17. The data were compared using a two-tailed analysis with a 95% confidence interval. The $t_{critical}$ value for this dataset was equal to 2.23 and the t-statistic was calculated to be 0.744. The average QI for cores obtained from the two types of bridge decks were deemed statistically similar, as the t-statistic was less than $t_{critical}$.

The variation of pulse velocity with depth was investigated by dividing the cores into three equal regions with depth: top, middle, and bottom. The results of this analysis are presented in Tables 3.10 through 3.14, 3.16 and 3.18 for each bridge deck. Average QI is presented for each region of the cores. In addition, ratios of region-specific QI to average QI for a given bridge deck are provided. It was observed that average QI and region-specific QI were similar for cores from both bridge deck systems. Higher QI were generally measured on cores from decks with SIPMF, although the differences were minimal (Tables 3.16 and 3.18). A student's t-test was conducted to compare the region-specific QI for decks constructed with and without SIPMFs based on the values provided in Tables 3.16 and 3.18. The data were compared using a two-tailed analysis with a 95% confidence interval. The $t_{critical}$ value for this dataset was equal to 2.23 and the t-statistic values were calculated to be 0.58, 0.15, and 0.78 for QI of top, middle, and bottom regions respectively. The region-specific QI for cores obtained from the two types of bridge decks were considered statistically similar, as the t-statistic was less than $t_{critical}$. The region-specific analysis did not indicate specifically beneficial or adverse effects of the presence of SIPMF on the bridge decks as a function of the depth of the decks.

Further analysis was conducted using direct comparison decks. The variation in average QI between the paired direct comparison data sets (Bridge Deck Number 1 and 6; 2 and 7; and 3 and 8) was calculated by dividing the difference between the average QI of cores from the deck with SIPMF and deck without SIPMF with the average QI of the deck without SIPMF. The variation was determined to be in the range of -1.1% to +5.3%. The low variation in average QI between the paired deck systems also indicates the similarity of the two bridge deck systems.

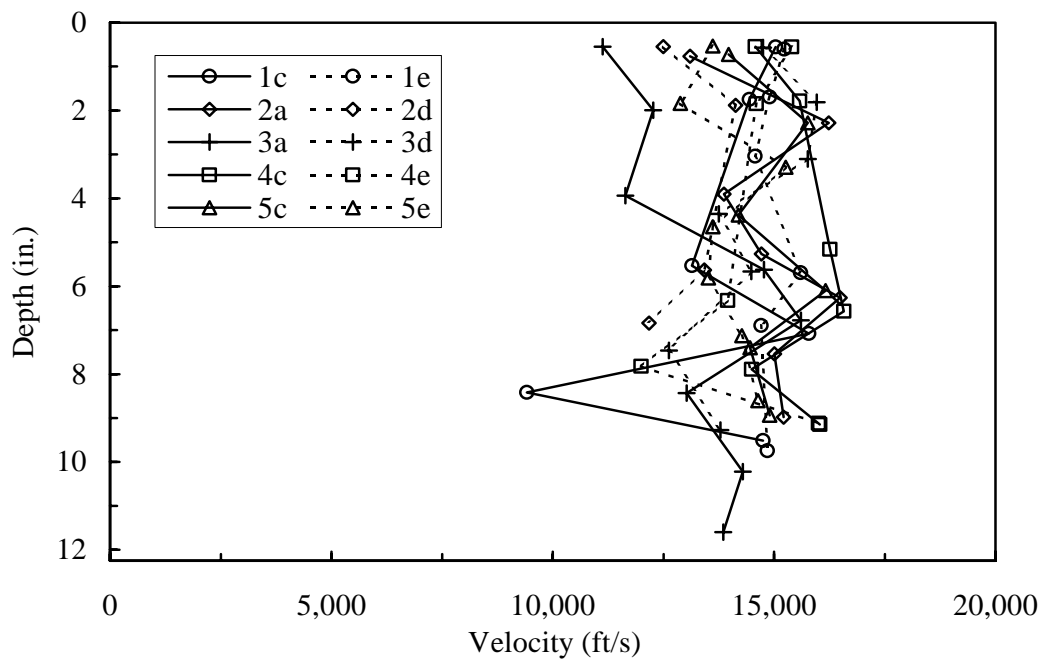


Figure 3.182. Velocity profiles for cores from bridge decks without SIPMF

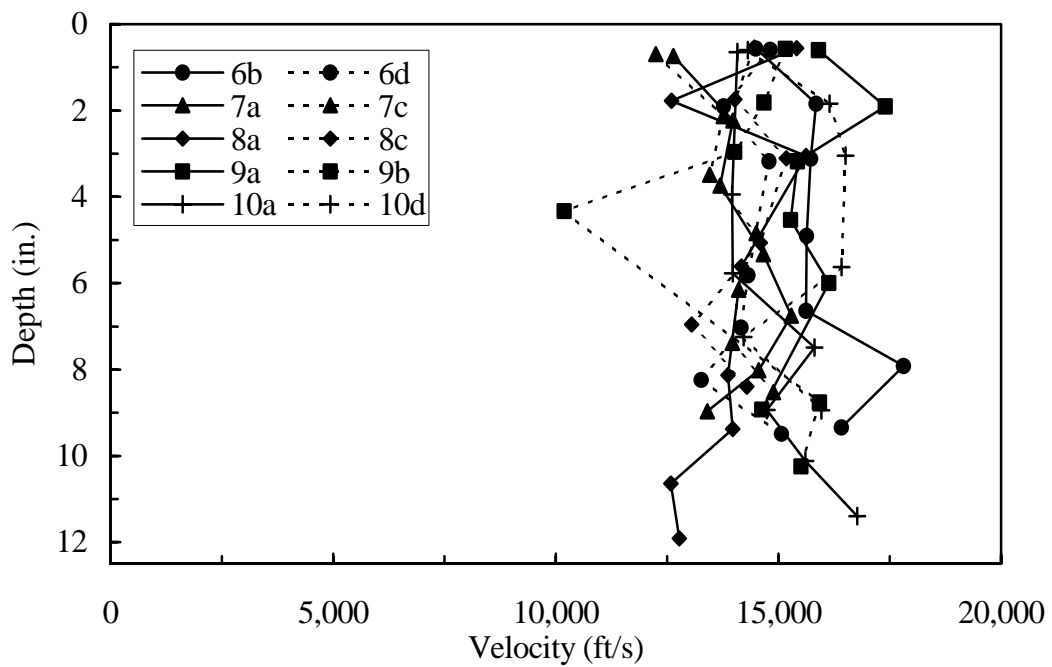


Figure 3.183. Velocity profiles for cores from bridge decks with SIPMF

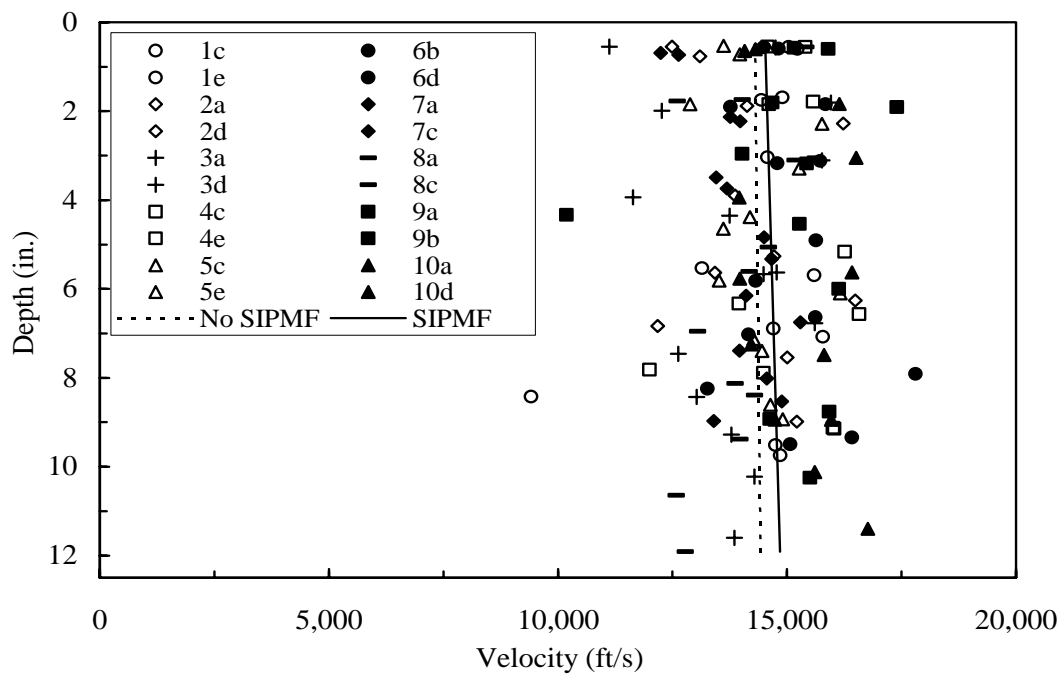


Figure 3.184. Summary of all ultrasonic pulse velocity measurements with depth

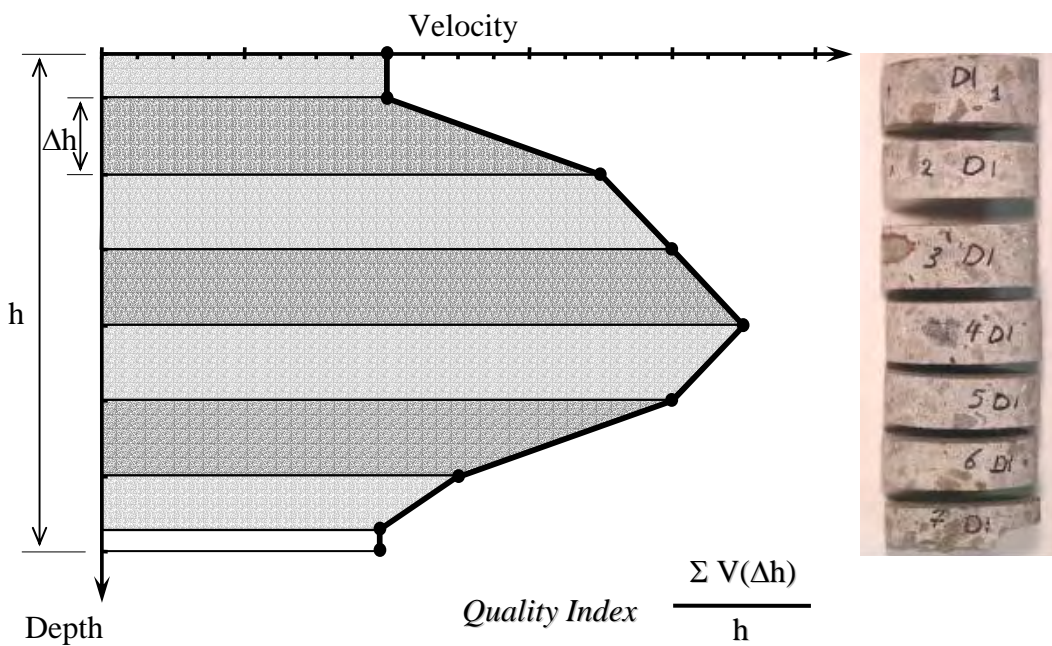


Figure 3.185. *Quality Index(QI)* calculation

Table 3.10. Ultrasonic velocity for Cores 1c, 1e, 2a, and 2d

Core 1c					Core 1e				
Slice No.	Thickness (in.)	Mid Point depth (h) (in.)	Velocity (V) (ft/s)	$\Sigma V(\Delta h)$ (in.ft/s)	Slice No.	Thickness (in.)	Mid Point depth (h) (in.)	Velocity (V) (ft/s)	$\Sigma V(\Delta h)$ (in.ft/s)
1	1.107	0.553	15,035	8,319.1	1	1.206	0.603	15,225	9,179.0
2	1.051	1.748	14,441	17,604.5	2	1.032	1.693	14,900	16,417.0
3	2.335	3.556	(--)	(--)	3	1.135	3.037	14,571	19,799.8
4					4	1.296	4.368	(--)	(--)
5	1.384	5.532	13,146	52,191.6	5	1.128	5.695	15,597	40,098.3
6	1.475	7.076	15,781	22,344.5	6	1.035	6.892	14,706	18,137.1
7	0.981	8.420	9,416	16,922.5	8	1.645	8.347	(--)	(--)
8	0.975	9.513	14,747	20,392.7	9				
					10	0.915	9.740	14,852	48,923.8
$\Sigma =$	10.00			137,774.8	$\Sigma =$	10.20			152,554.9
$V_{\max} =$			15,781		$V_{\max} =$			15,597	
$QI_{\text{avg}} =$				13,777.5	$QI_{\text{avg}} =$				14,956.4
$QI_{\text{top}} =$				14,517.1	$QI_{\text{top}} =$				14,917.0
$QI_{\text{mid}} =$				13,724.0	$QI_{\text{mid}} =$				15,164.7
$QI_{\text{bot}} =$				13,091.3	$QI_{\text{bot}} =$				14,787.5
$QI_{\text{top}} / V_{\max} =$				0.92	$QI_{\text{top}} / V_{\max} =$				0.96
$QI_{\text{top}} / QI_{\text{avg}} =$				1.05	$QI_{\text{top}} / QI_{\text{avg}} =$				1.00
$QI_{\text{mid}} / V_{\max} =$				0.87	$QI_{\text{mid}} / V_{\max} =$				0.97
$QI_{\text{mid}} / QI_{\text{avg}} =$				1.00	$QI_{\text{mid}} / QI_{\text{avg}} =$				1.01
$QI_{\text{bot}} / V_{\max} =$				0.83	$QI_{\text{bot}} / V_{\max} =$				0.95
$QI_{\text{bot}} / QI_{\text{avg}} =$				0.95	$QI_{\text{bot}} / QI_{\text{avg}} =$				0.99

Core 2a					Core 2d				
Slice No.	Thickness (in.)	Mid Point depth (h) (in.)	Velocity (V) (ft/s)	$\Sigma V(\Delta h)$ (in.ft/s)	Slice No.	Thickness (in.)	Mid Point depth (h) (in.)	Velocity (V) (ft/s)	$\Sigma V(\Delta h)$ (in.ft/s)
1	1.532	0.766	13,100	10,036.1	1	1.093	0.547	12,493	6,830.0
2	1.293	2.280	16,231	22,202.6	2	1.336	1.880	14,131	17,749.7
3	1.746	3.901	13,868	24,395.1	3	2.274	3.804	(--)	(--)
4	0.782	5.266	14,714	19,509.0	4				
5	1.005	6.261	16,494	15,520.9	5	1.145	5.632	13,426	51,690.7
6	1.350	7.539	15,008	20,139.5	6	1.026	6.836	12,179	15,414.9
7	1.536	8.982	15,212	33,480.3	7	2.283	8.609	(--)	(--)
					8				
$\Sigma =$	9.75			145,283.4	$\Sigma =$	9.75			127,178.9
$V_{\max} =$			16,494		$V_{\max} =$			14,131	
$QI_{\text{avg}} =$				14,900.9	$QI_{\text{avg}} =$				13,044.0
$QI_{\text{top}} =$				14,522.9	$QI_{\text{top}} =$				13,465.1
$QI_{\text{mid}} =$				14,855.1	$QI_{\text{mid}} =$				13,470.0
$QI_{\text{bot}} =$				15,294.6	$QI_{\text{bot}} =$				12,196.9
$QI_{\text{top}} / V_{\max} =$				0.88	$QI_{\text{top}} / V_{\max} =$				0.95
$QI_{\text{top}} / QI_{\text{avg}} =$				0.98	$QI_{\text{top}} / QI_{\text{avg}} =$				1.03
$QI_{\text{mid}} / V_{\max} =$				0.90	$QI_{\text{mid}} / V_{\max} =$				0.95
$QI_{\text{mid}} / QI_{\text{avg}} =$				1.00	$QI_{\text{mid}} / QI_{\text{avg}} =$				1.03
$QI_{\text{bot}} / V_{\max} =$				0.93	$QI_{\text{bot}} / V_{\max} =$				0.86
$QI_{\text{bot}} / QI_{\text{avg}} =$				1.03	$QI_{\text{bot}} / QI_{\text{avg}} =$				0.94

{(--) Indicates no available data}

Table 3.11. Ultrasonic velocity for Cores 3a, 3d, 4c, and 4e

Core 3a					Core 3d				
Slice No.	Thickness (in.)	Mid Point depth (h) (in.)	Velocity (V) (ft/s)	$\Sigma V(\Delta h)$ (in.ft/s)	Slice No.	Thickness (in.)	Mid Point depth (h) (in.)	Velocity (V) (ft/s)	$\Sigma V(\Delta h)$ (in.ft/s)
1	1.093	0.547	11,126	6,080.3	1	1.140	0.570	14,750	8,406.9
2	1.596	1.993	12,266	16,920.4	2	1.096	1.808	15,963	19,016.4
3	2.084	3.935	11,640	23,214.8	3	1.256	3.105	15,761	20,561.9
4	1.092	5.626	14,773	22,324.9	4	0.994	4.350	13,751	18,381.0
5	0.996	6.773	15,606	17,416.6	5	1.400	5.668	14,490	18,609.0
6	2.117	8.432	13,025	23,754.5	6	1.944	7.461	12,627	24,302.1
7	1.253	10.220	14,294	24,421.1	7				
8	1.301	11.599	13,854	28,432.1	8	1.447	9.276	13,788	33,960.0
$\Sigma =$	12.25			162,564.5	$\Sigma =$	10.00			143,237.2
$V_{\max} =$			15,606		$V_{\max} =$			15,963	
$QI_{\text{avg}} =$				13,270.6	$QI_{\text{avg}} =$				14,323.7
$QI_{\text{top}} =$				11,738.8	$QI_{\text{top}} =$				15,464.6
$QI_{\text{mid}} =$				14,289.5	$QI_{\text{mid}} =$				14,213.1
$QI_{\text{bot}} =$				13,783.5	$QI_{\text{bot}} =$				13,293.4
$QI_{\text{top}} / V_{\max} =$				0.75	$QI_{\text{top}} / V_{\max} =$				0.97
$QI_{\text{top}} / QI_{\text{avg}} =$				0.89	$QI_{\text{top}} / QI_{\text{avg}} =$				1.08
$QI_{\text{mid}} / V_{\max} =$				0.92	$QI_{\text{mid}} / V_{\max} =$				0.89
$QI_{\text{mid}} / QI_{\text{avg}} =$				1.08	$QI_{\text{mid}} / QI_{\text{avg}} =$				0.99
$QI_{\text{bot}} / V_{\max} =$				0.88	$QI_{\text{bot}} / V_{\max} =$				0.83
$QI_{\text{bot}} / QI_{\text{avg}} =$				1.04	$QI_{\text{bot}} / QI_{\text{avg}} =$				0.93

Core 4c					Core 4e				
Slice No.	Thickness (in.)	Mid Point depth (h) (in.)	Velocity (V) (ft/s)	$\Sigma V(\Delta h)$ (in.ft/s)	Slice No.	Thickness (in.)	Mid Point depth (h) (in.)	Velocity (V) (ft/s)	$\Sigma V(\Delta h)$ (in.ft/s)
1	1.101	0.550	14,576	8,022.8	1	1.109	0.554	15,401	8,538.4
2	1.176	1.785	15,576	18,605.8	2	1.054	1.846	14,604	19,370.2
3	1.952	3.444	(--)	(--)	3	2.845	4.005	(--)	(--)
4					4				
5	1.293	5.162	16,263	53,770.3	5	1.379	6.327	13,948	63,973.1
6	1.329	6.569	16,576	23,096.4	6	1.182	7.817	11,997	19,338.0
7	1.118	7.887	14,490	20,483.8	7	1.007	9.122	16,007	26,318.4
8	1.208	9.146	16,034	28,893.7					
$\Sigma =$	9.75			152,872.8	$\Sigma =$	9.63			137,538.0
$V_{\max} =$			16,576		$V_{\max} =$			16,607	
$QI_{\text{avg}} =$				15,679.3	$QI_{\text{avg}} =$				14,289.7
$QI_{\text{top}} =$				15,284.2	$QI_{\text{top}} =$				14,859.4
$QI_{\text{mid}} =$				16,210.5	$QI_{\text{mid}} =$				14,168.2
$QI_{\text{bot}} =$				15,543.2	$QI_{\text{bot}} =$				13,841.4
$QI_{\text{top}} / V_{\max} =$				0.92	$QI_{\text{top}} / V_{\max} =$				0.93
$QI_{\text{top}} / QI_{\text{avg}} =$				0.98	$QI_{\text{top}} / QI_{\text{avg}} =$				1.04
$QI_{\text{mid}} / V_{\max} =$				0.98	$QI_{\text{mid}} / V_{\max} =$				0.89
$QI_{\text{mid}} / QI_{\text{avg}} =$				1.03	$QI_{\text{mid}} / QI_{\text{avg}} =$				0.99
$QI_{\text{bot}} / V_{\max} =$				0.94	$QI_{\text{bot}} / V_{\max} =$				0.87
$QI_{\text{bot}} / QI_{\text{avg}} =$				0.99	$QI_{\text{bot}} / QI_{\text{avg}} =$				0.97

{(--) Indicates no available data}

Table 3.12. Ultrasonic velocity for Cores 5c, 5e, 6b, and 6d

Core 5c					Core 5e				
Slice No.	Thickness (in.)	Mid Point depth (h) (in.)	Velocity (V) (ft/s)	$\Sigma V(\Delta h)$ (in.ft/s)	Slice No.	Thickness (in.)	Mid Point depth (h) (in.)	Velocity (V) (ft/s)	$\Sigma V(\Delta h)$ (in.ft/s)
1	1.446	0.723	13,970	10,101.2	1	1.061	0.531	13,618	7,224.9
2	1.415	2.283	15,764	23,189.2	2	1.152	1.842	12,881	17,380.3
3	2.525	4.382	14,193	31,445.2	3	1.334	3.290	15,267	20,380.1
4					4	0.972	4.648	13,613	19,609.0
5	0.647	6.097	16,163	26,031.1	5	0.950	5.814	13,518	15,815.7
6	1.693	7.396	14,457	19,888.1	6	1.260	7.124	14,271	18,203.3
7	1.128	8.936	14,904	31,008.8	7	1.290	8.605	14,635	30,839.3
$\Sigma =$	9.50			141,663.6	$\Sigma =$	9.25			129,452.6
$V_{\max} =$			16,163		$V_{\max} =$			15,267	
$QI_{\text{avg}} =$				14,912.0	$QI_{\text{avg}} =$				13,994.9
$QI_{\text{top}} =$				14,820.3	$QI_{\text{top}} =$				13,576.1
$QI_{\text{mid}} =$				15,036.3	$QI_{\text{mid}} =$				14,059.4
$QI_{\text{bot}} =$				14,879.3	$QI_{\text{bot}} =$				14,349.1
$QI_{\text{top}} / V_{\max} =$				0.92	$QI_{\text{top}} / V_{\max} =$				0.89
$QI_{\text{top}} / QI_{\text{avg}} =$				0.99	$QI_{\text{top}} / QI_{\text{avg}} =$				0.97
$QI_{\text{mid}} / V_{\max} =$				0.93	$QI_{\text{mid}} / V_{\max} =$				0.92
$QI_{\text{mid}} / QI_{\text{avg}} =$				1.01	$QI_{\text{mid}} / QI_{\text{avg}} =$				1.01
$QI_{\text{bot}} / V_{\max} =$				0.92	$QI_{\text{bot}} / V_{\max} =$				0.94
$QI_{\text{bot}} / QI_{\text{avg}} =$				1.00	$QI_{\text{bot}} / QI_{\text{avg}} =$				1.03

Core 6b					Core 6d				
Slice No.	Thickness (in.)	Mid Point depth (h) (in.)	Velocity (V) (ft/s)	$\Sigma V(\Delta h)$ (in.ft/s)	Slice No.	Thickness (in.)	Mid Point depth (h) (in.)	Velocity (V) (ft/s)	$\Sigma V(\Delta h)$ (in.ft/s)
1	1.127	0.564	14,493	8,167.0	1	1.190	0.595	14,816	8,815.4
2	1.184	1.845	15,843	19,443.5	2	1.168	1.900	13,768	18,647.1
3	1.114	3.121	15,722	20,131.8	3	1.124	3.171	14,787	18,155.7
4	2.201	4.905	15,631	27,968.1	4	1.230	4.474	(--)	(--)
5					5				
6	1.010	6.637	15,621	27,060.1	6	1.205	5.817	14,318	38,505.7
7	1.291	7.913	17,808	21,338.9	7	0.961	7.026	14,161	17,213.6
8	1.315	9.343	16,416	35,248.5	8	1.229	8.247	13,264	16,739.9
					9	1.013	9.494	15,069	25,290.4
$\Sigma =$	10.00			159,357.9	$\Sigma =$	10.00			14,3367.6
$V_{\max} =$			17,808		$V_{\max} =$			15,068.45	
$QI_{\text{avg}} =$				15,935.8	$QI_{\text{avg}} =$				14,336.8
$QI_{\text{top}} =$				15,324.3	$QI_{\text{top}} =$				14,403.1
$QI_{\text{mid}} =$				15,647.5	$QI_{\text{mid}} =$				14,468.0
$QI_{\text{bot}} =$				16,835.7	$QI_{\text{bot}} =$				14,139.2
$QI_{\text{top}} / V_{\max} =$				0.86	$QI_{\text{top}} / V_{\max} =$				0.96
$QI_{\text{top}} / QI_{\text{avg}} =$				0.96	$QI_{\text{top}} / QI_{\text{avg}} =$				1.01
$QI_{\text{mid}} / V_{\max} =$				0.88	$QI_{\text{mid}} / V_{\max} =$				0.96
$QI_{\text{mid}} / QI_{\text{avg}} =$				0.98	$QI_{\text{mid}} / QI_{\text{avg}} =$				1.01
$QI_{\text{bot}} / V_{\max} =$				0.95	$QI_{\text{bot}} / V_{\max} =$				0.94
$QI_{\text{bot}} / QI_{\text{avg}} =$				1.06	$QI_{\text{bot}} / QI_{\text{avg}} =$				0.99

{(--) Indicates no available data}

Table 3.13. Ultrasonic velocity for Cores 7a, 7c, 8a, and 8c

Core 7a					Core 7c				
Slice No.	Thickness (in.)	Mid Point depth (h) (in.)	Velocity (V) (ft/s)	$\Sigma V(\Delta h)$ (in.ft/s)	Slice No.	Thickness (in.)	Mid Point depth (h) (in.)	Velocity (V) (ft/s)	$\Sigma V(\Delta h)$ (in.ft/s)
1	1.472	0.736	12,637	9,301.1	1	1.381	0.691	12,244	8,455.6
2	1.257	2.229	13,980	19,864.5	2	1.348	2.134	13,764	18,773.0
3	1.503	3.736	13,690	20,861.6	3	1.201	3.488	13,457	18,424.9
4	1.429	5.330	14,661	22,590.7	4	1.341	4.838	14,503	18,879.2
5	1.162	6.754	15,292	21,318.4	5	1.129	6.152	14,106	18,796.5
6	1.102	8.014	14,559	18,807.3	6	1.184	7.388	13,962	17,338.4
7	0.557	8.971	13,400	17,123.2	7	0.941	8.53	14,888	23,471.9
$\Sigma =$	9.25			129,866.7	$\Sigma =$	9.00			124,139.4
$V_{\max} =$			15,292.1		$V_{\max} =$			14,888	
$QI_{\text{avg}} =$				14,039.7	$QI_{\text{avg}} =$				13,793.3
$QI_{\text{top}} =$				13,311.8	$QI_{\text{top}} =$				13,020.0
$QI_{\text{mid}} =$				14,268.1	$QI_{\text{mid}} =$				13,884.7
$QI_{\text{bot}} =$				14,539.0	$QI_{\text{bot}} =$				14,475.1
$QI_{\text{top}} / V_{\max} =$				0.87	$QI_{\text{top}} / V_{\max} =$				0.88
$QI_{\text{top}} / QI_{\text{avg}} =$				0.95	$QI_{\text{top}} / QI_{\text{avg}} =$				0.94
$QI_{\text{mid}} / V_{\max} =$				0.93	$QI_{\text{mid}} / V_{\max} =$				0.93
$QI_{\text{mid}} / QI_{\text{avg}} =$				1.02	$QI_{\text{mid}} / QI_{\text{avg}} =$				1.01
$QI_{\text{bot}} / V_{\max} =$				0.95	$QI_{\text{bot}} / V_{\max} =$				0.97
$QI_{\text{bot}} / QI_{\text{avg}} =$				1.04	$QI_{\text{bot}} / QI_{\text{avg}} =$				1.05

Core 8a					Core 8c				
Slice No.	Thickness (in.)	Mid Point depth (h) (in.)	Velocity (V) (ft/s)	$\Sigma V(\Delta h)$ (in.ft/s)	Slice No.	Thickness (in.)	Mid Point depth (h) (in.)	Velocity (V) (ft/s)	$\Sigma V(\Delta h)$ (in.ft/s)
1	1.105	0.552	15,410	8,511.0	1	1.085	0.542	14,455	7,839.7
2	1.127	1.777	12,601	17,152.3	2	0.945	1.741	14,024	17,067.0
3	1.202	3.050	15,617	17,965.5	3	1.413	3.104	15,178	19,900.2
4	3.696	5.608	14,172	38,097.8	4	2.129	5.059	14,591	29,102.3
5					5				
6	1.127	8.129	13,868	35,336.0	6	1.295	6.955	13,050	26,201.1
7	1.158	9.380	13,972	17,420.1	7	1.214	8.393	14,289	19,659.8
8	1.150	10.643	12,583	16,765.5					
9	1.174	11.913	12,778	23,607.0					
$\Sigma =$	12.50			174,855.3	$\Sigma =$	9.00			119,770.1
$V_{\max} =$			15,617		$V_{\max} =$			15,178	
$QI_{\text{avg}} =$				13,988.4	$QI_{\text{avg}} =$				13,307.8
$QI_{\text{top}} =$				14,570.6	$QI_{\text{top}} =$				14,411.7
$QI_{\text{mid}} =$				14,206.1	$QI_{\text{mid}} =$				14,681.4
$QI_{\text{bot}} =$				13,188.6	$QI_{\text{bot}} =$				10,830.3
$QI_{\text{top}} / V_{\max} =$				0.93	$QI_{\text{top}} / V_{\max} =$				0.95
$QI_{\text{top}} / QI_{\text{avg}} =$				1.04	$QI_{\text{top}} / QI_{\text{avg}} =$				1.08
$QI_{\text{mid}} / V_{\max} =$				0.91	$QI_{\text{mid}} / V_{\max} =$				0.97
$QI_{\text{mid}} / QI_{\text{avg}} =$				1.02	$QI_{\text{mid}} / QI_{\text{avg}} =$				1.10
$QI_{\text{bot}} / V_{\max} =$				0.84	$QI_{\text{bot}} / V_{\max} =$				0.71
$QI_{\text{bot}} / QI_{\text{avg}} =$				0.94	$QI_{\text{bot}} / QI_{\text{avg}} =$				0.81

{(--)} Indicates no available data}

Table 3.14. Ultrasonic velocity for Cores 9a, 9b, 10a, and 10d

Core 9a					Core 9b				
Slice No.	Thickness (in.)	Mid Point depth (h) (in.)	Velocity (V) (ft/s)	$\Sigma V(\Delta h)$ (in.ft/s)	Slice No.	Thickness (in.)	Mid Point depth (h) (in.)	Velocity (V) (ft/s)	$\Sigma V(\Delta h)$ (in.ft/s)
1	1.198	0.599	15,900	9,525.5	1	1.147	0.573	15,155	17,380.8
2	1.108	1.905	17,401	21,738.5	2	1.075	1.809	14,675	17,889.1
3	1.128	3.175	15,430	20,857.8	3	0.985	2.963	14,021	15,909.0
4	1.295	4.539	15,274	20,943.1	4	1.504	4.331	10,189	10,602.8
5	1.314	5.996	16,132	22,878.8	5	3.070	6.742	(--)	(--)
6	1.226	7.419	(--)	(--)	6				
7					7	0.724	8.762	15,922	57,850.9
8	1.491	8.930	14,624	56,007.7	8				
					9	2.002	10.249	15,505	38,882.7
$\Sigma =$	9.68			151,951.4	$\Sigma =$	11.25			158,515.3
$V_{\max} =$			17,401		$V_{\max} =$			15,922	
$QI_{\text{avg}} =$				15,705.6	$QI_{\text{avg}} =$				14,090.3
$QI_{\text{top}} =$				16,399.6	$QI_{\text{top}} =$				14,700.0
$QI_{\text{mid}} =$				15,602.9	$QI_{\text{mid}} =$				12,118.1
$QI_{\text{bot}} =$				15,114.3	$QI_{\text{bot}} =$				15,453.2
$QI_{\text{top}} / V_{\max} =$				0.94	$QI_{\text{top}} / V_{\max} =$				0.92
$QI_{\text{top}} / QI_{\text{avg}} =$				1.04	$QI_{\text{top}} / QI_{\text{avg}} =$				1.04
$QI_{\text{mid}} / V_{\max} =$				0.90	$QI_{\text{mid}} / V_{\max} =$				0.76
$QI_{\text{mid}} / QI_{\text{avg}} =$				0.99	$QI_{\text{mid}} / QI_{\text{avg}} =$				0.86
$QI_{\text{bot}} / V_{\max} =$				0.87	$QI_{\text{bot}} / V_{\max} =$				0.97
$QI_{\text{bot}} / QI_{\text{avg}} =$				0.96	$QI_{\text{bot}} / QI_{\text{avg}} =$				1.10

Core 10a					Core 10d				
Slice No.	Thickness (in.)	Mid Point depth (h) (in.)	Velocity (V) (ft/s)	$\Sigma V(\Delta h)$ (in.ft/s)	Slice No.	Thickness (in.)	Mid Point depth (h) (in.)	Velocity (V) (ft/s)	$\Sigma V(\Delta h)$ (in.ft/s)
1	1.291	0.645	14,078	9,085.4	1	1.207	0.603	14,310	8,633.1
2	1.481	2.145	(--)	(--)	2	1.054	1.839	16,146	18,816.9
3	1.886	3.942	13,957	46,216.4	3	1.154	3.049	16,509	19,748.6
4					4	1.307	4.384	(--)	(--)
5	1.536	5.767	13,974	25,480.6	5				
6	1.677	7.487	15,811	25,619.7	6	0.967	5.627	16,419	42,445.8
7	1.000	8.940	14,738	22,181.7	7	2.070	7.251	14,220	24,878.8
8	1.129	10.117	15,606	17,870.5	8				
9	1.205	11.398	16,768	30,822.9	9	1.109	8.946	15,967	34,435.2
$\Sigma =$	12.00			177,277.1	$\Sigma =$	9.50			148,958.4
$V_{\max} =$			16,768		$V_{\max} =$			16,509	
$QI_{\text{avg}} =$				14,773.1	$QI_{\text{avg}} =$				15,679.8
$QI_{\text{top}} =$				14,026.4	$QI_{\text{top}} =$				15,520.6
$QI_{\text{mid}} =$				14,576.4	$QI_{\text{mid}} =$				16,345.5
$QI_{\text{bot}} =$				15,716.5	$QI_{\text{bot}} =$				15,173.4
$QI_{\text{top}} / V_{\max} =$				0.84	$QI_{\text{top}} / V_{\max} =$				0.94
$QI_{\text{top}} / QI_{\text{avg}} =$				0.95	$QI_{\text{top}} / QI_{\text{avg}} =$				0.99
$QI_{\text{mid}} / V_{\max} =$				0.87	$QI_{\text{mid}} / V_{\max} =$				0.99
$QI_{\text{mid}} / QI_{\text{avg}} =$				0.99	$QI_{\text{mid}} / QI_{\text{avg}} =$				1.04
$QI_{\text{bot}} / V_{\max} =$				0.94	$QI_{\text{bot}} / V_{\max} =$				0.92
$QI_{\text{bot}} / QI_{\text{avg}} =$				1.06	$QI_{\text{bot}} / QI_{\text{avg}} =$				0.97

{(--) Indicates no available data}

Table 3.15. Summary of pulse velocity test results for No SIPMF Bridge Decks

Bridge Deck Number	Core	Height, h (in.)	$\Sigma V(\Delta h)$ (in.ft/s)	QI_{avg} for Core (ft/s)	QI_{avg} for Bridge Deck (ft/s)
1	1c	10.00	137,774.8	13,777	14,366
	1e	10.20	152,554.9	14,956	
2	2a	9.75	145,283.4	14,900	13,972
	2d	9.75	127,178.9	13,044	
3	3a	12.25	162,564.5	13,270	13,797
	3d	10.00	143,237.2	14,324	
4	4c	9.75	152,872.8	15,679	14,985
	4e	9.63	137,538.0	14,290	
5	5c	9.50	141,663.6	14,912	14,454
	5e	9.25	129,452.6	13,995	
Average				14,315	
Standard Deviation				821	
Σ		100.08	1,430,120		
QI (ft/s)	14,290				

Table 3.16. Summary of region-specific pulse velocity analysis for No SIPMF Bridge Decks

Bridge Deck Number	Core	QI_{avg} (ft/s)	QI_{top} (ft/s)	QI_{top} / QI_{avg}	QI_{mid} (ft/s)	QI_{mid} / QI_{avg}	QI_{bot} (ft/s)	QI_{bot} / QI_{avg}
1	1c	13,777	14,517	1.05	13,724	1.00	13,091	0.95
	1e	14,956	14,917	1.00	15,165	1.01	14,787	0.99
2	2a	14,900	14,553	0.98	14,855	0.98	15,295	1.03
	2d	13,044	13,465	1.03	13,470	1.03	12,197	0.94
3	3a	13,270	11,739	0.89	14,289	1.08	13,783	1.04
	3d	14,324	15,465	1.08	14,213	0.99	13,293	0.93
4	4c	15,679	15,284	0.98	16,210	1.03	15,543	0.99
	4e	14,290	14,859	1.04	14,168	0.99	13,841	0.97
5	5c	14,912	14,820	0.99	15,036	1.01	14,879	1.00
	5e	13,995	13,576	0.97	14,059	1.01	14,349	1.03
Average		14,315	14,320	1.00	14,519	1.02	14,106	0.99

Table 3.17. Summary of pulse velocity test results for SIPMF Bridge Decks

Bridge Deck Number	Core	Height, h (in.)	$\Sigma V(\Delta h)$ (in.ft/s)	QI_{avg} for Core (ft/s)	QI_{avg} for Bridge Deck (ft/s)
6	6b	10.00	159,357.9	15,936	15,137
	6d	10.00	143,367.6	14,337	
7	7a	9.25	129,866.7	14,040	13,917
	7c	9.00	124,139.4	13,793	
8	8a	12.50	174,855.3	13,988	13,648
	8c	9.00	119,770.1	13,308	
9	9a	9.68	151,951.4	15,706	14,898
	9b	11.25	158,515.3	14,090	
10	10a	12.00	177,277.1	14,773	15,227
	10d	9.50	148,958.4	15,680	
Average				14,565	
Standard Deviation				915	
Σ		102.18	1,488,059		
QI (ft/s)	14,564				

Table 3.18. Summary of region-specific pulse velocity analysis for SIPMF Bridge Decks

Bridge Deck Number	Core	QI_{avg} (ft/s)	QI_{top} (ft/s)	QI_{top} / QI_{avg}	QI_{mid} (ft/s)	QI_{mid} / QI_{avg}	QI_{bot} (ft/s)	QI_{bot} / QI_{avg}
6	6b	15,936	15,324	0.96	15,647	0.98	16,836	1.06
	6d	14,337	14,403	1.01	14,468	1.01	14,139	0.99
7	7a	14,040	13,312	0.95	14,268	1.02	14,539	1.04
	7c	13,793	13,020	0.94	13,885	1.01	14,475	1.05
8	8a	13,988	14,571	1.04	14,206	1.02	13,189	0.94
	8c	13,308	14,412	1.08	14,681	1.10	10,830	0.81
9	9a	15,706	16,400	1.04	15,603	0.99	15,114	0.96
	9b	14,090	14,700	1.04	12,118	0.86	15,453	1.10
10	10a	14,773	14,026	0.95	14,576	0.99	15,717	1.06
	10d	15,680	15,521	0.99	16,346	1.04	15,173	0.97
Average		14,565	14,569	1.00	14,580	1.00	14,547	1.00

3.5 SUMMARY OF INSPECTION AND CORING

A study was conducted to evaluate the performance of concrete bridge decks constructed using SIPMFs. Comparisons were made between decks without SIPMF and decks with SIPMF. The test program was conducted on bridge decks located in Michigan. The decks were exposed to high seasonal temperature variations and cyclic freeze thaw due to the prevailing climatic conditions in the state. Evaluations were made using visual field inspection and analysis of cores obtained from bridge decks. The cores were investigated using visual inspection, compressive strength tests, and ultrasonic tests. The compressive strength tests provided overall strength for a given core. The ultrasonic tests provided a means for evaluating the response of cores with depth of bridge deck. The test results were analyzed initially to compare all bridge decks without SIPMF to bridge decks with SIPMF. Then, three bridges that were constructed using a combination of formwork systems were analyzed. This paired analysis allowed for direct comparison of measured parameters eliminating the effects of bridge age, traffic loading, and environmental conditions.

Based on the visual field inspection and visual inspection of cores, it was determined that the two bridge deck systems were similar. Statistical analysis of compressive strength and ultrasonic pulse velocity tests also indicated similarity of the bridge deck systems for all of the decks and paired, direct comparison decks. The ultrasonic test results with depth did not indicate specifically beneficial or adverse effects of the presence of SIPMF on the bridge decks. Overall, the performance of concrete bridge decks constructed with SIPMFs was determined to be similar to the performance of concrete bridge decks constructed without SIPMFs in this test program.

CHAPTER 4 : TEST PROGRAM

4.1 INTRODUCTION

The experimental program was designed to provide an investigation of the performance and durability of bridge decks constructed using Stay-In-Place Metal Forms (SIPMFs) and epoxy-coated reinforcement under different environmental exposure conditions. A total of 24 specimens were designed and constructed for this purpose. Twelve specimens were constructed using SIPMFs and twelve specimens were constructed using conventional removable wooden forms to allow for comparison between the two types of formwork methods on bridge deck performance. Epoxy-coated reinforcement bars were used for all of the 24 specimens. Several destructive and nondestructive tests were conducted at the different stages of the environmental conditioning to evaluate the degree of degradation and deterioration, and the influence of various types of environmental exposures on load carrying capacity. The environmental exposure conditions included: service load exposure, freeze/thaw exposure, salt-water exposure, and repeated load cycles.

4.2 OVERVIEW OF TEST PROGRAM

A summary flow chart for the experimental program is shown in Figure 4.1. The chart includes the chronological application of environmental exposure conditions, the number of specimens assigned for each exposure, the duration of each exposure, and the different types of destructive and nondestructive tests conducted at various stages of the test program.

All of the specimens were subjected to service load application before any further environmental conditioning. The purpose of this load application was to create full-depth cracks in all of the specimens to allow water to fully penetrate the concrete during the freeze/thaw and salt-water exposures. Specimens were initially loaded to create cracks along the bottom side and then loaded again to create cracks along the top side to form full depth cracks. The concrete with full-depth cracks simulates in-service concrete bridge decks.

A total of 12 specimens were constructed using SIPMFs and a total of 12 specimens were constructed using conventional removable wooden forms. This arrangement allowed for

determination of the effects of formwork on performance of the varying bridge decks. The various types of environmental exposure conditioning and the number of specimens designated for each exposure are shown in Table 4.1. Two specimens from each set were designated as control specimens. These specimens were used to establish baseline values for the mechanical and ultrasonic properties of the concrete. These specimens were not subjected to any freeze/thaw, salt-water, or repeated load exposure.

Six specimens from each set were exposed to a combined effect of salt-water and repeated load (termed salt-water specimens). Two salt-water specimens from each set were exposed to salt-water for 1,000 hours and also exposed to 250,000 cycles of repeated load. Two salt-water specimens from each set were exposed to salt-water for 3,000 hours and also exposed to 500,000 cycles of repeated load. The final two salt-water specimens from each set were exposed to salt-water for 10,000 hours and also exposed to 750,000 cycles of repeated load.

Four specimens from each set were exposed to a combined effect of freeze/thaw cycles and repeated load (termed freeze/thaw specimens). Two freeze/thaw specimens from each set were exposed to freeze/thaw for 300 cycles and also exposed to 250,000 cycles of repeated load. The final two freeze/thaw specimens from each set were exposed to freeze/thaw for 600 cycles and also exposed to 500,000 cycles of repeated load.

Two specimens were constructed for preliminary tests to evaluate nominal ultimate strength of the specimens. These specimens are termed reference specimens and are not part of the comparative experimental test program. These specimens were only used to establish suitable levels of loading for repeated load cycles for the remaining specimens in the test program.

Ultrasonic test methods were used throughout the test program. Ultrasonic pulse-echo testing was used during environmental exposure tests to determine the quality of contact between the SIPMFs and the concrete for the first set of 12 specimens. Ultrasonic through-transmission testing was used subsequent to environmental exposure to evaluate the condition of concrete for all of the 24 specimens in the test program. All of the specimens were tested for ultimate

load subsequent to exposure tests. Results of ultrasonic and mechanical tests were used to compare the bridge decks using SIPMF and conventional formwork.

Each specimen was given a name that identified its type, the kind of environmental exposure condition it was exposed to, and the duration of this exposure. The first two letters of the labels identified the type of the specimen; specimens with SIPMFs were labeled “WI”, while specimens without SIPMFs were labeled “WO”. The next letter of the label identified the kind of environmental exposure for the specimen; control specimens were labeled “C”, salt-water specimens were labeled “S”, and freeze/thaw specimens were labeled “F”. For the freeze/thaw specimens, the number after the letter “F” identified the number of freeze/thaw cycles (in hundreds) for the specimen. For the salt-water specimens, the number after the letter “S” identified the time for the salt-water exposure (in thousands of hours) for the specimen. The final number in the specimen label identified the specimen number (1 or 2) for a given set of exposure conditions.

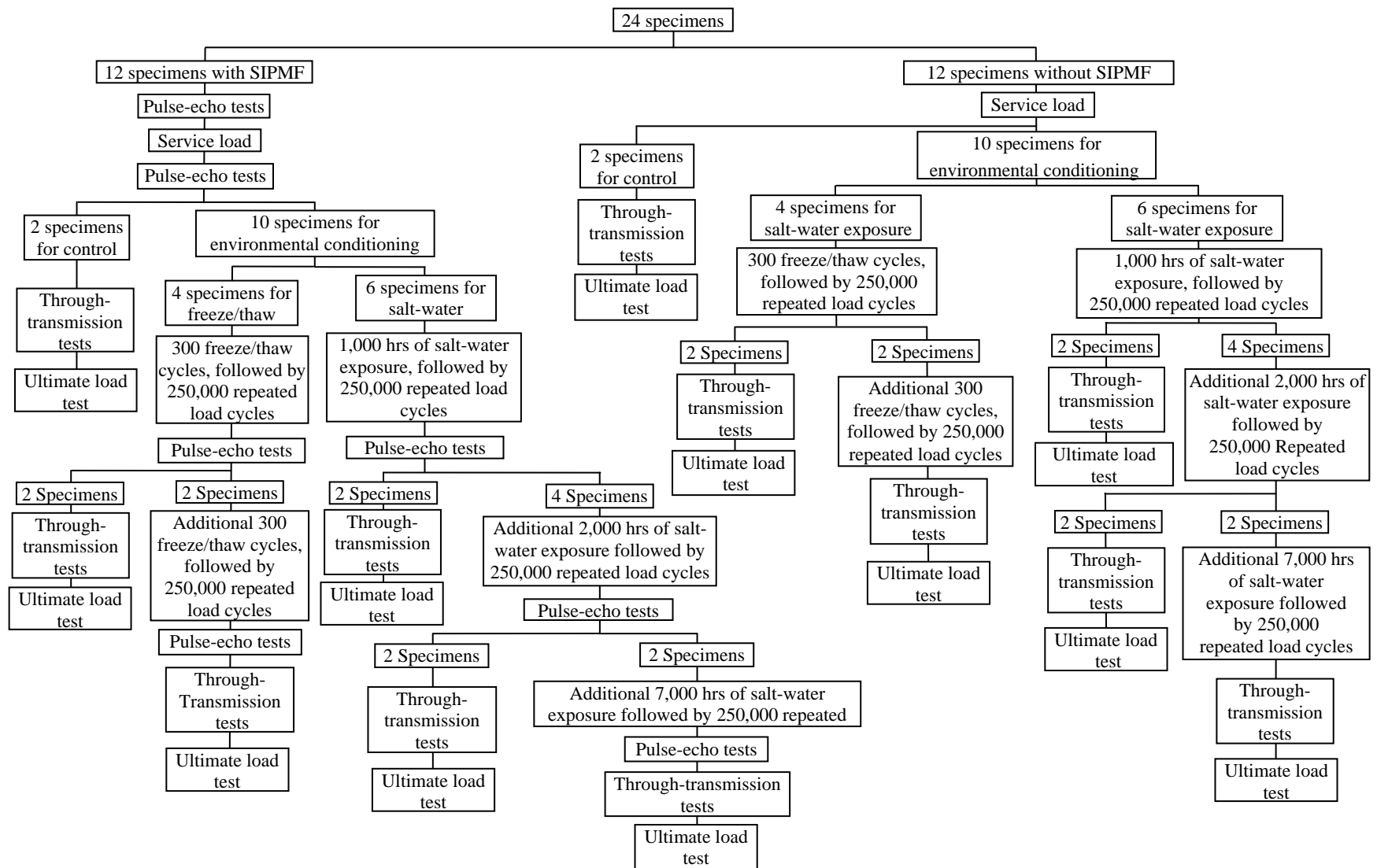


Figure 4.1. Summary flow chart for the experimental test program

Table 4.1. Specimens labeling and the types of exposure conditioning

Environmental Exposure Condition	Labels for Specimens with SIPMF	Labels for Specimens without SIPMF	Sequence of Environmental Exposure Conditioning
Control	WI-C-1 WI-C-2	WO-C-1 WO-C-2	Service Load
1,000 Hour Salt-Water	WI-S-1-1 WI-S-1-2	WO-S-1-1 WO-S-1-2	Service Load 1,000 hours of salt-water 250,000 repeated load cycles
3,000 Hour Salt-Water	WI-S-3-1 WI-S-3-2	WO-S-3-1 WO-S-3-2	Service Load 1,000 hours of salt-water 250,000 repeated load cycles 2,000 hours of salt-water 250,000 repeated load cycles
10,000 Hour Salt-Water	WI-S-10-1 WI-S-10-2	WO-S-10-1 WO-S-10-2	Service Load 1,000 hours of salt-water 250,000 repeated load cycles 2,000 hours of salt-water 250,000 repeated load cycles 7,000 hours of salt-water 250,000 repeated load cycles
300 Cycles Freeze/Thaw	WI-F-3-1 WI-F-3-2	WO-F-3-1 WO-F-3-2	Service Load 300 freeze/thaw cycles 250,000 repeated load cycles
600 Cycles Freeze/Thaw	WI-F-6-1 WI-F-6-2	WO-F-6-1 WO-F-6-2	Service Load 300 freeze/thaw cycles 250,000 repeated load cycles 300 freeze/thaw cycles 250,000 repeated load cycles

4.3 TEST SPECIMENS

The specimens were designed to simulate typical bridge decks commonly used in Michigan. All of the specimens were constructed to have similar depth and span as the typical bridge decks used by the Michigan Department of Transportation. Similar dimensions, in particular similar depths, were used to simulate the conditions for water infiltration through the depth of an in-service bridge deck.

4.3.1 Materials

The concrete mix used for constructing the specimens was MDOT Mix D (Limestone aggregate, air entrainment, and water reducing admixture) obtained from a single truck mixer. The concrete mix was used to construct test specimens as well as cylinders. The cylinders were used to evaluate the compressive strength of the concrete during the entire test program. The design mixture had a water-cement ratio of 0.40. The sand used in the mixture was 2NS Levy Oxford (Pit #63-4) and the coarse aggregate used was 6AA Limestone Presque Isle (Pit #71-47). The cement – sand – coarse aggregate ratio by weight was 1.00 – 1.70 – 2.69 (658 lb - 1119 lb - 1768 lb). The mixture included 0.5 lb/ cubic yard of air entraining admixture and 1.23 lb/ cubic yard of water reducer admixture. The air content was 6.5% (+/-1.5%), as provided by the concrete supplier. The measured slump, as determined using ASTM C143/ C143M-98, was 3.5 in. The compressive strength tests for cylinders were conducted according to ASTM C39/ C39M-99. The cylinders were 6 in. diameter and 12 in. height. The average 28-day strength for the concrete was 5760 psi.

The SIPMFs used in the test program were constructed of 22 gage galvanized steel. The forms contained a zinc coating that conformed to ASTM A653/ A653M-99 (A525-94), A924/ A924M-99. The SIPMFs had a 5.0 in. pitch and a 2.5 in. depth. These forms are termed “Wheeling Bridge Forms” and are commonly used in bridge deck construction in Michigan. The SIPMF had a 5.0 in. pitch and 2.5 in. depth.

Epoxy-coated steel was used for all of the reinforcement bars in the test program. The main reinforcement for top and bottom of the specimens was #5 bars. This size conforms to the minimum slab reinforcement requirements of the Michigan Department of Transportation. The

secondary reinforcement was #5 bars for the bottom reinforcement bars and #3 bars for the top reinforcement. The nominal yield strength of the reinforcement was 60 ksi. A tensile test conducted on a sample bar resulted in a yield strength of approximately 69 ksi and a modulus of elasticity (Young's modulus) of approximately 30,000 ksi. The stress-strain curve is presented in Figure 4.2. The epoxy-coated reinforcement steel bars were provided by Dayton-Richmond Corporation. The cut ends of the bars were painted with epoxy paint to avoid any exposed steel area.

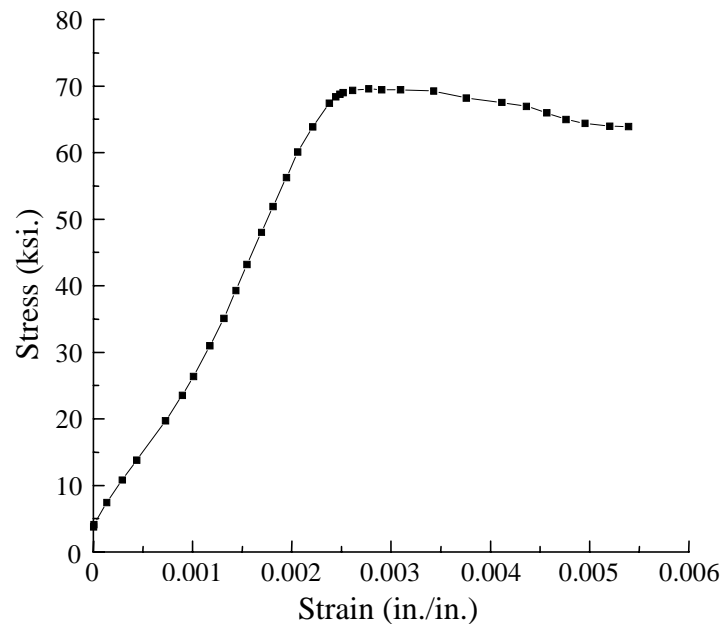


Figure 4.2. Stress-strain curve for steel reinforcement bars

4.3.2 Specimens Geometry and Fabrication

Specimens were fabricated to represent typical bridge deck sections for Michigan bridges. Twelve identical specimens were constructed using conventional removable wooden forms. The dimensions and reinforcement details for specimens without SIPMFs are presented in Figure 4.3. The specimens had a depth of 7.5 in., a width of 18.0 in., and a length of 72.0 in.

Twelve identical specimens were constructed using SIPMFs. The dimensions and reinforcement details for specimens with SIPMF are presented in Figure 4.4. The specimen depth varied from 7.5 in. to 10.0 in. due to the corrugation of the SIPMF. The specimen width was 18.0 in. and length was 72.0 in.

An 18.0 in. long galvanized steel angle was provided at each end of the specimen in order to connect the vertical sides of the formwork (wooden) to the SIPMF base. The cross sectional dimensions of the angle were 3.0 in. x 2.5 in. and the thickness of the angle was 0.25 in.

Shear connectors were used to provide anchorage between the SIPMF and the concrete at the ends of the specimens. The shear connectors were # 3 self-drilling zinc-plated steel screws (hexagonal head) with a length of 4.0 in. The role of the shear connectors was to prevent complete pullout of the SIPMF during the various stages of the test program. The shear connectors were provided only at the ends of the specimen in order not to influence the contact between the concrete and the SIPMF. The detail for the shear connector and the steel angles at the end of the specimens is presented in Figure 4.5.

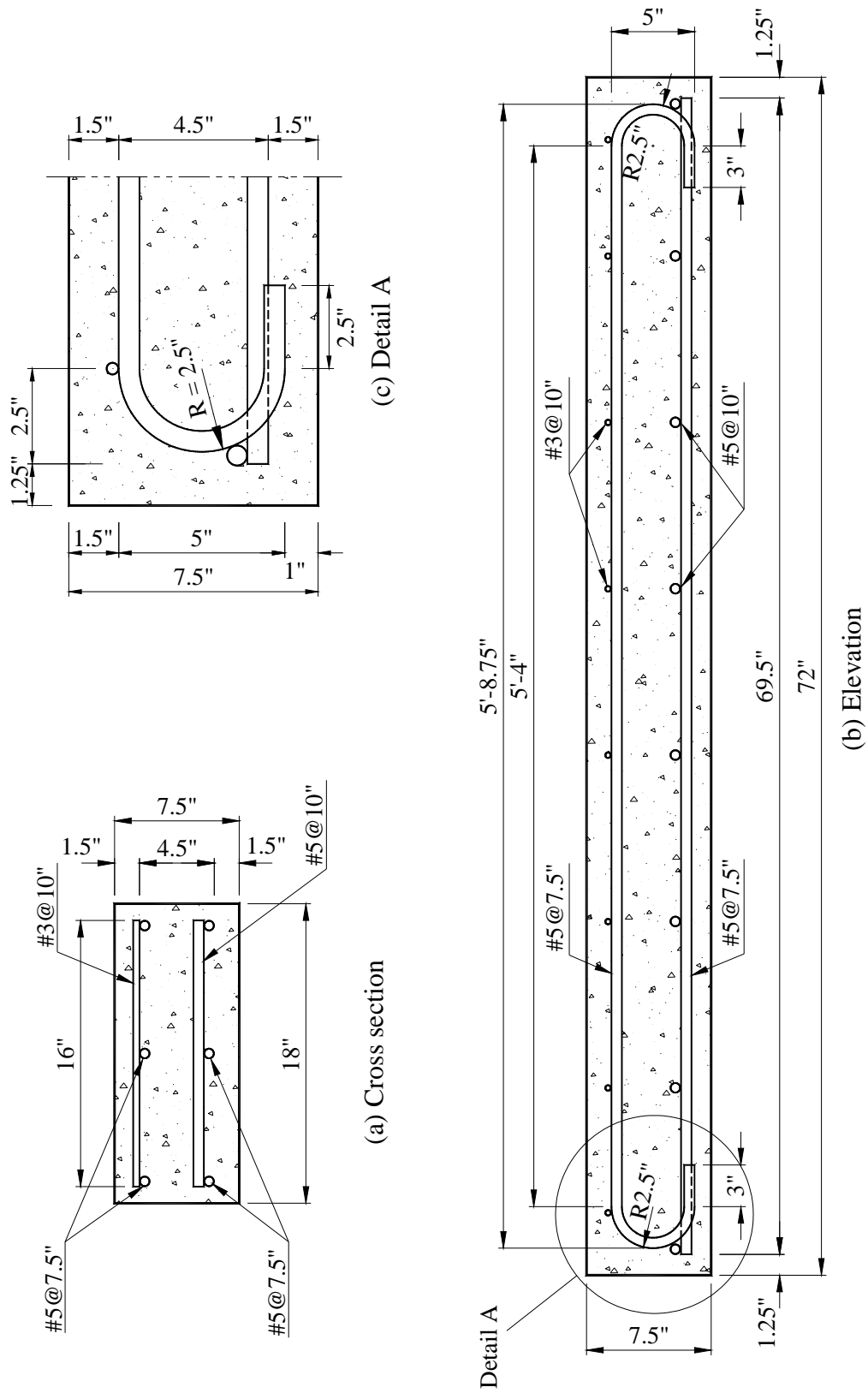


Figure 4.3. Dimensions and reinforcement details for specimens without SIPMF

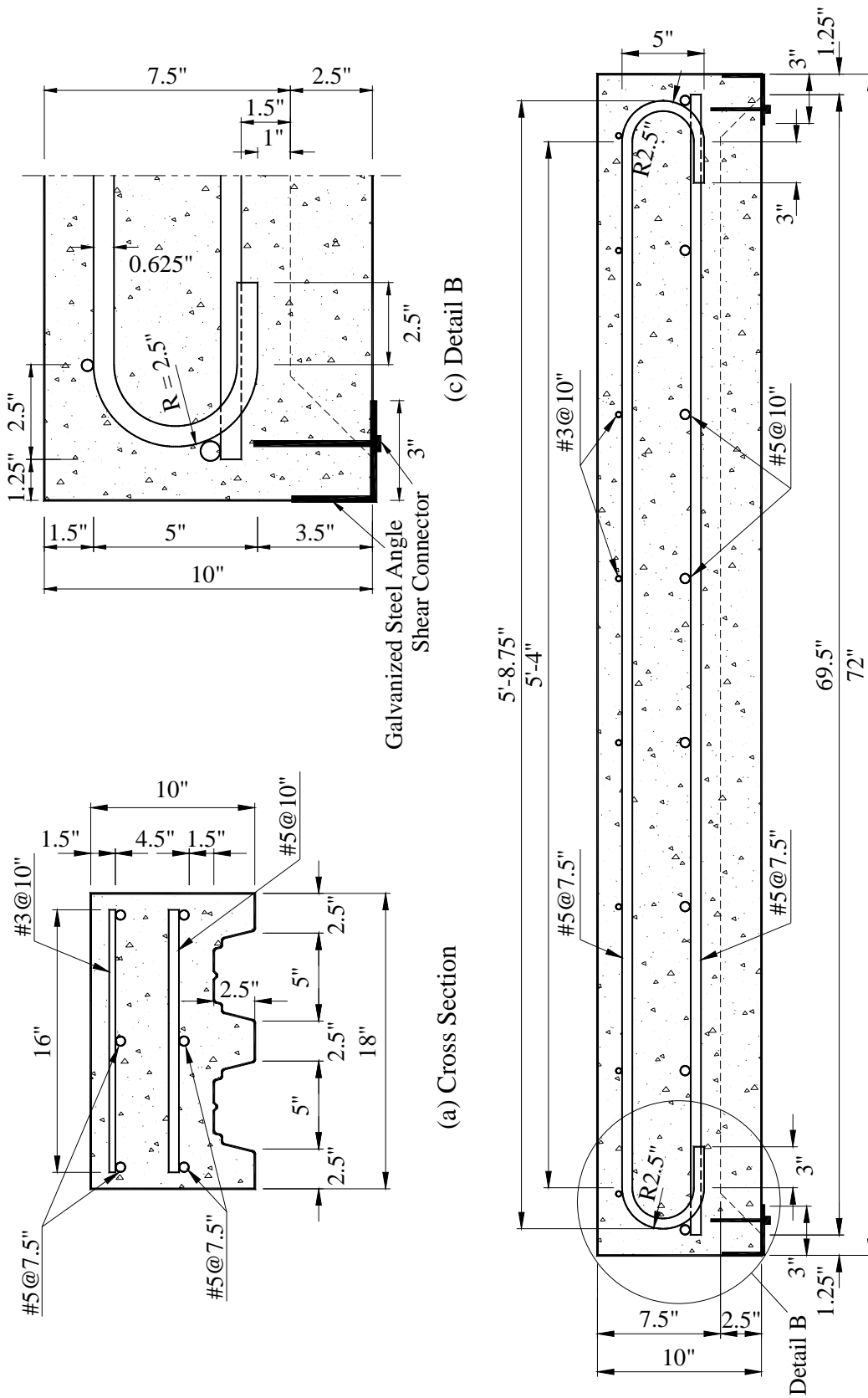


Figure 4.4. Dimensions and reinforcement details for specimens with SIPMF



Figure 4.5. Shear connectors

The reinforcement cages for both types of specimens were identical. The top and bottom longitudinal reinforcement layers consisted of three # 5 epoxy-coated steel bars with center-to-center spacing of 7.5 in. The top transverse reinforcement bars were # 3 epoxy-coated steel bars with 10 in. spacing between the centerlines of the bars. The bottom transverse reinforcement bars were # 5 epoxy-coated steel bars with 10 in. spacing between the centerlines of the bars. The thickness of the clear concrete cover for the longitudinal reinforcement was 1.5 in. for the top and bottom faces, while for the ends the clear cover had a thickness of 1.25 in. The reinforcement details are shown in Figures 4.3 and 4.4. The top longitudinal reinforcement was bent with a radius of 2.5 in. to form a hook to provide sufficient development length. Twenty-four cages were assembled using 0.08 in. diameter epoxy-coated steel wire to tie the reinforcement bars together as shown in Figure 4.6. The bottom and top reinforcement layers were assembled first then tied together to form the cage.



Figure 4.6. Epoxy-coated tying wire

Two hangers were made for each specimen to facilitate the handling of the specimens during environmental exposure testing. A 36 in. long steel cable of zinc-coated 3/16" in. diameter steel cable with a specified working load limit of 840 lb was used for constructing the hangers. The cable was tied to the reinforcement steel bars using the epoxy-coated steel wire (used for tying the reinforcement bars together) as shown in Figure 4.7.

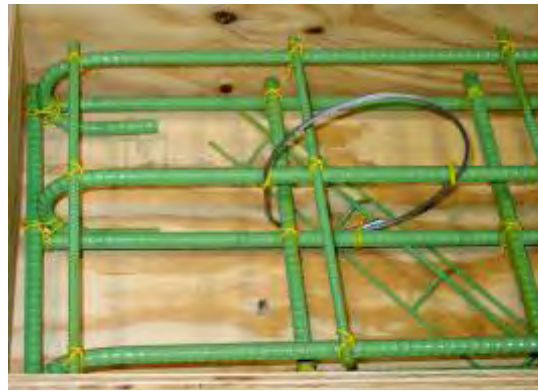


Figure 4.7. Specimen hanger

Epoxy-coated steel chairs were used to maintain the vertical distances for the reinforcement cage (Figure 4.8). Chairs with height of 3.25 in. were used to maintain the distance between the top and bottom reinforcement layers. Chairs of 1.5 in. height were placed under the bottom reinforcement layer to maintain the clear concrete cover. Five chairs were placed inside a form such that 2 were located 90° from the main reinforcement alignment and 3 were located 45° from the main reinforcement alignment.



a. Epoxy-coated steel chairs



b. Chairs inside the form

Figure 4.8. Epoxy-coated steel chairs

Box-shaped forms were made using 0.75 in. thick plywood reinforced with wooden bars with a cross-section of 2.0 in. x 4.0 in. The forms were constructed to have internal dimensions equal to the dimensions of the specimens. For the specimens without SIPMFs, the bottom of the form was made from sheets of plywood as shown in Figure 4.9. For the specimens with SIPMF, the bottom of the form consisted of the SIPMF as shown in Figure 4.10. The concrete from a single ready-mix truck was placed in the 24 forms on the same day. Concrete was compacted inside the forms using mechanical vibrators.



Figure 4.9. Complete forms with the cages (without SIPMF)

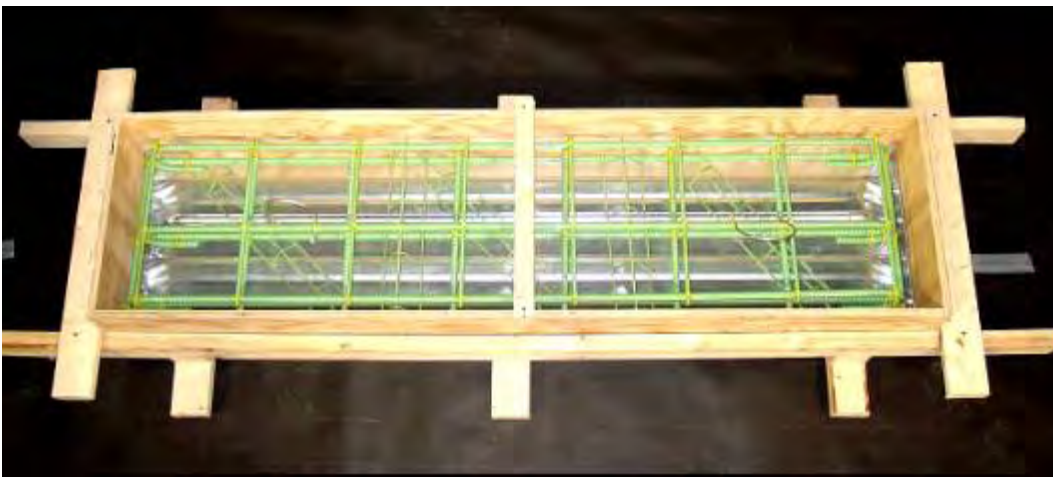


Figure 4.10. Complete forms with the cages (with SIPMF)

In addition, 90 standard size concrete cylinders (6 in. diameter, 12 in. length) were cast from the same batch of concrete according to ASTM C31/ C31M-98.

4.4 ENVIRONMENTAL CONDITIONING

The environmental exposure tests were designed to subject the specimens to conditions that simulate the exposure conditions for bridge deck slabs in Michigan. All specimens were subjected to service load exposure. Four specimens were used as control specimens and the remaining 20 specimens were subjected to the following two categories of environment conditionings: 1) freeze/thaw exposure and repeated load cycles, 2) salt-water exposure and repeated load cycles (Table 4.1 and Figure 4.1).

Specimens were weighed prior to the environmental exposure tests. The weight of the specimens after exposure tests was compared to the initial weight of the specimens to ensure complete drying of the specimens between exposure tests.

4.4.1 Service Load Exposure

The specimens were subjected to service load. This step was used to induce cracking through the entire thickness of the specimens. The loading setup consisted of two types of setup configurations:

Positive moment load setup and negative moment load setup. The positive moment caused cracking in the bottom regions of the specimens whereas the negative moment caused cracking in the top regions of the specimens.

Positive Moment Load Setup

The positive moment load setup consisted of a four-point loading system as shown in Figures 4.11 and 4.12. The distance between the left and right supports was 63.0 in. Each of the left and right loads was equal to half of the total load ($P/2$), and the loads were applied at the third distances of the span L (at $L/3 = 21.0$ in. and at $2*L/3 = 42.0$ in.). The edges of each specimen were 4.5 in. away from the left and right supports.

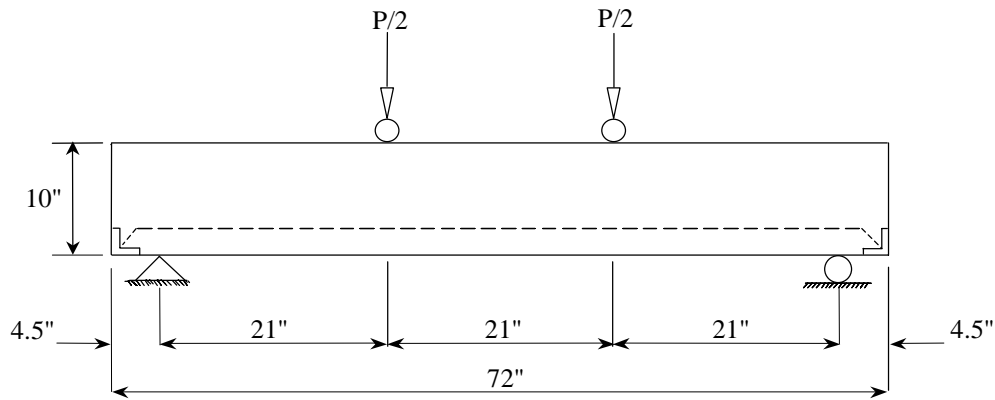


Figure 4.11. Positive moment load setup for specimens with SIPMF

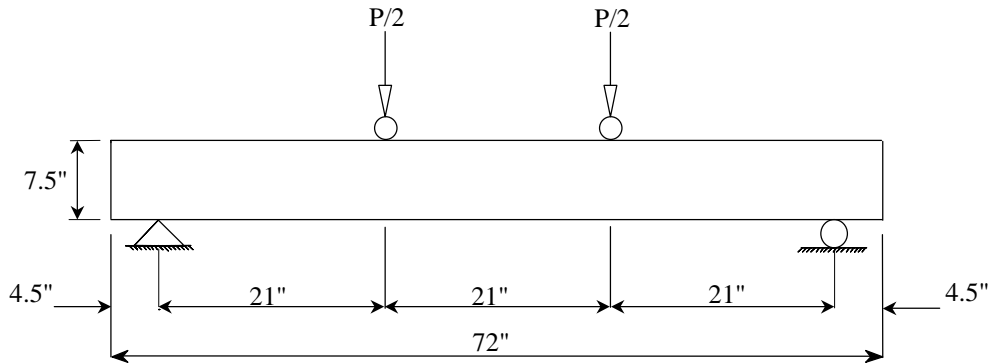


Figure 4.12. Positive moment load setup for specimens without SIPMF

The vertical and horizontal alignments of the load setups were verified prior to initiation of the service load application. Supports for the setup were designed to provide a hinged support on one end and a roller support on the other end of the specimen. Customized contour bearings were fabricated for use with the specimens containing SIPMF. The design of the bearing allowed for good contact between the specimens and the supports (Figure 4.16). Each specimen was instrumented with 2 linear potentiometers at the left and right midspan edges to monitor vertical displacement during a test. Load was applied using a 20 kip actuator. A data acquisition system was used to monitor the load-displacement response of a specimen during a test (Figure 4.13).



a. Actuator applying load on the specimen



b. Controllers and data acquisition

Figure 4.13. Actuators, controllers, and data acquisition

Negative Moment Load Setup

The load setup consisted of an inverted four-point loading system as shown in Figures 4.14 and 4.15. The length of each specimen was 72 in. The loaded span L was equal to 63 in. The left and right supports were separated by a distance of 21 in. and were located at the third points of the span L ($L/3 = 21$ in. and $2*L/3 = 42$ in.). The left and right loads were each equal to half of the total load ($P/2$), and were applied at 4.5 in. away from the left and right edges of the specimens.

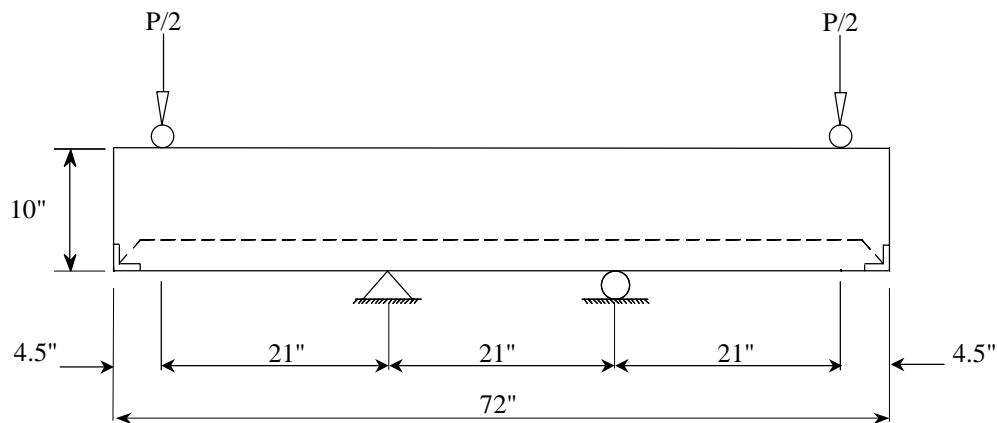


Figure 4.14. Negative moment load setup for specimens with SIPMF

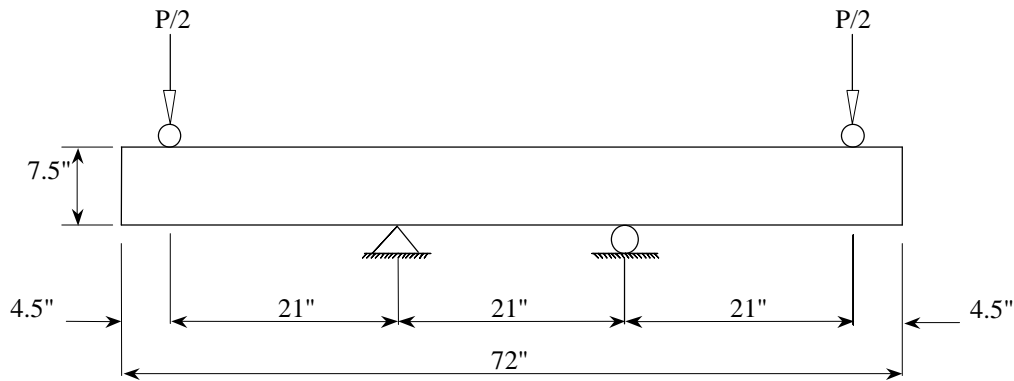


Figure 4.15. Negative moment load setup for specimens without SIPMF

The general specimen setup including supports, instrumentation, and load application system was similar to the positive moment loading setup with the exception of the inverted position of the setup. A photo showing the custom contour bearing for the specimens with SIPMF is presented in Figure 4.16. A photo showing the negative moment loading setup is presented in Figure 4.17.



Figure 4.16. Alignment of the custom fabricated contour bearing underneath the specimen on top of the support



Figure 4.17. Negative moment loading setup

Application of Service Load

Service load application for specimens with SIPMF consists of two steps. Initially, positive moment is applied to the specimens. The load was maintained on a specimen until cracking of the specimen was observed. The load increased with increasing displacement initially, which was followed by constant load with increasing displacement indicating presence of cracking in the specimens (Figure 4.18). Negative moment is applied to the specimens subsequent to observation of cracking during positive moment application. The load was increased on a specimen until full-depth cracks were observed in a specimen (Figure 4.19). A similar procedure was used for specimens without SIPMF (Figures 4.20 and 4.21).



Figure 4.18. Positive moment application
(cracking along the bottom of specimen with SIPMF)



Figure 4.19. Negative moment application
(cracking along the top of specimen with SIPMF)



Figure 4.20. Positive moment application
(cracking along the bottom of specimen without SIPMF)



Figure 4.21. Negative moment application
(cracking along the top of specimen without SIPMF)

A quantitative criterion was developed to determine the initiation and presence of cracks in a specimen using the load-displacement curves obtained in a test. A crack is identified when displacement increased by more than 0.002 in. with no increase in load (Figure 4.22). The example in Figure 4.22 identifies the presence of 3 incidents of cracking in the specimen. Generally, multiple cracks were generated in a specimen during both positive and negative moment stages of load application. Presence of cracks was confirmed visually and by sound.

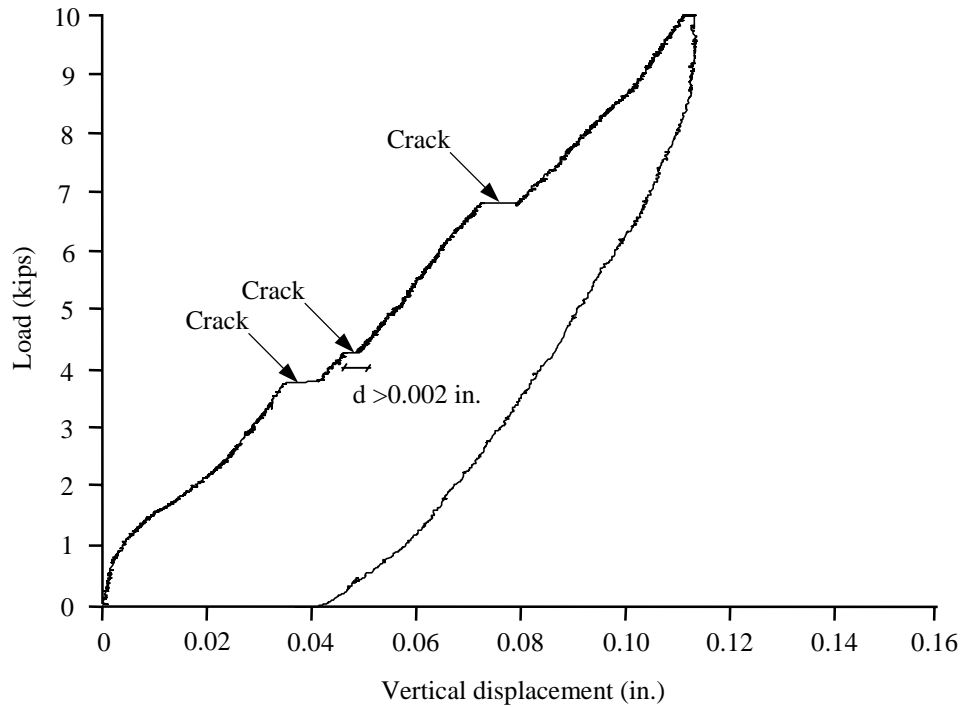


Figure 4.22. Criteria for crack determination

4.4.2 Freeze/Thaw Cycles

Freeze/thaw exposure represents one of the environmental conditions that Michigan bridges are exposed to during their service life. In this test program, eight bridge deck specimens were subjected to freeze/thaw exposure. Four specimens were exposed to 300 freeze/thaw cycles and the remaining four specimens were exposed to 600 freeze/thaw cycles (Table 4.1).

The specimens were subjected to the freeze/thaw cycles in a large (19.5 ft x 11.75 ft x 8.92 ft) walk-in environmental chamber (Figure 4.23). The specimens were placed inside a holding tank in the chamber. The holding tank had dimensions of 6.5ft x 4.0 ft x 5.0 ft and eight specimens could be placed in the tank at a given time.



Figure 4.23. Freeze/Thaw system

Specimens were subjected to freeze/thaw cycles subsequent to initial service load exposure (and resulting cracking of the specimens). Thermocouples were installed in the specimens to monitor the temperature of the specimens during exposure. Most of the specimens were instrumented with 2 thermocouples: one near the corner of the specimen (3 in. x 3 in. x 3 in. from the corner) and one at the center (and mid-depth) of the specimen. The specimens were drilled, then the thermocouples were placed at the specified location, and then they were coated with epoxy. The thermocouples were extended and connected to a data acquisition system located outside of the chamber. All of the 8 freeze/thaw specimens were placed in the holding tank subsequent to installation of the thermocouples (Figure 4.24 and 4.25). The specimens were separated by wooden platforms to allow exposure to the entire surface of each specimen. In addition to the bridge deck specimens, 20 cylinders were placed in the tank for freeze/thaw exposure. Special provisions, such as air ducts and fans above the holding tanks were used to improve circulation of air in the holding tank and thus exposure of the specimens.



a. Custom-designed crane system



b. Moving specimens to holding tank



c. Placement of bridge deck specimens in holding tank



d. Placement of cylinders in holding tank

Figure 4.24. Placement of the 8 freeze/thaw specimens in the holding tank

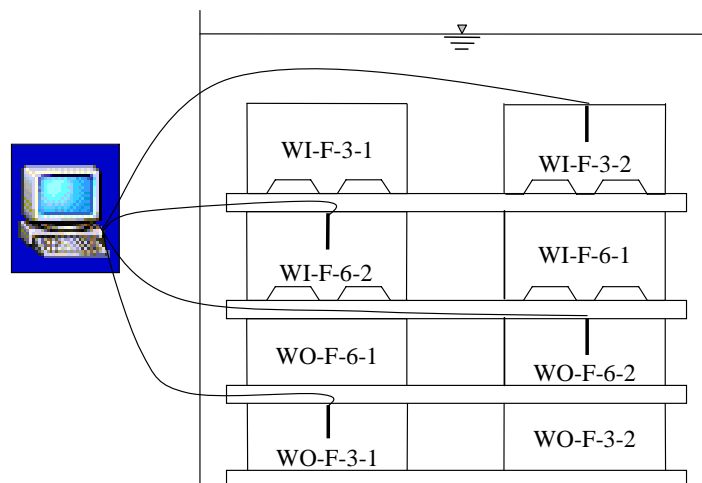


Figure 4.25. Arrangement of specimens in holding tank inside environmental chamber (concrete cylinders not shown for clarity)

The freeze/thaw exposure was applied according to ASTM C666-97 with three deviations. First, the cycle time was increased due to the large size of the specimens. Second, the specimens did not remain completely surrounded by water for the entire duration of the cycles. Third, the specimens were exposed to a temperature of approximately 20-25 °F during the first 190 freezing cycles for cycle durations of 6.5 hr. In the modified procedure, the specimens were subjected to a 3-stage cycle: freezing period, thawing period, and soaking period. The total duration of the freeze/thaw cycles was approximately 7 hr. and 45 min. The freezing period had a duration of approximately 3 hr. and 30 min. and was applied using flowing air, which had temperatures reaching approximately -70 °F. The thawing period of the cycle had a duration of approximately 3 hr. and was applied using flowing air, which had temperatures reaching approximately 145 °F. The soaking period of the cycle had a duration of approximately 1 hr. 30 min. and consisted of soaking the specimens by immersion in the water at a temperature of approximately 42 °F. Exact durations of the freezing and thawing periods were controlled to induce internal temperatures of the specimens of 0°F and 40°F for freezing and thawing, respectively. The variations of temperatures with time during the modified freeze/thaw test procedure are provided in Figure 4.26.

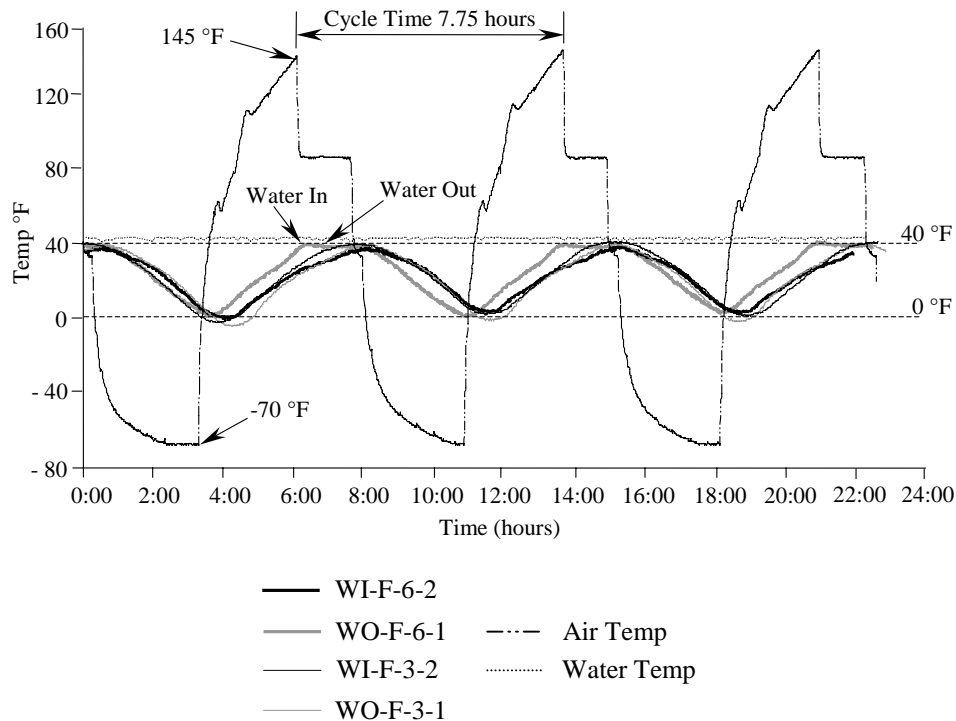


Figure 4.26. Temperature variations for freeze/thaw cycles (for 300- and 600-cycle specimens)

All of the bridge deck specimens were removed from the holding tank subsequent to exposure to 300 freeze/thaw cycles. All 8 specimens were then subjected to 250,000 repeated load cycles. The repeated load cycles are described in detail in Section 4.4.4. The quality of bond between the bridge deck specimens and the SIPMF was determined for the 4 specimens with SIPMF using ultrasonic pulse-echo testing. A slice with 3 in. thickness was cut from the long edge of each 300-cycle freeze/thaw specimen, and ultrasonic through-transmission testing was used on the slices to determine the quality of the concrete. The 300-cycle freeze/thaw specimens were then subjected to ultimate load test. Ten concrete cylinders were tested for compressive strength according to ASTM C39/ C39M-99 at the same time as the ultimate load tests were conducted.

The remaining freeze/thaw specimens were returned to the holding tank (Figure 4.27). These specimens were subjected to an additional 300 freeze/thaw cycles (Figure 4.28). The 4 bridge deck specimens were removed from the holding tank subsequent to these cycles. All 4 specimens were then subjected to 250,000 repeated load cycles, and pulse echo testing was used for the 2 specimens with SIPMF. A slice with 3 in. thickness was cut from the long edge of each 600-cycle freeze/thaw specimen, and ultrasonic through-transmission testing was used on the slices. Finally, the specimens were subjected to ultimate load test. The remaining concrete cylinders were tested for compressive strength according to ASTM C39/ C39M-99 at the same time the ultimate load tests were conducted.

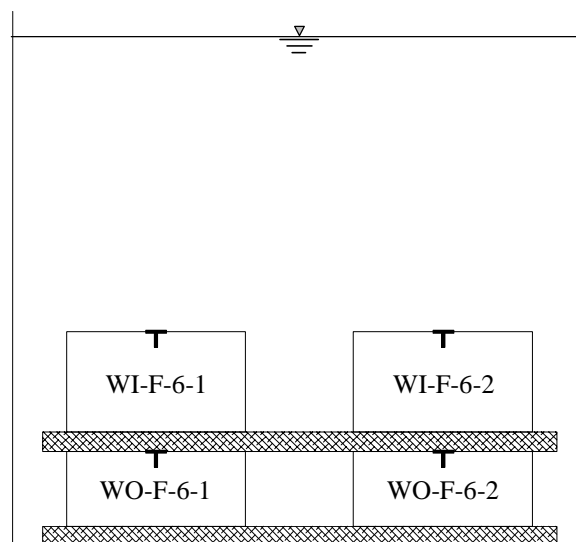


Figure 4.27. Holding tank inside the environmental chamber with the 600-cycle freeze/thaw specimens

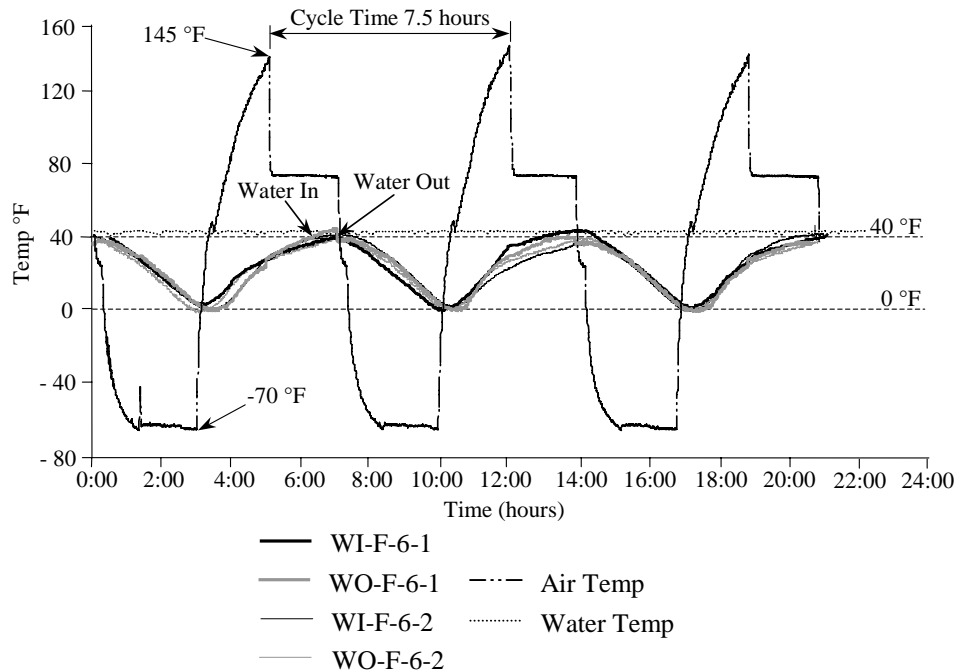


Figure 4.28. Temperature variations for freeze/thaw cycles (for 600- cycle specimens)

4.4.3 Salt-Water Exposure

Salt is used as deicing material in winter months on bridges in Michigan. In this test program, 12 bridge deck specimens were exposed to salt-water: Four specimens were subjected to 1,000 hours of salt-water exposure, four specimens were subjected to 3,000 hours of salt-water exposure, and four specimens were subjected to 10,000 hrs of salt-water exposure.

The salt used contained primarily NaCl in addition to other ions (Appendix C). The salt was mixed with the water to obtain a specific gravity of approximately 1.025. The consistency of the salt solution concentration was monitored indirectly by measuring the specific gravity of the solution, which was maintained at 1.025 ± 0.005 throughout the test program.

Specimens were exposed to salt-water in 2 tanks (A and B), each of which held 6 specimens at a given time. The holding tanks had dimensions of 10.0 ft x 4.0 ft x 4.0 ft. The specimens in a single tank were separated using wooden platforms to allow exposure to the entire surface of each specimen. In addition to the bridge deck specimens, 30 concrete cylinders were placed in the tanks for 1,000-, 3,000-, and 10,000-hours of salt-water exposure, each in

groups of 10 (Figures 4.29 and 4.30). The salt solution was added to the tanks to entirely cover all of the specimens. Submersible pumps were used in the tanks to promote circulation and air pumps were used to maintain adequate levels of oxygen in the solution. Plastic tarps were placed over the tanks to prohibit growth of algae. The specific gravity and the temperature of the solution were weekly measured during the test program.

Specimens WI-S-1-1, WI-S-1-2, WO-S-1-1, and WO-S-1-2 were exposed to salt-water for 1,000 hours. Subsequently, the specimens were removed from the salt-water solution and subjected to 250,000 cycles of repeated load. Ultrasonic pulse-echo tests were conducted on the 2 specimens with SIPMF. A slice with 3 in. thickness was cut from the long edge of each specimen, and ultrasonic through-transmission tests were used on these slices. Finally, the 4 specimens were tested for ultimate load. Ten concrete cylinders were similarly subjected to 1,000 hours of salt-water exposure and then were tested for compressive strength at the same time ultimate load tests were conducted.

Specimens WI-S-3-1, WI-S-3-2, WO-S-3-1, and WO-S-3-2 were exposed to salt-water for 1,000 hours. Subsequently, the specimens were removed from the salt-water solution and subjected to the first 250,000 cycles of repeated load. Ultrasonic pulse-echo tests were conducted on 2 specimens with SIPMF. All of the specimens were returned to salt-water and subjected to the remaining 2,000 hours of exposure. At the end of the 2,000 hours in salt-water solution, specimens were removed from the solution and subjected to the second 250,000 cycles of repeated load. Ultrasonic pulse-echo tests were conducted on the 2 specimens with SIPMF. A slice with 3 in. thickness was cut from the long edge of each specimen, and ultrasonic through-transmission tests were conducted on these slices. Finally, the 4 specimens were tested for ultimate load. Ten concrete cylinders were similarly subjected to a total of 3,000 hours of salt-water exposure and then were tested for compressive strength at the same time ultimate load tests were conducted.



a. Placement of specimens and cylinders in the tank



b. Final arrangement of specimens before filling tank with salt-water



c. Specimens in tank after filling with salt-water

Figure 4.29. Placement of specimens inside salt-water tanks

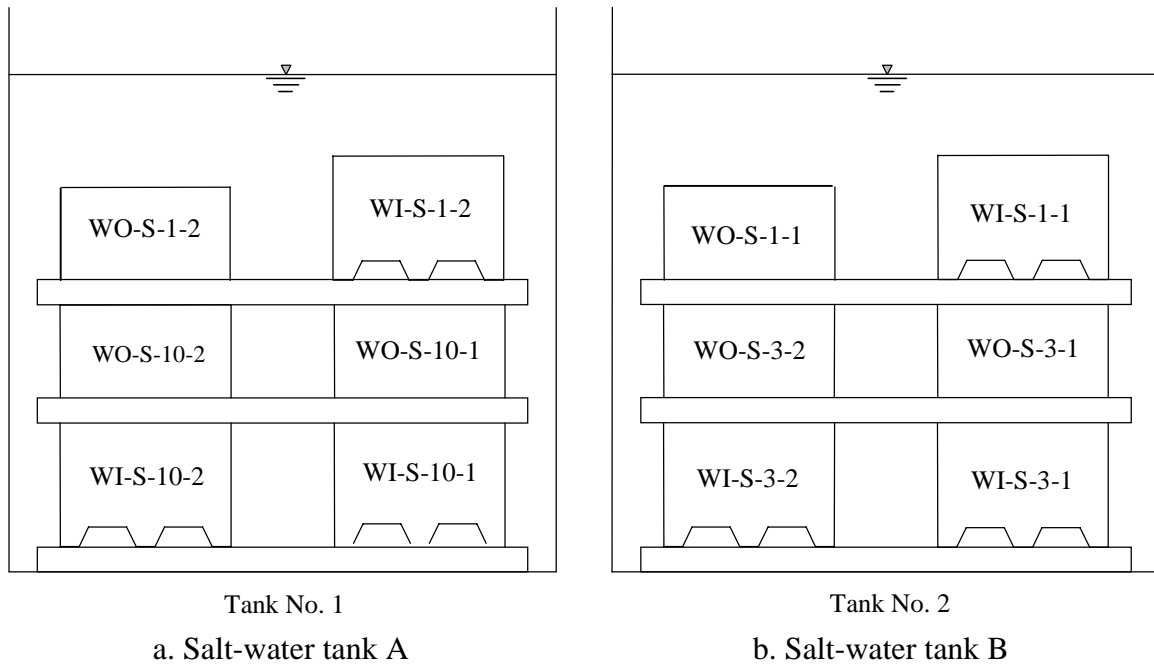


Figure 4.30. Arrangement of salt-water exposure specimens

Specimens WI-S-10-1, WI-S-10-2, WO-S-10-1, and WO-S-10-2 were exposed to salt-water for 1,000 hours. Subsequently, the specimens were removed from the salt-water solution and were subjected to the first 250,000 cycles of repeated load. Ultrasonic pulse-echo tests were conducted on 2 specimens with SIPMF. All of the specimens were returned to the salt-water and subjected to an additional 2,000 hours of exposure. At the end of the 2,000 hours in salt-water solution, specimens were removed from the salt-water solution and subjected to the second 250,000 cycles of repeated load. Ultrasonic pulse-echo tests were conducted on the 2 specimens with SIPMF. The specimens were returned to the tank to be subjected to an additional 7,000 hours in salt-water solution. At the end of the 7,000 hours, specimens were removed from the solution and were subjected to the third 250,000 cycles of repeated load. Ultrasonic pulse-echo tests were conducted on the 2 specimens with SIPMF. A slice with 3 in. thickness was cut from the long edge of each specimen, and ultrasonic through-transmission tests were conducted on these slices. Finally, the 4 specimens were tested for ultimate load. Ten concrete cylinders were similarly subjected to 10,000 total hours of salt-water exposure and then were tested for compressive strength at the same time ultimate load tests were conducted.

4.4.4 Repeated Load Cycles

Repeated load cycles represent live loads that act on bridge decks. In this test program, repeated loads were applied in intervals of 250,000 cycles at a time. Repeated load cycles were used in combination with either freeze/thaw exposure or salt-water exposure tests.

Repeated load cycles were applied with a frequency of 3.5 Hz. The amplitudes of the repeated loads were determined using ultimate load tests conducted on reference specimens. The ultimate load for the specimen with SIPMF was 42 kips and the value of the ultimate load for the specimen without SIPMF was 34.5 kips (Figures 4.31 and 4.32).

The amplitude of the cyclic load was taken as 25% of the ultimate load obtained using reference specimens. This corresponded to load amplitudes of 10.5 kips and 8.5 kips for specimens with and without SIPMF, respectively. A minimum load of 2.5 kips was maintained during the tests (which is presenting a minimum load applied on bridge deck slabs) and the upper limits of applied load were 13 kips and 11 kips for specimens with and without SIPMF, respectively (Figure 4.35).

The negative moment load setup was used for the repeated load exposure tests, which was “TW” (negative moment) for specimens with SIPMF (Figure 4.33a) and was “T” (negative moment) for specimens without SIPMF (Figure 4.34a). A specimen with SIPMF under repeated load exposure is shown in Figure 4.33b, and a specimen without SIPMF under repeated load exposure is shown in Figure 4.34b. The diagram for cycles of repeated load for specimens with SIPMF is shown in Figure 4.35a, and the diagram for cycles of repeated load for specimens without SIPMF is shown in Figure 4.35b.

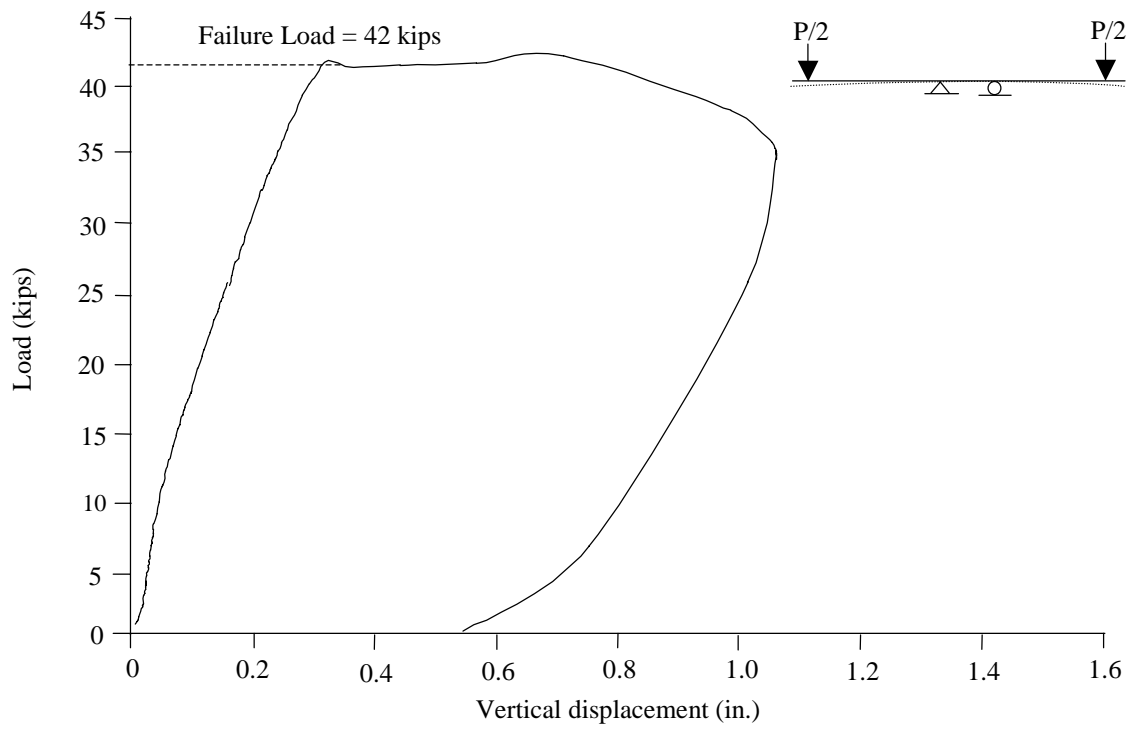


Figure 4.31. Load-displacement curve for reference specimen with SIPMF

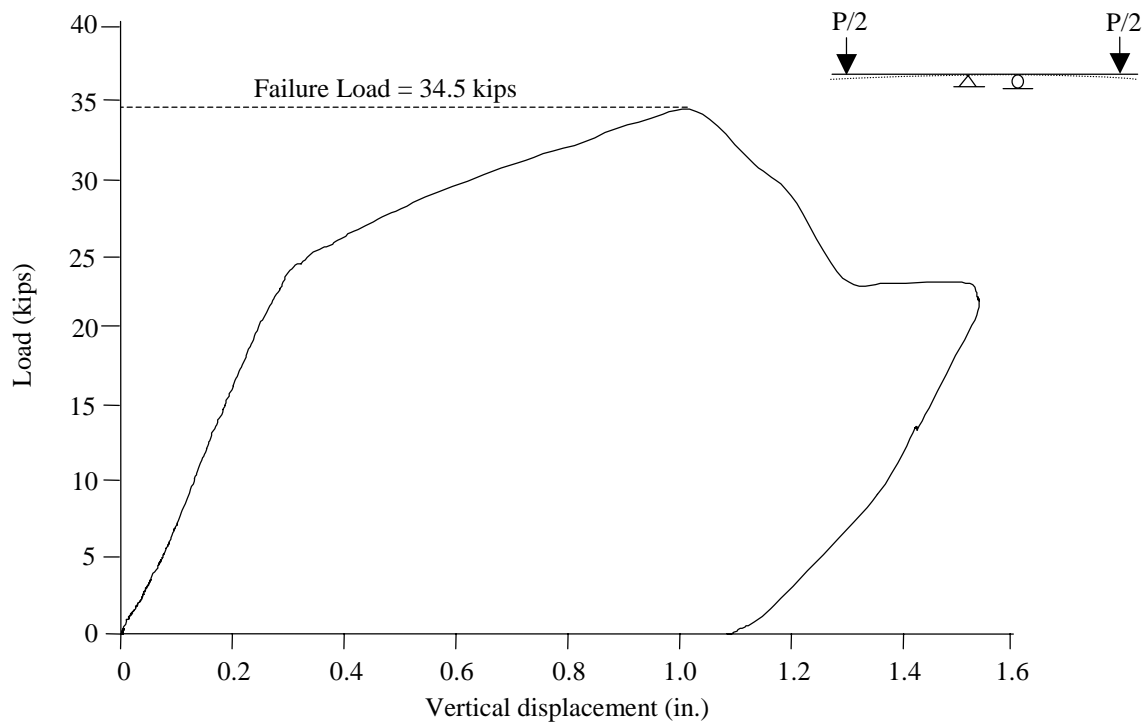


Figure 4.32. Load-displacement curve for reference specimen without SIPMF

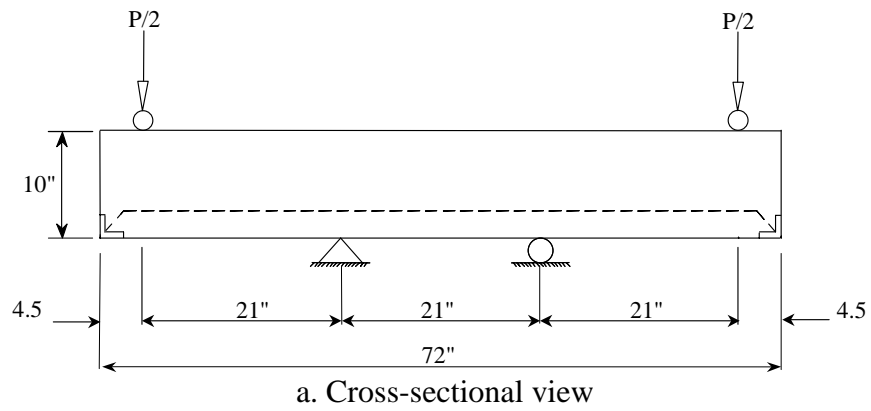


Figure 4.33. Repeated load for specimen with SIPMF

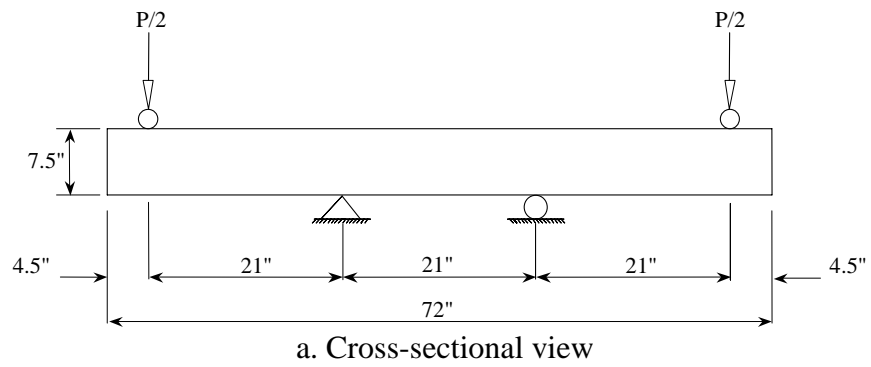
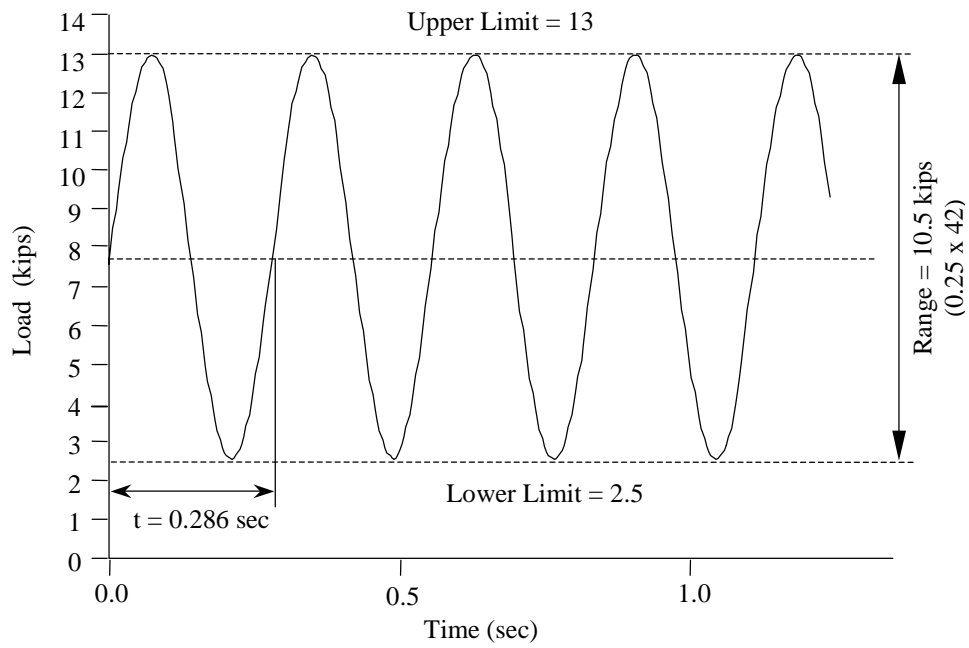
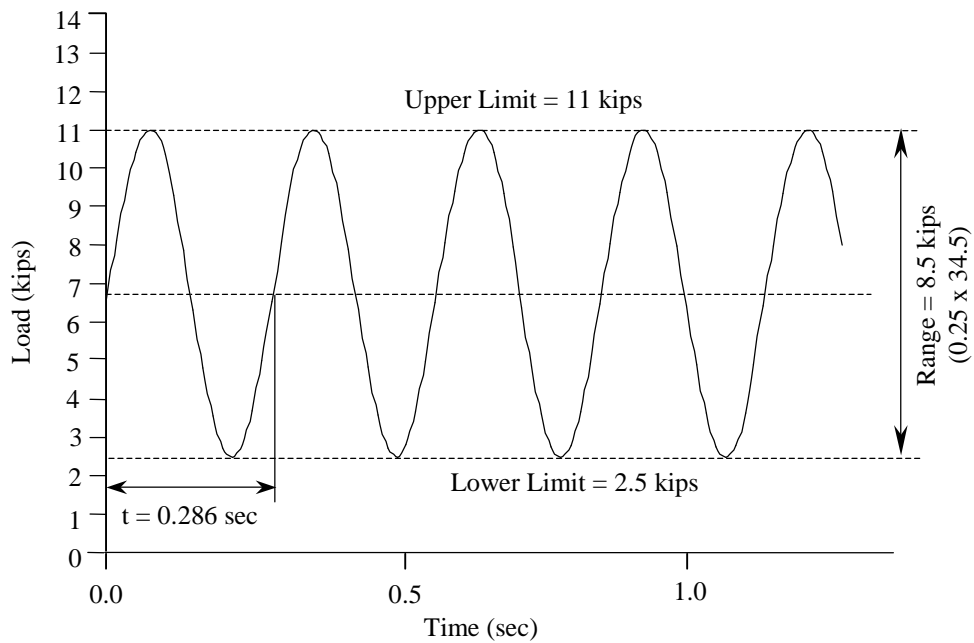


Figure 4.34. Repeated load for specimen without SIPMF



a. Specimen with SIPMF



b. Specimen without SIPMF

Figure 4.35. Diagram for repeated load cycles

4.5 ULTRASONIC TESTS

4.5.1 Pulse-Echo

Ultrasonic pulse-echo tests were used to evaluate the contact between the SIPMF and the concrete deck. The tests were used to assess the bond between the SIPMF and the concrete and to evaluate the effects of the environmental exposure conditions on the quality of contact between the SIPMF and concrete deck.

Description of the Method

Tests were conducted using a setup that consisted on an ultrasonic transducer, a pulser-receiver, and a digital oscilloscope. A 2.25-MHz-center frequency broadband transducer was used in the tests. A delay line (plastic spacer) was attached to the transducer for the tests. The delay line was used to improve the nearfield resolution through the thin SIPMF. A high-gain, low-noise broadband (10 MHz) pulser-receiver with a signal repetition rate of 20 Hz is used to excite the transducer and send waves to the test material and also to receive the reflections from the test material. The digital oscilloscope was used to view the waveforms and also to obtain a digital record of the waveforms for further processing. The tests were conducted using the following settings on the pulser-receiver (Table 4.2). The settings were kept constant throughout the test program to ensure consistency of the measured waveforms.

Table 4.2. Equipment settings for pulse-echo tests

Parameter	Setting
Repetition Rate (Hz)	20
Damping (Ω)	50
Pulse height	Variable
Attenuator Left (dB)	0
Attenuator Right (dB)	1
High Pass Filter (MHz)	0.1
Low Pass Filter (MHz)	Out
Vernier (dB)	0
Gain (dB)	40
Phase	Normal (0°)

A test is conducted by placing the transducer on the SIPMF on the underside of a bridge deck specimen and then sending and receiving waves at the measurement location. The transducer is used to both send and receive the waves. A couplant is placed between the transducer and SIPMF to ensure full transmission of the waves into the test material (Figure 4.36). Each measurement consisted of the average of 10 waveforms obtained at a time. Grids were drawn on the test specimens to mark the measurement locations (Figure 4.37). The grid was divided into 64 segments with 1-in. spacing along the length of the specimen. The grid was divided into 11 segments following the contour of the SIPMF along the width of a specimen as following: one segment at each of the 3 ribs, one segment at each of the 4 slopes, and 2 segments at the 2 flat areas (Figure 4.37). The transverse gridlines were labeled 1 through 64 and the longitudinal gridlines were labeled A through K. The grid contained a total of 704 measurement points at the intersections of transverse and longitudinal gridlines.

A custom-built transducer holder was used in the tests (Figure 4.38). Contact pressure between the transducer and the SIPMF can affect the transmission of waveforms into the test materials. This is particularly a concern when the amplitude measurements are conducted on the waveforms. The transducer holder has a spring-loaded mechanism that allows for application of a constant pressure to the test material at each measurement location. In addition, the holder is designed to ensure perpendicularity of the transducer to the SIPMF. The angle of incidence can also affect the transmission of waveforms into the test material. The holder allows for maintaining a constant incidence angle at each measurement location. The holder also eliminates operator variability in the pulse-echo tests.

Data Analysis

Wave transmission and reflection occurs when an incident wave encounters a boundary between materials. The relative proportions of transmission and reflection depend on the acoustic properties (namely, acoustic impedance) of the materials at the boundary. It is possible to distinguish the type of materials at a boundary by quantifying the amplitude of reflected waves at the boundary. The waveforms generated in a specimen as a result of a single excitation of the transducer are presented in Figure 4.39. In this arrangement, wave transmission and reflection

occur at the two boundaries: between delay line and SIPMF and between SIPMF and concrete. The amplitude of the waveforms received in this arrangement depends on the quality of contact at these two boundaries. Since the specimen holder applies a constant pressure and the same type of couplant (gel type) was used in all of the tests, the contact in the transducer-SIPMF boundary was essentially constant throughout the test program. In contrast, various factors can affect the contact between SIPMF and concrete and the contact at this boundary varies in the test program. A data analysis procedure was used to quantify the quality of contact at this boundary. A typical waveform obtained in the tests is presented in Figure 4.40.

Low transmission and high reflection occur at the SIPMF-concrete boundary when poor contact (e.g., air gaps) is present between the two materials. High transmission and low reflection occur at the SIPMF-concrete boundary when good contact is present between the two materials. Typical waveforms obtained for poor and good contact conditions are presented in Figure 4.41. The conditions at the SIPMF-concrete boundary are quantified by determining the area under the reflections obtained from this boundary in a waveform. The area is determined in the zone of interest (Figure 4.40), and is termed waveform area. The waveform in this region is divided into segments that are $0.04 \mu\text{s}$ apart and the area is calculated by multiplying $8.92 \mu\text{s}$ by the average absolute value of the amplitude of the waveform in this interval (Figure 4.42).

Baseline values of waveform area for poor contact were established by obtaining ultrasonic measurements on a stand-alone SIPMF (not connected to concrete). This extreme condition represented SIPMF-air boundary, which is expected to occur when the concrete separates entirely from the SIPMF. Measurements from 100 locations were quantified to provide the baseline values for poor contact. The statistical analysis for establishing the baseline values is presented in Figure 4.43. The threshold value of waveform areas for poor contact was set at $18.8 \text{ mV-}\mu\text{s}$, which corresponds to 2 standard deviations below the mean of the baseline measurements.

Similarly, an analysis was conducted to establish baseline values of waveform area for good contact between SIPMF and concrete. This was done by conducting measurements on samples specifically prepared for this analysis. The quality of bond between the SIPMF and concrete in these forms was verified using conventional sounding techniques. Special care was

taken in the preparation of the specimens to ensure good contact between the SIPMF and concrete. Measurements from 100 locations were quantified to provide the baseline values for good contact. The statistical analysis for establishing the baseline values is presented in Figure 4.44. The threshold value of waveform areas for good contact was set at 11.6 mV- μ s, which corresponds to 2 standard deviations above the mean of the baseline measurements.

Overall, waveform area measurements above 18.8 mV- μ s indicate poor contact, waveform area measurements between 11.6 and 18.8 mV- μ s indicate fair contact, and waveform area measurements below 11.6 mV- μ s indicate good contact. The validity of the threshold values was monitored throughout the test program. An example of an analysis of a bridge deck specimen is presented in Figure 4.45. The ultrasonic measurements conducted on 704 points on a grid are used to generate a contour map of the quality of contact between SIPMF and concrete. The comparison of measured waveform area values with threshold values is automated in the analysis. The contour maps were further analyzed by determining the relative proportion of the locations with varying levels of contact (Figure 4.46). This analysis was used throughout the test program to monitor the changes occurring in SIPMF-concrete contact due to various exposure mechanisms.

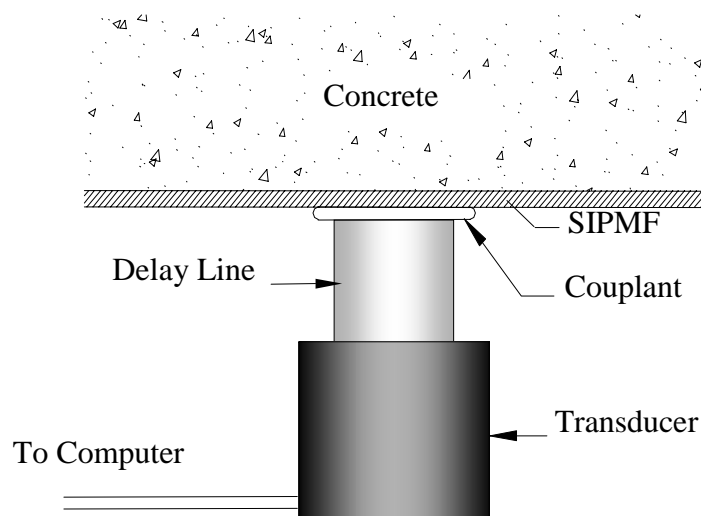


Figure 4.36. Ultrasonic pulse-echo test setup



Figure 4.37. Grid for ultrasonic pulse-echo measurements for specimens with SIPMF



a. Transducer unit



b. Close-up of transducer holder



c. Use of transducer holder in tests

Figure 4.38. Pulse-echo method

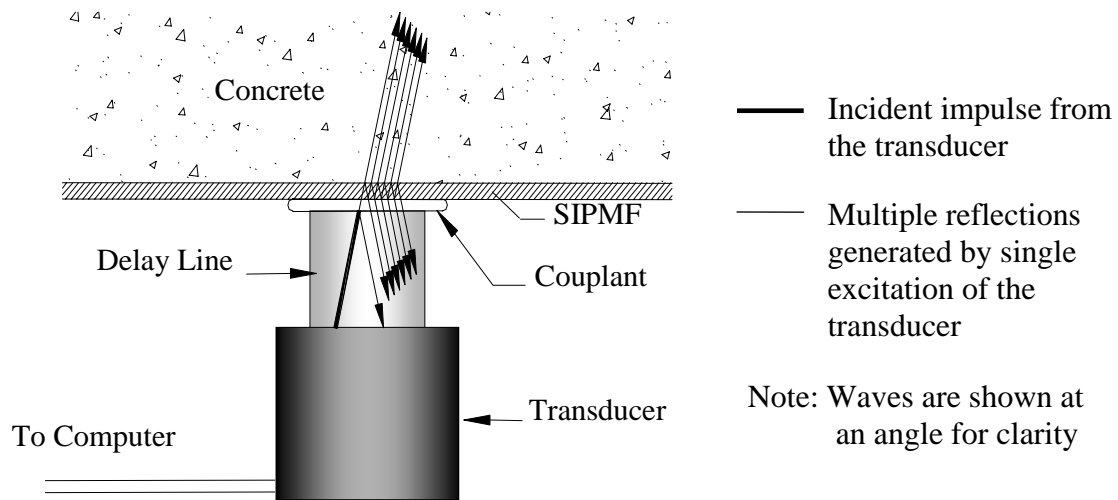


Figure 4.39. Transmission and reflections at boundaries (from Yesiller and Sungur, 2001)

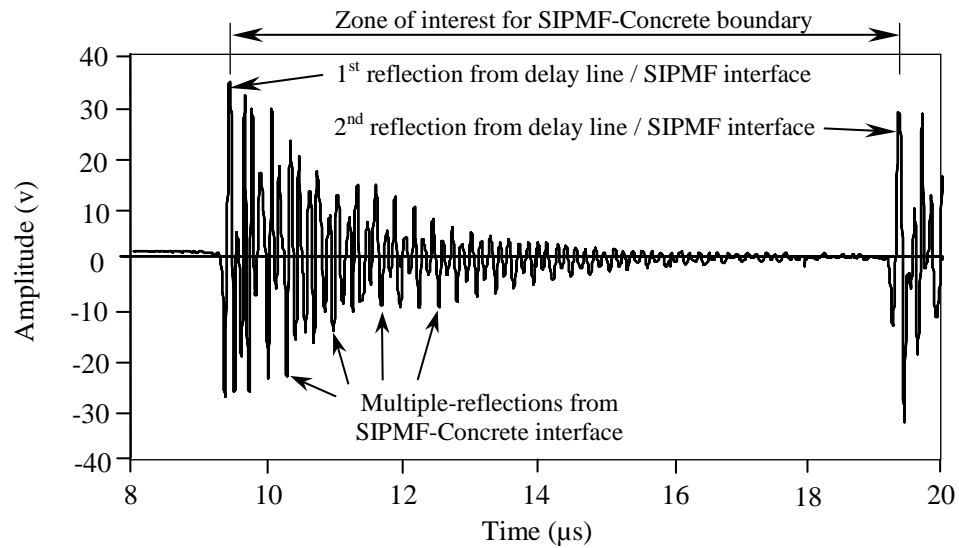
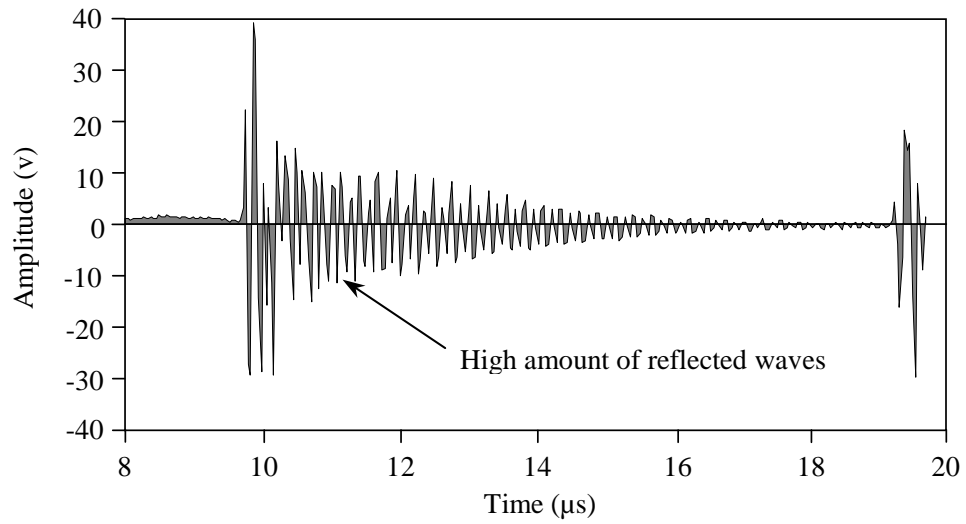
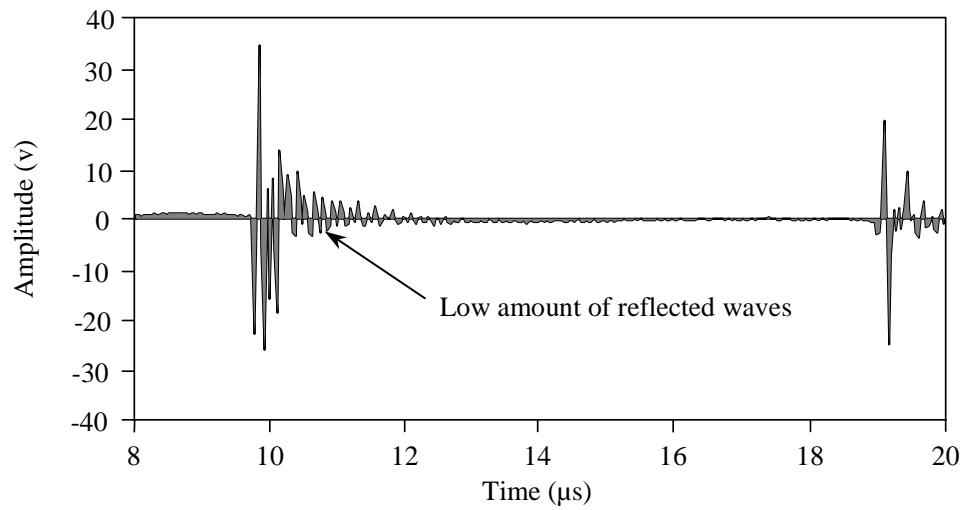


Figure 4.40. Ultrasonic waveform from pulse-echo test



a. Poor contact



b. Good contact

Figure 4.41. Typical waveforms for poor and good contact

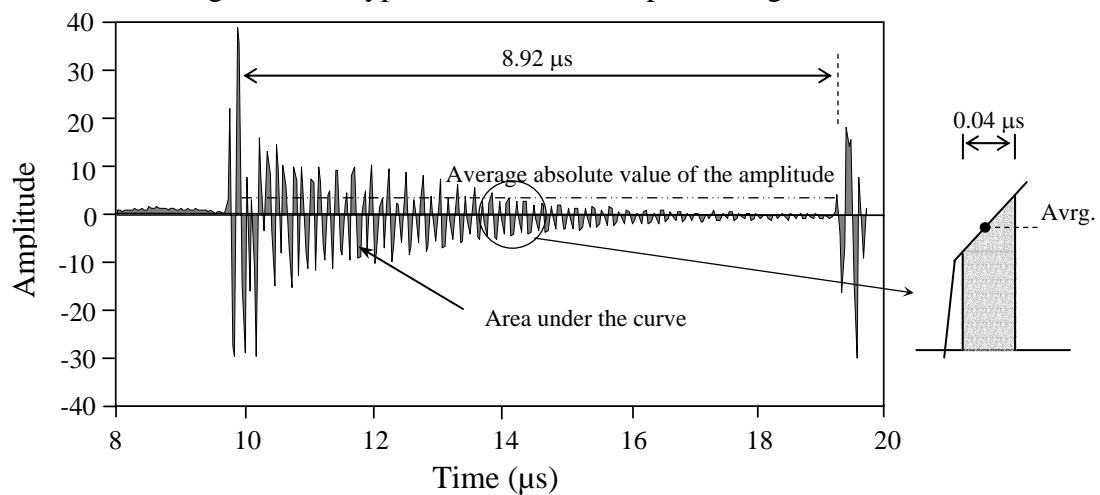


Figure 4.42. Pulse echo calculation

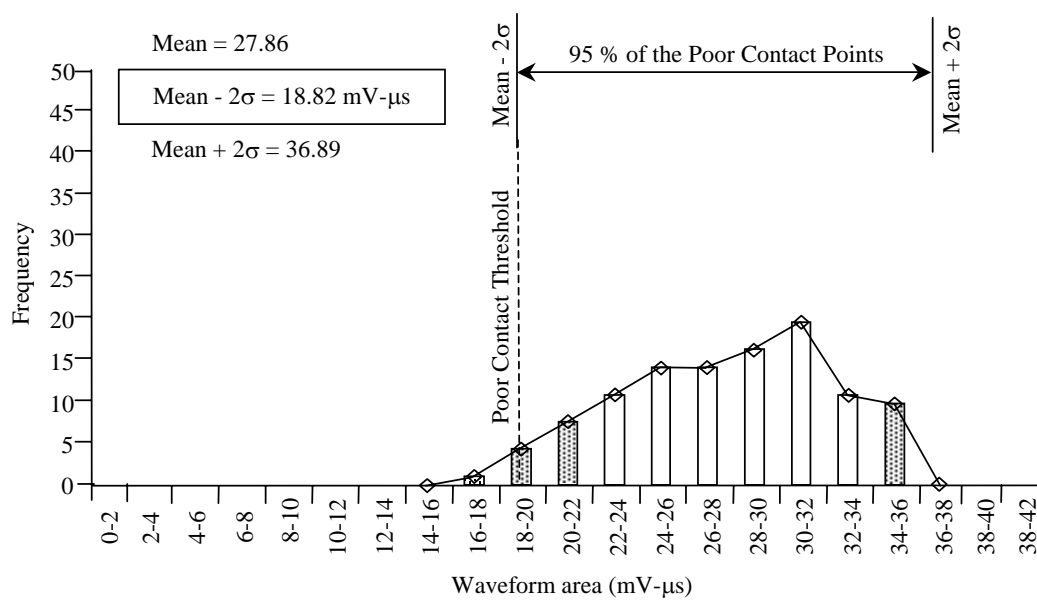


Figure 4.43. Statistical analysis for poor contact criteria

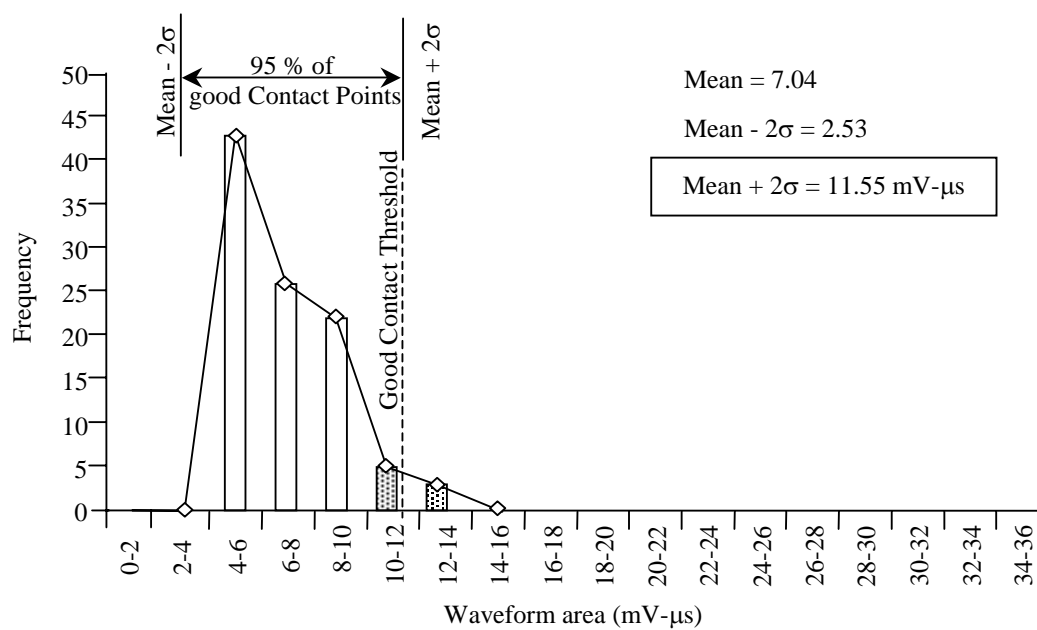


Figure 4.44. Statistical analysis for good contact criteria

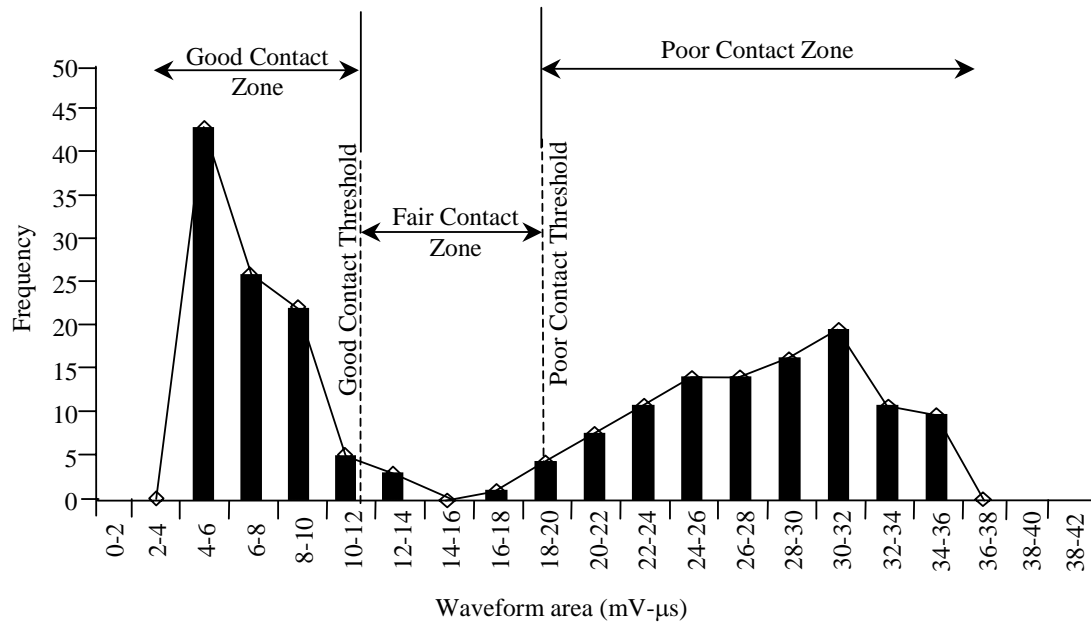


Figure 4.45. Statistical analysis for good and poor contact criteria

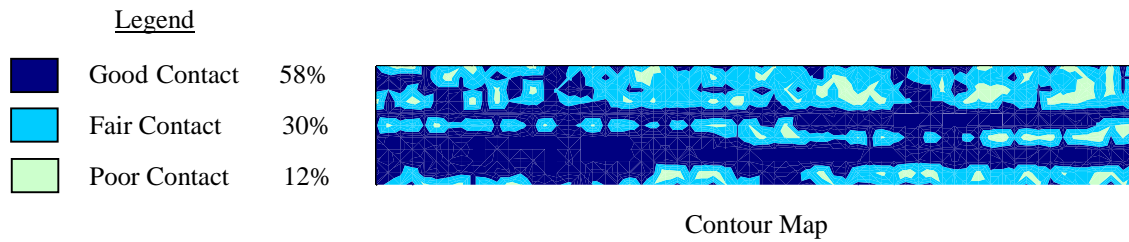


Figure 4.46. Typical pulse-echo analysis of a specimen

4.5.2 Through-Transmission

Ultrasonic through-transmission technique was used in the test program to evaluate the quality and condition of the concrete in the bridge deck specimens. The tests were used to evaluate the effects of the environmental exposure conditions on the quality of the concrete (Figure 4.47).



a. Transducers



b. Through-transmission test setup



c. Through-transmission measurements apparatus

Figure 4.47. Transducers and testing setup

Description of the Method

Tests were conducted using a setup that consisted of 2 transducers, a pulser-receiver, and a digital oscilloscope. Two 100-kHz-center frequency narrowband transducers were used in the

tests. The low frequency of the transducers was selected to investigate concrete, which is a high attenuation material. The pulser-receiver and the oscilloscope were the same devices that were used in the pulse-echo tests. The pulser-receiver has a high-voltage pulser and a high-gain receiver, which are appropriate for testing high attenuation materials. The tests were conducted using the following settings on the pulser-receiver (Table 4.3). The settings were kept constant throughout the test program to ensure consistency of the measured waveforms.

Table 4.3. Equipment settings for through-transmission tests

Parameter	Setting
Repetition Rate (Hz)	20
Damping (Ω)	50
Pulse height	400
Attenuator Left (dB)	0
Attenuator Right (dB)	0
High Pass Filter (MHz)	0.03
Low Pass Filter (MHz)	1
Vernier (dB)	0
Gain (dB)	40
Phase	Normal (0°)

A through-transmission test is conducted by placing one transducer on one surface of a test material and the second transducer on the opposite surface of the test material (directly across from the first transducer) (Figure 4.48). In this arrangement, one transducer is used to transmit waves and the other transducer is used to receive the transmitted waves. Each measurement consisted of the average of 10 waveforms obtained at a time. Tests were conducted on bridge deck specimens subsequent to exposure tests. A 3 in. wide section was cut from the long edge of specimens prior to ultimate load tests to conduct the ultrasonic through-transmission tests (Figure 4.49). These slices had dimensions of 72.0 in. length, 3.0 in. width, and 7.5 in. depth for specimens without SIPMF and 10.0 in. depth for specimens with SIPMF.

Grids were constructed on side surfaces of each slice to mark the measurement locations (Figure 4.50). The grid was divided into 41 segments with 1.75 in. spacing along the length of the specimen. The grid was divided into 4 segments with 1.75 in. spacing along the depth of a

specimen. The transverse gridlines were labeled 1 through 41 and the longitudinal gridlines were labeled A through D. The grid contained a total of 164 measurement points at the intersections of transverse and longitudinal gridlines.

A custom-built micrometer was used to measure the distance between the transducers (i.e., thickness of a slice) at each measurement location. The micrometer had a 0.001 in. resolution (Figure 4.51). The tests were conducted using a custom-designed and built transducer guide setup (Figure 4.52). The setup was designed to fully align the transducers on both sides of a specimen and also to apply constant pressure to the transducers. Misalignment of transducers across a test materials and variations in pressure applied to the transducers can affect transmission of waves and thus results obtained in a test program. The guide setup allowed for maintaining full alignment and constant pressure at each measurement location (Figure 4.53).

Data Analysis

Through-transmission tests were used to determine ultrasonic pulse velocity in the test program. The velocity was determined as the quotient of travel distance to travel time of waves. Ultrasonic pulse velocity has commonly been used for concrete in the past. Propagation of ultrasonic waves is correlated to mechanical properties of test materials, including concrete. Qualitative correlations have been established between pulse velocity and quality of concrete (*Krautkramer and Krautkramer, 1990, Table 4.3*), which were linked with the Young's modulus, but not completely.

In the tests on slices from bridge deck specimens, the travel distances for the waves were determined using mechanical measurements (micrometer thickness measurements on slices) and travel time for waves as determined using the ultrasonic tests. A typical waveform obtained in the through-transmission tests is presented in Figure 4.54. The resolution of the time measurements was 0.04 μs (based on an adaptation of Taylor's Theorem to the propagation of uncertainty, the maximum error in pulse velocity calculations was 1.2%). The travel time for the waves corresponds to the arrival time shown in the figure. Arrival time was identified as the first major deviation in the amplitude of a waveform (on an amplitude vs. time record) using statistical analysis. The details for the analysis procedure are presented in Appendix B. A

computer program that was written to determine the arrival times based on the detailed statistical analysis is also presented in Appendix B. The ultrasonic velocity of the wave through the concrete was calculated for each point on the grid using the calculated arrival time and the measured thickness. Contour maps were further analyzed by determining the proportion of the locations with varying levels of velocity (concrete quality) (Figure 4.55).

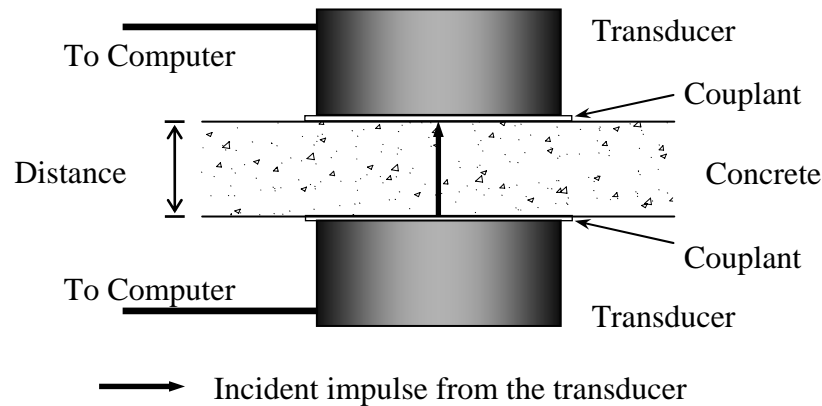


Figure 4.48. Through-transmission technique



a. Cutting a 3 in. slice



b. Partially cut slice

Figure 4.49. Removal of slices from bridge deck specimens



a. Grid on slice from specimen with SIPMF



b. Grid on slice from specimen without SIPMF

Figure 4.50. Grids for through-transmission tests

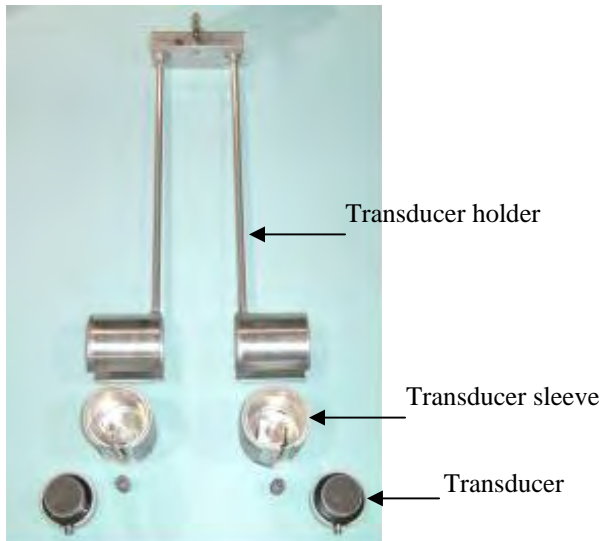


a. Custom-made micrometer



b. Measuring thickness at a measurement location on a slice

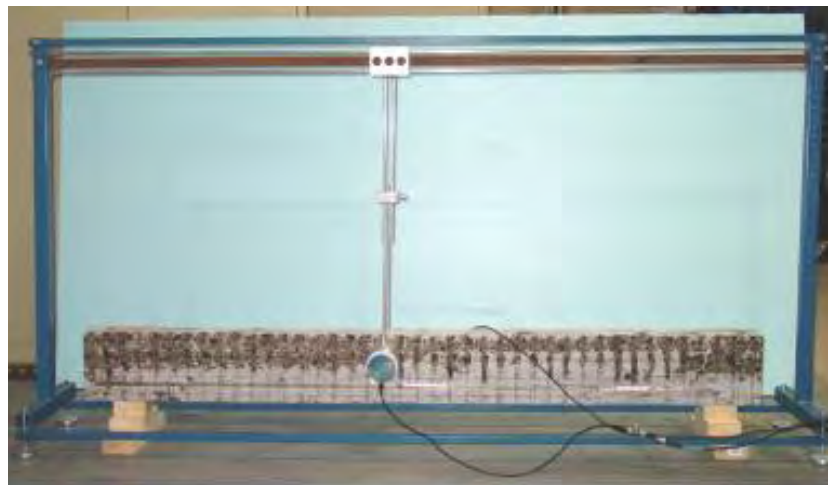
Figure 4.51. Thickness measurement



a. Parts of the transducer guide assembly



b. Assembled transducer guide



c. Transducer guide setup used for a slice

Figure 4.52. Transducer guide setup

Table 4.4. Ultrasonic velocity versus quality of concrete
(from Krautkramer and Krautkramer, 1990)

Pulse Velocity (ft/sec)	Quality of Concrete
Above 15,000	Very Good
12,000 – 15,000	Good
9,000 – 12,000	Moderate to Questionable
6,000 – 9,000	Poor
Below 6,000	Very Poor



Figure 4.53. Transducers applied to specimen with transducer guide

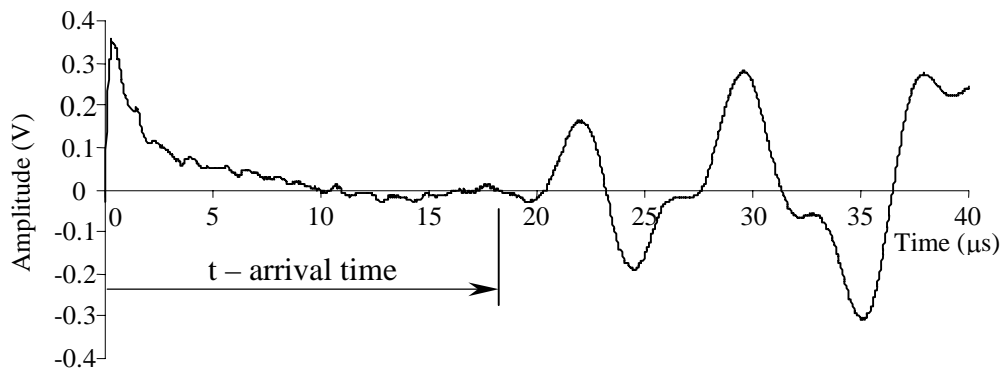
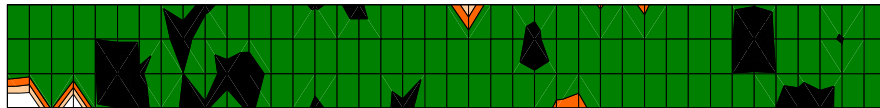
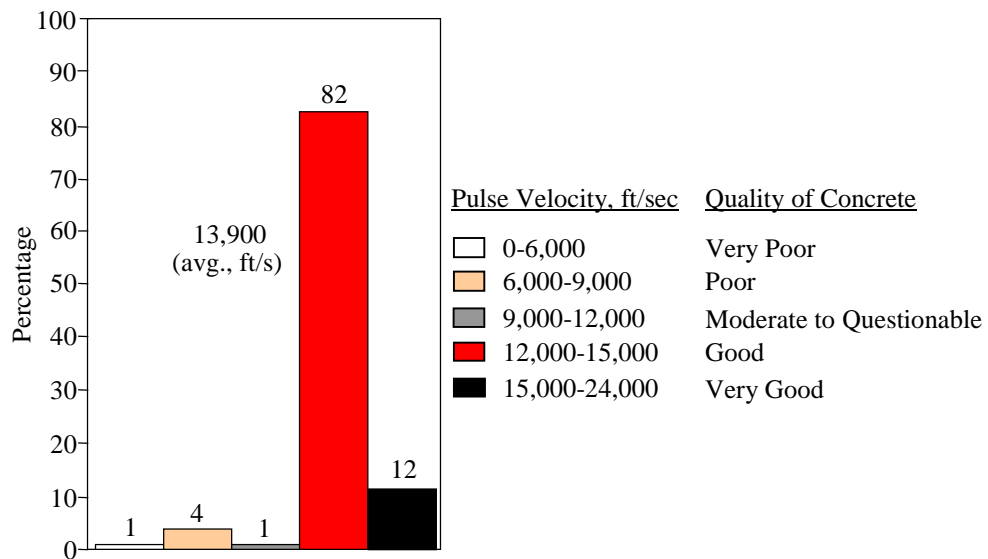


Figure 4.54. Typical waveform obtained in the tests



a. Contour map



b. Bar chart to quantify quality of concrete

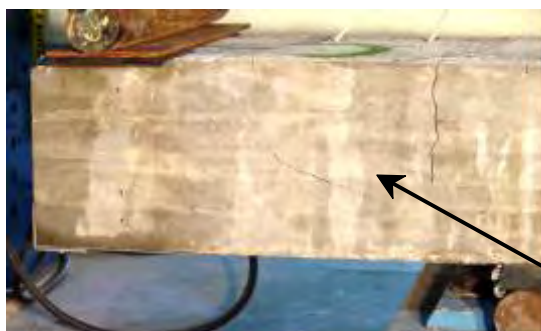
Figure 4.55. Typical through-transmission analysis of a specimen

4.6 ULTIMATE LOAD TESTS

All specimens were subjected to ultimate load test subsequent to their respective environmental exposure. The ultimate load tests were conducted after the removal of 3 in. slices from the long edge of the bridge deck specimens. Negative moment test setup was used for ultimate load tests (Figures 4.14 and 4.15) with a 200 kip actuator. The loading was in the range of 2.4 to 3.2 kips/min, and 1.6 to 2.3 kips/min for specimens with and without SIPMF, respectively. The load rate ranges were calculated for the specimens, after having been sliced, to have a stress in the extreme fiber in the range from 125 to 175 psi/min (ASTM C78-94). The ultimate failure mode for any specimen was as one of the following modes: flexural mode (Figure 4.56 a), shear mode (Figure 4.56 b), or combined flexural/shear mode (Figure 4.56 c). A load-displacement curve is generated for each test to determine the ultimate load (Figure 4.57).



a. Flexural failure mode for a specimen



Front face



Rear face



Entire specimen

b. Shear failure mode for a specimen



c. Combined flexural/shear failure mode

Figure 4.56. Failure modes for ultimate load tests

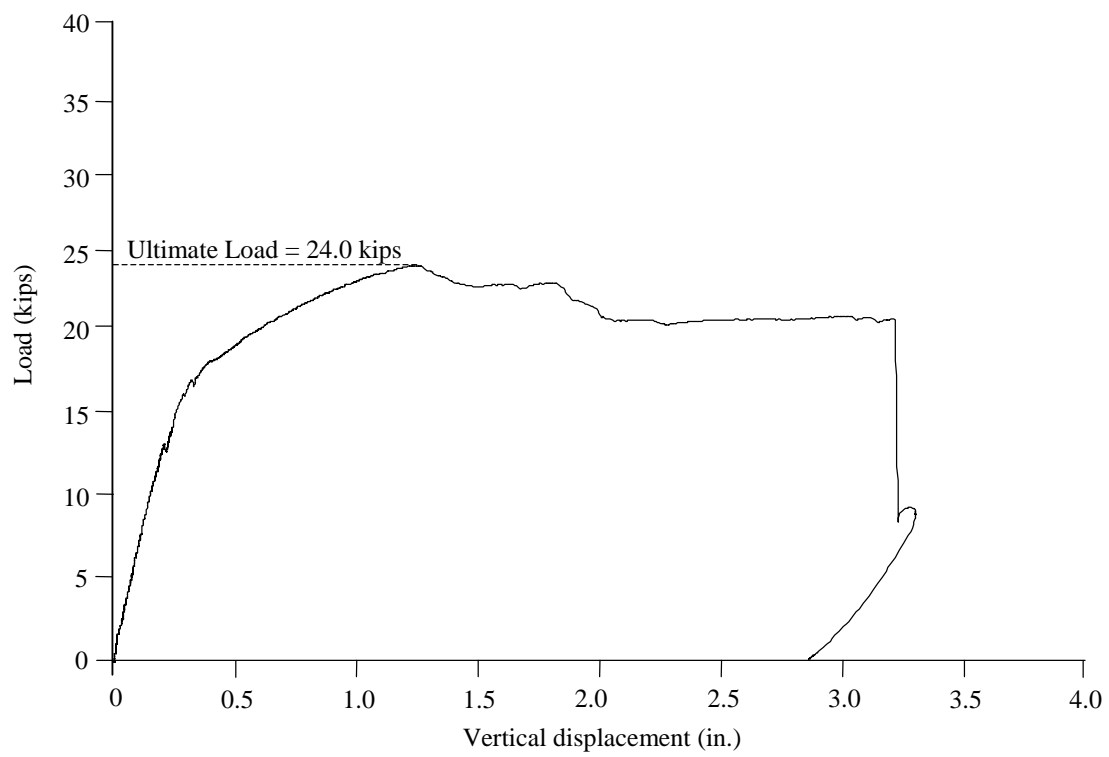


Figure 4.57. Example load-displacement curve for ultimate load test

CHAPTER 5 : RESULTS AND DISCUSSION

5.1 INTRODUCTION

Results of the laboratory experimental program are presented in this chapter. First, results related to the compressive strength of concrete cylinders are presented. Next, the results of the exposure tests and load tests for laboratory deck slab specimens are presented. Results for specimens with SIPMF are presented for ultrasonic pulse-echo tests, ultrasonic through-transmission tests, and loading tests. Results for specimens without SIPMF are presented for ultrasonic through-transmission tests and loading tests. A comparison of laboratory results is provided at the end of the chapter.

5.2 COMPRESSIVE STRENGTH OF CONCRETE

The compressive strength of concrete was evaluated throughout the test program using concrete cylinders. Cylinders were prepared to assess strength gain with time under controlled curing conditions as well as for the various exposure conditions. The compressive strength tests were conducted at approximately the same time as the ultimate load tests for specimens. Results of the compressive strength tests are presented in Table 5.1 and Figure 5.1.

The average compressive strength of the cylinders that were cured under controlled conditions increased to a maximum value of 5,760 psi at 28 days. A slight decrease in compressive strength was observed for further curing times up to 568 days (4,800 psi). The average compressive strength of the cylinders subjected to 300 freeze/thaw cycles was 5,800 psi. The compressive strength decreased with further freeze/thaw cycles (4,100 psi after 600 freeze/thaw cycles). The average compressive strength of the cylinders for salt-water exposure increased with increasing time of exposure. The average compressive strengths were 6,470 psi, 6,600 psi, and 7,055 psi for 1,000; 3,000; and 10,000 hours of salt-water exposure, respectively.

Several cylinders deteriorated entirely due to freeze/thaw exposure. The level of deterioration was sufficient to prevent compressive strength testing. Four of the ten cylinders subjected to 300 cycles were deteriorated (one cylinder was deteriorated after 150 cycles and

3 cylinders after 300 cycles). Eight of the ten cylinders subjected to 600 cycles were deteriorated (3 cylinders were deteriorated after 350 cycles and 5 additional cylinders were deteriorated after 600 cycles).

Table 5.1. Compressive strength test results for cylinders

Name of Environmental Exposure	Specimens Tested with Cylinders	Age (days)	Number of Cylinders	Compressive Strength (psi)			
				Maximum	Minimum	Standard Deviation	Average
Control	---	7	5	5,065	4,510	209	4,790
	---	14	5	5,660	4,800	324	5,235
	---	28	5	6,030	5,430	260	5,760
	---	90	5	5,840	5,230	212	5,500
	WI-C-1 WO-C-1	287	5	5,160	4,760	177	4,980
	WI-C-2 WO-C-2	568	5	5,000	4,435	252	4,795
1,000 Hours of Salt-Water Exposure	WI-S-1-1 WI-S-1-2 WO-S-1-1 WO-S-1-2	287	10	6,980	5,520	504	6,470
300 Freeze/Thaw Cycles	WI-F-3-1 WI-F-3-2 WO-F-3-1 WO-F-3-2	375	10 * (6)	6,800	4,520	759	5,800
3,000 Hours of Salt-Water Exposure	WI-S-3-1 WI-S-3-2 WO-S-3-1 WO-S-3-2	375	10	6,880	6,120	249	6,600
600 Freeze/Thaw Cycles	WI-F-6-1 WI-F-6-2 WO-F-6-1 WO-F-6-2	480	10 * (2)	4,210	4,000	151	4,100
10,000 Hours of Salt-Water Exposure	WI-S-10-1 WI-S-10-2 WO-S-10-1 WO-S-10-2	606	10	7,490	6,635	278	7,055

* some of the cylinders were completely deteriorated during the environmental conditioning.

(#) actual number of cylinder tests

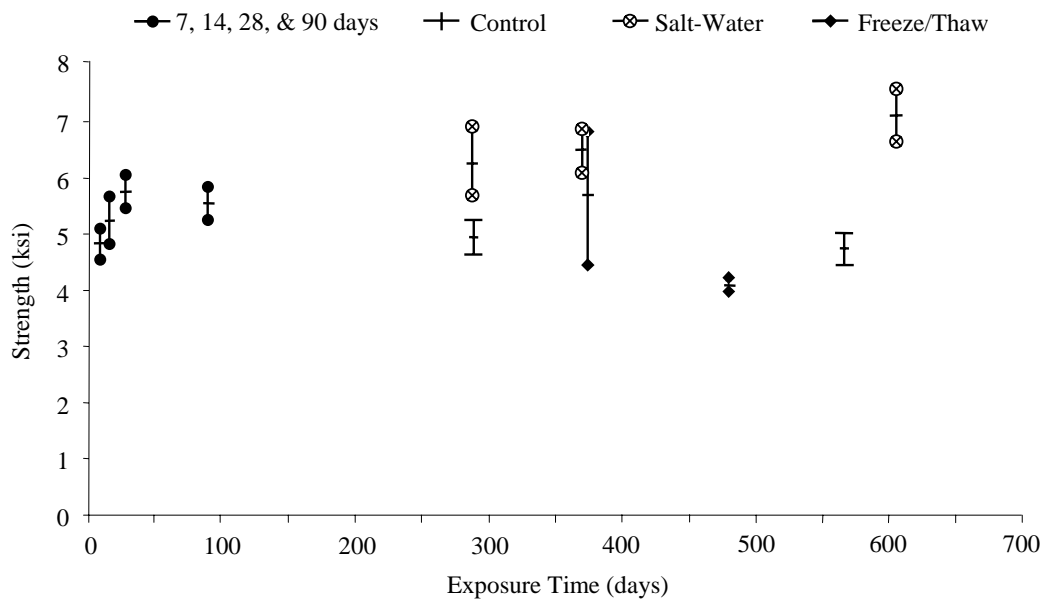


Figure 5.1. Compressive strength for cylinders

5.3 SPECIMENS WITH SIPMF

Results of exposure and load tests for specimens with SIPMFs are presented in this section. First, results from the service load tests are presented. Next, ultrasonic pulse-echo test results are presented to provide assessment of the quality of bond between the concrete and the SIPMFs after various exposure conditions. Third, ultrasonic through-transmission test results are presented to provide assessment of the quality of concrete over the longitudinal cross sections of all specimens following exposure tests. Finally, ultimate load test results are presented to evaluate the influence of various exposure conditions on the ultimate load capacity of the specimens.

5.3.1 Service Load Test Results

All 12 specimens with SIPMF were subjected to a service load test at the beginning of the test program to promote full depth cracks. The service load test consisted of two steps: positive moment (bottom cracking) and negative moment (top cracking) applications. The load-displacement curves for the service load tests for specimens with SIPMF are presented in Figures 5.2 and 5.3. The bottom and top cracking loads for specimens with SIPMF are presented in Table 5.2. The onset of cracking for the positive moment application for specimens with SIPMF occurred at loads between 9.71 kips to 12.49 kips. The onset of cracking for the

negative moment application occurred at loads between 3.23 kips to 7.12 kips. The range of loads associated with onset of cracking is shown as a shaded envelope on Figures 5.2 and 5.3. The theoretical cracking load was determined for specimens with SIPMF using the elastic theory with the compressive strength f_c' data from the 28-day compressive strength test cylinders. The measured loads for positive moment cracking were generally consistent with theoretical calculations of cracking loads. The theoretical prediction was 9.83 kips, which was within 14% of the average measured value for all specimens (11.21 kips). The measured loads for negative moment cracking were lower than theoretical predictions. The difference in measured and predicted values was attributed to the weakened overall structure due to presence of positive moment cracks at the time of negative moment application. The average measured value for all specimens was 5.20 kips, whereas the theoretical predicted ultimate load was 13.14 kips.

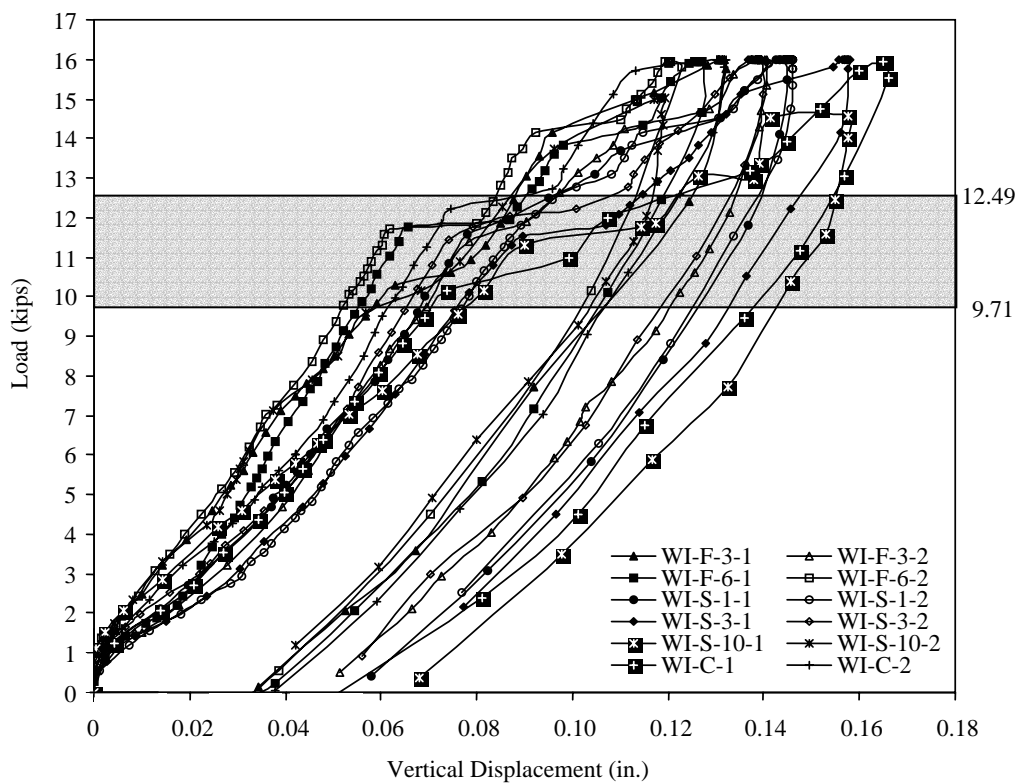


Figure 5.2. Load-displacement curves for positive moment application (bottom cracking) for specimens with SIPMF

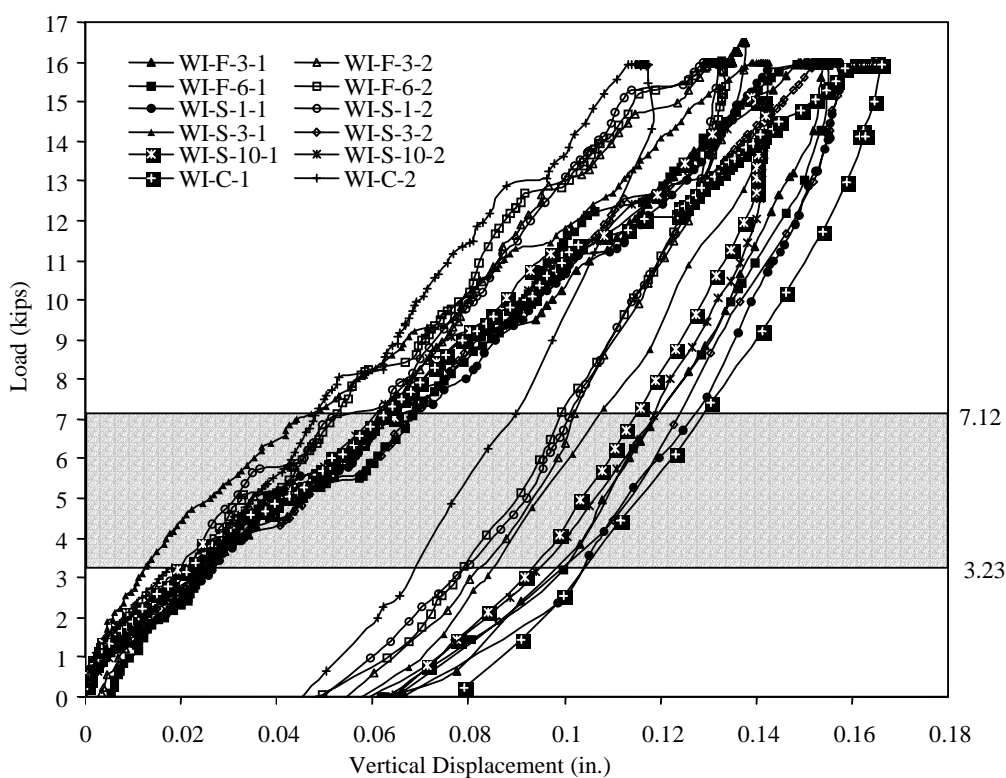


Figure 5.3. Load-displacement curves for negative moment application (top cracking) for specimens with SIPMF

Table 5.2. Top and bottom cracking load for the specimens with SIPMF

Type of specimens			Cracking Load (kips)	
			Top Cracking	Bottom Cracking
Specimens with SIPMF	Control	WI-C-1	4.59	10.62
		WI-C-2	3.23	12.49
	Freeze/Thaw 300 cycle	WI-F-3-1	4.48	10.49
		WI-F-3-2	5.12	11.71
		WI-F-6-1	5.31	11.88
		WI-F-6-2	5.18	11.89
	Salt-Water	WI-S-1-1	5.59	11.98
		WI-S-1-2	5.83	12.42
		WI-S-3-1	7.12	11.62
		WI-S-3-2	4.17	11.93
		WI-S-10-1	4.11	11.74
		WI-S-10-2	5.61	9.71

5.3.2 Ultrasonic Pulse-Echo Test Results

The ultrasonic pulse-echo test results are presented in the form of contour maps that represent quality of contact between the concrete and SIPMF and in the form of bar charts that summarize the findings of the analysis.

Control Specimens

Ultrasonic pulse-echo test results for control specimens are presented in Figures 5.4 to 5.9. Results for control specimens are presented for Before Cracking and After Cracking (due to service load application).

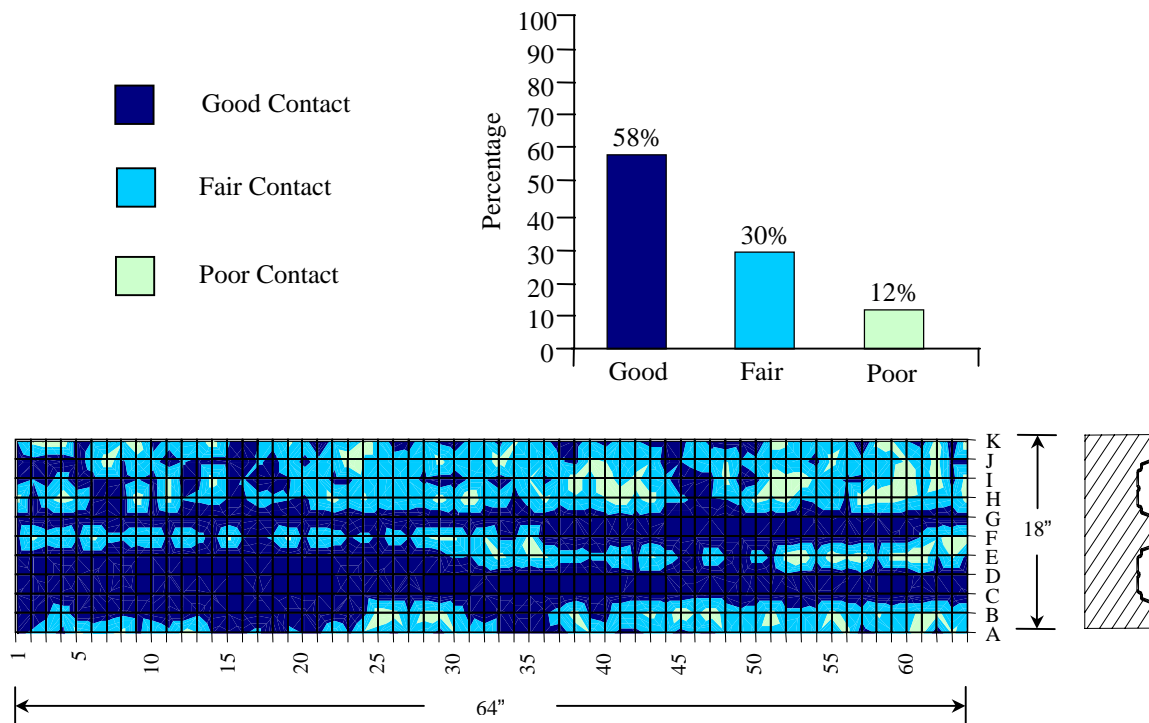


Figure 5.4. Pulse-echo contour map and bar chart for Before Cracking for specimen WI-C-1

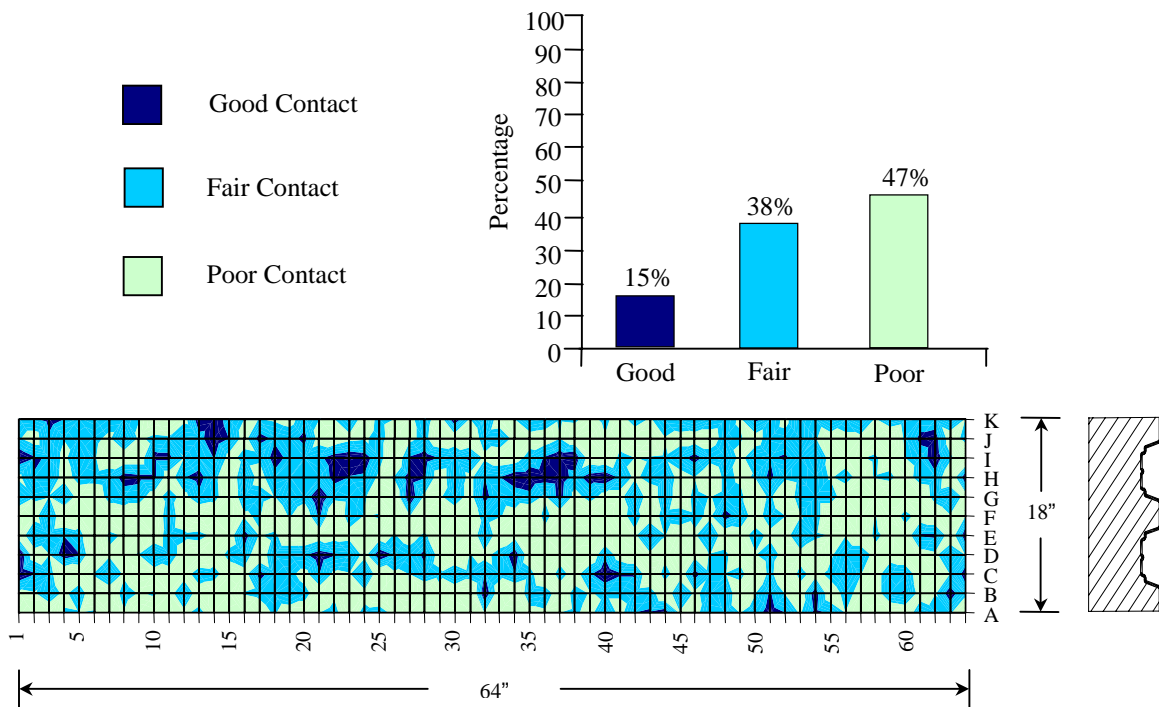


Figure 5.5. Pulse-echo contour map and bar chart for After Cracking for specimen WI-C-1

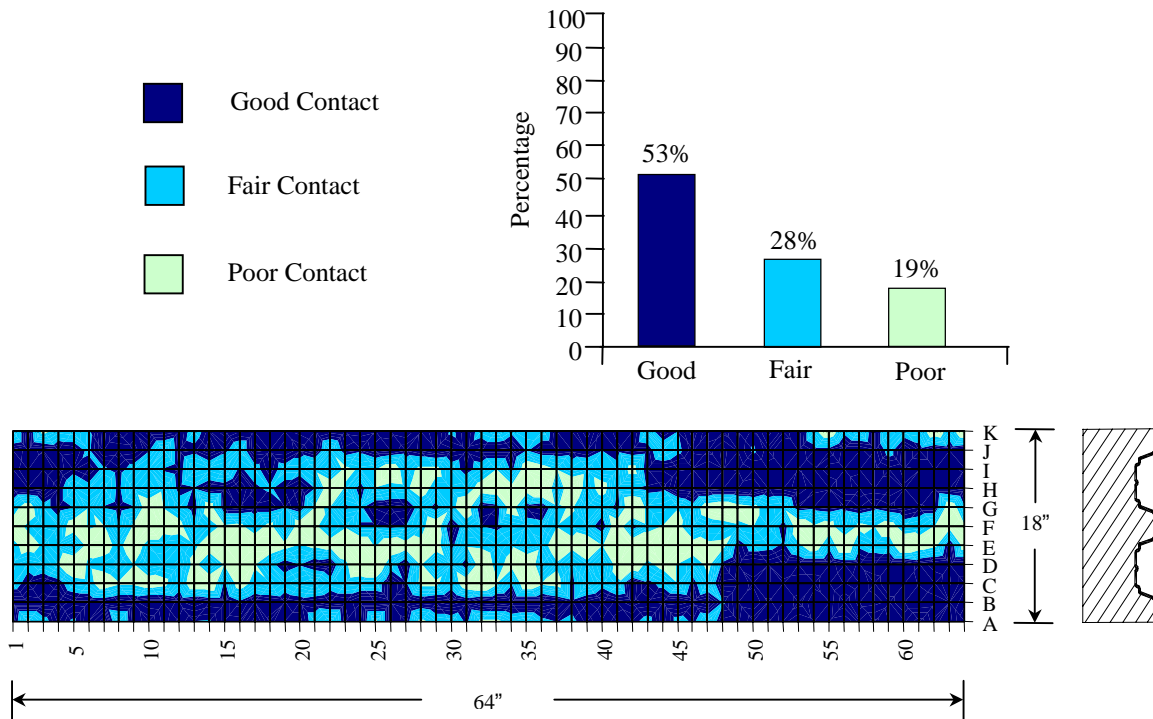


Figure 5.6. Pulse-echo contour map and bar chart for Before Cracking for specimen WI-C-2

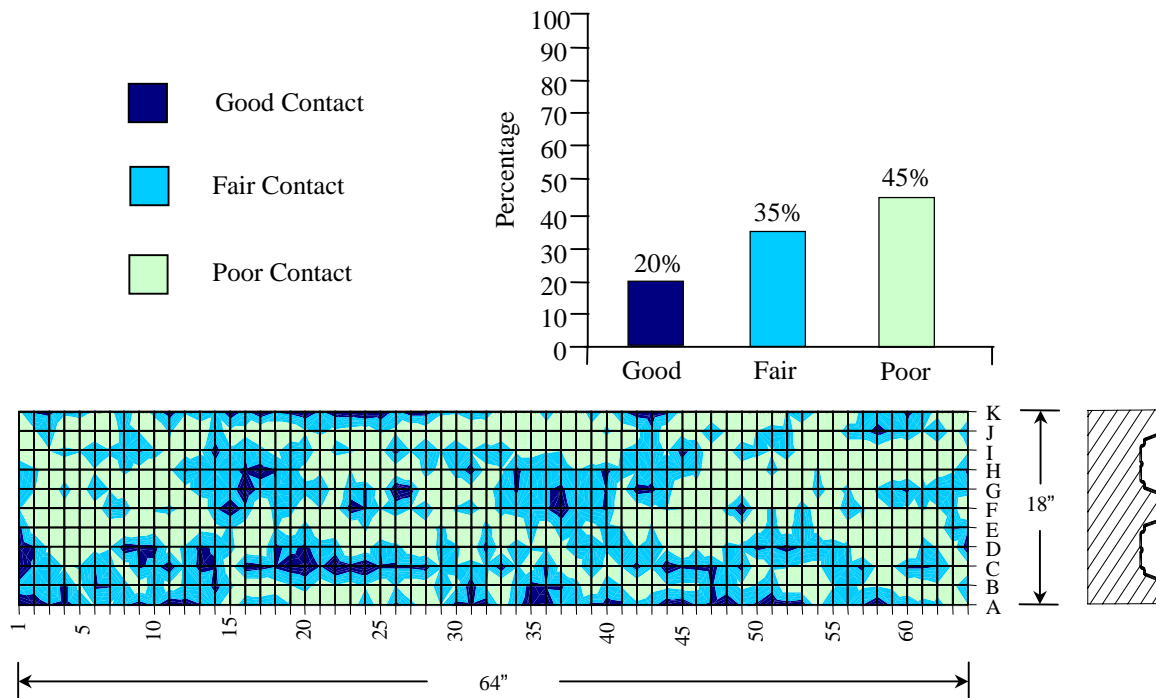


Figure 5.7. Pulse-echo contour map and bar chart for After Cracking for specimen WI-C-2

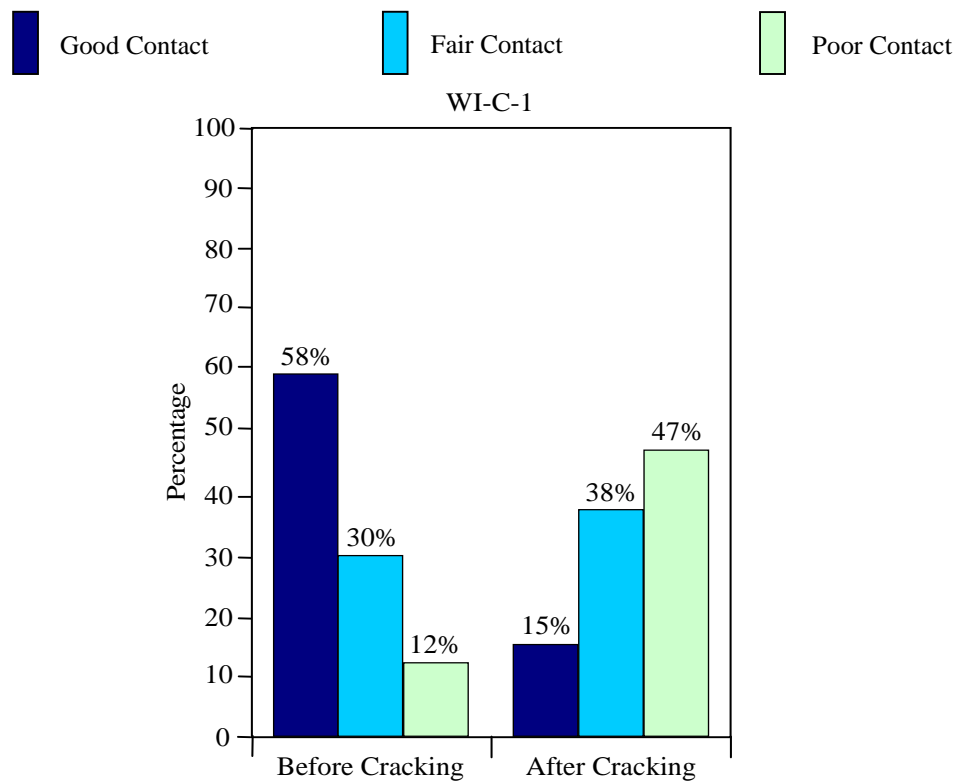


Figure 5.8. Summary of pulse-echo results for specimen WI-C-1

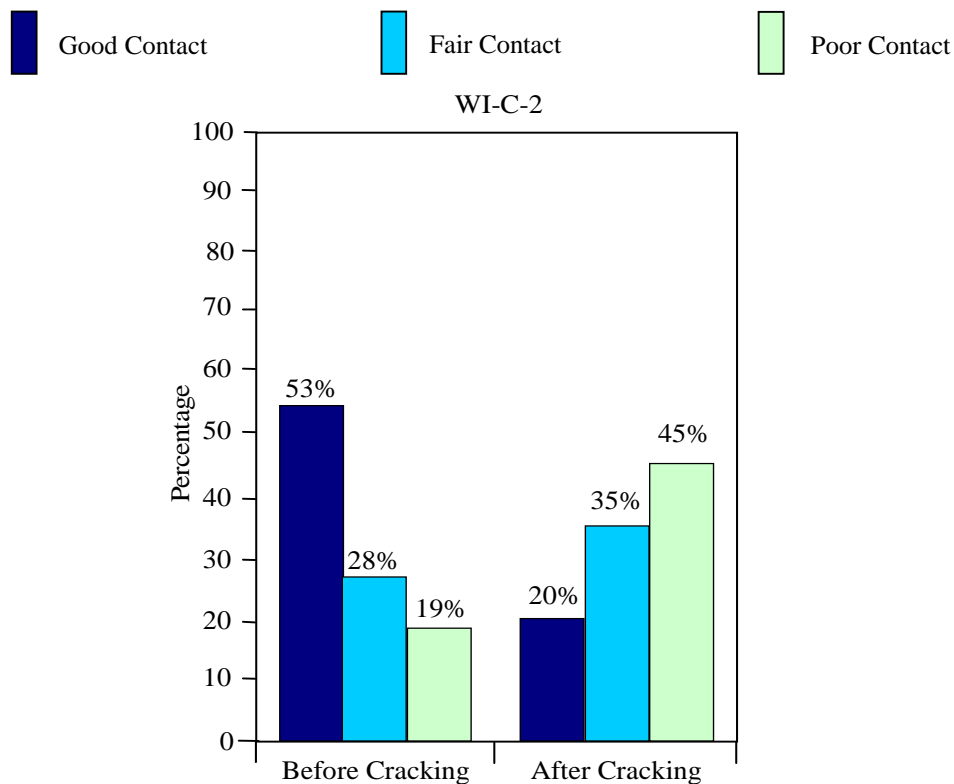


Figure 5.9. Summary of pulse-echo results for specimen WI-C-2

The pulse-echo test results are generally similar for both control specimens. More than half of the measurement points for each control specimen are associated with good contact before cracking. Service load tests caused significant decreases in the quality of contact between the concrete and the SIPMF. After cracking, only 15% and 20% of the measurement points for the control specimens were associated with good contact, whereas nearly half of the measurement points (45% and 47%) were associated with poor contact.

Freeze/Thaw Specimens

Ultrasonic pulse-echo test results for freeze/thaw specimens are presented in Figures 5.10 to 5.27. Pulse-echo results for the 300-cycle freeze/thaw specimens are presented for Before Cracking, After Cracking (due to service load application), and After 300 Freeze/Thaw Cycles (Figures 5.10 to 5.17). Pulse-echo results for the 600-cycle freeze/thaw specimens are presented for Before Cracking, After Cracking, After 300 Freeze/Thaw Cycles, and After 600 Freeze/Thaw Cycles (Figures 5.18 to 5.27).

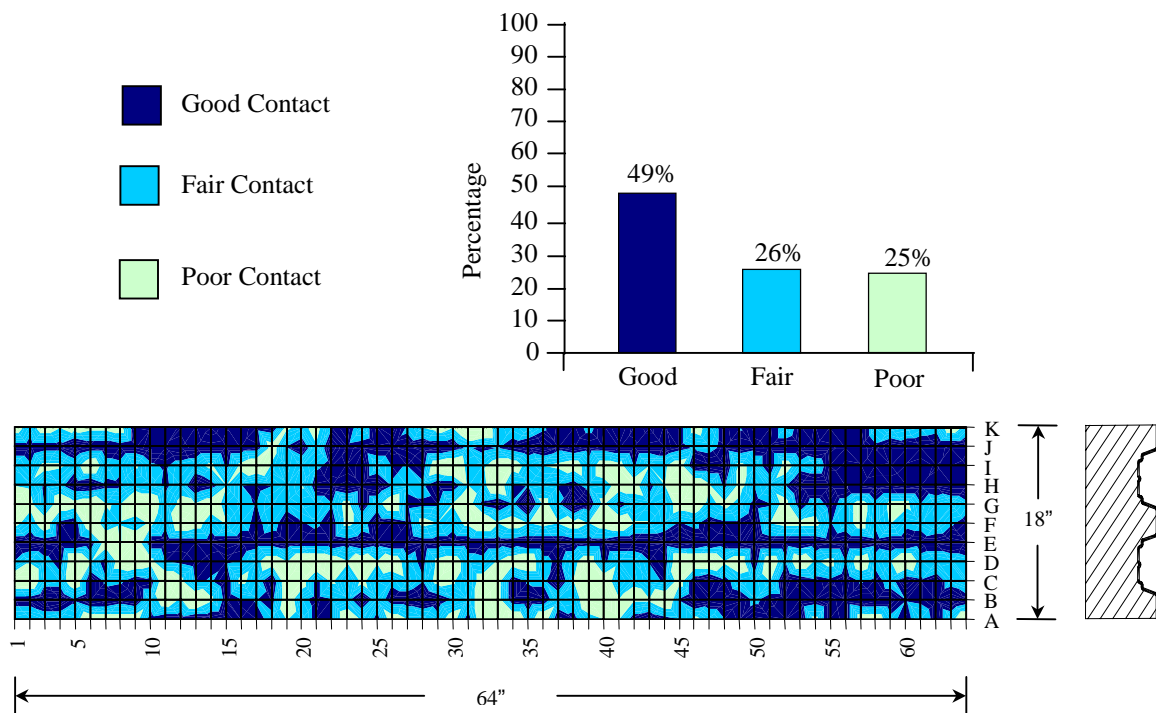


Figure 5.10. Pulse-echo contour map and bar chart for Before Cracking for specimen WI-F-3-1

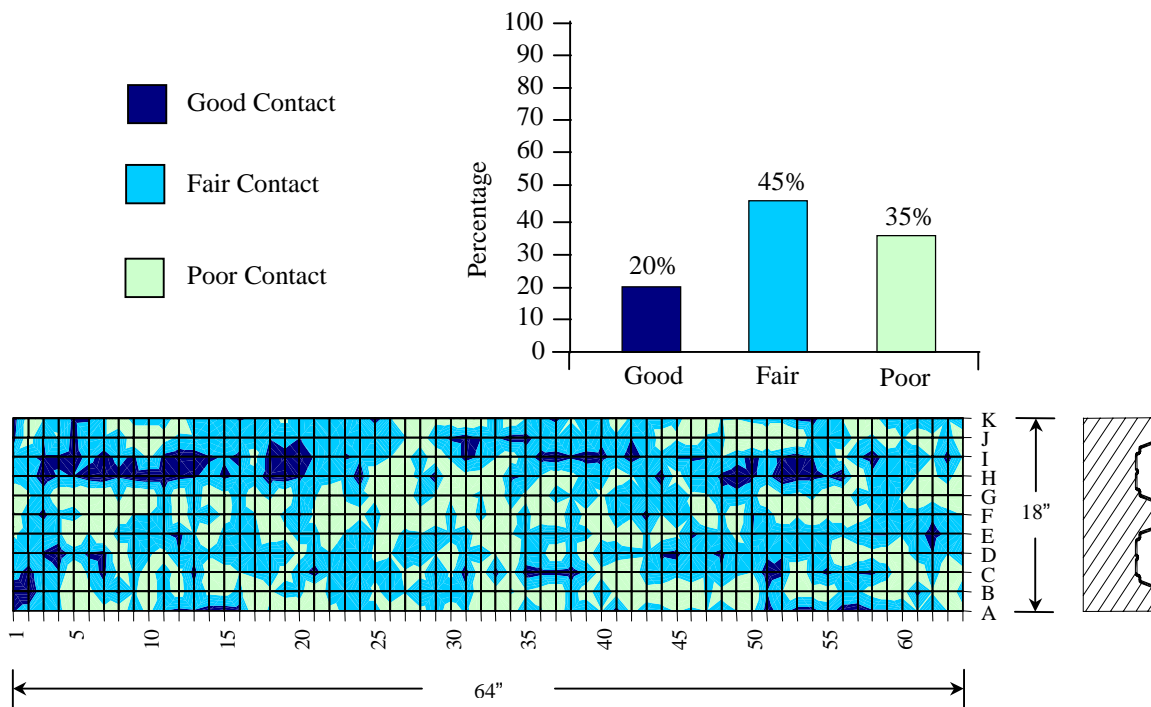


Figure 5.11. Pulse-echo contour map and bar chart for After Cracking for specimen WI-F-3-1

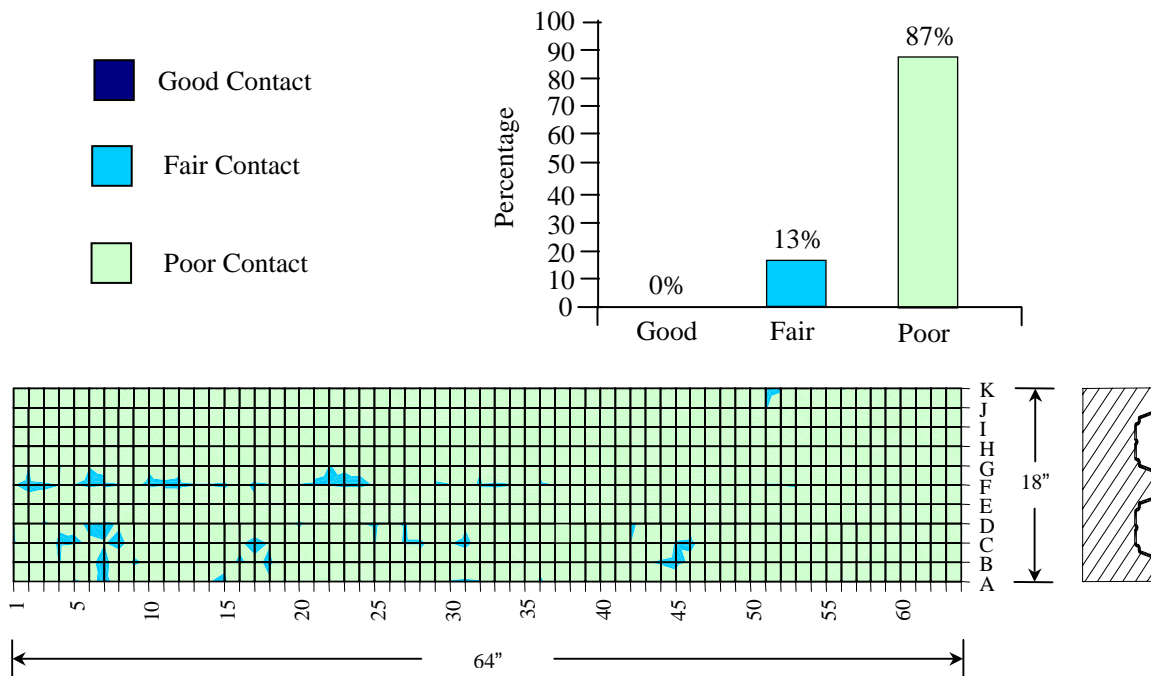


Figure 5.12. Pulse-echo contour map and bar chart for After 300 Freeze/Thaw Cycles for specimen WI-F-3-1

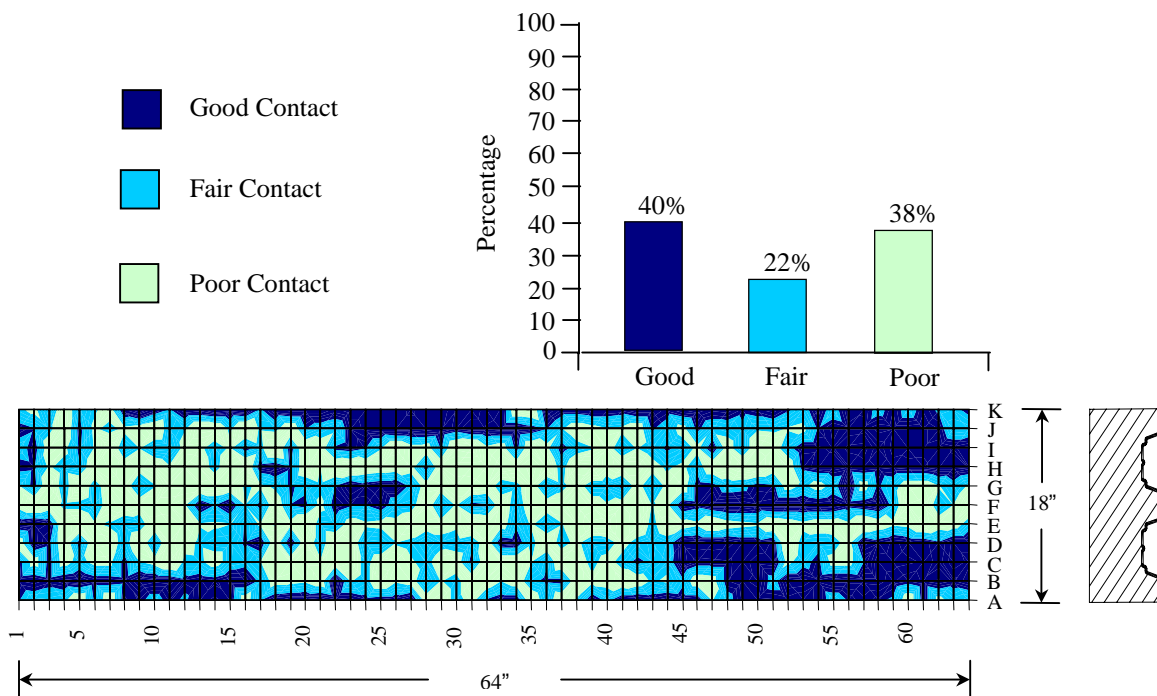


Figure 5.13. Pulse-echo contour map and bar chart for Before Cracking for specimen WI-F-3-2

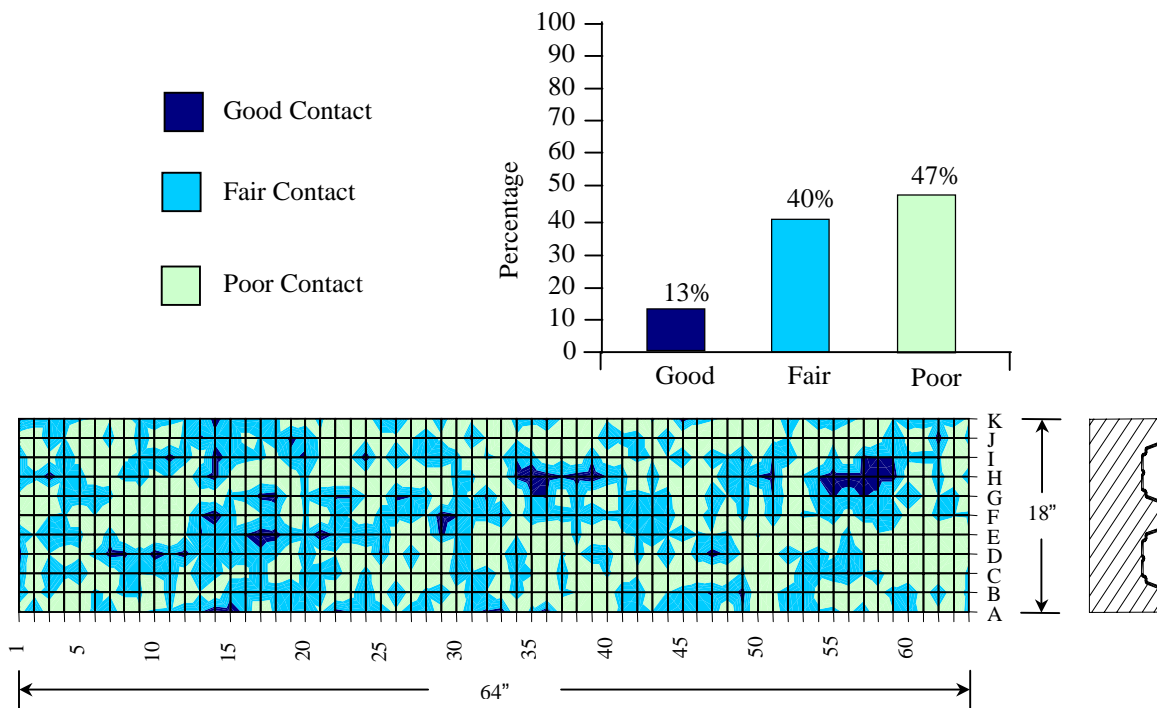


Figure 5.14. Pulse-echo contour map and bar chart for After Cracking for specimen WI-F-3-2

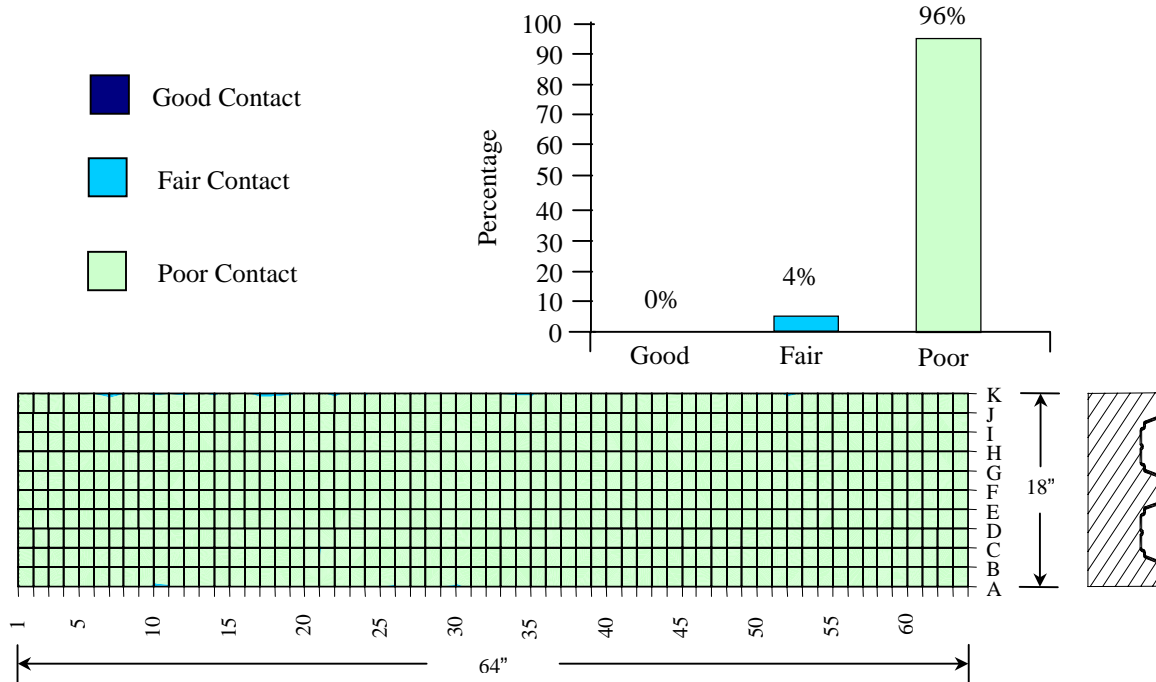


Figure 5.15. Pulse-echo contour map and bar chart for After 300 Freeze/Thaw Cycles for specimen WI-F-3-2

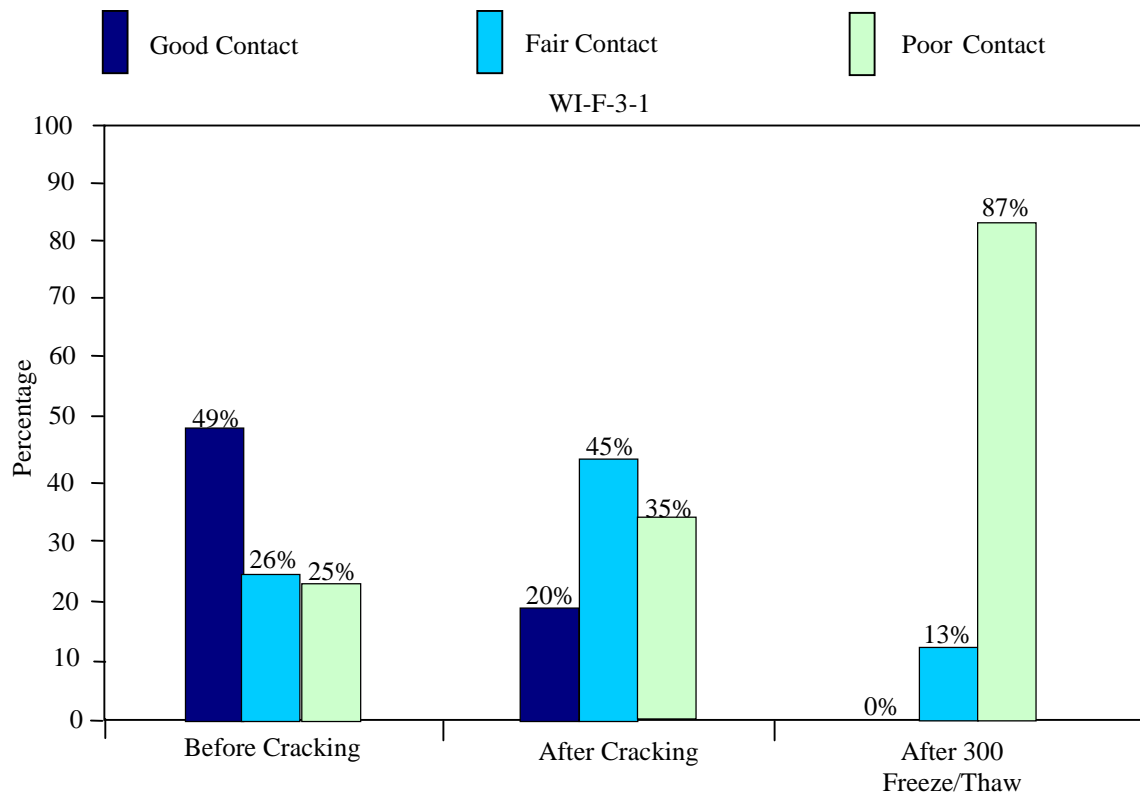


Figure 5.16. Summary of pulse-echo results for specimen WI-F-3-1

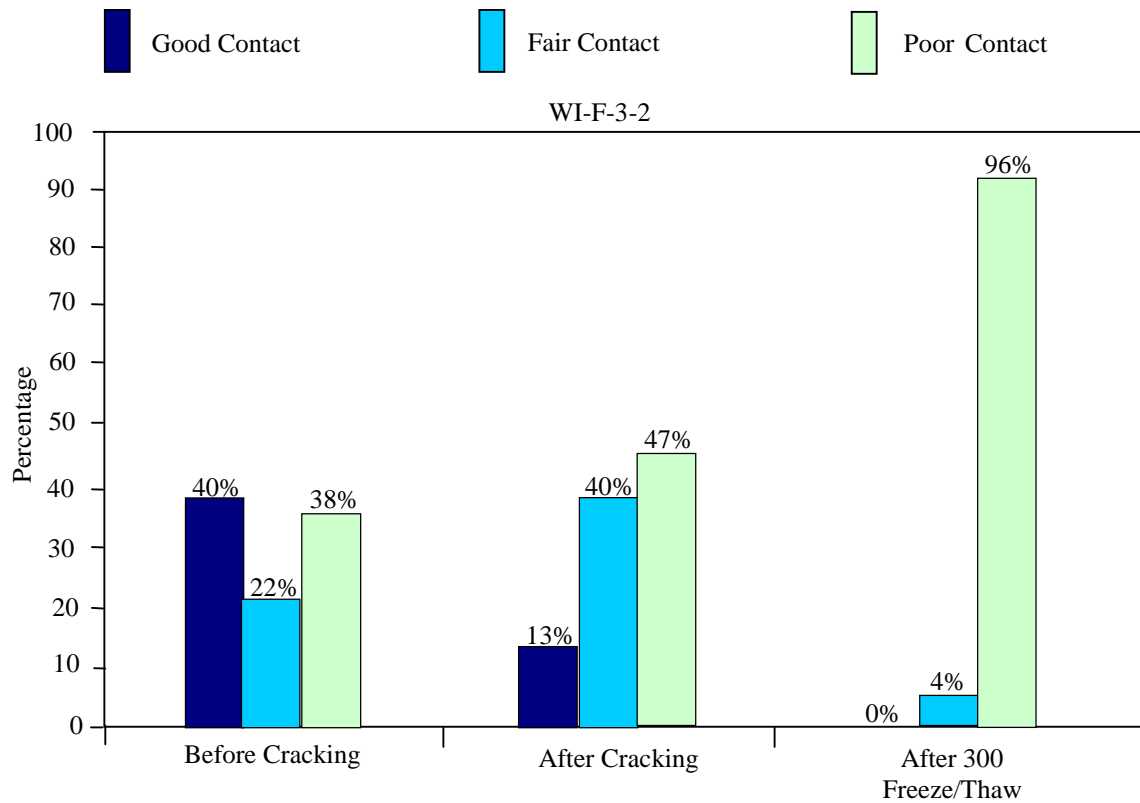


Figure 5.17. Summary of pulse-echo results for specimen WI-F-3-2

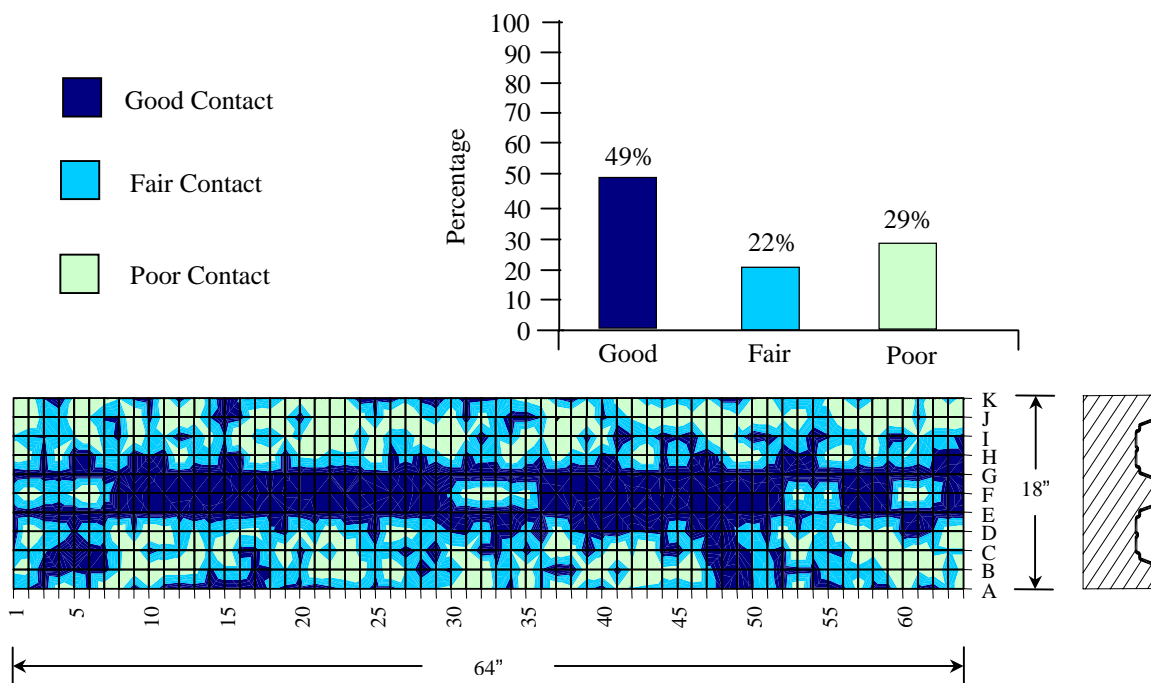


Figure 5.18. Pulse-echo contour map and bar chart for Before Cracking for specimen WI-F-6-1

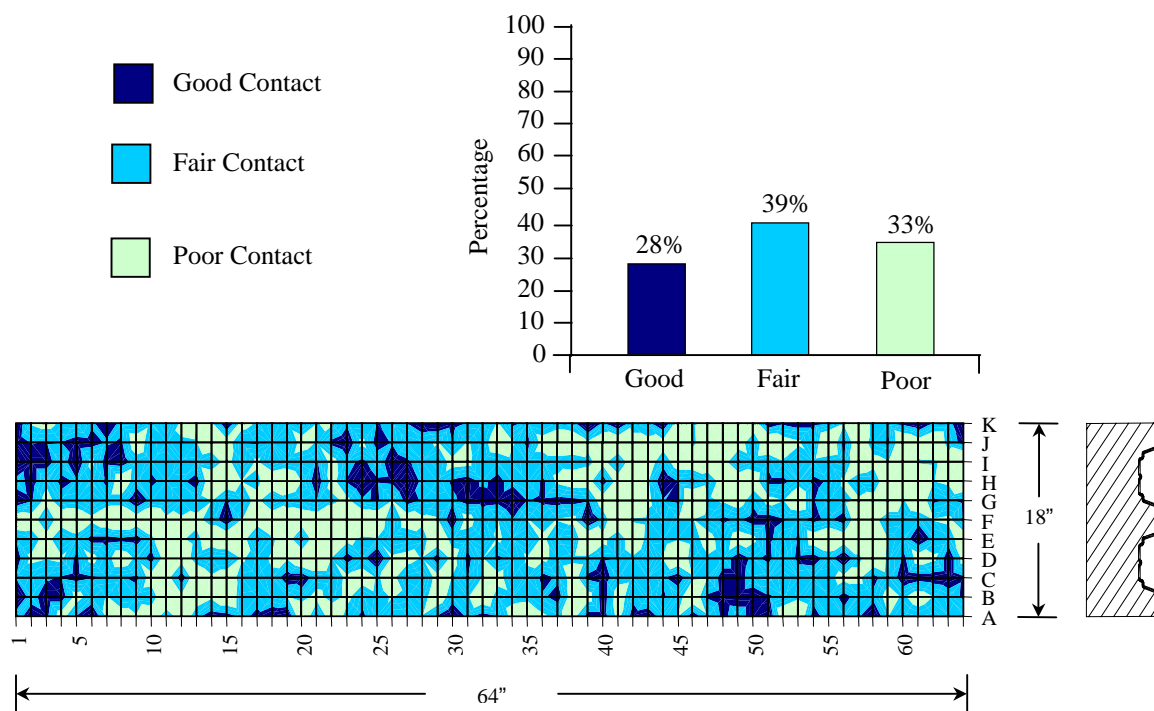


Figure 5.19. Pulse-echo contour map and bar chart for After Cracking for specimen WI-F-6-1

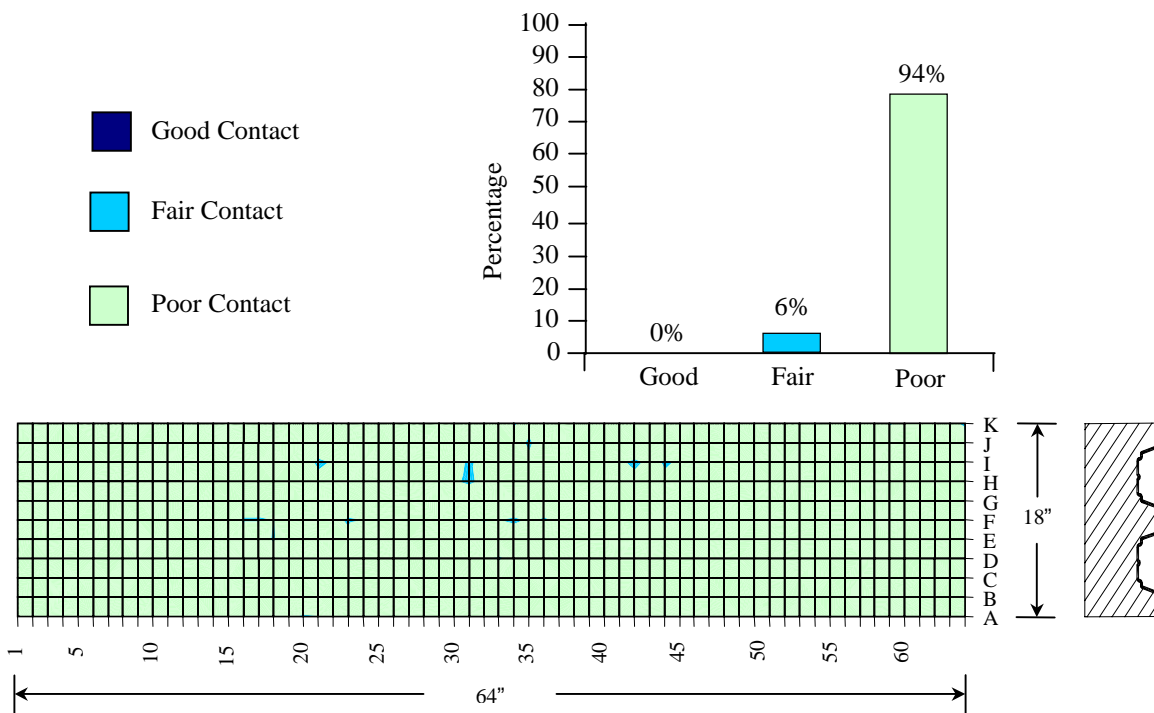


Figure 5.20. Pulse-echo contour map and bar chart for After 300 Freeze/Thaw Cycles for specimen WI-F-6-1

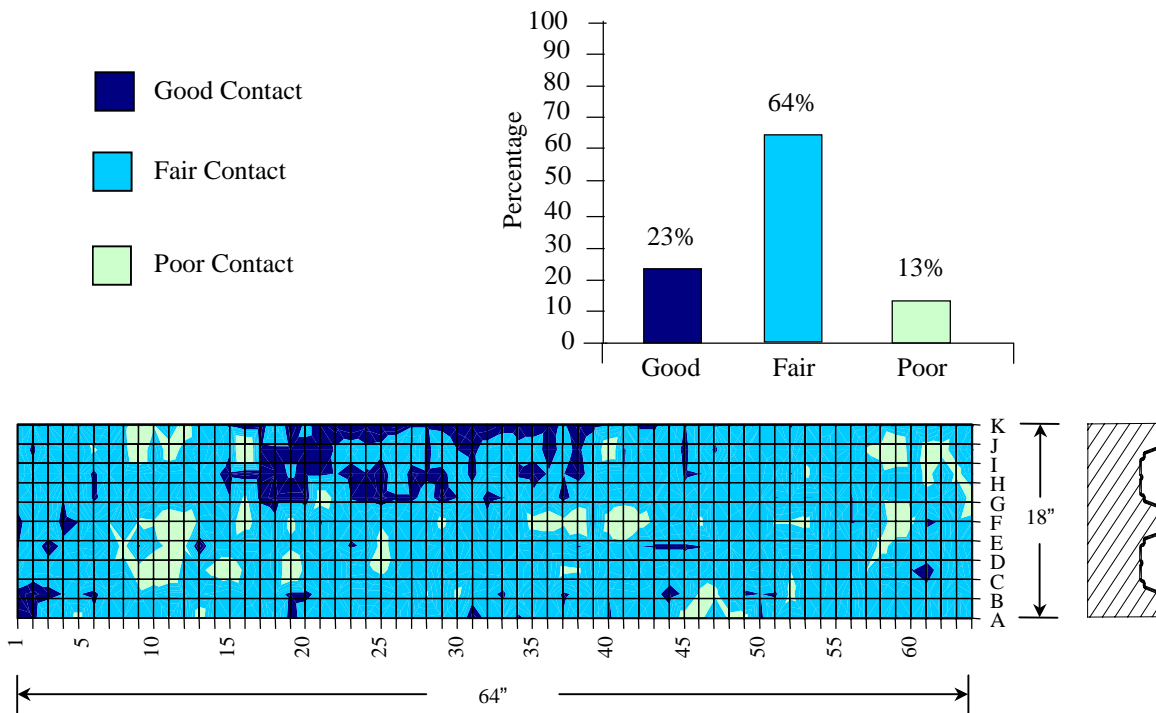


Figure 5.21. Pulse-echo contour map and bar chart for After 600 Freeze/Thaw Cycles for specimen WI-F-6-1

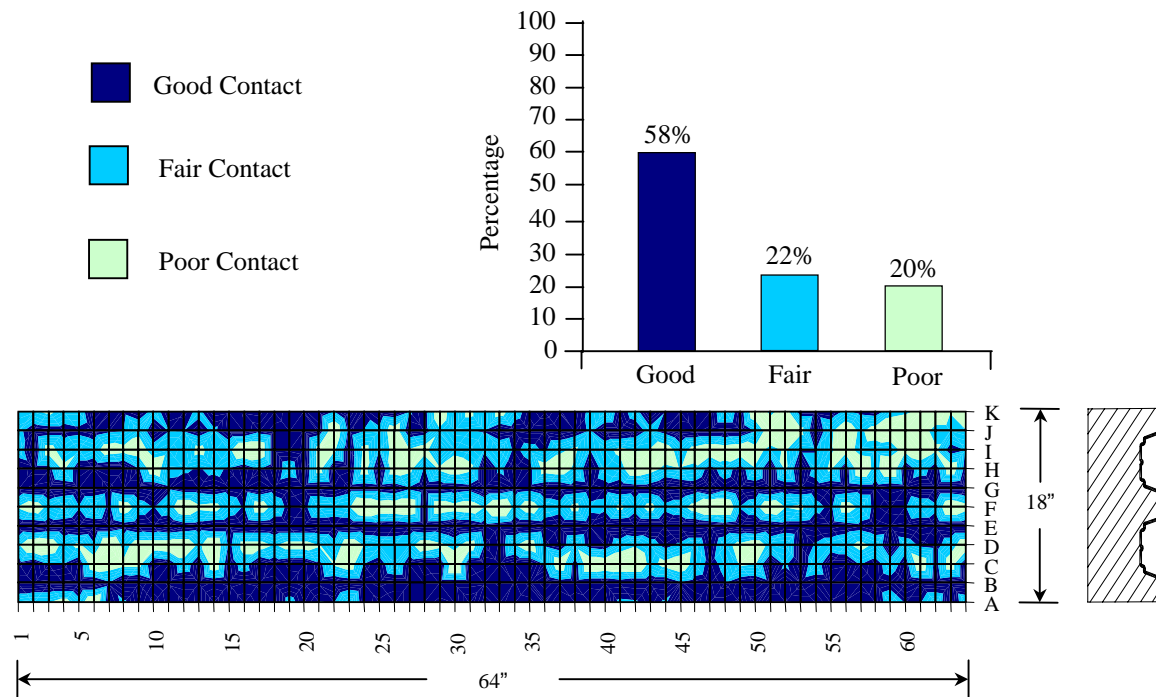


Figure 5.22. Pulse-echo contour map and bar chart for Before Cracking for specimen WI-F-6-2

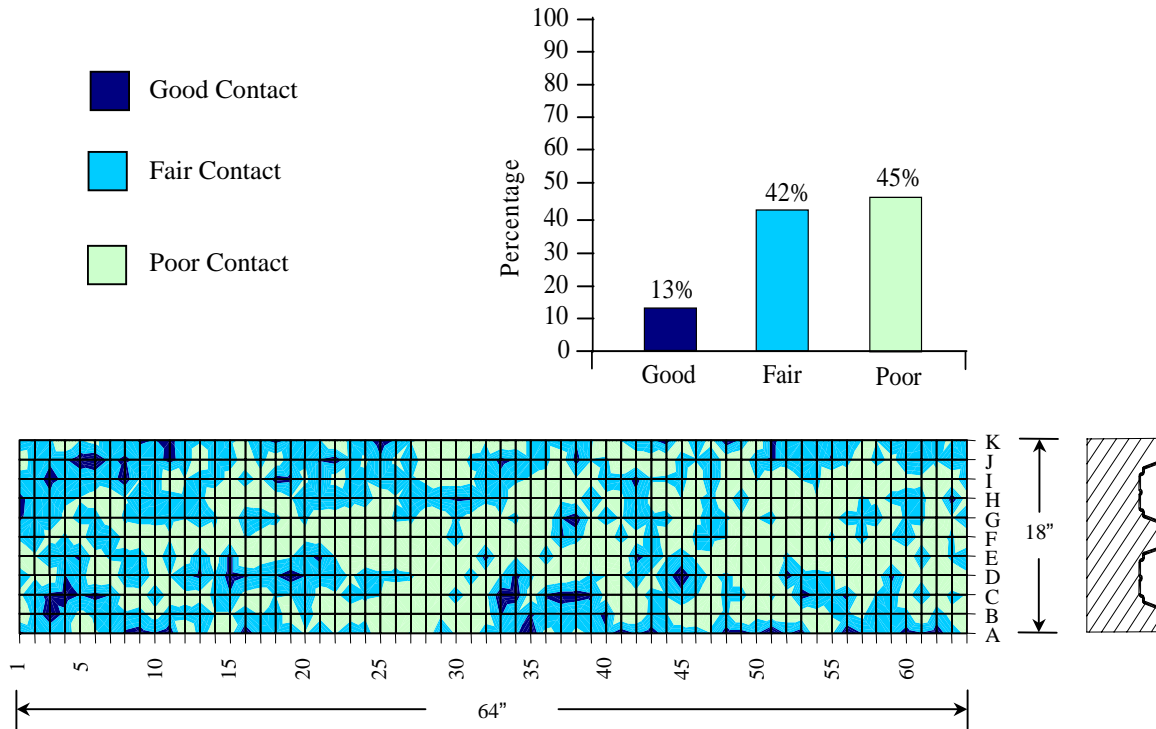


Figure 5.23. Pulse-echo contour map and bar chart for After Cracking for specimen WI-F-6-2

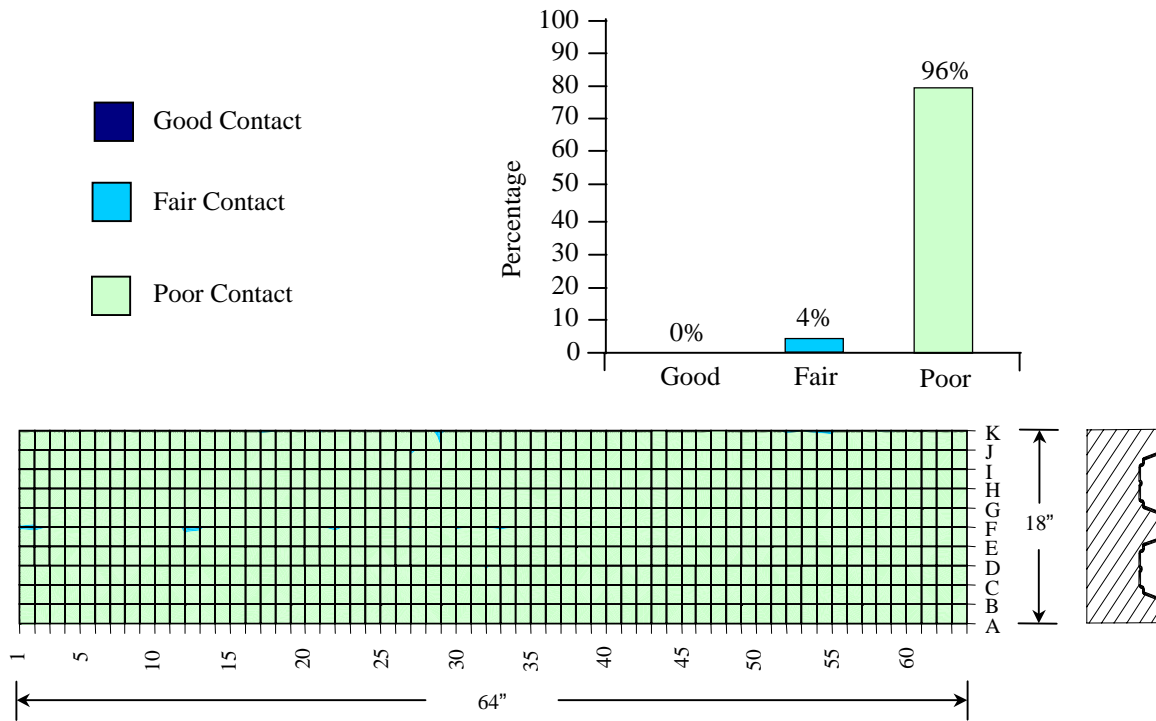


Figure 5.24. Pulse-echo contour map and bar chart for After 300 Freeze/Thaw Cycles for specimen WI-F-6-2

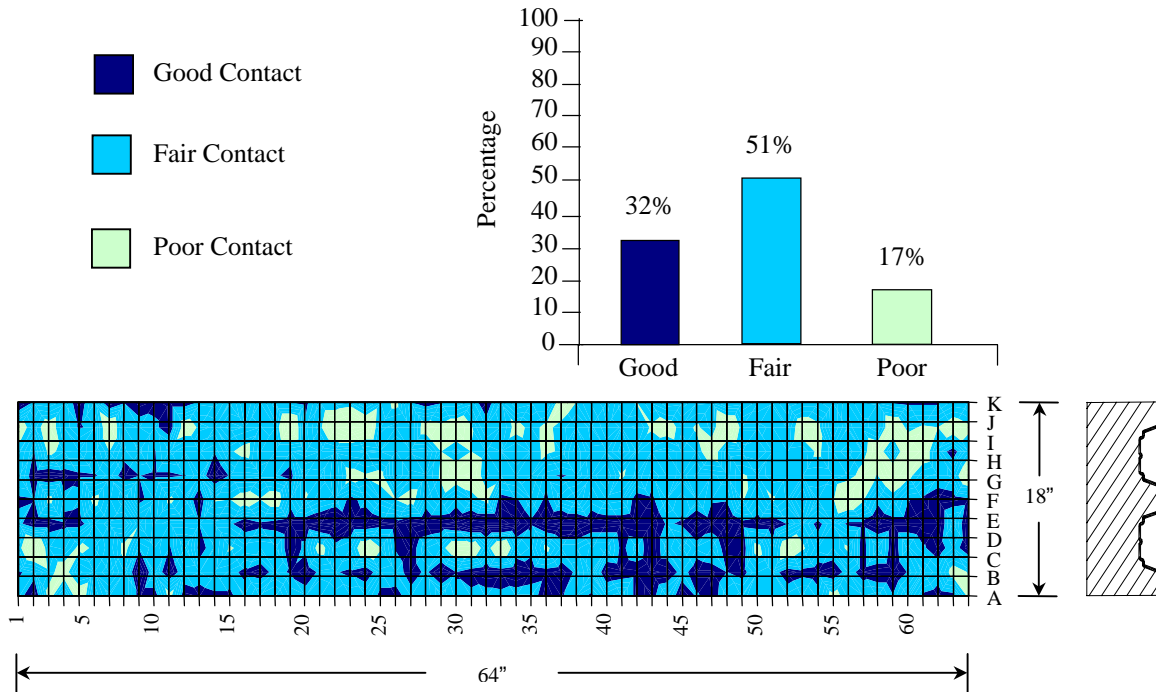


Figure 5.25. Pulse-echo contour map and bar chart for After 600 Freeze/Thaw Cycles for specimen WI-F-6-2

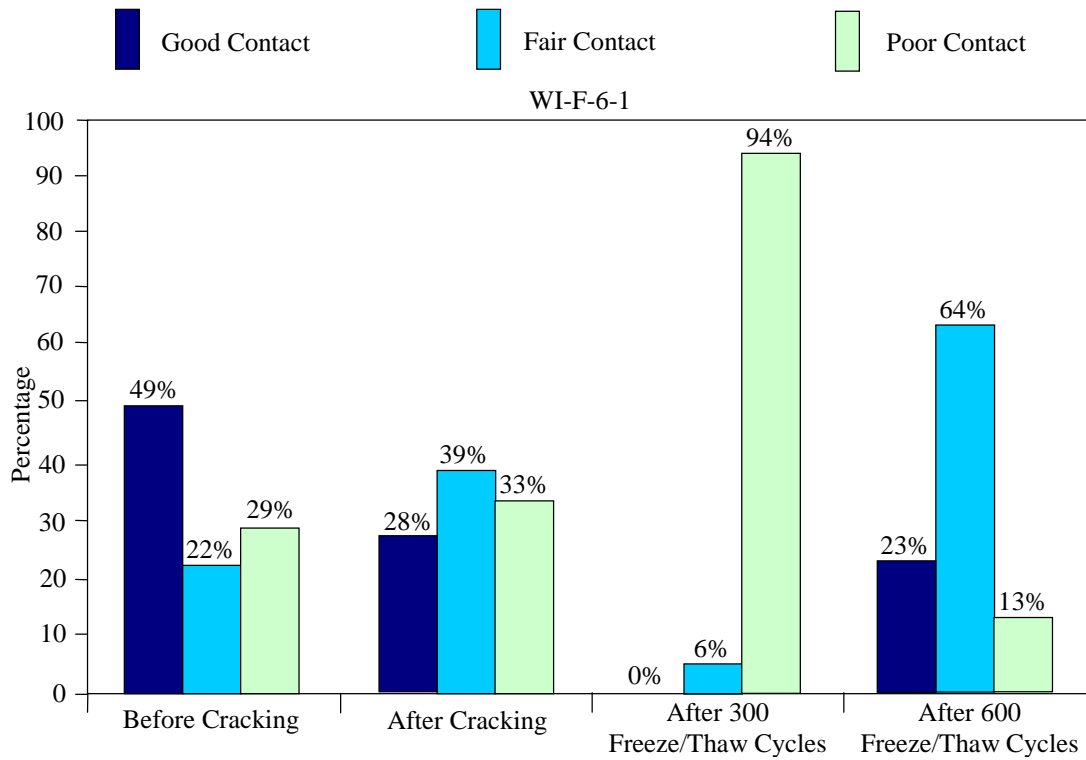


Figure 5.26. Summary of pulse-echo results for specimen WI-F-6-1

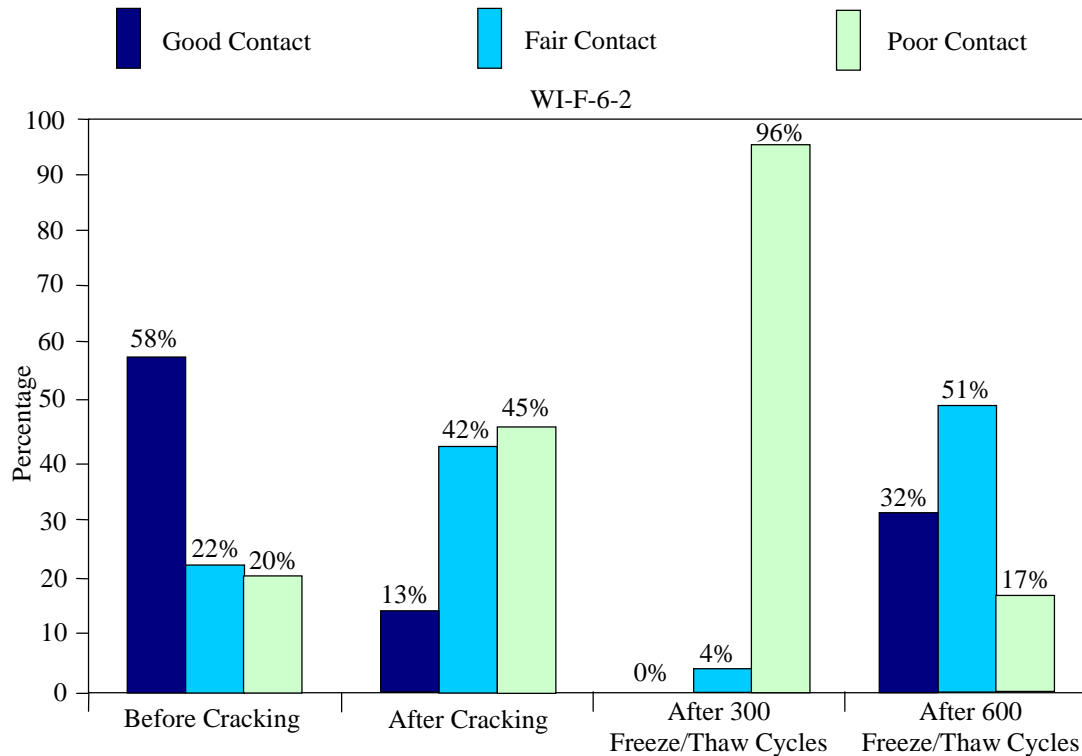


Figure 5.27. Summary of pulse-echo results for specimen WI-F-6-2

The overall trend of quality of contact between SIPMF and concrete is generally consistent for all freeze/thaw exposure specimens. The initial contact (before cracking) is consistently good, a significant loss of contact occurs upon service load cracking, essentially all contact is lost after 300 freeze/thaw cycles, and an apparent improvement of contact is observed after 600 freeze/thaw cycles. The average contact ratings for all freeze/thaw specimens before cracking were 49% good, 23% fair, and 28% poor. After cracking, the average contact ratings measured were 19% good, 42% fair, and 40% poor. After the first 300 freeze/thaw cycles, nearly all contact was lost as the average poor contact rating for all specimens subjected to 300 freeze/thaw cycles was 93%. An apparent regain of contact was observed after 600 cycles. For those specimens subjected to 600 freeze/thaw cycles, the average contact ratings were 28% good, 58% fair, and 15% poor. The apparent improvement in contact is attributed to accumulation of mineral precipitate between the SIPMF and the concrete. Some similarity of spatial patterns of contact ratings were observed for the before cracking specimens. Regions of consistent contact rating appear to follow generally longitudinal trends. After cracking (and for further stages of conditioning), no distinct or consistent spatial trends were observed in the regions of similar contact ratings.

Mineral precipitate on the freeze/thaw exposure specimens was observed for both monitored exposure periods. SIPMFs were removed from the specimens after ultimate load tests for inspection. Some precipitate was observed on the top side of the SIPMF (side in contact with concrete) after 300 freeze/thaw cycles. Noticeably more precipitate was observed on the removed forms after 600 freeze/thaw cycles. Qualitative chemical analysis conducted on precipitate collected from between the SIPMF and concrete for 600-cycle freeze/thaw specimens indicated presence of Calcium, Iron, Aluminum, and Magnesium. The precipitate can be traced to concrete/cement origin from i) lime, ii) tetracalcium aluminoferrite, and iii) magnesium oxide.

Salt-Water Specimens

Ultrasonic pulse-echo test results for salt-water specimens are presented in Figures 5.28 to 5.57. Pulse-echo results for the 1,000-hour salt-water exposures specimens are presented for Before Cracking, After Cracking, and After 1,000 Hours of Salt-Water Exposure (Figures 5.28 to 5.35). Pulse-echo results for the 3,000-hour salt-water exposures specimens are presented for Before Cracking, After Cracking, After 1,000 Hours of Salt-Water Exposure, and After 3,000 Hours of Salt-Water Exposure (Figures 5.36 to 5.45). Pulse-echo results for the 10,000-hour salt-water exposures specimens are presented for Before Cracking, After Cracking, After 1,000 Hours of Salt-Water Exposure, After 3,000 Hours of Salt-Water Exposure, and After 10,000 Hours of Salt-Water Exposure (Figures 5.46 to 5.57).

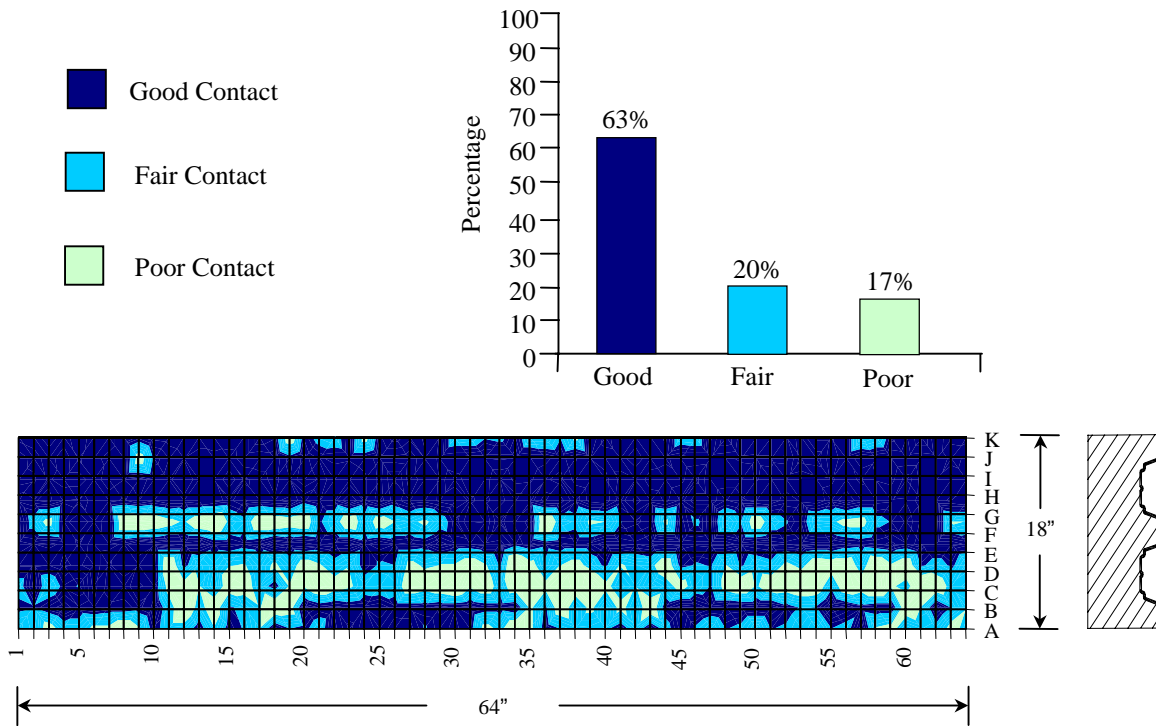


Figure 5.28. Pulse-echo contour map and bar chart for Before Cracking for specimen WI-S-1-1

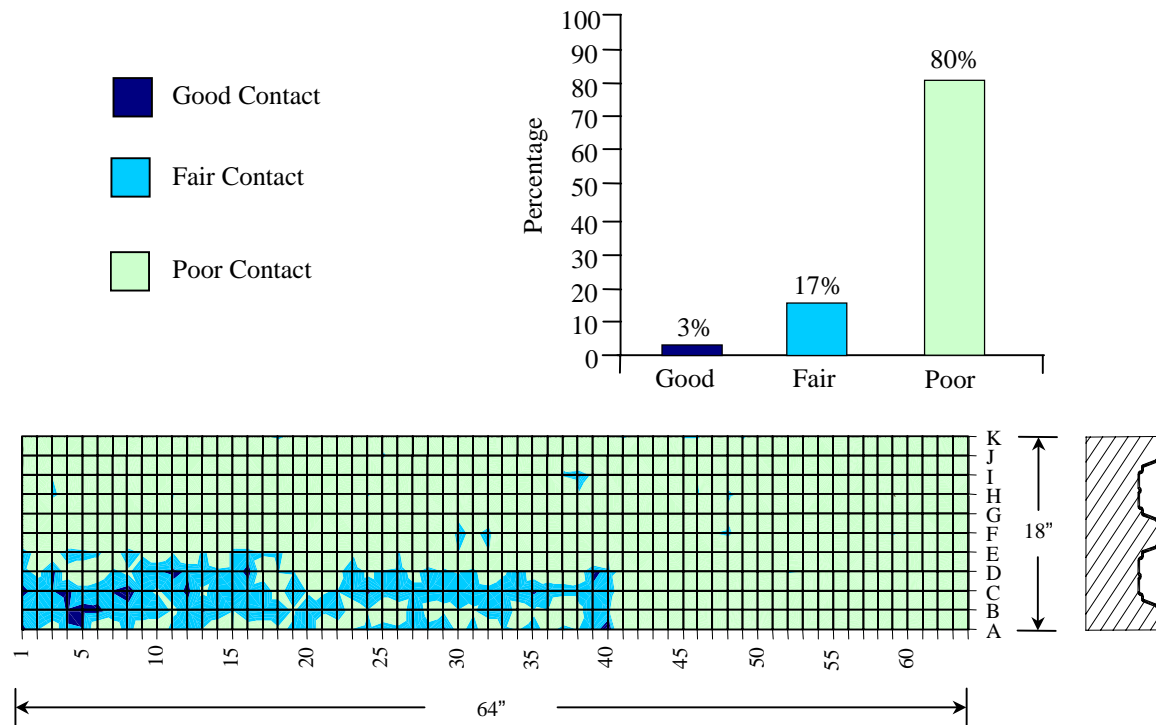


Figure 5.29. Pulse-echo contour map and bar chart for After Cracking for specimen WI-S-1-1

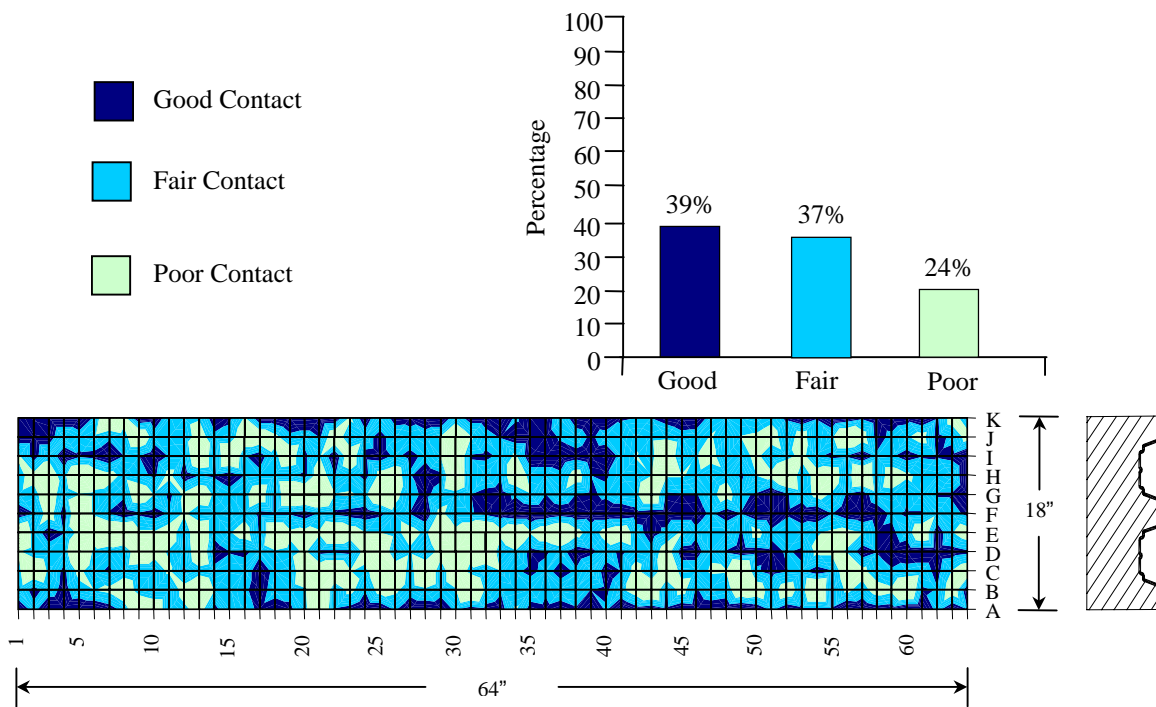


Figure 5.30. Pulse-echo contour map and bar chart for After 1,000 hrs Salt-Water for specimen WI-S-1-1

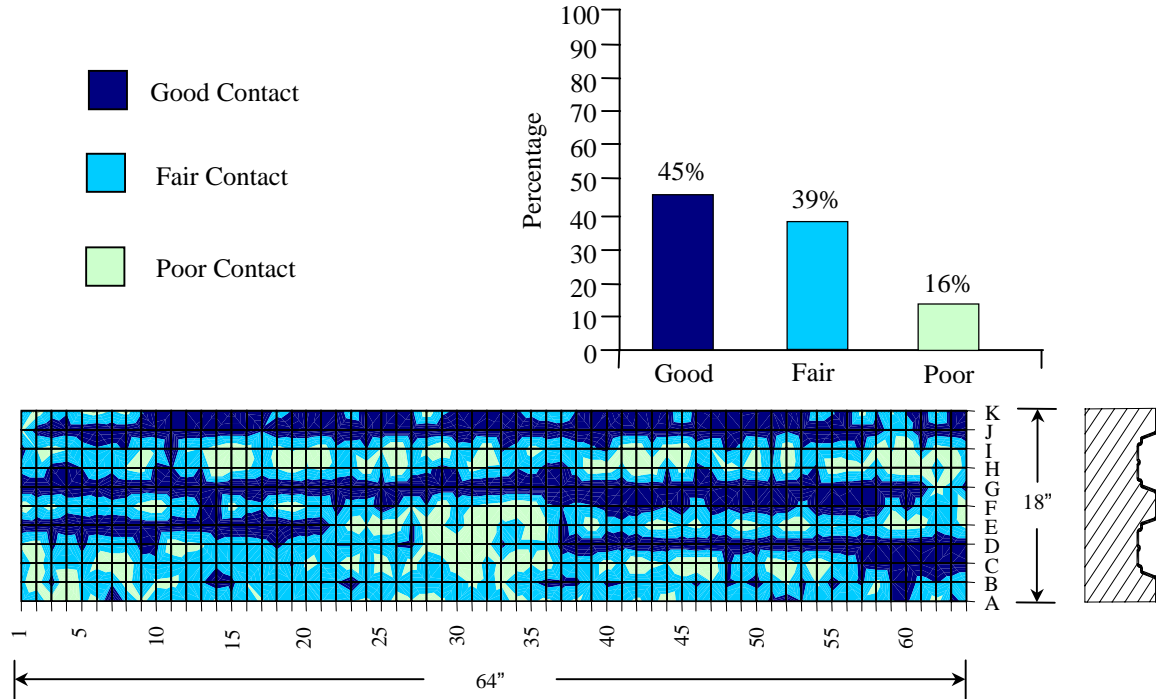


Figure 5.31. Pulse-echo contour map and bar chart for Before Cracking for specimen WI-S-1-2

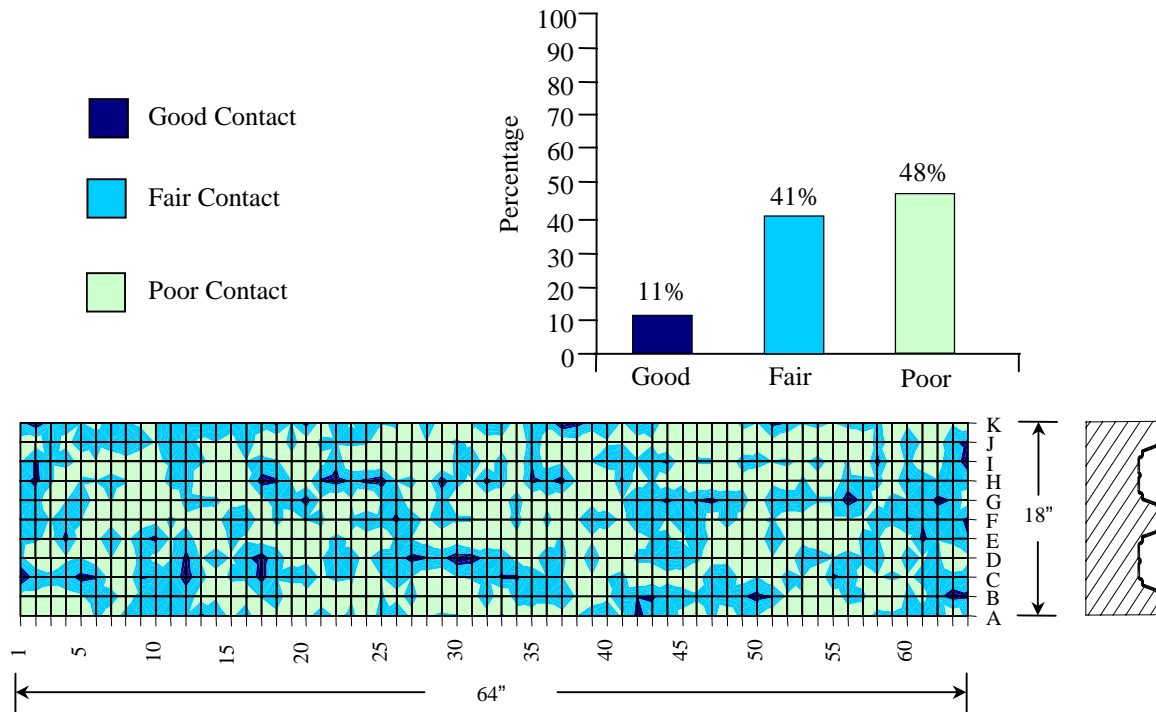


Figure 5.32. Pulse-echo contour map and bar chart for After Cracking for specimen WI-S-1-2

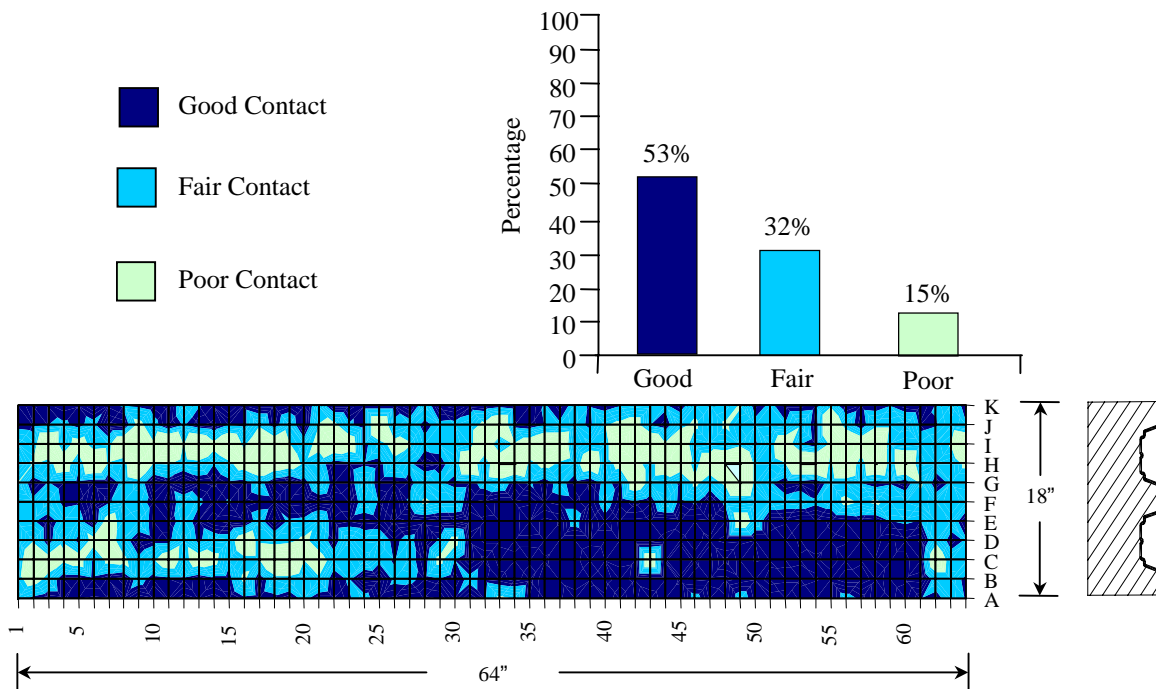


Figure 5.33. Pulse-echo contour map and bar chart for After 1,000 hrs Salt-Water for specimen WI-S-1-2

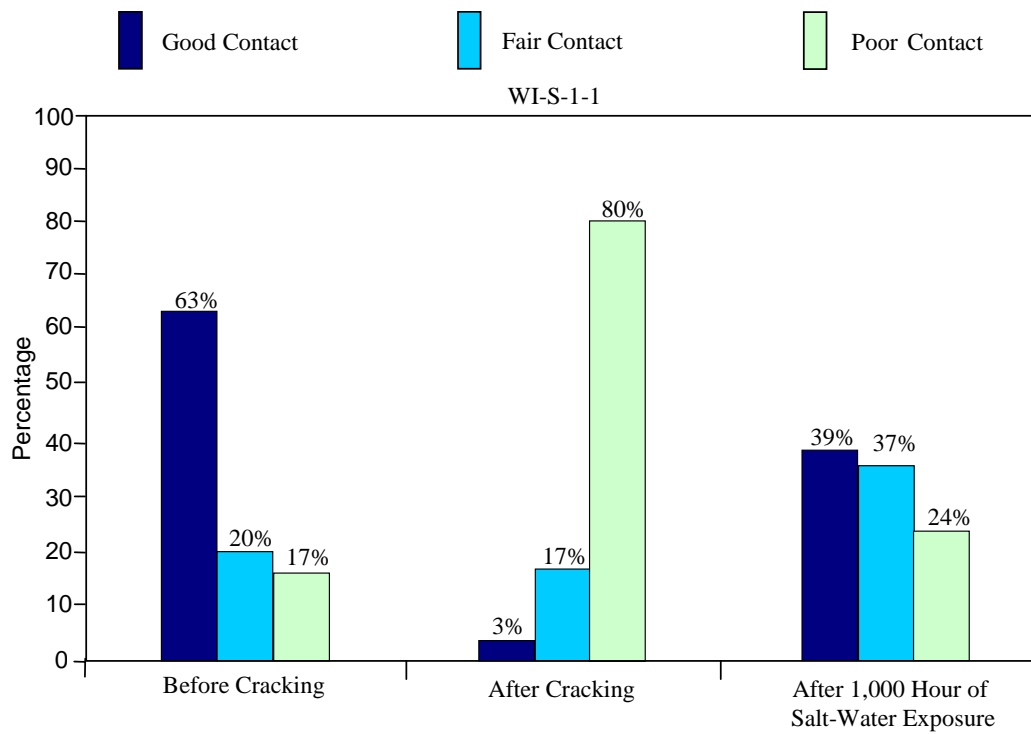


Figure 5.34. Summary of pulse-echo results for specimen WI-S-1-1

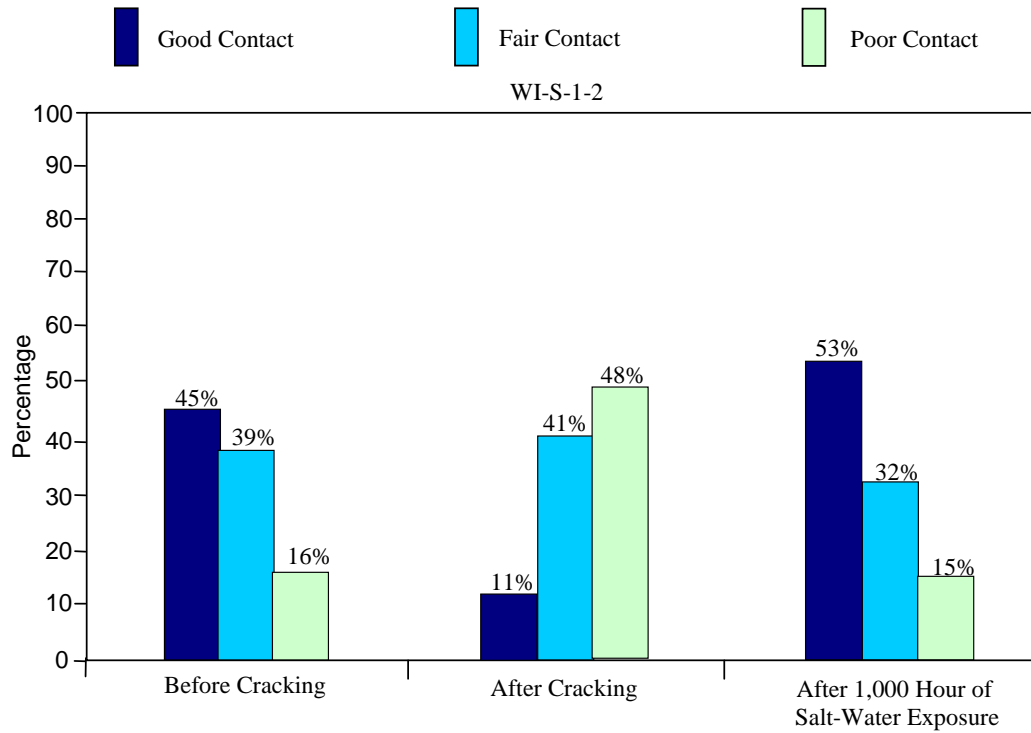


Figure 5.35. Summary of pulse-echo results for specimen WI-S-1-2

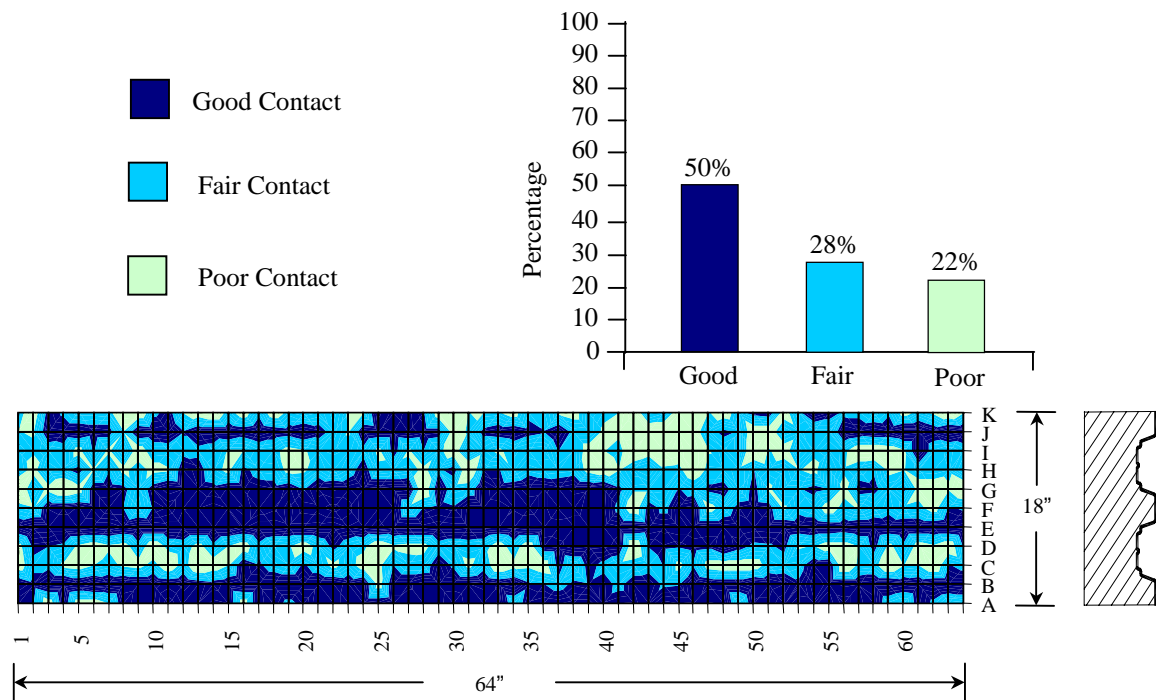


Figure 5.36. Pulse-echo contour map and bar chart for Before Cracking for specimen WI-S-3-1

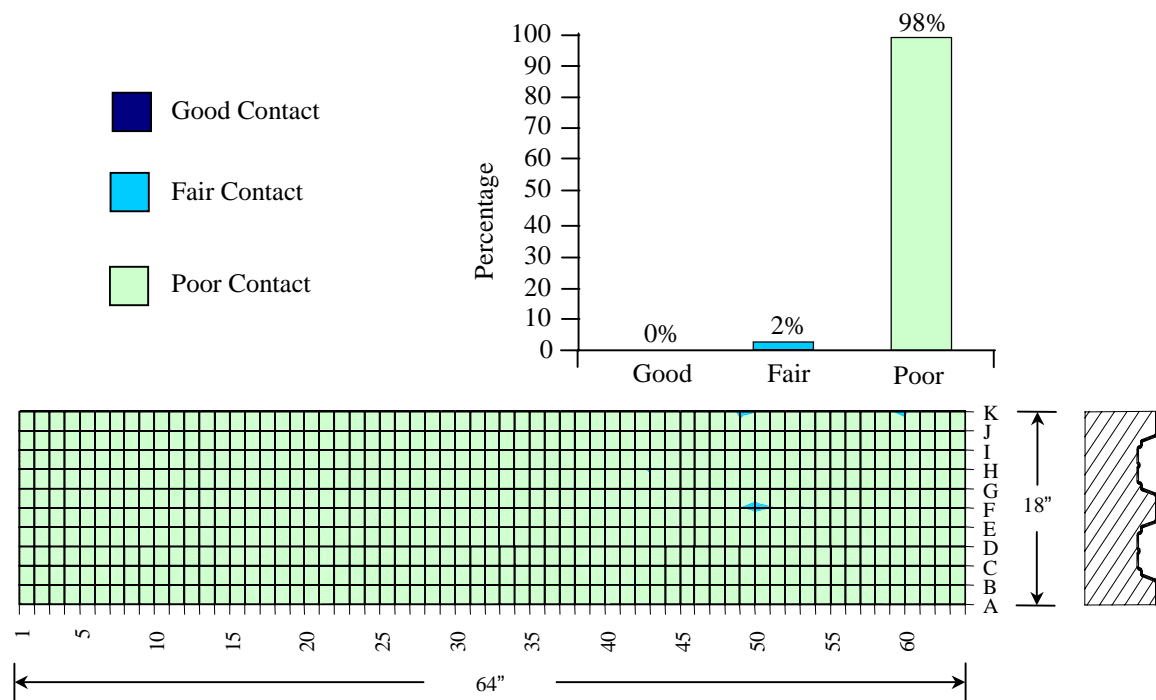


Figure 5.37. Pulse-echo contour map and bar chart for After Cracking for specimen WI-S-3-1

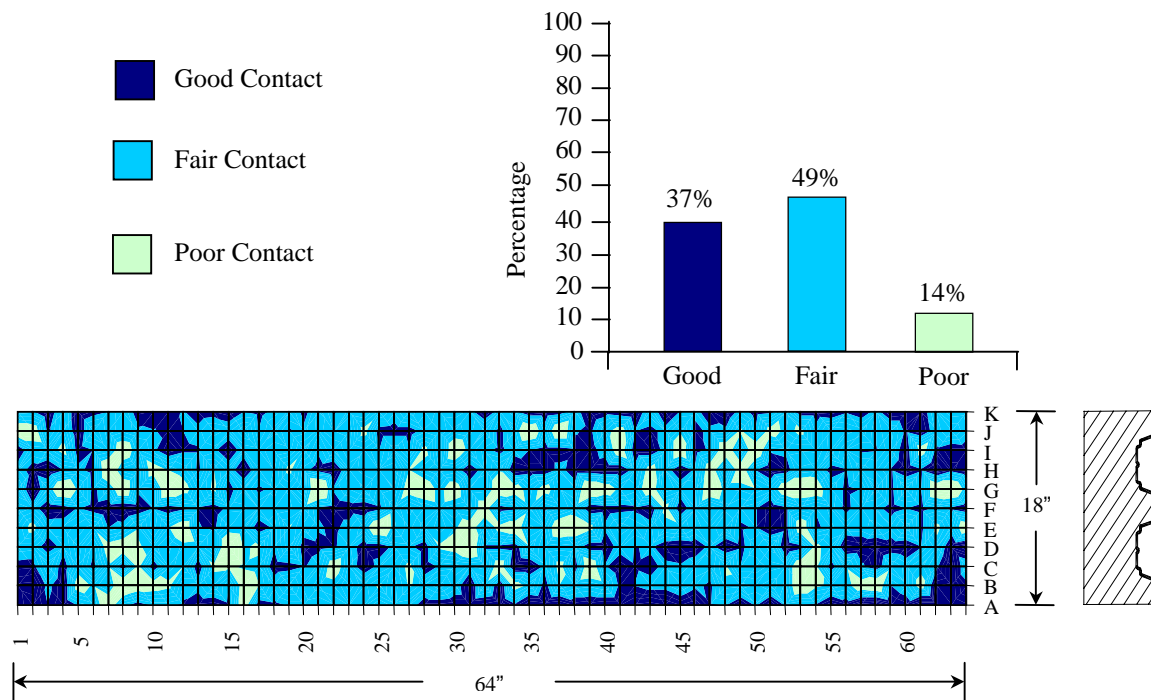


Figure 5.38. Pulse-echo contour map and bar chart for After 1,000 hrs Salt-Water for specimen WI-S-3-1

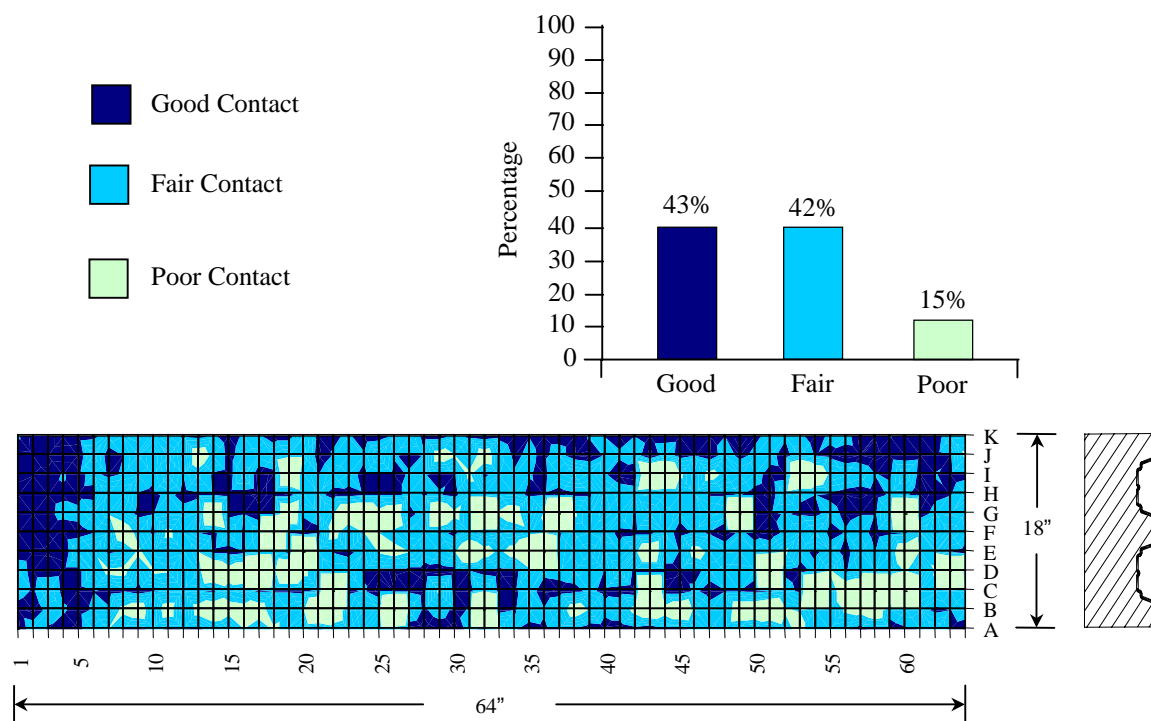


Figure 5.39. Pulse-echo contour map and bar chart for After 3,000 hrs Salt-Water for specimen WI-S-3-1

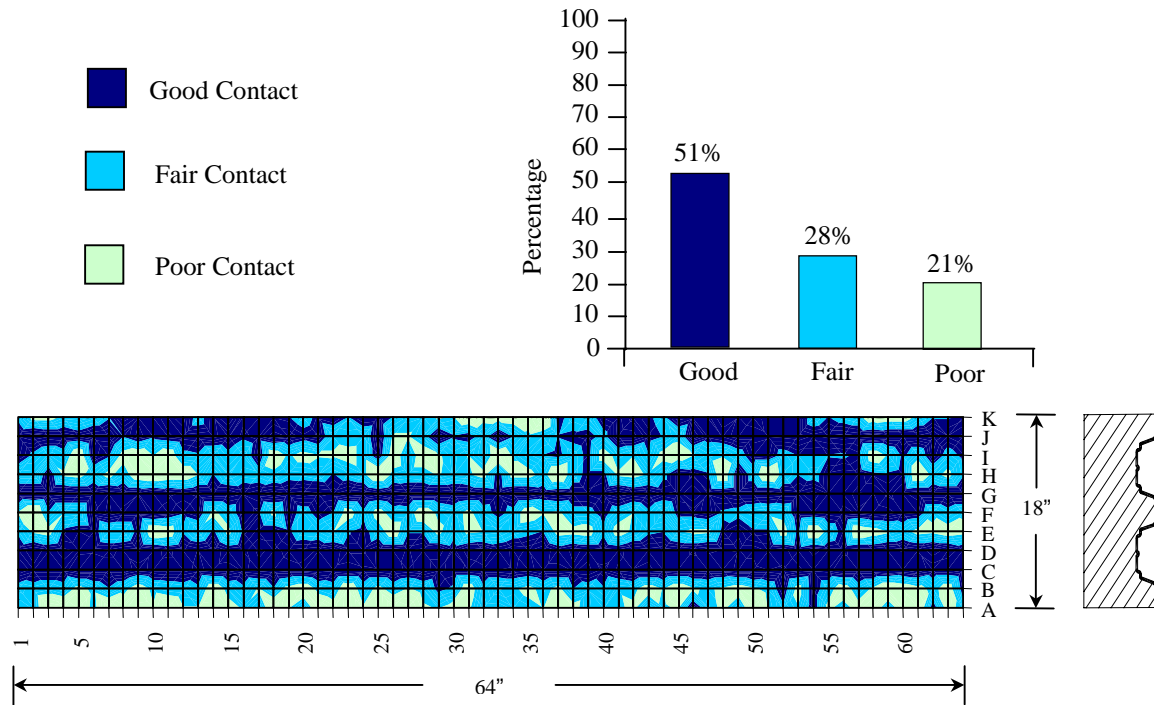


Figure 5.40. Pulse-echo contour map and bar chart for Before Cracking for specimen WI-S-3-2

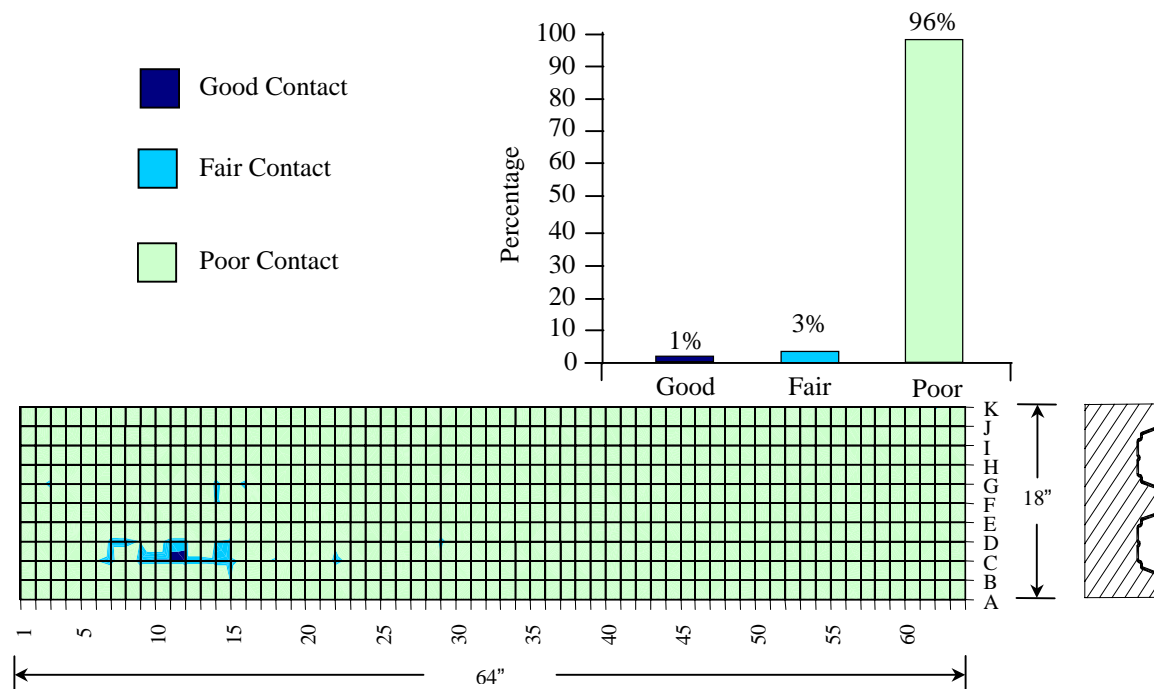


Figure 5.41. Pulse-echo contour map and bar chart for After Cracking for specimen WI-S-3-2

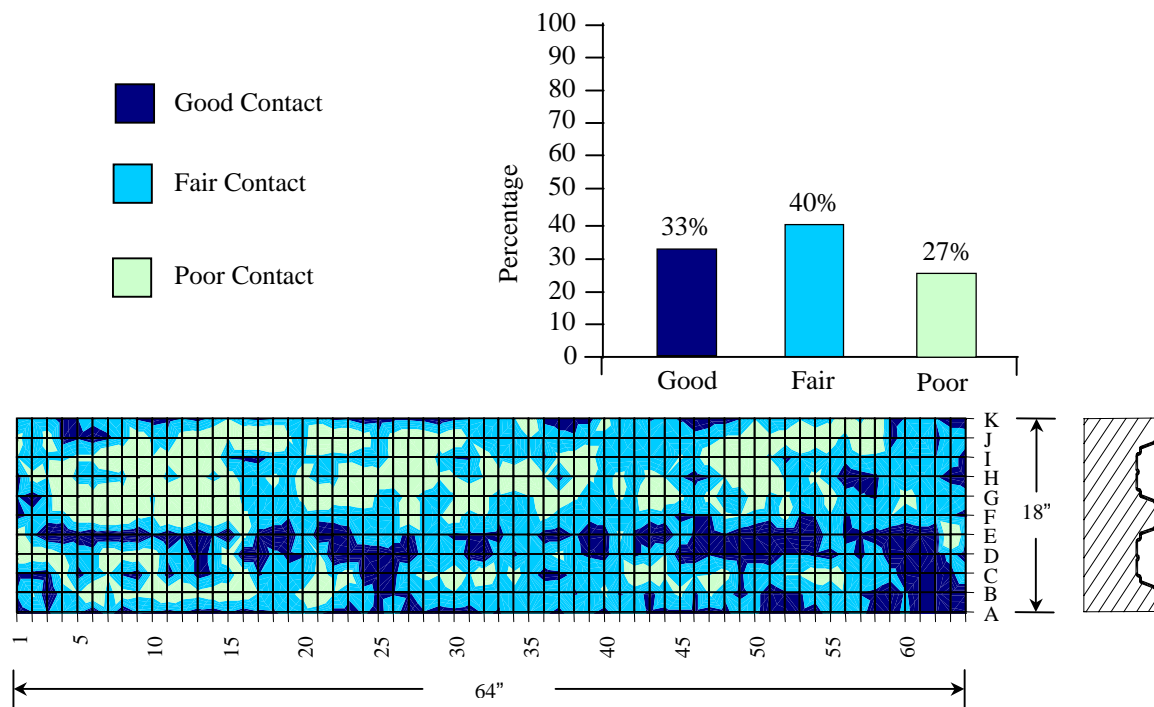


Figure 5.42. Pulse-echo contour map and bar chart for After 1,000 hrs Salt-Water for specimen WI-S-3-2

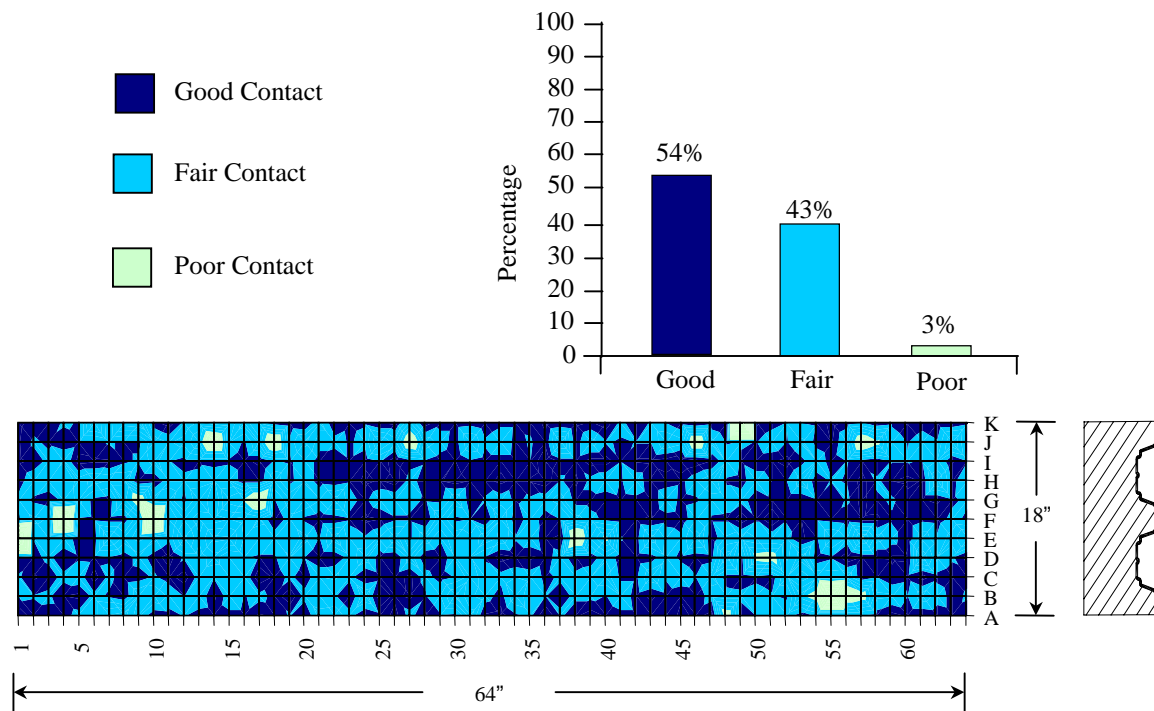


Figure 5.43. Pulse-echo contour map and bar chart for After 3,000 hrs Salt-Water for specimen WI-S-3-2

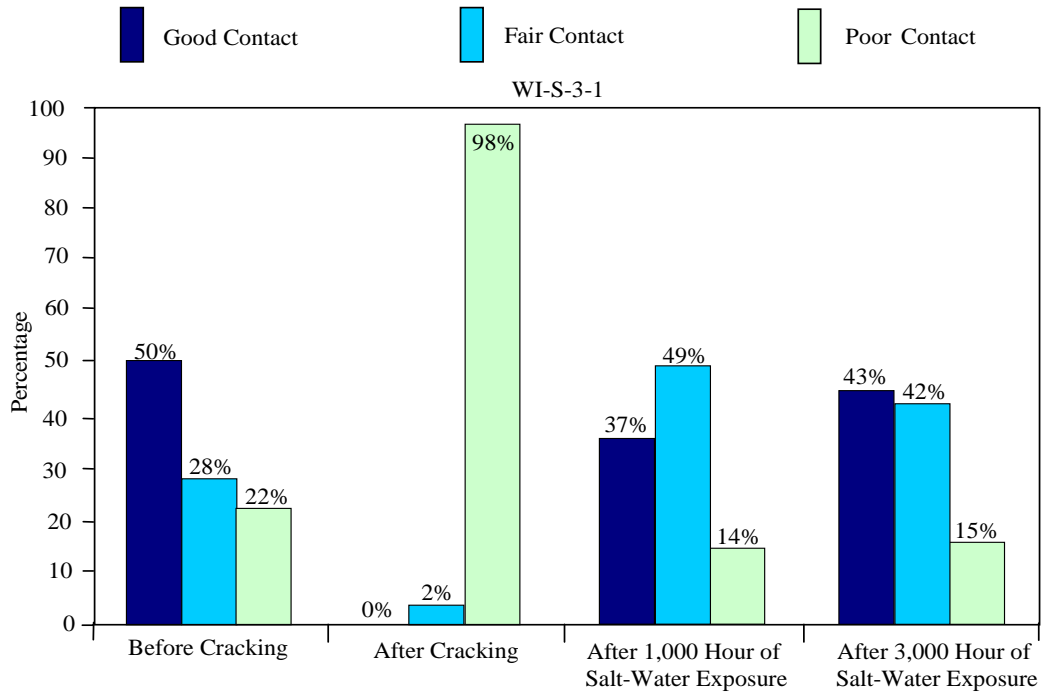


Figure 5.44. Summary of pulse-echo results for specimen WI-S-3-1

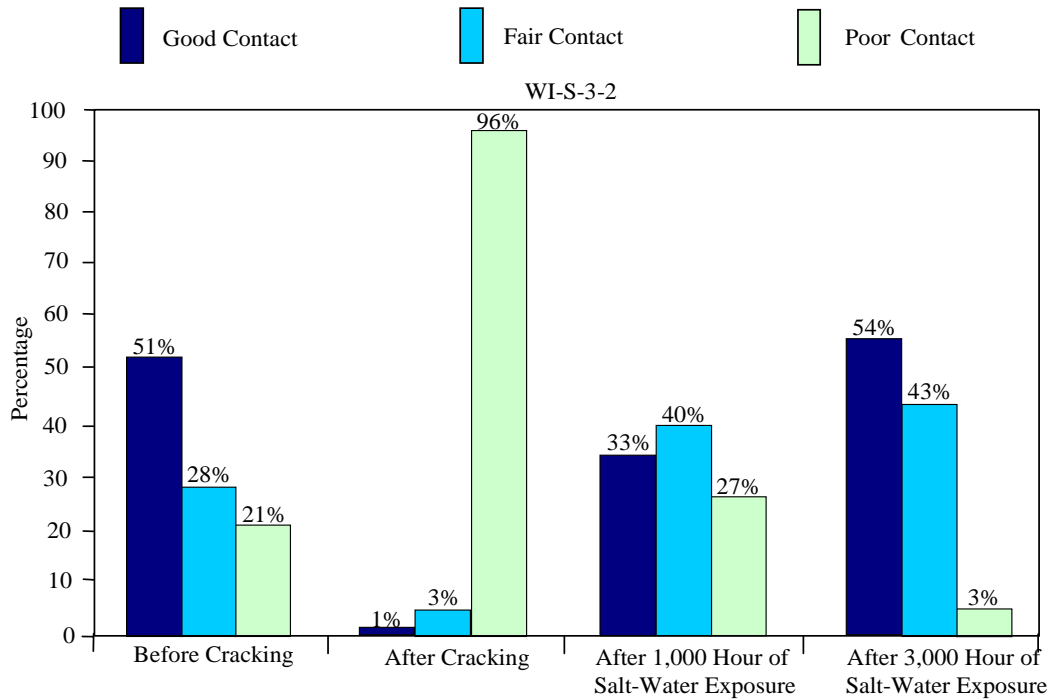


Figure 5.45. Summary of pulse-echo results for specimen WI-S-3-2

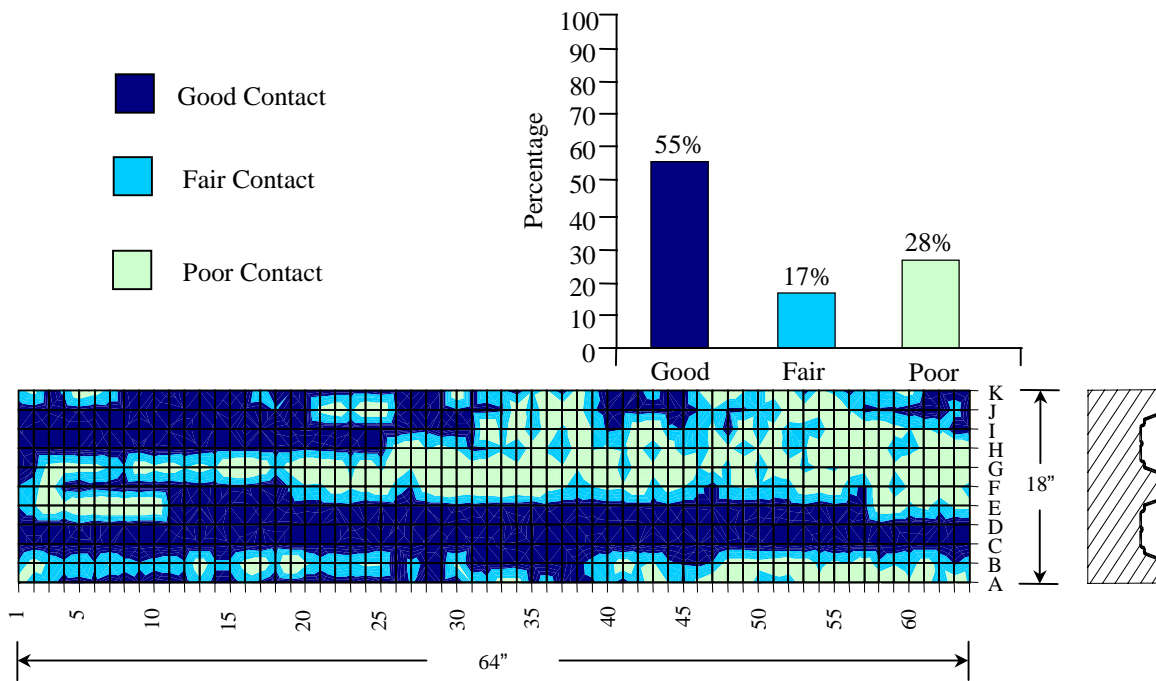


Figure 5.46. Pulse-echo contour map and bar chart for Before Cracking for specimen WI-S-10-1

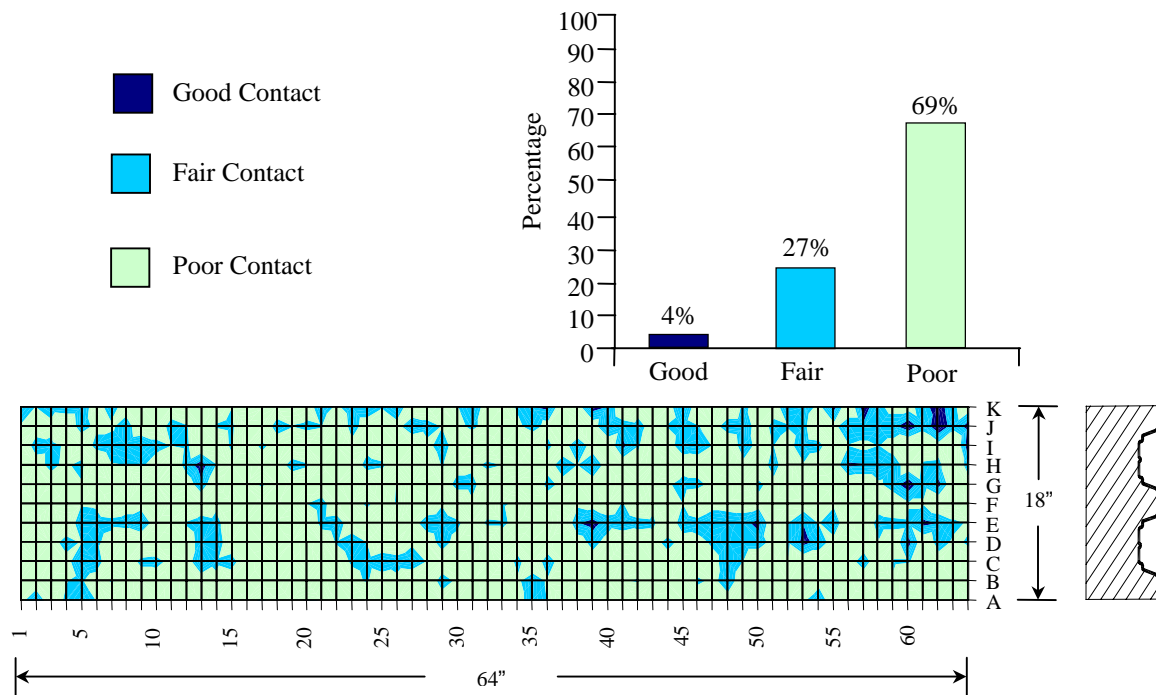


Figure 5.47. Pulse-echo contour map and bar chart for After Cracking for specimen WI-S-10-1

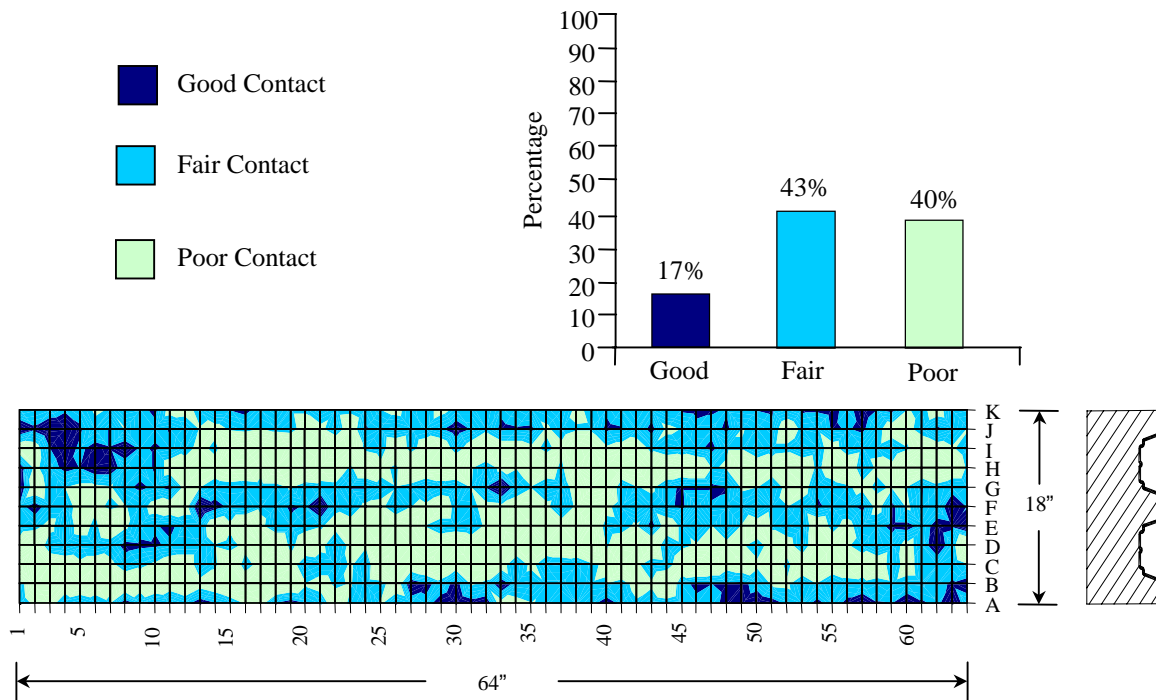


Figure 5.48. Pulse-echo contour map and bar chart for After 1,000 hrs Salt-Water for specimen WI-S-10-1

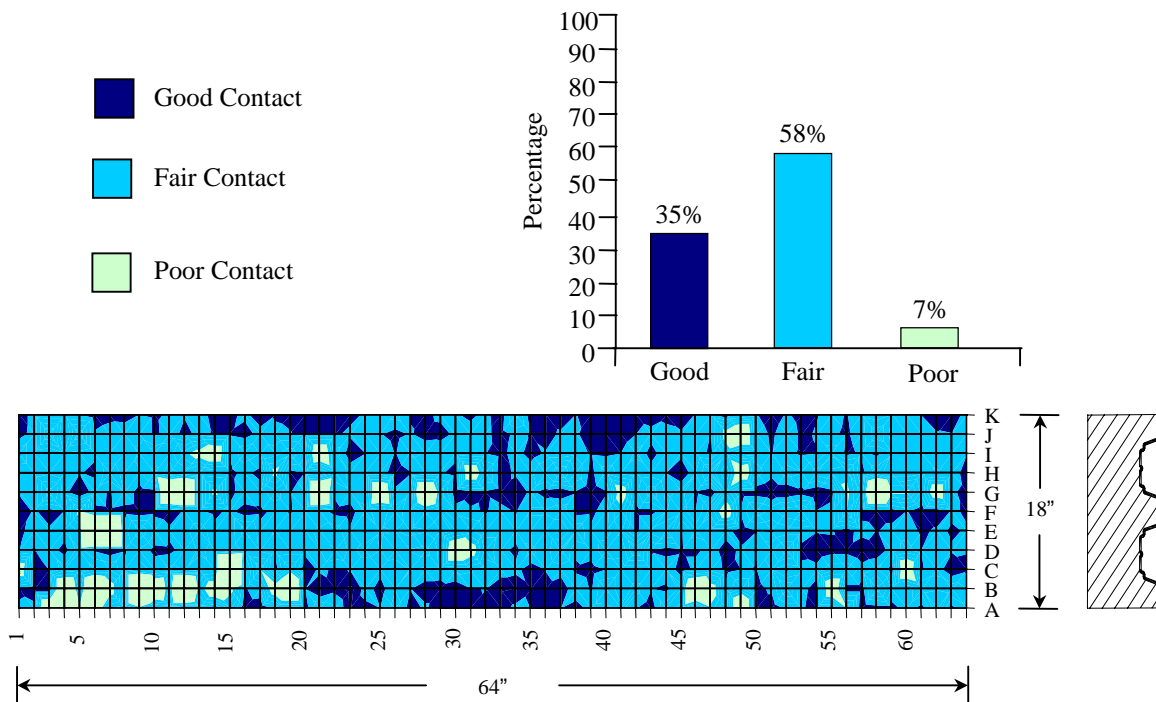


Figure 5.49. Pulse-echo contour map and bar chart for After 3,000 hrs Salt-Water for specimen WI-S-10-1

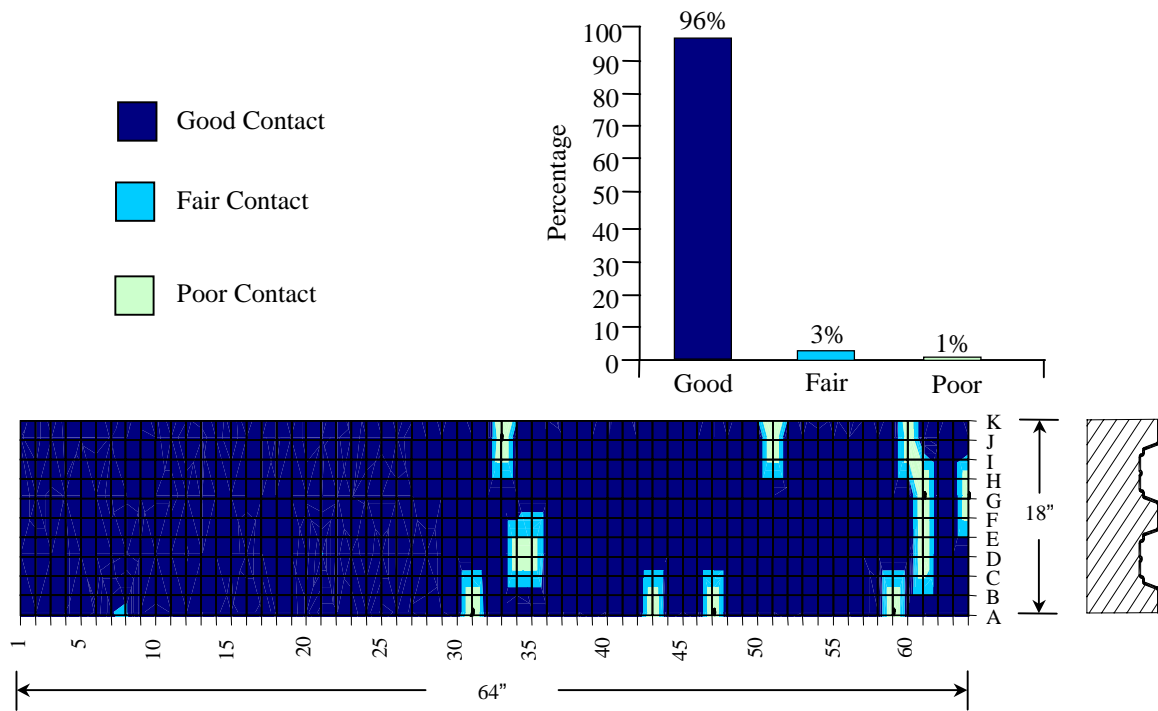


Figure 5.50. Pulse-echo contour map and bar chart for After 10,000 hrs Salt-Water for specimen WI-S-10-1

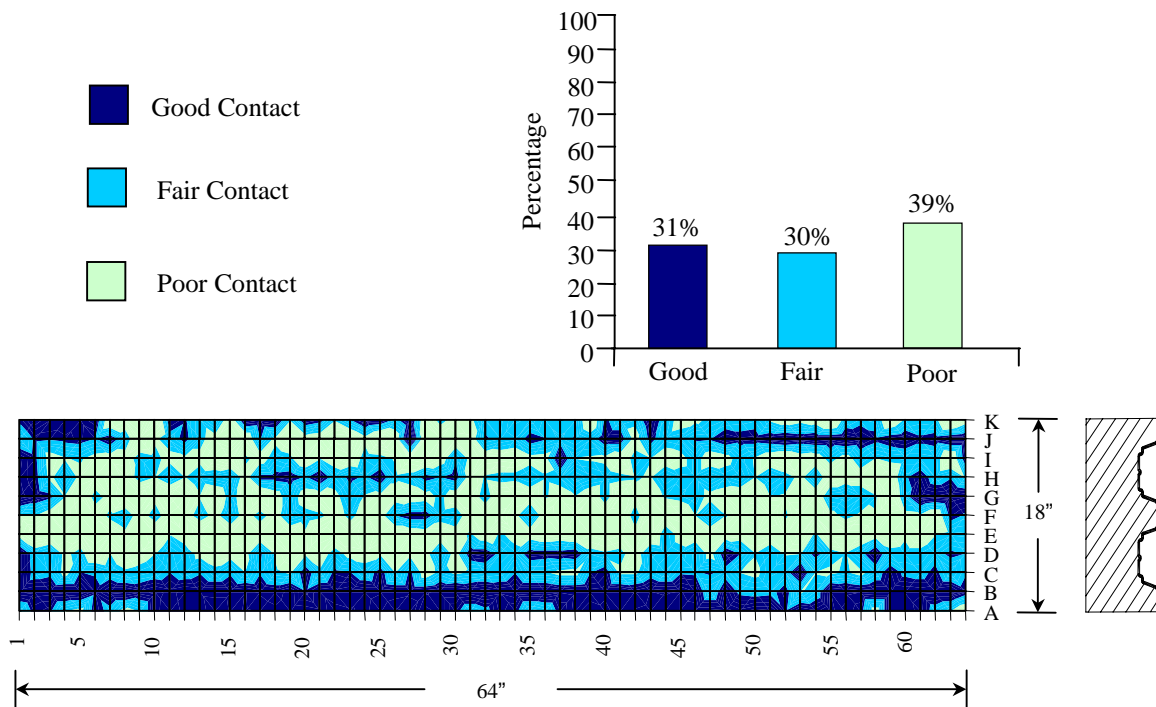


Figure 5.51. Pulse-echo contour map and bar chart for Before Cracking for specimen WI-S-10-2

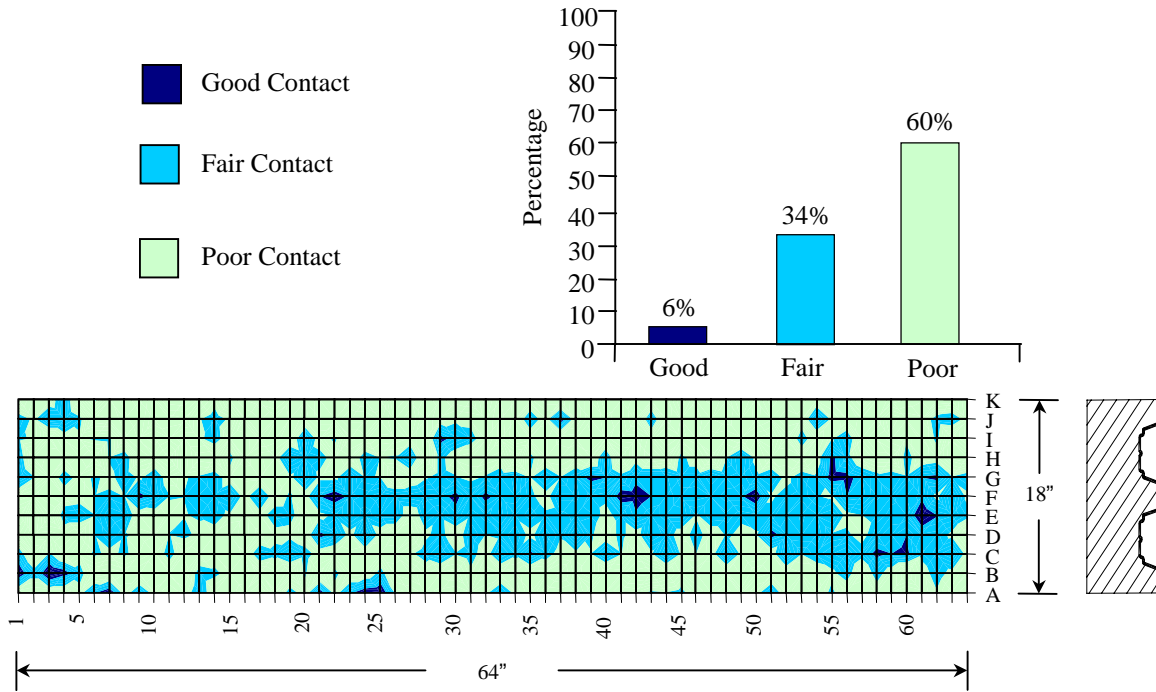


Figure 5.52. Pulse-echo contour map and bar chart for After Cracking for specimen WI-S-10-2

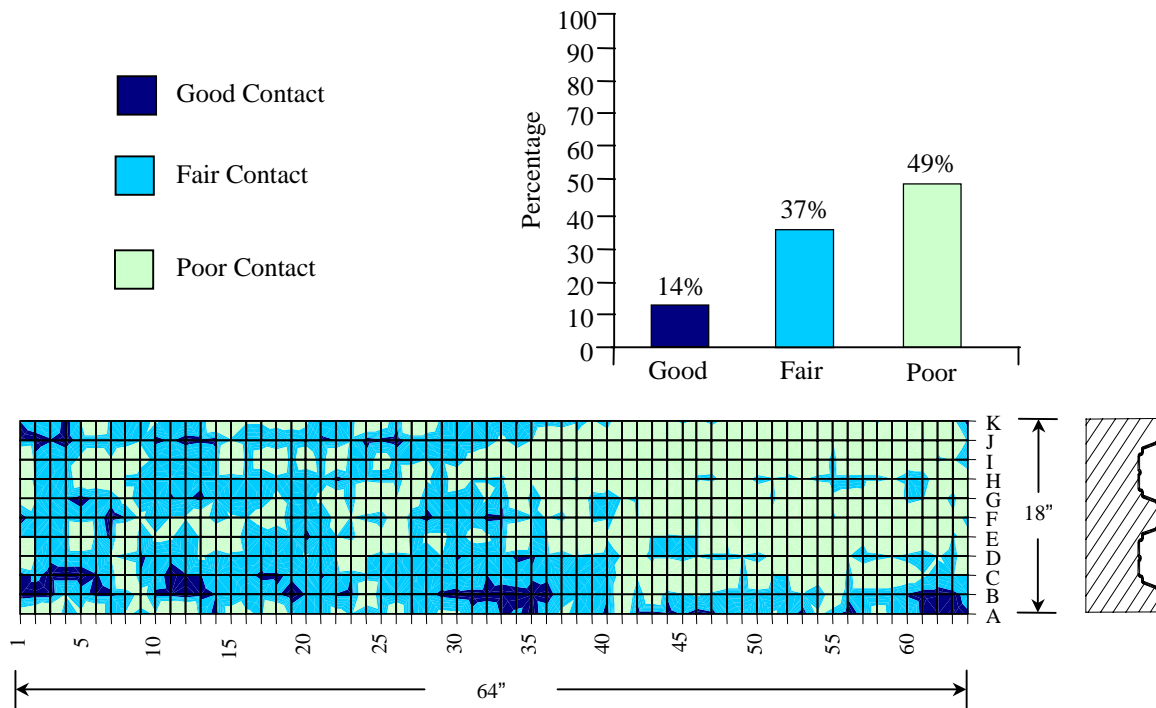


Figure 5.53. Pulse-echo contour map and bar chart for After 1,000 hrs Salt-Water for specimen WI-S-10-2

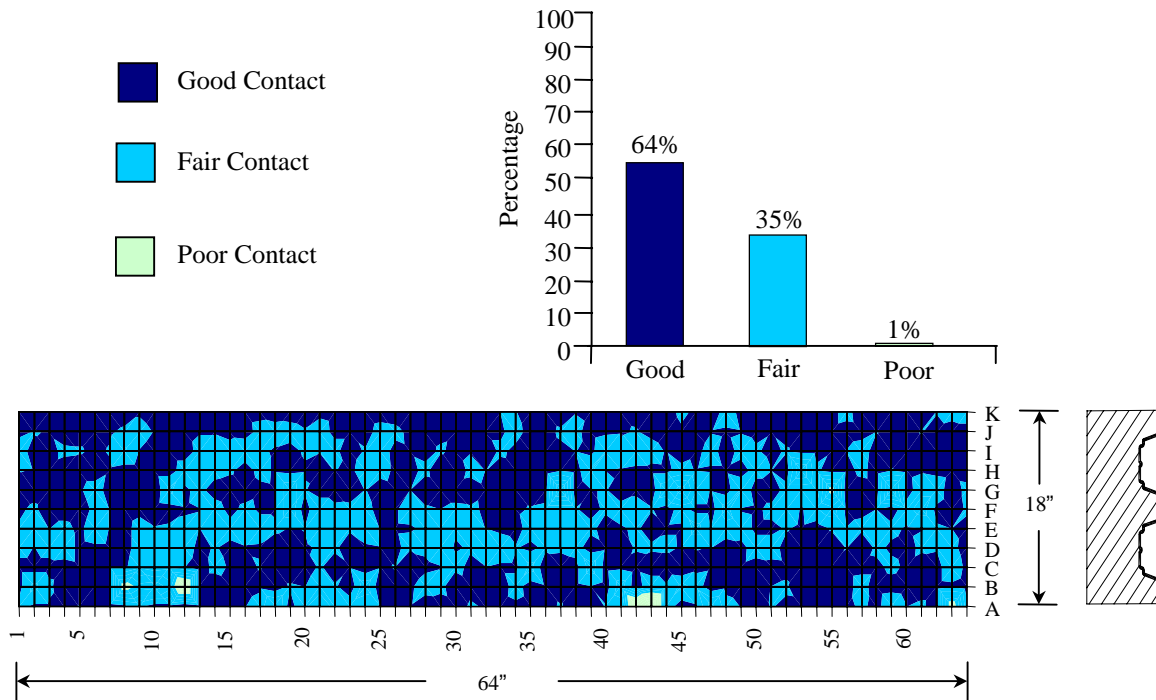


Figure 5.54. Pulse-echo contour map and bar chart for After 3,000 hrs Salt-Water for specimen WI-S-10-2

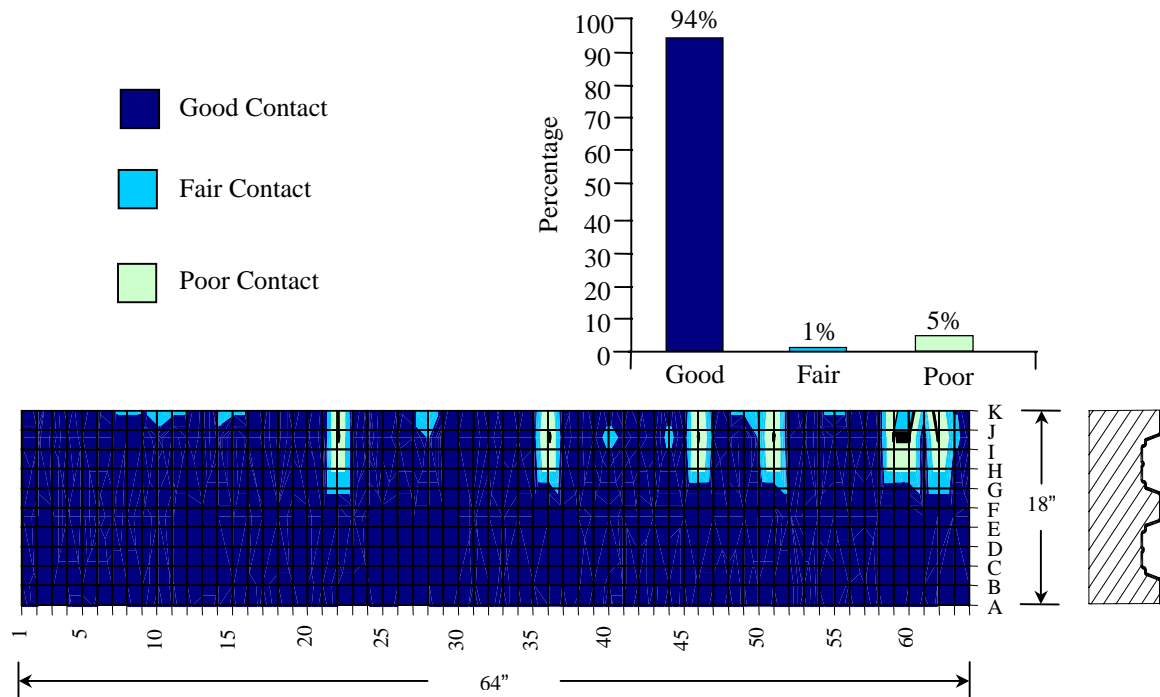


Figure 5.55. Pulse-echo contour map and bar chart for After 10,000 hrs Salt-Water for specimen WI-S-10-2

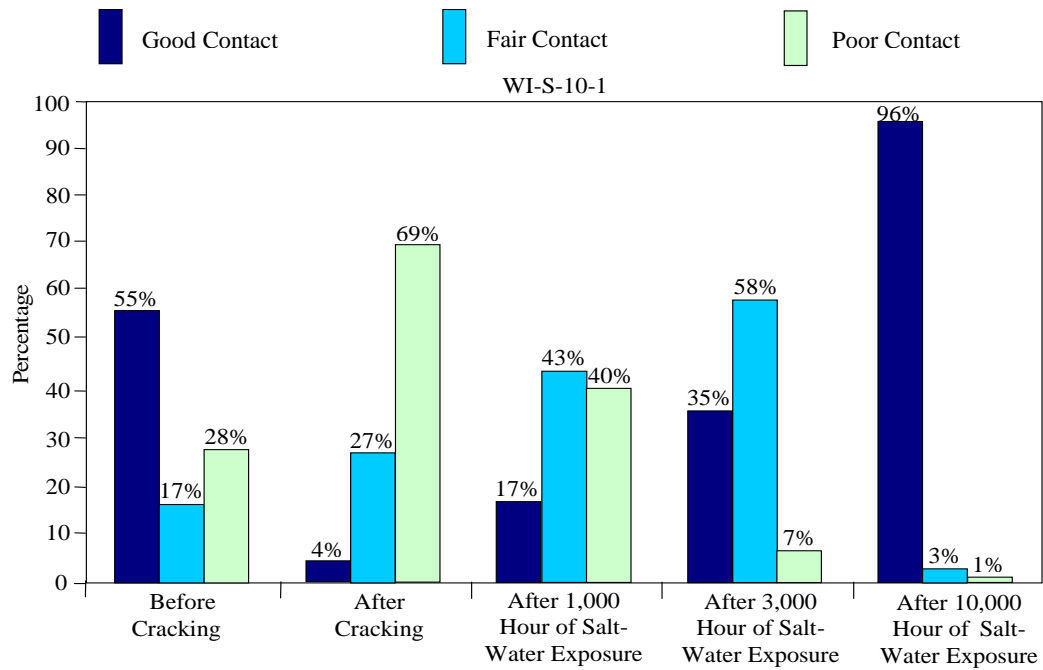


Figure 5.56. Summary of pulse-echo results for specimen WI-S-10-1

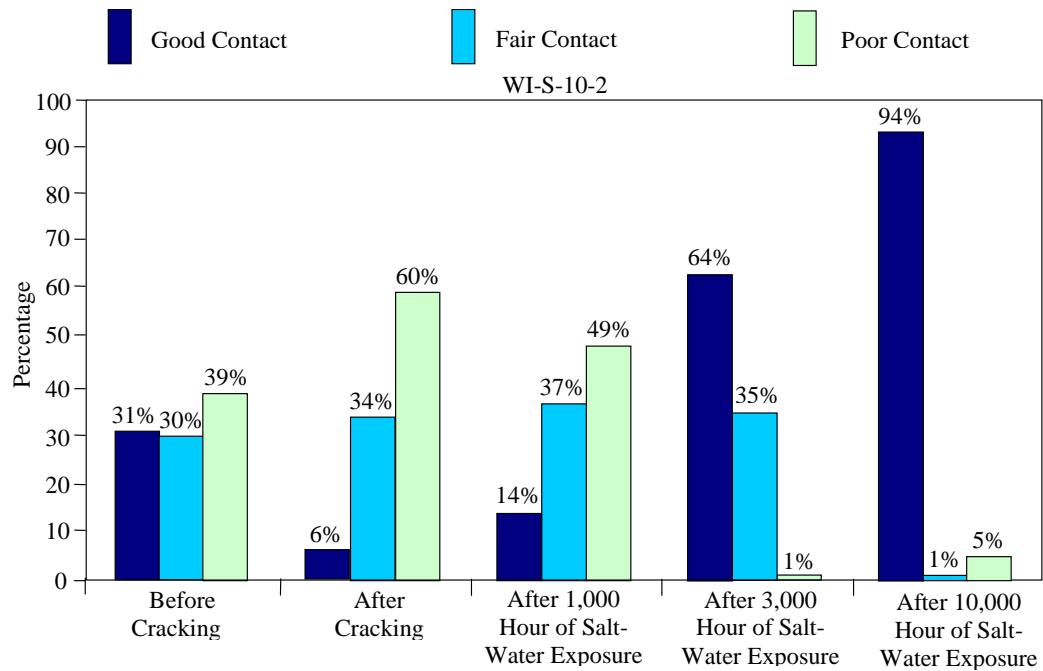


Figure 5.57. Summary of pulse-echo results for specimen WI-S-10-2

The overall trend of quality of contact between the SIPMF and the concrete is generally consistent for all salt-water exposure specimens. The initial contact (before cracking) is consistently good, a significant loss of contact occurs upon service load cracking, and an apparent improvement of contact is observed with continued salt-water exposure. The average contact ratings for all salt-water specimens before cracking were 49% good, 27% fair, and 24% poor. After cracking, the average contact ratings measured were 4% good, 21% fair, and 75% poor. After the first 1,000 hours of salt-water exposure, the average good contact rating for all specimens increased to 32%. The average good contact rating increased to 49% and 95% for 3,000 and 10,000 hours of salt-water exposure, respectively. The apparent improvement in contact is attributed to accumulation of mineral precipitate between the SIPMF and the concrete. Some similarity of spatial patterns of contact ratings are observed for the before cracking specimens. Regions of consistent contact rating appear to follow generally longitudinal trends. After cracking (and for further stages of salt-water conditioning), no distinct or consistent spatial trends are observed in the regions of consistent contact ratings.

Mineral precipitate on the salt-water exposure specimens was observed for all monitored exposure periods. SIPMFs were removed from the specimens after ultimate load tests for inspection. Some precipitate was observed on the top side of the SIPMF (side in contact with concrete) after 1,000 hours of salt-water exposure. Noticeably more precipitate was observed on the removed forms after 3,000 hours, and a similar high amount of precipitation was observed on the 10,000-hour salt-water exposures specimens. Qualitative chemical analysis conducted on precipitate collected from between the SIPMF and the concrete for 10,000-hour salt-water exposures specimens indicated presence of Calcium and Iron (traced to concrete/cement origin from lime and tetracalcium aluminoferrite), Zinc (traced to galvanized coating of SIPMF). Tests conducted on precipitate collected on the underside of the SIPMF (exposed side) on 3,000-hour salt-water exposures specimens indicated presence of Calcium, Iron, and Magnesium (traced to concrete/cement origin from i) lime, ii) tetracalcium aluminoferrite, and iii) magnesium oxide), as well as Sodium (traced to salt solution). A noteworthy observation of the analysis of the presence of precipitate is that sodium was not detected in the area between the SIPMF and the concrete.

5.3.3 Ultrasonic Through-Transmission Results

Ultrasonic through-transmission tests were conducted on a 3-in. slice removed from each specimen before ultimate load testing. Conducting through-transmission tests over a grid pattern on each slice allowed for determination of pulse-velocity over the entire longitudinal cross section of each specimen. Through-transmission test results are presented in Figures 5.58 to 5.71 for specimens with SIPMF. Results of the through-transmission tests are presented as contour maps representing various ranges of pulse-velocity. Cracks are shown as white lines in figures. The pulse velocity can be correlated to quality of concrete as presented in Chapter 4. The contour maps provide graphical representation of the spatial distribution of quality of concrete. In addition to the contour maps, these figures include profiles of average pulse velocity through the depth ($v_{ave-depth}$) and along the length ($v_{ave-longitudinal}$) of the specimens. Further interpretation of the through-transmission data is presented at the end of this chapter (chronological summaries and comparison of average pulse velocity for entire cross section, perimeter region, interior region, and bottom region of the specimens).

Control Specimens

Through-transmission test results for control specimens with SIPMF are presented in Figures 5.58 and 5.59. The average ultrasonic velocity for the entire cross sections of control specimens with SIPMF was 13,727 ft/sec. The average ultrasonic velocity for the points on the perimeter (rows A and D and points: B1, C1, B41, and C41) for control specimens with SIPMF was 13,577 ft/sec. The average ultrasonic velocity for the interior points (rows B and C except points: B1, C1, B41, and C41) for control specimens with SIPMF was 13,891 ft/sec. The average ultrasonic velocity for the bottom points (rows D) for control specimens with SIPMF was 13,663 ft/sec. Essentially, the distribution of pulse velocity over the cross section is uniform for the control specimens.

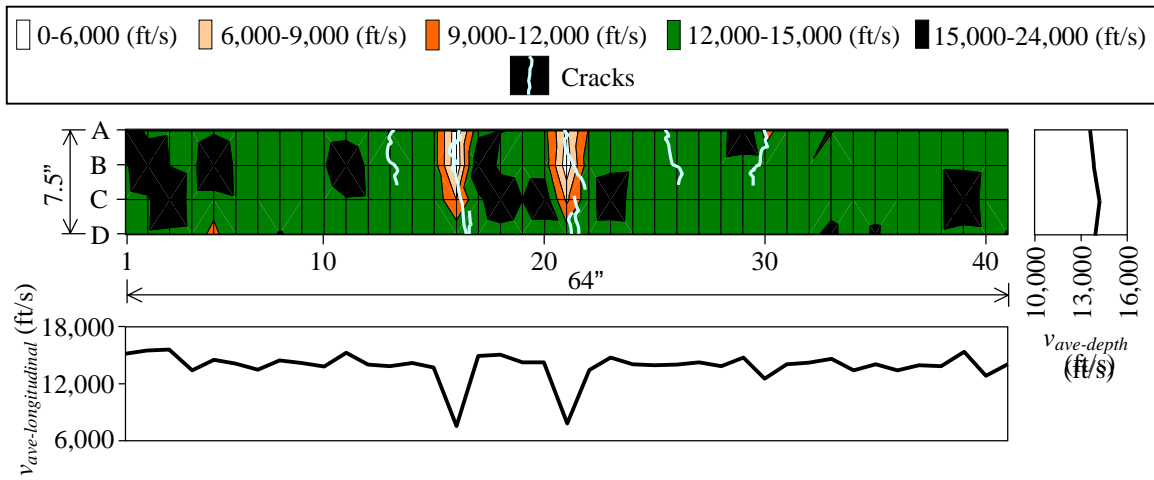


Figure 5.58. Through-transmission test results for slice from specimen WI-C-1

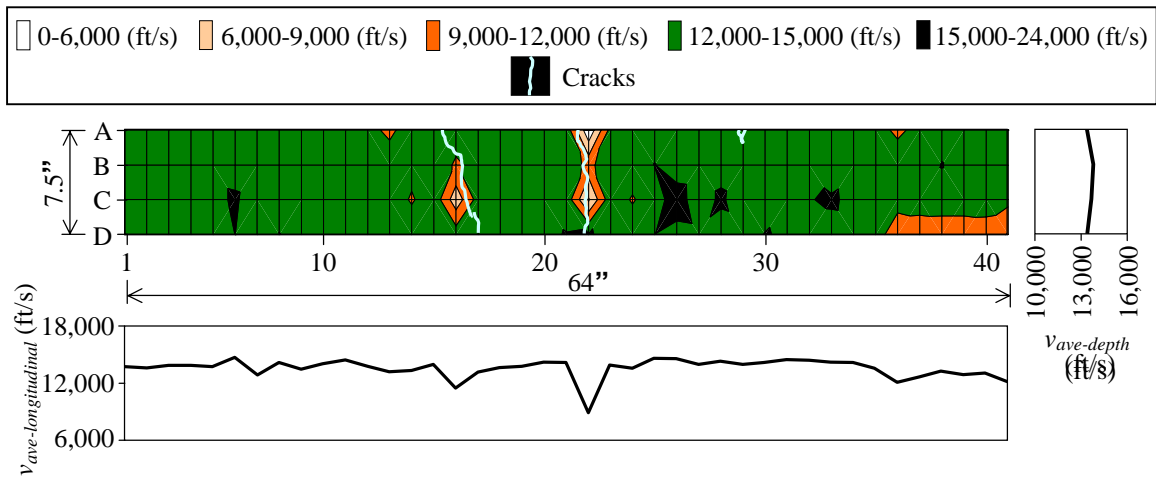


Figure 5.59. Through-transmission test results for slice from specimen WI-C-2

Freeze/Thaw Specimens

Through-transmission test results for 300-cycle freeze/thaw specimens with SIPMF are presented in Figures 5.60 and 5.61. The average ultrasonic velocity for the entire cross sections of 300-cycle freeze/thaw specimens with SIPMF was 14,525 ft/sec. The average ultrasonic velocity for the points on the perimeter (rows A and D and points: B1, C1, B41, and C41) for 300-cycle freeze/thaw specimens with SIPMF was 14,384 ft/sec. The average ultrasonic velocity for the interior points (rows B and C except points: B1, C1, B41, and C41) for 300-cycle freeze/thaw specimens with SIPMF was 14,681 ft/sec. The average ultrasonic velocity for the bottom points (rows D) for 300-cycle freeze/thaw specimens with SIPMF was 14,742 ft/sec. Essentially, the distribution of pulse velocity over the cross section is uniform for the 300-cycle freeze/thaw specimens with SIPMF.

Through-transmission test results for 600-cycle freeze/thaw specimens with SIPMF are presented in Figures 5.62 and 5.63. The average ultrasonic velocity for the entire cross sections of 600-cycle freeze/thaw specimens with SIPMF was 13,979 ft/sec. The average ultrasonic velocity for the points on the perimeter (rows A and D and points: B1, C1, B41, and C41) for 600-cycle freeze/thaw specimens with SIPMF was 13,595 ft/sec. The average ultrasonic velocity for the interior points (rows B and C except points: B1, C1, B41, and C41) for 600-cycle freeze/thaw specimens with SIPMF was 14,404 ft/sec. The average ultrasonic velocity for the bottom points (rows D) for 600-cycle freeze/thaw specimens with SIPMF was 13,412 ft/sec. Essentially, the distribution of pulse velocity over the cross section is uniform for the 600-cycle freeze/thaw specimens with SIPMF.

A summary of through-transmission test results for control specimens and freeze/thaw specimens with SIPMF is presented in Figure 5.64. The average percentages of measurement points for the control specimens with SIPMF were 2% very poor, 1% poor, 4% moderate to questionable, 84% good, and 9% very good. The average percentages of measurement points for the 300-cycle freeze/thaw specimens with SIPMF were 0% very poor, 0% poor, 1% moderate to questionable, 83% good, and 17% very good. The average percentages of measurement points

for the 600-cycle freeze/thaw specimens with SIPMF were 1% very poor, 2% poor, 2% moderate to questionable, 86% good, and 9% very good.

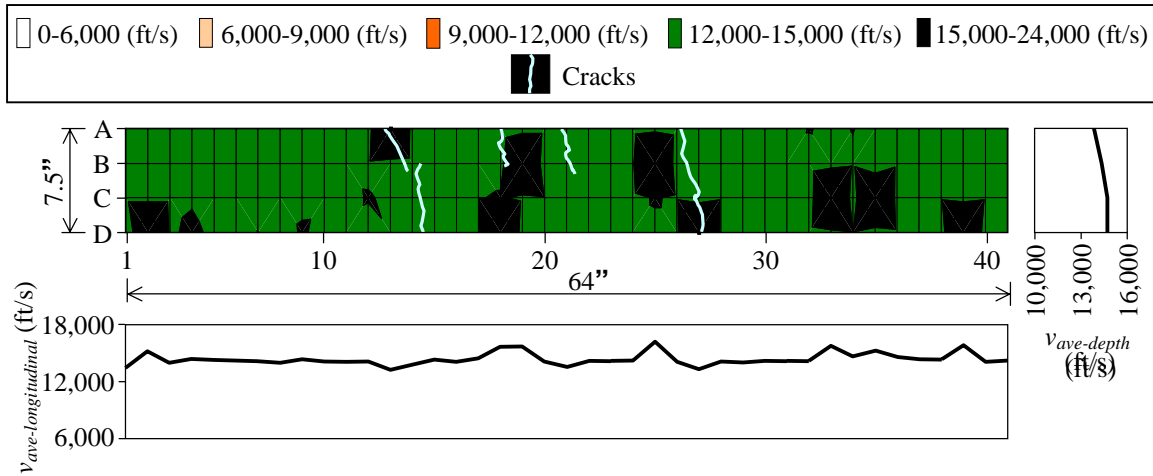


Figure 5.60. Through-transmission test results for slice from specimen WI-F-3-1

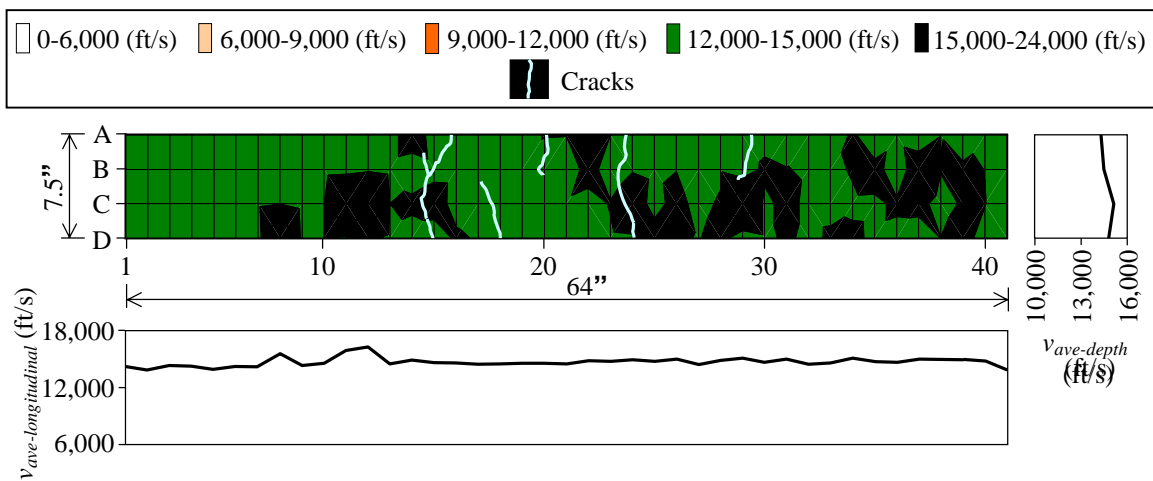


Figure 5.61. Through-transmission test results for slice from specimen WI-F-3-2

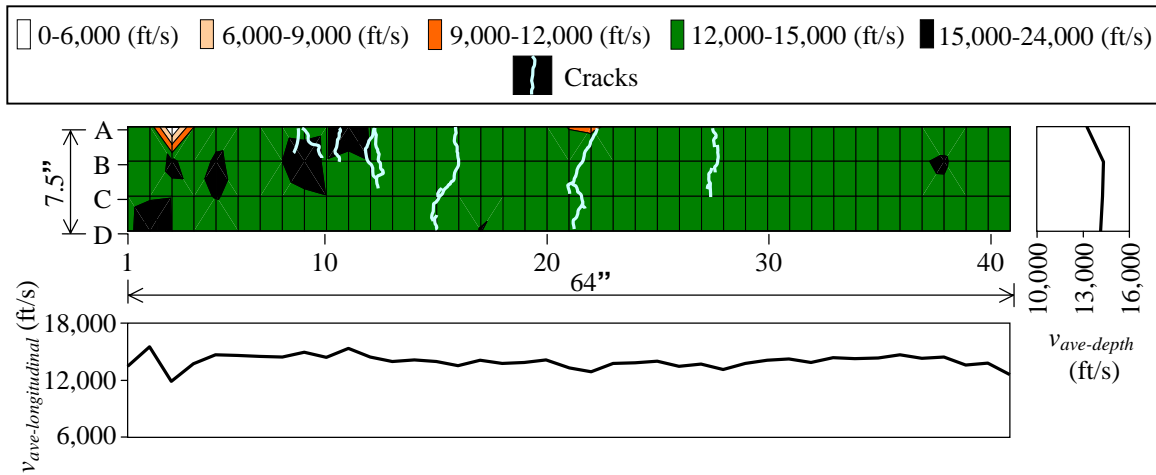


Figure 5.62. Through-transmission test results for slice from specimen WI-F-6-1

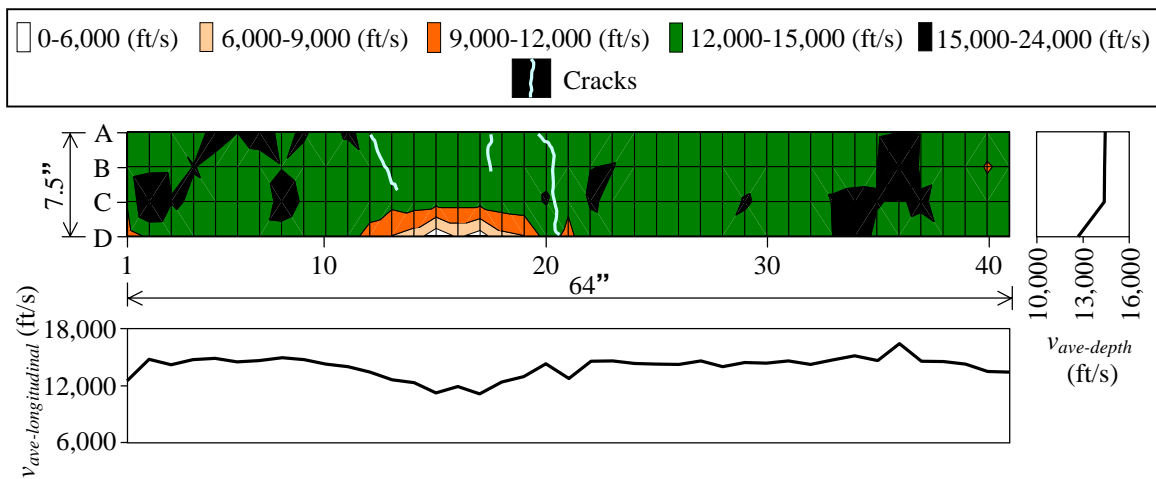


Figure 5.63. Through-transmission test results for slice from specimen WI-F-6-2

The average pulse velocity for the entire cross sections of the freeze/thaw specimens with SIPMF increased to 14,525 ft/s after 300 cycles of freeze/thaw exposure (compared to 13,727 ft/s for control specimens). A subsequent decrease in average pulse velocity to 13,979 ft/s was measured for the 600 cycle specimens, although the average pulse velocity after 600 cycles was still greater than that for the control specimens. The overall increase in pulse velocity after freeze/thaw exposure is attributed to improved hydration conditions in the presence of frequent wetting of the specimens.

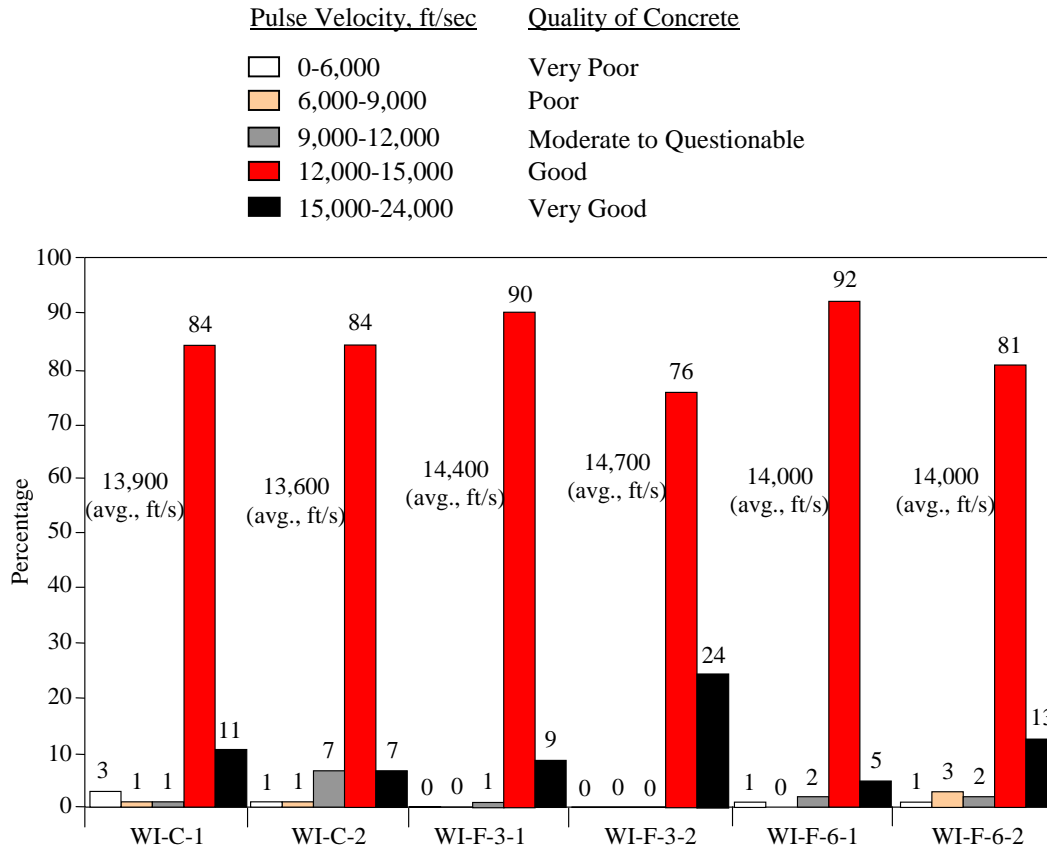


Figure 5.64. Summary of through-transmission test results for control and freeze/thaw exposure specimens with SIPMF

Salt-Water Specimens

Through-transmission test results for 1,000-hour salt-water exposures specimens with SIPMF are presented in Figures 5.65 and 5.66. The average ultrasonic velocity for the entire cross sections of 1,000-hour salt-water exposures specimens with SIPMF was 13,575 ft/sec. The average ultrasonic velocity for the points on the perimeter (rows A and D and points: B1, C1, B41, and C41) for 1,000-hour salt-water exposures specimens with SIPMF was 13,487 ft/sec. The average ultrasonic velocity for the interior points (rows B and C except points: B1, C1, B41, and C41) for 1,000-hour salt-water exposures specimens with SIPMF was 13,673 ft/sec. The average ultrasonic velocity for the bottom points (rows D) for 1,000-hour salt-water exposures specimens with SIPMF was 13,275 ft/sec. Essentially, the distribution of pulse velocity over the cross section is uniform for the 1,000-hour salt-water exposures specimens with SIPMF.

Through-transmission test results for 3,000-hour salt-water exposures specimens with SIPMF are presented in Figures 5.67 and 5.68. The average ultrasonic velocity for the entire cross sections of 3,000-hour salt-water exposures specimens with SIPMF was 14,056 ft/sec. The average ultrasonic velocity for the points on the perimeter (rows A and D and points: B1, C1, B41, and C41) for 3,000-hour salt-water exposures specimens with SIPMF was 14,081 ft/sec. The average ultrasonic velocity for the interior points (rows B and C except points: B1, C1, B41, and C41) for 3,000-hour salt-water exposures specimens with SIPMF was 14,029 ft/sec. The average ultrasonic velocity for the bottom points (rows D) for 3,000-hour salt-water exposures specimens with SIPMF was 13,876 ft/sec. Essentially, the distribution of pulse velocity over the cross section is uniform for the 3,000-hour salt-water exposures specimens with SIPMF.

Through-transmission test results for 10,000-hour salt-water exposures specimens with SIPMF are presented in Figures 5.69 and 5.70. The average ultrasonic velocity for the entire cross sections of 10,000-hour salt-water exposures specimens with SIPMF was 15,025 ft/sec. The average ultrasonic velocity for the points on the perimeter (rows A and D and points: B1, C1, B41, and C41) for 10,000-hour salt-water exposures specimens with SIPMF was 14,987ft/sec. The average ultrasonic velocity for the interior points (rows B and C except points: B1, C1, B41, and C41) for 10,000-hour salt-water exposures specimens with SIPMF was 15,067ft/sec. The average ultrasonic velocity for the bottom points (rows D) for 10,000-hour salt-water exposures specimens with SIPMF was 15,198 ft/sec. Essentially, the distribution of pulse velocity over the cross section is uniform for the 10,000-hour salt-water exposures specimens with SIPMF.

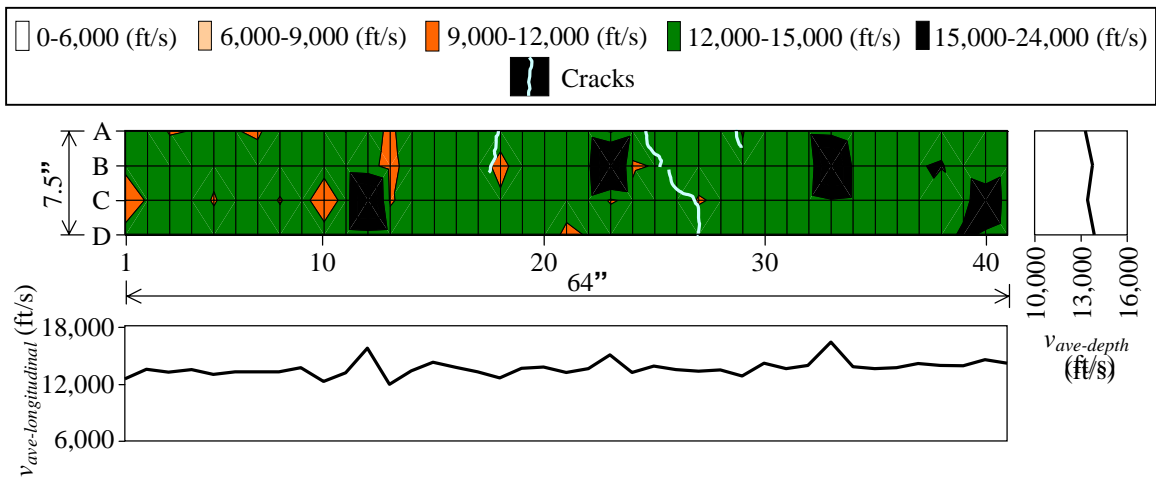


Figure 5.65. Through-transmission test results for slice from specimen WI-S-1-1

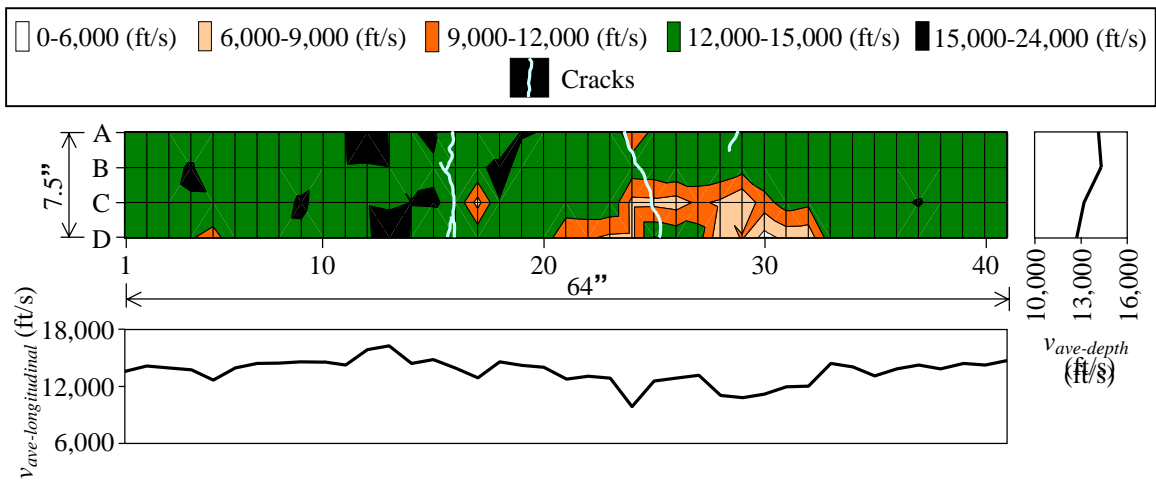


Figure 5.66. Through-transmission test results for slice from specimen WI-S-1-2

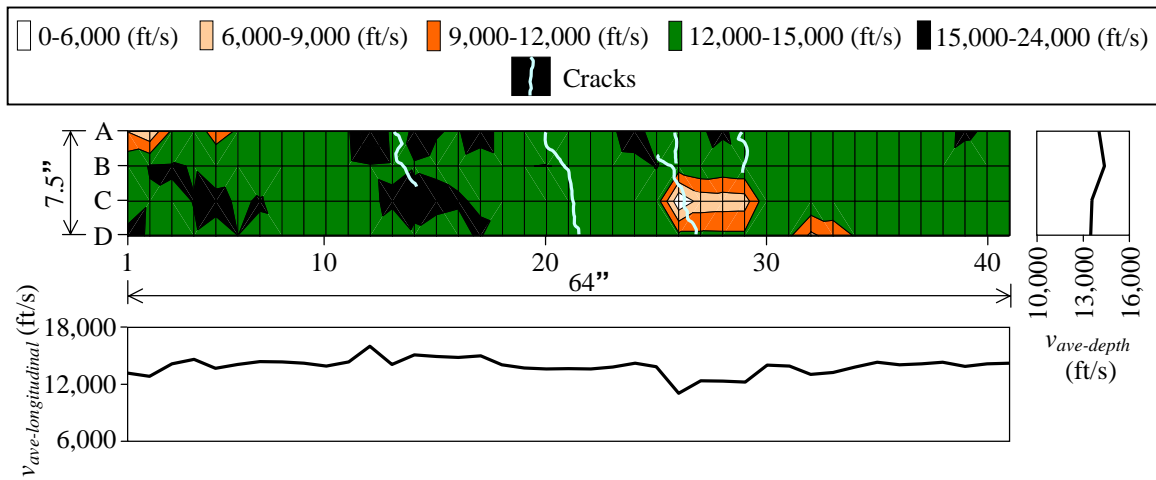


Figure 5.67. Through-transmission test results for slice from specimen WI-S-3-1

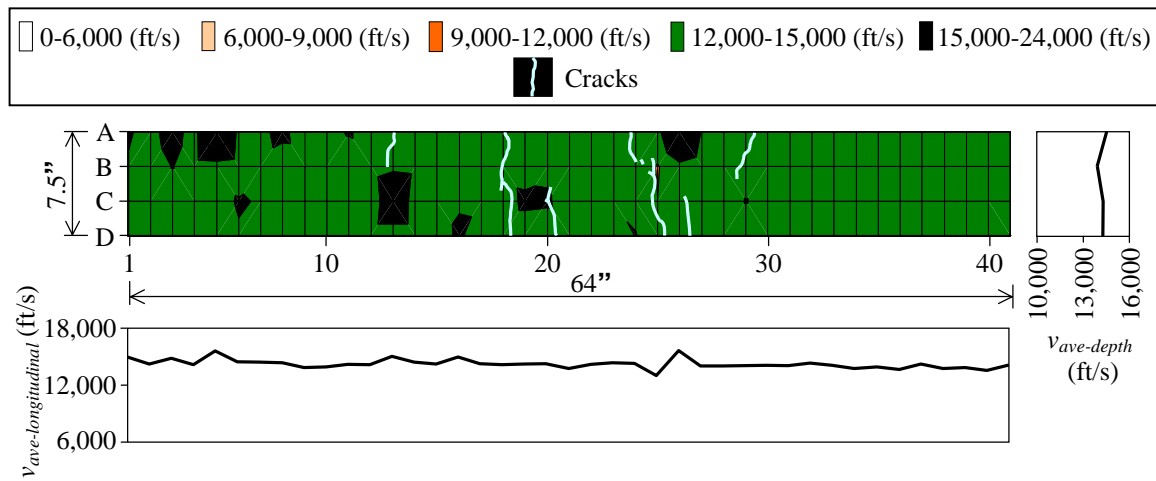


Figure 5.68. Through-transmission test results for slice from specimen WI-S-3-2

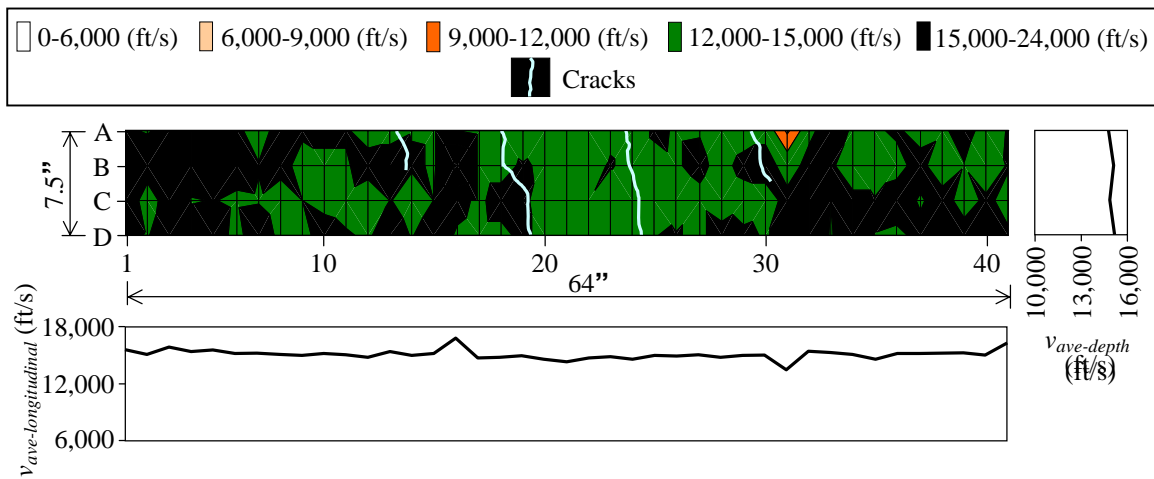


Figure 5.69. Through-transmission test results for slice from specimen WI-S-10-1

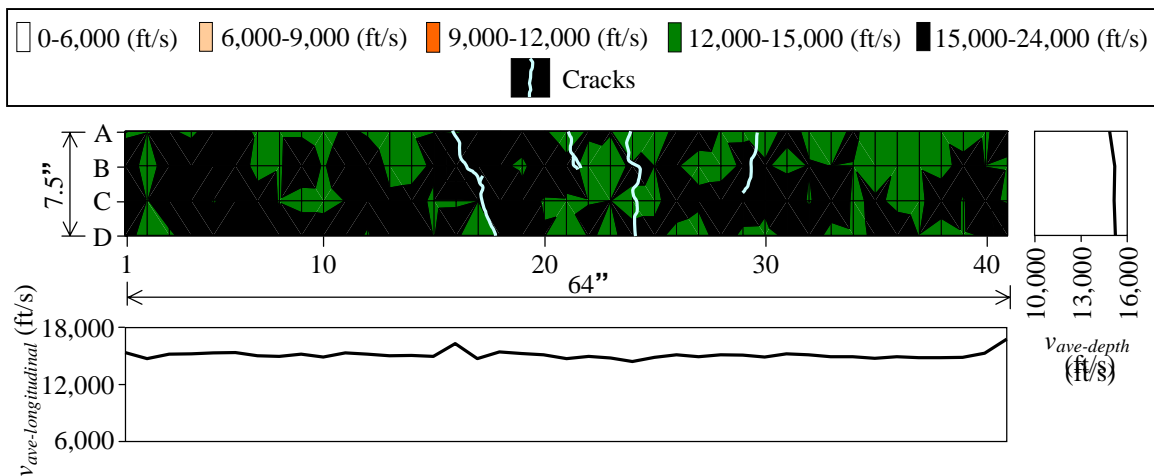


Figure 5.70. Through-transmission test results for slice from specimen WI-S-10-2

A summary of through-transmission test results for control specimens and salt-water specimens with SIPMF is presented in Figure 5.71. The average percentages of measurement points for the control specimens with SIPMF were 2% very poor, 1% poor, 4% moderate to questionable, 84% good, and 9% very good. The average percentages of measurement points for the 1,000-hour salt-water exposures specimens with SIPMF were 0% very poor, 4% poor, 7% moderate to questionable, 84% good, and 5% very good. The average percentages of measurement points for the 3,000-hour salt-water exposures specimens with SIPMF were 0%

very poor, 2% poor, 1% moderate to questionable, 86% good, and 11% very good. The average percentages of measurement points for the 10,000-hour salt-water exposures specimens with SIPMF were 0% very poor, 1% poor, 0% moderate to questionable, 54% good, and 46% very good.

The average pulse velocity for the entire cross sections of the 1,000-hour salt-water specimens (13,575 ft/s) was similar to the control specimens (13,727 ft/s). The average pulse velocity for the entire cross sections increased monotonically with further salt-water exposure (14,056 ft/s for the 3,000-hour salt-water specimens and 15,025 ft/s for the 10,000-hour salt-water specimens). The consistent increase in pulse velocity after salt-water exposure is attributed to improved hydration conditions for specimens submerged in a tank.

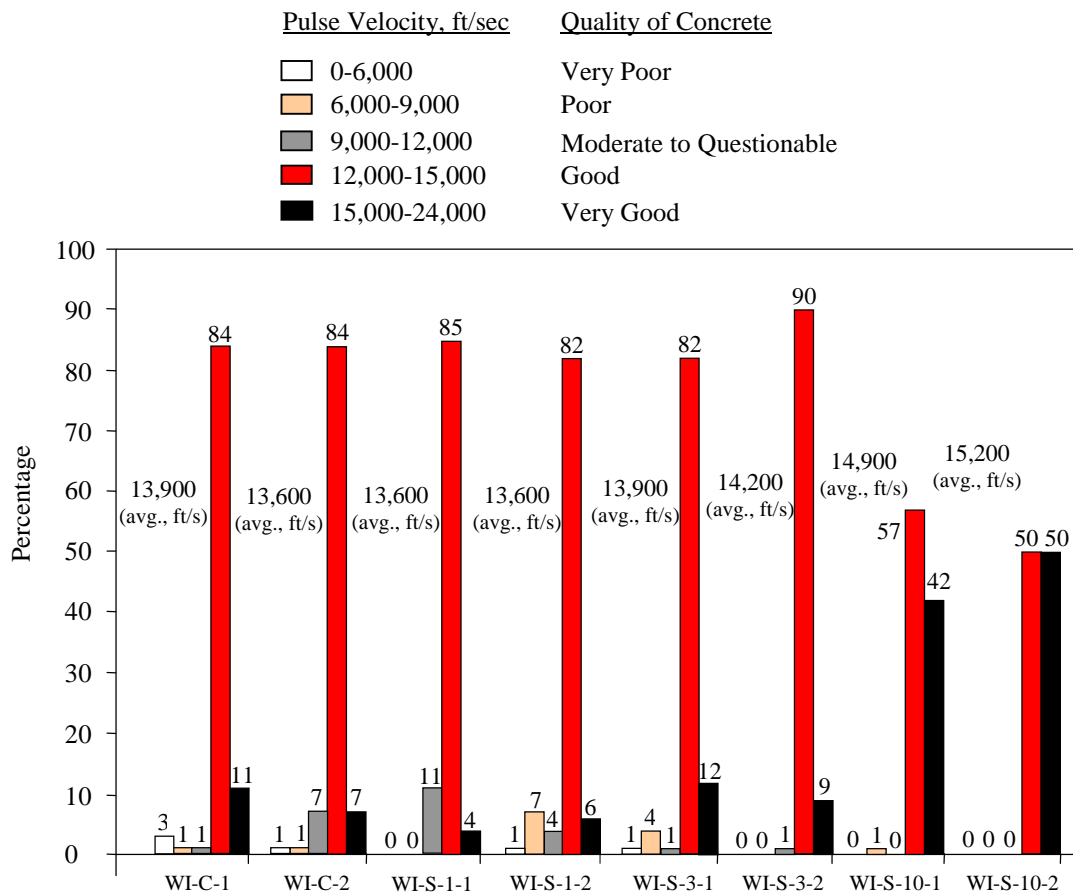
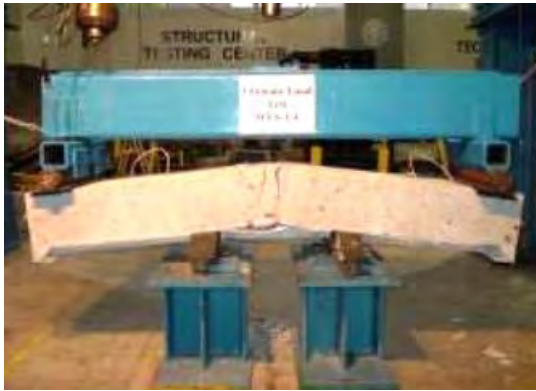


Figure 5.71. Summary of through-transmission test results for control and salt-water exposure specimens with SIPMF

5.3.4 Ultimate Load Test Results

Ultimate load test was applied on each specimen at the end of the environmental exposures, and the load setup “TW” was used for ultimate load tests. Ultimate load test results are presented for control specimens, freeze/thaw specimens, and salt-water specimens with SIPMF in this section. For ultimate load tests on specimens with SIPMF, failure modes observed were flexural, shear, and flexural/shear (Figure 5.72).



a. Flexural failure mode



b. Shear failure mode



c. Flexural/shear failure mode

Figure 5.72. Mode of failures for specimens with SIPMF

Control Specimens

The ultimate load tests were conducted for control specimens with SIPMF after 287 days of curing (WI-C-1) and 568 days of curing (WI-C-2). The failure mode for both control specimens was a shear failure mode. The ultimate load was 33.25 kips and the deflection corresponding to peak load was 0.49 in. for WI-C-1. The ultimate load was 36.71 kips, and the

deflection corresponding to peak load was 0.60 in. for WI-C-2. Graphical and tabular summaries of the control specimen results are presented in comparison to the environmental exposure tests in the following sections.

Additional strength was achieved over the extended curing period for WI-C-2. The ultimate load of control specimens was estimated using either the strength design method for flexural capacity or the shear strength calculation for shear capacity and the results from corresponding compressive strength (cylinder) tests. The predicted strengths for the control specimens were 33.32 kips/ 34.67 kips (flexural/shear) for WI-C-1 and 33.79 kips/ 34.02 kips (flexural/shear) for WI-C-2, respectively. Generally, good agreement is observed between predicted and experimental results.

Results from the control specimens were used as baseline values for comparison to the specimens that were subjected to environmental exposure. Ultimate load tests were conducted on the control specimens on dates that coincided with tests for the shortest environmental exposure conditions (1,000 hour salt-water exposure) and for the longest environmental exposure conditions (10,000 hour salt-water exposure) to account for expected changes in baseline strength with time due to curing. Linear interpolation was applied to data from the control specimens to estimate baseline values for comparative tests conducted at intermediate stages (300 and 600 freeze/thaw cycle and 3,000 hour salt-water specimens) [Figure 5.73].

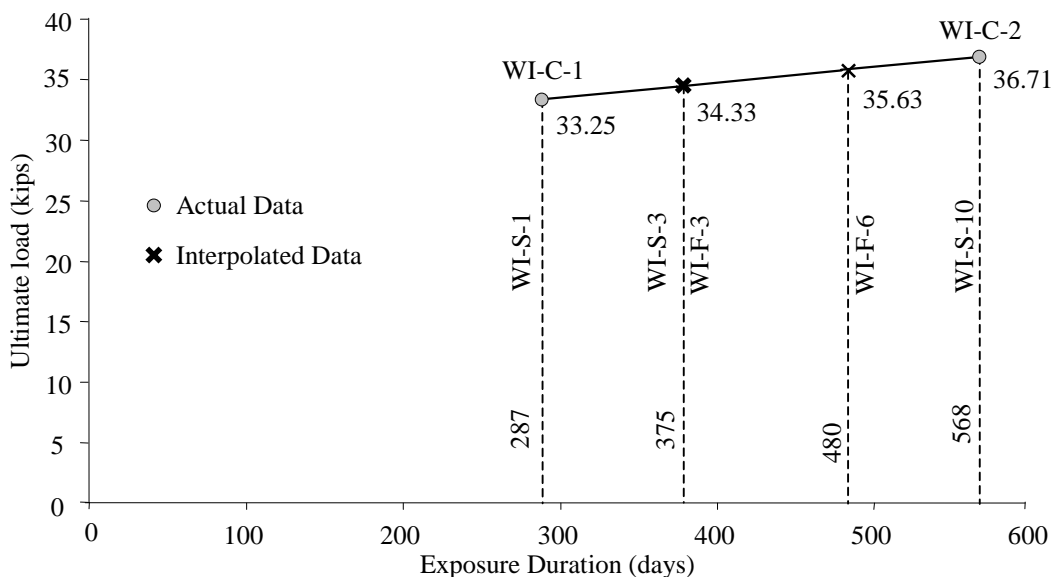


Figure 5.73. Interpolation of control values for freeze/thaw and salt-water specimens with SIPMF

Freeze/Thaw Specimens

The ultimate load tests were conducted for Freeze/Thaw specimens with SIPMF after 375 days of curing (300 cycles) and 480 days of curing (600 cycles). The failure mode for all freeze/thaw specimens was flexural failure mode with the exception of WI-F-6-1, which failed in flexural/shear failure mode. For WI-F-3-1, the ultimate load was 31.52 kips and the deflection corresponding to peak load was 0.82 in. For WI-F-3-2, the ultimate load was 33.05 kips and the deflection corresponding to peak load was 0.75 in. For WI-F-6-1, the ultimate load was 34.64 kips and the deflection corresponding to peak load was 0.73 in. For WI-F-6-2, the ultimate load was 32.78 kips and the deflection corresponding to peak load was 0.52 in. A graph containing all ultimate load test results for freeze/thaw and control specimens with SIPMFs is presented in Figure 5.74. A summary of results is presented in Table 5.3.

A comparison was made to determine the effect of freeze/thaw exposure on ultimate load of specimens with SIPMF (Figure 5.75). Appropriate baseline values for comparison were determined from control specimens. A reduction in ultimate load as compared to baseline values was observed for all freeze/thaw specimens with SIPMFs. After 300 cycles of freeze/thaw exposure, reductions in ultimate load as compared to baseline values were 8.2% and 3.7% for an average reduction of 5.9%. After 600 cycles of freeze/thaw exposure, reductions in ultimate load as compared to baseline values were 8.0% and 2.8% for an average reduction of 5.4%. These data indicate that deterioration of specimens occurs due to freeze/thaw exposure. Minimal difference is observed between 300 and 600 freeze/thaw cycles.

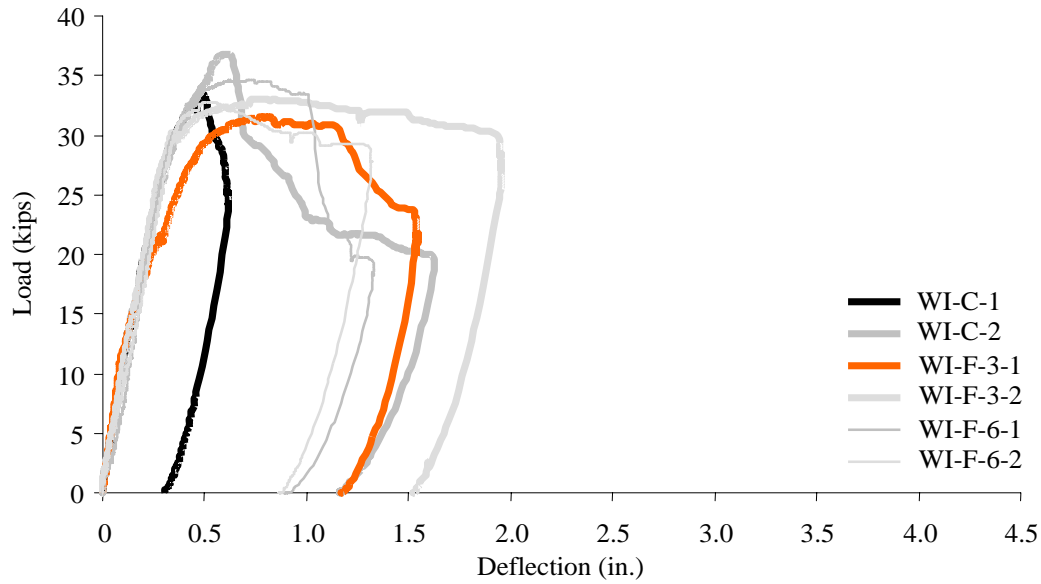


Figure 5.74. Load-deflection curves for ultimate load of control and freeze/thaw exposure specimens with SIPMF

Table 5.3. Ultimate load results for control and freeze/thaw exposure specimens with SIPMF

Specimen	Mode of Failure	Failure Load (kips)		Baseline Value (kips)	Deflection at Ultimate Load (in.)	Percentage of Change in Deflection		Percentage of Change in Capacity	
WI-C-1	Shear	33.25	(--)	(--)	0.49	(--)		(--)	
WI-C-2	Shear	36.71			0.60				
WI-F-3-1	Flexural	31.52	Average 32.29	34.33 ^a	0.82	56.5%	Average 49.8%	- 8.2%	Average - 5.9%
WI-F-3-2	Flexural	33.05			0.75	43.1%		- 3.7%	
WI-F-6-1	Flexural/Shear	34.64	Average 33.71	35.63 ^a	0.73	29.0%	Average 10.5%	- 2.8%	Average - 5.4%
WI-F-6-2	Flexural	32.78			0.52	-8.1%		- 8.0%	

^a Linear interpolation used between control specimens to estimate baseline value

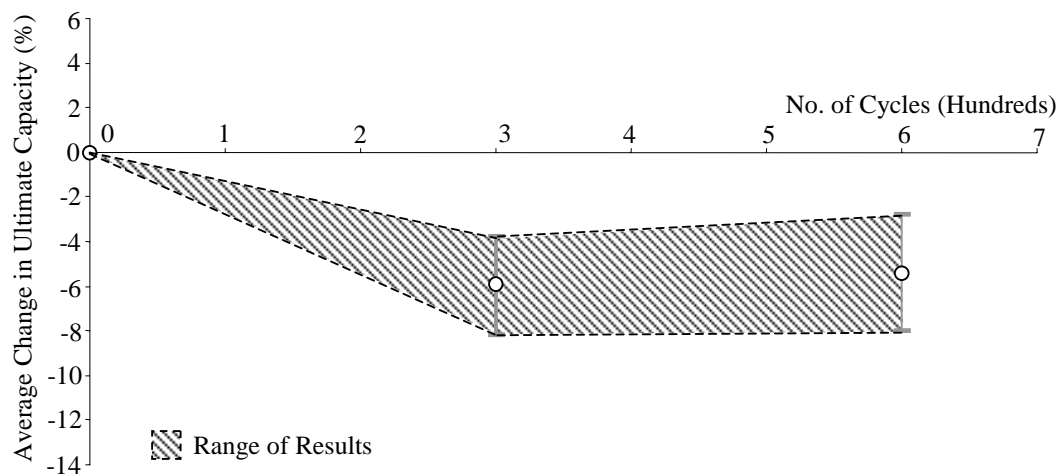


Figure 5.75. Percentage of change in ultimate load carrying capacity for freeze/thaw exposure specimens with SIPMF

Salt-Water Specimens

The ultimate load tests were conducted for Salt-Water specimens with SIPMF after 287 days of curing (1,000 hour specimens), 375 days of curing (3,000 hour specimens) and 586 days of curing (10,000 hour specimens). The failure mode for all salt-water specimens was flexural failure mode with the exception of WI-S-10-1, which failed in shear failure mode. For WI-S-1-1, the ultimate load was 33.35 kips and the deflection corresponding to peak load was 0.53 in. For WI-S-1-2, the ultimate load was 35.81 kips and the deflection corresponding to peak load was 0.54 in. For WI-S-3-1, the ultimate load was 32.80 kips and the deflection corresponding to peak load was 0.70 in. For WI-S-3-2, the ultimate load was 32.56 kips and the deflection corresponding to peak load was 0.82 in. For WI-S-10-1, the ultimate load was 35.13 kips and the deflection corresponding to peak load was 0.71 in. For WI-S-10-2, the ultimate load was 32.70 kips and the deflection corresponding to peak load was 0.73 in. A graph containing all ultimate load test results for salt-water and control specimens with SIPMFs is presented in Figure 5.76. A summary of results is presented in Table 5.4.

A comparison was made to determine the effect of salt-water exposure on ultimate load of specimens with SIPMF (Figure 5.77). Appropriate baseline values for comparison were determined from control specimens. An initial increase in ultimate load is observed after 1,000

hours of salt-water exposure as compared to baseline values followed by a decrease in ultimate load due to further salt-water exposure. After 1,000 hours of salt-water exposure, increases in ultimate load as compared to baseline values were 0.3% and 7.7% for an average increase of 4.0%. After 3,000 hours of salt-water exposure, reductions in ultimate load as compared to baseline values were 4.5% and 5.2% for an average reduction of 4.8%. After 10,000 hours of salt-water exposure, further reductions in ultimate load as compared to baseline values were observed as 4.3% and 10.9% for an average reduction of 7.6%. These data indicate that structural deterioration of specimens occurs due to salt-water exposure. The observed reduction in ultimate load was most prominent between specimens exposed to 1,000 and 3,000 hours of salt-water.

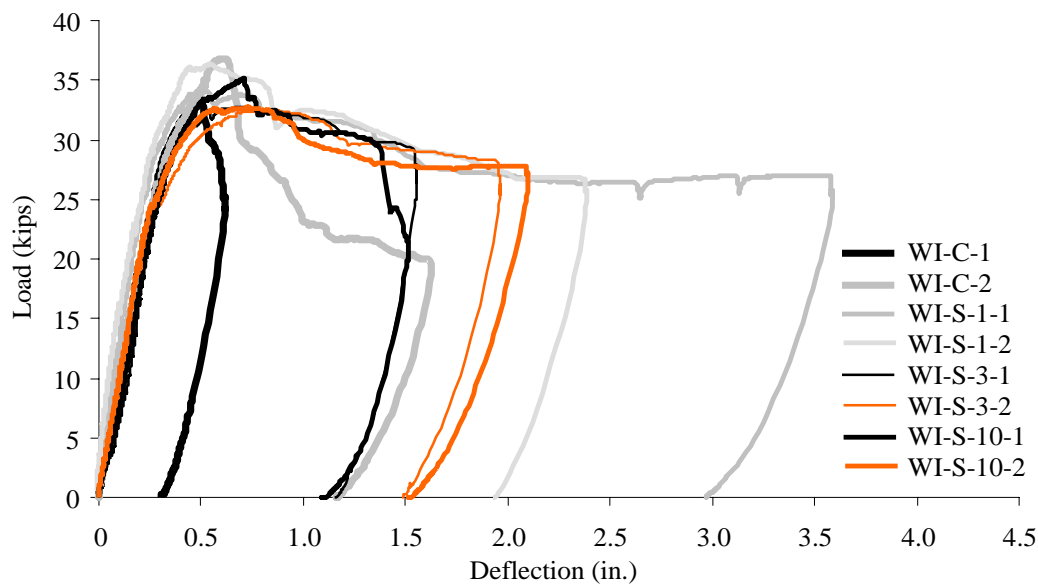


Figure 5.76. Load-deflection curves for ultimate load of 1,000-, 3,000-, 10,000-hour salt-water exposures, and control specimens with SIPMF

Table 5.4. Ultimate load results for 1,000-, 3,000-, 10,000-hour salt-water exposures, and control specimens with SIPMF

Specimen	Mode of Failure	Failure Load (kips)		Baseline Value (kips)	Deflection at Ultimate Load (in.)	Percentage of Change in Deflection		Percentage of Change in Capacity	
WI-C-1	Shear	33.25	(--)	(--)	0.49	(--)		(--)	
WI-C-2	Shear	36.71			0.60				
WI-S-1-1	Flexural	33.35	Average 34.58	33.25	0.53	8.2%	Average 9.2%	+ 0.3%	Average + 4.0%
WI-S-1-2	Flexural	35.81			0.54	10.2%		+ 7.7%	
WI-S-3-1	Flexural	32.80	Average 32.68	34.33 ^a	0.70	33.6%	Average 45.1%	- 4.5%	Average - 4.8%
WI-S-3-2	Flexural	32.56			0.82	56.5%		- 5.2%	
WI-S-10-1	Shear	35.13	Average 33.92	36.71	0.71	18.3%	Average 20.0%	- 4.3%	Average - 7.6%
WI-S-10-2	Flexural	32.70			0.73	21.7%		- 10.9%	

^a Linear interpolation used between control specimens to estimate baseline value

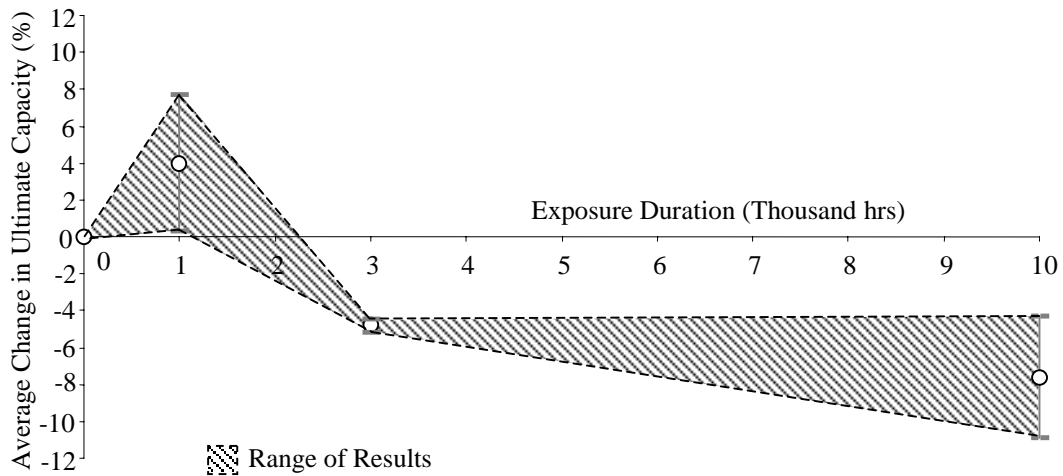


Figure 5.77. Percentage of change in ultimate load carrying capacity for salt-water exposure specimens with SIPMF

5.4 SPECIMENS WITHOUT SIPMF

Results of exposure and load tests for specimens without SIPMFs are presented in this section. First, results from the service load tests are presented. Next, ultrasonic through-transmission test results are presented to provide assessment of the quality of concrete over the longitudinal cross sections of all specimens following exposure tests. Finally, ultimate load test results are presented to evaluate the influence of various exposure conditions on the ultimate load capacity of the specimens.

5.4.1 Service Load Test Results

All 12 specimens without SIPMF were subjected to a service load test at the beginning of the test program to promote full depth cracks. The service load test consisted of two steps: positive moment (bottom cracking) and negative moment (top cracking) applications. The load-displacement curves for the service load tests for specimens without SIPMF are presented in Figures 5.78 and 5.79. The bottom and top cracking loads for specimens without SIPMF are presented in Table 5.5. The onset of cracking for the positive moment application for specimens without SIPMF occurred at loads between 6.23 kips to 7.59 kips. The onset of cracking for the negative moment application occurred at loads between 3.15 kips to 5.17 kips. The range of loads associated with onset of cracking is shown as a shaded envelope on Figures 5.78 and 5.79. The theoretical cracking load was determined for specimens without SIPMF using the elastic theory with the compressive strength f_c' data from the 28-day compressive strength test cylinders. The measured loads for positive moment cracking were generally consistent with theoretical calculations of cracking loads. The theoretical prediction was 8.81 kips, which was within 27% of the average measured value for all specimens (6.90 kips). The measured loads for negative moment cracking were lower than theoretical predictions. The difference in measured and predicted values was attributed to the weakened overall structure due to presence of positive moment cracks at the time of negative moment application. The average measured value for all specimens was 4.17 kips, whereas the theoretical predicted ultimate load was 8.81 kips.

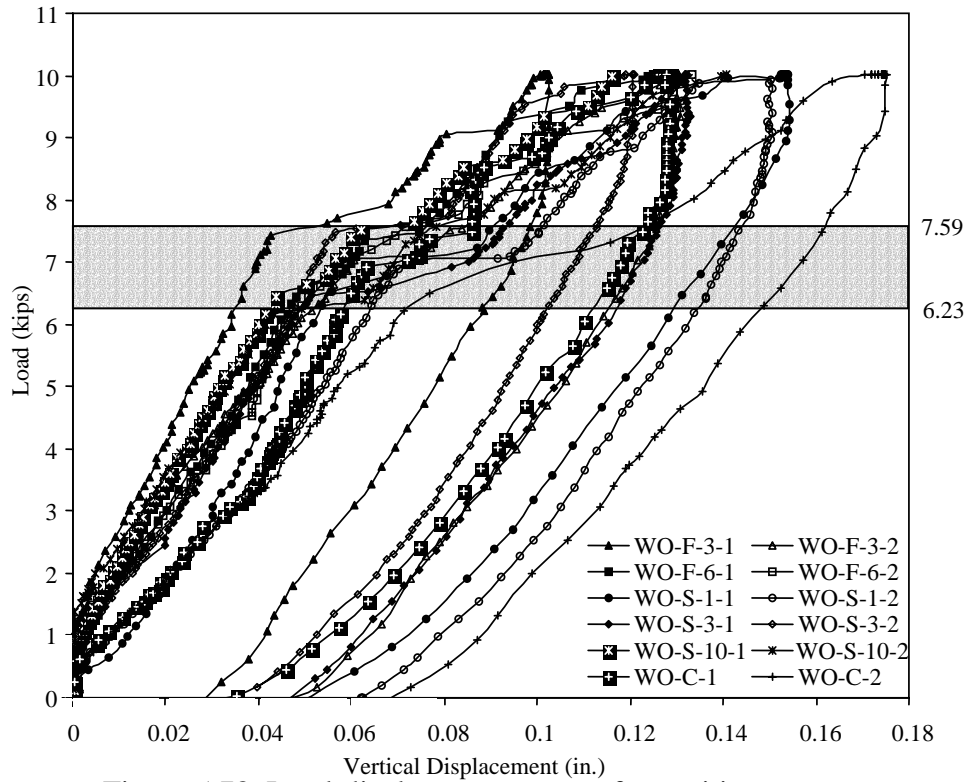


Figure 5.78. Load-displacement curves for positive moment application (bottom cracking) for specimens without SIPMF

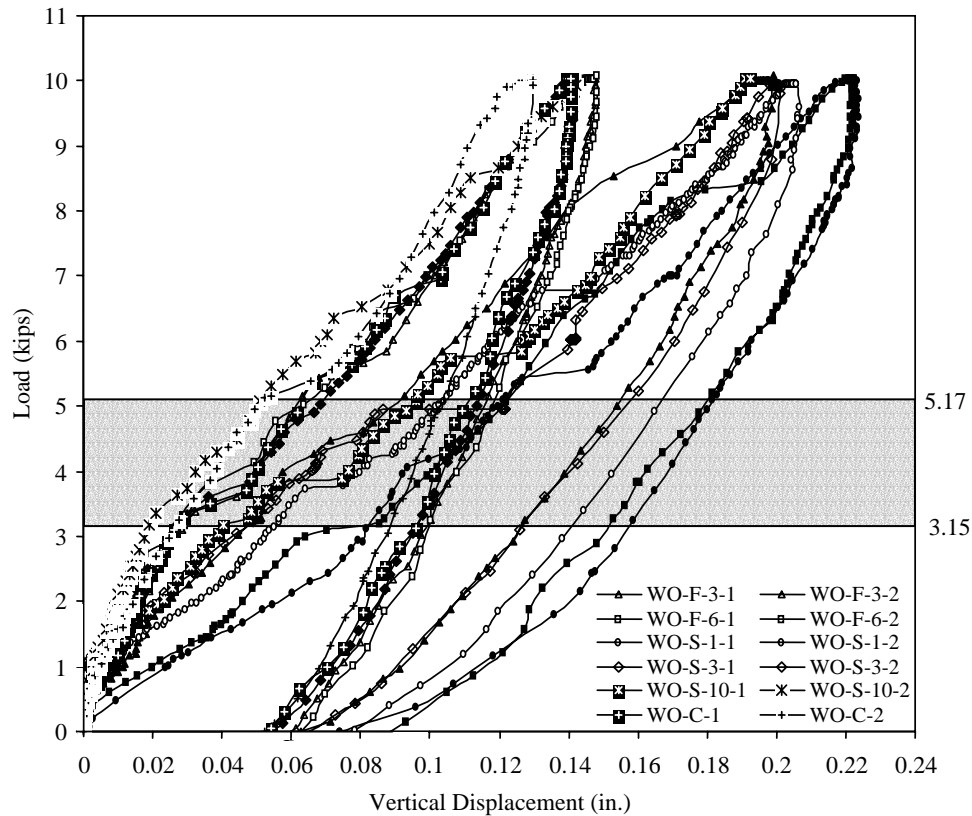


Figure 5.79. Load-displacement curves for negative moment application (top cracking) for specimens without SIPMF

Table 5.5. Top and bottom cracking load for the specimens without SIPMF

Type of specimens			Cracking Load (kips)	
			Top Cracking	Bottom Cracking
Specimens without SIPMF	Control		WO-C-1	3.45
			WO-C-2	5.17
	Freeze/Thaw	300 cycle	WO-F-3-1	3.25
			WO-F-3-2	3.59
		600 cycle	WO-F-6-1	3.15
			WO-F-6-2	3.82
	Salt-Water	1,000 hr	WO-S-1-1	4.12
			WO-S-1-2	3.74
		3,000 hr	WO-S-3-1	3.64
			WO-S-3-2	4.46
		10,000 hr	WO-S-10-1	3.21
			WO-S-10-2	3.42

5.4.2 Ultrasonic Through-Transmission Results

Ultrasonic through-transmission tests were conducted on a 3-in. slice removed from each specimen before ultimate load testing. Conducting through-transmission tests over a grid pattern on each slice allowed for determination of pulse-velocity over the entire longitudinal cross section of each specimen. Through-transmission test results are presented in Figures 5.80 to 5.93 for specimens without SIPMF. Results of the through-transmission tests are presented as contour maps representing various ranges of pulse-velocity. The pulse velocity can be correlated to quality of concrete as presented in Chapter 4. The contour maps provide graphical representation of the spatial distribution of quality of concrete. In addition to the contour maps, these figures include profiles of average pulse velocity through the depth ($v_{ave-depth}$) and along the length ($v_{ave-longitudinal}$) of the specimens. Further interpretation of the through-transmission data is presented at the end of this chapter (chronological summaries and comparison of average pulse velocity for entire cross section, perimeter region, interior region, and bottom region of the specimens).

Control Specimens

Through-transmission test results for control specimens without SIPMF are presented in Figures 5.80 and 5.81. The average ultrasonic velocity for the entire cross sections of control specimens without SIPMF was 13,244 ft/sec. The average ultrasonic velocity for the points on the perimeter (rows A and D and points: B1, C1, B41, and C41) for control specimens without SIPMF was 12,894 ft/sec. The average ultrasonic velocity for the interior points (rows B and C except points: B1, C1, B41, and C41) for control specimens without SIPMF was 13,691 ft/sec. The average ultrasonic velocity for the bottom points (rows D) for control specimens without SIPMF was 12,535 ft/sec. Essentially, the distribution of pulse velocity over the cross section is uniform for the control specimens.

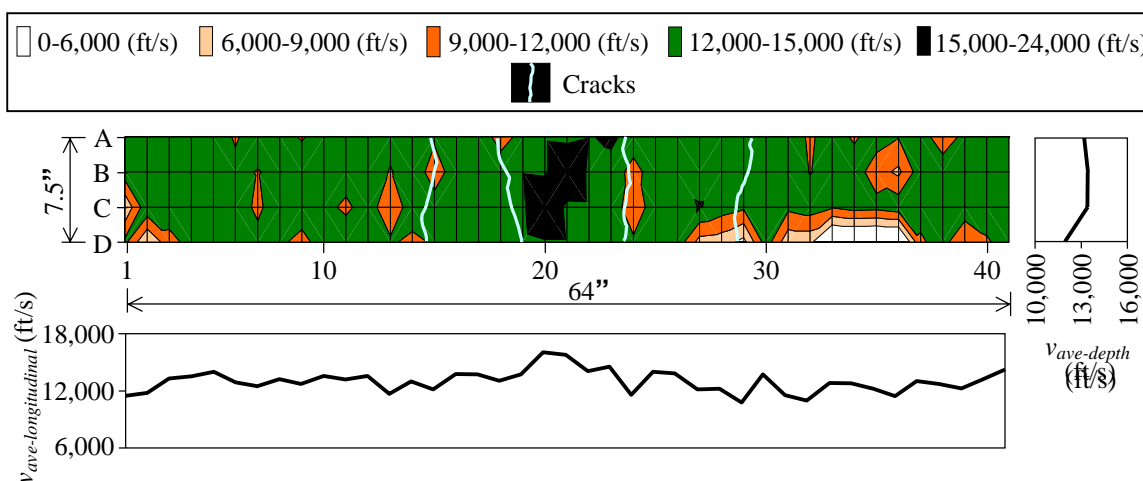


Figure 5.80. Through-transmission test results for slice from specimen WO-C-1

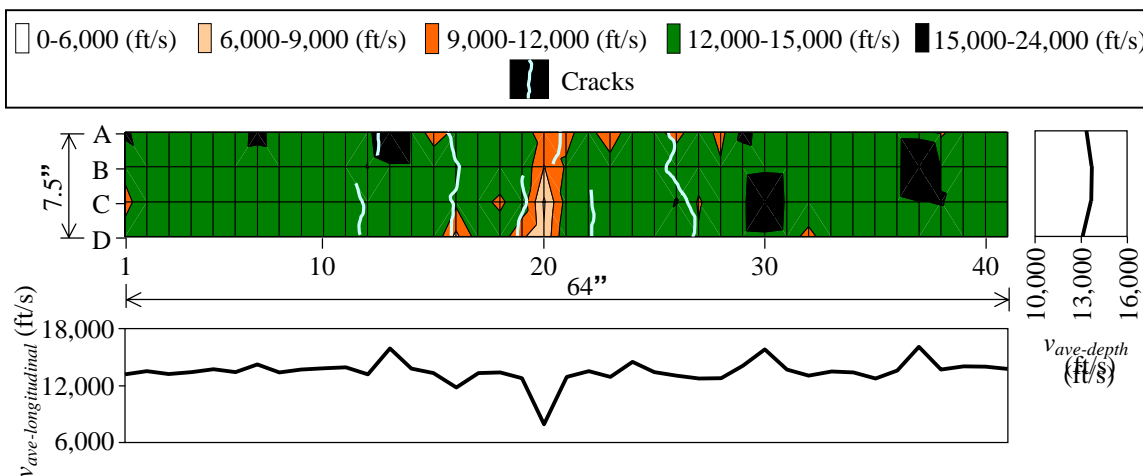


Figure 5.81. Through-transmission test results for slice from specimen WO-C-2

Freeze/Thaw Specimens

Through-transmission test results for 300-cycle freeze/thaw specimens without SIPMF are presented in Figures 5.82 and 5.83. The average ultrasonic velocity for the entire cross sections of 300-cycle freeze/thaw specimens without SIPMF was 13,360 ft/sec. The average ultrasonic velocity for the points on the perimeter (rows A and D and points: B1, C1, B41, and C41) for 300-cycle freeze/thaw specimens without SIPMF was 13,279 ft/sec. The average ultrasonic velocity for the interior points (rows B and C except points: B1, C1, B41, and C41) for 300-cycle freeze/thaw specimens without SIPMF was 13,449 ft/sec. The average ultrasonic velocity for the bottom points (rows D) for 300-cycle freeze/thaw specimens without SIPMF was 13,449 ft/sec. Essentially, the distribution of pulse velocity over the cross section is uniform for the 300-cycle freeze/thaw specimens without SIPMF.

Through-transmission test results for 600-cycle freeze/thaw specimens without SIPMF are presented in Figures 5.84 and 5.85. The average ultrasonic velocity for the entire cross sections of 600-cycle freeze/thaw specimens without SIPMF was 14,457 ft/sec. The average ultrasonic velocity for the points on the perimeter (rows A and D and points: B1, C1, B41, and C41) for 600-cycle freeze/thaw specimens without SIPMF was 14,324 ft/sec. The average ultrasonic velocity for the interior points (rows B and C except points: B1, C1, B41, and C41) for 600-cycle freeze/thaw specimens without SIPMF was 14,600 ft/sec. The average ultrasonic velocity for the bottom points (rows D) for 600-cycle freeze/thaw specimens without SIPMF was 14,575 ft/sec. Essentially, the distribution of pulse velocity over the cross section is uniform for the 600-cycle freeze/thaw specimens without SIPMF.

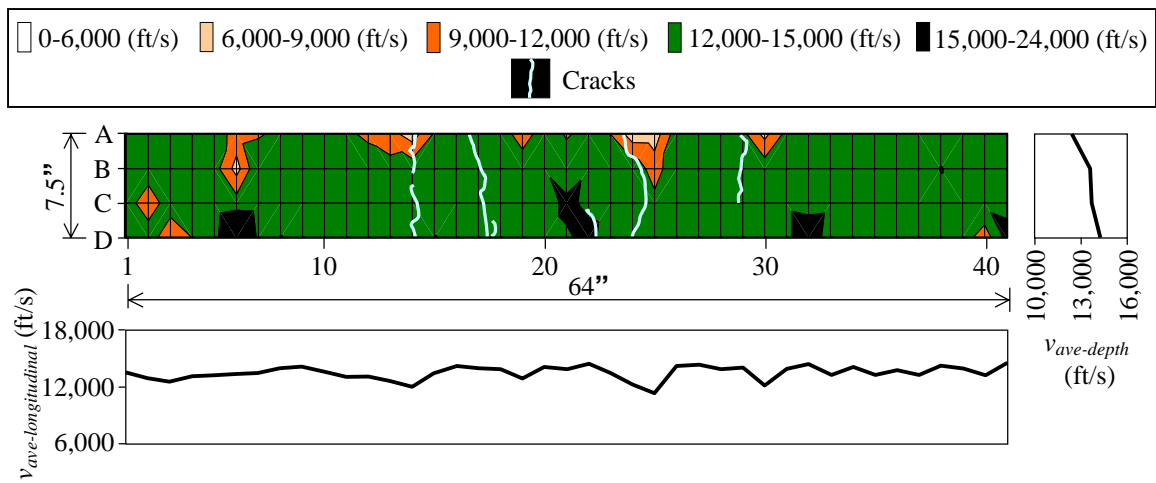


Figure 5.82. Through-transmission test results for slice from specimen WO-F-3-1

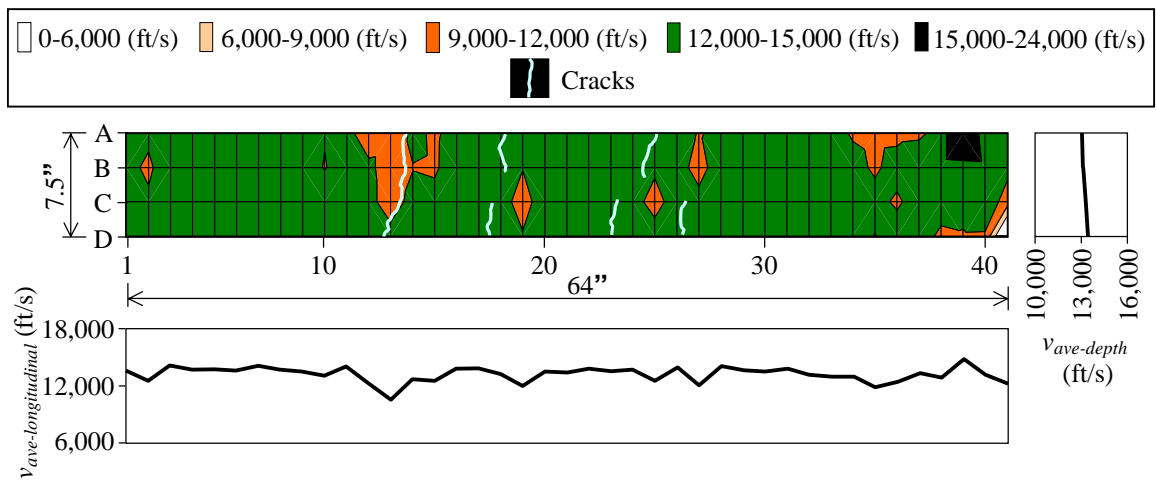


Figure 5.83. Through-transmission test results for slice from specimen WO-F-3-2

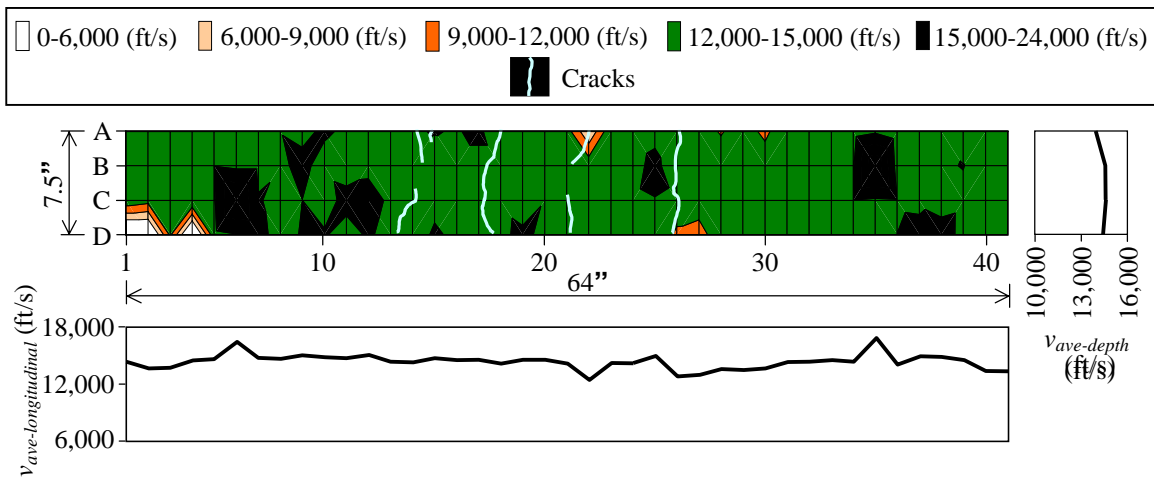


Figure 5.84. Through-transmission test results for slice from specimen WO-F-6-1

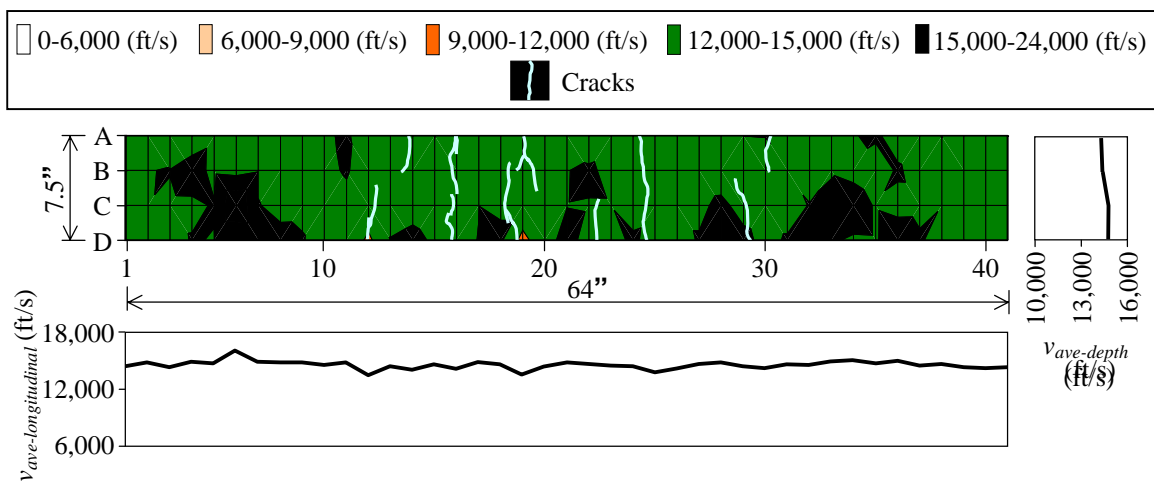


Figure 5.85. Through-transmission test results for slice from specimen WO-F-6-2

A summary of through-transmission test results for control specimens and freeze/thaw specimens without SIPMF is presented in Figure 5.86. The average percentages of measurement points for the control specimens without SIPMF were 1% very poor, 3% poor, 11% moderate to questionable, 81% good, and 4% very good. The average percentages of measurement points for the 300-cycle freeze/thaw specimens without SIPMF were 0% very poor, 2% poor, 10% moderate to questionable, 85% good, and 3% very good. The average percentages of measurement points for the 600-cycle freeze/thaw specimens without SIPMF were 0% very poor, 0% poor, 2% moderate to questionable, 81% good, and 17% very good.

The average pulse velocity for the entire cross sections of the freeze/thaw specimens without SIPMF increased to 13,360 ft/s after 300 cycles of freeze/thaw exposure (compared to 13,244 ft/s for control specimens). A subsequent increase in average pulse velocity to 14,457 ft/s was measured for the 600 cycle specimens. The overall increase in pulse velocity after freeze/thaw exposure is attributed to improved hydration conditions in the presence of frequent wetting of the specimens.

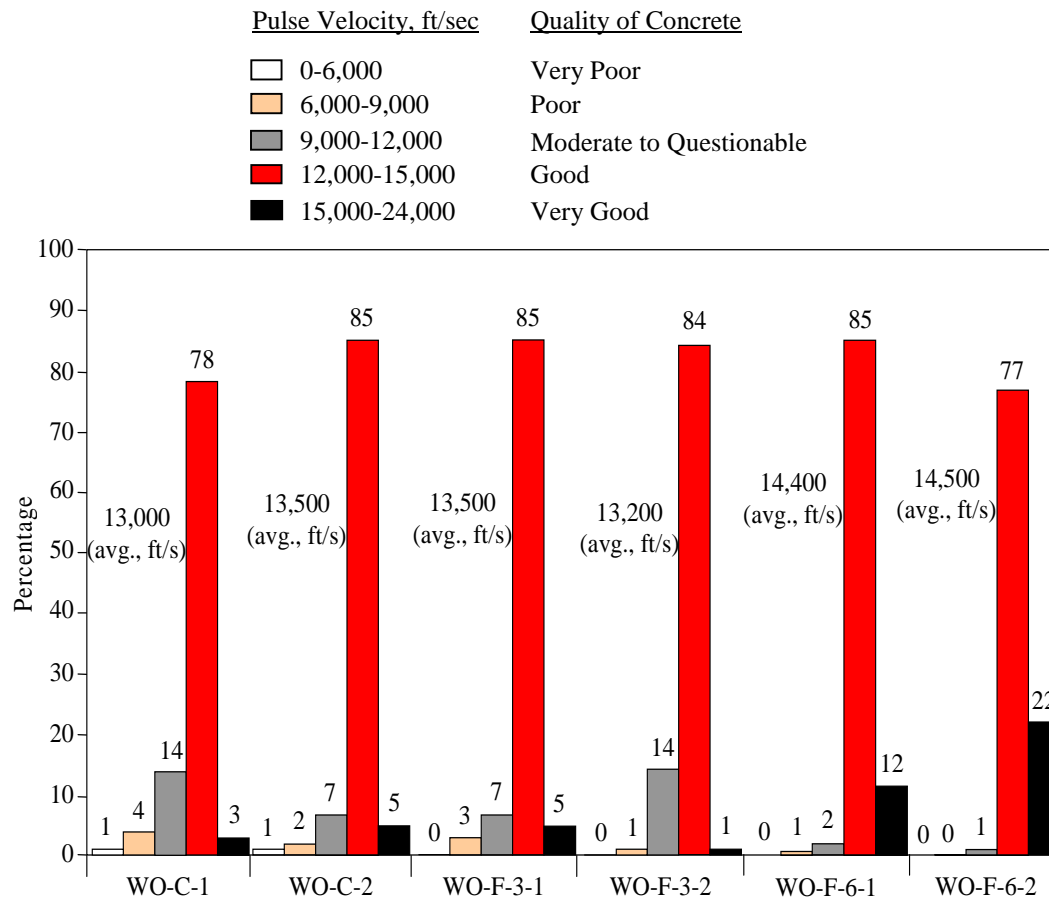


Figure 5.86. Summary of through-transmission test results for control and freeze/thaw specimens without SIPMF

Salt-Water Specimens

Through-transmission test results for 1,000-hour salt-water exposures specimens without SIPMF are presented in Figures 5.87 and 5.88. The average ultrasonic velocity for the entire cross sections of 1,000-hour salt-water exposures specimens without SIPMF was 14,087 ft/sec. The average ultrasonic velocity for the points on the perimeter (rows A and D and points: B1,

C1, B41, and C41) for 1,000-hour salt-water exposures specimens without SIPMF was 14,052 ft/sec. The average ultrasonic velocity for the interior points (rows B and C except points: B1, C1, B41, and C41) for 1,000-hour salt-water exposures specimens without SIPMF was 14,124 ft/sec. The average ultrasonic velocity for the bottom points (rows D) for 1,000-hour salt-water exposures specimens without SIPMF was 14,061 ft/sec. Essentially, the distribution of pulse velocity over the cross section is uniform for the 1,000-hour salt-water exposures specimens without SIPMF.

Through-transmission test results for 3,000-hour salt-water exposures specimens without SIPMF are presented in Figures 5.89 and 5.90. The average ultrasonic velocity for the entire cross sections of 3,000-hour salt-water exposures specimens without SIPMF was 14,449 ft/sec. The average ultrasonic velocity for the points on the perimeter (rows A and D and points: B1, C1, B41, and C41) for 3,000-hour salt-water exposures specimens without SIPMF was 14,500 ft/sec. The average ultrasonic velocity for the interior points (rows B and C except points: B1, C1, B41, and C41) for 3,000-hour salt-water exposures specimens without SIPMF was 14,394 ft/sec. The average ultrasonic velocity for the bottom points (rows D) for 3,000-hour salt-water exposures specimens without SIPMF was 14,754 ft/sec. Essentially, the distribution of pulse velocity over the cross section is uniform for the 3,000-hour salt-water exposures specimens without SIPMF.

Through-transmission test results for 10,000-hour salt-water exposures specimens without SIPMF are presented in Figures 5.91 and 5.92. The average ultrasonic velocity for the entire cross sections of 10,000-hour salt-water exposures specimens without SIPMF was 14,581 ft/sec. The average ultrasonic velocity for the points on the perimeter (rows A and D and points: B1, C1, B41, and C41) for 10,000-hour salt-water exposures specimens without SIPMF was 14,649 ft/sec. The average ultrasonic velocity for the interior points (rows B and C except points: B1, C1, B41, and C41) for 10,000-hour salt-water exposures specimens without SIPMF was 14,506 ft/sec. The average ultrasonic velocity for the bottom points (rows D) for 10,000-hour salt-water exposures specimens without SIPMF was 14,787 ft/sec. Essentially, the distribution of pulse velocity over the cross section is uniform for the 10,000-hour salt-water exposures specimens without SIPMF.

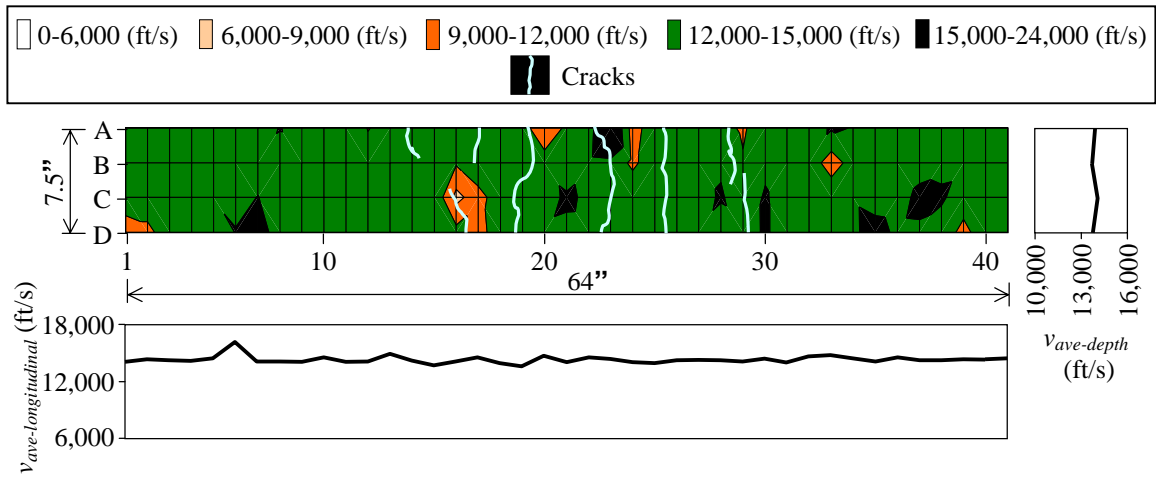


Figure 5.87. Through-transmission test results for slice from specimen WO-S-1-1

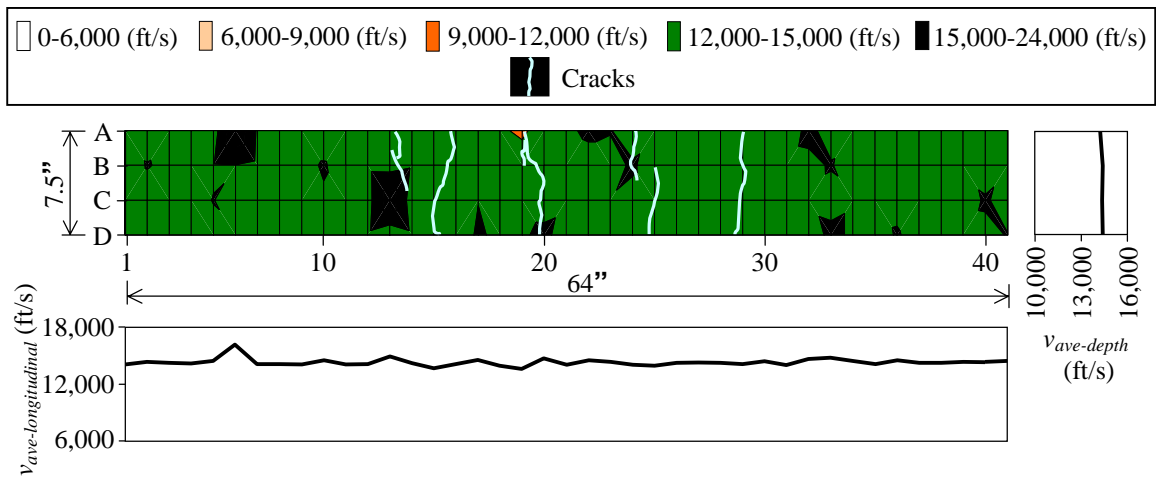


Figure 5.88. Through-transmission test results for slice from specimen WO-S-1-2

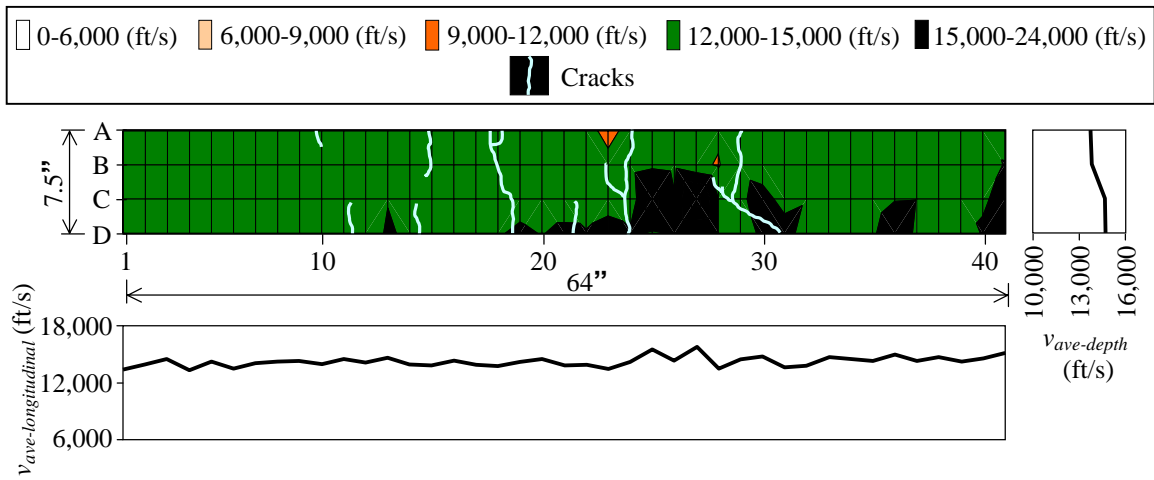


Figure 5.89. Through-transmission test results for slice from specimen WO-S-3-1

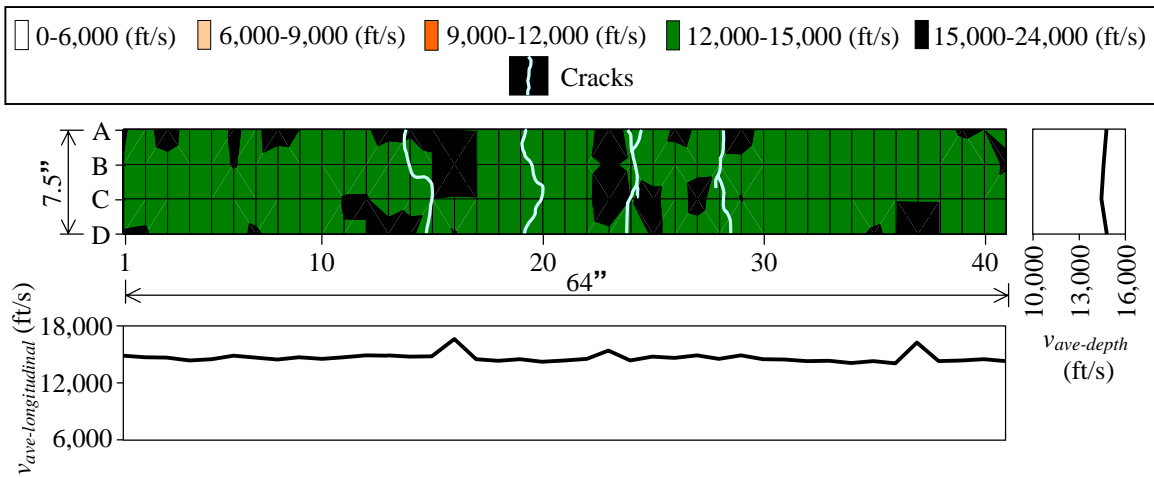


Figure 5.90. Through-transmission test results for slice from specimen WO-S-3-2

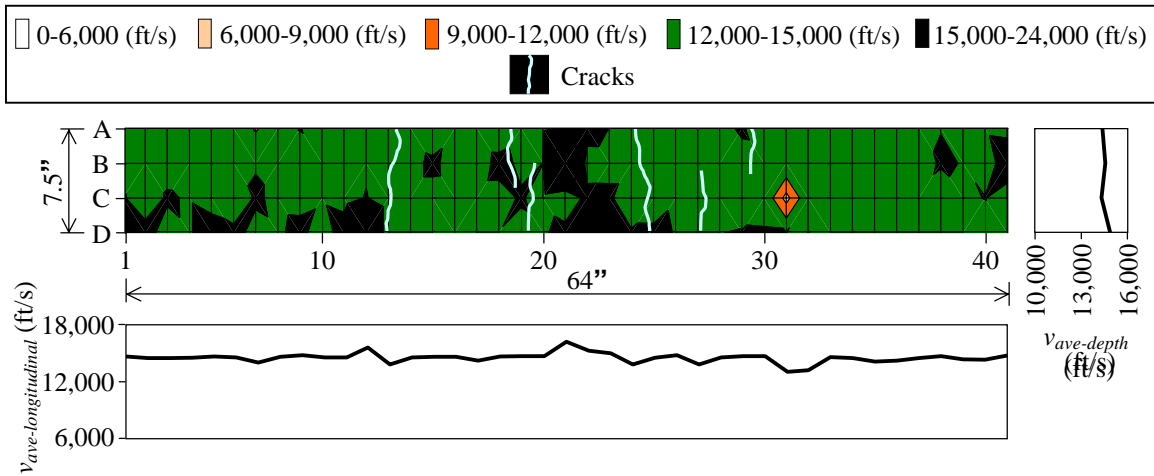


Figure 5.91. Through-transmission test results for slice from specimen WO-S-10-1

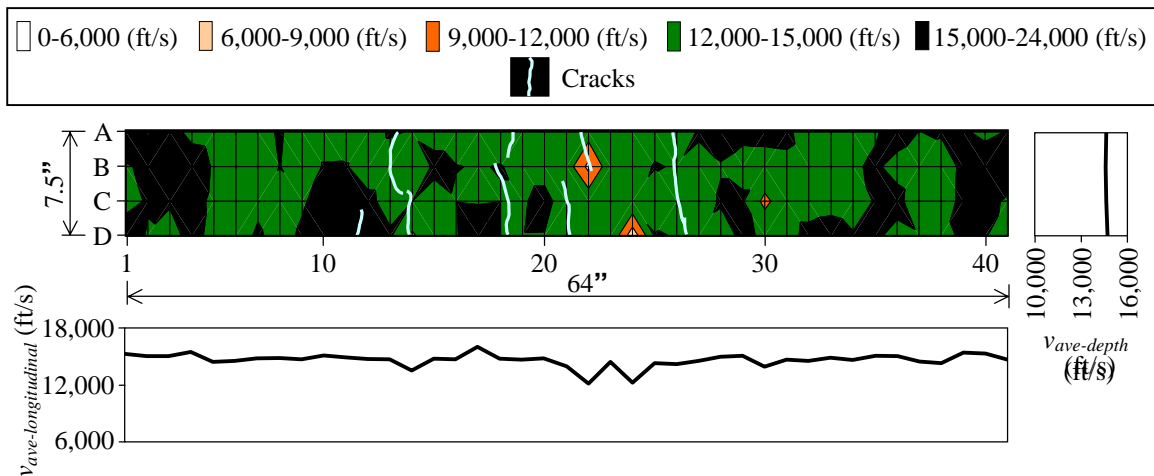


Figure 5.92. Through-transmission test results for slice from specimen WO-S-10-2

A summary of through-transmission test results for control specimens and salt-water specimens without SIPMF is presented in Figure 5.93. The average percentages of measurement points for the control specimens without SIPMF were 1% very poor, 3% poor, 11% moderate to questionable, 81% good, and 4% very good. The average percentages of measurement points for the 1,000-hour salt-water exposures specimens without SIPMF were 0% very poor, 1% poor, 3% moderate to questionable, 87% good, and 9% very good. The average percentages of measurement points for the 3,000-hour salt-water exposures specimens without SIPMF were 0% very poor, 0% poor, 1% moderate to questionable, 85% good, and 15% very good. The average percentages of measurement points for the 10,000-hour salt-water exposures specimens without

SIPMF were 0% very poor, 1% poor, 1% moderate to questionable, 70% good, and 27% very good.

The average pulse velocity for the entire cross sections of the salt-water exposures specimens without SIPMF increased to 14,087 ft/s after 1,000-hour of salt-water exposure (compared to 13,244 ft/s for control specimens). The average pulse velocity for the entire cross sections increased monotonically and fraction of “very good” concrete is increasing with further salt-water exposure (14,449 ft/s for the 3,000-hour salt-water specimens and 14,581 ft/s for the 10,000-hour salt-water specimens). The consistent increase in pulse velocity after salt-water exposure is attributed to improved hydration conditions for specimens submerged in a tank.

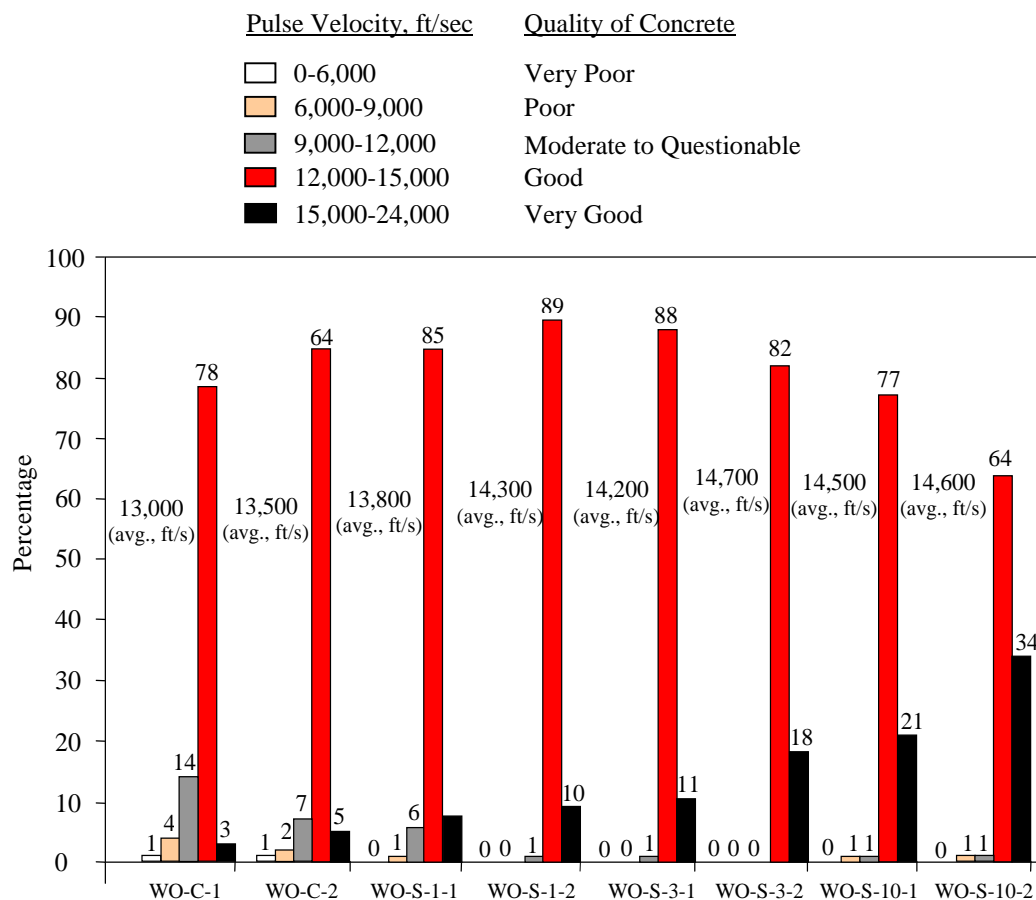


Figure 5.93. Summary of through-transmission test results for control and salt-water exposure specimens without SIPMF

5.4.3 Ultimate Load Test Results

Ultimate load test was applied on each specimen at the end of the environmental exposures, and the load setup “T” was used for ultimate load. Ultimate load test results are presented for control specimens, freeze/thaw specimens, and salt-water specimens without SIPMF in this section. For ultimate load tests on specimens with SIPMF, failure modes observed were flexural, shear, and flexural/shear (Figure 5.94).



a. Flexural failure mode



b. Shear failure mode



c. Flexural/shear failure mode

Figure 5.94. Modes of failure for specimens without SIPMF

Control Specimens

The ultimate load tests were conducted for control specimens without SIPMF after 287 days of curing (WO-C-1) and 568 days of curing (WO-C-2). The failure mode for WO-C-1 specimen was a flexural/shear failure mode whereas the failure mode for WO-C-2 specimen was a flexural failure mode. The ultimate load was 24.02 kips and the deflection corresponding to

peak load was 1.11 in. for WO-C-1. The ultimate load was 24.04 kips, and the deflection corresponding to peak load was 1.00 in. for WO-C-2. Graphical and tabular summaries of the control specimen results are presented in comparison to the environmental exposure tests in the following sections.

No additional strength was achieved over the extended curing period for WO-C-2. The ultimate load of control specimens was estimated using either the strength design method for flexural capacity or the shear strength calculation for shear capacity and the results from corresponding compressive strength (cylinder) tests. The predicted strengths for the control specimens were 23.70 kips/ 24.1 kips (flexural/shear) for WO-C-1 and 23.65 kips/ 23.63 kips (flexural/shear) for WO-C-2, respectively. Generally, good agreement is observed between predicted and experimental results.

Results from the control specimens were used as baseline values for comparison to the specimens that were subjected to environmental exposure. Ultimate load tests were conducted on the control specimens on dates that coincided with tests for the shortest environmental exposure conditions (1,000 hour salt-water exposure) and for the longest environmental exposure conditions (10,000 hour salt-water exposure) to account for expected changes in baseline strength with time due to curing. Linear interpolation was applied to data from the control specimens to estimate baseline values for comparative tests conducted at intermediate stages (300 and 600 freeze/thaw cycle and 3,000 hour salt-water specimens) [Figure 5.95].

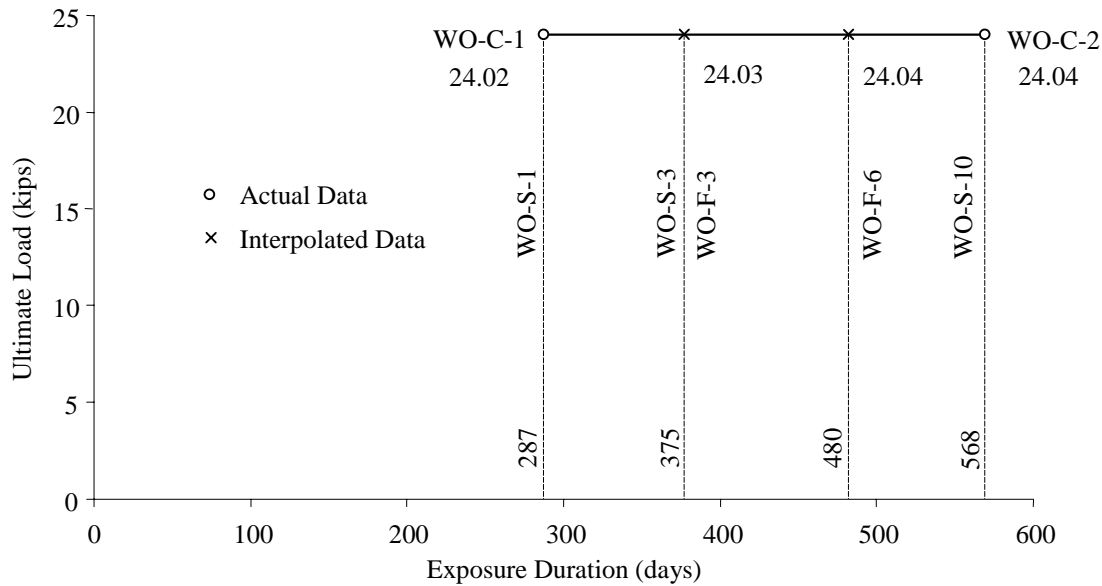


Figure 5.95. Interpolation of control values for freeze/thaw and salt-water specimens without SIPMF

Freeze/Thaw Specimens

The ultimate load tests were conducted for Freeze/Thaw specimens without SIPMF after 375 days of curing (300 cycles) and 480 days of curing (600 cycles). The failure mode for all freeze/thaw specimens was flexural failure mode with the exception of WO-F-6-1 which failed in flexural/shear failure mode. For WO-F-3-1, the ultimate load was 22.66 kips and the deflection corresponding to peak load was 1.11 in. For WO-F-3-2, the ultimate load was 24.91 kips and the deflection corresponding to peak load was 0.77 in. For WO-F-6-1, the ultimate load was 23.89 kips and the deflection corresponding to peak load was 0.65 in. For WO-F-6-2, the ultimate load was 20.94 kips and the deflection corresponding to peak load was 0.44 in. A graph containing all ultimate load test results for freeze/thaw and control specimens without SIPMFs is presented in Figure 5.96. A summary of results is presented in Table 5.6.

A comparison was made to determine the effect of freeze/thaw exposure on ultimate load of specimens without SIPMF (Figure 5.97). Appropriate baseline values for comparison were determined from control specimens. A reduction in ultimate load as compared to baseline values was observed for all freeze/thaw specimens without SIPMFs except for WO-F-3-2. After 300

cycles of freeze/thaw exposure, a reduction in the ultimate load for WO-F-3-1 as compared to baseline value was 5.7% and an increase in the ultimate load for WO-F-3-2 as compared to baseline value was 3.7% for an average reduction of 1.0%. After 600 cycles of freeze/thaw exposure, reductions in ultimate load as compared to baseline values were 0.7% and 12.9% for an average reduction of 6.7%. These data indicate that deterioration of specimens occurs due to freeze/thaw exposure. Apparent difference is observed between 300 and 600 freeze/thaw cycles.

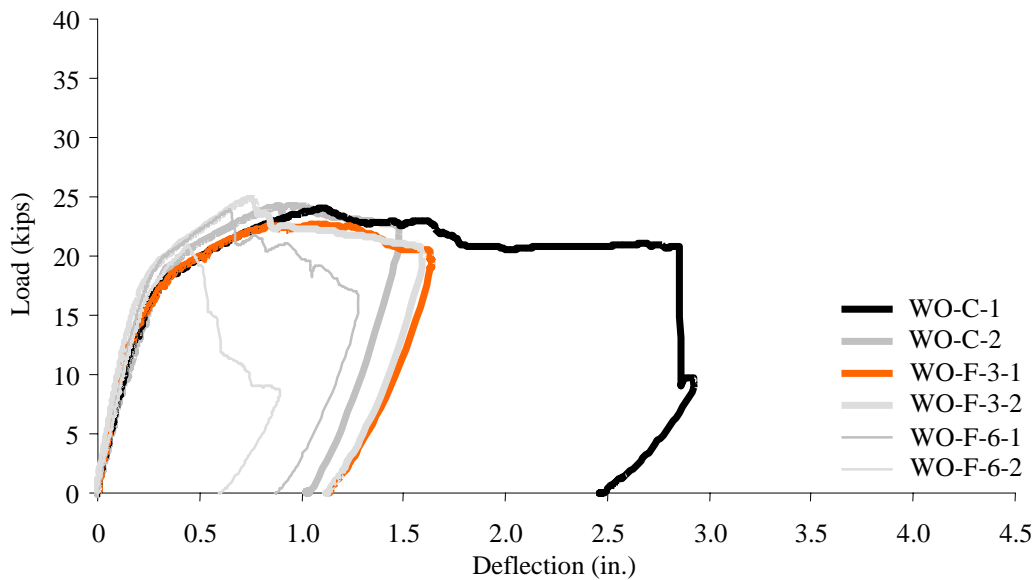


Figure 5.96. Load-deflection curves for ultimate load of 300-, 600-cycle, and control specimens without SIPMF

Table 5.6. Ultimate load results for control, 300-, and 600-cycle freeze/thaw specimens without SIPMF

Specimen	Mode of Failure	Failure Load (kips)		Comparable Control Value (kips)	Deflection at Ultimate Load (in.)	Percentage of Change in Deflection		Percentage of Change in Capacity	
WO-C-1	Flexural/Shear	24.02	(--)	(--)	1.11	(--)	(--)	(--)	(--)
WO-C-2	Flexural	24.04			1.00				
WO-F-3-1	Flexural	22.66	Average 23.79	24.03 ^a	1.11	+ 3.2%	-12.6%	- 5.7%	Average - 1.0%
WO-F-3-2	Flexural	24.91			0.77	-28.4%		+ 3.7%	
WO-F-6-1	Flexural	23.89	Average 22.42	24.04 ^a	0.65	-37.1%	-47.3%	- 0.7%	Average - 6.7%
WO-F-6-2	Shear	20.94			0.44	-57.4%		- 12.9%	

^a Linear interpolation used between control specimens to estimate baseline value

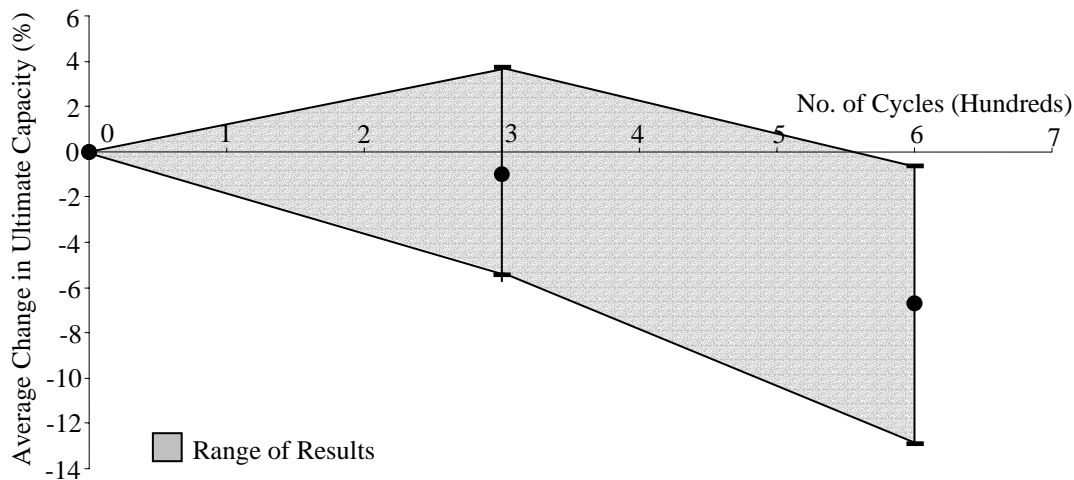


Figure 5.97. Percentage of change in ultimate load carrying capacity for freeze/thaw exposure specimens without SIPMF

Salt-Water Specimens

The ultimate load tests were conducted for Salt-Water specimens without SIPMF after 287 days of curing (1,000 hour exposure specimens), 375 days of curing (3,000 hour exposure specimens) and 586 days of curing (10,000 hour exposure specimens). The failure mode for all salt-water specimens was flexural failure mode with the exception of WO-S-10-1, which failed in flexural/shear failure mode. For WO-S-1-1, the ultimate load was 26.78 kips and the deflection corresponding to peak load was 1.13 in. For WO-S-1-2, the ultimate load was 25.61 kips and the deflection corresponding to peak load was 1.04 in. For WO-S-3-1, the ultimate load was 25.76 kips and the deflection corresponding to peak load was 0.87 in. For WO-S-3-2, the ultimate load was 25.64 kips and the deflection corresponding to peak load was 0.82 in. For WO-S-10-1, the ultimate load was 25.02 kips and the deflection corresponding to peak load was 0.79 in. For WO-S-10-2, the ultimate load was 25.73 kips and the deflection corresponding to peak load was 0.87 in. A graph containing all ultimate load test results for salt-water and control specimens without SIPMFs is presented in Figure 5.98. A summary of results is presented in Table 5.7.

A comparison was made to determine the effect of salt-water exposure on ultimate load of specimens without SIPMF (Figure 5.99). Appropriate baseline values for comparison were

determined from control specimens. An initial increase in ultimate load is observed after 1,000 hours of salt-water exposure as compared to baseline values followed by a lesser amount of increase in ultimate load due to further salt-water exposure. After 1,000 hours of salt-water exposure, increases in ultimate load as compared to baseline values were 11.4% and 6.6% for an average increase of 9.0%. After 3,000 hours of salt-water exposure, increases in ultimate load as compared to baseline values were 7.2% and 6.7% for an average increase of 7.0%. After 10,000 hours of salt-water exposure, further increases in ultimate load as compared to baseline values were observed as 4.1% and 7.1% for an average increase of 5.6%. These data indicate that structural improvement of specimens occurs due to salt-water exposure. The observed increase in ultimate load was most prominent for specimens exposed to 1,000 hours of salt-water.

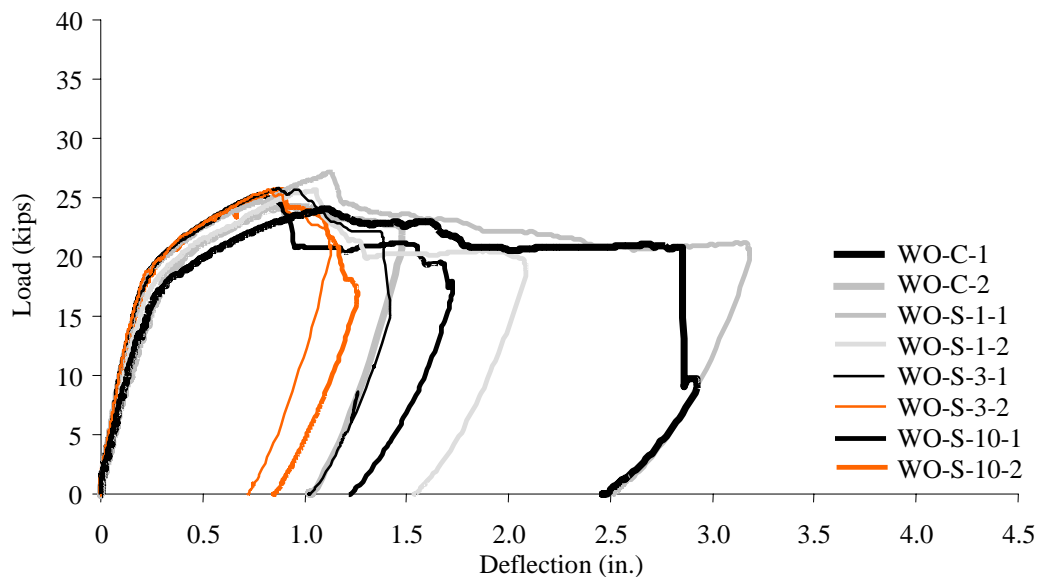


Figure 5.98. Load-deflection curves for ultimate load of 1,000-, 3,000-, 10,000-hour salt-water exposures, and control specimens without SIPMF

Table 5.7. Ultimate load results for control, 1,000-, 3,000-, 10,000-hour salt-water exposures specimens without SIPMF

Specimen	Mode of Failure	Failure Load (kips)		Comparable Control Value (kips)	Deflection at Ultimate Load (in.)	Percentage of Change in Deflection		Percentage of Change in Capacity	
WO-C-1	Flexural/Shear	24.02	(--)	(--)	1.11	(--)	(--)	(--)	(--)
WO-C-2	Flexural	24.04			1.00				
WO-S-1-1	Flexural	26.78	Average 26.20	24.02	1.13	1.8%	-2.3%	+ 11.4%	Average + 9.0%
WO-S-1-2	Flexural	25.61			1.04	-6.3%		+ 6.58%	
WO-S-3-1	Flexural	25.76	Average 25.70	24.03 ^a	0.87	-19.1%	-21.5%	+ 7.20%	Average + 7.0%
WO-S-3-2	Flexural	25.64			0.82	-23.8%		+ 6.70%	
WO-S-10-1	Flexural/Shear	25.02	Average 25.38	24.04	0.79	-21.0%	-17.0%	+ 4.12%	Average + 5.6%
WO-S-10-2	Flexural	25.73			0.87	-13.0%		+ 7.07%	

^a Linear interpolation used between control specimens to estimate baseline value

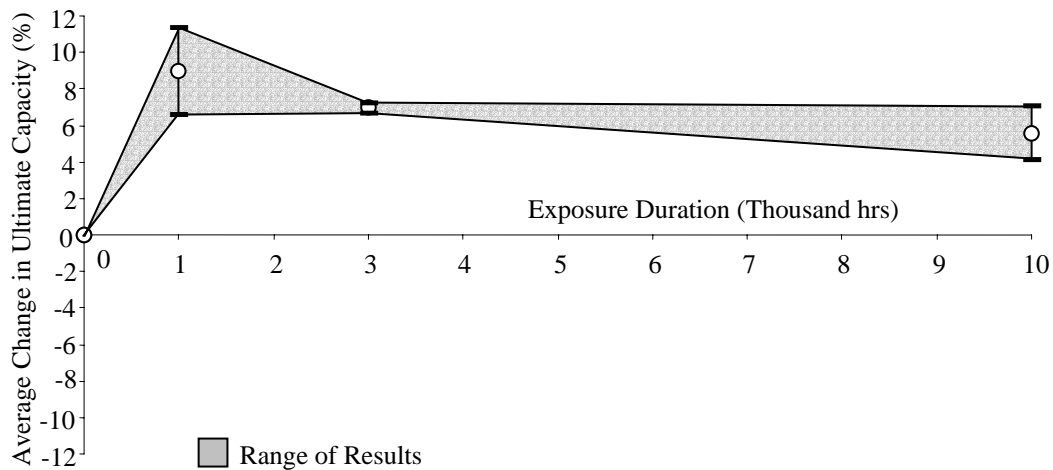


Figure 5.99. Percentage of change in ultimate load carrying capacity for salt-water exposures specimens without SIPMF

5.5 COMPARISON BETWEEN SPECIMENS WITH AND WITHOUT SIPMF

5.5.1 Ultrasonic Through-Transmission Results Comparison

Comparisons of the results of the ultrasonic through-transmission tests are presented as bar charts representing the numerical distribution of pulse-velocities for all measurement points. A summary bar chart for the comparison between the ranges for control specimens with and without SIPMF is presented in Figure 5.100. A summary bar chart for the comparison between the ranges for 300-cycle freeze/thaw specimens with and without SIPMF is presented in Figure 5.101. A summary bar chart for the comparison between the ranges for 600-cycle freeze/thaw specimens with and without SIPMF is presented in Figure 5.102. A summary bar chart for the comparison between the ranges for 1,000-hour salt-water exposures specimens with and without SIPMF is presented in Figure 5.103. A summary bar chart for the comparison between the ranges for 3,000-hour salt-water exposures specimens with and without SIPMF is presented in Figure 5.104. A summary bar chart for the comparison between the ranges for 10,000-hour salt-water exposures specimens with and without SIPMF is presented in Figure 5.105. The average velocities for the perimeter, interior, bottom, and total points of the control, freeze/thaw, and salt-water specimens with and without SIPMF are presented in Table 5.8.

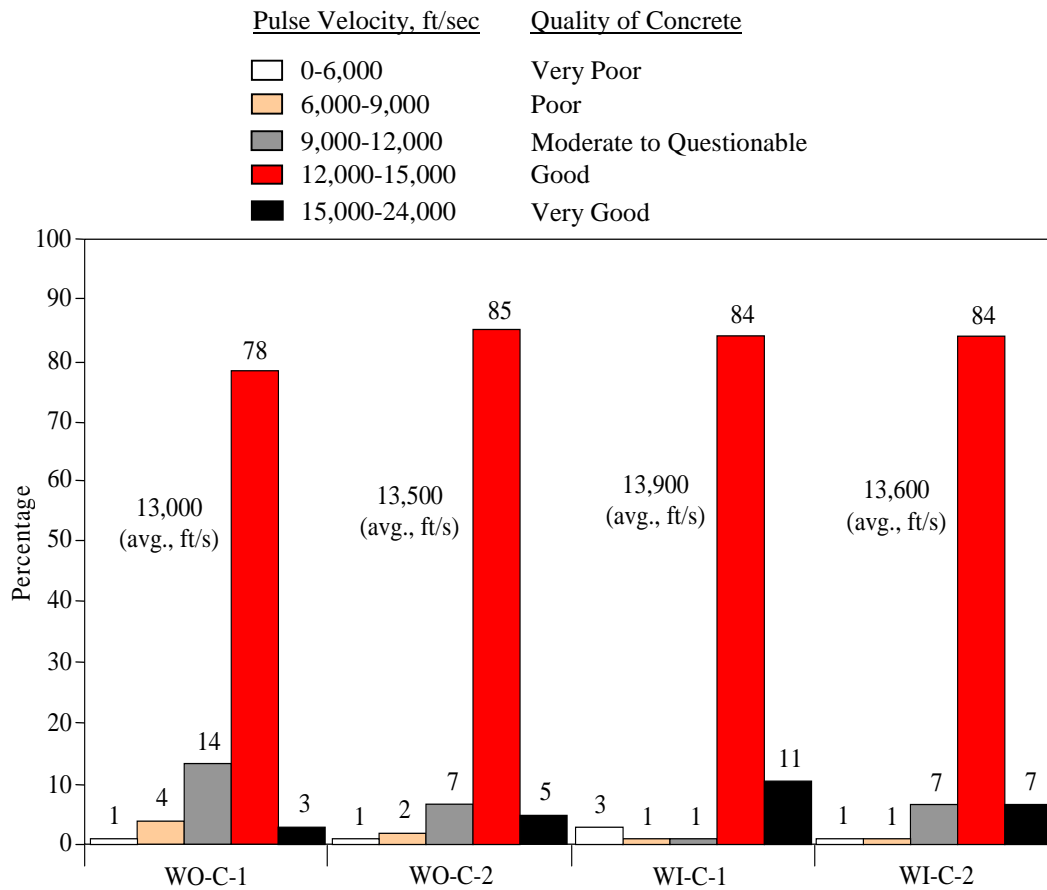


Figure 5.100. Summary of through-transmission test results for control specimens with and without SIPMF

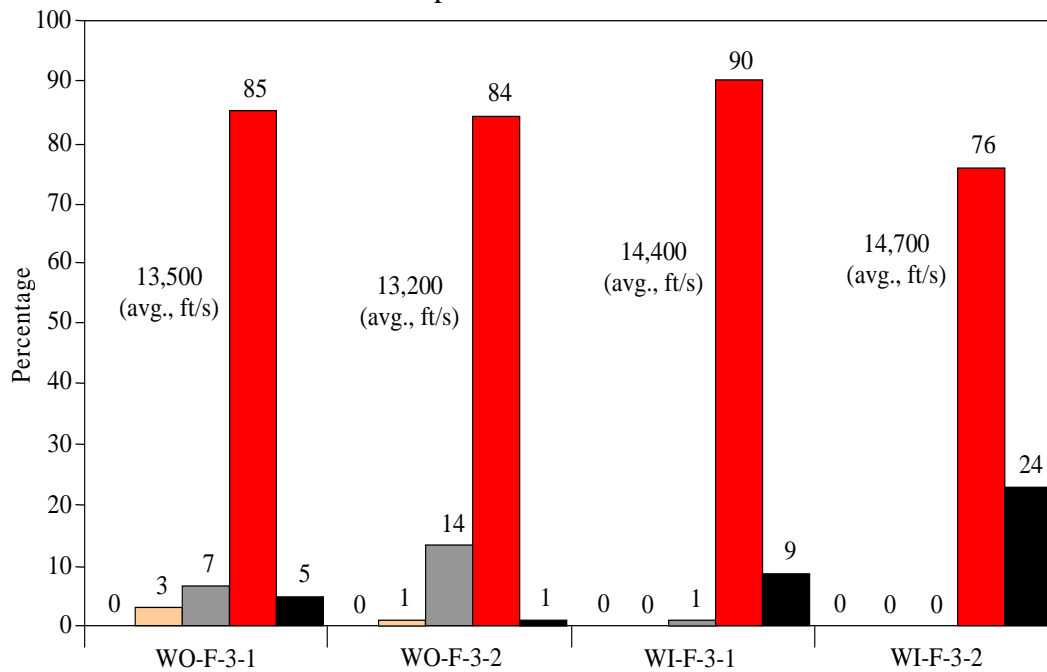


Figure 5.101. Summary of through-transmission test results for 300-cycle freeze/thaw specimens with and without SIPMF

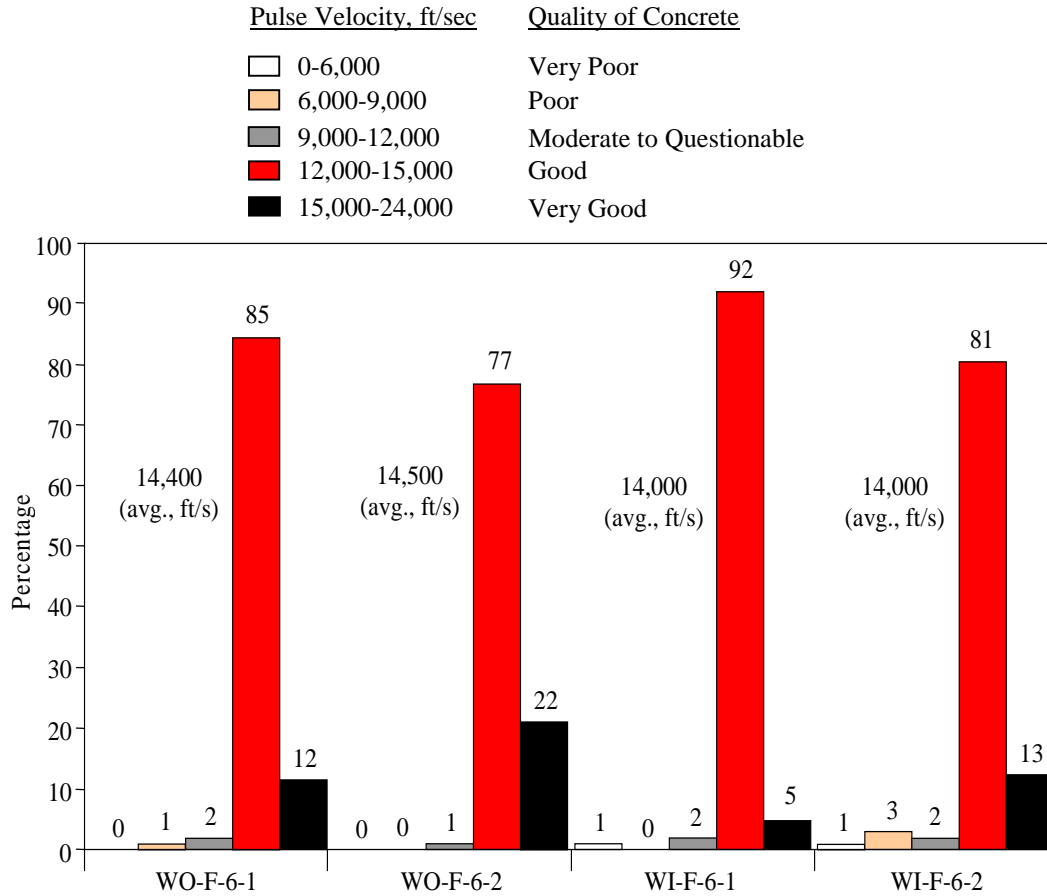


Figure 5.102. Summary of through-transmission test results for 600-cycle freeze/thaw specimens with and without SIPMF

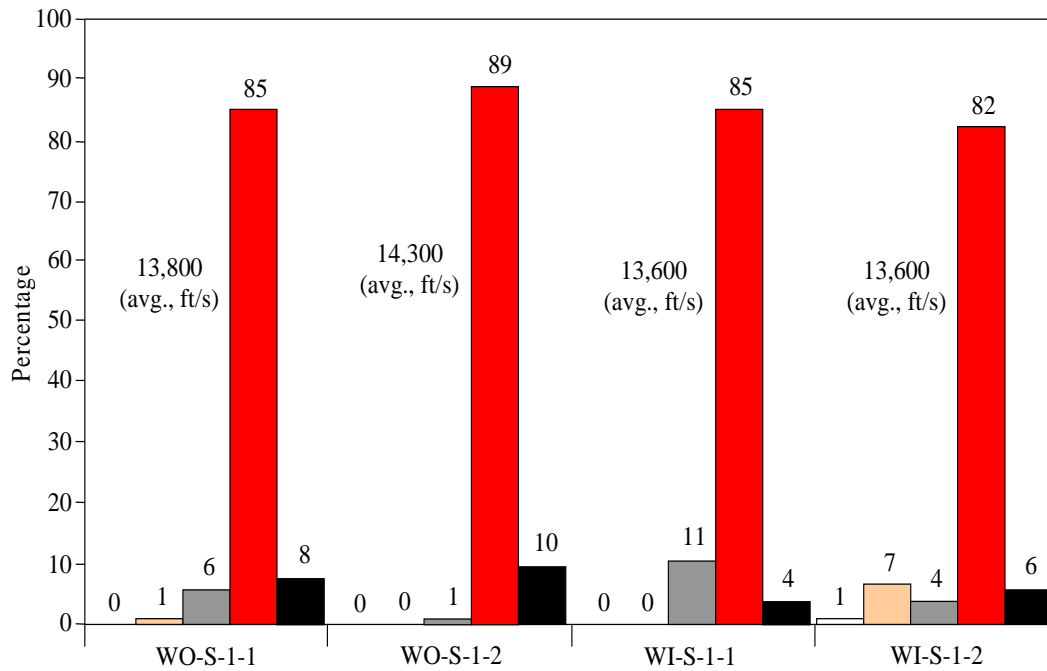


Figure 5.103. Summary of through-transmission test results for 1,000-hour salt-water exposures specimens with and without SIPMF

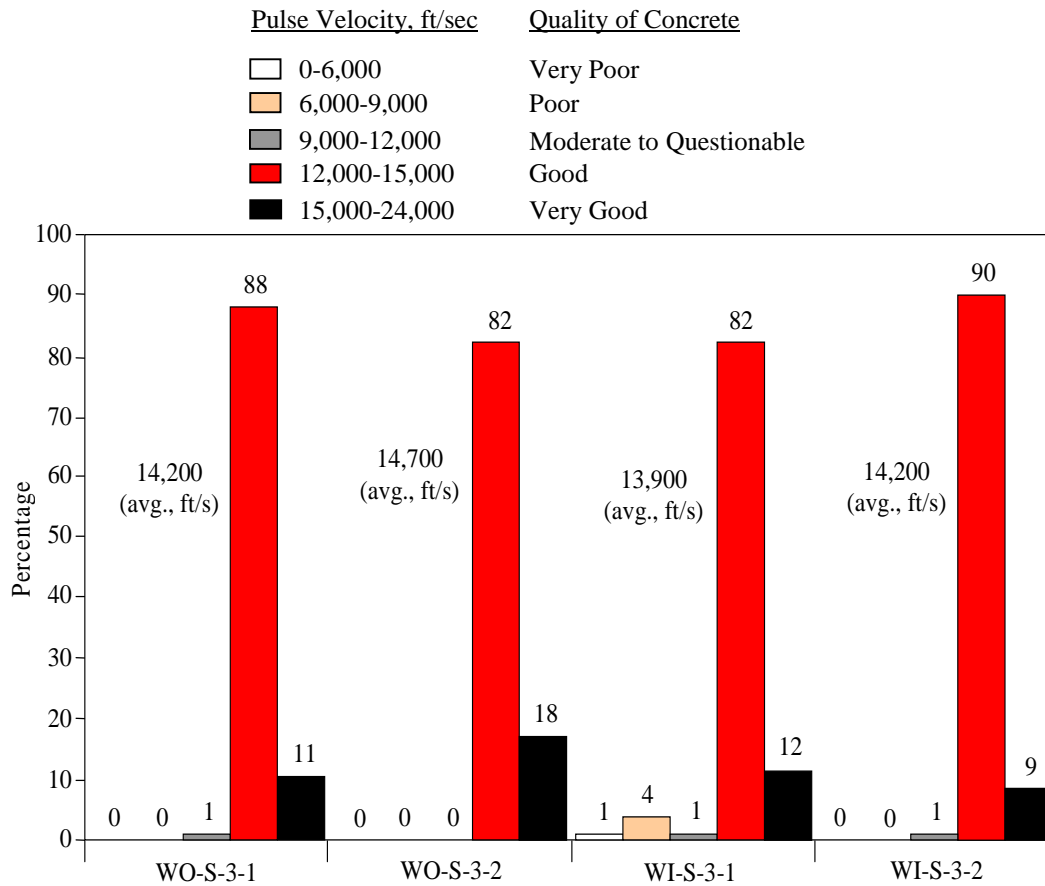


Figure 5.104. Summary of through-transmission test results for 3,000-hour salt-water exposures specimens with and without SIPMF

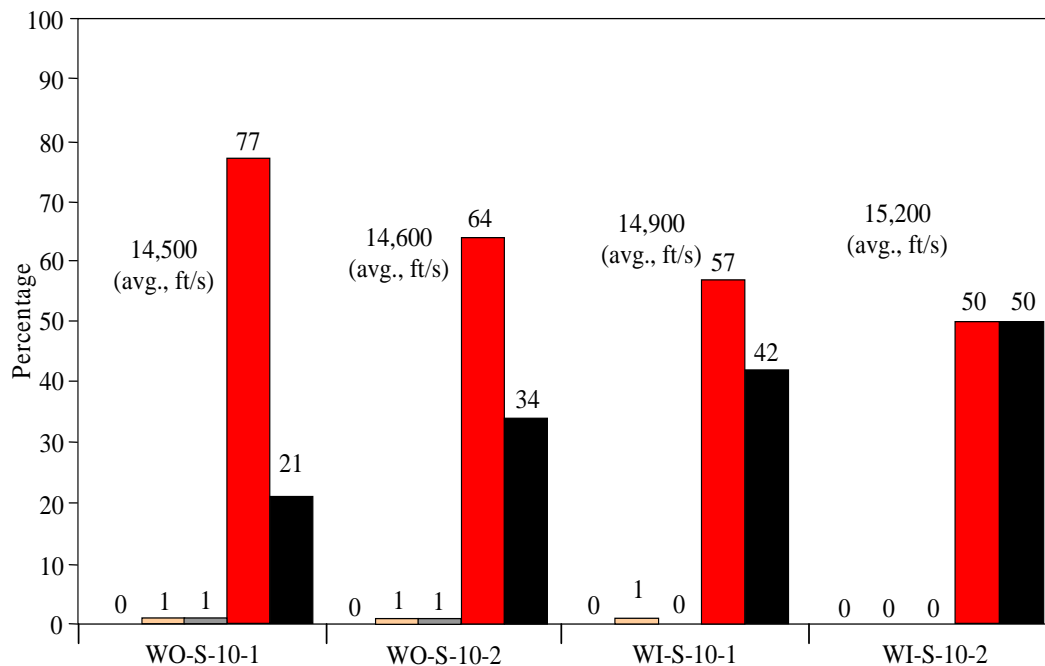


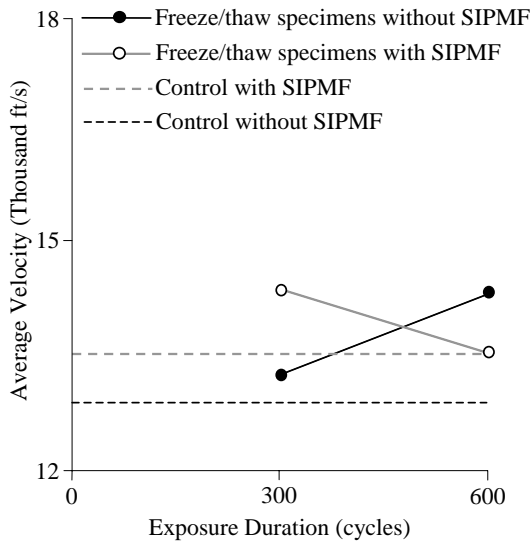
Figure 5.105. Summary of through-transmission test results for 10,000-hour salt-water exposures specimens with and without SIPMF

Table 5.8. Average velocities for the control, freeze/thaw, and salt-water specimens with and without SIPMF

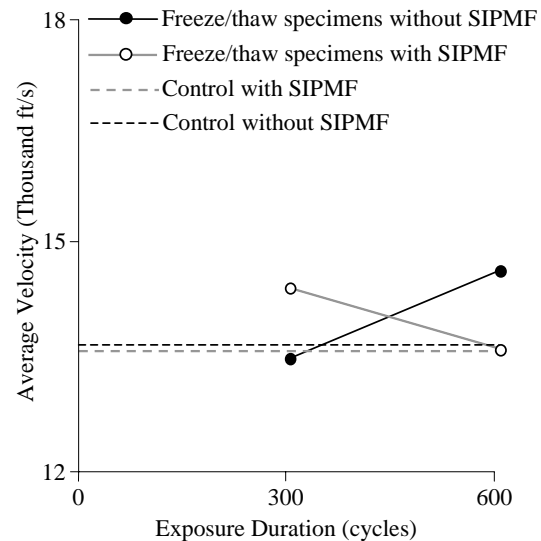
Type of specimens			Average Velocity (ft/s)							
			Perimeter Points		Interior Points		Bottom Points		Total Points	
			Specimen	Avrg.	Specimen	Avrg.	Specimen	Avrg.	Specimen	Avrg.
Specimens with SIPMF	Control	WI-C-1	13,746	13,577	14,047	13,891	13,922	13,663	13,889	13,727
		WI-C-2	13,408		13,735		13,404		13,564	
	Freeze/Thaw	300 cycle	WI-F-3-1	14,384	14,513	14,681	14,677	14,742	14,364	14,525
			WI-F-3-2		14,849		14,806		14,686	
		600 cycle	WI-F-6-1	13,595	14,360	14,404	14,129	13,412	13,982	13,979
			WI-F-6-2		14,447		12,696		13,976	
	Salt-Water	1,000 hr	WI-S-1-1	13,487	13,631	13,673	13,857	13,275	13,574	13,575
			WI-S-1-2		13,714		12,694		13,575	
		3,000 hr	WI-S-3-1	14,081	13,972	14,029	13,489	13,876	13,871	14,056
			WI-S-3-2		14,085		14,263		14,241	
		10,000 hr	WI-S-10-1	14,987	14,953	15,067	15,153	15,198	14,934	15,025
			WI-S-10-2		15,180		15,244		15,115	
Specimens without SIPMF	Control	WO-C-1	12,576	12,894	13,501	13,619	11,951	12,535	13,027	13,244
		WO-C-2	13,211		13,737		13,119		13,461	
	Freeze/Thaw	300 cycle	WO-F-3-1	13,279	13,648	13,449	14,257	13,853	13,492	13,360
			WO-F-3-2		13,249		13,448		13,227	
		600 cycle	WO-F-6-1	14,324	14,610	14,600	14,410	14,575	14,373	14,457
			WO-F-6-2		14,589		14,741		14,540	
	Salt-Water	1,000 hr	WO-S-1-1	14,052	13,877	14,124	13,747	14,061	13,849	14,087
			WO-S-1-2		14,371		14,375		14,324	
		3,000 hr	WO-S-3-1	14,500	14,256	14,394	14,704	14,754	14,236	14,449
			WO-S-3-2		14,531		14,803		14,662	
		10,000 hr	WO-S-10-1	14,649	14,427	14,506	14,865	14,787	14,526	14,581
			WO-S-10-2		14,584		14,709		14,636	

The graphs for the comparison between the average velocities for the perimeter, interior, bottom, and total points of the control and freeze/thaw specimens with and without SIPMF are shown in Figure 5.106. A comparison of average rates of change for pulse velocity is presented in Table 5.9 for freeze/thaw exposure for specimens with and without SIPMF. The rates of change for pulse velocity are calculated from slopes of the average curves in Figure 5.106. The

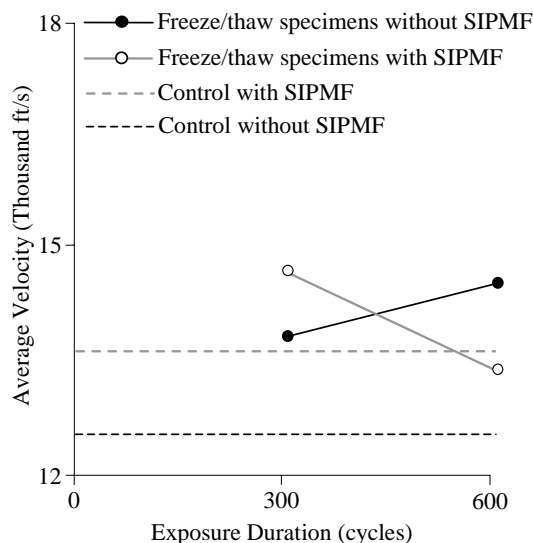
rates of change in pulse velocity for specimens with and without SIPMF for the period between zero and 300 freeze/thaw cycles were positive (indicating an apparent improvement in the quality of concrete). The rate of change in pulse velocity was greater for specimens with SIPMF for this period. For the period between 300 and 600 freeze/thaw cycles, the rate of change was negative for specimens with SIPMF and positive for specimens without SIPMF.



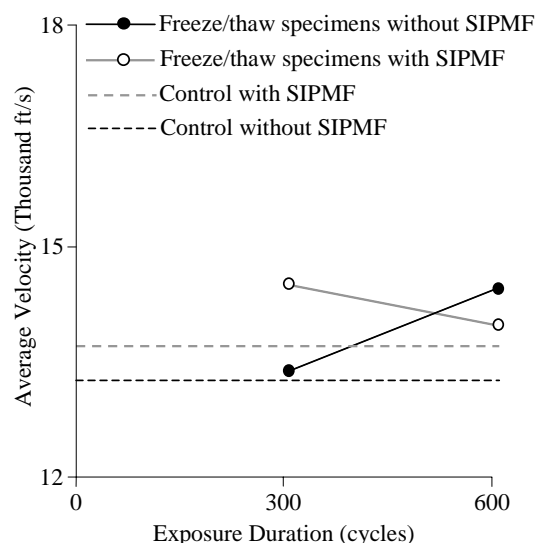
a. Average velocity for perimeter points



b. Average velocity for interior points



c. Average velocity for bottom points



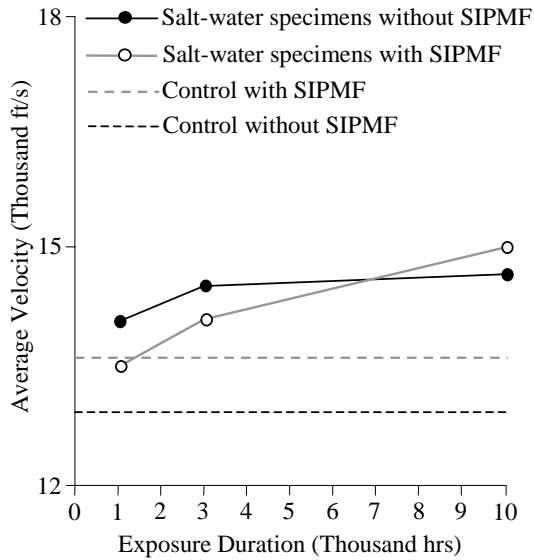
d. Average velocity for total points

Figure 5.106. Average velocity for freeze/thaw exposure specimens

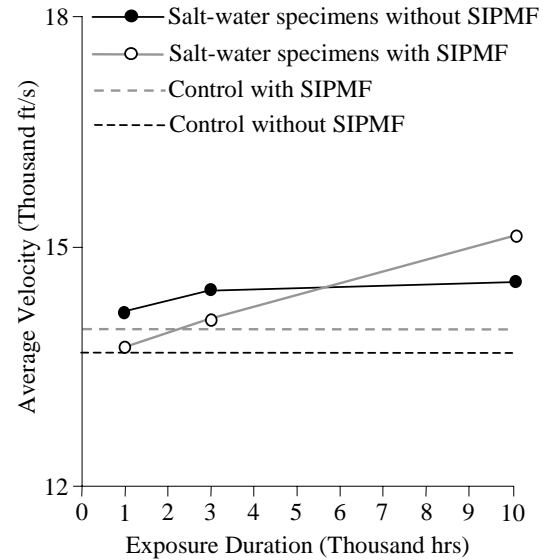
Table 5.9. Rates of change of pulse velocity for freeze/thaw exposure for specimens with and without SIPMF

Freeze/Thaw Exposure period	Rate of Change of Pulse Velocity [(ft/s) / cycle]	
	SIPMF	No SIPMF
0 to 300 cycles	+ 2.7	+ 0.4
300 to 600 cycles	- 1.8	+ 3.7

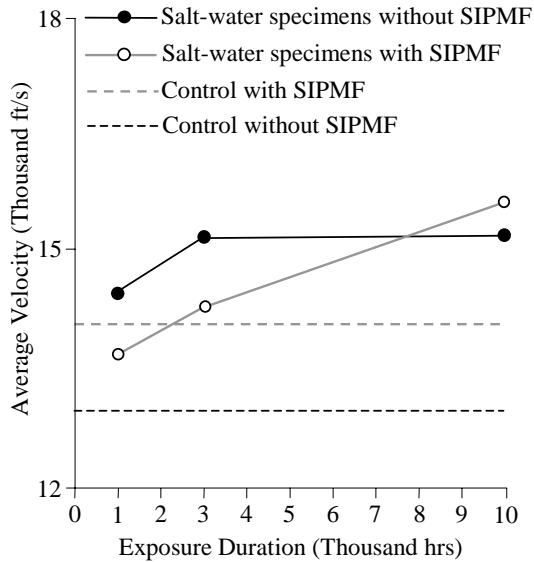
The graphs for the comparison between the average velocities for the perimeter, interior, bottom, and total points of the control and salt-water specimens with and without SIPMF are shown in Figure 5.107. A comparison of average rates of change for pulse velocity is presented in Tables 5.10 for salt-water exposure for specimens with and without SIPMF. The rates of change for pulse velocity are calculated from slopes of the average curves in Figure 5.107. In most cases the rates of change in the pulse velocity were small positive values. For the period between zero and 1,000 hours, a small negative rate of change was observed for specimens with SIPMF. The average rates of change for all specimens for periods between 1,000 and 3,000 hours as well as between 3,000 and 10,000 hours were positive.



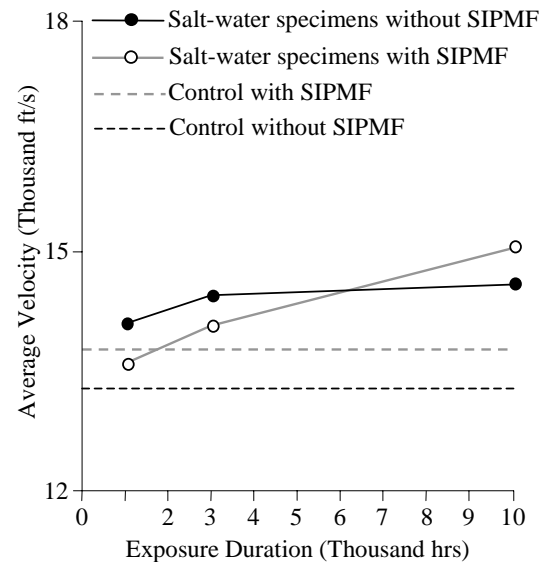
a. Average velocity for perimeter points



b. Average velocity for interior points



c. Average velocity for bottom points



d. Average velocity for total points

Figure 5.107. Average velocity for salt-water exposure specimens

Table 5.10. Rates of change of pulse velocity for salt-water exposure for specimens with and without SIPMF

Salt-Water Exposure period	Rate of Change of Pulse Velocity [(ft/s) / hours]	
	SIPMF	No SIPMF
0 to 1,000 hours	- 0.2	+ 0.8
1,000 to 3,000 hours	+ 0.2	+ 0.2
3,000 to 10,000 hours	+ 0.1	+ 0.0

5.5.2 Ultimate Load Test Results Comparison

A comparison was made to determine the effect of freeze/thaw exposure on ultimate load of specimens with and without SIPMF (Figure 5.108). Appropriate baseline values for comparison were determined from control specimens. A reduction in ultimate load as compared to baseline values was observed for all freeze/thaw specimens with and without SIPMFs except for WO-F-3-2. After 300 cycles of freeze/thaw exposure, reductions in ultimate load as compared to baseline values were greater for specimens with SIPMF than for specimens without SIPMF. In general, after 600 cycles of freeze/thaw exposure, reductions in ultimate load for all specimens with and without SIPMF, as compared to baseline values, were within the same range. These data indicate that deterioration of specimens occurs due to freeze/thaw exposure.

A comparison of average rates of change for ultimate load is presented in Table 5.11 for freeze/thaw exposure for specimens with and without SIPMF. The rates of change for ultimate load are calculated from slopes of the average curves in Figure 5.108. The rates of change in ultimate load for specimens with and without SIPMF for the period between zero and 300 freeze/thaw cycles were negative (indicating a decrease in ultimate load capacity). The rate of change in ultimate load was greater for specimens with SIPMF for this period. For the period between 300 and 600 freeze/thaw cycles, the rate of change in ultimate load was a small positive value for specimens with SIPMF and negative for specimens without SIPMF. Analysis and comparison of ductility for the specimens were not provided due to the different failure modes experienced by the specimens exposed to different environmental conditions.

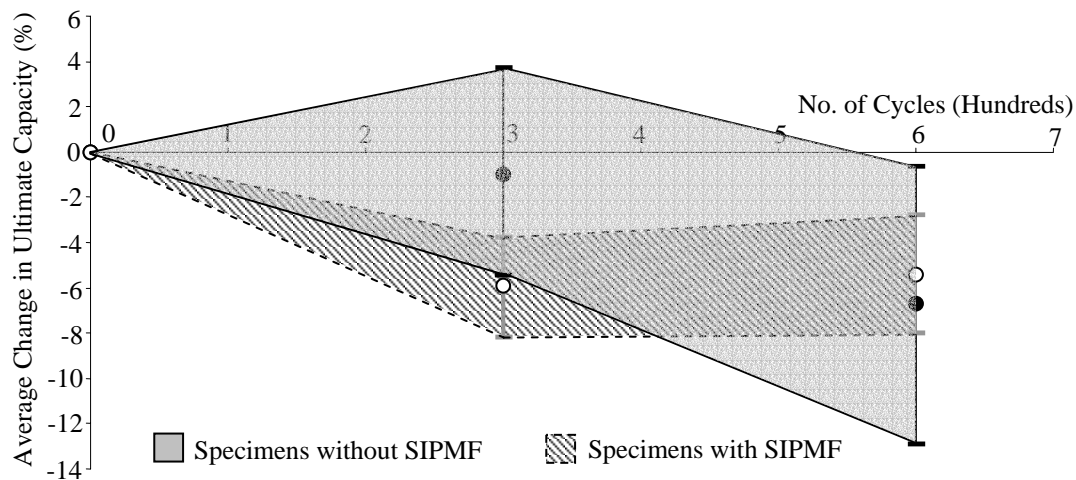


Figure 5.108. Percentage of change in ultimate load carrying capacity for freeze/thaw exposure specimens with and without SIPMF

Table 5.11. Rates of change of ultimate load for freeze/thaw exposure for specimens with and without SIPMF

Freeze/Thaw Exposure period	Rate of Change of Ultimate Load (% change / 100 cycles)	
	SIPMF	No SIPMF
0 to 300 cycles	- 2.0	- 0.3
300 to 600 cycles	+ 0.2	- 1.9

A comparison was made to determine the effect of salt-water exposure on ultimate load of specimens with and without SIPMF (Figure 5.109). Appropriate baseline values for comparison were determined from control specimens. An initial increase in ultimate load is observed after 1,000 hours of salt-water exposure as compared to baseline values followed by a lesser increase (for specimens without SIPMF) or a decrease (for specimens with SIPMF) in ultimate load due to further salt-water exposure. The average change in ultimate load carrying capacity for specimens with and without SIPMF between 3,000 and 10,000 hours of salt-water exposure was not significant. In general, the percentages of change in ultimate load carrying capacity for specimens without SIPMF are greater after salt-water exposure when compared to specimens with SIPMF.

A comparison of average rates of change for ultimate load is presented in Tables 5.12 for salt-water exposure for specimens with and without SIPMF. The rates of change for ultimate

load are calculated from slopes of the average curves in Figure 5.109. The trends of the rates of change of ultimate load with salt-water exposure for specimens with and without SIPMF were similar. For both cases positive rates of change were observed from zero to 1,000 hours, negative rates of change were observed between 1,000 and 3,000 hours, and small negative rates of change were observed between 3,000 and 10,000 hours. The long-term rates of change (as measured between 3,000 and 10,000 hours) were similar.

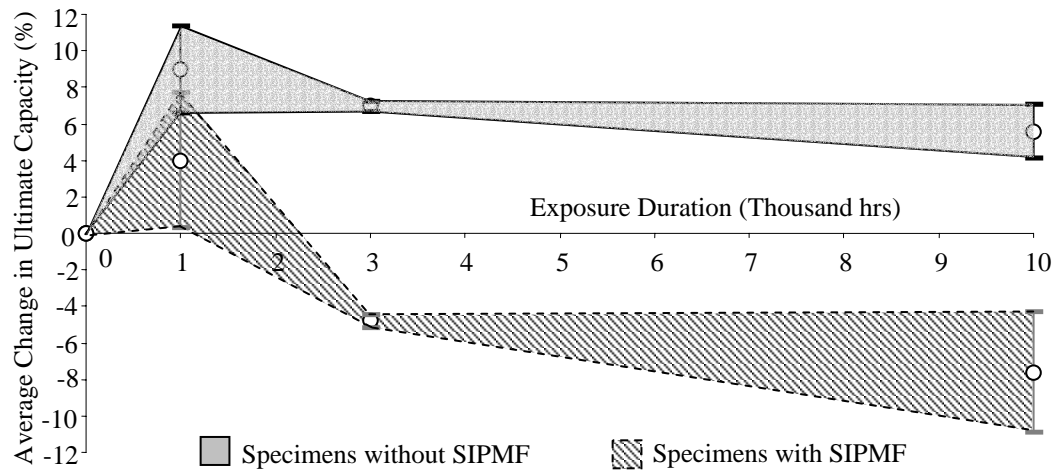


Figure 5.109. Percentage of change in ultimate load carrying capacity for salt-water exposures specimens with and without SIPMF

Table 5.12. Rates of change of ultimate load for salt-water exposure specimens with and without SIPMF

Salt-Water Exposure period	Rate of Change of Ultimate Load (% change / 1,000 hours)	
	SIPMF	No SIPMF
0 to 1,000 hours	+ 4.0	+ 9.0
1,000 to 3,000 hours	- 4.4	- 1.0
3,000 to 10,000 hours	- 0.4	- 0.2

5.5.3 Correlation between Ultrasonic and Structural Test Results

A strong correlation between trends in ultimate load and average pulse velocity was not observed in the test program. For specimens subjected to environmental exposure, a decrease in ultimate load capacity is observed for the majority of specimens whereas an increase in average pulse velocity was observed for the majority of specimens. The overall increase in pulse velocity after environmental exposure is attributed to extended curing duration and improved hydration conditions in the presence of frequent wetting of the specimens. Despite the apparent increase in the quality of concrete, a decrease in ultimate load is observed for these same specimens. The decrease in ultimate load is attributed to presence of macrofeatures such as cracks that would influence large-scale structural behavior (i.e., ultimate load), but not influence the majority of discrete ultrasonic measurements over the cross section.

CHAPTER 6 : FIELD IMPLEMENTATION

6.1 INTRODUCTION

The ultrasonic inspection methods developed and used in this test program can be implemented for field inspection. Both the through-transmission technique and pulse-echo technique can be used for normal field inspection. The equipment and software needed to implement these methods in the field are described in this chapter.

6.2 THROUGH-TRANSMISSION TECHNIQUE

The through-transmission ultrasonic test method provides for assessment of pulse velocity through the depth of concrete bridge decks. Ultrasonic through-transmission tests conducted on slices of full-depth cores provide a profile of pulse velocity. The hardware required for this method is described in chapter 4. The software required to identify the first arrival time is presented in Appendix B. First arrival time is used to identify travel time for the waveform. Thickness of the slice can be measured using a micrometer. The quotient of thickness to travel time is defined as pulse velocity. The pulse velocity can be related to the quality of concrete using empirical relationships (Krautkramer and Krautkramer 1990). The methodology for determining the Quality Index (QI) for a core is presented in Chapter 4. The distribution of pulse-velocity with depth as well as the QI for cores can be used for determining the influence of the presence of SIPMFs.

6.3 PULSE-ECHO TECHNIQUE

The method developed for analyzing the contact between SIPMFs and concrete can be adopted for field use. The method for field implementation is demonstrated below:

- 1) The hardware used for the laboratory experiments is directly transferable to field use. Detailed specifications for the transducer, delay line, and pulser-receiver are presented in Chapter 4. Detailed plans for construction of a transducer holder that provides a repeatable load application (identical to what was used in the laboratory test program) is presented in Figures 6.1 to 6.6. The addition of an extension rod to the transducer holder or an automated track mounting

system to the underside of the bridge deck slab may provide added flexibility for field implementation. A longer cable and a power source (generator) would be required for field implementation.

2) The software used for analysis of laboratory test results is directly transferable to field use. The area confined by the waveform curve is calculated using the trapezoidal method. Threshold values for area confined by the curves are presented for idealized (and controlled) conditions in the laboratory in Chapter 4.

3) The sampling grid used for the laboratory test program is presented in Figure 6.7. Random sampling locations on the underside of the SIPMF can be used in the field to provide statistically representative results. Distribution of sampling locations across the profile of the section should be maintained for selection of measurement locations (columns A through K, Figure 6.7). The number of samples required to achieve representative results was determined using statistical analysis on the results from the laboratory test program. The following steps were used to produce a chart that can be used to identify a suitable number of measurement points for field bridge deck inspection:

- a) The finely spaced grid used for the laboratory tests (704 measurement locations) was assumed to provide statistically representative results for defining the percentage of total area classified as good, fair, and poor contact. Therefore, the results from each specimen can be considered statistically “true” in that they provide a valid determination of percentages of area classified as good, fair, and poor contact. In addition, it was assumed that the large-scale laboratory samples provided representative results for assessment of contact. Therefore, equivalency of large-scale laboratory specimens and full-size bridge decks is assumed.
- b) Random sampling locations are assumed to be representative for measurement locations. The non-biased spatial distribution of contact quality regions (good, fair, and poor) for laboratory results supports this premise.
- c) The results determined in the laboratory investigation for full data sets (704 measurement points) were compared to results from subsets of selected measurement locations from varying numbers of random sampling points on the same specimen. The percentages of areas corresponding to good, fair, and poor contact were determined for the subset of data points. The difference for each

category (good, fair, and poor contact) between the true values (as determined using 704 points) and the given number of measurement points was calculated. A plot was produced representing the percentage difference for each category (good, fair, and poor) from true value versus the number of random measurement points (Figure 6.8).

- d) The plot presented in Figure 6.8 was constructed to provide determination of the required number of measurements to adequately represent spatial distribution of quality of contact between SIPMF and concrete. A higher number of measurement locations allows for higher precision in determining the percentage of points corresponding to the various degrees of quality of contact between the concrete and the SIPMF. An envelope is presented in Figure 6.8 that contains the great majority of laboratory test data (several outlying datapoints are outside the envelope). The envelope in Figure 6.8 can be used to directly determine (either graphically or by using the equation in Figure 6.8) the minimum number of measurement locations to achieve a given degree of precision in establishing the regions of varying degrees of contact.
- 4) Timing of measurements in the field relates to the perceived importance of good contact between the SIPMF and the concrete as discussed in Chapter 4. Measurements may be taken shortly following construction to provide baseline values and allow for an assessment of any change occurring over the service life of the bridge deck. Measurements can be taken at any time during the service life of a bridge deck and the after-construction baseline values are not required for interpretation of the results. Assessment of quality of contact over time would require repeated measurements to be taken. Since statistically representative results are achieved using random sampling locations, it is not necessary that sampling locations be the same between various surveys. A series of ultrasonic pulse-echo measurements could be incorporated into a normal bridge deck inspection routine.

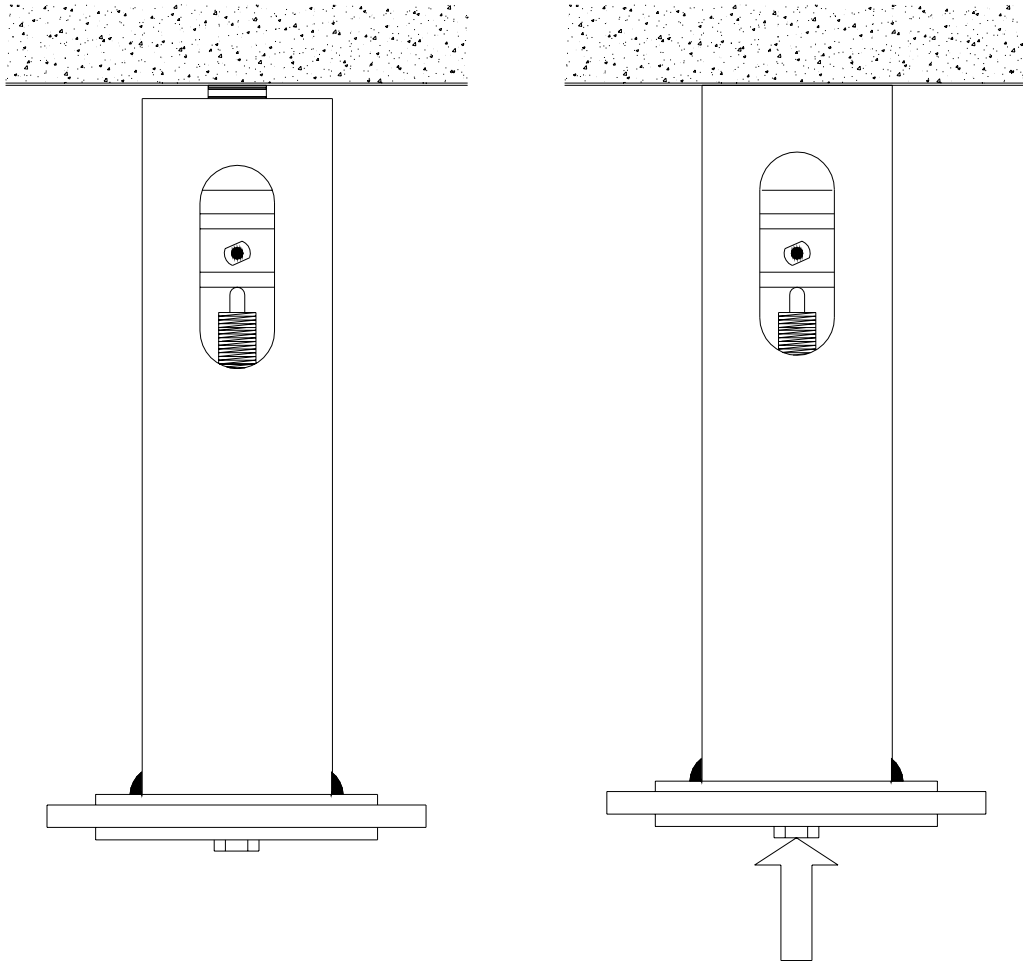


Figure 6.1. Application of transducer for pulse-echo testing using transducer holder

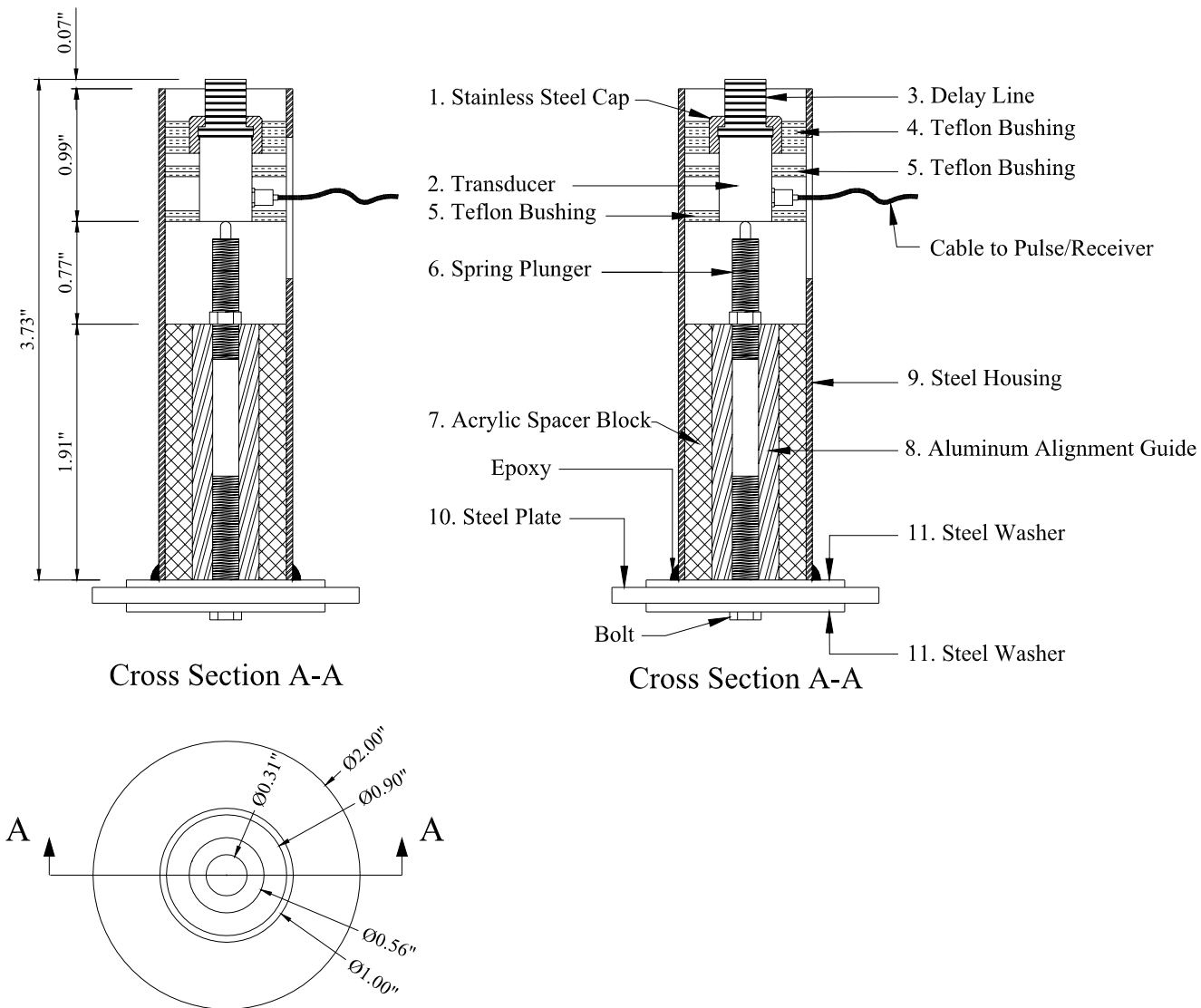


Figure 6.2. Transducer holder details

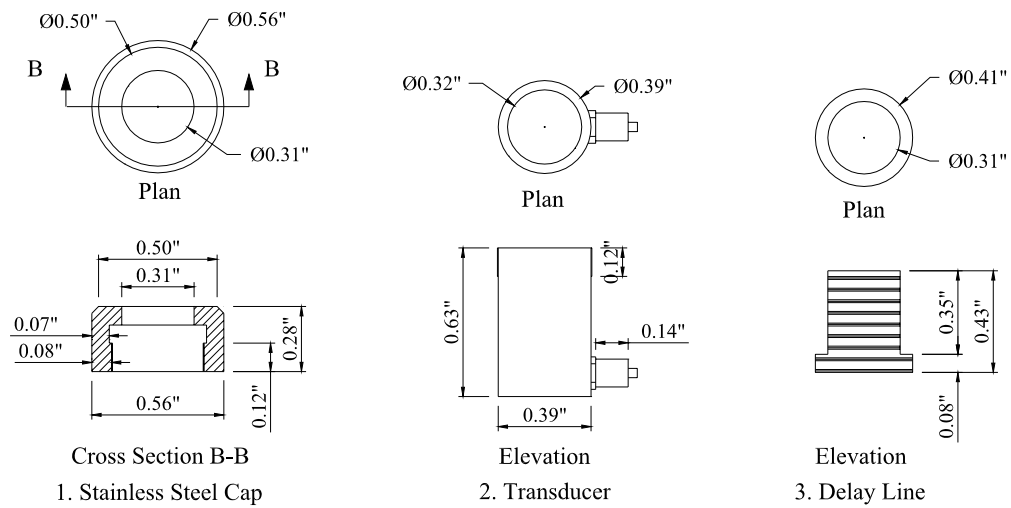


Figure 6.3. Transducer and delay line details

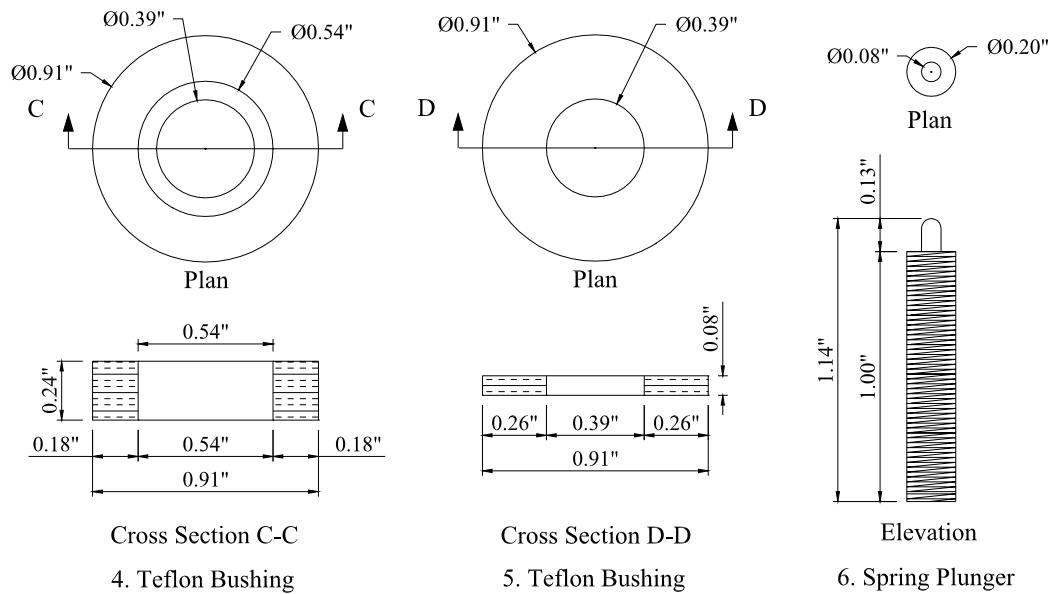


Figure 6.4. Teflon bushing and spring plunger details

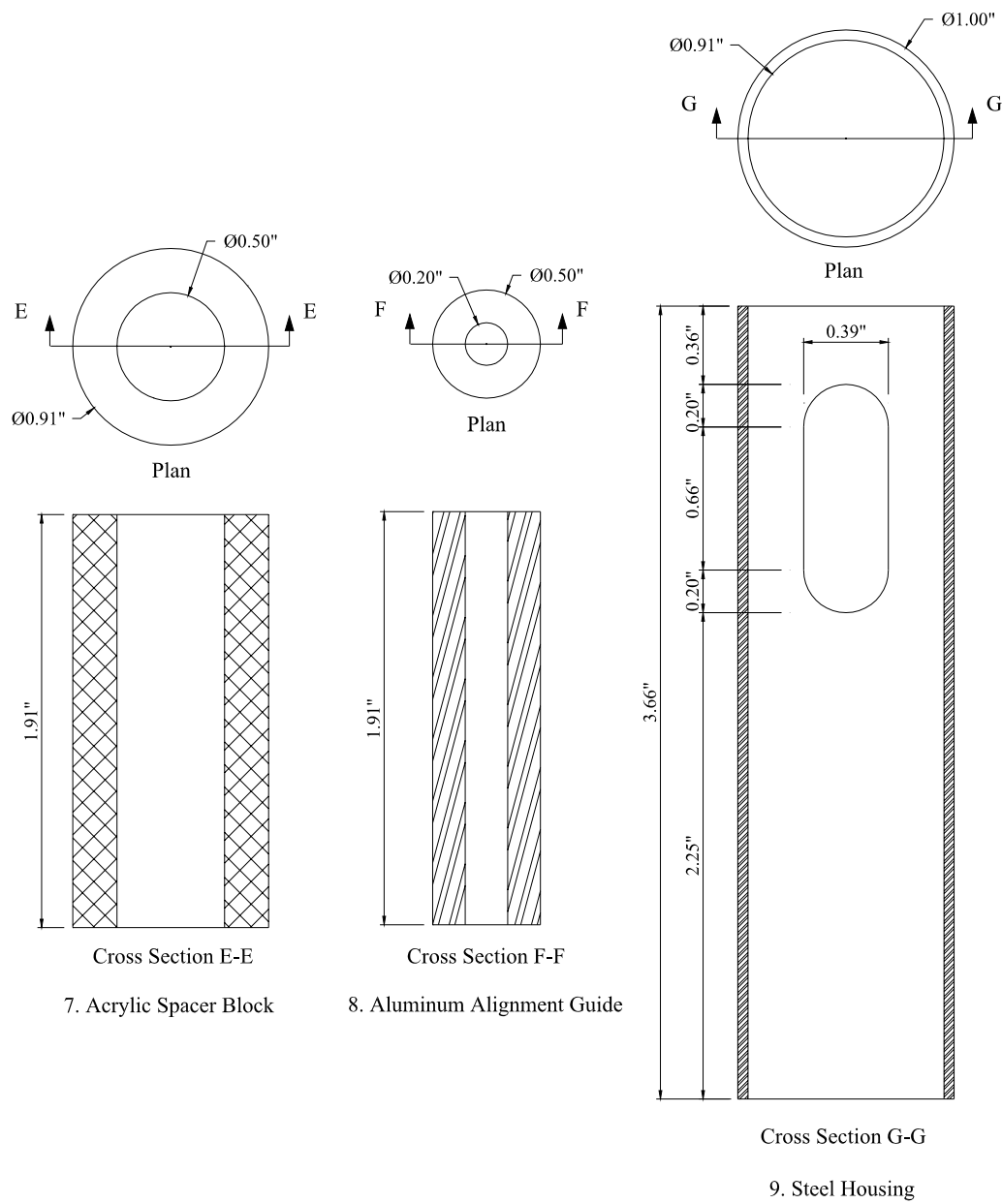


Figure 6.5. Spacer block, alignment guide, and housing details

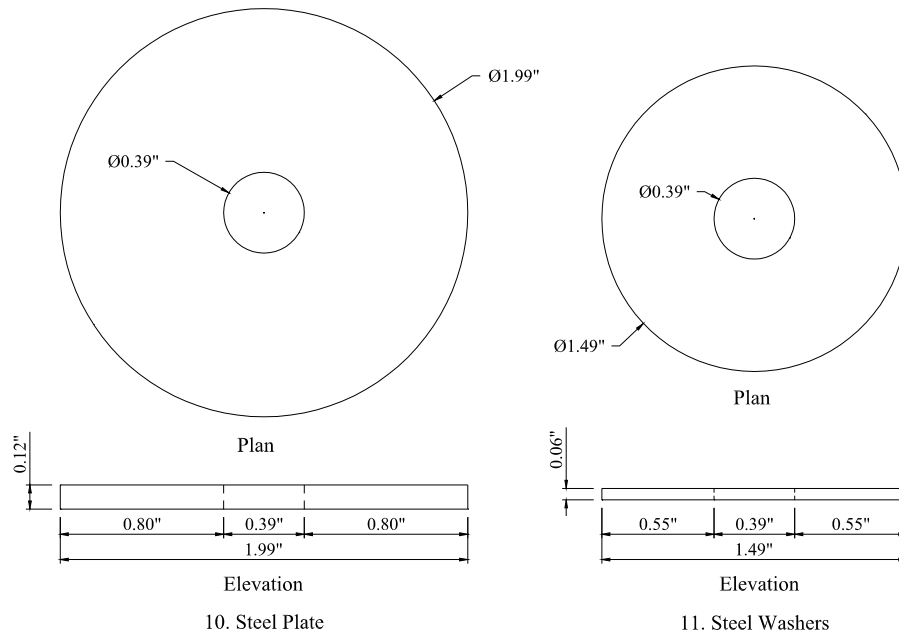


Figure 6.6. Transducer holder base details

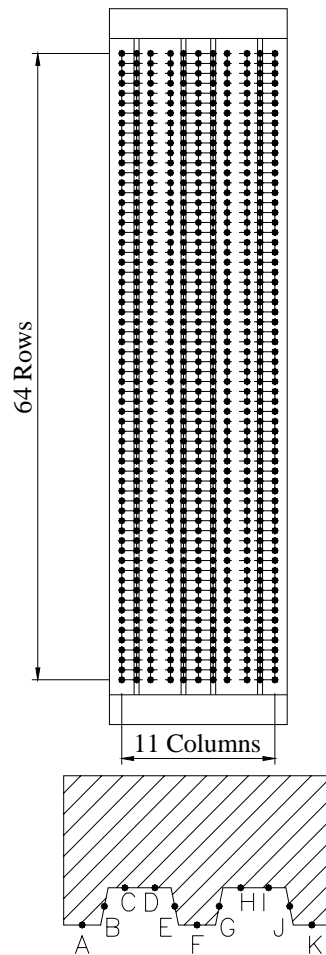


Fig 6.7. Measurement locations for laboratory test specimens

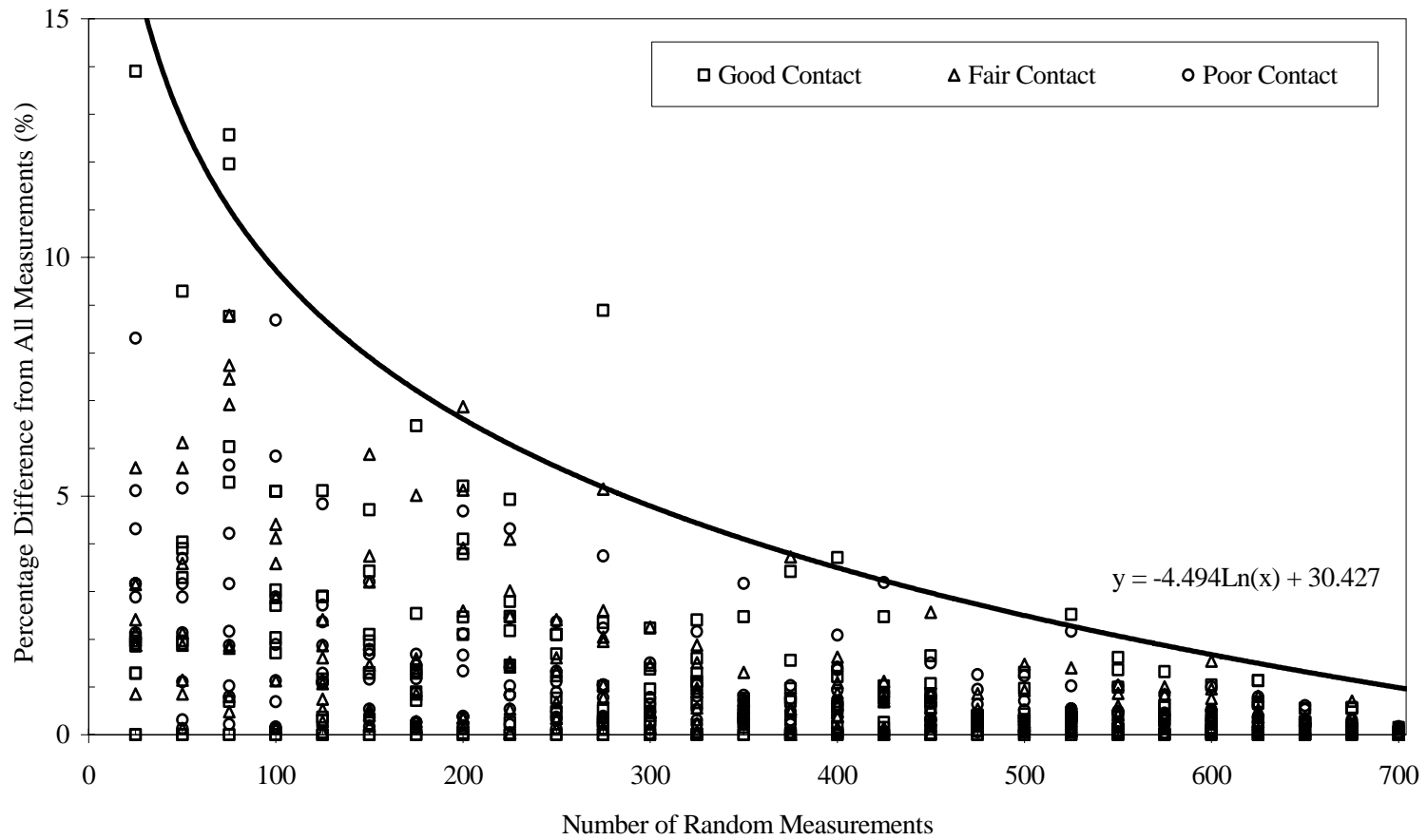


Figure 6.8. Statistical determination of number of measurement points

6.4 SUITABILITY OF FIELD IMPLEMENTATION

The two inspection and evaluation methods used in this research program are both suitable for field implementation. A recommendation is made for MDOT to incorporate through-transmission testing of sliced cores into normal field inspection techniques. This method is straightforward and allows for determination of quality of concrete through the entire bridge deck thickness. Comparative analyses can be conducted to evaluate the influence of SIPMFs on bridge deck performance. A lower priority exists for incorporating pulse-echo inspection of the contact between the SIPMF and the concrete. The importance of intimate contact on bridge deck performance is somewhat debatable. High quality contact between SIPMF and concrete is beneficial, as no space exists for excess ponding of water directly beneath the concrete bridge deck. However, high quality contact could be considered detrimental, as this condition would prevent convection of air for potentially drying out the lower region of the concrete bridge deck. Furthermore, the logistics of field inspection using this technique are somewhat complex. Therefore, the through-transmission technique should be considered the priority for the near future.

CHAPTER 7 : SUMMARY AND CONCLUSIONS

A comprehensive research investigation was conducted to evaluate the use of SIPMFs in construction of concrete bridge decks. A survey was developed and administered to all DOTs to examine the state of the practice of using SIPMFs for concrete bridge deck construction. Additionally, a field investigation was conducted to evaluate the performance of existing concrete bridge decks constructed with and without SIPMFs. This field investigation included visual inspection of 10 bridge decks and laboratory investigation of full-depth cores obtained from the inspected bridge decks. The cores were investigated using visual inspection, compressive strength tests, and ultrasonic tests. The compressive strength tests provided overall strength for the concrete used in the inspected bridges. The ultrasonic tests provided means for evaluating the quality of concrete through the depth of bridge deck. A laboratory durability investigation was conducted on 24 large-scale bridge deck slab specimens with and without SIPMF. Four specimens were used as control specimens, and the remaining 20 specimens were subjected to either freeze/thaw exposure and repeated load cycles or salt-water exposure and repeated load cycles. At various stages before, during, and after the environmental exposure, ultrasonic pulse-echo testing was used to determine the quality of contact between the SIPMFs and concrete for specimens with SIPMF. Furthermore, after the completion of the environmental exposure, ultrasonic through-transmission testing was used to assess the condition of the concrete for all specimens. These tests were followed by the ultimate load tests. Conclusions from each phase of the research investigation are outlined below.

Based on the survey responses provided by 39 DOTs, the following conclusions were drawn:

- 1) Two-thirds of responding DOTs allow the use and one-third of responding DOTs do not allow the use of SIPMFs in concrete bridge deck construction. Most of the DOTs that use SIPMFs are satisfied with the performance of this bridge deck system.
- 2) The majority of DOTs that do not use SIPMFs are concerned with the inability to visually examine and access the bottom of the deck slabs.
- 3) The majority of DOTs use conventional inspection approaches such as visual inspection, and hammer sounding for periodic examination of their SIPMF bridge decks.

- 4) Most of the DOTs do not believe that the SIPMF increases the long-term durability of bridge decks. The majority of DOTs reported that the use of SIPMFs is not linked to any deck deterioration.
- 5) Statistical bias is present in the data with regard to climatic region. The overall acceptance of use of SIPMFs and satisfaction with performance of SIPMF decks is generally higher for the Southern region compared to the Northern region of the country.
- 6) By comparing results of the survey to a similar survey administered in 1974, an increase in the overall use of SIPMFs is observed. However, some DOTs remain hesitant to adopt widespread use of SIPMFs for concrete bridge deck construction.

Based on the field inspection and coring of bridge deck slabs, the following conclusions were drawn:

- 1) From the visual field inspection and visual inspection of cores, it was determined that the two bridge deck systems were similar. Statistical analysis of compressive strength and ultrasonic pulse velocity tests also indicated similarity of the bridge deck systems for all of the decks as well as for direct comparison decks (for which traffic and environmental loads were identical).
- 2) The ultrasonic test results through the depth of the cores did not indicate specifically beneficial or adverse effects of the presence of SIPMF on the bridge decks.
- 3) Overall, the performance of concrete bridge decks constructed with SIPMFs was determined to be similar to the performance of concrete bridge decks constructed without SIPMFs.

Based on results of the laboratory structural test program, the following conclusions were drawn:

- 1) The average compressive strength of the cylinders that were cured under controlled conditions increased for curing periods up to 28 days, and decreased slightly for further curing times. The average compressive strength of the cylinders decreased with freeze/thaw exposure, and several cylinders deteriorated entirely. The average compressive strength of the cylinders for salt-water exposure increased with increasing time of exposure.

- 2) Generally, a reduction in the ultimate load carrying capacity was observed for all freeze/thaw specimens with and without SIPMFs except for specimen WO-F-3-2. After 300 cycles of freeze/thaw exposure, greater reduction in the ultimate load carrying capacity was observed for specimens with SIPMF than for specimens without SIPMF (approximately 5%). After further freeze/thaw exposure (600 total cycles), similar reduction in the ultimate load carrying capacity for all specimens with and without SIPMF was observed. This reduction was attributed to the deterioration of specimens with and without SIPMF due to freeze/thaw exposure.
- 3) An initial increase in ultimate load carrying capacity was observed after 1,000 hours of salt-water exposure for specimens with and without SIPMF. For further salt-water exposure, a relative decrease in ultimate load was observed for specimens with and without SIPMF. A larger decrease in ultimate load between 1,000 and 3,000 hours of salt-water exposure was observed for specimens with SIPMF than specimens without SIPMF. The average change in ultimate load carrying capacity for specimens with and without SIPMF between 3,000 and 10,000 hours of salt-water exposure was not significant. After 10,000 hours of salt-water exposure, the ultimate loads for specimens with SIPMF were less than baseline values, whereas ultimate loads for specimens without SIPMF were greater than baseline values.

Based on the ultrasonic pulse-echo tests on laboratory specimens the following conclusions were drawn:

- 1) The regions of consistent contact rating (good, fair, and poor) were generally well distributed over the entire area of SIPMF.
- 2) The overall trend of quality of contact between SIPMF and concrete was generally consistent for all freeze/thaw exposure specimens. The initial contact (before cracking) was consistently good, whereas a significant loss of contact occurred upon service load cracking. Essentially all contact was lost after 300 freeze/thaw cycles, and an apparent improvement of contact was observed after 600 freeze/thaw cycles. The apparent improvement in contact was attributed to accumulation of mineral precipitate between the SIPMF and concrete, which was traced to concrete/cement origin.

- 3) A similar trend of quality of contact between SIPMF and concrete was generally observed for all salt-water exposure specimens. The initial contact (before cracking) was consistently good, a significant loss of contact occurred upon service load cracking, and an apparent improvement of contact was observed with continued salt-water exposure (1,000, 3000, and 10,000 hours of salt-water exposure). The apparent improvement in contact was attributed to accumulation of mineral precipitate on the top and bottom surfaces of the SIPMF, which was traced to cement and salt origin.

Based on the ultrasonic through-transmission tests on laboratory specimens the following conclusions were drawn:

- 1) With the exception of generally lower pulse-velocities in regions containing cracks, the pulse-velocities were generally well distributed over the entire longitudinal cross section of the specimens. Average pulse-velocity for perimeter, interior, bottom, and total regions were generally similar.
- 2) An increase in the average pulse-velocity was observed for all freeze/thaw specimens with and without SIPMFs compared to the average pulse-velocity of the respective control specimens with and without SIPMFs. For specimens without SIPMFs, a continual increase in pulse-velocity was observed for freeze/thaw exposure. For specimens with SIPMFs, an increase in pulse-velocity was observed after 300 freeze/thaw cycles. A decreasing trend of pulse-velocity was observed for specimens with SIPMFs after further freeze/thaw exposure (600 total cycles), although the average pulse-velocity remained greater than the average control pulse-velocity (approximately 6%).
- 3) Relatively small changes in pulse-velocity were observed in response to salt-water exposure. Measured average pulse-velocities after 1,000 hours of salt-water exposure were close to values determined using control specimens. In all cases, the average pulse-velocity increased with further duration of salt-water exposure (3,000 and 10,000 hours total exposure). After 10,000 hours of salt-water exposure, the average pulse-velocity for specimens with SIPMF was higher than the average pulse-velocity for specimens without SIPMF (approximately 3%).

Overall, apparent equivalency of deck performance was observed using field inspection, visual inspection of cores, compressive strength of cores, and pulse-velocity profile of the cores. Small changes in the performance of bridge deck specimens with and without SIPMFs were measured during the structural and ultrasonic laboratory test programs.

REFERENCES

- Ahmed, I. and Ahmed, M. Z. (1996). "Premature Deterioration of Concrete Structures – Case Study." *Journal of Performance of Constructed Facilities*, ASCE, 10(4), 164-170.
- Alampalli, S., Owens, F., Sandhu, D., and Haddock, J. (2002). "A Qualitative Study of Correlation between Bridge Vibration and Bridge Deck Cracking," *Transportation Research Board Annual Meeting CD-ROM*.
- Almusallam, A. A., Al-Gahtani, A. S., Aziz, A. R., Dakhil, F. H., and Rasheeduzzafar. (1996). "Effect of Reinforcement Corrosion on Flexural Behavior of Concrete Slabs." *Journal of Materials in Civil Engineering*, ASCE, 8(3), 123-127.
- ASTM Standard (2000). A653/ A653M-99: Standard Specification for Steel Sheet, Zinc-Coated (Galvanized) or Zinc-Iron Alloy-Coated (Galvannealed) by the Hot-Dip Process. *Annual Book of ASTM Standards*, Vol. 01.06, ASTM International, West Conshohocken, PA.
- ASTM Standard (2000). A924/ A924M-99: Standard Specification for General Requirements for Steel Sheet, Metallic-Coated by the Hot-Dip Process. *Annual Book of ASTM Standards*, Vol. 01.06, ASTM International, West Conshohocken, PA.
- ASTM Standard (2000). C31/ C31M-98: Standard Practice for Making and Curing Concrete Test Specimens in the Field. *Annual Book of ASTM Standards*, Vol. 04.02, ASTM International, West Conshohocken, PA.
- ASTM Standard (2000). C39/ C39M-99: Standard Test Method for Compressive Strength of Cylindrical Concrete Specimens. *Annual Book of ASTM Standards*, Vol. 04.02, ASTM International, West Conshohocken, PA.
- ASTM Standard (2000). C78-94: Standard Test Method for Flexural Strength of Concrete (Using Simple Beam with Third-Point Loading). *Annual Book of ASTM Standards*, Vol. 04.02, ASTM International, West Conshohocken, PA.
- ASTM Standard (2000). C143/ C143M-98: Standard Test Method for Slump of Hydraulic-Cement Concrete. *Annual Book of ASTM Standards*, Vol. 04.02, ASTM International, West Conshohocken, PA.
- ASTM Standard (2000). C597-97: Standard Test Method for Pulse Velocity Through Concrete. *Annual Book of ASTM Standards*, Vol. 04.02, ASTM International, West Conshohocken, PA.
- ASTM Standard (2000). C617-98: Practice for Capping Cylindrical Concrete Specimens. *Annual Book of ASTM Standards*, Vol. 04.02, ASTM International, West Conshohocken, PA.

- ASTM Standard (2000). C666-97: Standard Test Method for Resistance of Concrete to Rapid Freezing and Thawing. *Annual Book of ASTM Standards*, Vol. 04.02, ASTM International, West Conshohocken, PA.
- Benson, C. H., Gunter, J. A., Trautwein, S. J. and Berzanskis, P. H. (1997). "Comparison of Four Methods to Assess Hydraulic Conductivity," *Journal of Geotechnical and Geoenvironmental Engineering*, ASCE, Vol. 123, No. 10, pp. 929-937.
- Bray, D. E. and McBride, D. (Eds.) (1992). *Nondestructive Testing Techniques*, John Wiley and Sons, Inc., New York.
- Cady, P. D. and Carrier, R. E. (1971). *Moisture Content of Bridge Decks*, Report, The Pennsylvania State University.
- Cady, P. D. and Renton, J. B. (1975). *Durability of Steel-Formed, Sealed Bridge Decks*, Final Report, The Pennsylvania State University, University Park, Pennsylvania.
- Callister, W. D., Jr. (1997). *Materials Science and Engineering*. John Wiley and Sons, Inc., New York.
- Chamberlin, W. P., Amsler, D. E., and Jaqueway, J. K. (1972). *A Condition Survey of Monolithic Bridge Decks in New York State, Special Report 11*, Engineering Research and Development Bureau.
- Chaigon, F. (2002). Colas, Inc., Personal Communication.
- Cordon, W.A. (1979) *Properties, Evaluation, and Control of Engineering Materials*, McGraw-Hill, New York, New York.
- Davis, A. G. (1999). "Review of Nondestructive Evaluation Techniques of Civil Infrastructure," Discussion, *Journal of Performance of Constructed Facilities*, ASCE, Vol. 11, No. 4, p. 47.
- Ensminger, D. (1998). *Ultrasonics: Fundamentals, Technology, Applications*. Marcel Decker, New York, New York.
- Enright, M. P., and Frangopol, D. M. (2000). "Survey and Evaluation of Damaged Concrete Bridges." *Journal of Bridge Engineering*, ASCE, 5(1), 31-38.
- FHWA Instructional Memorandum 40-3-72 (1972). Federal Highway Administration, United States Federal Highway Association, Washington, D.C.
- Francois, R., and Arligui, G. (1998). "Influence on Service Cracking on Reinforcement Steel Corrosion." *Journal of Materials in Civil Engineering*, ASCE, 10(1), 14-20.

- Hearn, G., and Shim, H. (1998). "Integration of Bridge Management Systems and Nondestructive Evaluations." *Journal of Infrastructure Systems*, ASCE, 4(2), 49-55.
- Hilton, M. H. (1975). *An Experience Survey on the Use of Permanent Steel Bridge Deck Forms*, Virginia Highway & Transportation Research Council, Charlottesville, Virginia.
- Hurd, M. K. (1995). *Formwork for Concrete*. American Concrete Institute, Farmington Hills, Michigan.
- Ibrahim, M., Al-Gahtani, A. S., Maslehuddin, M., and Dakhil, F. H. (1999). "Use of Surface Treatment Materials to Improve Concrete Durability." *Journal of Materials in Civil Engineering*, ASCE, 11(1), 36-40.
- Inci, G. (2001). "Nondestructive Evaluation of Compacted Soils," *Ph.D. Dissertation*, Department of Civil and Environmental Engineering, Wayne State University, Detroit, Michigan.
- Kamada, T., Nagataki, S., and Iwanami, M. (1997). "Evaluation of Material Deterioration in Concrete by Nondestructive Testing Methods," *International Conference on Engineering Materials*, Ottawa, Canada, 453-466.
- Kirkpatrick, T. J., Weyers, R. E., Sprinkel, M. M., and Anderson-Cook, C. M. (2001). "Impact of Specification Changes on Chloride Induced Corrosion Service Life of Bridge Decks," *Transportation Research Board 2002 Annual Meeting CD-ROM*.
- Kosmatka, S. H. and Panarese, W. C. (1988). *Design and Control of Concrete Mixtures*. Portland Cement Association, Skokie, Illinois.
- Koubaa, A., and Snyder, M. B. (2001). "Assessing Frost Resistance of Concrete Aggregates in Minnesota." *Journal of Cold Regions Engineering*, ASCE, 15(4), 187-210.
- Krautkramer, J. and Krautkramer, H. (1990). *Ultrasonic Testing of Materials*. Springer-Verlag, Berlin.
- Leung, C. K. Y. (2001). "Modeling of Concrete Cracking Induced by Steel Expansion," *Journal of Materials in Civil Engineering*, ASCE, 13(3), 169-175.
- Mamlouk, M. S. and Zaniewski, J. P. (1999). *Materials for Civil and Construction Engineers*. Addison Wesley Longman, Inc., Menlo Park, California.
- Mays, G. (1992). *Durability of Concrete Structures: Investigation, Repair, Protection*. Chapman Hall, London.
- Millstien, L. and Sabnis, G. M. (1983). "Determination of Concrete Strengths Using Ultrasonic Waves," *Recent Advances in Engineering Mechanics and Their Impact on Civil*

- Engineering Practice*, Chen, W. F. and Lewis, A. D. M., Eds., ASCE, Reston, Virginia, 561-564.
- Mohamed, O. A., Rens, K. L., and Stalnaker, J. J. (2000). "Factors Affecting Resistance of Concrete to Freezing and Thawing Damage," *Journal of Materials in Civil Engineering*, ASCE, 12(1), 26-32.
- Olson, L. D., (1992). "Sonic NDE of Structural Concrete." *Nondestructive Testing of Concrete Elements and Structures*, ASCE, Reston, Virginia, pp 70-81.
- Pilson, M.E.Q., (1998). "*An Introduction to the Chemistry of the Sea*".
- Pla-Rucki, G. F., and Eberhard, M. O. (1995). "Imaging of Reinforced Concrete: State-of-the-Art Review." *Journal of Infrastructure Systems*, ASCE, 1(2), 134-141.
- Popovics, S. and Popovics, J. S. (1992). "A Critique of Ultrasonic Pulse Velocity Method for Testing Concrete," *Nondestructive Testing of Concrete Elements and Structures*, Ansari, F. and Sture, S. Eds., ASCE, Reston, Virginia, pp 94-103.
- Ramey, G. E., and Wright, R. L. (1997). "Structural Design Actions to Mitigate Bridge Deck Cracking." *Practice Periodical on Structural Design and Construction*, ASCE, 2(3), 118-124.
- Ramey, G. E., Wolff, A. R., and Wright, R. L. (1997). "DOT Management Actions to Enhance Bridge Durability/Longevity." *Practice Periodical on Structural Design and Construction*, ASCE, 2(3), 125-130.
- Rangaraju, P. R. (2001). "Investigation into Premature Deterioration of Concrete on USTH 169 Near Hibbing, Minnesota," *Transportation Research Board 2001 Annual Meeting CD-ROM*.
- Ravindrarajah, R. S. (1992) "Evaluation of Compressive Strength for High-Strength Concrete by Pulse Velocity Method," *Nondestructive Testing of Concrete Elements and Structures*, Ansari, F. and Sture, S. Eds., ASCE, Reston Virginia, pp. 115-126.
- Rens, K. L., and Greimann, L. F. (1997). "Ultrasonic Approach for Nondestructive Testing of Civil Infrastructure." *Journal of Performance of Constructed Facilities*, ASCE, 11(3), 97-104.
- Rens, K. L., and Transue, D. J. (1998). "Recent Trends in Nondestructive Inspections in State Highway Agencies." *Journal of Performance of Constructed Facilities*, ASCE, 12(2), 94-96.
- Rens, K. L., Wipf, T. J., and Klaiber, F. W. (1997). "Review of Nondestructive Evaluation Techniques of Civil Infrastructure." *Journal of Performance of Constructed Facilities*, ASCE, 11(4), 152-160.

- Sarja, A. and Vesikari, E., Eds. (1996). *Durability Design of Concrete Structures*. Chapman and Hall, London.
- Sorum, C. H. and Lagowski, J. J. (1983). *Introduction to Semimicro Qualitative Analysis*. Prentice Hall, Inc. Englewood Cliffs, New Jersey.
- Stewart, M. G. and Rosowsky, D. V. (1998). "Structural Safety and Serviceability of Concrete Bridges Subject to Corrosion," *Journal of Infrastructure Systems*, ASCE, Vol. 4, No. 4, 146-155.
- Taly, N. (1998). *Design of Modern Highway Bridges*. McGraw Hill, New York.
- Tsiatas, G. and Robinson, J. (2002). "Durability Evaluation of Concrete Crack Repair Systems," *Transportation Research Board 2002 Annual Meeting CD-ROM*.
- Waddell, J. J. and Dobrowolski, J. A. (1993). *Concrete Construction Handbook*, McGraw Hill, New York.
- Wei-Du, L. (1992). "Frequency Spectrum Analysis of Ultrasonic Testing Signal in Concrete," *Nondestructive Testing of Concrete Elements and Structures*, Ansari, F. and Sture, S. Eds., ASCE, Reston, Virginia, pp. 104-114.
- Yaman, I. O., Aktan, H. M., Staton, J. F. (2001). "Relationship between Concrete Permeability and Ultrasonic Pulse Velocity," *Transportation Research Board 2001 Annual Meeting CD-ROM*.
- Yesiller, N. and A. Cekic, (2001), "Determination of Thickness of Smooth Geomembranes," *Geotechnical Testing Journal*, GTJODJ, ASTM, Vol. 24, No. 4, pp. 359-369.
- Yesiller, N., Hanson, J. L., Renner, A. T., and Usman, M. A. (2001). "Ultrasonic Testing for Evaluation of Stabilized Mixtures," *Transportation Research Record*, No. 1757, pp. 32-39.
- Yesiller, N. and S. Sungur, (2001), "Evaluation of Geomembranes Using an Ultrasonic Method," *Geotechnical Testing Journal*, GTJODJ, ASTM, Vol. 24, No. 3, pp. 273-287.
- Young, J. F., Mindess, S., Gray, R. J., and Bentur, A. (1998). *The Science and Technology of Civil Engineering Materials*. Prentice Hall, Upper River Saddle, New Jersey.

APPENDIX A: SURVEY REPORT

Survey on the Performance and Inspection Techniques for Bridge Decks Constructed with Stay-in-place-Metal-Forms

Report submitted to
Mr. Roger Till, PE
Engineer of Testing and Research
Michigan Department of Transportation
Construction and Technology Division
Secondary Government Complex
8885 Ricks Rd.
P.O. Box 30049
Lansing, Michigan 48909

Report submitted
by

Nabil F. Grace, Ph.D., PE
Professor and Chairman

James Hanson, Ph.D., PE
Associate Professor

Civil Engineering Department
Lawrence Technological University
21000 W. Ten Mile Rd.
Southfield, MI 48075-1058

Tel: 248-204-2556
Fax: 248-204-2568
E-mail: NABIL@LTU.EDU

June 26, 2002

Table of Contents

List of Figures	303
Introduction.....	305
Survey	305
Discussion of DOT Responses.....	305
Conclusions.....	308
Appendix A.....	336
Survey Cover Letter.....	336
Copy of the survey	337

List of Figures

Figure 1	Does Your state use SIPMFs for constructing deck slab bridges?	309
Figure 2	What is your state's policy concerning the use of permanent SIPMF?	310
Figure 3	In the case that your state does not use SIPMF, please specify the reasons.....	311
Figure 4	Approximately how many bridges having decks with SIPMF does your state Have?	312
Figure 5	Approximately how long have decks with SIPMF been used by your state in bridges?.....	313
Figure 6	Is your department satisfied by the performance of SIPMF?	314
Figure 7	Does your state fill corrugations of SIPMF with Styrofoam to reduce dead load?.....	315
Figure 8	Does your state use epoxy-coated steel in bridges with SIPMF?	316
Figure 9	Beside visual inspection and hammer sounding of the surface, what other techniques does your department use to inspect SIPMF bridge decks?	317
Figure 10	Does your state gather specific data related to SIPMF bridge decks?	318
Figure 11	What is the typical period between each inspection of decks with SIPMF?	319
Figure 12	How can you describe the status of SIPMF bridge decks in your state?.....	320
Figure 13	Do you believe that SIPMF increase the long term durability of bridge decks?	321
Figure 14	Has your state observed a difference in performance of decks with SIPMF constructed with bare steel reinforcement versus epoxy-coated reinforcement?.....	322
Figure 15	As a result of using SIPMF, what types of deterioration of bridge decks have been observed?	323
Figure 16	What is the cause of the bridge deck deteriorations when constructed using SIPMF?	324
Figure 17	What is the most type of deck cracking observed in SIPMF bridge decks?	325
Figure 18	Has any corrosion in the SIPMF been observed?	326
Figure 19	Where on the bridge was the most extensive corrosion of SIPMF concentrated?.....	327

Figure 20	Is there any corrosion observed in the deck reinforcement?	328
Figure 21	Where on the bridge was the most extensive corrosion of deck reinforcement concentrated?	329
Figure 22	After how long did the extensive corrosion occur?	330
Figure 23	Has any effect of joint leakage on the SIPMF been observed?	331
Figure 24	Were there any problems observed a direct result of using SIPMF?	332
Figure 25	Are you aware of any research reports in your state related to using SIPMF for bridge deck construction?	333
Figure 26	Is there any information that you would like to share with the research team related to your experience with observations of SIPMF?	334

Survey on the Performance and Inspection Techniques for Bridge Decks Constructed with Stay-in-Place Metal Forms

Introduction:

In December 2001, the Michigan Department of Transportation (MDOT) awarded the Structural Testing Center at Lawrence Technological University of Southfield, Michigan, a research contract to investigate the use of stay-in-place metal forms (SIPMFs) in bridge deck slabs. This research included the investigation of inspection procedures and deterioration modes of this type of bridge deck. One of the major tasks of this investigation was to conduct a nationwide survey on the performance and inspection techniques for bridge decks constructed with SIPMF. A comprehensive survey was developed, approved by MDOT Engineers, and delivered via e-mail to all fifty-two DOTs. A total of 38 DOTs responded to the survey. These DOTs are: Alabama, Alaska, Arizona, Arkansas, California, Connecticut, Delaware, Florida, Georgia, Hawaii, Idaho, Illinois, Iowa, Kansas, Kentucky, Maine, Massachusetts, Michigan, Minnesota, Mississippi, Missouri, Montana, Nebraska, Nevada, New Hampshire, New Jersey, New Mexico, New York, North Carolina, Ohio, Oklahoma, Oregon, Tennessee, Texas, Washington, West Virginia, Wyoming, and Virginia. This report summarizes the findings of this survey. The responses from the 38 DOTs are summarized and presented in this report along with the survey.

Survey:

The survey consisted of a variety of questions that were tailored to address the following issues:

1. The policy of various states on the use of SIPMF.
2. Reasons for not allowing the use of SIPMF.
3. Number and status of bridge decks constructed with SIPMF.
4. The age of available SIPMF bridge decks.
5. Satisfaction of the performance of SIPMF.
6. Use of filling material (Styrofoam) in SIPMF corrugations.
7. Use of epoxy-coated reinforcement with SIPMF.
8. Methods and interval periods of inspection.
9. Types and causes of deterioration of deck slabs and corrosion of SIPMF.
10. Effect of joint leakage on SIPMF.

A copy of the survey is included in Appendix A.

Discussion of DOT Responses:

The responses from the 38 DOTs were analyzed and presented in Figures 1-25. The number assigned to each figure matches the number assigned to the questions listed in the survey. Also, the title given to each figure is taken from the questions that were listed in the survey. It should be pointed out that the discussion and conclusions drawn from this survey pertain only to the DOTs that responded.

Examination of Figures 1-3 indicates that 26 states allow and 12 states do not allow the use of SIPMF. This policy may be attributed to the weather and the environmental conditions of the location of each state. Furthermore, Figure 3 suggests that the main reason that some states don't allow the use of SIPMF is that the presence of SIPMF may interfere with the inspection of bridge decks. Another reason cited by DOTs for not allowing the use of SIPMF is its susceptibility to potential corrosion problems due to the trapped water and salt between the forms and concrete. Also, it was indicated that Florida DOT doesn't allow the use of the SIPMF on bridges crossing over water.

As presented in Figure 4, only five states have more than 1000 bridges constructed with SIPMF, 3 states have between 500 and 1000 bridges, 8 states have between 100 and 500 bridges, and 15 states have less than 100 bridges. This suggests that SIPMF bridge decks are not commonly used in a majority of the bridges in each state. Only 11 states, including Alaska, Arizona, Alabama, California, Connecticut, Georgia, Idaho, Michigan, New York, Tennessee, and Virginia, have been using this type of bridge deck for more than 30 years, as presented in Figure 5. However, it should be pointed out that some of these states, such as Alaska, Arizona, California, Connecticut, and Idaho, each have less than 100 bridges of this type (Figure 4).

The level of satisfaction with the performance of this type of bridge deck is presented in Figure 6. The majority of the DOTs are satisfied with various levels. Four states are very satisfied, 10 states are satisfied and 15 states are neutral with regard to satisfaction. OHDOT is only DOT that is very dissatisfied and CTDOT is not satisfied with the SIPMF performance. Apparently, most of the very satisfied and satisfied DOTs are in the southern states. This suggests that level of satisfaction is dependent on the climatic and environmental conditions of each state.

Out of the 29 DOTs that use SIPMF, 20 DOTs do not fill the corrugations of the forms with Styrofoam to reduce the dead load, as presented in Figure 7. Only 6 DOTs indicated that they do fill the corrugations with Styrofoam and the remaining 3 DOTs sometimes fill the corrugations. This suggests that filling the corrugations of the forms is not a common practice in most of the states that use SIPMF.

An assessment of the use of epoxy-coated steel bars with SIPMF in this type of bridge deck is presented in Figure 8. From the 28 DOTs that responded to this question, 25 DOTs use epoxy-coated steel bars and only 3 DOTs do not use epoxy-coated steel bars. Only 4 DOTs reported a difference in performance between decks with SIPMF constructed with black steel bars and those constructed with epoxy-coated steel reinforcement (Figure 14).

The various reported methods of inspection for SIPMF deck slabs are presented in Figure 9. Only 5 DOTs use inspection methods other than the traditional visual inspection and hammer sounding of the surface. These methods include chain-drag, form-cut-out, full-depth coring, and mapping cracks. It is evident that there is no nondestructive inspection approach used for inspection for this type of bridge deck. Perhaps that explains the reason for the lack of gathering adequate and specific data related to the SIPMF bridge deck

slabs (Figure 10). This lack of gathering adequate information may be attributed to the lack of the widespread use of the SIPMF for bridge construction in all states. The period between each inspection of decks is generally from 1 to 3 years, as shown in Figure 11.

Figure 12 presents the status of existing SIPMF decks in different areas of the country. Four DOTs reported that their bridges are in excellent conditions and 15 DOTs indicated that their bridges are in good condition. Examining this Figure suggests that most of these 19 DOTs are in the southern states. However, 7 DOTs, most of them are in northern states, reported that their bridges are in fair condition. Climatic and environmental conditions are likely the major contributing factors for the deterioration. It should be pointed out that the majority of the DOTs do not believe that the use of SIPMF increases the long-term durability of bridge decks. Only NMDOT and NJDOT believe that the SIPMF increases the durability of bridge decks, as shown in Figure 13.

The types of and extent of both deterioration and corrosion of this type of bridge deck are shown in Figures 15 and 18, respectively. Fifteen DOTs reported no deterioration in their bridges, whereas 4 DOTs reported corrosion in the forms (Figures 15). IDOT indicated that they have light rusting between the overlap of the SIPMF, and rusting of SIPMF due to the trapping of moisture between the forms and the deck. TXDOT stated that they have some of the SIPMF corroded but with no deterioration in the deck that can be related to the use of SIPMF. Also, NYDOT reported rusting in the forms. ORDOT reported that they have pop-outs in the forms. Michigan is the only state that reported that their bridges have concrete cracking directly related to the orientation of the angle used for attaching the forms to the beams.

The majority of the DOTs acknowledged that the causes of this deterioration are unknown (Figure 16). However, IDOT and ORDOT reported that the surface loads are the cause of deterioration. Furthermore, Idaho and New York DOTs reported that environmental conditions are the causes of deterioration. Transverse cracking is the most common type of cracking in this type of bridge deck (Figure 17). In general, 12 DOTs observed corrosion and 14 DOTs observed no corrosion in the SIPMF (Figure 18). Examination of Figure 19 suggests that the locations of most extensive corrosion in the SIPMF are at areas of water leakage and the joints. These corroded areas are at the ends of the spans, along the fascia girders, drop inlet on bridge decks, joints with sealing materials, and joints without sealing materials.

Figures 20-22 address the extent and location of corrosion of the deck reinforcements. Eighteen DOTs observed no corrosion and 6 states observed corrosion in the deck reinforcements, as shown in Figure 20. Figure 21 suggests that the top reinforcements and the span-ends experienced the most extensive concentration of corrosion. This reported extensive corrosion occurred after more than ten years of service (Figure 22).

Figure 23 indicates that 6 DOTs in the northern states reported an effect of joint leakage on the SIPMF whereas 17 DOTs in the southern states reported no observation of such leakage effect on the forms. In conclusion, as presented in figure 24, only three DOTs observed problems as a direct result of using SIPMF in bridge decks.

None of the DOTs, with the exception of MIDOT and IADOT, were aware of any research reports in their states related to using SIPMF for bridge deck construction (Figure 25).

Conclusions:

Based on the responses provided by 38 DOTs, the following conclusions can be drawn:

1. A total of 26 DOTs allow the use and 12 DOTs do not allow the use of SIPMF. This policy may be attributed to climatic and environmental conditions in each state. Most of 26 DOTs are satisfied with the performance of this bridge deck system. The majority of DOTs that do not use SIPMF are concerned with the lack of visual examination and accessibility to the bottom of the deck slab.
2. Only five states located on the eastern region of the country have more than 1000 bridges each, whereas 15 states have less than 100 bridges each. Of the remaining states allowing the use of SIPMF, each has between 100 and 1000 SIPMF bridge decks. Eleven DOTs have been using SIPMF for more than 30 years and some of them have reported less than 100 bridges of this type.
3. Filling the corrugations of SIPMF with Styrofoam to reduce the dead weight of bridge decks is not a common practice among the majority of the DOTs that allow their use in bridge decks.
4. The use of epoxy-coated steel bars in bridges with SIPMF is a common practice in most states. The majority of the DOTs did not observe a difference in performance between decks with SIPMF constructed with bare steel reinforcement and those constructed with epoxy-coated steel reinforcement.
5. The majority of the DOTs use conventional inspection approaches such as visual inspection, and hammer sounding for periodic examination of their SIPMF bridge decks. The typical period between each inspection is from 1-3 years. However, none of these DOTs gather specific data related to this type of bridge deck.
6. Most of the DOTs do not believe that the SIPMF increases the long-term durability of bridge decks. The majority of the DOTs reported that the use of SIPMF is not linked to any deck deterioration and the causes of this deterioration are unknown. However, 12 DOTs observed corrosion and 14 DOTs observed no corrosion in the SIPMF. Most of the reported zones of corrosion are located at places of water leakage and joints.
7. Only six DOTs observed corrosion and 18 DOTs observed no corrosion in the deck reinforcement. The reported corrosion is in the top reinforcement and at the span ends.
8. Three DOTs observed problems as a direct result of using SIPMF.
9. There is no significant research work/report available on this type of bridge decks.

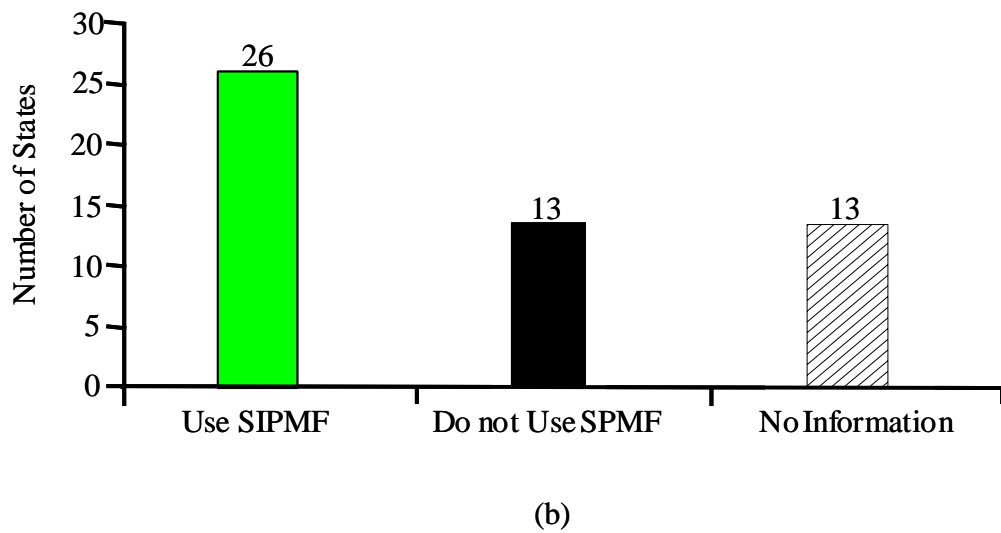
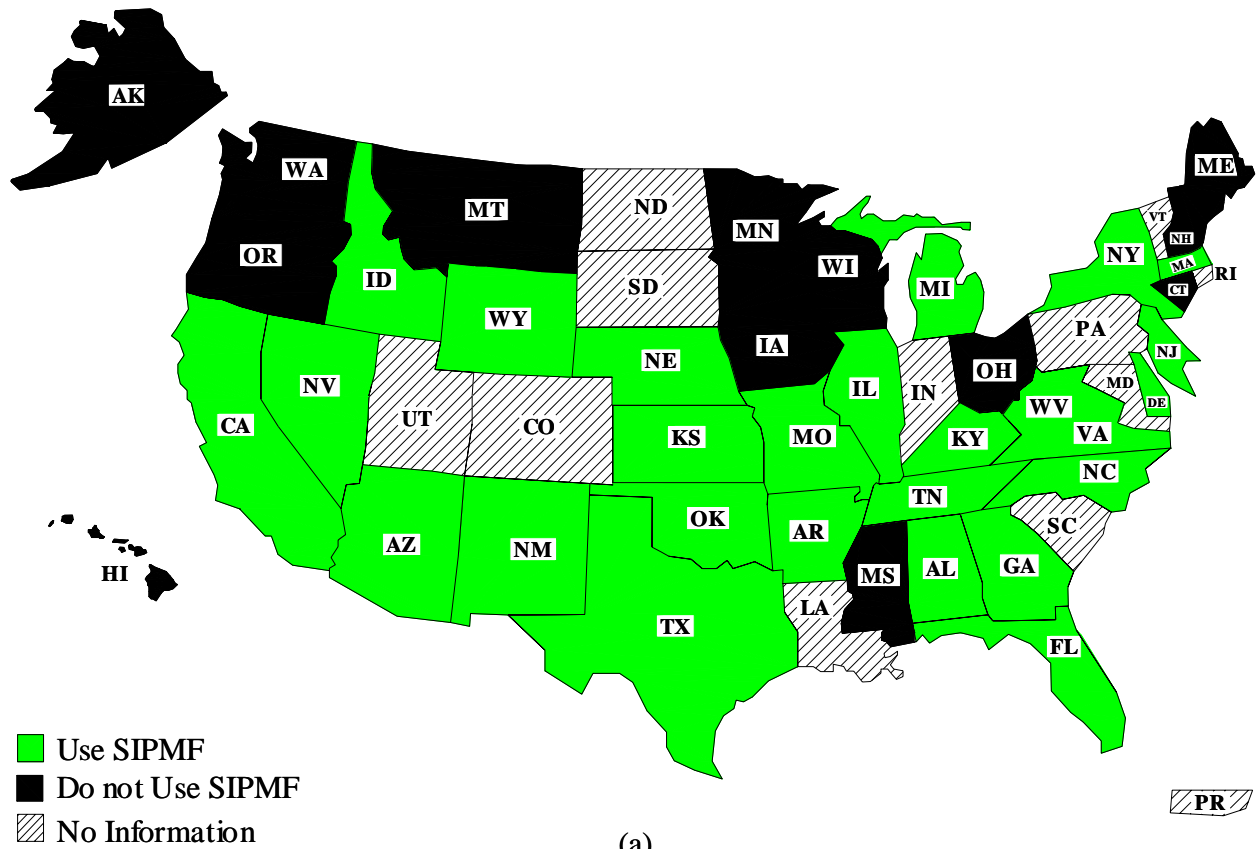
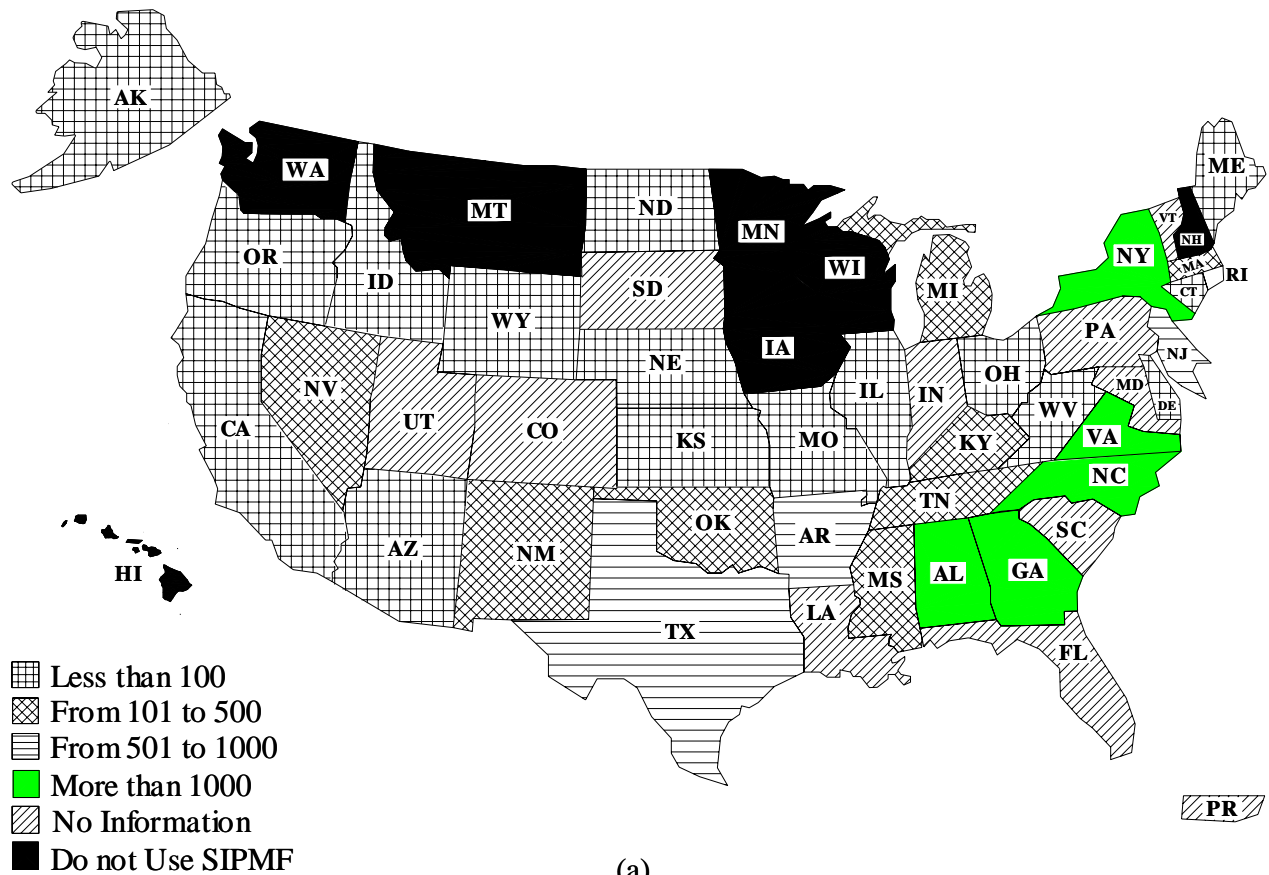
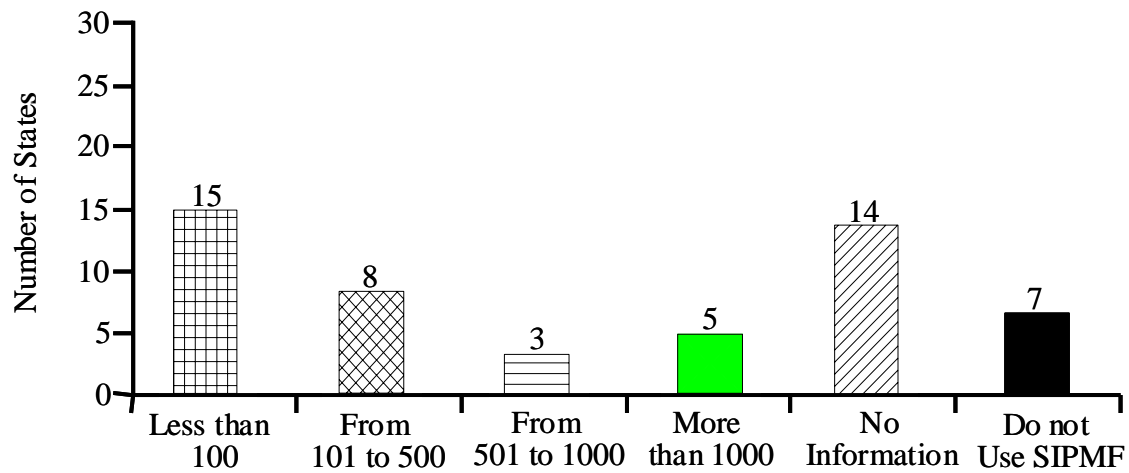


Figure 1. Does your state use SIPMFs for constructing deck slab bridges?



(a)



(b)

Figure 4. Approximately how many bridges having decks with SIPMF does your state have?

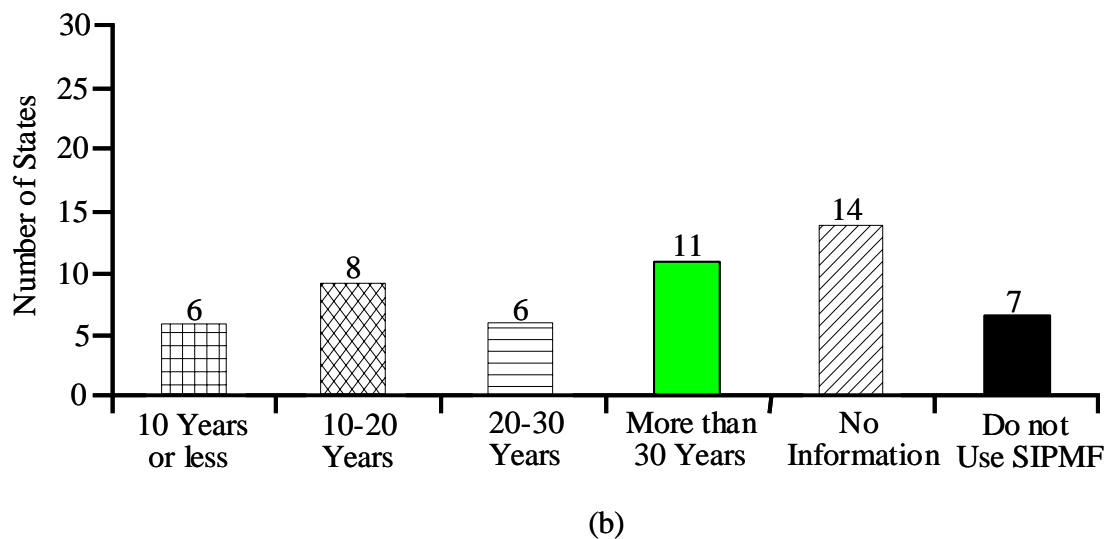
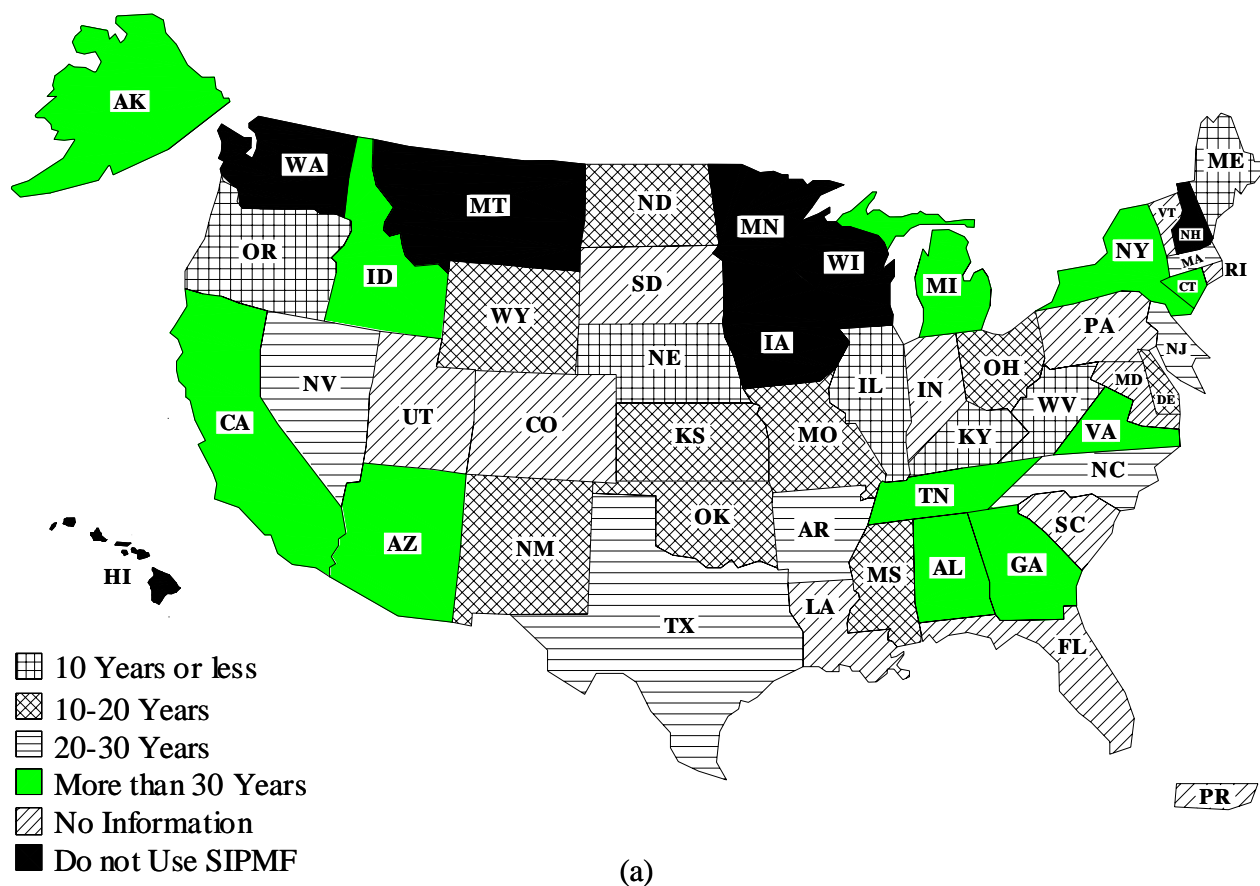


Figure 5. Approximately how long have decks with SIPMF been used by your state in bridges?

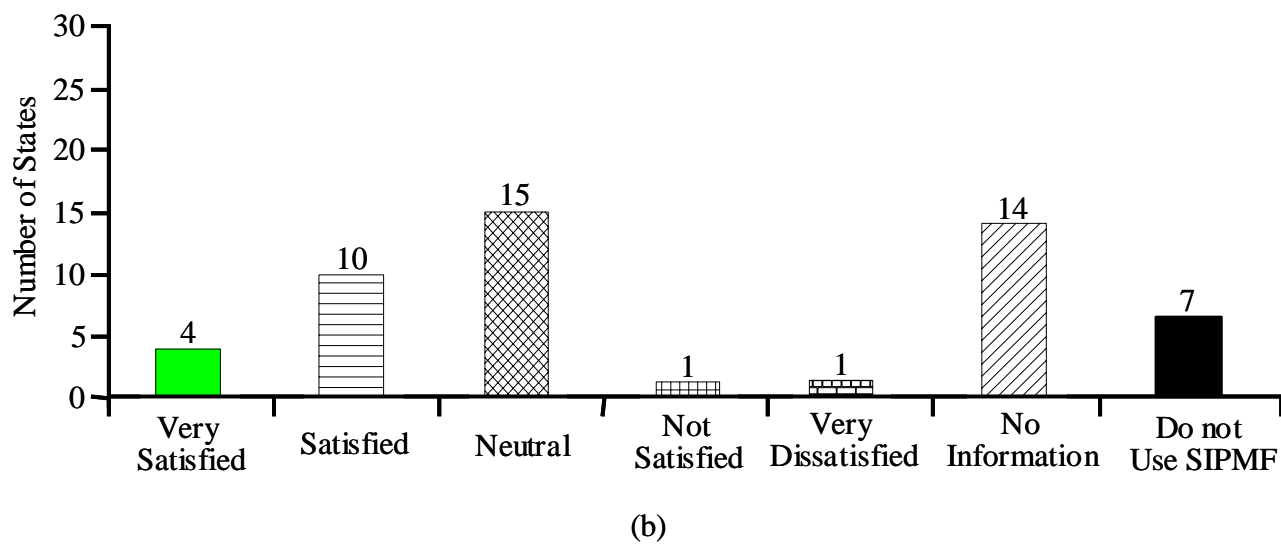
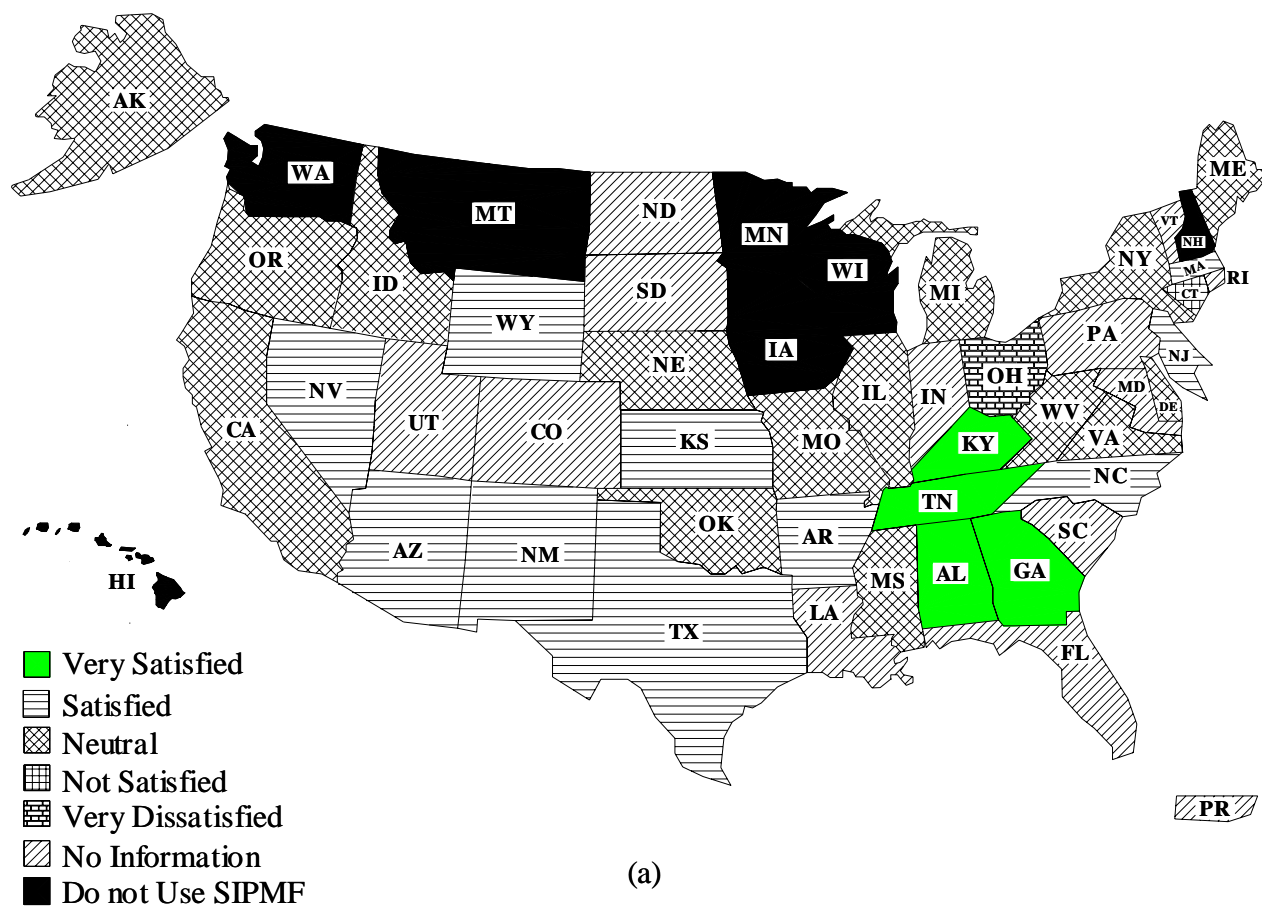


Figure 6. Is your department satisfied by the performance of SIPMF?

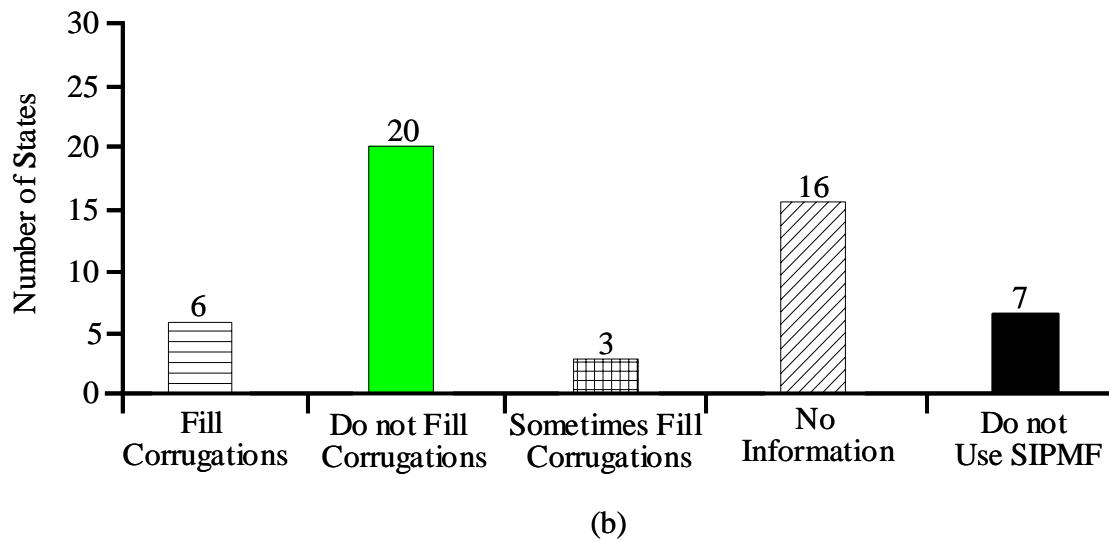
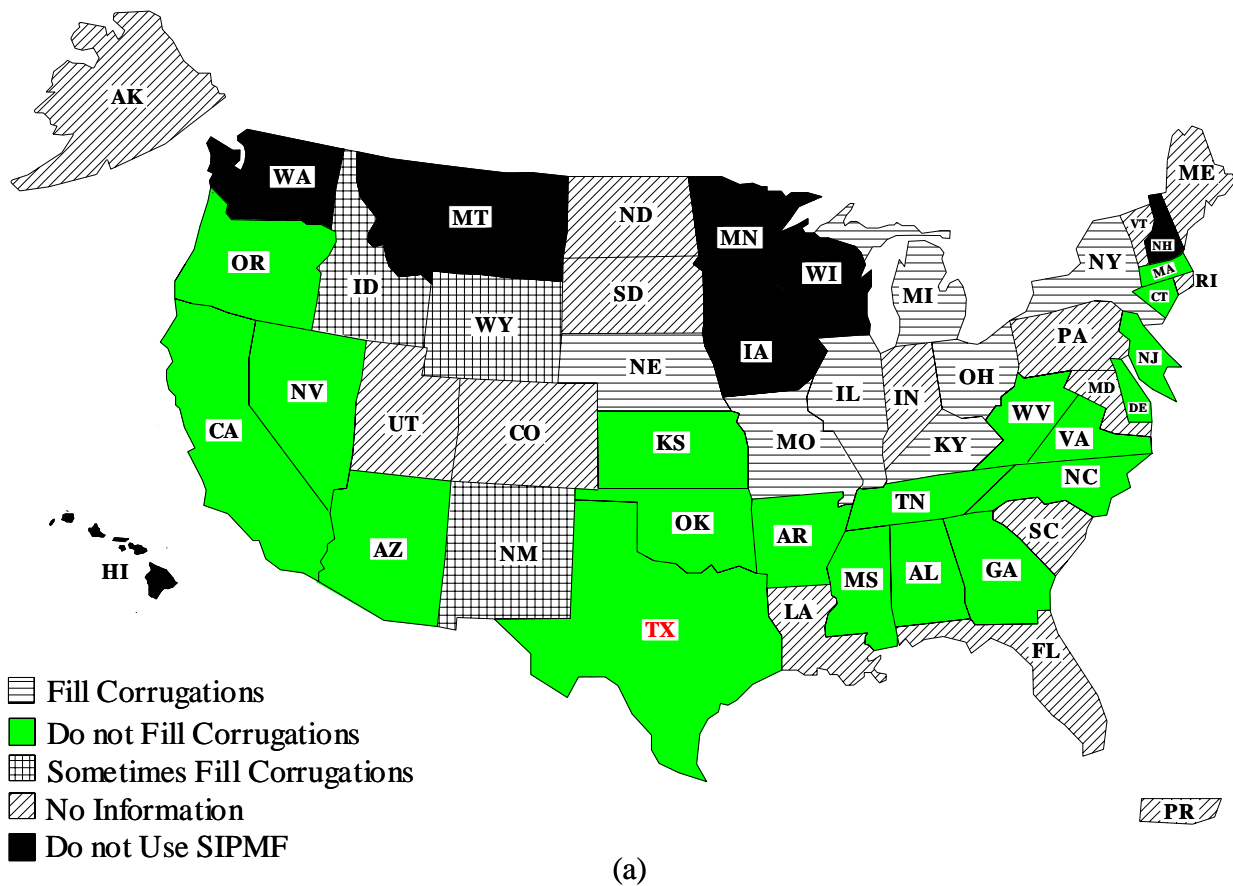


Figure 7. Does your state fill corrugations of SIPMF with Styrofoam to reduce dead load?

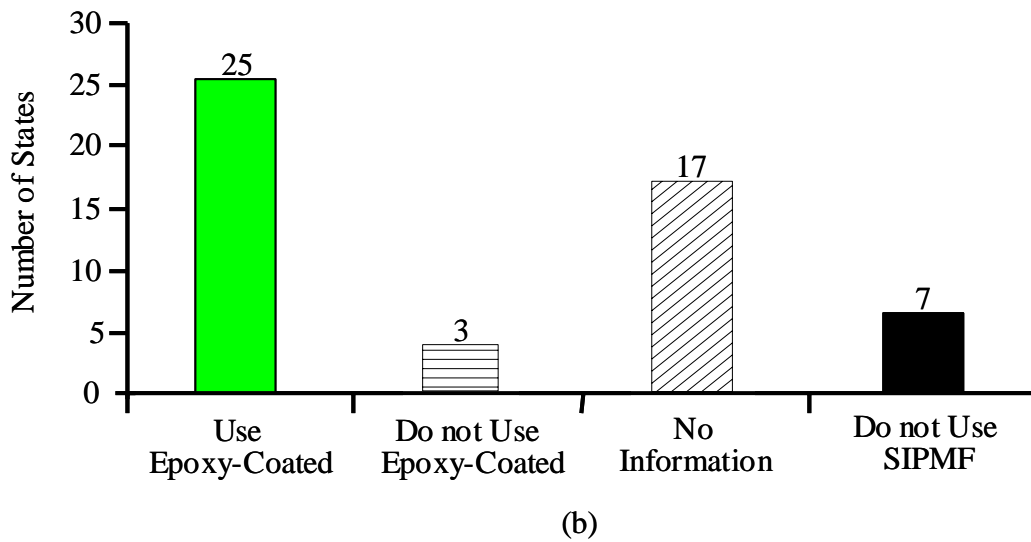
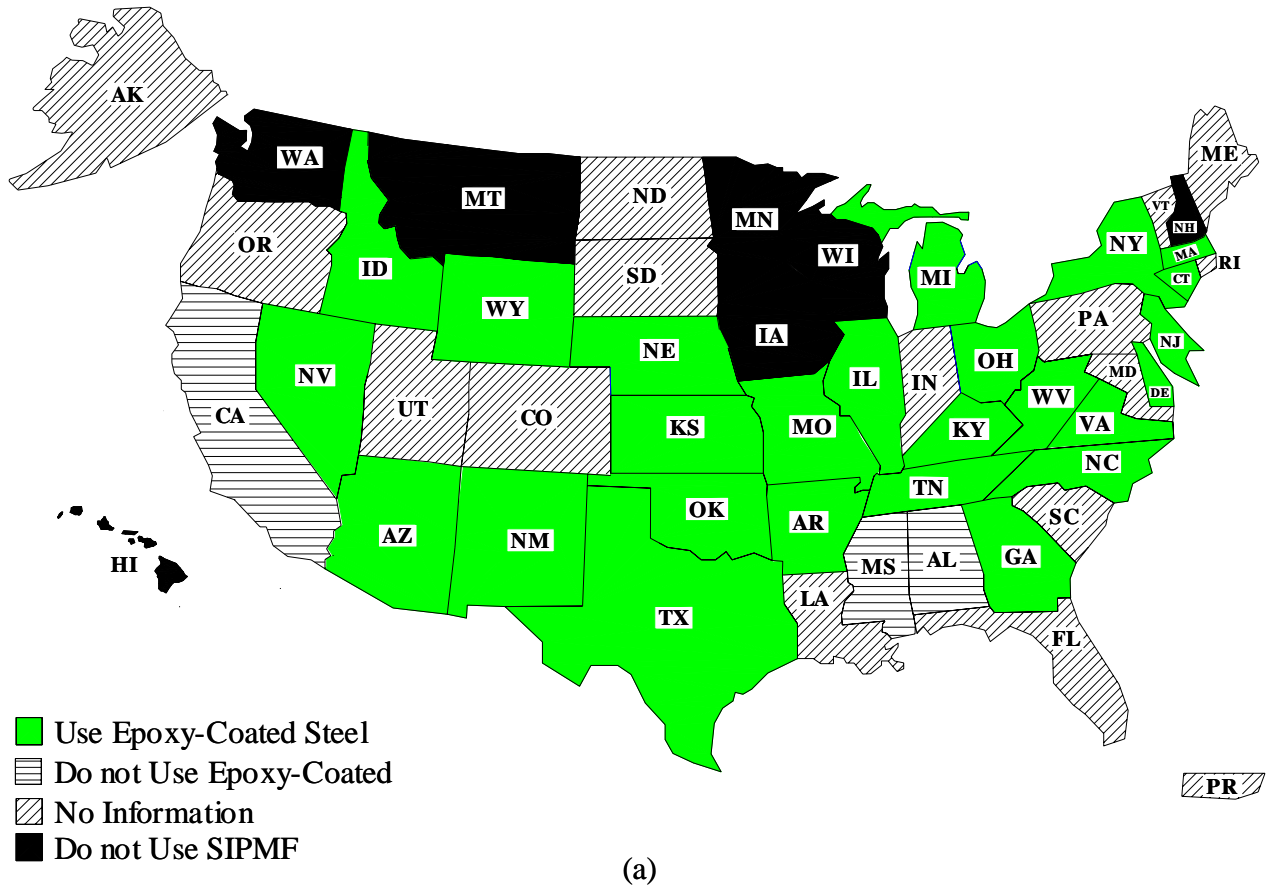


Figure 8. Does your state use epoxy-coated steel in bridges with SIPMF?

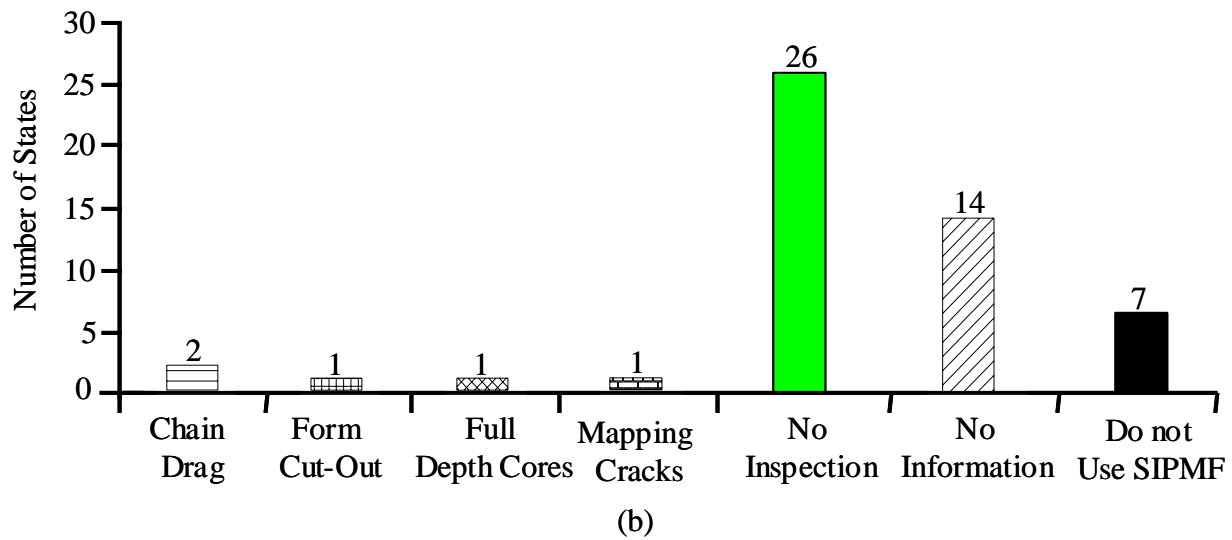
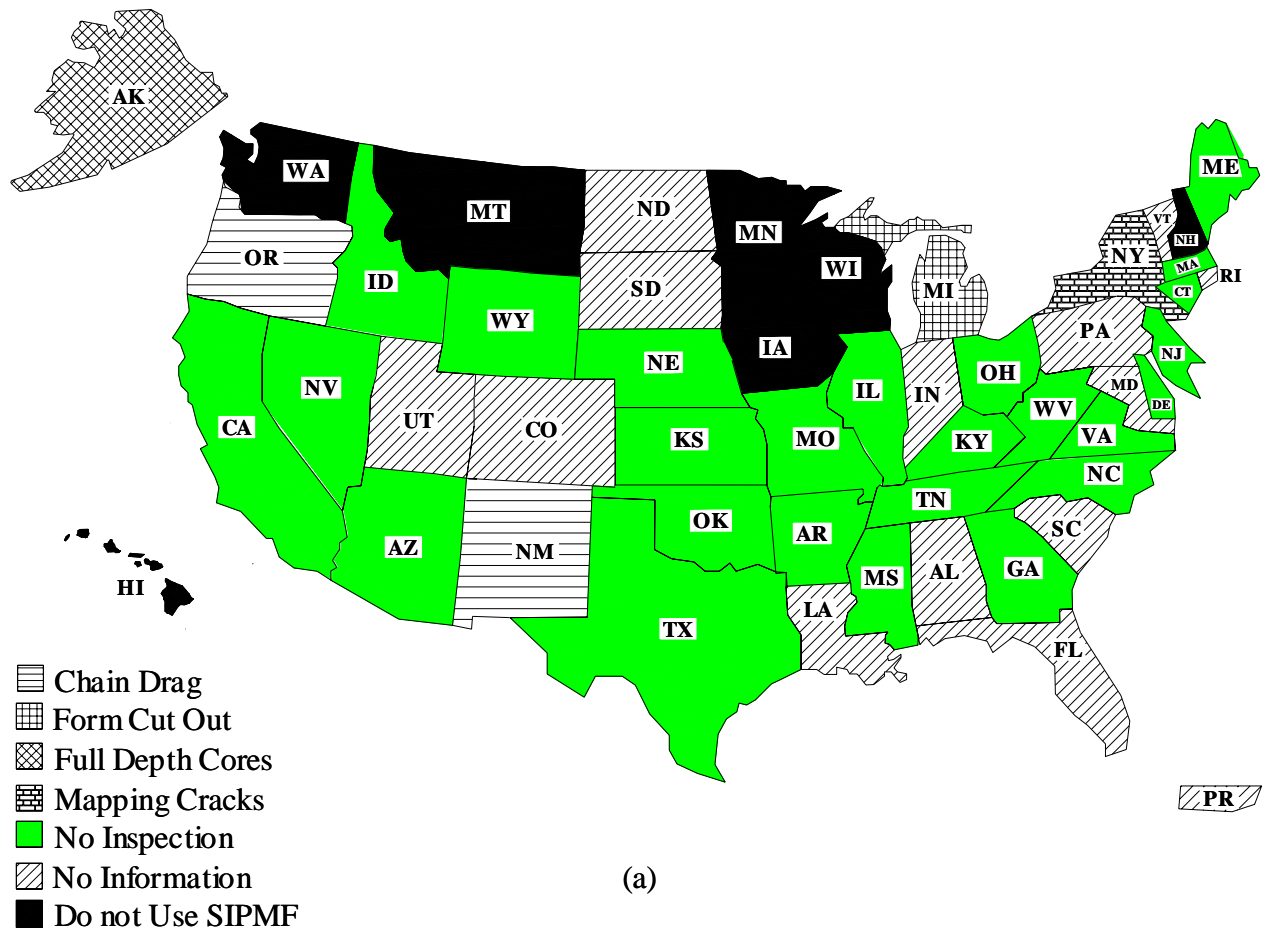


Figure 9. Beside visual inspection and hammer sounding of the surface, what other techniques does your department use to inspect SIPMF bridge decks?

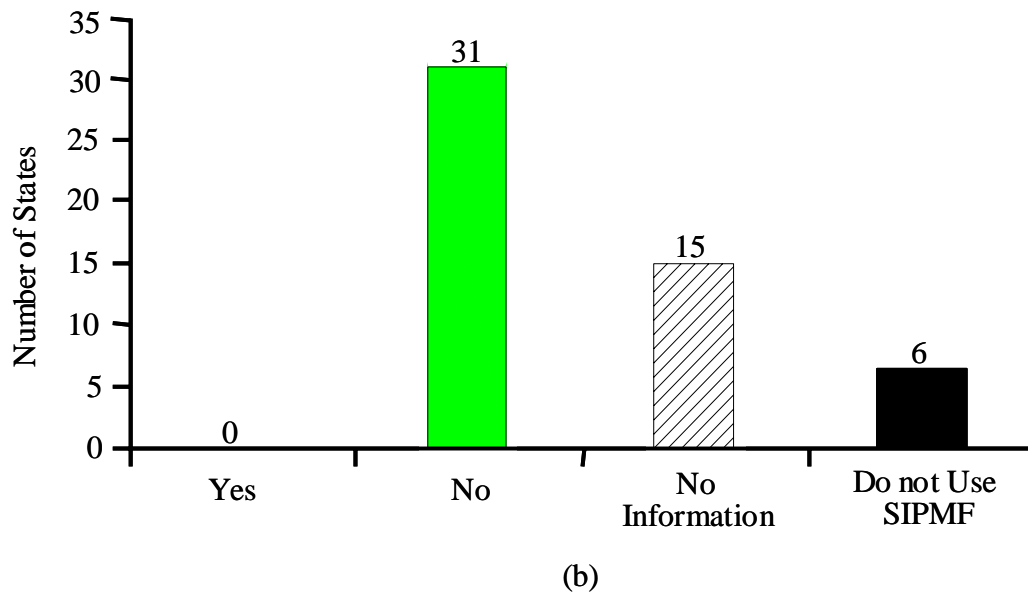
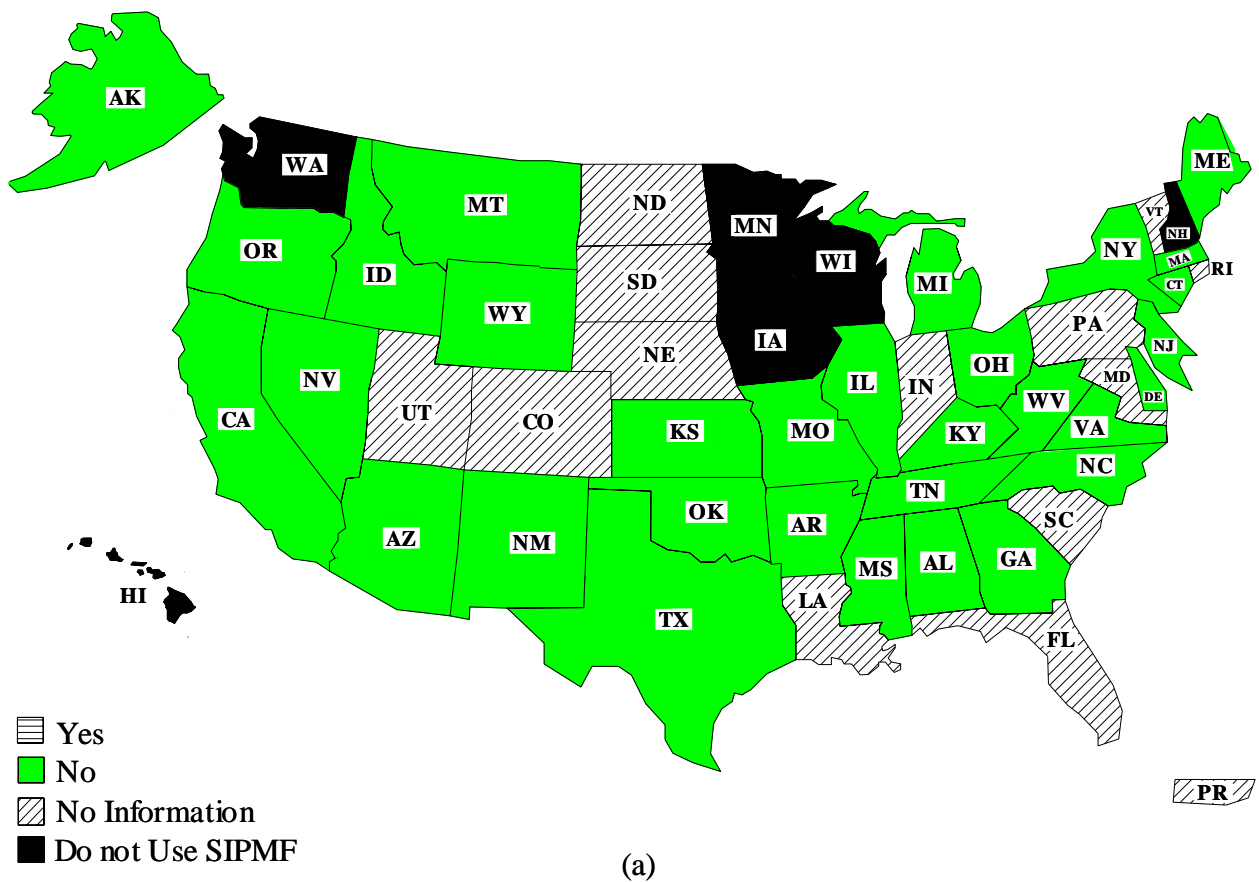


Figure 10. Does your state gather specific data related to SIPMF bridge decks?

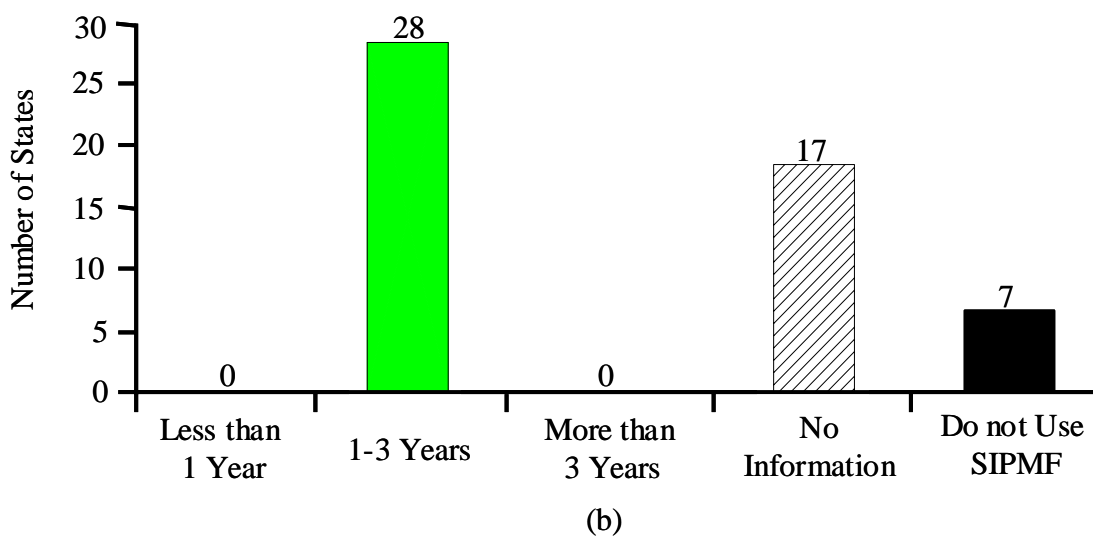
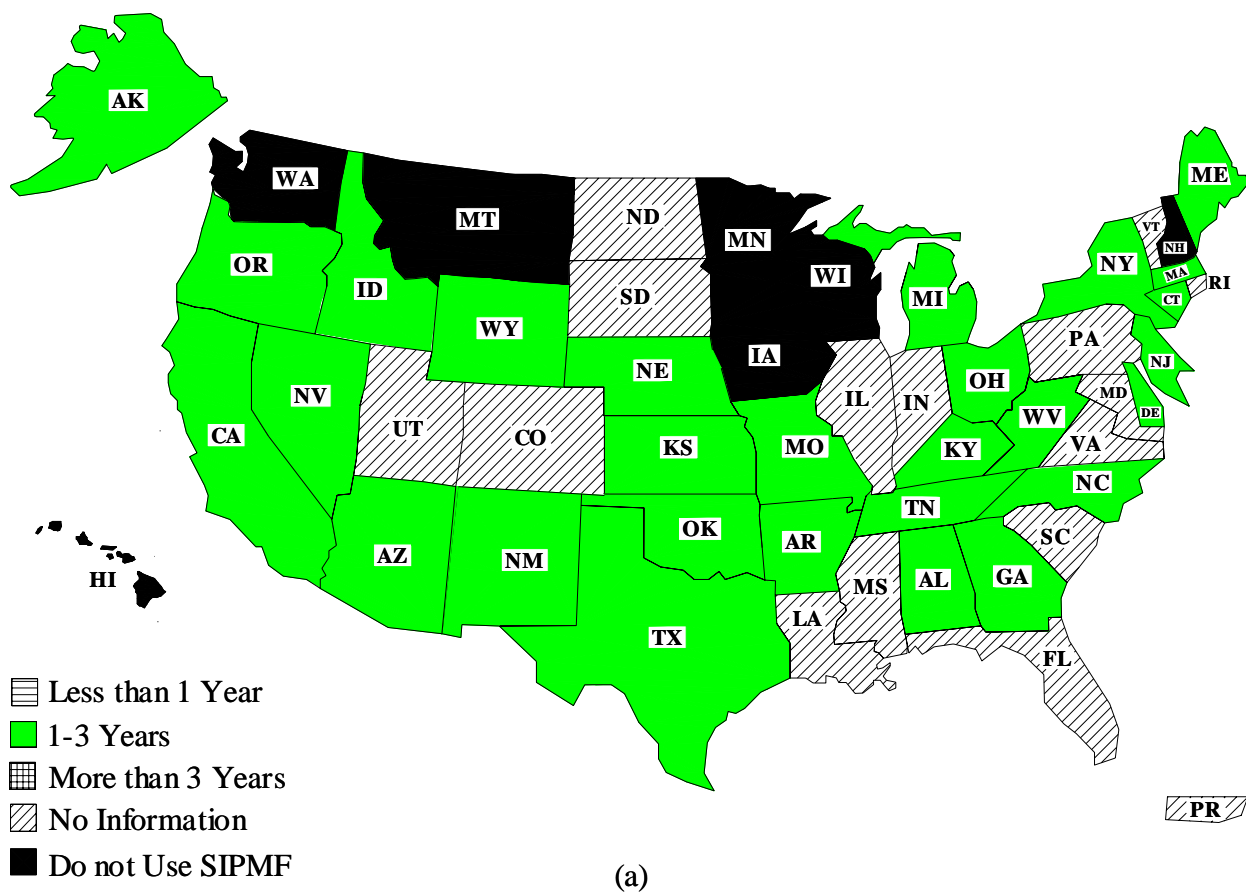


Figure 11. What is the typical period between each inspection of decks with SIPMF?

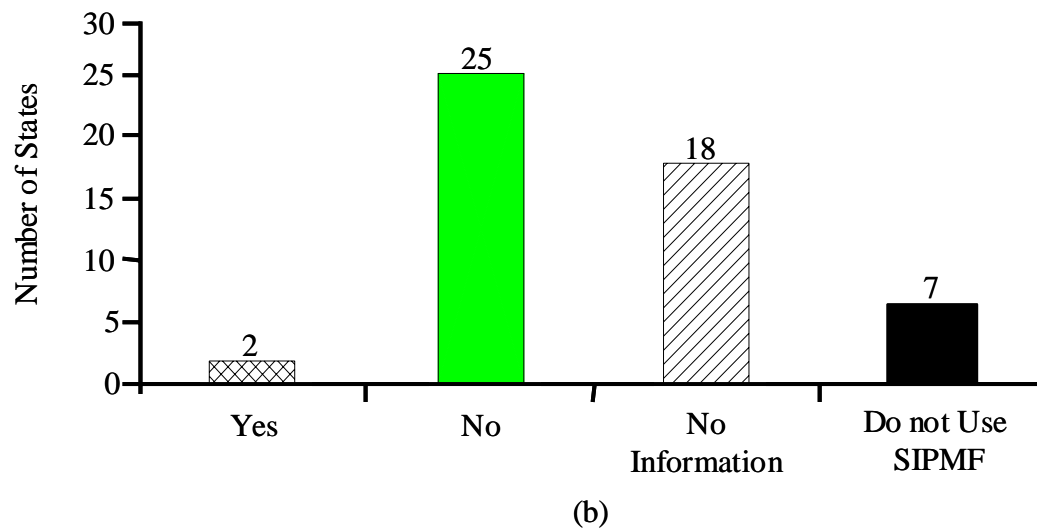
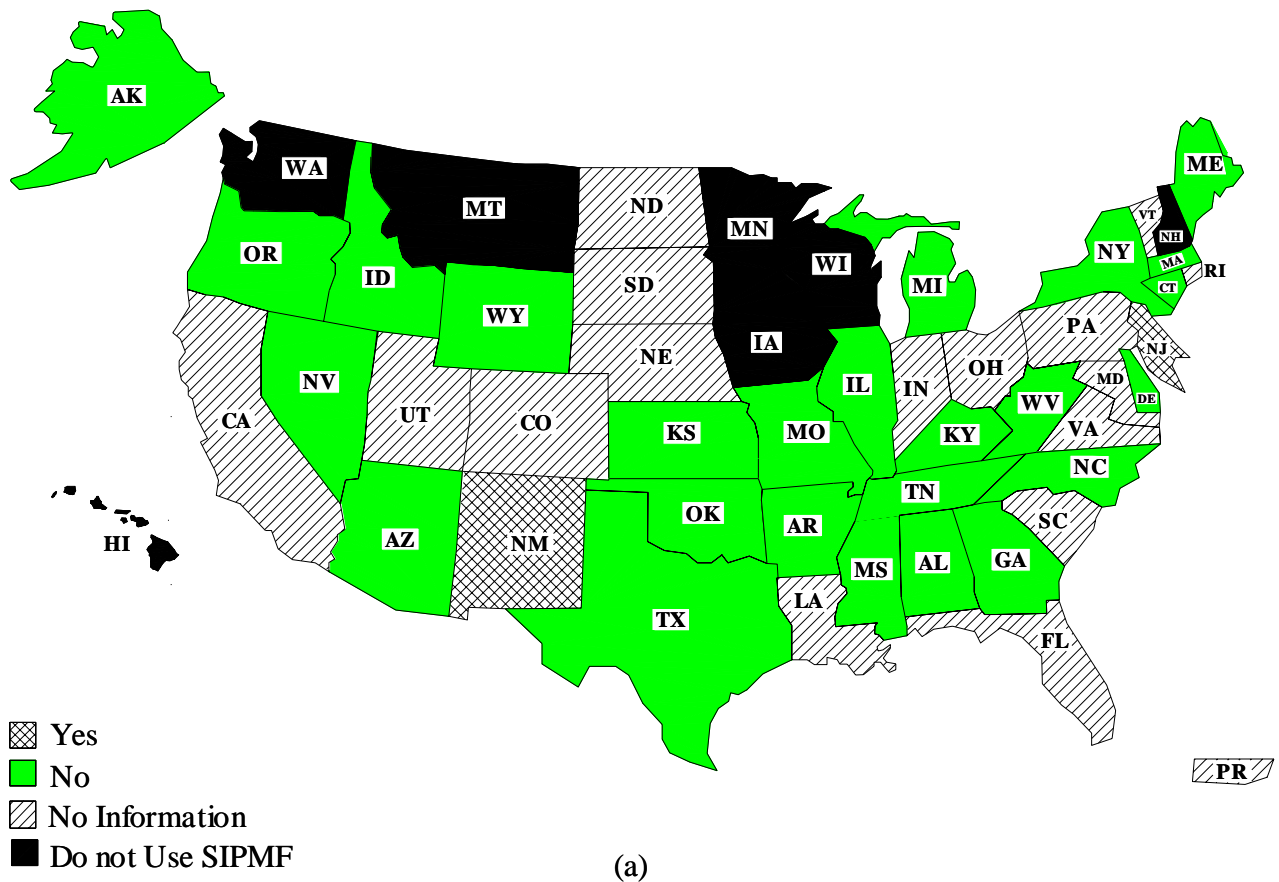


Figure 13. Do you believe that SIPMF increase the long term durability of bridge decks?

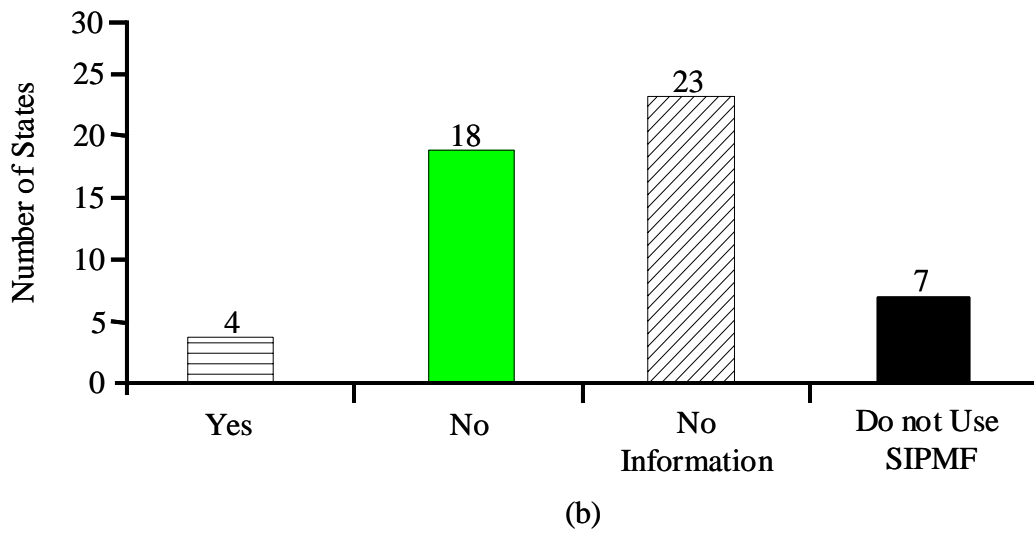
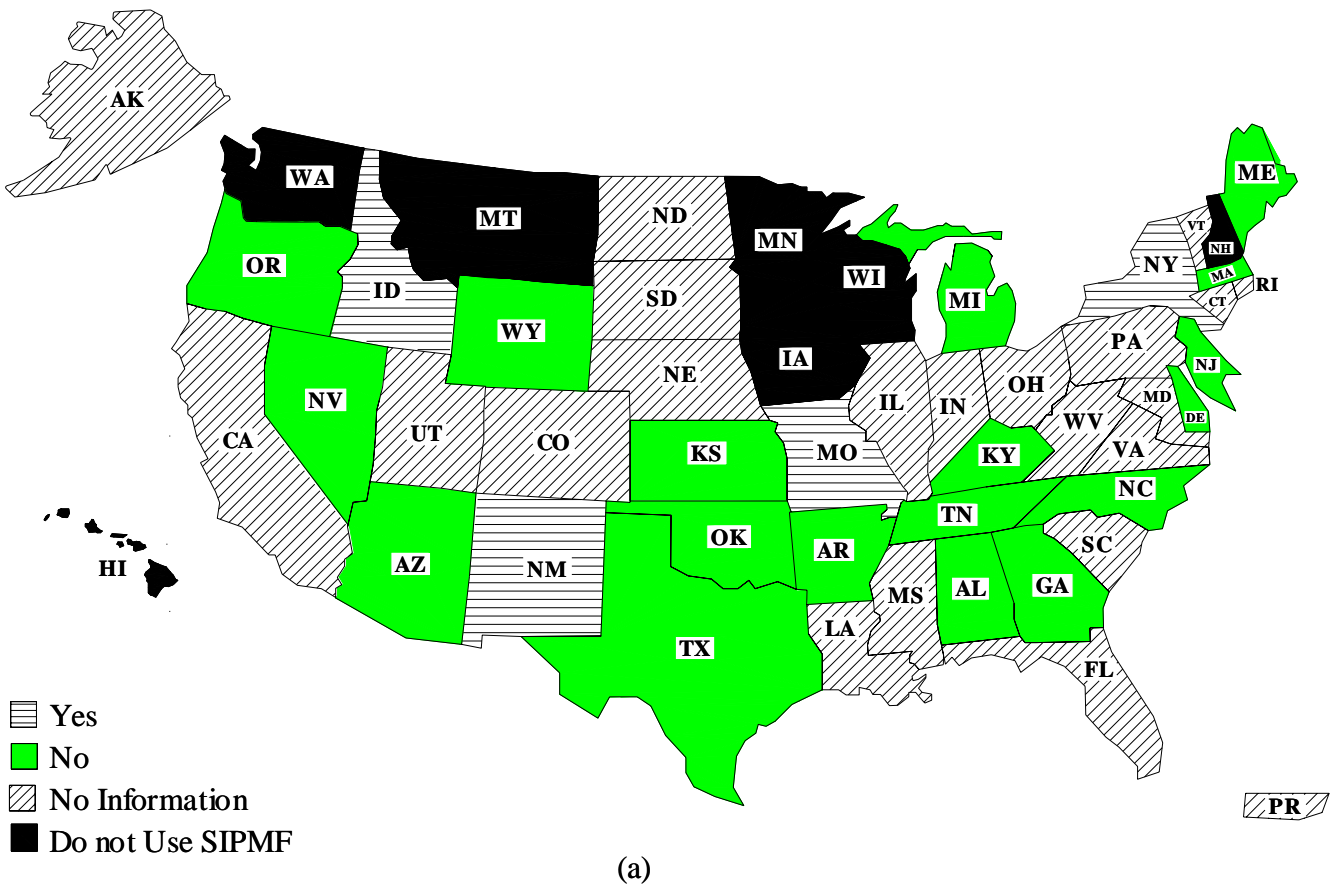


Figure 14. Has your state observed a difference in performance of decks with SIPMF constructed with bare steel reinforcement versus epoxy-coated reinforcement?

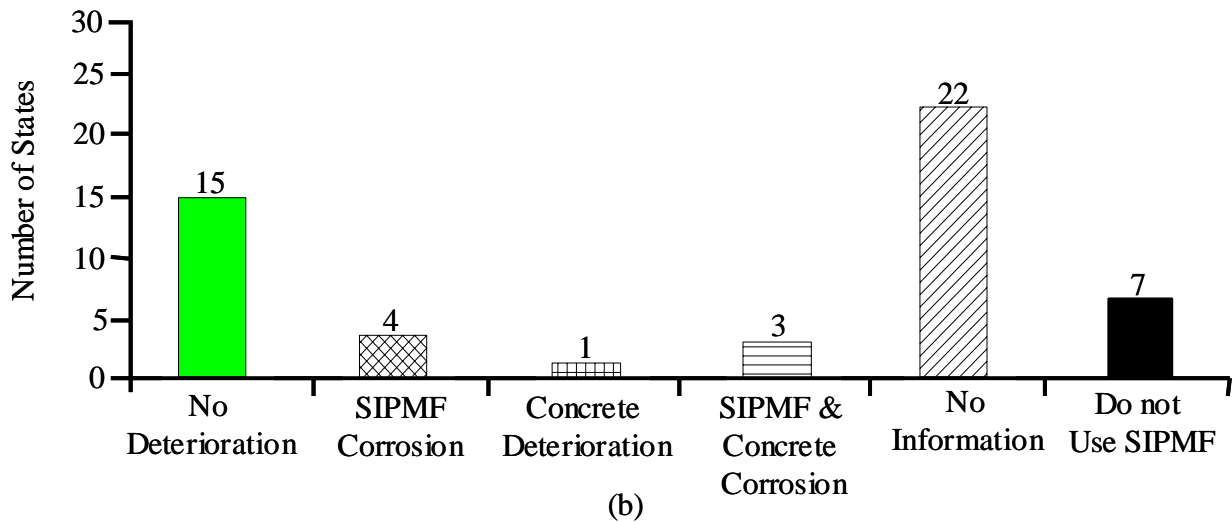
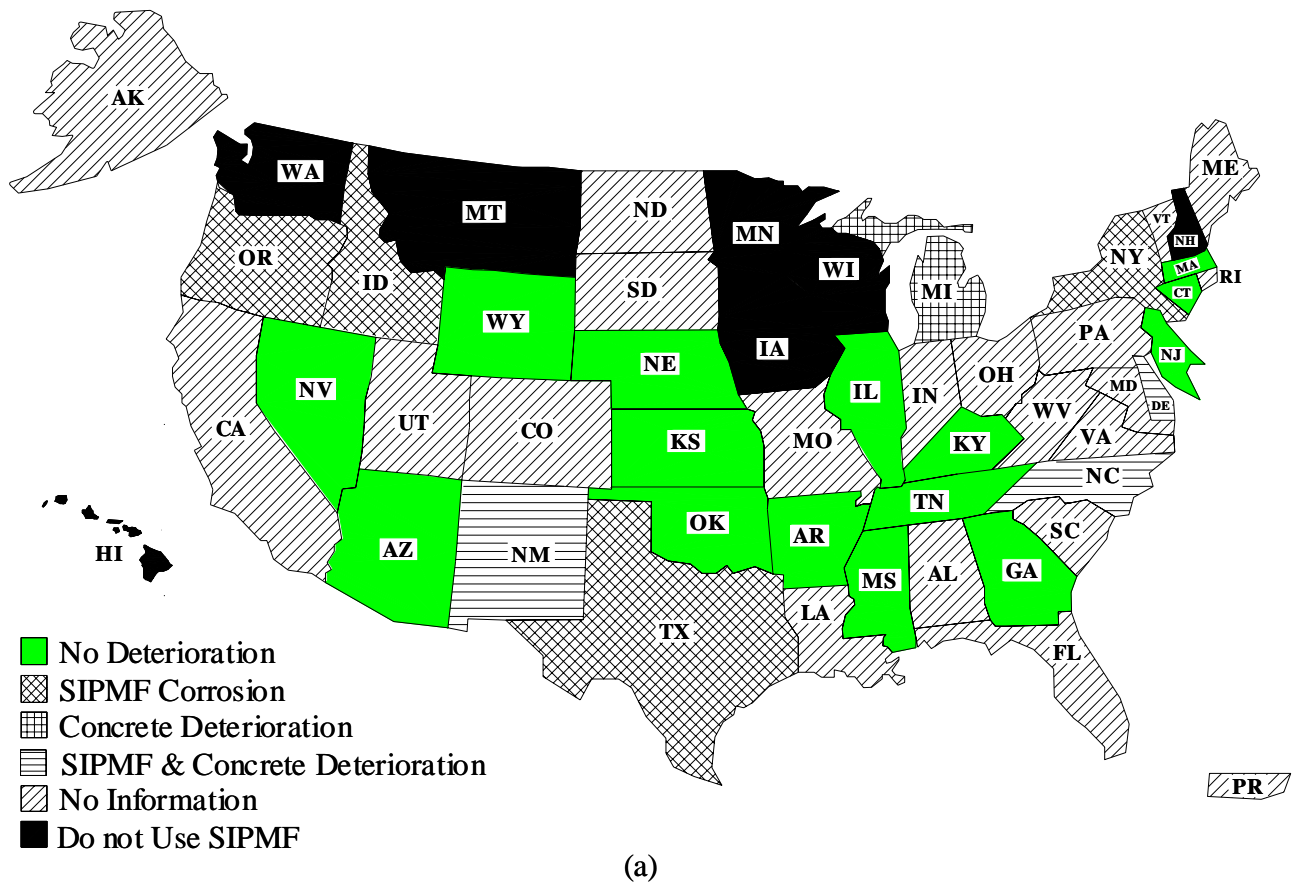


Figure 15. As a result of using SIPMF, what types of deterioration of bridge decks have been observed?

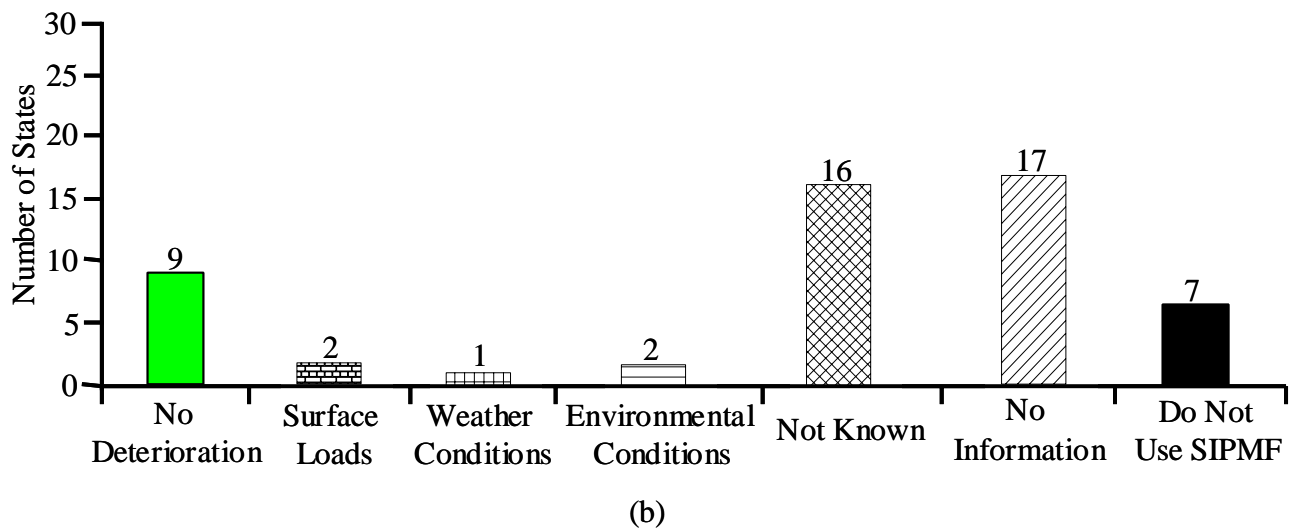
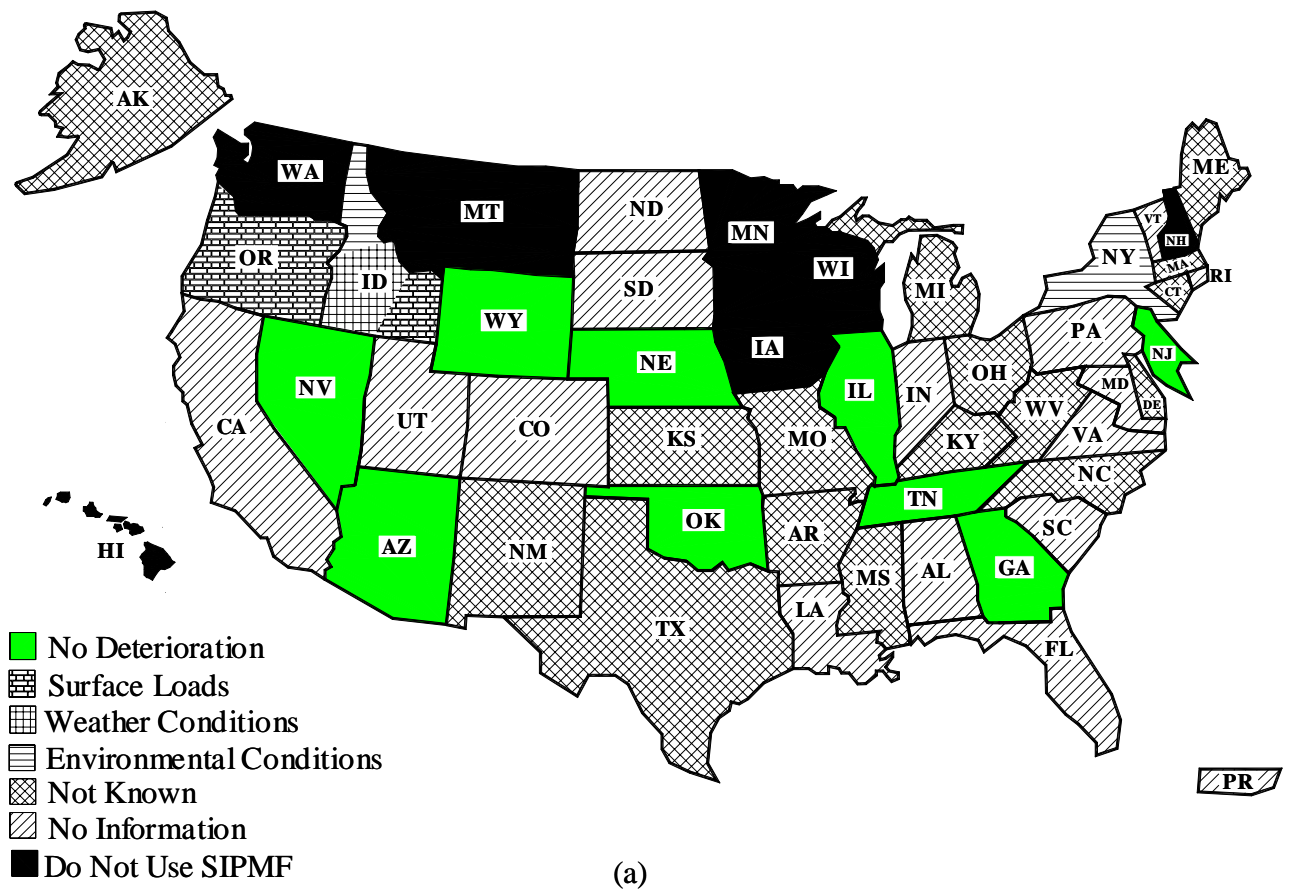


Figure 16. What is the cause of the bridge deck deteriorations when constructed using SIPMF?

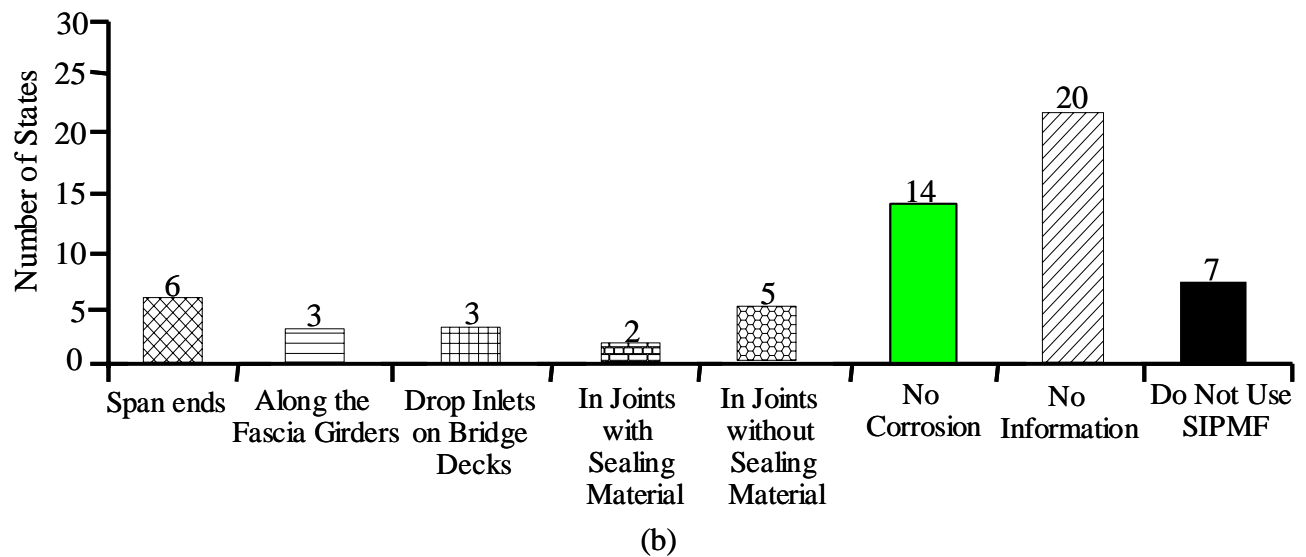
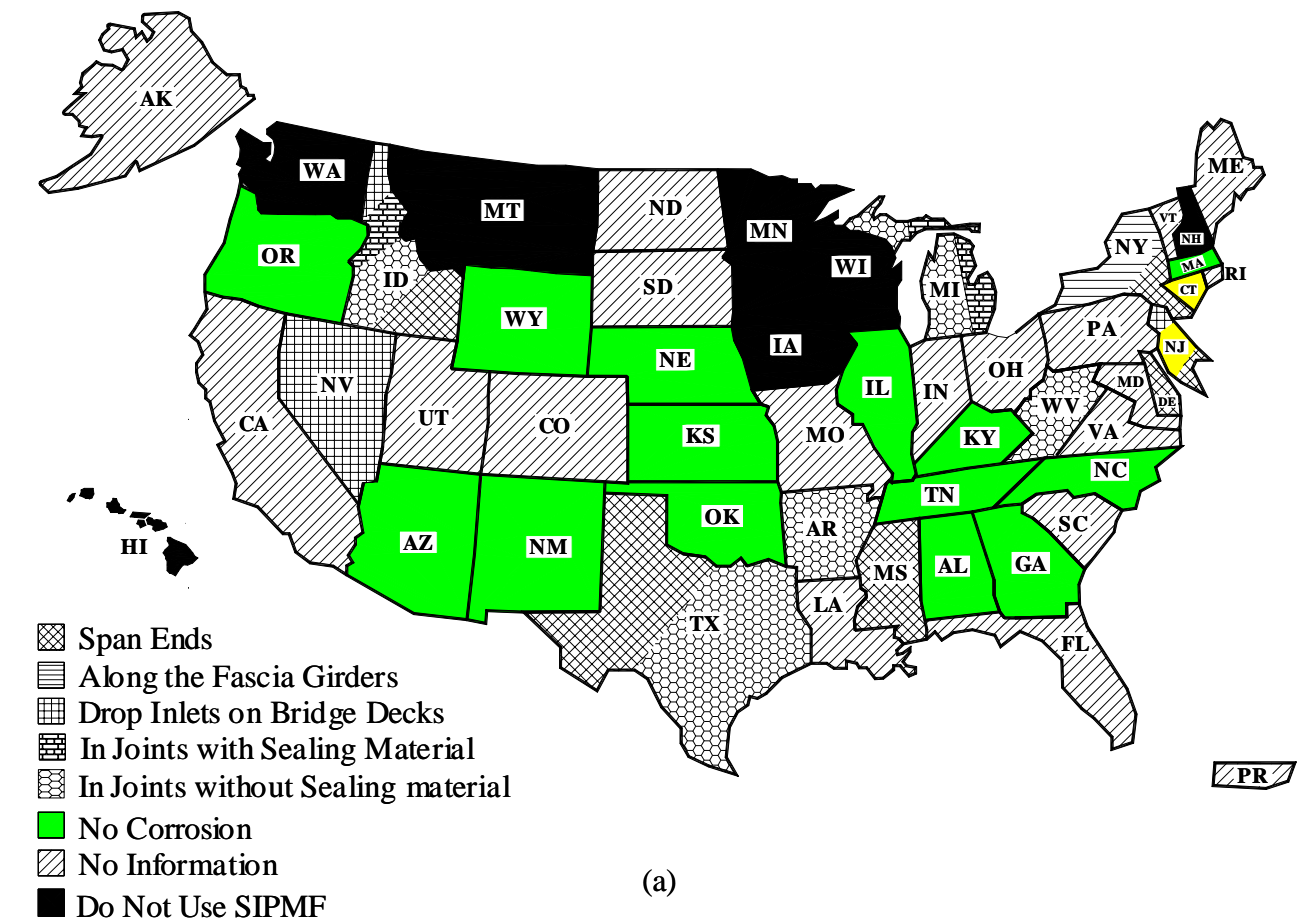


Figure 19. Where on the bridge was the most extensive corrosion of SIPMF concentrated?

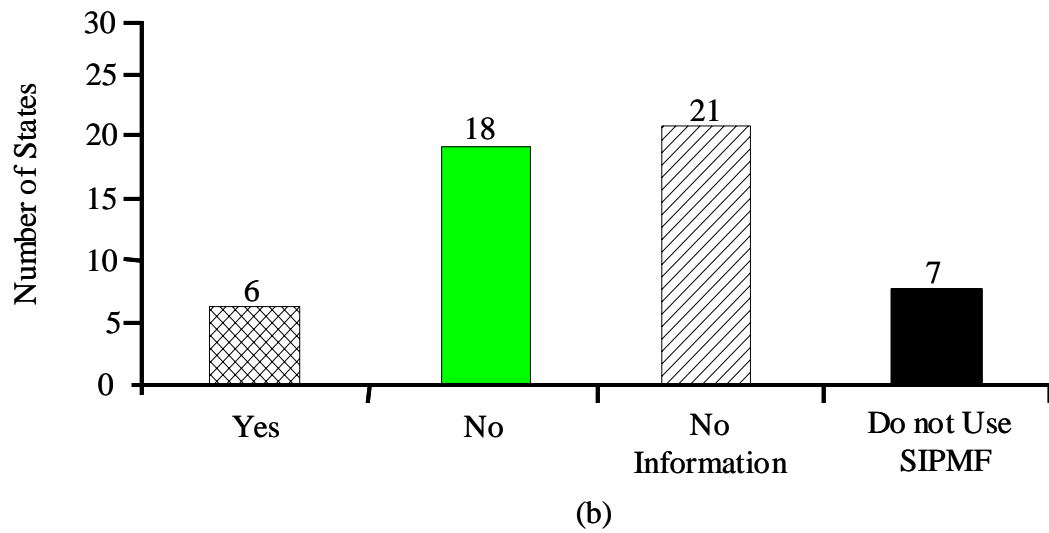
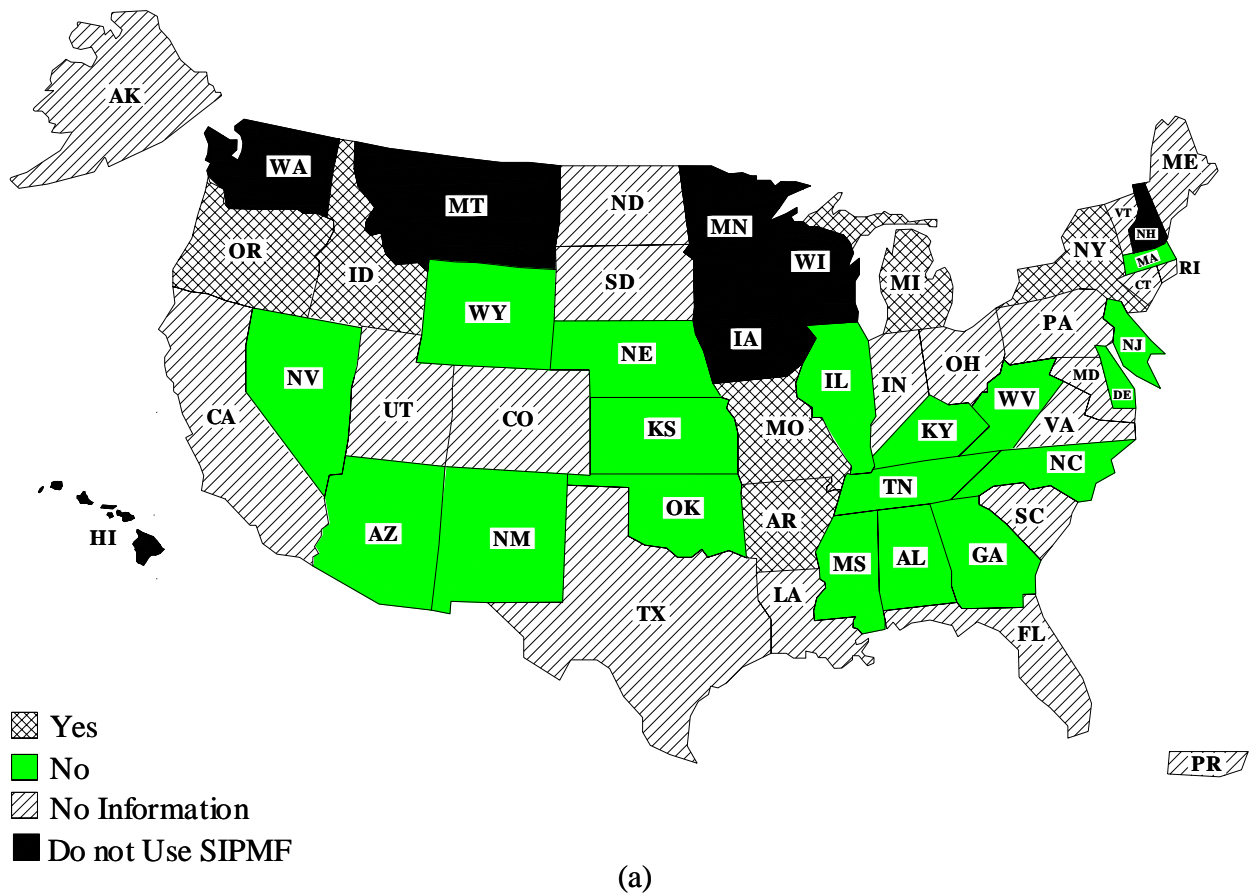


Figure 20. Is there any corrosion observed in the deck reinforcement?

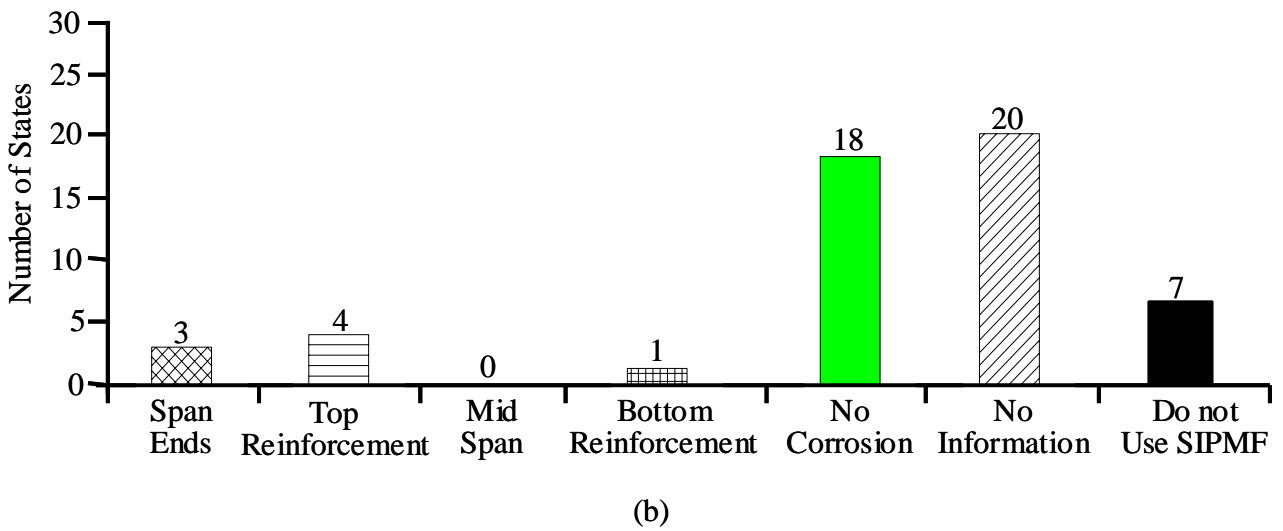
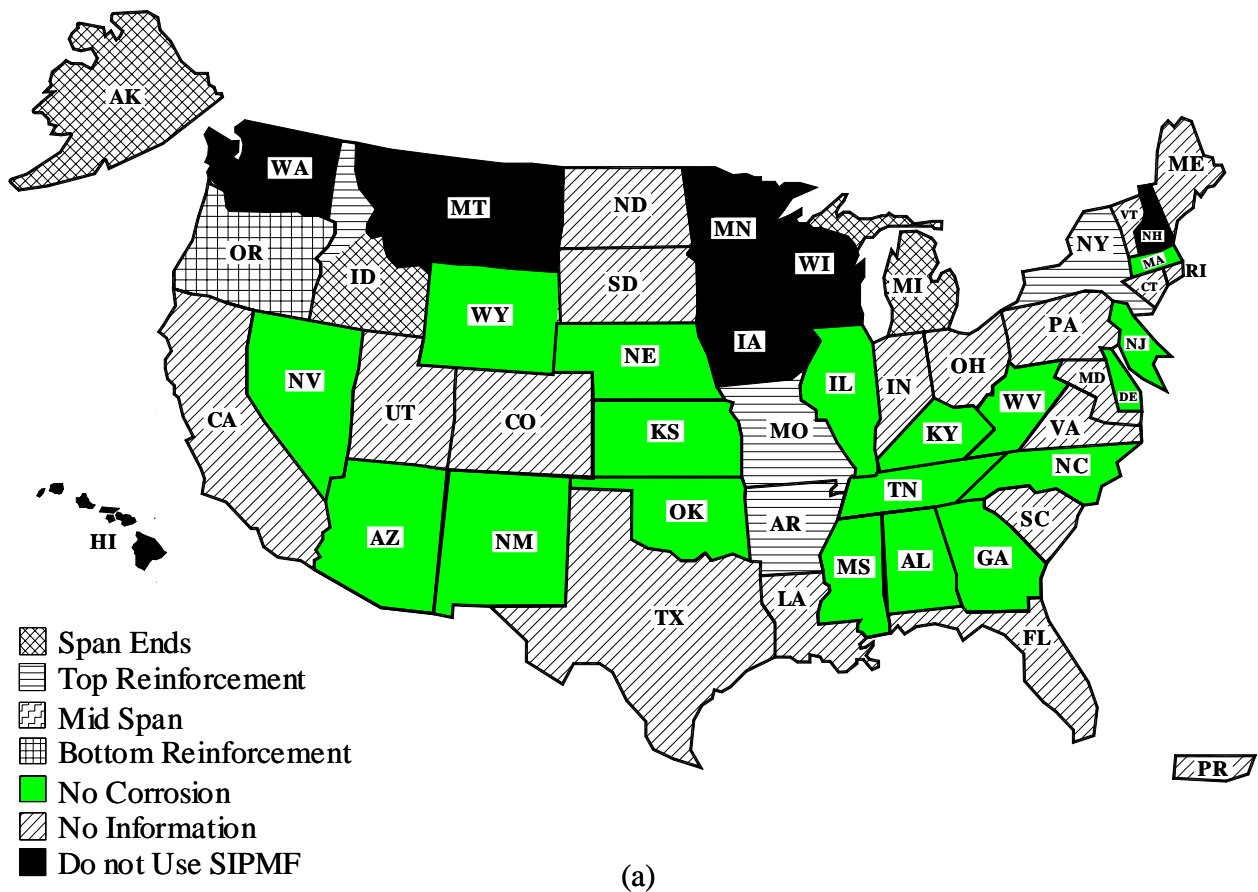
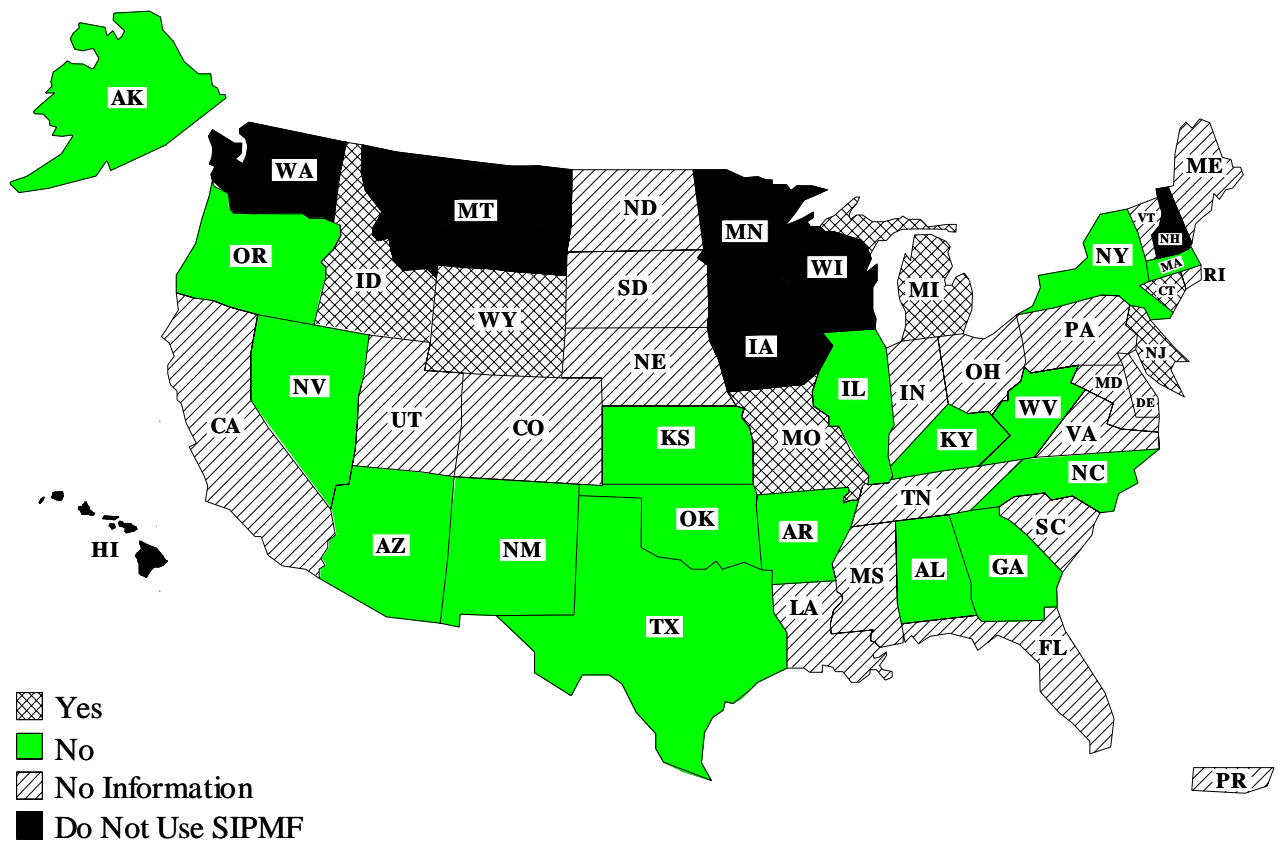
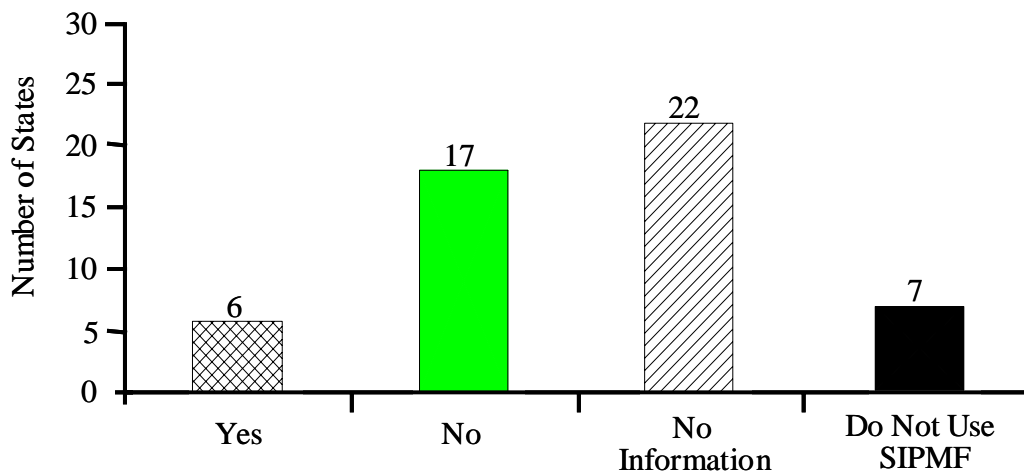


Figure 21. Where on the bridge was the most extensive corrosion of deck reinforcement concentrated?

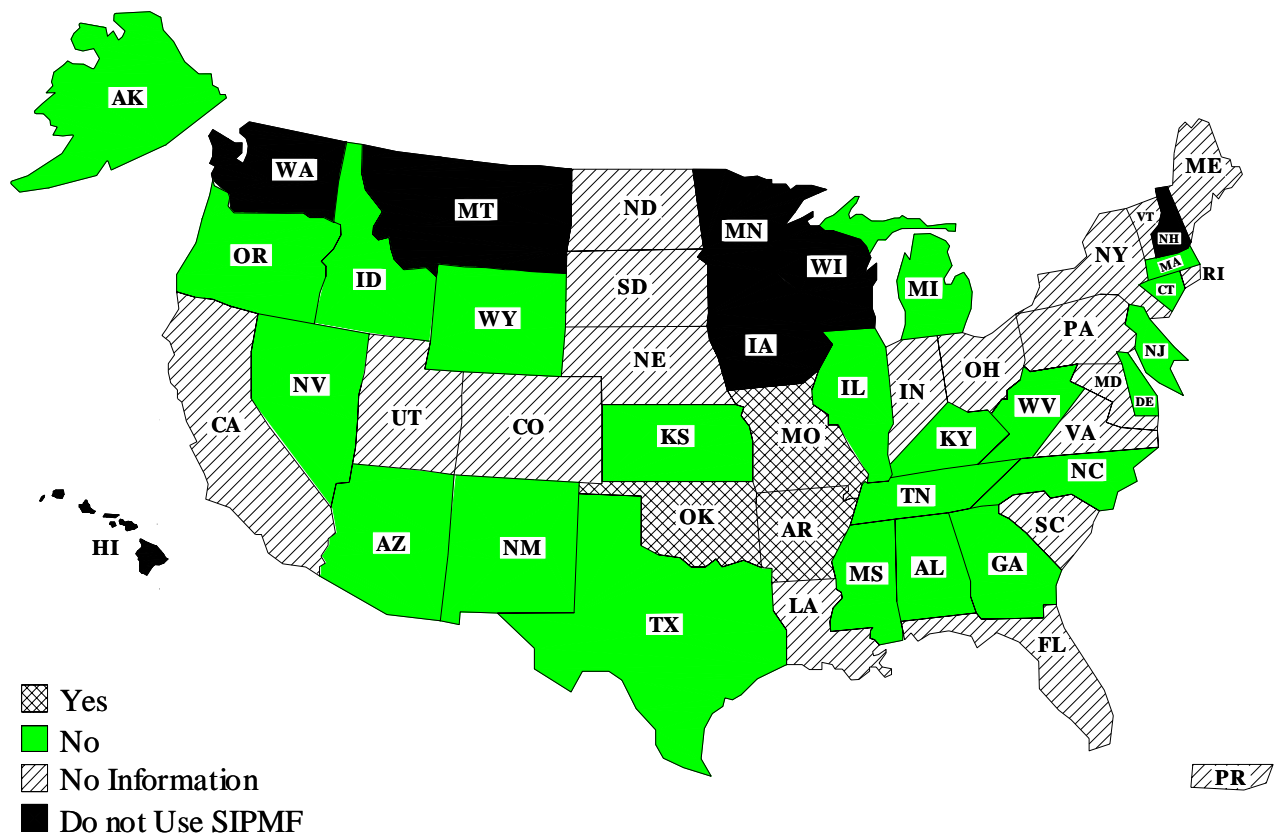


(a)

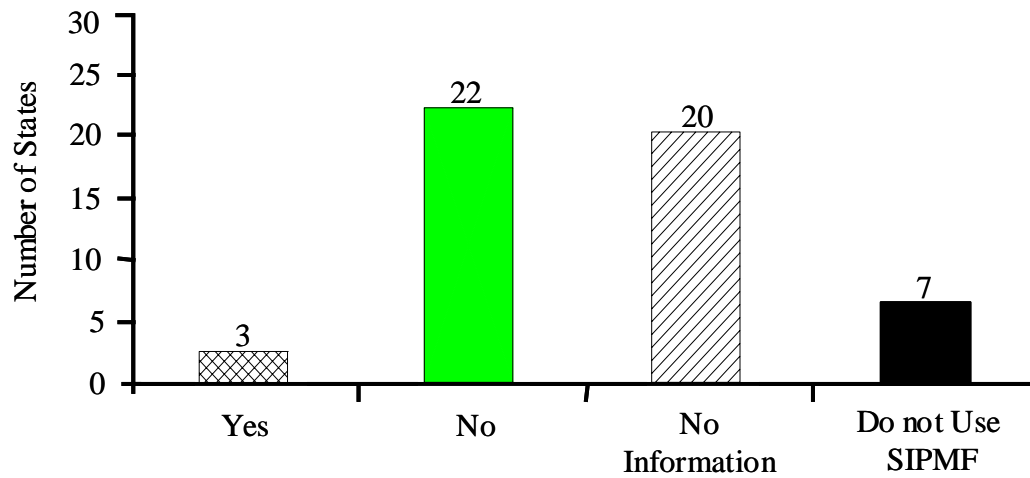


(b)

Figure 23. Has any effect of joint leakage on the SIPMF been observed?

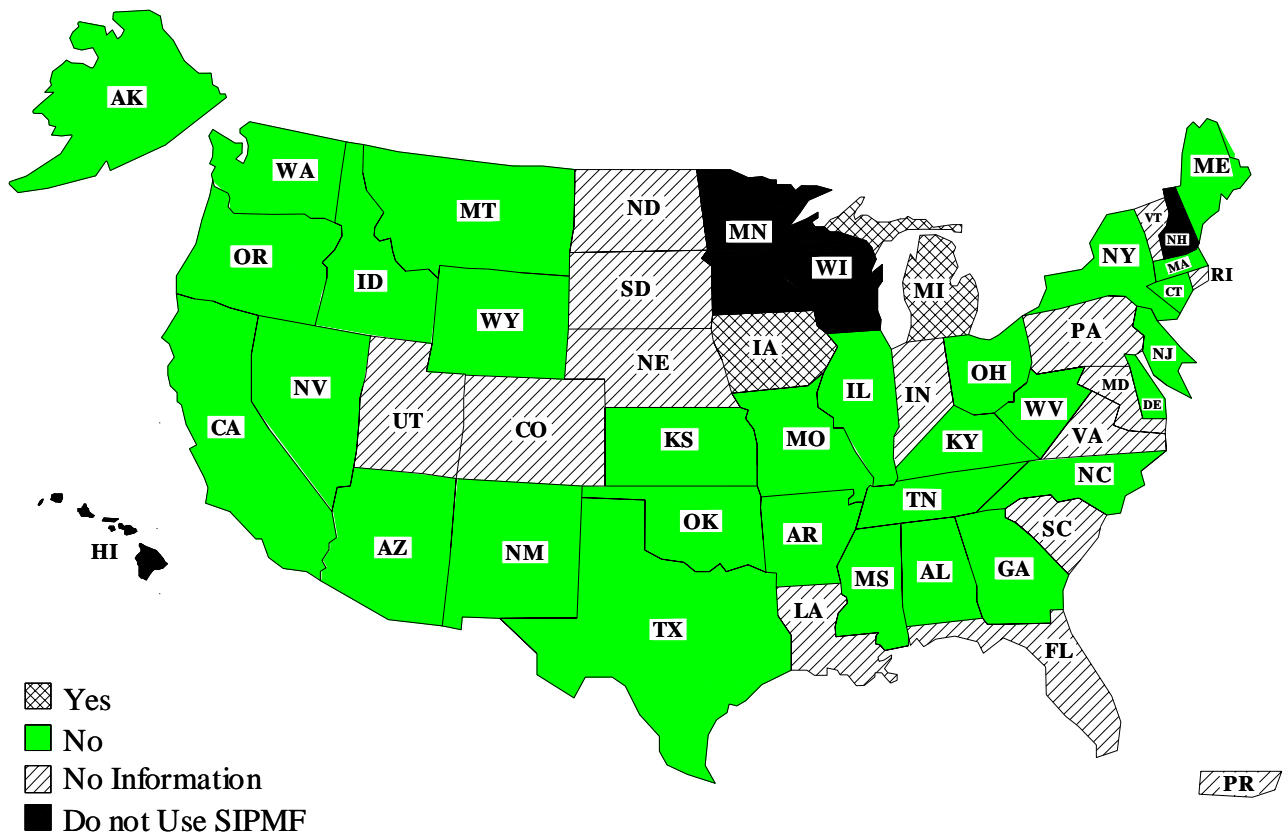


(a)

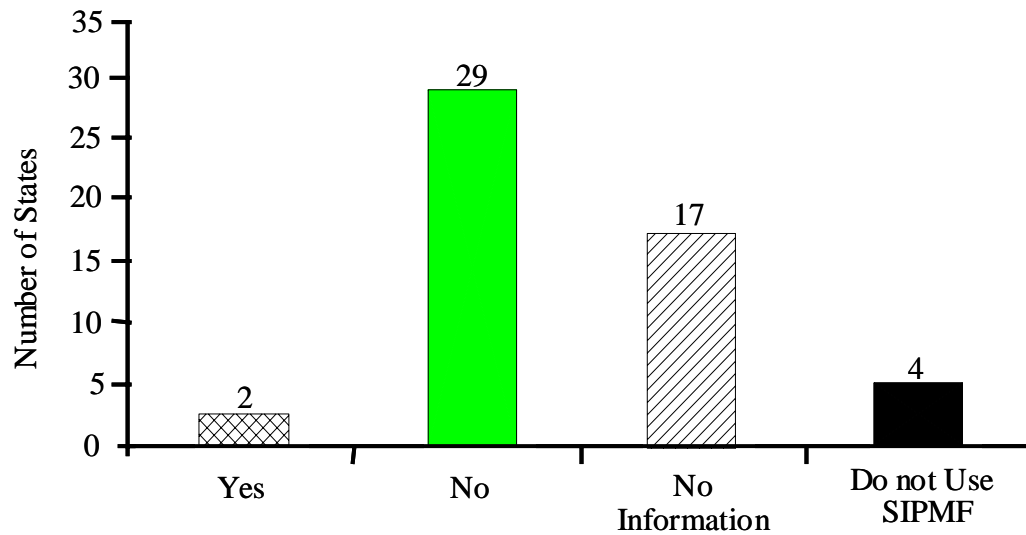


(b)

Figure 24. Were there any problems observed a direct result of using SIPMF?



(a)



(b)

Figure 25. Are you aware of any research reports in your state related to using SIPMF for bridge deck construction?

Additional Comments

State	Comment
Alabama	We have both transverse and longitudinal cracking in some of our bridge decks, but I do not attribute it to use of SIPMF. Shrinkage cracking occurs with all types of deck forms.
Arizona	<p>Epoxy-Coated deck reinforcement is used at elevations over 5000 feet, regardless whether SIPMF are used.</p> <p><u>SIPMF systems are considered for the following situations:</u></p> <ol style="list-style-type: none"> 1) When bridges span high traffic volume roadways, deep canyons or live streams. 2) When removal of conventional formwork would be difficult or hazardous. 3) When use of SIPMF system for long bridges with simple geometry could save time and/or money. 4) Where time is a critical element of the project.
California	SIPMF is not allowed on California bridges in areas where snowfall occurs. In general, on State-owned bridges (which are in the tens), the SIPMF is not included in capacity estimation. There are about tow hundred county-owned bridges in California, often single span bridges, where AC is placed directly on corrugated metals decking which acts as “forms” as well as a structure element.
Connecticut	SIPMF are only allowed over electrified rail lines or in bays over utilities where removal of conventional formwork is not feasible.
Illinois	So far our experience with SIPMF is very limited.
Maine	We have constructed only one deck with SIPMF, in 1959. It was recently replaced. We frequently use prestressed concrete slab panels in lieu of SIPMF.
Mississippi	We are concerned that with the transverse deck cracking problem we are experiencing, the use of SIPMF will contribute to premature deck deterioration due to water trapped in the forms.
Nevada	<p>No specific cracking type (longitudinal, transverse or diagonal) has been typical of decks cast with SIPMF.</p> <p>Rust areas in SIPMF have typically been associated with drain cuts which have not had galvanized repairs made thereby exposing uncoated steel to drain leakage.</p>

Figure 26. Is there any other information that you would like to share with the research team related to your experiences with observations of SIPMF?

Additional Comments

State	Comment
New Jersey	The use of SIPMF in New Jersey has been very successful with no notable deterioration of deck slabs that can be attributed to their use.
New Mexico	Since about 1990 we allowed contractors to use SIPMF or removable forms. Almost all bridges built after 1990 used SIPMF. We also require Epoxy-Coated rebar w/both mats w/SIPMF. For removable forms we require Epoxy-Coated rebar in top mat only. Contractors preferred SIPMF. Almost 100% of bridges built in New Mexico since 1990.
Ohio	We are currently examining SIPMF and trying pilot projects FY 02-06. Your research will be an important benchmark.
Oregon	When repairing a concrete deck blowout/delam using a full depth patch the delams tend to migrate outward from the original hole. The deck tends to deteriorate at an accelerated rate around the repair patch. However, when the repair included a SIPMF on the bottom side of the deck the repair seems to last much longer.
Washington	We have one state owned bridge that I know with SIPMF. The bridge was built in 1930 and rebuilt in 1949. I am assuming that the SIPMF were used in the 1949 rebuilding. This bridge is over a body of salt water and the metal forms are severely rusted out. Based on this experience as a bridge inspector, I am not in favor of ever allowing them to be used on one of our bridges.
Wyoming	Wyoming allows, but not require, the contractor to use SIPMF. We design our bridges with 15 lbs/SF additional dead load to account for the forms in most cases. However, if the actual dead load increase from filling these forms with concrete will exceed 15 lbs/SF, then the contractor is required to fill or partially fill the voids with Styrofoam. Dead load calculations not only take into account the weight of the field forms, but also the weight of additional concrete resulting from deflection of the forms, which we limit to ½ inch.

Figure 26. Is there any other information that you would like to share with the research team related to your experiences with observations of SIPMF? (Continued)

Appendix A

Survey

The Michigan Department of Transportation (MDOT) is engaged in a research project with the Structural Testing Center at Lawrence Technological University. This project involves the investigation of inspection procedures and deterioration modes of bridge decks constructed with Stay-In-Place Metal Forms (SIPMF) and epoxy-coated reinforcement.

One phase of the research program is to acquire data and experiences related to SIPMFs from state engineers representing all 50 states. Please find a survey in Word and pdf format attached to this e-mail message. Your response to this survey is important for advancing the state of practice of this bridge construction technique. The multiple choice portion of the survey can be completed electronically by clicking on the selected box.

You may either indicate your responses to the survey directly as a reply to this e-mail or as a hardcopy. Hardcopy responses should be faxed or mailed to Dr. Grace's attention at Lawrence Technological University. We anticipate this survey will take approximately 10 minutes to complete. Additional information and survey results may be obtained through Dr. Grace at Lawrence Technological University. His Contact Information is listed at the end of the attached file.

We would appreciate having the completed survey returned by March 1, 2002. Thank you for your cooperation in completing this survey.

Best Regards,

Roger D. Till, PE
Engineer of Structural Research
Michigan Department of Transportation
Construction and Technology Division
8885 Ricks Road
Lansing, Michigan 48909
Phone: (517) 322-5682
Fax: (517) 322-5664

Nabil F. Grace, Ph.D., PE
Director of Structural Testing Center
Lawrence Technological University
21000 W. Ten Mile Rd.
Southfield, MI 48075
Tel: (248) 204-2556
Fax: (248) 204-2568
E- mail: NABIL@LTU.edu

Multi-State Survey for Practices of Departments of Transportation Related to the Inspection and Deterioration of Bridge Decks Constructed with Stay-In-Place Metal Forms (SIPMF) and Epoxy-Coated Reinforcement.

CONTACT INFORMATION

State:

Please tell us about yourself:

Name:

Title /

position:

Department:

Telephone No:

Fax:

E-mail Address:

Mailing

Address:

City:

Zip Code:

PRACTICES

1- Does your state use Stay-In- Place Metal Forms (SIPMF) for constructing deck slab bridges?

☐ Yes ☐ No

2- What is your state's policy concerning the use of permanent SIPMF?

☐ Not permitted ☐ Permitted ☐ Permitted in special situation

3- In the case that your state does not permit the use of SIPMF, please specify the reasons.

4- Approximately how many bridges having decks with SIPMF does your state have?

- ☐ Less than 100 ☐ From 101 To 500 ☐ From 501 to 1000 ☐ Greater than 1000

5- Approximately how long have decks with SIPMF been used by your state in bridges?

- ☐ 10 years or less ☐ 10-20 years ☐ 20-30 years ☐ More than 30 years

6- Is your department satisfied by the performance of SIPMF?

- ☐ Very satisfied ☐ Satisfied ☐ Neutral ☐ Not satisfied ☐ Very dissatisfied

7- Does your state fill corrugations of the SIPMF with Styrofoam to reduce dead load?

- ☐ Yes ☐ No

8- Does your state use epoxy-coated steel in bridge decks with SIPMF?

- ☐ Yes ☐ No

INSPECTION

9- Besides visual inspection and hammer sounding of the surface, what other techniques does your department use to inspect SIPMF bridge decks?

- ☐ Ultrasonic methods
☐ Acoustic Tomography
☐ Ground-Penetrating Radar
☐ Infrared Thermography
☐ Laser Crack Detection
☐ Petrographic examination
☐ No inspection conducted
☐ Other Please describe:

10- Does your state gather specific data related to SIPMF bridge decks?

☐ Yes ☐ No

If yes please provide:

Contact person:

Phone number:

11- What is the typical period between each inspection of decks with SIPMF?

☐ Less than 1 year

☐ From 1-3 years

☐ More than 3 years

PERFORMANCE

12- How can you describe the status of SIPMF bridge decks in your state?

☐ Excellent

☐ Good

☐ Fair

☐ Poor

13- Do you believe that SIPMFs increase the long-term durability of bridge decks?

☐ Yes ☐ No

14- Has your state observed a difference in performance of decks with SIPMF constructed with bare steel reinforcement versus epoxy-coated reinforcement?

☐ Yes ☐ No

15- As a result of using SIPMF, what types of deterioration of bridge decks have been observed?

☐ No deterioration

☐ Cracking

☐ Low surface mortar deterioration

☐ Spalling

☐ High surface mortar deterioration

☐ Popouts

☐ Scaling

☐ Delamination

☐ Rubblized concrete adjacent to form

☐ Other Please describe:

16- What is the cause of the bridge deck deteriorations when constructed using SIPMF?

☐ Surface load

☐ Weather conditions

☐ Environmental conditions

☐ Not known

Explain:

17- What is the most common type of deck cracking observed in SIPMF bridge decks?

☐ Longitudinal

☐ Transverse

☐ Diagonal

18- Has any corrosion in the SIPMF been observed?

☐ Yes ☐ No

If no, skip to question 20

19- Where on the bridge was the most extensive corrosion of SIPMF concentrated?

☐ Span ends

☐ Along the fascia girders

☐ Drop inlets on bridge decks

☐ In joints with sealing material

☐ In joints without sealing material

20- Is there any corrosion observed in the deck reinforcement?

☐ Yes ☐ No

If no, skip to question 23

21- Where on the bridge was the most extensive corrosion of deck reinforcement concentrated?

☐ Span ends

☐ Mid span

☐ Top reinforcement

☐ Bottom reinforcement

☐ Others Please describe:

22- After how long did the extensive corrosion occur?

☐ 1-5 years

☐ 5-10 years

☐ More than 10 years

23- Has any effect of joint leakage on the SIPMF been observed?

☐ Yes ☐ No

If yes, please describe briefly:

24- Were there any other problems observed as a direct result of using SIPMF?

☐ Yes ☐ No

If yes, please specify this problem

REPORTS

25- Are you aware of any research reports in your state related to using SIPMF for bridge deck construction?

☐ Yes ☐ No

If yes please list or provide contact information :

OTHER COMMENTS

26- Is there any other information that you would like to share with the research team related to your experiences with observations of SIPMF?

Thank you for your time in completing the survey.

For additional information and survey results, you may contact Dr. Nabil Grace at Lawrence

Technological University. His contact information is listed below.

Nabil F. Grace, Ph.D., PE
Director of Structural Testing Center
Lawrence Technological University
21000 W. Ten Mile Rd.
Southfield, MI 48075
Tel: (248) 204-2556
Fax:(248) 204-2568
E- mail: Nabil@LTU.edu

APPENDIX B: PROGRAM FOR ARRIVAL TIME CALCULATION

Summary of steps to determine first arrival time from through-transmission tests (from Inci, 2001)

1. $FW_{avg.} = W_{avg.} - AW_{avg.}$
2. The waveform $FW_{avg.}$ is divided into regional division.
3. First $FW_{avg.}$ is divided into regions of 20 points.
4. For each region the following terms were calculated:
 - i. $ABS \mid 1^{st} - last \mid = ABS_{20}$
 - ii. Avg. (1st to last) “Mean” $= M_{20}$
 - iii. (Max – Min) $= MM_{20}$
 - iv. Standard deviation of the region $= \sigma_{20}$
5. Same as in step 3, $FW_{avg.}$ is divided into regions of 40, 60, 80,, 1000 points.
6. Same as in step 4, each region the following terms were calculated:
 - i. $ABS \mid 1^{st} - last \mid = ABS_{40, 60, 80, \dots, 1000}$
 - ii. Avg. (1st to last) “Mean” $= M_{40, 60, 80, \dots, 1000}$
 - iii. (Max – Min) $= MM_{40, 60, 80, \dots, 1000}$
 - iv. Standard deviation of the region $= \sigma_{40, 60, 80, \dots, 1000}$
7. For each region division eight criteria were applied:
 - i. If $M_i < [\text{Mean of } (M_1 \rightarrow M_{i-1}) - 3 * \text{Mean of } (\sigma_1 \rightarrow \sigma_{i-1})]$
or $M_i > [\text{Mean of } (M_1 \rightarrow M_{i-1}) + 3 * \text{Mean of } (\sigma_1 \rightarrow \sigma_{i-1})]$,
then the first point in region “i” will be the “time base point t_1 ”.
 - ii. If $ABS_i > 4 * [\text{Mean of } (ABS_1 \rightarrow ABS_{i-1})]$,
then the first point in region “i” will be the “time base point t_2 ”.
 - iii. If $M_i > 4 * [\text{Mean of } (M_1 \rightarrow M_{i-1})]$,
then the first point in region “i” will be the “time base point t_3 ”.
 - iv. If $MM_i > 4 * [\text{Mean of } (MM_1 \rightarrow MM_{i-1})]$,
then the first point in region “i” will be the “time base point t_4 ”.

v. If $MM_i > 4 * MM_{i-1}$,
then the first point in region “i” will be the “time base point t_5 ”.

vi. If $M_i > 4 * M_{i-1}$,
then the first point in region “i” will be the “time base point t_6 ”.

vii. If $ABS_i > 4 * ABS_{i-1}$,
then the first point in region “i” will be the “time base point t_7 ”.

viii. If $M_i < [M_{i-1} - 3 * \sigma_{i-1}]$
or $M_i > [M_{i-1} + 3 * \sigma_{i-1}]$,
then the first point in region “i” will be the “time base point t_8 ”.

8. After calculating all of the eight time base points for each region division, the t-base matrix (8 x 50) is built as following:

i. Region division: 20 40 60 80.....1000

$$\begin{pmatrix} t_1 & t_1 & t_1 & t_1 \dots\dots\dots t_1 \\ t_2 & t_2 & t_2 & t_2 \dots\dots\dots t_2 \\ t_3 & t_3 & t_3 & t_3 \dots\dots\dots t_3 \\ t_4 & t_4 & t_4 & t_4 \dots\dots\dots t_4 \\ t_5 & t_5 & t_5 & t_5 \dots\dots\dots t_5 \\ t_6 & t_6 & t_6 & t_6 \dots\dots\dots t_6 \\ t_7 & t_7 & t_7 & t_7 \dots\dots\dots t_7 \\ t_8 & t_8 & t_8 & t_8 \dots\dots\dots t_8 \end{pmatrix}$$

9. The average for all time base t_i from the matrix was calculated to get
“Time Base Value = t_f ”.

10. A “Base Region” was decided to be:

$$[(^{1/3}) t_f \rightarrow (^{2/3}) t_f]$$

11. For the Base Region the following terms were calculated:

i. Maximum = Max_{BR}

ii. Minimum = Min_{BR}

iii. Mean = M_{BR}

12. The waveform $FW_{avg.}$ is adjusted by doing the following correction:

$$FW_{new} = [FW_{avg.} - M_{BR}]$$

13. A filtration is done by taking the reading each 10 points.

14. The filtered adjusted new waveform " FW_{filt} " is inverted with respect to the x-axis to get the waveform " FW_{inv} ".

15. A threshold was determined to be:

$$\text{Threshold value } Th = 1.1 * [Max_{BR} - Min_{BR}]$$

16. The arrival time is determined to be:

t_{arr} = the first intersection point of the waveform " FW_{inv} " with the threshold value "Th".

$FW_{avg.}$: Filtered average wave
 $W_{avg.}$: Average wave
 $AW_{avg.}$: Average air wave
ABS : Absolute value
Avg. : Average value
 1^{st} : First value in the region
last : Last value in the region
(Max – Min) : Maximum value – minimum value

Automated Program for Calculating Arrival Time Across Entire Specimen:

```
Sub ultrasonicII()  
,  
' ultrasonicII Macro  
' Macro recorded 9/23/2003 by Administrator  
,  
' Keyboard Shortcut: Ctrl+r  
,
```

```
For J = 1 To 4  
    Select Case J  
        Case 1  
            Beam = "A"  
  
        Case 2
```

```

    Beam = "B"

Case 3
    Beam = "C"

Case 4
    Beam = "D"
End Select

Workbooks.Open Filename:= _
"C:\MDot_WH\Project\Specimens Slices\WO-C-1\Ultrasonic Readings\Time
Values.xls"

If J = 1 Then
    Range("B2").Select
ElseIf J = 2 Then
    Range("B3").Select
ElseIf J = 3 Then
    Range("B4").Select
ElseIf J = 4 Then
    Range("B5").Select
End If

ActiveWorkbook.Save
ActiveWorkbook.Close

For i = 1 To 41
'Select files A1-A41...
Application.ScreenUpdating = True
    dSource = Beam & i & ".asc"

    ChDir "C:\MDot_WH\Project\Specimens Slices\WO-C-1\Ultrasonic Readings"
    Workbooks.OpenText Filename:= _
        "C:\MDot_WH\Project\Specimens Slices\WO-C-1\Ultrasonic Readings\" &
dSource, Origin _
        :=xlWindows, StartRow:=1, DataType:=xlDelimited, TextQualifier:= _
        xlDoubleQuote, ConsecutiveDelimiter:=False, Tab:=True, Semicolon:=False, _
        Comma:=False, Space:=False, Other:=False, FieldInfo:=Array(Array(1, 1), _
        Array(2, 1))
    Columns("A:B").Select
    Selection.Copy
    Windows("Arrival time Fin.xls").Activate
    ActiveWindow.Panes(1).Activate
    Columns("A:B").Select
    ActiveSheet.Paste
    ActiveWindow.Panes(2).Activate

```



```

Range("FT32").Select
Application.CutCopyMode = False
Selection.Copy
Workbooks.Open Filename:= _
    "C:\MDot_WH\Project\Specimens Slices\WO-C-1\Ultrasonic Readings\Time
Values.xls"
Selection.PasteSpecial Paste:=xlValues, Operation:=xlNone, SkipBlanks:= _
    False, Transpose:=False
Application.CutCopyMode = False

ActiveCell.Offset(0, 1).Select

ActiveWorkbook.Save
ActiveWorkbook.Close
Windows(Beam & i & ".asc").Activate
ActiveWorkbook.Close

Next i
Next J

End Sub

```


APPENDIX C: SALT SOLUTION COMPOSITION

Typical Composition of Instant Ocean Salt Solution at Approximate Salinity of 35ppt

Ion	Instant Ocean (ppm)	Seawater* (ppm)
Chloride	19,290	19,353
Sodium	10,780	10,781
Sulfate	2,660	2,712
Magnesium	1,320	1,284
Potassium	420	399
Calcium	400	412
Carbonate/bicarbonate	200	126
Bromide	56	67
Strontium	8.8	7.9
Boron	5.6	4.5
Fluoride	1.0	1.28
Lithium	0.3	0.173
Iodide	0.24	0.06
Barium	less than 0.04	0.014
Iron	less than 0.04	less than 0.001
Manganese	less than 0.025	less than 0.001
Chromium	less than 0.015	less than 0.001
Cobalt	less than 0.015	less than 0.001
Copper	less than 0.015	less than 0.001
Nickel	less than 0.015	less than 0.001
Selenium	less than 0.015	less than 0.001
Vanadium	less than 0.015	less than 0.002
Zinc	less than 0.015	less than 0.001
Molybdenum	less than 0.01	0.01
Aluminum	less than 0.006	less than 0.001
Lead	less than 0.005	less than 0.001
Arsenic	less than 0.004	0.002
Cadmium	less than 0.002	less than 0.001
Nitrate	None	1.8
Phosphate	None	0.2

* Data for seawater values taken from Pilson (1998).